

**Modulation of Brain Chemistry with Small Molecule Probes: From Opioid to
Growth Factor Signaling Systems**

Madalee M. Gassaway

Submitted in partial fulfillment of the
requirements for the degree of
Doctor of Philosophy
in the Graduate School of Arts and Sciences

COLUMBIA UNIVERSITY

2016

© 2016
Madalee M. Gassaway
All rights reserved

Abstract

Modulation of Brain Chemistry with Small Molecule Probes: From Opioid to Growth Factor Signaling Systems

Madalee M. Gassaway

This report describes the use of small molecule probes in the modulation of brain chemistry with the ultimate goal of developing novel therapeutics for the treatment of mood disorders. With an increasing number of people suffering from depression, there is a need to explore more diverse mechanisms of these diseases to better understand their cause and therefore provide insight into their treatment. Chapter 1 serves as an introduction and describes the current understanding of depression mechanisms, as well as a history of antidepressant therapeutics. The chapter then goes on to discuss, in depth, the mechanisms of G Protein-Coupled Receptor (GPCR) function and the implications of biased signaling. There is also an introductory overview of basic pharmacological terms. The chapter finishes with a summary of current technology available to measure GPCR function, including those utilized in the rest of this report.

The remainder of the report is broken up into two parts. In the first part, I will describe my work to understand the opioid receptor system in the context of mood disorders. In Chapter 2, the atypical antidepressant tianeptine is discovered to act through the mu-opioid receptor (MOR), and a biochemical exploration is reported including an exploration of its unique properties in the context of G protein-dependent and -independent signaling, as well as preliminary *in vivo* and structure activity relationship studies into the mechanism of action. In Chapter 3, I will describe the biological characterization of the *Mitragyna speciosa* alkaloids at the opioid receptors. In particular, the major alkaloids mitragynine and 7-OH mitragynine are found to be partial agonists at the MOR and antagonists at the kappa-opioid receptor (KOR) with

apparent G protein bias. In Chapter 4, alkaloids inspired by those found in *Tabernanthe iboga*, such as ibogaine, are synthesized and characterized at the opioid receptors. Through a novel 12-hydroxy-oxaibogamine scaffold, opioid activity is uncovered that is greatly increased in comparison to the ibogaine metabolite noribogaine. Analogs tested have varying degrees of potency and efficacy at all three opioid receptors, and one analog in particular is found to be a selective G protein biased partial KOR agonist. In Chapter 5, I will conclude the opioid section by taking a critical examination of commonly used assays for measuring arrestin recruitment by dissecting assay components and analyzing what is necessary to determine accurate calculations of bias within a cellular system. The alleged G protein bias of KOR agonist dynorphin is studied at great length, and a discussion on the future of understanding ligand bias is presented.

In the second part of this report, I move away from opioids and instead focus on the growth factor signaling system as a second approach to uncovering novel therapeutics for depression. In Chapter 6, I describe a second potential mechanism of action of the natural product ibogaine in the context of glial cell line-derived neurotrophic factor (GDNF) signaling. The deconstructed *iboga* analog XL-008 is studied that is a superior releaser of GDNF and potentiates the signaling of a second growth factor, fibroblast growth factor 2 (FGF2). In the final Chapter 7, I look to the FGF family, both receptor and growth factor, as a novel target for depression. In order to identify small molecule modulators of the FGF receptor 1 (FGFR1), cell-based assays are developed and validated in a pilot screen. The strength of these assays are assessed, and the initial results from a full high throughput screen are presented.

Table of Contents

Chapter 1 – An Introduction into Depression, Opioids, and Pharmacology	1
Depression: Symptoms and Mechanisms	1
Symptoms of Depression	1
Monoamine Hypothesis of Depression.....	1
Glutamate Signaling in Depression	2
Mesolimbic Rewards Pathway.....	4
Neurotrophin Hypothesis	6
Current Treatment Options for Depression are Limited.....	8
Monoamine Oxidase Inhibitors (MAOIs).....	8
Tricyclic Antidepressants (TCAs)	9
Selective Serotonin Reuptake Inhibitors (SSRIs)	9
Atypical Classes of Antidepressants	10
Filling the Void in Antidepressant Therapeutics	11
G Protein-Coupled Receptor (GPCR) Signaling – The Opioid Receptors.....	12
Signaling Cascades of GPCRs	12
Unconventional Signaling of GPCRs	15
Understanding Ligand Bias: Pharmacology, Definitions, and Evidence.....	16
A Lesson in Pharmacology Terms.....	16
Defining Functional Selectivity/Ligand Bias.....	17
Distinguishing the Level of Bias for a Ligand.....	22
Examples of Ligand Bias	25
Tools to Study Pharmacology	29

Assays Available for the Measure of GPCR Functional Activity	29
Current Work.....	35
References.....	36

Part I – The Opioid Receptor Signaling System

Chapter 2 – Uncovering the Mechanism of Action of the Atypical

Antidepressant Tianeptine.....48

Introduction.....48

Results52

Identifying the Molecular Target of Tianeptine52

Tianeptine Binds to the Opioid Receptors.....52

Tianeptine is an Agonist at the MOR.....53

Functional Activity of Tianeptine Metabolites.....57

Measuring Other Signaling Pathways.....58

In Vitro Pharmacokinetic Data on Tianeptine and MC5.....60

Discussion60

Mechanism of Action.....60

Preliminary *In Vivo* Results Implicate MOR in Behavioral Effects of Tianeptine and

MC5.....65

Goals for Structure Activity Relationship (SAR) Studies.....66

Abuse Potential of Tianeptine.....67

Conclusions.....68

Experimental68

Preparation of MC3 and MC5 Metabolites.....	68
Biology.....	72
References.....	75
<u>Chapter 3 – Exploring the Biological Activity of the <i>Mitragyna speciosa</i></u>	
<u>Alkaloids at the Opioid Receptors</u>	81
<u>Introduction.....</u>	81
<u>Results</u>	84
Biological Activity of <i>Mitragyna</i> Alkaloids at Rodent Opioid Receptors.....	84
Isolation of the Alkaloids From the Plant Material	84
Binding Affinity.....	85
Functional Activity	86
Biological Activity of <i>Mitragyna</i> Alkaloids at the Human Opioid Receptors.....	87
Binding Affinity.....	88
Functional Activity	88
Exploring Other Isomers of Mitragynine	91
Synthesis of Mitragynine Isomers	92
Functional Activity of Mitragynine Isomers.....	93
Mitragynine Pseudoindoxyl is an Interesting Pharmacological Tool	94
Synthesis of Mitragynine Pseudoindoxyl	95
Functional Activity of Mitragynine Pseudoindoxyl	95
Exploring G Protein Independent Signaling Pathways of <i>Mitragyna</i> Alkaloids.....	97
<i>Mitragyna</i> Alkaloids do not Signal Through Arrestin.....	97
Calculating the Bias Factors of <i>Mitragyna</i> Alkaloids.....	98

Mitragynine Pseudoindoxyl is a Potential Imaging Agent.....	100
Mitragynine Pseudoindoxyl as an Imaging Agent.....	100
Molecular Docking of <i>Mitragyna</i> Alkaloids at the MOR	102
Mitragynine Scaffold has Unique Binding Pose at MOR.....	102
Biological Activity of <i>Mitragyna</i> Alkaloids at Non-Opioid Receptors.....	105
Binding Affinity at Human α_2R	105
Functional Activity at Human α_2R	106
Functional Activity at Vesicular Monoamine Transporter 2 (VMAT2).....	107
<u>Discussion</u>	108
Opioid Activity of <i>Mitragyna</i> Alkaloids.....	108
G Protein Bias of Three Alkaloids.....	110
<i>Mitragyna</i> Alkaloids Have a Unique Binding Pose at MOR.....	110
Variation Between Rodent and Human Data.....	111
7-OH as a Natural Alkaloid of <i>Mitragyna speciosa</i>	112
Pharmacological Consequences of Adrenergic Activity	112
<u>Conclusions</u>.....	116
<u>Experimental</u>	117
Chemistry	117
Biological Procedures	119
Calculations.....	124
<u>References</u>.....	124
<u>Chapter 4 – 12-Hydroxy-Oxaibogamine as a Novel Scaffold for Opioid Receptor Modulation.....</u>	130

<u>Introduction</u>	130
<u>Results</u>	133
Biological Activity of Noribogaine at the Opioid Receptors	133
Discovery and Biological Activity of Novel Oxaibogamine Analogs	136
Initial Structure Activity Relationships (SAR) Reveal Alternate Scaffold	136
Synthesis of 12-Hydroxy-Oxaibogamine Analogs	137
Functional Activity of Novel 12-Hydroxy-Oxaibogamine Analogs	139
Exploring the SAR of <i>Exo</i>- and <i>Endo</i>-Substituents Within the Oxaibogamine Scaffold....	142
Synthesis of Analogs Beyond the Ethyl Substituent.....	142
Functional Activity of Second Generation 12-Hydroxy-Oxaibogamine Analogs at the Opioid Receptors	145
Synthesis and SAR of Oxaibogamines Leads to Novel Analogs with Biased Receptor Signaling	147
Synthesis of Bridgehead-Substituted Analogs.....	147
Functional Activity of Bridgehead-Substituted Analogs.....	148
New Analog Shows G Protein Biased Signaling.....	150
Enantioselective Synthesis of Oxaibogamine Analog (<i>5S</i>)-46	152
Oxaibogamine Enantiomer Has Similar Functional Activity to Its Racemic Analog	155
<u>Discussion</u>	156
Mechanism of Action of Ibogaine	156
Important SAR of <i>Iboga</i> Scaffold.....	158
Implications of Polypharmacology	158
Biased Signaling as a Path to Better Therapeutics?.....	160

<u>Conclusions</u>	162
<u>Experimental</u>	162
Chemistry.....	162
X-ray Structure Determination	180
Biological Procedures	181
<u>References</u>	184
¹ H and ¹³ C NMR.....	191
 <u>Chapter 5 – A Tale of a Tail: Understanding the Tools Available to Measure</u>	
<u>Ligand Bias</u>	231
<u>Introduction</u>	231
<u>Results</u>	232
Uncovering the “Bias” of Endogenous KOR Agonist Dynorphin A	232
Initial Findings in the Tango Assay.....	232
Researching Dynorphin Results Further.....	233
Assessing the Stability of Dynorphin A in the Tango Assay Set-up	234
Dissecting the Role of the V₂ Tail in Arrestin Recruitment	238
Removing the V ₂ Tail From the Tango Construct.....	238
Utilizing the Tango Construct in Another Arrestin Assay.....	240
Bringing the V ₂ Tail into a Different KOR Construct	241
Interpreting the Data in Terms of Bias Factors	243
G Protein Activation Data Provides Comparison for Bias Factor Calculations	243
Calculating Ligand Bias From the Data.....	244
Summary of Bias Factor Calculations	245

<u>Discussion</u>	246
Interpreting the Variation of Arrestin Recruitment by Dynorphin Between Assays	246
Uncovering True Example of Biased Ligands	247
Applying Assays Principles to Specific Ligands	248
Correctly Interpreting Results for a Meaningful Bias Factor	249
Moving Assays Closer to <i>In Vivo</i>	250
Testing Ligands <i>In Vivo</i>	251
<u>Conclusions</u>	252
<u>Experimental</u>	253
Tango Assay	254
BRET	254
Cloning	255
Calculations	256
<u>References</u>	257

Part II – The Growth Factor Signaling System

Chapter 6 – Potentiation of FGF2-Induced Glial Cell Line-Derived

Neurotrophic Factor Release by a Novel Deconstructed *Iboga* Alkaloid

<u>Analog</u>	260
<u>Introduction</u>	260
<u>Results</u>	263
Synthesis and Initial Biological Studies on Deconstructed <i>Iboga</i> Alkaloid Analogs	263
Synthesis of XL-008 and Ibogamine	263

GDNF Release From C6 Glioma Cells.....	264
XL-008 Potentiation of FGF2-Induced GDNF Release.....	265
XL-008 Induces Potentiation of GDNF Release From FGF2	266
Understanding the Signaling Pathways Involved in FGF2-Induced GDNF Release	269
Cell Viability and Toxicity Effects From Treatment with XL-008 and FGF2	273
<u>Discussion</u>	277
Mechanism of Action.....	277
Difficulty in Working with C6 Cells	279
Use of Pharmacological Inhibitors.....	279
<u>Conclusion</u>	280
<u>Experimental</u>	281
<u>References</u>.....	286
 <u>Chapter 7 – Identifying Small Molecule Modulators of the Fibroblast Growth</u>	
<u>Factor Receptor</u>	
<u>Introduction</u>.....	
<u>Results</u>	
<u>Developing Assays for the Measurement of FGFR1 Activation</u>.....	
Stably Expressing FGFR1 Cell Line.....	296
Detecting Receptor Phosphorylation	296
Detecting Downstream Signaling Events	299
Phenotypic Screen for Receptor Activation.....	302
Reported Small Molecule Agonists are Inactive in Assays	302
<u>Putting Assays in Place for HTS</u>.....	304

The Primary Assay for FGFR1 Activation	304
Adaptation of the Primary Assay to HTS Format.....	304
Using the Library of Pharmacologically Active Compounds (LOPAC) for an Initial Screen.....	305
Determining Hit Selection From Screening Results	306
Validating the Agonist Activity of LOPAC Hit.....	307
Small Molecule Hit From LOPAC Screen	307
Measuring Downstream Signaling From Naloxonazine.....	309
Neurite Outgrowth From Naloxonazine	310
Exploring the Mechanism of Action of Naloxonazine	311
Visualizing Receptor Phosphorylation Through Western Blot	313
Continuing Forward with HTS	315
<u>Discussion</u>	316
Mechanism of Action of Naloxonazine	316
Advantages of Using a Small Molecule Modulator.....	317
The Difficulty and Likelihood of Developing Small Molecule Agonists for RTKs	318
FGFR1 Activation and Cancer.....	319
<u>Conclusions</u>.....	320
<u>Experimental</u>	321
<u>References</u>.....	326

Acknowledgements

I would like to begin by thanking my research advisor, Dalibor Sames, for his unending support and inspiration during my graduate studies at Columbia University. When I joined the group five years ago, I had many stipulations – very forward of me as a first year graduate student. I was adamant that I wanted to work on something unstudied in the lab and that I also wanted to pursue both chemistry and biology research interests. Dali never wavered in helping me fulfill these interests, and together we were able to bring some unbelievable science into the lab as a result. I have become a much more critical scientist in fields of study I never thought possible as a young graduate student, and I will carry these interdisciplinary goals with me for the rest of my career. Through our expanding research interests, I had the fortune of working with Jonathan Javitch, Professor of Psychiatry and Pharmacology at CUMC. Jonathan has truly acted as a second research advisor to me, providing space and resources for me to work freely as a member of his lab. Between our numerous emails, meetings, and discussions, Jonathan has taught me everything I know about pharmacology and being a proficient biologist. I would definitely not be here today without his continuous generosity and encouragement in learning numerous new techniques.

I would also like to thank Mark Sonders, an unofficial member of our lab, who has provided interesting discussion over the years on my research, which has always been thoroughly appreciated. I am honored to have him as a member of my thesis committee, as well. To my other thesis committee members (both present and past), thank you for participating in this momentous occasion in my education and career: Ronald Breslow, Mary Sever, James Leighton, and Virginia Cornish. Your critique of my research over the years has been much appreciated.

I also need to acknowledge my scientific roots. My early interest in chemistry and biology started at Soquel High School under the instruction of Dan Siddens and Gail Alaimo. At UC Berkeley, I would like to thank Ming Hammond, who took a big risk by allowing me to be the first member of her research lab. Under Ming's mentorship, I learned the foundations of scientific research and the importance of work ethic and time management. These skills have proved invaluable during graduate school and allowed me the ability to work on so many research projects simultaneously. I also had the opportunity to work a summer internship at Plexxikon, Inc. under the guidance of Wayne Spevak and Jiazhong Zhang. During my time at Plexxikon, I was first exposed to pharmaceutical science and medicinal chemistry, which has thoroughly shaped my research and career interests.

Among my immediate research colleagues, I would like to thank Andrew Kruegel. Without his synthetic expertise and sharp intellect, none of my research would be possible. He remains one of the smartest people I know and have been able to work with, and I will always value and respect his opinions. I am very excited to see where he takes our research projects! I also need to thank Teresa Jacques, my first mentor in the Sames lab and a dear friend. She has always been a good sounding board when research became difficult and has truly been a wonderful presence in my life. Adam Henke, Umed Boltaev, and Rich Karpowicz have also played important roles in my graduate career, as direct collaborators, bench mates, and friends.

My collaborations have allowed me contact with many talented scientists to whom I am grateful. In the Javitch lab, Marie-Laure Rives taught me the essentials to running my opioid experiments, which has shaped my entire thesis. Prashant Donthamsetti and Steve Grinnell provided helpful insight into assays, pharmacology, and the opioid systems. Maria Hague Pedersen held my hand as I struggled through my first cloning project, and I will be indebted to

her patience and guidance. I would also like to thank Rene Hen and the members of his lab, Benjamin Samuels and Kate Nautiyal, for taking interest in our opioid project and signing on full time to perform the *in vivo* experiments.

I certainly would not be here today without the love and support of so many friends and family members. I am truly grateful to have so many people in my life who support my goals. To my New York family, I would like to thank Helen Tran and Dejai and Alanna Barnes for providing unforgettable memories each and every day that have made getting through the good and bad times possible. I also need to thank my college partner-in-crime Louise Goupil, whose numerous Skype sessions have always been a welcome distraction and a necessary part of my life. To my oldest friend Heddy Hill, who can never cease to make me laugh, thank you.

To my parents Dave and Jean Gassaway and my brother Michael Gassaway, thank you for supporting me and never questioning my life choices – even when those took me across the country. I cannot thank you enough, Mom and Dad, for instilling the importance of education and independence in us from an early age. These are qualities I hope to pass to my children one day. I also would like to thank my in-laws, Carl and Barbara Wulf, for their continuous love and support. To Bruce and Heidi Jensen and TJ Gassaway, thank you for always being available for a heartfelt chat and visit when needed. You have helped keep me sane when life was busy and chaotic, and I appreciate our relationships more than words can say. And finally, to my husband Kevin – I love you. Getting a PhD comes with many sacrifices, whether it be the long hours, the weekends spent in the lab, or bringing work home time and again, and you have never once made me feel bad for being ambitious. I brought you along on this long journey with me all the way from California, and having you in my life has always made me feel that I can accomplish anything. I cannot wait to see where life takes us next.

Chapter 1 – An Introduction into Depression, Opioids, and Pharmacology

Depression: Symptoms and Mechanisms

Symptoms of Depression. Depression is a debilitating psychiatric disorder associated with feelings of melancholy, anxiety, helplessness, and general aversion to activity. It can also negatively affect sleep, energy levels, as well as psychomotor and cognitive functions. Depression (and major depressive disorder, MDD) also carries a high risk of morbidity and recurrence, making it an immense public health cost.^{1,2} One additional danger associated with depression is suicide, which is the third leading cause of death among 15-24 year olds. Slow onset of antidepressant efficacy of currently available therapeutics, therefore, becomes particularly dangerous as it is well documented to be associated with high levels of suicidal behavior.³ The World Health Organization estimates that at least 120 million people worldwide suffer from depression, and for these reasons it is estimated to be the leading cause of global burden of disease by 2030.

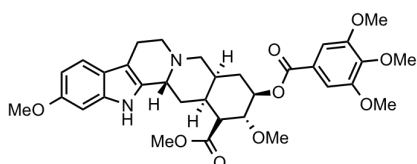


Figure 1. Chemical Structure of Indole Alkaloid Reserpine.

Monoamine Hypothesis of Depression. Since the 1960s, the monoamine hypothesis has been the leading theory of depression, namely that depressed patients have low concentrations of serotonin, norepinephrine,

and dopamine.⁴⁻⁶ This hypothesis was initially developed based on two lines of evidence: 1) the alkaloid reserpine (**Figure 1**), a vesicular monoamine transporter inhibitor, caused depression in some patients and depression-like symptoms in animals^{7,8}, and 2) the primary target of many antidepressants is to increase the synaptic concentration of monoamine neurotransmitters for activation at postsynaptic receptors. This mechanistic hypothesis has been the basis for the development of numerous modern day antidepressants (see below). However, more recent

clinical evidence suggests that depression is probably not simply caused by a depletion of monoamine neurotransmitters but that monoamine depletion plays a modulatory role on other neurobiological systems. For instance, depletion of monoamines in healthy subjects does not necessarily lead to depression.⁹ Further, in patients with untreated MDD, further depletion of monoamines does not increase depressive symptoms.¹⁰ Thus, the original monoamine hypothesis had to be revised.

Glutamate Signaling in Depression. As the major excitatory neurotransmitter in the central nervous system (CNS), glutamate signaling contributes to more than half of the synapses in the brain. The ionotropic glutamate receptors, N-methyl-D-aspartate (NMDA), α -amino-3-hydroxy-5-methyl-4-isoxazolepropionic acid (AMPA), and kainate receptors, are ion channels that are permeable to sodium (Na^+) and calcium (Ca^{2+}) cations and depolarize neurons in response mostly to extracellular neurotransmitters (e.g. glutamate and Zn^{2+}).¹¹ There are also eight metabotropic glutamate receptors (mGluR1-8), located pre- and post-synaptically, that can mediate intracellular signaling through their activation of G protein signaling (see below). NMDA receptors, in particular, require co-agonist binding to both glycine and glutamate binding sites for ion channel opening, as well as dislodging of the magnesium ion (Mg^{2+}) from the channel by depolarization (consequent to AMPA receptor activation); these channels are nonselective for Na^+ and Ca^{2+} .¹¹ AMPA receptors mediate fast synaptic transmission, with the GluR2 subunit mediating ion permeability and phosphorylation of serine 818 by CaMKII leading to long-term potentiation (a persistent strengthening of synapses that is a fundamental mechanism for learning and memory formation).¹¹

Given the important role that glutamate signaling plays in synaptic function, there is little surprise of its role in MDD. For instance, clinical studies analyzing plasma, cerebrospinal fluid,

and serum, have found increased concentrations of both glutamate and glutamine in patients with MDD compared to healthy controls, as well as decreased serum and plasma glutamate levels following antidepressant treatment.¹² In more direct measurements, proton magnetic resonance spectroscopy has found reduced glutamate/glutamine exchange in both subcortical and cortical regions of the brain in patients suffering from MDD.¹² Additionally, postmortem studies of MDD patients have shown changes in NMDA receptor subunit expression, suggesting that depression might be associated with NMDA receptor hyperfunction in subcortical regions of the

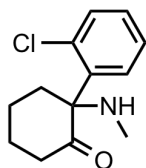


Figure 2. Structure of Ketamine.

brain (hippocampus, locus coeruleus, and amygdala) and hypofunction in cortical regions of the brain (prefrontal, perirhinal, temporal cortices).¹² These hypotheses are further supported by the clinical results with noncompetitive NMDA receptor antagonist ketamine, a dissociative anesthetic and phencyclidine derivative (**Figure 2**). In a proof of concept randomized, double-blind study, a single subanesthetic dose (0.5 mg/kg) of ketamine produced rapid antidepressant effects (within four hours) that lasted up to 72 hours compared to the placebo control¹³ (with the caveat that it is hard to control these trials as the placebo lacks the dissociative effects) – in contrast to the 4-12 week delay of other antidepressants currently available (see below).¹⁴ Patients still experienced hallucinogenic effects at this dose, but these subsided within two hours prior to the onset of antidepressant effects. Follow-up studies have shown the effectiveness of ketamine in treatment resistant patients¹⁵⁻¹⁷ and alternate routes of administration, including oral.¹⁸⁻²¹ The positive results of ketamine highlight the importance of the glutamatergic system in understanding and treating depression, and offers a refreshing divergence from the heavily studied monoamine hypothesis.

Mesolimbic Rewards Pathway. The mesolimbic dopamine rewards pathway is traditionally linked to the rewarding effects of food, drugs of abuse, and sex – often through activation of dopaminergic transmission or by direct activation of mu-opioid receptors (MOR) in relevant brain regions (see below).²² However, many symptoms of depression, including anhedonia (the inability to feel pleasure), reduced motivation, and decreased energy levels, are in fact mediated by the nucleus accumbens (NAc) and the ventral tegmental area (VTA), two key players in the mesolimbic pathway.²² It therefore seems plausible that the dopaminergic reward circuit could be another key player in the mechanisms behind depression. Unfortunately, the exact involvement of the VTA-NAc pathway in mood disorders is not well understood. Through sporadic studies over the past several decades, researchers have found that in animal models of depression, stress potently activates dopaminergic neurons in the VTA and stimulates dopaminergic transmission to limbic targets in the NAc.^{23–25} Additionally, reports show that antidepressant treatments can actually alter dopaminergic activity in the VTA or its targets, while experimental manipulation of dopaminergic signaling in the VTA-NAc can modulate depression-like behaviors in animal models.^{22–25} In humans, magnetic resonance imaging, MRI, and positron emission tomography, PET, have shown that depressed patients have decreased activity in the NAc and prefrontal cortex (PFC), as well as increased activity in the amygdala (important in fear responses).^{26–29} More recent optogenetic studies in mice on the VTA-NAc circuits reveal that selective inhibition of VTA dopamine neurons induces a depression-like phenotype that can be rescued with photoactivation³⁰, while in contrast, phasic stimulation of these neurons during social-interaction tests induces a depression-susceptible phenotype³¹, indicating contradictory roles of these circuits. Additionally, a separate study showed that the mesoaccumbens glutamatergic input into the NAc actually mediated aversion rather than award, indicating

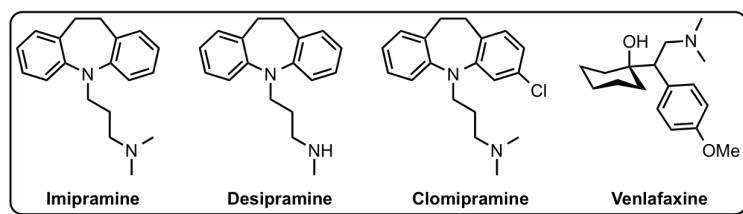


Figure 3. Structures of Antidepressants Inhibited by Naloxone.

instead an excitatory input on the GABAergic interneurons studied.³² Due to the strong mechanistic focus on the other monoamine systems,

like serotonin and norepinephrine, and brain regions (i.e. hippocampus) in depression, studies in the VTA-NAc regions have largely concentrated on addiction or schizophrenia. Additionally it is not well understood why aversive stimuli (i.e. stress) would produce a drug-like (or drug of abuse-like) response in the VTA dopaminergic system. One possibility is that stress activation of the VTA is a positive, coping mechanism that helps increase an individual's motivation to cope actively to the current threat. Another possibility is that longer-term exposure to stress may cause pathological adaptations in the VTA-NAc pathway, which can sensitize individuals to drugs of abuse or contribute to depressive behaviors.^{22,33}

In any case, it is possible that in depressed individuals, there may be a dysfunctional or underactive rewards pathway, which would consequently exhibit a decreased ability to respond to natural rewards. Therefore, increasing the activity of the rewards pathway (e.g., through exogenous opioid administration) could offer a potential antidepressant therapy. For example, the effects of many antidepressants (**Figure 3**), such as imipramine, desipramine, clomipramine,

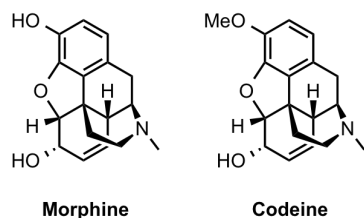


Figure 4. Main Opioid Constituents from *Papaver somniferum*.

and venlafaxine (see below), can be partially inhibited by naloxone, an opioid antagonist.^{34,35} Additionally, some antidepressants cause increased enkephalin (endogenous opioid) levels (both protein and mRNA) in the rewards circuits and other brain areas^{36,37}, and imipramine increases

MOR expression in several brain regions.³⁸ Although not well understood, there is a clear connection between antidepressants and the opioid system. In fact, until the 1950s, the “opium cure,” a low dose of opium, was quite effective at treating symptoms of depression.³⁹ Opium, isolated from *Papaver somniferum*, and its constituent opioids, morphine and codeine, have been recognized for centuries as the leading therapeutics for pain and the inspiration for many semi-

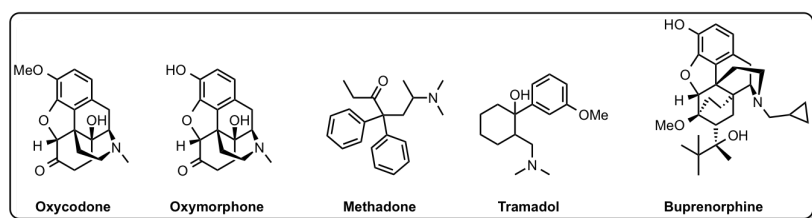


Figure 5. Opioids with Clinical Evidence of Antidepressant Activity.

synthetic opioids (Figure 4). While compounds like morphine are effective analgesics, they suffer

from serious drawbacks including addiction potential, tolerance build-up, constipation, and respiratory depression – the latter being the key effect leading to overdose and death.⁴⁰ Therefore, opioids as antidepressants have largely fallen out of favor due to the negative perceptions from their abuse potential. However, there have also been a few infrequent reports (case studies and small controlled clinical trials) that indicate MOR agonists as being antidepressants, including the endogenous peptide β -endorphin, oxycodone, oxymorphone, methadone, tramadol, and buprenorphine (Figure 5).^{41–48} Additionally, many studies in animals have identified delta-opioid receptor (DOR) agonists with antidepressant-like effects.^{49,50} A better understanding of this mechanism in depression might allow the discovery of new, safe opioid antidepressants.

Neurotrophin Hypothesis. Moving further away from monoamines, glutamate, and opioids, the growth factor systems offer yet another interesting possibility for understanding depression. Increasing evidence now suggests that a decrease of neurotrophic factors (NFs),

particularly brain-derived neurotrophic factor (BDNF), and therefore impaired synaptic plasticity may be responsible for some cases of depression. As small proteins with neurotrophic functions, NFs include nerve growth factor (NGF), BDNF, glial cell line-derived neurotrophic factor (GDNF, see Chapter 6), insulin-like growth factor (IGF), and fibroblast growth factor (FGF, see Chapter 7).⁵¹ Given their biological roles in maintaining neuronal survival, promoting differentiation, facilitating axonal growth, maintaining survival of mature neurons, and neurogenesis, it is no surprise that NFs may also mediate some symptoms of depression and other neuropsychiatric disorders.⁵¹ In the clinic, reduced BDNF mRNA levels have been identified in the hippocampus of animal models for depression⁵², as well as decreased serum BDNF levels in untreated depressed patients.⁵³ Further, administration of BDNF directly to the animal brain produces antidepressant-like effects.⁵⁴ Similar evidence is also being found for the FGF system, as well (see Chapter 7). Interestingly, BDNF levels are used as a biomarker for depression⁵⁵, and the BDNF Met allele is associated with an increased risk of suicide in patients with MDD.^{56,57}

Through this growing body of evidence, Duman has suggested a neurotrophin hypothesis to explain the onset of depression, whereby NFs help to promote synaptic growth and maintain neuronal survival, and in contrast, decreased levels of NFs contribute to the hippocampal and prefrontal cortical atrophy observed in depressed patients.⁵⁸ In this way, the actions of NFs may reverse the damage caused by depression, indicating an antidepressant therapeutic role for these proteins and interpretation of depression as a neurodegenerative disorder.⁵⁹ Relying solely on increased NF expression to combat depression may be challenging, however. For instance, cAMP response element-binding protein (CREB)-mediated BDNF expression usually takes 2-3 weeks to show antidepressant effects, which is not conducive with a rapid-acting response.⁶⁰

Another alternative would be to target instead the receptors that NFs act upon, termed receptor tyrosine kinases (RTKs), as a more direct way to increase the signaling (see Chapter 7). Although the mechanisms of NF's role in depression are still not fully understood, there is precedent to study this hypothesis further.

Current Treatment Options for Depression are Limited

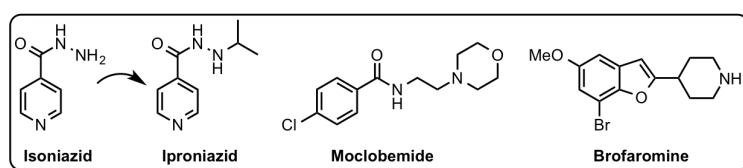


Figure 6. Structures of Notable MAOIs.

Monoamine Oxidase Inhibitors (MAOIs). The first pharmacological treatment for depression was

discovered somewhat serendipitously. Isoniazid (**Figure 6**) was first developed for the treatment of tuberculosis, significantly decreasing the mortality rate of this disease after only one year on the market.⁶¹ In 1953, a monoalkyl derivative of isoniazid, iproniazid (**Figure 6**), was developed that showed interesting euphoric and psychostimulating side effects in the clinic.⁶¹ These effects were analyzed in a separate clinical trial for patients with depression and remarkable improvements were visible in 70% of patients tested. Iproniazid was continually used, off-label, in patients suffering from MDD. This class of antidepressants is known as monoamine oxidase inhibitors (MAOI). MAO is an enzyme that oxidatively deaminates biogenic amines, and therefore an MAOI helps to increase the levels of these biogenic amines in presynaptic terminals. Unfortunately for long-term use, MAOIs have their own side effects. For example, iproniazid was ultimately removed from the market due to it causing hypertensive crises; in the presence of certain foods, like cheese or dairy products, which contain high levels of tyramine, irreversible MAOIs like iproniazid can further increase the levels of tyramine and norepinephrine in the

sympathetic nervous system, leading to increased heart rate, hypertension, and sweating.⁶¹ While some reversible and selective MAOIs have been developed (see moclobemide and brofaromine, **Figure 6**), which are effective and do not carry the risk of hypertensive crisis, they do still have some side effects and are not available for use in the United States.

Tricyclic Antidepressants (TCAs). TCAs are characterized by their fused three-ring structure (see examples in **Figure 3** above). Inspired by the success of the drug chlorpromazine in the treatment of schizophrenia, there was a push in the early 1950s by Roland Kuhn and Geigy Ltd in Basel, Switzerland to find more antipsychotic drugs.⁶² The tricyclic drug imipramine was developed in 1958, and while not effective as an antipsychotic, it showed improvements in patients suffering from depression.⁶³ In comparison to MAOIs, imipramine showed improved side effects, and in 1959 became the first antidepressant approved for use by the Food and Drug Administration (FDA). TCAs are the only antidepressants classified by their structure rather than by their mechanism of action, as the mechanism of action of imipramine was not known. It is now widely recognized that TCAs bind quite promiscuously in the central nervous system (CNS), and are not limited to inhibition of norepinephrine and serotonin transporters (which likely contribute to the antidepressant effects); other effects include blocking adrenergic α_1 and α_2 receptors, muscarinic receptors, and histamine H_1 receptors.⁶⁴ Based on the often non-selective actions of TCAs, the side effects are numerous and debilitating, including dizziness,

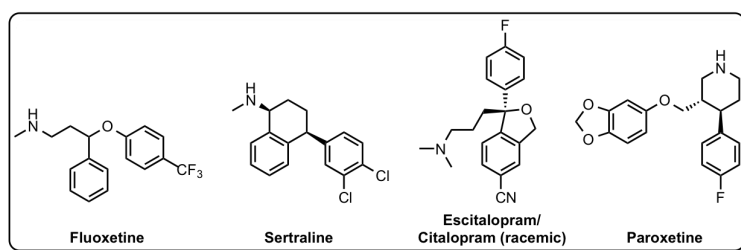


Figure 7. Structures of Notable SSRIs.

memory impairments, and drowsiness.

Selective Serotonin Reuptake Inhibitors (SSRIs).

Following the identification

of the monoamine hypothesis for depression, serotonin was identified as a clear player in MDD. For instance, a postmortem study on patients who suffered depressive suicides revealed decreased concentrations of serotonin.⁶⁵ Based on these findings, Eli Lilly began developing drugs that would selectively inhibit the reuptake of serotonin at serotonin transporters, thus increasing presynaptic concentrations of serotonin to act upon postsynaptic serotonin receptors. In 1974, fluoxetine became the first SSRI to be published. (**Figure 7**).⁶⁶ Given its increased selectivity in comparison to other antidepressants, fluoxetine was approved by the FDA in 1987 and is currently marketed under the trade name Prozac[®]. Other well-known SSRIs include sertraline (Zoloft[®]), citalopram (Celexa[®]), paroxetine (Paxil[®]), and escitalopram (Lexapro[®]) (**Figure 7**). While more selective than other drugs, SSRIs still suffer from side effects, including nausea, insomnia, and sexual dysfunction.⁶⁷ Additionally there are an increasing number of patients with MDD termed “SSRI-resistant,” indicating that these drugs are not effective in all populations of patients.⁶⁸

Atypical Classes of Antidepressants.

There are a few additional classes of more atypical antidepressants available. Bupropion (Wellbutrin[®], **Figure 8**) is primarily a dopamine-norepinephrine reuptake inhibitor with low risk of sexual dysfunction and limited dry mouth, nausea, and insomnia.^{69–71} Serotonin-norepinephrine reuptake inhibitors (SNRIs) have also been

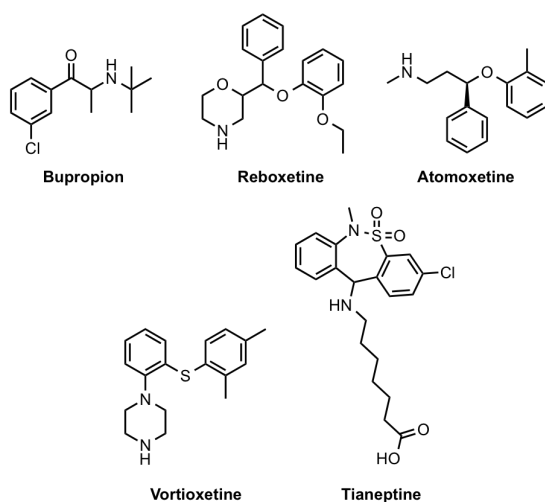


Figure 8. Structures of Some Atypical Antidepressants.

developed, including venlafaxine (Effexor[®]), which act mechanistically similar to TCAs without

off-target activity at adrenergic, histamine, muscarinic, dopamine, and serotonin receptors.⁶⁹ The side effects, though, are similar to other antidepressants.⁷¹ Selective norepinephrine reuptake inhibitors, like reboxetine and atomoxetine (**Figure 8**), have been developed.⁷² One of the more recent antidepressants to be approved by the FDA is vortioxetine (Brintellix[®], **Figure 8**), a more multi-action drug functioning as an agonist at 5-HT_{1A}, a partial agonist at 5-HT_{1B}, an antagonist at 5-HT_{3A} and 5-HT₇, and a serotonin reuptake inhibitor with considerable affinity for dopamine and norepinephrine transporters.⁷³ Vortioxetine is supposed to have a lower risk for sexual dysfunction and weight gain, and offers potential improvements to cognitive function. Ketamine has been shown clinically to have fast-acting antidepressant effects (see above).^{12,74,75} Although promising, ketamine is not currently FDA-approved for general use as an antidepressant (only off-label). Another atypical antidepressant is tianeptine (**Figure 8**). Marketed in non-English speaking countries as a serotonin reuptake enhancer, tianeptine is known to modulate the glutamatergic system and have numerous neurorestorative properties.^{76,77} Until recently, its mechanism of action has remained elusive (see Chapter 2) and its approval in the United States has not been pursued.⁷⁸

Filling the Void in Antidepressant Therapeutics

Although the use of antidepressants continues to rise, and our general understanding of the mechanisms behind depression continues to improve, the development of new antidepressant drugs has faltered. There remain populations of patients who are resistant to these medications, and with less than a third of patients gaining remission, the low rate of response, slow onset of improvements, and staggering number of side effects make current depression therapeutics unacceptable.⁷⁵ As we move forward, more effort should be devoted to developing these

promising antidepressants, like ketamine and tianeptine, which offer a refreshing view on treating depression and may fill the void in available therapeutics. The main obstacle to overcome, however, is understanding better the direct molecular mechanisms of depression; current treatments work upstream of the target that actually mediates the depressive responses, which slows down effects significantly. If we can better understand the direct causes for depression among different populations of patients, then we will be better equipped to develop more effective drugs that will provide rapid relief.

In gaining inspiration for new antidepressant therapeutics, one can look to several interesting scaffolds from nature and beyond. In addition to the atypical antidepressant tianeptine described above, alkaloids from both *Mitragyna speciosa* and *Tabernanthe iboga* have been utilized for centuries for their intriguing psychological and physiological properties. Ibogaine, in particular, from *Tabernanthe iboga*, has shown numerous clinical and preclinical results indicating its effects on drug abuse and addiction.⁷⁹ In trying to understand the mechanism of action of both tianeptine and these alkaloids, the complex signaling of G Protein-Coupled Receptors emerges – in particular that of the opioid neurochemical system. By studying the signaling of these compounds further in the context of their obvious effects on neurochemistry and depression, a viable target emerges for advanced mechanistic understanding of mood disorders.

G Protein-Coupled Receptor (GPCR) Signaling – the Opioid Receptors

Signaling Cascades of GPCRs. The signaling cascades initiated by GPCRs are complex, and the study of these processes can be quite complicated. Activation of the GPCR first leads to the G protein (guanine nucleotide-binding protein) dependent signaling pathways (**Figure 9**),

beginning with dissociation of the alpha G protein subunit from the beta-gamma G protein subunits, which then go on to activate their respective downstream targets. There are many downstream targets for the alpha G proteins depending on the subtype. For instance, downstream targets can include adenylyl cyclase (activation to produce more cyclic AMP (cAMP) in G_{α_s} -coupled GPCRs (stimulation = G_{α_s}); or inhibition to produce less cAMP in $G_{\alpha_{i/o}}$ -coupled GPCRs (inhibition = $G_{\alpha_{i/o}}$)), phospholipase C (activation by $G_{\alpha_{q/11}}$ -coupled GPCRs to cause increased calcium levels within the cell), or RhoGEF (rho guanine nucleotide exchange factor; activation by $G_{\alpha_{12/13}}$ -coupled GPCRs leads to Rho kinase activation, ROCK 1/2).⁸⁰⁻⁸² For the beta-gamma G protein subunits, depending on the GPCR subtype, downstream targets include ion channels, adenylyl cyclase (indirectly), phosphatidylinositol-4,5-bisphosphate 3-kinase (PI3K) regulation, and extracellular signal-regulated kinases (ERK) regulation. They also are inhibitors of the alpha

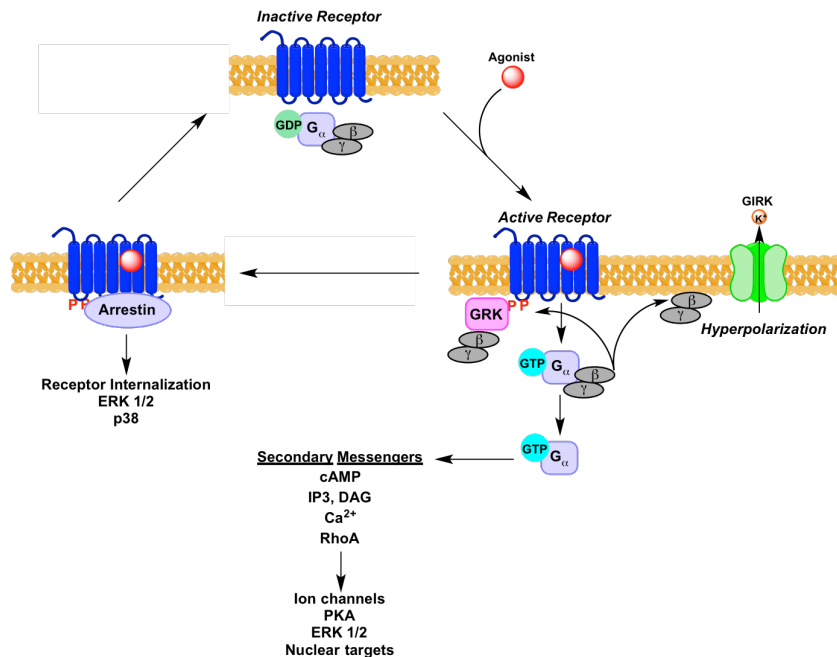


Figure 9. Summary of G Protein- and Arrestin-Dependent Signaling Pathways Following GPCR Activation.

G protein subunits, where association of the beta-gamma complex to a GDP-bound alpha G protein leads to inactivation of the G proteins. Additionally, the beta-gamma G protein subunits are responsible for bringing G Protein-Coupled Receptor Kinases

(GRKs) to the receptor for phosphorylation of the serine and threonine residues.^{83,84} Upon GPCR phosphorylation, arrestins can be recruited to the receptor, thus activating the G protein independent signaling cascades (**Figure 9**).

Arrestins are important proteins for signaling within the cell, as well. Arrestins have classically been divided into two distinct subtypes, visual arrestins and non-visual arrestins simply due to the fact that the first arrestins were identified in photoreceptors. Arrestin-1 (or S-antigen) and arrestin-4 (or X-arrestin, cone arrestin) are mainly expressed in rod and cone photoreceptors of the eye retina and bind to rhodopsin, cone opsins, and various downstream signaling targets, including c-Jun N-terminal kinase 3 (JNK3), microtubules, Mdm2, parkin, and calmodulin.⁸⁵ The non-visual arrestins, arrestin-2 (or β -arrestin, β -arrestin1) and arrestin-3 (or β -arrestin2, hTHY-ARRX) are expressed in virtually all cell types and bind many non-visual GPCRs (i.e. non-rhodopsin receptors). Additionally, these non-visual arrestins activate other downstream signaling pathways, including mitogen-activated protein kinases (MAPK) (apoptosis signal regulated kinase 1, ASK1; mitogen-activated protein kinase 4 and 7, MMK4/7; JNK1/2/3; proto-oncogene, c-Raf1; mitogen-activated protein kinase kinase, MEK1; extracellular signal-regulated kinases 1/2, ERK1/2; p38), ubiquitin ligases (mouse double minute 2 homolog, Mdm2; atrophin-1-interacting protein 4, AIP4; parkin) for receptor recycling, calmodulin, and others.⁸⁵ Arrestins play key roles in mediating receptor desensitization (tolerance build-up to receptor activation by blocking GPCR coupling to G proteins) and downregulation (decrease of surface levels of receptor, via arrestin-catalyzed receptor internalization or clathrin-dependent endocytosis of receptors from the cell surface).

In the context of a specific GPCR, opioid receptors like MOR, KOR, or DOR, are $G_{i/o}$ coupled GPCRs. Activation of this GPCR leads to dissociation of the G_α from the $G_{\beta\gamma}$, which

goes on to suppress adenylyl cyclase activity, resulting in decreased cAMP levels.⁸⁶ The $G_{\beta\gamma}$ proteins go on to open G protein-coupled inwardly-rectifying potassium channels (GIRKs), causing hyperpolarization of the cells (and possibly resulting in acute analgesic effects).⁸⁷ The $G_{\beta\gamma}$ proteins also help sequester GRKs to phosphorylate the serine and threonine residues on the receptor, providing a binding site for arrestin 3. The arrestin 3 signaling cascade ultimately leads to receptor internalization.⁸⁶

Unconventional Signaling of GPCRs. Signaling is additionally complex by more unconventional signaling networks of GPCRs. For example, GPCRs can directly interact with downstream effectors through specific protein-protein interaction domains such as the PDZ domain.⁸⁸ Additionally, there is emerging evidence that downstream effectors might also be mediated through transactivation of other receptors by GPCRs. For instance, some ERK signaling by GPCRs may in fact be mediated through transactivation of receptor tyrosine kinases (RTKs).⁸⁹ This transactivation usually occurs via two distinct mechanisms. One mechanism is ligand-independent and involves the physical association of the RTK and GPCR in a complex with downstream second messengers like Ca^{2+} and kinase Src.⁸⁹ The second mechanism requires a GPCR-mediated untethering of a membrane-bound RTK ligand that, once released, will activate the RTK and lead to downstream signaling (“inside-out” model; named because an untethered membrane-bound RTK factor *inside* the cell is released and act on the *outside* face of the RTK).⁸⁹ Recent examples for the first mechanism show that the epidermal growth factor receptor (EGFR) might be able to form a complex with either the angiotensin AT_1 receptor⁹⁰ or the β_2 adrenoceptors, leading to Src-dependent activation of ERK pathways and other cascades.⁹¹ However RTK activation more likely occurs through an inside-out mechanism by which the GPCR activates a metalloprotease that causes proteolytic release of the membrane-bound EGFR

pro-ligand (heparin-binding EGF, Hb-EGF), which then activates EGFR and causes ERK signaling.⁸⁹ Additionally, there are reports of the mu-opioid receptor (MOR) leading to transactivation of the fibroblast growth factor receptor in C6 glioma cells⁹², as well as adenosine A_{2A} mediated transactivation of Trk receptors.⁹³

In addition to transactivation mechanisms, some receptors are reported to form heteromers, or two different receptors physically associating to make a dimer. There are many examples of MOR-DOR heteromers, which may hold potential for improving analgesic therapeutics. For example, morphine-induced analgesia can be potentiated by DOR ligands, and an alleged MOR-DOR specific agonist is being developed that avoids the unwanted side effects associated with chronic morphine use.⁹⁴⁻⁹⁶ Heteromer theories should, however, be approached with caution as there are some questions as to whether these complexes exist in native tissues or are physiologically relevant.^{97,98} Additionally some splice variants of GPCRs can elicit interesting signaling cascades. For instance, the truncated six-transmembrane splice variant of MOR (lacking exon 1) has been reported to induce potent analgesia in mice without unwanted side effects like respiratory depression, constipation, dependence, and reinforcing behavior.⁹⁹⁻¹⁰¹ Additionally, small molecule IBNtxA has been reported to activate this MOR splice variant¹⁰⁰, suggesting potential for pharmacological targeting.

Understanding Ligand Bias: Pharmacology, Definitions, and Evidence

A Lesson in Pharmacology Terms. Ligand interactions with a receptor are traditionally viewed as a function of two parameters: affinity (defines how tightly a ligand and receptor interact) and intrinsic efficacy (ability of a ligand to elicit a biological response once bound to a receptor).¹⁰² Ligand potency is thus defined as a measure of both affinity and efficacy and should

be compared to a reference ligand acting on the same receptor. Each receptor can have orthosteric ligands, which bind to the same site as the endogenous agonist, or allosteric ligands, which bind to a site separate from the endogenous agonist. Within each of these categories, ligands are typically designated into four categories: a. full agonists, which activate the receptor to elicit the highest biological responses possible; b. partial agonists, which activate the receptor to a fraction of the full response; c. antagonists, which inhibit the activation of the receptor by an agonist; and d. inverse agonists, which inhibit the constitutive activity of the receptor.¹⁰² It was classically thought that the efficacy of an agonist was linear (with receptor binding) and could be predicted by receptor occupancy theory, which states that receptors have either an active or inactive conformation with full/partial agonists and inverse agonists stabilizing the active and inactive conformations, respectively. According to this view, the response elicited by a ligand through the different signaling pathways should always be the same and be a function of the intrinsic efficacy of the agonist. Experimental evidence, however, suggests that this view of receptor/ligand interaction may be misleading. An increasing number of ligands are showing so-called “imbalanced efficacies” for the different receptor-activated signaling pathways and suggests that efficacy might actually be pluridimensional rather than linear. For instance, some proteins that interact with GPCRs can affect receptor activation, producing differences in efficacy for the same ligand^{103,104}, a phenomenon known as conditional efficacy. Additionally, one ligand can act by different mechanisms within the same cellular context, acting as an agonist for one pathway and an antagonist for another^{105–107}. Due to the high complexity with which signaling can occur in spite of traditional views of receptor occupancy, a more comprehensive view of receptor activation needs to be defined.

Defining Functional Selectivity/Ligand Bias. The idea of ligand bias or functional

selectivity emerges from the interplay of multiple signaling cascades. An unbiased or balanced ligand is one that signals comparably through all the major signaling pathways of receptor activation, as suggested by receptor occupancy theory, or the concept of a single active and inactive receptor state. Often times, unbiased ligands are denoted full agonists and used as a reference for comparing the bias of new ligands. In the case of GPCRs, this feature would include signaling through both the G protein and arrestin pathways. Therefore a compound that shows preferences for one signaling cascade over another would be considered biased. In the context of GPCRs, the most common biased ligands are G protein biased or arrestin biased ligands, however one can envision a bias possible between any number of the downstream signaling pathways. One of the first examples of signal bias in a biological system was observed at MOR: Laura Bohn and co-workers found that mice lacking the β -arrestin2 (arrestin-3) gene showed a potentiated and prolonged analgesic effect from morphine. This suggested that inhibiting the β -arrestin2 signaling (as in the case of a G protein biased ligand) could greatly increase the effectiveness of morphine as an analgesic, a highly desirable characteristic for treating many opioid related side effects¹⁰⁸ (see below).

Given that the classical two-state model for receptor activation is likely too simple to explain such diverse signaling effects, multiple receptor conformations responsible for the activation and signaling must be taken into account. According to this model, there are many different active conformations for a receptor, whereby a particular ligand might be able to activate (or inhibit) the different downstream effectors to varying degrees through initial interactions with the receptor. Arguably the most-studied GPCR in terms of structural connections to ligand bias is the β_2 adrenergic receptor (β_2 AR). Kashai and co-workers showed that the weakly arrestin biased ligand carvedilol (**Figure 10**) caused Cys²⁶⁵ to become more

buried within the core of the receptor than the reference ligand isoproterenol using a chemical-labeling approach coupled with mass spectrometry.¹⁰⁹ Additionally, they showed that Lys²⁶³ near the edge of the third intracellular loop became more exposed. In a separate study, a covalently attached ¹⁹F-labeled NMR probe was used to observe differences in the motions of cytoplasmically facing cysteines (including Cys²⁶⁵) in the presence of different ligands, with carvedilol showing a shift in conformational equilibrium of transmembrane domain 6 (TM6) and transmembrane domain 7 (TM7).¹¹⁰ These studies are quite impressive considering that there is no strongly biased ligand known for the receptor and a crystal structure with these ligands is not yet available.

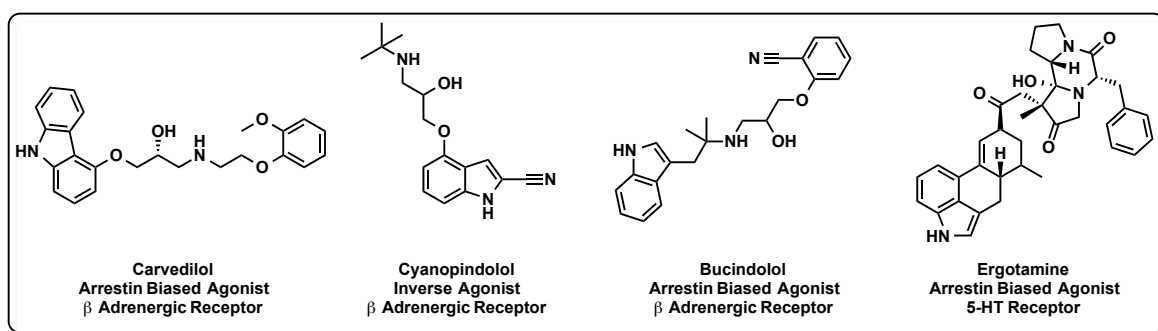


Figure 10. Chemical Structures of Biased Ligands Discussed in this Introductory Chapter.

Some receptors with solved crystal structures have been studied to determine effects from biased ligands. The crystal structure of thermo-stabilized turkey β_1 adrenergic receptor (β_1 AR) bound to weakly arrestin-biased carvedilol showed that, compared to an inverse agonist-bound structure (cyanopindolol, **Figure 10**), global conformations remained the same, except for some additional van der Waals contacts made with Leu¹⁰¹ in TM2, Asp²⁰⁰ and Tyr²⁰⁷ in the extracellular loop 2 (ECL2), Trp³³⁰ in TM7, and a hydrogen bond with Phe²⁰¹ in ECL2 – all of which are similar to the structure obtained by crystallization with bucindolol (**Figure 10**), a different arrestin-biased ligand.^{111,112} There is overlap of these interactions with the known inactive β_2 AR crystal structure¹¹³, which suggests that these interactions might also be observed

in a crystal structure of active β_2 AR. Structural differences have also been noted between the 5-HT_{1B} and 5-HT_{2B} receptors bound to an ergotamine ligand, which has shown a strong arrestin bias for the 5-HT_{2B} receptor and a weak arrestin bias for the 5-HT_{1B} receptor. Some of the additional contacts made in the presence of the ergotamine ligand with the 5-HT_{2B} receptor are strikingly similar to those seen with carvedilol-bound β_1 AR.^{114,115} Although understanding the structural conformations within a receptor of ligand bias is in the early stages and will likely be a receptor-specific process, these studies provide evidence for a physical component to biased signaling.

There is also an important structural role for GRKs in arrestin recruitment to the GPCRs. So called “barcodes” for GRK-induced receptor phosphorylation on the C terminal end of GPCRs have been recognized that can regulate or even enhance arrestin recruitment to receptors.¹¹⁶ These results are generally supported by experiments showing that lack of GRKs or even deletion of serine or threonine phosphorylation sites on the C terminus can affect the affinity of arrestin for the receptor, thus modulating the downstream signaling of arrestin recruitment.^{117,118} Further, studies have shown that GRK-specific phosphorylation sites can account for different downstream signaling cascades. For instance, in the β_2 AR, GRK2 phosphorylation sites lead to receptor internalization while GRK6 sites lead to ERK activation.¹¹⁶ Further, arrestin biased ligand carvedilol was shown to only induce phosphorylation of the GRK6 sites on β_2 AR, thus highlighting that even within the same signaling pathway (i.e. arrestin signaling) there may be some bias between downstream effectors – furthering the complexity with which receptors function. These results also suggest that perhaps ligands are capable of preferentially recruiting distinct GRKs to the receptors, leading to distinct phosphorylation barcodes that will ultimately impart unique arrestin function.

There is also a concept of “endogenous bias” whereby endogenous ligands for a receptor can have inherent bias for one signaling pathway over another. For example, CCL19 and CCL21, two endogenous ligands for the CC chemokine receptor 7, activate receptor desensitization, arrestin recruitment, and ERK1/2 signaling to a different degree even though they have similar G protein coupling efficiency.^{119,120} Additionally, there is known differential activation of the serotonin receptor, 5HT_{2A}, in the presence of “trace amines.” Serotonin-induced receptor activation can trigger Akt signaling through an arrestin-3/Src-dependent pathway in mouse cortex and cortical neurons but not when N-methyltryptamines activate the receptor.¹²¹ Finally, even in the context of opioids, there is a possibility that endogenous peptide endomorphin-1 might be G protein biased (when compared to control agonist DAMGO) – though the authors suggest that true bias cannot be determined until *in vivo* studies are performed.¹²²

In the context of opioid receptors, there have been serious efforts to develop G protein biased ligands as better therapeutics for pain that avoid the unwanted side effects of morphine use (respiratory depression, constipation, tolerance, physical dependence)^{40,86}. G protein biased MOR agonists are reported with reduced respiratory depression and constipation, suggesting that these deleterious side effects are mediated through arrestin signaling.¹²³ Additionally, KOR agonists can provide similar analgesic relief when compared to morphine and have the added benefit of not activating the dopamine reward pathway.¹²⁴ However, KOR activation leads to dysphoria, or a feeling of helplessness, as well as hallucination.^{124–126} These effects, evident in potent compounds such as the KOR agonist salvinorin A¹²⁷, lead to a particularly frightening experience for someone needing simple relief from pain. There are reports, however, that suggest these dysphoric effects are mediated through arrestin-dependent activation of the p38 MAPK pathway.^{125,126} Therefore, an agonist that is biased to the G protein-dependent signaling pathway

(and therefore has little to no signaling in the arrestin pathway) may offer a unique solution to some of these aversive effects from opioid signaling and represent a novel therapeutic avenue worth pursuing further.

Distinguishing the Level of Bias for a Ligand. When studying a potentially unbalanced or biased ligand, it is important to determine the level to which the bias occurs. Often times for different experimental systems, whether due to receptor reserve (extra or unused receptors present in the cell) or signal amplification (one molecule activating many of the same downstream effectors), the biological response from a particular ligand may be completely different, with partial agonists appearing full and full agonists appearing partial, which ultimately makes it difficult to accurately determine the level of bias for one pathway over another. Therefore, the proper tools are needed to accurately quantify the bias from a particular compound. Always a ligand should be compared with an unbiased reference agonist, often the standard full agonist of the receptor. Without this comparison, there is little hope in gleaning meaningful information on the test ligand. Additionally, while it can be useful to see how a ligand compares to the control on one signaling pathway, in terms of potency and efficacy, at least two signaling pathways need to be analyzed in order to denote a ligand bias. Researchers have proposed many ways to quantify ligand bias into a so-called “bias factor” with mixed results. Some of the early attempts at quantification required either a rigorous comparison of efficacies from different ligands at equimolar concentrations or ligand concentrations that result in equiactive responses.¹²⁸ These methods suffer in that they do not inherently take into account the affinity of a ligand for a receptor, which could greatly alter the downstream signaling outcomes.

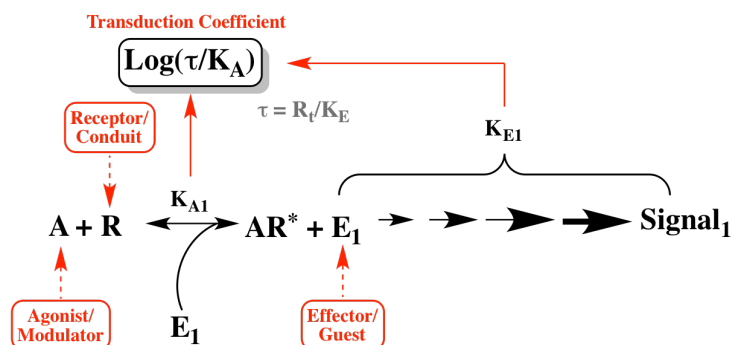


Figure 11. Schematic Diagram of the Black-Leff Operational Model in the Quantification of Ligand Bias. In this model, a receptor conformation will be stabilized by the agonist, leading to a particular interaction with downstream signaling proteins (effectors). The affinity and efficacy (a measure of the “quality” of the receptor conformation) is dependent upon the signaling protein, which is unique to each pathway. The transduction coefficient of an agonist takes into account both the affinity and the efficacy for a particular pathway. R_t = receptor density; K_E = ability of system to convert receptor stimulus into a response. Adapted from Kenakin.¹³¹

A better approach can be found by utilizing the operational model developed by Black and Leff.^{129,130} The operational model examines the agonism of a compound by carefully analyzing the dose response curve, taking into account the ligand affinity (K_A) for the receptor and the

efficacy (τ) to activate a signaling pathway. The τ factor takes into account both receptor density, $[R_t]$, and K_E , which denotes the intensity of a response and the system’s ability to convert the receptor stimulus into a response (**Figure 11**). It then must be assumed that a ligand bias can be characterized by different active states of the receptor, each with their own ligand affinity or efficacy. Therefore the most common representation of the Black-Leff operational model for dose response curves can be seen in equation 1 below.^{131,132}

$$\text{Response} = \frac{E_m [A]^n \tau^n}{[A]^n \tau^n + ([A]^n + K_A)^n} \quad (1)$$

where $[A]$ denotes the agonist concentration, E_m denotes the maximal response of the system, and n is the transducer slope, which links agonist concentration to the observed response (distinct from the Hill slope¹³³, which describes instead the midpoint gradient derived from fitting a concentration-response curve). **Figure 11** summarizes the ability of the Black-Leff operational model to quantify agonist bias. When data is fit using the operational model, agonism can be characterized as a function of both τ and K_A , and a so-called transduction coefficient, $\text{log}(\tau/K_A)$,

can characterize the agonism of any pathway within a cellular system where an agonist interacts with a receptor. When the transduction coefficient is normalized to a control, unbiased ligand (see below), a normalized factor, or $\Delta\log(\tau/K_A)$, can be used to account for any natural bias within the system. Thus the bias for an agonist between distinct signaling pathways, p_1 and p_2 , can be defined as follows in equations 2 and 3 as

$$bias = 10^{\Delta\log(\tau/K_A)_{p_1-p_2}} \quad (2)$$

where

$$\begin{aligned} & \Delta\log(\tau/K_A)_{p_1-p_2} \\ & = \log bias \\ & = \Delta\log(\tau/K_A)_{p_1} - \Delta\log(\tau/K_A)_{p_2} \end{aligned} \quad (3)$$

and where

$$\begin{aligned} & \Delta\log(\tau/K_A) \\ & = \log(\tau/K_A)_{Ligand} - \log(\tau/K_A)_{Control} \end{aligned} \quad (4)$$

A simplified version of the Black-Leff model uses a calculation of both efficacy and potency called the activity ratio or RA, which is denoted as the maximal response of an agonist divided by the EC_{50} (ligand concentration of half maximal response, a measure of potency). When properly compared to a control and analyzed through multiple pathways, a reasonable calculation for a ligand bias (Log[RA]) can be obtained (Equation 5).^{129,134,135}

$$\text{Ligand bias} = \text{Log} \left[\left(\frac{Emax_{pathway 1}}{EC50_{pathway 1}} \cdot \frac{EC50_{pathway 2}}{Emax_{pathway 2}} \right)_{Ligand} \times \left(\frac{Emax_{pathway 2}}{EC50_{pathway 2}} \cdot \frac{EC50_{pathway 1}}{Emax_{pathway 1}} \right)_{Reference} \right] \quad (5)$$

There are many ways to represent bias factors such that comparisons between ligands are easy to follow and interpret. Most commonly used are graphical representations showing the mean values and error for $\Delta\log(\tau/K_A)$ ¹³¹, heat maps showing bias for any number of signaling

pathways represented by changing color¹³⁶, and so-called webs of bias.¹³⁷ No matter what method is chosen to calculate a bias factor for a particular ligand, there will always be a question of what level of bias is significant and will lead to differential effects in signaling.

Examples of Ligand Bias. 6'-GNTI (**Figure 12**) has been reported by various scientists to be G protein biased at the KOR. Utilizing the same BRET assays described here, 6'-GNTI was initially found to be not only biased for the G protein signaling pathway but also an antagonist of the arrestin pathway.¹³⁸ In a follow-up study from a different lab, the authors found that G protein signaling could not be recapitulated in mouse striatal membranes, an endogenous source of receptors rather than an overexpressed system, while downstream signaling (Akt pathway) in overexpressed CHO cells and native systems (striatal membranes) was consistent with previous reports.¹³⁹ These results highlight that the *in vitro* pharmacology observed for 6'-GNTI might not be relevant *in vivo* or might be tissue or cell-specific. A more recent study tested 6'-GNTI *in vivo* for convulsant/seizure effects (likely in regard to reports that it activates KOR-DOR heteromers¹⁴⁰), as well as aversive effects from KOR signaling. Mice given an intra-hippocampal injection of the drug were found to have an increased threshold for seizure and no conditioned place avoidance, a measure of aversion, indicating promise that some *in vitro* bias effects may be translatable into behavioral effects (although the latter may be related to completely different pharmacological/signaling phenomena).¹⁴¹

Another example of ligand bias at KOR shows that at least for this receptor, bias is not limited to G protein versus arrestin signaling. The natural product collybolide (**Figure 12**), isolated from the mushroom *Collybia maculata*, is an agonist acting at KOR that shows greatly increased potency through the mitogen-activated protein kinase (ERK) pathway than does salvinorin A in human KOR expressing HEK cells using the [³⁵S]GTPγS binding assay and

western blotting (see below discussion of assays).¹⁴² The *in vitro* signaling bias was supported *in vivo* by a 10-fold higher potency for blocking non-histamine mediated itch (or pruritus) in comparison to salvinorin A. This example highlights that ligand bias can exist between any two or more signaling pathways and ideally are supported by both *in vitro* and *in vivo* results.

RB-64 (**Figure 12**), a diterpene salvinorin A analog and KOR agonist, has also been studied *in vivo* for potential behavioral effects of receptor signaling bias. Identified to have a bias

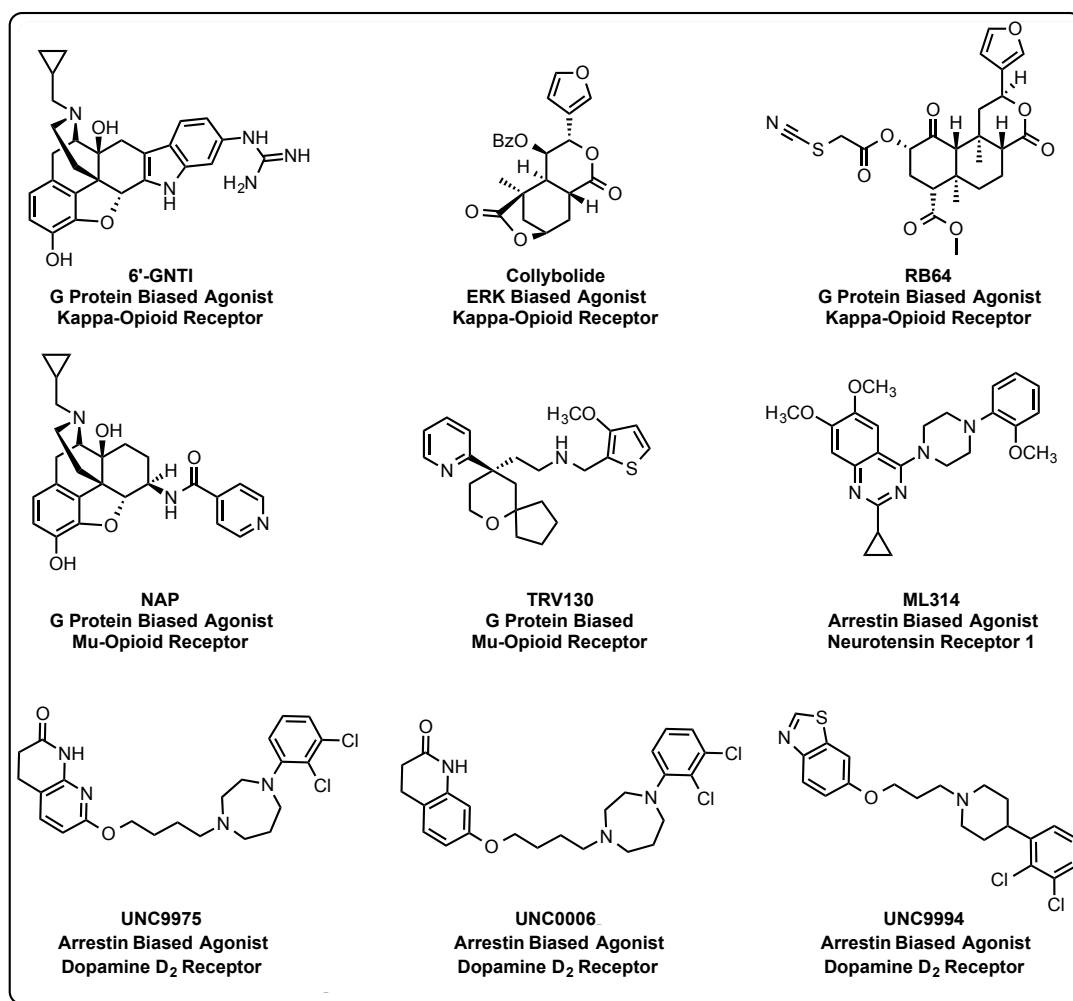


Figure 12. Structures of Reported Biased Agonists Discussed.

factor of 35 for G protein (measured in overexpressed cells using a cAMP sensor assay for G protein and reporter gene assay for arrestin, see below for more detail)¹⁴³, there has since been

some attempt to understand both the structural effects on the receptor from this compound¹⁴⁴, as well as *in vivo* behavioral effects.¹⁴⁵ It has been hypothesized that a G protein biased ligand would avoid aversive effects from KOR signaling¹²⁵, but evidence is still limited to fully support such claims *in vivo*. RB-64 is one such compound that provides some insight into the behavioral effects of possible G protein bias. When administered to mice, RB-64 did induce potent analgesia without inducing any sedation or anhedonia-like symptoms, consistent with reports that arrestin-3 activity is essential for the sedative and anhedonia-like effects from KOR agonists. Unfortunately aversive effects were still present in a conditioned place aversion assay. This may not be surprising, however, as initial signaling bias was determined in artificial systems, and the compound likely has different signaling properties in brain tissue or cells. Therefore, RB-64 as a tool does help to resolve some of the mystery surrounding the behavioral effects of an *in vitro* G protein biased compound, however it does also suggest that, not surprisingly, even among G protein biased compounds there may be some distinction in their ultimate behavioral effects.

Biased ligands are also reported at other opioid receptors, like MOR. NAP (**Figure 12**), a naltrexamine derivative, was recently reported to be a partial MOR agonist for G protein activation ($[^{35}\text{S}]\text{GTP}\gamma\text{S}$ binding assay, see below) and an arrestin-3 (β -arrestin2, determined in PathHunter[®], see below) and intracellular calcium flux antagonist (calcium indicator used) in human MOR-CHO cells.¹⁴⁶ As it is hypothesized that G protein-biased MOR agonists might have effects on blocking constipation symptoms, researchers tested NAP on *ex vivo* mouse colons and found that the compound reversed morphine-induced reduction in colon motility, though no comparison was made to other partial MOR agonists. NAP therefore represents an interesting lead as a treatment for opioid-induced constipation, although no evidence is provided about whether the compound has analgesic properties.

Trevena's compound TRV130 (**Figure 12**) is currently in clinical trials as a G protein biased MOR agonist for pain, as preliminary *in vivo* results were promising and showed less risk of respiratory depression and constipation.¹²³ This profile has largely shown to translate into humans with lower incidence of nausea and vomiting, an indication that functional selectivity may improve some opioid side effects.¹⁴⁷ Additionally, noribogaine, the active metabolite of the natural product ibogaine, has been reported to be a G protein biased KOR agonist.¹⁴⁸ Given the weak agonism we observed from noribogaine at KOR (see Chapter 4), it seems unlikely that noribogaine represents a true biased ligand (for further discussion on these compounds, see Chapter 4).

However, biased ligands are not limited to the opioid receptors or even to the G protein signaling pathway. ML314 (**Figure 12**) is an arrestin-biased neurotensin receptor (NTR1) agonist (arrestin-3 translocation measurements in arrestin-3-GFP expressing cells and aequorin-based calcium reporter assay for G protein) that shows promise in the treatment of methamphetamine addiction while inhibiting the G protein signaling pathway.¹⁴⁹ In a rigorous study utilizing multiple animal models, researchers showed that ML314 attenuated methamphetamine-induced hyperlocomotion (excessive movement usually in response to increased stimulation of the nervous system and a positive phenotype of schizophrenia in some mice models) in both wildtype and dopamine transporter knock out mice, and reduced conditioned place preference from methamphetamine. Additionally, in rats ML314 blocked methamphetamine self-administration and acted as an allosteric enhancer of endogenous neurotensin binding. Not only then is ML314 an arrestin biased ligand, but it also seems to be an allosteric compound, which may help to account for its unique signaling and behavioral effects.

Arrestin bias is also found at other GPCRs, including the dopamine D₂ receptor (D₂R), where it has been found to be particularly interesting as an anti-psychotic therapeutic. Three aripiprazole ligands (**Figure 12**), UNC9975, UNC0006, and UNC9994, were found to be arrestin biased D₂R ligands that inhibited G protein signaling.¹⁵⁰ Interestingly, UNC9975 showed potent anti-psychotic-like activity but did not have motoric side effects in mice, consistent with blockade of the G protein pathway. The anti-psychotic effects from these compounds were completely abolished in mice lacking arrestin-3 (β -arrestin2) with the addition of catalepsy effects. These effects were recapitulated favorably in mice with schizophrenia-like behaviors.¹⁵¹

Understanding the structural components of the receptor that lead to functional selectivity would show significant progress in the field. Rather than searching tirelessly for the next biased ligand, looking instead to the receptor might provide a more directed approach to developing improved therapeutics. Some attempts at elucidating the portions of receptors involved in dictating bias have been made. For example, at the D₂R, important residues in the third intracellular loop were identified that could be mutated in such a way as to create a receptor with decreased arrestin recruitment which was unable to internalize.¹⁵² This example highlights the possibility of identifying receptor features key for functional selectivity. One can envision that if a biased receptor could be crystalized, computational predictions could be made to design ligands that would selectively activate it or mimic the mutation, thus inducing the same bias.

Tools to Study Pharmacology

Assays Available for the Measure of GPCR Functional Activity. Since the discovery of GPCRs in the late 1980s¹⁵³, scientists have been striving for new and improved ways to measure the functional activity of GPCRs, both through G protein dependent and G protein independent

pathways. The first example of measuring G protein activation utilized radioactive GTP. Known

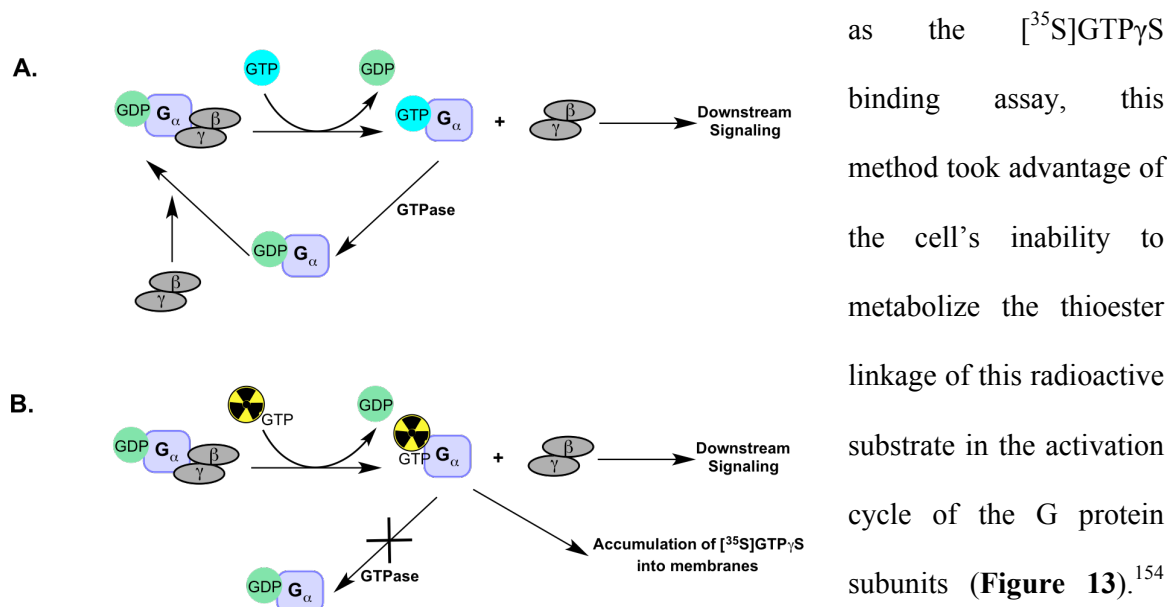


Figure 13. Mechanism of the $[^{35}\text{S}]\text{GTP}\gamma\text{S}$ Binding Assay for Measuring Functional Activity of GPCRs.

as the $[^{35}\text{S}]\text{GTP}\gamma\text{S}$ binding assay, this method took advantage of the cell's inability to metabolize the thioester linkage of this radioactive substrate in the activation cycle of the G protein subunits (**Figure 13**).¹⁵⁴

Rather than converting the active GTP-bound G_{α} subunit to the inactive GDP-bound G_{α} subunit via the actions of GTPase, the $[^{35}\text{S}]\text{GTP}\gamma\text{S}$ -bound G_{α} subunit accumulates in the cell membranes, leading to an increased signal that can be detected with a scintillation counter. Although this method is still used by researchers today, it suffers from lack of sensitivity, even in over-expressed systems. Western blots have also been utilized since the early days of GPCR study to measure the activation of downstream signaling pathways such as ERK1/2 and Akt, however again this method is not particularly sensitive and is ultimately not appropriate for measuring subtle dose responses. These methods do have an advantage however that they can be performed in either endogenous or over-expressed systems, albeit with varying degrees of success.

While radioligand binding assays still remain the gold standard for measuring ligand affinity for a receptor, the tools available to measure receptor signaling continue to become increasingly sophisticated. Assay options in genetically modified systems are plentiful, offering

robust and reproducible measurement in clever and easy to use methods. The explosion of bioluminescent resonance energy transfer (BRET) assays is apparent in the numerous examples of their usage in measuring the pharmacology of ligands at GPCRs.^{155,156} Resonance energy transfer (RET) is an energy transfer mechanism possible between two light-sensitive molecules.

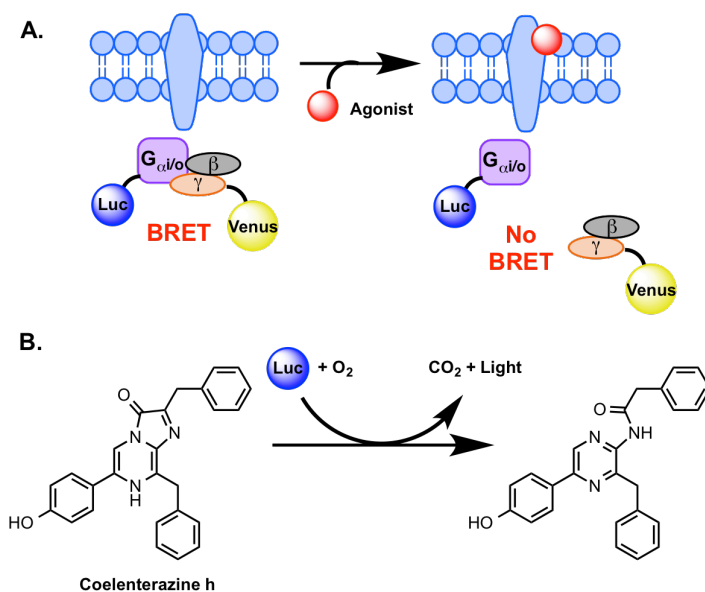


Figure 14. Mechanism of the BRET-based G Protein Activation Assay. A. Schematic depiction of G protein activation assay. B. Production of light from luciferase and coelenterazine h.

An excited donor chromophore may transfer energy to an acceptor chromophore through nonradiative dipole-dipole coupling, provided that the donor and acceptor have adequate match of their spectra and orientation. Because the energy transfer is inversely proportional to the sixth power of the distance between the two chromophores,

these RET techniques are sensitive to small changes in distance.¹⁵⁷ As such, the BRET-based assays rely upon close proximity between the donor and acceptor molecules. Featured heavily in Chapters 2-5 is a G protein activation assay where the G_{α} subunit is tagged with RLuc8¹⁵⁸, a BRET donor, and the G_{γ} subunit is tagged with mVenus¹⁵⁹, a BRET acceptor. Luciferase converts the substrate coelenterazine h into an excited state intermediate that emits light when relaxing to its ground state, making a BRET interaction possible. In the presence of agonist, and

subsequent dissociation of the α from the $\beta\gamma$ subunits, the BRET donor signal increases and the

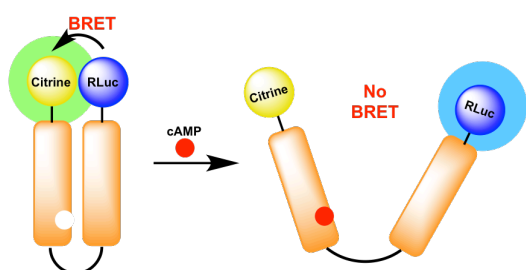


Figure 15. Mechanism of BRET-based cAMP sensor, CAMYEL.

BRET acceptor signal decreases, and an overall loss of the BRET signal (donor/acceptor) can be detected (**Figure 14**). BRET methods also exist to detect cAMP levels in cells, which are particularly useful for $G_{\alpha S}$ - and $G_{\alpha i/o}$ -coupled GPCRs, such as the CAMYEL (cAMP sensor

using YFP-Epac-RLuc) cAMP sensor (**Figure 15**). There are also virally delivered cAMP sensors that can be administered to more natural systems, like primary neurons, where receptors are expressed at endogenous levels and may better recapitulate signaling *in vivo*.¹⁶⁰ These sensors, however, can be particularly difficult to utilize for measuring $G_{\alpha i/o}$ -coupled GPCRs, since basal levels of cAMP may be too low to observe cAMP inhibition in response to receptor activation. Additionally there are numerous reporter gene assays available that couple receptor activation to expression of a gene that codes for an enzyme that can act upon an exogenous reporter substrate added to the cells (**Figure 16**).

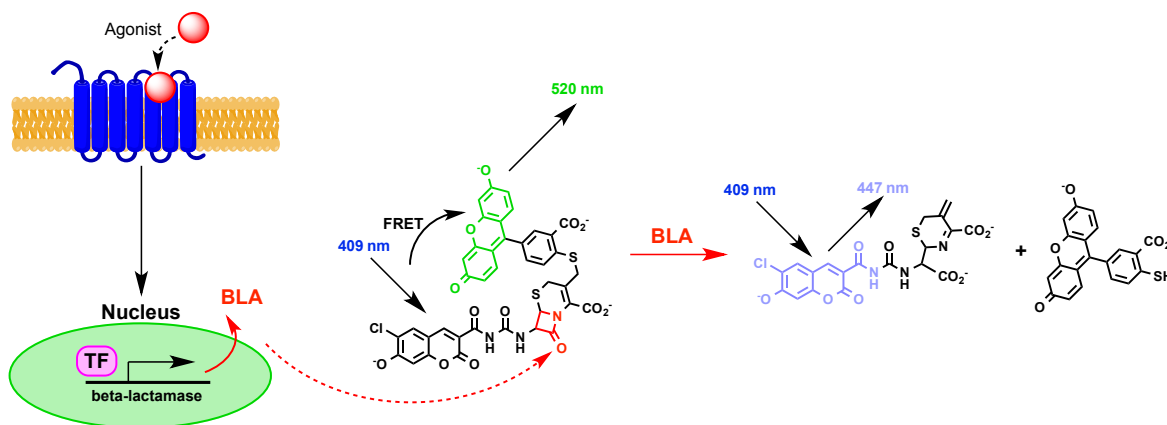


Figure 16. Mechanism of Action for Reporter Gene Based G Protein Activation Assays. Activation of the GPCR leads to increased expression of beta-lactamase, which then reacts with an added substrate, creating a change in FRET measurements. BLA = beta-lactamase.

Invitrogen has a commercially available kit in which beta-lactamase is expressed in response to GPCR activation, which then can react with a FRET substrate, thus correlating agonist activity with changes in FRET dynamics.¹⁶¹ The FRET signal is buffered by the time required for protein synthesis and thus is a temporarily imprecise reporter of GPCR activation. While these methods are useful for initial *in vitro* pharmacology analysis of drugs and can often times have a large dynamic range, they are highly modified and thus may not be good models of the relevant endogenous systems. These assays are certainly a helpful starting point for understanding receptor signaling but of course should be used simultaneously with other assays, too.¹⁶²

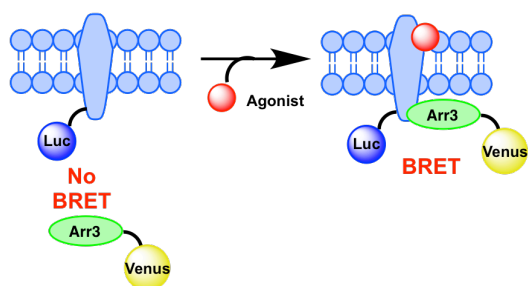


Figure 17. Mechanism of the BRET-based Arrestin Recruitment Assay.

An equally numerous amount of assays exist for measuring arrestin recruitment. Some early examples of arrestin measurement relied upon western blotting to look at downstream targets (such as p38 MAPK) or even arrestin itself.^{108,163} Others utilized imaging based

approaches or receptor internalization as a way to infer the arrestin activity.^{138,164} However while useful, these techniques are not necessarily direct measures of arrestin recruitment. Much like for G protein activation, there are several BRET-based assays for monitoring arrestin recruitment *in*

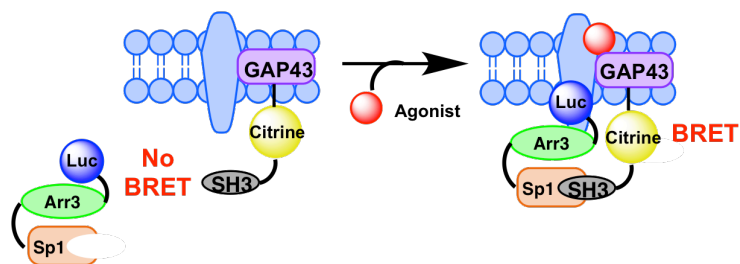


Figure 18. Mechanism of the BRET-based Arrestin GAP43 Translocation Assay.

vitro. The first (*BRET recruitment assay*) utilizes receptors tagged with a BRET donor, like RLuc8, and arrestin tagged with the BRET acceptor, mVenus.

Upon receptor activation and arrestin recruitment, a BRET signal can be detected (**Figure 17**).¹³⁸ This method is limited by the ability to clone receptors tagged with the BRET donor, which can be challenging. As a complementary approach (*BRET GAP43 translocation assay*), the BRET acceptor, fluorescent protein citrine, is tethered to the membrane by the doubly palmitoylated fragment of GAP43, found in virtually all cells, and fused to an SH3 domain. The arrestin protein is then sandwiched between both the BRET donor RLuc8 and a low affinity SH3-binding peptide, Sp1. Upon arrestin recruitment to the receptor, Sp1 and SH3 bind, causing a proximity-based BRET signal (**Figure 18**).¹⁵² The advantage of this method is that native receptors can be utilized, making the assay easily translatable over many GPCRs. Unfortunately, the assay is not necessarily compatible with every receptor construct, as varying levels of receptor expression in the cells seems to affect the success of the assay (see Chapter 5).

Reporter gene assays, such as the Tango assay, exist for measuring arrestin recruitment, as well (see Chapter 5). Depending on the reporter gene chosen and the substrate used for

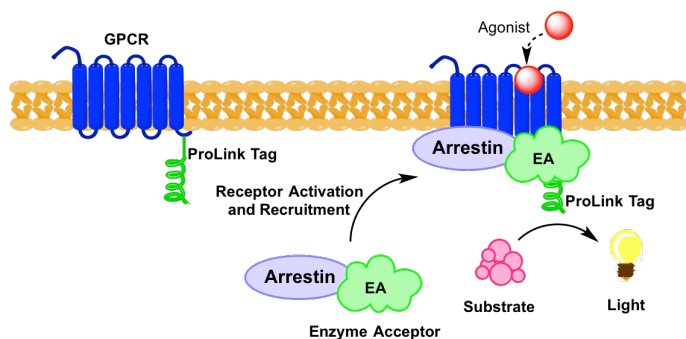


Figure 19. Mechanism of DiscoverX PathHunter® Assay for Arrestin Recruitment.

detection, it is possible to obtain quite a sensitive read-out for arrestin recruitment. DiscoverX also has a PathHunter® enzyme fragment complementation (EFC) assay for arrestin recruitment. In this assay, an N-terminal portion of

beta-galactosidase is fused to the C terminus of stably expressed β -arrestin 2 (arrestin 3). Then a mutated amino-terminal fragment of beta-galactosidase (ProLink/enzyme donor, PK) is fused to the C-terminus of the GPCR. When arrestin is recruited to the receptor upon activation, the beta-

galactosidase enzyme is reconstituted and able to act upon a substrate added to the cells (**Figure 19**).¹⁶⁵ Much like with measuring G protein activation, these systems are highly modified compared to *in vivo* systems and thus should be used with caution. If the assay is not sensitive enough (or too sensitive), bias calculations could be skewed.

Current Work

Given the complexity by which antidepressants elicit their behavioral effects and the clear need for better therapeutics, it is time to explore more exotic targets for treating depression. In particular, opioid and neurotrophin signaling offer two unique ways to tackle the poor therapeutics currently available for depression and anxiety. The literature precedent for such targets is clear, yet few researchers have given much attention to these understudied mechanisms. By studying these signaling cascades further, we can better understand how the different mechanisms overlap and therefore reveal the inner-workings of depression. In Part I, I will describe our efforts to understand the mechanisms of opioid receptor modulation in the context of depression and mood disorders, specifically through biochemical efforts that include *in vitro* pharmacology signaling studies, chemical synthesis, and some *in vivo* experiments. In particular, a significant effort is dedicated to exploring G protein bias within the various scaffolds as one solution to address the shortcomings of opioid receptor signaling, both for potential antidepressant and analgesic therapeutics. In Part II, I will describe the assay development and seminal work performed in our campaign to identify small molecule modulators of RTKs. Through these studies we have learned important indications that regulating brain chemistry through opioid receptor and RTK modulators reveals viable targets for antidepressant therapeutics, offering hope to those currently suffering from MDD.

References

- (1) Kessler, R. C.; Akiskal, H. S.; Ames, M.; Birnbaum, H.; Greenberg, P.; Hirschfeld, R. M. A.; Jin, R.; Merikangas, K. R.; Simon, G. E.; Wang, P. S. Prevalence and Effects of Mood Disorders on Work Performance in a Nationally Representative Sample of U.S. Workers. *Am. J. Psychiatry* **2006**, *163*, 1561–1568.
- (2) Baune, B. T.; Adrian, I.; Jacobi, F. Medical Disorders Affect Health Outcome and General Functioning Depending on Comorbid Major Depression in the General Population. *J. Psychosom. Res.* **2007**, *62*, 109–118.
- (3) Jick, H.; Kaye, J. A.; Jick, S. S. Antidepressants and the Risk of Suicidal Behaviors. *JAMA* **2004**, *292*, 338–343.
- (4) Bunney, W. E.; Davis, J. M. Norepinephrine in Depressive Reactions. *Arch. Gen. Psychiatry* **1965**, *13*, 483.
- (5) Schildkraut, J. J.; Kety, S. S. Biogenic Amines and Emotion. *Science* **1967**, *156*, 21–37.
- (6) Schildkraut, J. J. The Catecholamine Hypothesis of Affective Disorders. A Review of Supporting Evidence. *Int. J. Psychiatry* **1967**, *4*, 203–217.
- (7) Muller, J. C. Depression and Anxiety Occuring During Rauwolfia Therapy. *J. Am. Med. Assoc.* **1955**, *159*, 836.
- (8) Hirschfeld, R. M. History and Evolution of the Monoamine Hypothesis of Depression. *J. Clin. Psychiatry* **2000**, *61 Suppl 6*, 4–6.
- (9) Salomon, R. M.; Miller, H. L.; Krystal, J. H.; Heninger, G. R.; Charney, D. S. Lack of Behavioral Effects of Monoamine Depletion in Healthy Subjects. *Biol. Psychiatry* **1997**, *41*, 58–64.
- (10) Berman, R. M.; Sanacora, G.; Anand, A.; Roach, L. M.; Fasula, M. K.; Finkelstein, C. O.; Wachen, R. M.; Oren, D. A.; Heninger, G. R.; Charney, D. S. Monoamine Depletion in Unmedicated Depressed Subjects. *Biol. Psychiatry* **2002**, *51*, 469–473.
- (11) Kew, J. N.; Kemp, J. A. Ionotropic and Metabotropic Glutamate Receptor Structure and Pharmacology. *Psychopharmacol.* **2005**, *179*, 4–29.
- (12) Hillhouse, T. M.; Porter, J. H. A Brief History of the Development of Antidepressant Drugs: From Monoamines to Glutamate. *Exp. Clin. Psychopharmacol.* **2015**, *23*, 1–21.
- (13) Berman, R. M.; Cappiello, A.; Anand, A.; Oren, D. A.; Heninger, G. R.; Charney, D. S.; Krystal, J. H. Antidepressant Effects of Ketamine in Depressed Patients. *Soc. Biol. Psychiatry* **2000**, *47*, 351–354.
- (14) Schulberg, H. C.; Katon, W.; Simon, G. E.; Rush, A. J. Treating Major Depression in Primary Care Practice: An Update of the Agency for Health Care Policy and Research Practice Guidelines. *Arch. Gen. Psychiatry* **1998**, *55*, 1121–1127.
- (15) Zarate, C. A.; Singh, J. B.; Carlson, P. J.; Brutsche, N. E.; Ameli, R.; Luckenbaugh, D. A.; Charney, D. S.; Manji, H. K. A Randomized Trial of an N-Methyl-D-Aspartate Antagonist in Treatment-Resistant Major Depression. *Arch. Gen. Psychiatry* **2006**, *63*, 856–864.
- (16) Aan Het Rot, M.; Collins, K. A.; Murrrough, J. W.; Perez, A. M.; Reich, D. L.; Charney, D. S.; Mathew, S. J. Safety and Efficacy of Repeated-Dose Intravenous Ketamine for Treatment-Resistant Depression. *Biol. Psychiatry* **2010**, *67*, 139–145.
- (17) Murrrough, J. W.; Perez, A. M.; Pillemer, S.; Stern, J.; Parides, M. K.; Aan Het Rot, M.; Collins, K. A.; Mathew, S. J.; Charney, D. S.; Iosifescu, D. V. Rapid and Longer-Term Antidepressant Effects of Repeated Ketamine Infusions in Treatment-Resistant Major Depression. *Biol. Psychiatry* **2013**, *74*, 250–256.

- (18) Irwin, S. A.; Iglewicz, A. Oral Ketamine for the Rapid Treatment of Depression and Anxiety in Patients Receiving Hospice Care. *J Palliat Med* **2010**, *13*, 903–908.
- (19) McNulty, J. P.; Hahn, K. Compounded Oral Ketamine. *Int. J. Pharm. Compd.* **2012**, *16*, 364–368.
- (20) Irwin, S. a; Iglewicz, A.; Nelesen, R. A.; Lo, J. Y.; Carr, C. H.; Romero, S. D.; Lloyd, L. S. Daily Oral Ketamine for the Treatment of Depression and Anxiety in Patients Receiving Hospice Care: A 28-Day Open-Label Proof-of-Concept Trial. *J. Palliat. Med.* **2013**, *16*, 958–965.
- (21) Lara, D. R.; Bisol, L. W.; Munari, L. R. Antidepressant, Mood Stabilizing and Procognitive Effects of Very Low Dose Sublingual Ketamine in Refractory Unipolar and Bipolar Depression. *Int. J. Neuropsychopharmacol.* **2013**, *16*, 2111–2117.
- (22) Nestler, E. J.; Carlezon, W. A. The Mesolimbic Dopamine Reward Circuit in Depression. *Biol. Psychiatry* **2006**, *59*, 1151–1159.
- (23) Espejo, E. F.; Miñano, F. J. Prefrontocortical Dopamine Depletion Induces Antidepressant-like Effects in Rats and Alters the Profile of Desipramine during Porsolt's Test. *Neuroscience* **1999**, *88*, 609–615.
- (24) Yadid, G.; Overstreet, D. H.; Zangen, A. Limbic Dopaminergic Adaptation to a Stressful Stimulus in a Rat Model of Depression. *Brain Res.* **2001**, *896*, 43–47.
- (25) Cyr, M.; Morissette, M.; Barden, N.; Beaulieu, S.; Rochford, J.; Di Paolo, T. Dopaminergic Activity in Transgenic Mice Underexpressing Glucocorticoid Receptors: Effect of Antidepressants. *Neuroscience* **2001**, *102*, 151–158.
- (26) Mayberg, H. S.; Brannan, S. K.; Tekell, J. L.; Silva, J. A.; Mahurin, R. K.; McGinnis, S.; Jerabek, P. A. Regional Metabolic Effects of Fluoxetine in Major Depression: Serial Changes and Relationship to Clinical Response. *Biol. Psychiatry* **2000**, *48*, 830–843.
- (27) Sheline, Y. I.; Barch, D. M.; Donnelly, J. M.; Ollinger, J. M.; Snyder, A. Z.; Mintun, M. A. Increased Amygdala Response to Masked Emotional Faces in Depressed Subjects Resolves with Antidepressant Treatment: An fMRI Study. *Biol. Psychiatry* **2001**, *50*, 651–658.
- (28) Taylor Tavares, J. V.; Clark, L.; Furey, M. L.; Williams, G. B.; Sahakian, B. J.; Drevets, W. C. Neural Basis of Abnormal Response to Negative Feedback in Unmedicated Mood Disorders. *Neuroimage* **2008**, *42*, 1118–1126.
- (29) Drevets, W. C.; Price, J. L.; Simpson Jr., J. R.; Todd, R. D.; Reich, T.; Vannier, M.; Raichle, M. E. Subgenual Prefrontal Cortex Abnormalities in Mood Disorders. *Nature*, 1997, *386*, 824–827.
- (30) Tye, K. M.; Mirzabekov, J. J.; Warden, M. R.; Ferenczi, E. A.; Tsai, H.-C.; Finkelstein, J.; Kim, S.-Y.; Adhikari, A.; Thompson, K. R.; Andalman, A. S.; Gunaydin, L. A.; Witten, I. B.; Deisseroth, K. Dopamine Neurons Modulate Neural Encoding and Expression of Depression-Related Behaviour. *Nature* **2012**, *493*, 537–541.
- (31) Chaudhury, D.; Walsh, J. J.; Friedman, A. K.; Juarez, B.; Ku, S. M.; Koo, J. W.; Ferguson, D.; Tsai, H.-C.; Pomeranz, L.; Christoffel, D. J.; Nectow, A. R.; Ekstrand, M.; Domingos, A.; Mazei-Robison, M. S.; Mouzon, E.; Lobo, M. K.; Neve, R. L.; Friedman, J. M.; Russo, S. J.; Deisseroth, K.; Nestler, E. J.; Han, M.-H. Rapid Regulation of Depression-Related Behaviours by Control of Midbrain Dopamine Neurons. *Nature* **2013**, *493*, 532–536.
- (32) Qi, J.; Zhang, S.; Wang, H.-L.; Barker, D. J.; Miranda-Barrientos, J.; Morales, M. VTA Glutamatergic Inputs to Nucleus Accumbens Drive Aversion by Acting on GABAergic

- Interneurons. *Nat. Neurosci.* **2016**, *19*, 725–733.
- (33) Saal, D.; Dong, Y.; Bonci, A.; Malenka, R. C. Drugs of Abuse and Stress Trigger a Common Synaptic Adaptation in Dopamine Neurons. *Neuron* **2003**, *37*, 577–582.
- (34) Berrocoso, E.; Rojas-Corrales, M. O.; Micó, J. A. Non-Selective Opioid Receptor Antagonism of the Antidepressant-like Effect of Venlafaxine in the Forced Swimming Test in Mice. *Neurosci. Lett.* **2004**, *363*, 25–28.
- (35) Devoize, J. L.; Rigal, F.; Eschalier, A.; Trolese, J. F.; Renoux, M. Influence of Naloxone on Antidepressant Drug Effects in the Forced Swimming Test in Mice. *Psychopharmacology (Berl)*. **1984**, *84*, 71–75.
- (36) De Felipe, M. C.; De Ceballos, M. L.; Gil, C.; Fuentes, J. A. Chronic Antidepressant Treatment Increases Enkephalin Levels in N. Accumbens and Striatum of the Rat. *Eur. J. Pharmacol.* **1985**, *112*, 119–122.
- (37) Rossby, S.; Perrin, C.; Burt, A.; Nalepa, I.; Schmidt, D.; Sulser, F. Fluoxetine Increases Steady-State Levels of Preproenkephalin mRNA in Rat Amygdala by a Serotonin Dependent Mechanism. *J. Serotonin Res.* **1996**, *3*, 69–74.
- (38) de Gandarias, J. M.; Echevarria, E.; Acebes, I.; Silio, M.; Casis, L. Effects of Imipramine Administration on Mu-Opioid Receptor Immunostaining in the Rat Forebrain. *Arzneimittelforschung.* **1998**, *48*, 717–719.
- (39) Kraepelin, E. *Einführung in Die Psychiatrische Klinik: Zweiunddreissig Vorlesungen*; J.A. Barth: Leipzig, 1905.
- (40) Trang, T.; Al-Hasani, R.; Salvemini, D.; Salter, M. W.; Gutstein, H.; Cahill, C. M. Pain and Poppies: The Good, the Bad, and the Ugly of Opioid Analgesics. *J. Neurosci.* **2015**, *35*, 13879–13888.
- (41) Gerner, R. H.; Catlin, D. H.; Gorelick, D. A.; Hui, K. K.; Li, C. H. Beta-Endorphin. Intravenous Infusion Causes Behavioral Change in Psychiatric Inpatients. *Arch. Gen. Psychiatry* **1980**, *37*, 642–647.
- (42) Stoll, A. L.; Rueter, S. Treatment Augmentation with Opiates in Severe and Refractory Major Depression. *Am. J. Psychiatry* **1999**, *156*, 2017.
- (43) Dean, A. J.; Bell, J.; Christie, M. J.; Mattick, R. P. Depressive Symptoms during Buprenorphine vs. Methadone Maintenance: Findings from a Randomised, Controlled Trial in Opioid Dependence. *Eur. Psychiatry* **2004**, *19*, 510–513.
- (44) Shapira, N. A.; Verduin, M. L.; DeGraw, J. D. Treatment of Refractory Major Depression with Tramadol Monotherapy. *J. Clin. Psychiatry* **2001**, *62*, 205–206.
- (45) Shapira, N. A.; Keck, P. E.; Goldsmith, T. D.; McConville, B. J.; Eis, M.; McElroy, S. L. Open-Label Pilot Study of Tramadol Hydrochloride in Treatment-Refractory Obsessive-Compulsive Disorder. *Depress. Anxiety* **1997**, *6*, 170–173.
- (46) Emrich, H. M.; Vogt, P.; Herz, A. Possible Antidepressive Effects of Opioids: Action of Buprenorphine. *Ann. N. Y. Acad. Sci.* **1982**, *398*, 108–112.
- (47) Karp, J. F.; Butters, M. A.; Begley, A. E.; Miller, M. D.; Lenze, E. J.; Blumberger, D. M.; Mulsant, B. H.; Reynolds, C. F. Safety, Tolerability, and Clinical Effect of Low-Dose Buprenorphine for Treatment-Resistant Depression in Midlife and Older Adults. *J. Clin. Psychiatry* **2014**, *75*, e785–e793.
- (48) Bodkin, J. A.; Zornberg, G. L.; Lukas, S. E.; Cole, J. O. Buprenorphine Treatment of Refractory Depression. *J. Clin. Psychopharmacol.* **1995**, *15*, 49–57.
- (49) Jutkiewicz, E. M. The Antidepressant -like Effects of Delta-Opioid Receptor Agonists. *Mol. Interv.* **2006**, *6*, 162–169.

- (50) Peppin, J. F.; Raffa, R. B. Delta Opioid Agonists: A Concise Update on Potential Therapeutic Applications. *J. Clin. Pharm. Ther.* **2015**, *40*, 155–166.
- (51) Cai, S.; Huang, S.; Hao, W. New Hypothesis and Treatment Targets of Depression: An Integrated View of Key Findings. *Neurosci. Bull.* **2015**, *31*, 61–74.
- (52) Russo-Neustadt, A.; Ha, T.; Ramirez, R.; Kessler, J. P. Physical Activity-Antidepressant Treatment Combination: Impact on Brain-Derived Neurotrophic Factor and Behavior in an Animal Model. *Behav. Brain Res.* **2001**, *120*, 87–95.
- (53) Karege, F.; Perret, G.; Bondolfi, G.; Schwald, M.; Bertschy, G.; Aubry, J. M. Decreased Serum Brain-Derived Neurotrophic Factor Levels in Major Depressed Patients. *Psychiatry Res.* **2002**, *109*, 143–148.
- (54) Siuciak, J. A.; Lewis, D. R.; Wiegand, S. J.; Lindsay, R. M. Antidepressant-like Effect of Brain-Derived Neurotrophic Factor (BDNF). *Pharmacol. Biochem. Behav.* **1997**, *56*, 131–137.
- (55) Ihara, K.; Yoshida, H.; Jones, P. B.; Hashizume, M.; Suzuki, Y.; Ishijima, H.; Kim, H. K.; Suzuki, T.; Hachisu, M. Serum BDNF Levels before and after the Development of Mood Disorders: A Case-Control Study in a Population Cohort. *Transl. Psychiatry* **2016**, *6*, e782.
- (56) Sarchiapone, M.; Carli, V.; Roy, A.; Iacoviello, L.; Cuomo, C.; Latella, M. C.; Di Giannantonio, M.; Janiri, L.; De Gaetano, M.; Janal, M. N. Association of Polymorphism (Val66Met) of Brain-Derived Neurotrophic Factor with Suicide Attempts in Depressed Patients. *Neuropsychobiology* **2008**, *57*, 139–145.
- (57) Dwivedi, Y. Brain-Derived Neurotrophic Factor in Suicide Pathophysiology. In *The Neurobiological Basis of Suicide*; CRC Press/Taylor & Francis: Boca Raton, Florida, 2012.
- (58) Duman, R. S.; Monteggia, L. M. A Neurotrophic Model for Stress-Related Mood Disorders. *Biol. Psychiatry* **2006**, *59*, 1116–1127.
- (59) Lang, U. E.; Borgwardt, S. Molecular Mechanisms of Depression: Perspectives on New Treatment Strategies. *Cell. Physiol. Biochem.* **2013**, *31*, 761–777.
- (60) Duman, R. S.; Li, N. A Neurotrophic Hypothesis of Depression: Role of Synaptogenesis in the Actions of NMDA Receptor Antagonists. *Philos. Trans. R. Soc. Lond. B. Biol. Sci.* **2012**, *367*, 2475–2484.
- (61) López-Muñoz, F.; Alamo, C.; Juckel, G.; Assion, H.-J. Half a Century of Antidepressant Drugs: On the Clinical Introduction of Monoamine Oxidase Inhibitors, Tricyclics, and Tetracyclics. Part I: Monoamine Oxidase Inhibitors. *J. Clin. Psychopharmacol.* **2007**, *27*, 555–559.
- (62) Fangmann, P.; Assion, H.-J.; Juckel, G.; González, C. A.; López-Muñoz, F. Half a Century of Antidepressant Drugs: On the Clinical Introduction of Monoamine Oxidase Inhibitors, Tricyclics, and Tetracyclics. Part II: Tricyclics and Tetracyclics. *J. Clin. Psychopharmacol.* **2008**, *28*, 1–4.
- (63) Kuhn, R. The Treatment of Depressive States with G 22355 (Imipramine Hydrochloride). *Am. J. Psychiatry* **1958**, *115*, 459–464.
- (64) Cusack, B.; Nelson, A.; Richelson, E. Binding of Antidepressants to Human Brain Receptors: Focus on Newer Generation Compounds. *Psychopharmacology (Berl.)* **1994**, *114*, 559–565.
- (65) Shaw, D. M.; Camps, F. E.; Eccleston, E. G. 5-Hydroxytryptamine in the Hind-Brain of Depressive Suicides. *Br. J. Psychiatry* **1967**, *113*, 1407–1411.

- (66) Wong, D. T.; Horng, J. S.; Bymaster, F. P.; Hauser, K. L.; Molloy, B. B. A Selective Inhibitor of Serotonin Uptake: Lilly 110140, 3-(P-Trifluoromethylphenoxy)-N-Methyl-3-Phenylpropylamine. *Life Sci.* **1974**, *15*, 471–479.
- (67) Papakostas, G. I. Tolerability of Modern Antidepressants. *J. Clin. Psychiatry* **2008**, *69 Suppl E*, 8–13.
- (68) Preston, T. C.; Shelton, R. C. Treatment Resistant Depression: Strategies for Primary Care Topical Collection on Psychiatry in Primary Care. *Curr. Psychiatry Rep.* **2013**, *15*, 13–18.
- (69) Bymaster, F. P.; Dreshfield-Ahmad, L. J.; Threlkeld, P. G.; Shaw, J. L.; Thompson, L.; Nelson, D. L.; Hemrick-Luecke, S. K.; Wong, D. T. Comparative Affinity of Duloxetine and Venlafaxine for Serotonin and Norepinephrine Transporters in Vitro and in Vivo, Human Serotonin Receptor Subtypes, and Other Neuronal Receptors. *Neuropsychopharmacology* **2001**, *25*, 871–880.
- (70) Feighner, J.; Hendrickson, G.; Miller, L.; Stern, W. Double-Blind Comparison of Doxepin versus Bupropion in Outpatients with a Major Depressive Disorder. *J. Clin. Psychopharmacol.* **1986**, *6*, 27–32.
- (71) Clayton, A. H.; Pradko, J. F.; Croft, H. A.; Brendan Montano, C.; Leadbetter, R. A.; Bolden-Watson, C.; Bass, K. I.; Donahue, R. M. J.; Jamerson, B. D.; Metz, A. Prevalence of Sexual Dysfunction among Newer Antidepressants. *J. Clin. Psychiatry* **2002**, *63*, 357–366.
- (72) Montoya, A.; Bruins, R.; Katzman, M. A.; Blier, P. The Noradrenergic Paradox: Implications in the Management of Depression and Anxiety. *Neuropsychiatr. Dis. Treat.* **2016**, *12*, 541–557.
- (73) Bang-Andersen, B.; Ruhland, T.; Jørgensen, M.; Smith, G.; Frederiksen, K.; Jensen, K. G.; Zhong, H.; Nielsen, S. M.; Hogg, S.; Mørk, A.; Stensbøl, T. B. Discovery of 1-[2-(2,4-Dimethylphenylsulfanyl)phenyl]piperazine (Lu AA21004): A Novel Multimodal Compound for the Treatment of Major Depressive Disorder. *J. Med. Chem.* **2011**, *54*, 3206–3221.
- (74) Sanacora, G.; Schatzberg, A. F. Ketamine: Promising Path or False Prophecy in the Development of Novel Therapeutics for Mood Disorders? *Neuropsychopharmacology* **2014**, 1–31.
- (75) Martinowich, K.; Jimenez, D. V.; Zarate, C. A.; Manji, H. K. Rapid Antidepressant Effects: Moving Right Along. *Mol. Psychiatry* **2013**, *18*, 856–863.
- (76) McEwen, B. S.; Chattarji, S.; Diamond, D. M.; Jay, T. M.; Reagan, L. P.; Svenningsson, P.; Fuchs, E. The Neurobiological Properties of Tianeptine (Stablon): From Monoamine Hypothesis to Glutamatergic Modulation. *Mol. Psychiatry* **2010**, *15*, 237–249.
- (77) Svenningsson, P.; Bateup, H.; Qi, H.; Takamiya, K.; Haganir, R. L.; Spedding, M.; Roth, B. L.; McEwen, B. S.; Greengard, P. Involvement of AMPA Receptor Phosphorylation in Antidepressant Actions with Special Reference to Tianeptine. *Eur. J. Neurosci.* **2007**, *26*, 3509–3517.
- (78) Gassaway, M. M.; Rives, M.-L.; Kruegel, A. C.; Javitch, J. A.; Sames, D. The Atypical Antidepressant and Neurorestorative Agent Tianeptine Is a μ -Opioid Receptor Agonist. *Transl. Psychiatry* **2014**, *4*, e411.
- (79) Kroupa, B. P. K.; Wells, H. Ibogaine in the 21st Century: Boosters, Tune-Ups and Maintenance. *Maps* **2005**, *15*, 21–24.
- (80) Rosenbaum, D. M.; Rasmussen, S. G. F.; Kobilka, B. K. The Structure and Function of G-Protein-Coupled Receptors. *Nature* **2009**, *459*, 356–363.

- (81) Milligan, G.; Kostenis, E. Heterotrimeric G-Proteins: A Short History. *Br. J. Pharmacol.* **2009**, *147*, S46–S55.
- (82) Wu, D.; Lee, C. H.; Rhee, S. G.; Simon, M. I. Activation of Phospholipase C by the α Subunits of the Gq and G11 Proteins in Transfected Cos-7 Cells. *J. Biol. Chem.* **1992**, *267*, 1811–1817.
- (83) Khan, S. M.; Sleno, R.; Gora, S.; Zylbergold, P.; Laverdure, J.-P.; Labbé, J.-C.; Miller, G. J.; Hébert, T. E. The Expanding Roles of G $\beta\gamma$ Subunits in G Protein-Coupled Receptor Signaling and Drug Action. *Pharmacol. Rev.* **2013**, *65*, 545–577.
- (84) Luttrell, L. M.; Ferguson, S. S.; Daaka, Y.; Miller, W. E.; Maudsley, S.; Della Rocca, G. J.; Lin, F.; Kawakatsu, H.; Owada, K.; Luttrell, D. K.; Caron, M. G.; Lefkowitz, R. J. B-Arrestin-Dependent Formation of β_2 Adrenergic Receptor-Src Protein Kinase Complexes. *Science (80-.)*. **1999**, *283*, 655–661.
- (85) Gurevich, V. V.; Gurevich, E. V. Overview of Different Mechanisms of Arrestin-Mediated Signaling. *Curr. Protoc. Pharmacol.* **2014**, *2014*, 2.10.1–2.10.9.
- (86) Pasternak, G. W.; Pan, Y.-X. Mu Opioids and Their Receptors: Evolution of a Concept. *Pharmacol. Rev.* **2013**, *65*, 1257–1317.
- (87) Ikeda, K.; Kobayashi, T.; Kumanishi, T.; Yano, R.; Sora, I.; Niki, H. Molecular Mechanisms of Analgesia Induced by Opioids and Ethanol: Is the GIRK Channel One of the Keys? *Neurosci. Res.* **2002**, *44*, 121–131.
- (88) Bockaert, J.; Dumuis, A.; Fagni, L.; Marin, P. GPCR-GIP Networks: A First Step in the Discovery of New Therapeutic Drugs? *Curr. Opin. Drug Discov. Devel.* **2004**, *7*, 649–657.
- (89) Werry, T. D.; Sexton, P. M.; Christopoulos, A. “Ins and Outs” of Seven-Transmembrane Receptor Signalling to ERK. *Trends Endocrinol. Metab.* **2005**, *16*, 26–33.
- (90) Seta, K.; Sadoshima, J. Phosphorylation of Tyrosine 319 of the Angiotensin II Type 1 Receptor Mediates Angiotensin II-Induced Trans-Activation of the Epidermal Growth Factor Receptor. *J. Biol. Chem.* **2003**, *278*, 9019–9026.
- (91) Maudsley, S. The Beta 2-Adrenergic Receptor Mediates Extracellular Signal-Regulated Kinase Activation via Assembly of a Multi-Receptor Complex with the Epidermal Growth Factor Receptor. *J. Biol. Chem.* **2000**, *275*, 9572–9580.
- (92) Belcheva, M. M.; Haas, P. D.; Tan, Y.; Heaton, V. M.; Coscia, C. J. The Fibroblast Growth Factor Receptor Is at the Site of Convergence between Mu-Opioid Receptor and Growth Factor Signaling Pathways in Rat C6 Glioma Cells. *J. Pharmacol. Exp. Ther.* **2002**, *303*, 909–918.
- (93) Lee, F. S.; Chao, M. V. Activation of Trk Neurotrophin Receptors in the Absence of Neurotrophins. *Proc. Natl. Acad. Sci. U. S. A.* **2001**, *98*, 3555–3560.
- (94) Metcalf, M. D.; Yekkirala, A. S.; Powers, M. D.; Kitto, K. F.; Fairbanks, C. A.; Wilcox, G. L.; Portoghese, P. S. The δ Opioid Receptor Agonist SNC80 Selectively Activates Heteromeric μ - δ Opioid Receptors. *ACS Chem. Neurosci.* **2012**, *3*, 505–509.
- (95) Fujita, W.; Gomes, I.; Devi, L. A. Heteromers of μ - δ Opioid Receptors: New Pharmacology and Novel Therapeutic Possibilities. *Br. J. Pharmacol.* **2014**, 1–13.
- (96) Kabli, N.; Nguyen, T.; Balboni, G.; O’Dowd, B. F.; George, S. R. Antidepressant-like and Anxiolytic-like Effects Following Activation of the μ - δ Opioid Receptor Heteromer in the Nucleus Accumbens. *Mol. Psychiatry* **2013**, 1–9.
- (97) Lambert, N. A.; Javitch, J. A. CrossTalk Opposing View: Weighing the Evidence for Class A GPCR Dimers, the Jury Is Still Out. *J. Physiol.* **2014**, *592*, 2443–2445.

- (98) Lambert, N. A.; Javitch, J. A. Rebuttal from Nevin A. Lambert and Jonathan A. Javitch. *J. Physiol.* **2014**, *592*, 2449.
- (99) Majumdar, S.; Grinnell, S.; Le Rouzic, V.; Burgman, M.; Polikar, L.; Ansonoff, M.; Pintar, J.; Pan, Y.-X.; Pasternak, G. W. Truncated G Protein-Coupled Mu Opioid Receptor MOR-1 Splice Variants Are Targets for Highly Potent Opioid Analgesics Lacking Side Effects. *Proc. Natl. Acad. Sci.* **2011**, *108*, 19778–19783.
- (100) Grinnell, S. G.; Majumdar, S.; Narayan, A.; Le Rouzic, V.; Ansonoff, M.; Pintar, J. E.; Pasternak, G. W. Pharmacologic Characterization in the Rat of a Potent Analgesic Lacking Respiratory Depression, IBNtxA. *J. Pharmacol. Exp. Ther.* **2014**, *350*, 710–718.
- (101) Lu, Z.; Xu, J.; Rossi, G. C.; Majumdar, S.; Pasternak, G. W.; Pan, Y. Mediation of Opioid Analgesia by a Truncated 6-Transmembrane GPCR. *J. Clin. Invest.* **2015**, *125*, 2626–2630.
- (102) Kenakin, T. *A Pharmacology Primer: Theory, Applications, and Methods*; 3rd Editio.; Elsevier Academic Press: Burlington, MA, 2009.
- (103) Christopoulos, A.; Christopoulos, G.; Morfis, M.; Udawela, M.; Laburthe, M.; Couvineau, A.; Kuwasako, K.; Tilakaratne, N.; Sexton, P. M. Novel Receptor Partners and Function of Receptor Activity-Modifying Proteins. *J. Biol. Chem.* **2003**, *278*, 3293–3297.
- (104) Kenakin, T. Efficacy At G-Protein-Coupled Receptors. *Nat. Rev. Drug Discov.* **2002**, *1*, 103–110.
- (105) Wei, H.; Ahn, S.; Shenoy, S. K.; Karnik, S. S.; Hunyady, L.; Luttrell, L. M.; Lefkowitz, R. J. Independent Beta-Arrestin 2 and G Protein-Mediated Pathways for Angiotensin II Activation of Extracellular Signal-Regulated Kinases 1 and 2. *Proc. Natl. Acad. Sci. U. S. A.* **2003**, *100*, 10782–10787.
- (106) Gesty-Palmer, D.; Chen, M.; Reiter, E.; Ahn, S.; Nelson, C. D.; Wang, S.; Eckhardt, A. E.; Cowan, C. L.; Spurney, R. F.; Luttrell, L. M.; Lefkowitz, R. J. Distinct β -Arrestin- and G Protein-Dependent Pathways for Parathyroid Hormone Receptor-Stimulated ERK1/2 Activation. *J. Biol. Chem.* **2006**, *281*, 10856–10864.
- (107) Azzi, M.; Charest, P. G.; Angers, S.; Rousseau, G.; Kohout, T.; Bouvier, M.; Piñeyro, G. Beta-Arrestin-Mediated Activation of MAPK by Inverse Agonists Reveals Distinct Active Conformations for G Protein-Coupled Receptors. *Proc. Natl. Acad. Sci. U. S. A.* **2003**, *100*, 11406–11411.
- (108) Bohn, L. M.; Lefkowitz, R. J.; Gainetdinov, R. R.; Peppel, K.; Caron, M. G.; Lin, F. T. Enhanced Morphine Analgesia in Mice Lacking Beta-Arrestin 2. *Science* **1999**, *286*, 2495–2498.
- (109) Kahsai, A. W.; Xiao, K.; Rajagopal, S.; Ahn, S.; Shukla, A. K.; Sun, J.; Oas, T. G.; Lefkowitz, R. J. Multiple Ligand-Specific Conformations of the β 2-Adrenergic Receptor. *Nat. Chem. Biol.* **2011**, *7*, 692–700.
- (110) Liu, J. J.; Horst, R.; Katritch, V.; Stevens, R. C.; Wüthrich, K. Biased Signaling Pathways in β 2-Adrenergic Receptor Characterized by 19F-NMR. *Science* **2012**, *335*, 1106–1110.
- (111) Warne, T.; Edwards, P. C.; Leslie, A. G. W.; Tate, C. G. Crystal Structures of a Stabilized β 1-Adrenoceptor Bound to the Biased Agonists Bucindolol and Carvedilol. *Structure* **2012**, *20*, 841–849.
- (112) Warne, T.; Serrano-Vega, M. J.; Baker, J. G.; Moukhametzianov, R.; Edwards, P. C.; Henderson, R.; Leslie, A. G. W.; Tate, C. G.; Schertler, G. F. X. Structure of a β 1-Adrenergic G-Protein-Coupled Receptor. *Nature* **2008**, *454*, 486–491.
- (113) Shukla, A. K.; Singh, G.; Ghosh, E. Emerging Structural Insights into Biased GPCR

- Signaling. *Trends Biochem. Sci.* **2014**, *39*, 594–602.
- (114) Wacker, D.; Wang, C.; Katritch, V.; Han, G. W.; Huang, X.-P.; Vardy, E.; McCorvy, J. D.; Jiang, Y.; Chu, M.; Siu, F. Y.; Liu, W.; Xu, H. E.; Cherezov, V.; Roth, B. L.; Stevens, R. C. Structural Features for Functional Selectivity at Serotonin Receptors. *Science* **2013**, *340*, 615–619.
- (115) Wang, C.; Jiang, Y.; Ma, J.; Wu, H.; Wacker, D.; Katritch, V.; Han, G. W.; Liu, W.; Huang, X.-P.; Vardy, E.; McCorvy, J. D.; Gao, X.; Zhou, X. E.; Melcher, K.; Zhang, C.; Bai, F.; Yang, H.; Yang, L.; Jiang, H.; Roth, B. L.; Cherezov, V.; Stevens, R. C.; Xu, H. E. Structural Basis for Molecular Recognition at Serotonin Receptors. *Science* **2013**, *340*, 610–614.
- (116) Nobles, K. N.; Xiao, K.; Ahn, S.; Shukla, A. K.; Lam, C. M.; Rajagopal, S.; Strachan, R. T.; Huang, T.; Bressler, E. A.; Hara, M. R.; Shenoy, S. K.; Gygi, S. P.; Lefkowitz, R. J. Distinct Phosphorylation Sites on the $\beta(2)$ -Adrenergic Receptor Establish a Barcode That Encodes Differential Functions of β -Arrestin. *Sci. Signal.* **2011**, *4*, ra51.
- (117) Oakley, R. H.; Laporte, S. A.; Holt, J. A.; Caron, M. G.; Barak, L. S. Differential Affinities of Visual Arrestin, β arrestin1, and β arrestin2 for G Protein-Coupled Receptors Delineate Two Major Classes of Receptors. *J. Biol. Chem.* **2000**, *275*, 17201–17210.
- (118) Oakley, R. H.; Laporte, S. A.; Holt, J. A.; Barak, L. S.; Caron, M. G. Molecular Determinants Underlying the Formation of Stable Intracellular G Protein-Coupled Receptor- β -Arrestin Complexes after Receptor Endocytosis. *J. Biol. Chem.* **2001**, *276*, 19452–19460.
- (119) Kohout, T. A.; Nicholas, S. L.; Perry, S. J.; Reinhart, G.; Junger, S.; Struthers, R. S. Differential Desensitization, Receptor Phosphorylation, β -Arrestin Recruitment, and ERK1/2 Activation by the Two Endogenous Ligands for the CC Chemokine Receptor 7. *J. Biol. Chem.* **2004**, *279*, 23214–23222.
- (120) Zidar, D. a; Violin, J. D.; Whalen, E. J.; Lefkowitz, R. J. Selective Engagement of G Protein Coupled Receptor Kinases (GRKs) Encodes Distinct Functions of Biased Ligands. *Proc. Natl. Acad. Sci.* **2009**, *106*, 9649–9654.
- (121) Schmid, C. L.; Bohn, L. M. Serotonin, but Not N-Methyltryptamines, Activates the Serotonin 2A Receptor via a SS-arrestin2/Src/Akt Signaling Complex in Vivo. *J. Neurosci.* **2010**, *30*, 13513–13524.
- (122) Thompson, G. L.; Lane, J. R.; Coudrat, T.; Sexton, P. M.; Christopoulos, A.; Canals, M. Biased Agonism of Endogenous Opioid Peptides at the μ -Opioid Receptor. *Mol. Pharmacol.* **2015**, *88*, 335–346.
- (123) DeWire, S. M.; Yamashita, D. S.; Rominger, D. H.; Liu, G.; Cowan, C. L.; Graczyk, T. M.; Chen, X.-T.; Pitis, P. M.; Gotchev, D.; Yuan, C.; Koblish, M.; Lark, M. W.; Violin, J. D. A G Protein-Biased Ligand at the μ -Opioid Receptor Is Potently Analgesic with Reduced Gastrointestinal and Respiratory Dysfunction Compared with Morphine. *J. Pharmacol. Exp. Ther.* **2013**, *344*, 708–717.
- (124) Park, H. S.; Lee, H. Y.; Kim, Y. H.; Park, J. K.; Zvartau, E. E.; Lee, H. A Highly Selective κ -Opioid Receptor Agonist with Low Addictive Potential and Dependence Liability. *Bioorganic Med. Chem. Lett.* **2006**, *16*, 3609–3613.
- (125) Bruchas, M. R.; Macey, T. A.; Lowe, J. D.; Chavkin, C. Kappa Opioid Receptor Activation of p38 MAPK Is GRK3- and Arrestin-Dependent in Neurons and Astrocytes. *J. Biol. Chem.* **2006**, *281*, 18081–18089.
- (126) Bruchas, M. R.; Chavkin, C. Kinase Cascades and Ligand-Directed Signaling at the

- Kappa Opioid Receptor. *Psychopharmacology (Berl)*. **2010**, *210*, 137–147.
- (127) Yan, F.; Roth, B. L. Salvinorin A: A Novel and Highly Selective κ -Opioid Receptor Agonist. *Life Sci*. **2004**, *75*, 2615–2619.
- (128) Reiter, E.; Ahn, S.; Shukla, A. K.; Lefkowitz, R. J. Molecular Mechanism of β -Arrestin-Biased Agonism at Seven-Transmembrane Receptors. *Annu. Rev. Pharmacol. Toxicol.* **2012**, *52*, 179–197.
- (129) Rajagopal, S.; Ahn, S.; Rominger, D. H.; Gowen-Macdonald, W.; Lam, C. M.; Dewire, S. M.; Violin, J. D.; Lefkowitz, R. J. Quantifying Ligand Bias at Seven-Transmembrane Receptors. *Mol. Pharmacol.* **2011**, *80*, 367–377.
- (130) Black, J. W.; Leff, P. Operational Models of Pharmacological Agonism. *Proc. R. Soc. London. Ser. B, Biol. Sci.* **1983**, *220*, 141–162.
- (131) Kenakin, T.; Watson, C.; Muniz-Medina, V.; Christopoulos, A.; Novick, S. A Simple Method for Quantifying Functional Selectivity and Agonist Bias. *ACS Chem. Neurosci.* **2012**, *3*, 193–203.
- (132) Kenakin, T.; Christopoulos, A. Signalling Bias in New Drug Discovery: Detection, Quantification and Therapeutic Impact. *Nat. Rev. Drug Discov.* **2013**, *12*, 205–216.
- (133) Endrenyi, L.; Fajsz, C.; Kwong, F. H. Evaluation of Hill Slopes and Hill Coefficients When the Saturation Binding or Velocity Is Not Known. *Eur. J. Biochem.* **1975**, *51*, 317–328.
- (134) Griffin, M. T.; Figueroa, K. W.; Liller, S.; Ehlert, F. J. Estimation of Agonist Activity at G Protein-Coupled Receptors: Analysis of M2 Muscarinic Receptor Signaling through Gi/o, Gs, and G15. *J. Pharmacol. Exp. Ther.* **2007**, *321*, 1193–1207.
- (135) Stahl, E. L.; Zhou, L.; Ehlert, F. J.; Bohn, L. M. A Novel Method for Analyzing Extremely Biased Agonism at G Protein-Coupled Receptors. *Mol. Pharmacol.* **2015**, *87*, 866–877.
- (136) Kroeze, W. K.; Sassano, M. F.; Huang, X.-P.; Lansu, K.; McCorvy, J. D.; Giguère, P. M.; Sciaky, N.; Roth, B. L. PRESTO-Tango as an Open-Source Resource for Interrogation of the Druggable Human GPCRome. *Nat. Struct. Mol. Biol.* **2015**.
- (137) Zhou, L.; Lovell, K. M.; Frankowski, K. J.; Slauson, S. R.; Phillips, A. M.; Streicher, J. M.; Stahl, E.; Schmid, C. L.; Hodde, P.; Madoux, F.; Cameron, M. D.; Prisinzano, T. E.; Aubé, J.; Bohn, L. M. Development of Functionally Selective, Small Molecule Agonists at Kappa Opioid Receptors. *J. Biol. Chem.* **2013**, *288*, 36703–36716.
- (138) Rives, M.-L.; Rossillo, M.; Liu-Chen, L.-Y.; Javitch, J. A. 6'-Guanidinonaltrindole (6'-GNTI) Is a G Protein-Biased κ -Opioid Receptor Agonist That Inhibits Arrestin Recruitment. *J. Biol. Chem.* **2012**, *287*, 27050–27054.
- (139) Schmid, C. L.; Streicher, J. M.; Groer, C. E.; Munro, T. A.; Zhou, L.; Bohn, L. M. Functional Selectivity of 6'-guanidinonaltrindole (6'-GNTI) at κ -Opioid Receptors in Striatal Neurons. *J. Biol. Chem.* **2013**, *288*, 22387–22398.
- (140) Waldhoer, M.; Fong, J.; Jones, R. M.; Lunzer, M. M.; Sharma, S. K.; Kostenis, E.; Portoghese, P. S.; Whistler, J. L. A Heterodimer-Selective Agonist Shows in Vivo Relevance of G Protein-Coupled Receptor Dimers. *Proc. Natl. Acad. Sci. U. S. A.* **2005**, *102*, 9050–9055.
- (141) Zangrandi, L.; Burtscher, J.; MacKay, J. P.; Colmers, W. F.; Schwarzer, C. The G-Protein Biased Partial κ Opioid Receptor Agonist 6'-GNTI Blocks Hippocampal Paroxysmal Discharges without Inducing Aversion. *Br. J. Pharmacol.* **2016**, *173*, 1756–1767.
- (142) Gupta, A.; Gomes, I.; Bobeck, E. N.; Fakira, A. K.; Massaro, N. P.; Sharma, I.; Cavé, A.;

- Hamm, H. E.; Parello, J.; Devi, L. A. Collybolide Is a Novel Biased Agonist of κ -Opioid Receptors with Potent Antipruritic Activity. *Proc. Natl. Acad. Sci.* **2016**, 201521825.
- (143) White, K. L.; Scopton, A. P.; Rives, M.-L.; Bikbulatov, R. V.; Polepally, P. R.; Brown, P. J.; Kenakin, T.; Javitch, J. A.; Zjawiony, J. K.; Roth, B. L. Identification of Novel Functionally Selective κ -Opioid Receptor Scaffolds. *Mol. Pharmacol.* **2014**, *85*, 83–90.
- (144) Wu, H.; Wacker, D.; Mileni, M.; Katritch, V.; Han, G. W.; Vardy, E.; Liu, W.; Thompson, A. A.; Huang, X.-P.; Carroll, F. I.; Mascarella, S. W.; Westkaemper, R. B.; Mosier, P. D.; Roth, B. L.; Cherezov, V.; Stevens, R. C. Structure of the Human κ -Opioid Receptor in Complex with JD1c. *Nature* **2012**, *485*, 327–332.
- (145) White, K. L.; Robinson, J. E.; Zhu, H.; DiBerto, J. F.; Polepally, P. R.; Zjawiony, J. K.; Nichols, D. E.; Malanga, C. J.; Roth, B. L. The G Protein-Biased κ -Opioid Receptor Agonist RB-64 Is Analgesic with a Unique Spectrum of Activities In Vivo. *J. Pharmacol. Exp. Ther.* **2014**, *352*, 98–109.
- (146) Zhang, Y.; Williams, D. A.; Zaidi, S. A.; Yuan, Y.; Braithwaite, A.; Bilsky, E. J.; Dewey, W. L.; Akbarali, H. I.; Streicher, J. M.; Selley, D. E. 17-Cyclopropylmethyl-3,14 β -Dihydroxy-4,5 α -Epoxy-6 β -(4'-Pyridylcarboxamido)morphinan (NAP) Modulating the Mu Opioid Receptor in a Biased Fashion. *ACS Chem. Neurosci.* **2016**, *7*, 297–304.
- (147) Viscusi, E. R.; Webster, L.; Kuss, M.; Daniels, S.; Bolognese, J. A.; Zuckerman, S.; Soergel, D. G.; Subach, R. A.; Cook, E.; Skobieranda, F. A Randomized, Phase 2 Study Investigating TRV130, a Biased Ligand of the Mu-Opioid Receptor, for the Intravenous Treatment of Acute Pain. *Pain* **2016**, *157*, 264–272.
- (148) Maillet, E. L.; Milon, N.; Heghinian, M. D.; Fishback, J.; Schürer, S. C.; Garamszegi, N.; Mash, D. C. Noribogaine Is a G-Protein Biased κ -Opioid Receptor Agonist. *Neuropharmacology* **2015**, *99*, 675–688.
- (149) Barak, L. S.; Bai, Y.; Peterson, S.; Evron, T.; Urs, N.; Peddibhotla, S.; Hedrick, M. P.; Hershberger, P.; Maloney, P. R.; Chung, T. D. Y.; Rodriguiz, R. M.; Wetsel, W. C.; Thomas, J. B.; Hanson, G. R.; Pinkerton, A. B.; Caron, M. G. ML314: A Biased Neurotensin Receptor Ligand for Methamphetamine Abuse. *ACS Chem. Biol.* **2016**, acschembio.6b00291.
- (150) Allen, J. A.; Yost, J. M.; Setola, V.; Chen, X.; Sassano, M. F.; Chen, M.; Peterson, S.; Yadav, P. N.; Huang, X.; Feng, B.; Jensen, N. H.; Che, X.; Bai, X.; Frye, S. V.; Wetsel, W. C.; Caron, M. G.; Javitch, J. A.; Roth, B. L.; Jin, J. Discovery of β -Arrestin-Biased Dopamine D2 Ligands for Probing Signal Transduction Pathways Essential for Antipsychotic Efficacy. *Proc. Natl. Acad. Sci. U. S. A.* **2011**, *108*, 18488–18493.
- (151) Park, S. M.; Chen, M.; Schmerberg, C. M.; Dulman, R. S.; Rodriguiz, R. M.; Caron, M. G.; Jin, J.; Wetsel, W. C. Effects of β -Arrestin-Biased Dopamine D2 Receptor Ligands on Schizophrenia-Like Behavior in Hypoglutamatergic Mice. *Neuropsychopharmacology* **2015**, *41*, 1–12.
- (152) Clayton, C. C.; Donthamsetti, P.; Lambert, N. A.; Javitch, J. A.; Neve, K. A. Mutation of Three Residues in the Third Intracellular Loop of the Dopamine D2 Receptor Creates an Internalization-Defective Receptor. *J. Biol. Chem.* **2014**, *289*, 33663–33675.
- (153) De Lean, A.; Stadel, J. M.; Lefkowitz, R. J. A Ternary Complex Model Explains the Agonist-Specific Binding Properties of the Adenylate Cyclase-Coupled β -Adrenergic Receptor. *J. Biol. Chem.* **1980**, *255*, 7108–7117.
- (154) Pedersen, S. E.; Ross, E. M. Functional Activation of Beta-Adrenergic Receptors by Thiols in the Presence or Absence of Agonists. *J. Biol. Chem.* **1985**, *260*, 14150–14157.

- (155) Angers, S.; Salahpour, A.; Joly, E.; Hilairret, S.; Chelsky, D.; Dennis, M.; Bouvier, M. Detection of Beta 2-Adrenergic Receptor Dimerization in Living Cells Using Bioluminescence Resonance Energy Transfer (BRET). *Proc. Natl. Acad. Sci. U. S. A.* **2000**, *97*, 3684–3689.
- (156) Shukla, A. K.; Violin, J. D.; Whalen, E. J.; Gesty-Palmer, D.; Shenoy, S. K.; Lefkowitz, R. J. Distinct Conformational Changes in Beta-Arrestin Report Biased Agonism at Seven-Transmembrane Receptors. *Proc. Natl. Acad. Sci. U. S. A.* **2008**, *105*, 9988–9993.
- (157) Lohse, M. J.; Nuber, S.; Hoffmann, C. Fluorescence / Bioluminescence Resonance Energy Transfer Techniques to Study G-Protein-Coupled Receptor Activation and Signaling. *Pharmacol. Rev.* **2012**, *64*, 299–336.
- (158) Loening, A. M.; Fenn, T. D.; Wu, A. M.; Gambhir, S. S. Consensus Guided Mutagenesis of Renilla Luciferase Yields Enhanced Stability and Light Output. *Protein Eng. Des. Sel.* **2006**, *19*, 391–400.
- (159) Nagai, T.; Ibata, K.; Park, E. S.; Kubota, M.; Mikoshiba, K.; Miyawaki, A. A Variant of Yellow Fluorescent Protein with Fast and Efficient Maturation for Cell-Biological Applications. *Nat. Biotechnol.* **2002**, *20*, 87–90.
- (160) Mironov, S. L.; Skorova, E.; Taschenberger, G.; Hartelt, N.; Nikolaev, V. O.; Lohse, M. J.; Kügler, S. Imaging Cytoplasmic cAMP in Mouse Brainstem Neurons. *BMC Neurosci.* **2009**, *10*, 29.
- (161) Hanson, B. J. Multiplexing Fluo-4 NW and a GeneBLAzer Transcriptional Assay for High-Throughput Screening of G-Protein-Coupled Receptors. *J. Biomol. Screen. Off. J. Soc. Biomol. Screen.* **2006**, *11*, 644–651.
- (162) Javitch, J. A.; Han, Y. Functional Complementation Assay for Defined GPCR Oligomers. US 2011/0160081 A1, 2011.
- (163) Hurlé, M. A. Changes in the Expression of G Protein-Coupled Receptor Kinases and Beta-Arrestin 2 in Rat Brain during Opioid Tolerance and Supersensitivity. *J. Neurochem.* **2001**, *77*, 486–492.
- (164) Groarke, D. A.; Wilson, S.; Krasell, C.; Milligan, G. Visualization of Agonist-Induced Association and Trafficking of Green Fluorescent Protein-Tagged Forms of Both β -Arrestin-1 and the Thyrotropin- Releasing Hormone Receptor-1. *J. Biol. Chem.* **1999**, *274*, 23263–23269.
- (165) Burford, N. T.; Clark, M. J.; Wehrman, T. S.; Gerritz, S. W.; Banks, M.; O’Connell, J.; Traynor, J. R.; Alt, A. Discovery of Positive Allosteric Modulators and Silent Allosteric Modulators of the μ -Opioid Receptor. *Proc. Natl. Acad. Sci. U. S. A.* **2013**, *110*, 10830–10835.

Part I – The Opioid Receptor Signaling System

Chapter 2 – Uncovering the Mechanism of Action of the Atypical Antidepressant Tianeptine

Introduction

Tianeptine (**Figure 1**) is a tricyclic antidepressant that is atypical both in structure and function. With a substituted dibenzothiazepine core that contains two heteroatoms along with the aminoheptanoic side chain, the unusual structure of tianeptine separates it from other traditional tricyclic drugs. It was first discovered by the French Society of Medical Research in the 1960s

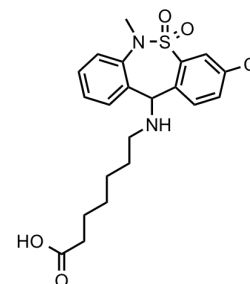


Figure 1. Structure of atypical antidepressant tianeptine.

and is currently manufactured by Servier.¹ In both controlled and open clinical trials, tianeptine has proven its efficacy as an antidepressant, including as a treatment in specific subsets of the population like elderly or alcoholic individuals.^{2,3} For these reasons, it is available for use in Europe and Asia (Coaxil), as well as in Latin America (Stablon).^{1,4} In terms of establishing better therapeutics for depression (see Introductory Chapter 1), researchers have identified three main goals which novel therapeutics should attain, including faster onset of antidepressant effects, efficacy in treatment-resistant subjects, and minimization of side effects, many of which tianeptine fulfills.^{5,6} First, tianeptine shows rapid efficacy against some depressive symptoms, both cognitive and anxiety. In patients with major depressive disorder (MDD) (aged 18 to 60 years), a 25 to 50 mg/day dose of tianeptine showed initial improvements after only 7 days, in contrast to other antidepressants that require weeks to months for real results.^{3,7} Additionally, anxiety was found to be lessened after seven days of treatment with tianeptine.² Second, tianeptine has shown promise in patients resistant to selective serotonin reuptake inhibitor (SSRI) therapy.⁸ In an open-label clinical trial, 150 patients with major depression who had partial to no response from SSRI therapy were given tianeptine in combination with an SSRI for six weeks,

and significant improvements were measured even from the first week.⁸ Double-blind clinical trials should be completed to fully demonstrate these results. Finally, in comparison to other SSRIs and tricyclic antidepressants, tianeptine shows a superior side effect profile.⁶ Tricyclics typically cause sedative, autonomic, cardiovascular, and attention/memory side effects, while SSRIs can cause nausea and sexual dysfunction. Tianeptine, however, is markedly better in comparison with few notable side effects.^{3,9-12} Additionally, these clinical effects are also prevalent in many preclinical studies, warranting the comprehensive examination of tianeptine in many animal models.^{6,13}

Tianeptine's effects extend beyond treatment of depression and anxiety. When studying the neuronal mechanisms behind depression, researchers are now uncovering a connection with loss of hippocampal volume, neuron dendrite shrinkage, glial cell loss, and impairments to neuroplasticity and cellular resilience.¹⁴⁻¹⁶ In several models, tianeptine has shown modulation of these effects. For example, tianeptine reversed the stress-induced decrease in hippocampal volume, as well as increased the concentration of cerebral metabolites and proliferation of granule precursor cells in the dentate gyrus in tree shrews that were subjected to psychological stress, highlighting its protective effect against stress-induced neuronal remodeling.¹⁷ Tianeptine has further been shown to modulate growth factor signaling in the hippocampus and amygdala of rodent models, specifically brain-derived neurotrophic factor (BDNF) and nerve growth factor (NGF), suggesting that tianeptine may promote neuroplasticity by increasing expression of these neuroplastic factors.^{18,19} Additionally, tianeptine reverses stress-induced inhibition of long-term potentiation (LTP) at excitatory synapses in the hippocampus and prefrontal cortex even after only hours of stress exposure.⁶ In terms of cognitive effects, tianeptine shows promising effects on spatial memory, focused attention behavior, learning, working memory, and memory

retention in rodents.⁶ Given the wide-ranging neurobiological effects of this neurorestorative agent, there is little surprise that much effort has been put into uncovering its mechanism of action.

In early studies with tianeptine, it was found to increase 5-hydroxytryptamine (5-HT, serotonin) uptake in rat brains from either acute or chronic dosing with the drug. This enhancement of 5-HT uptake was noted in the hippocampus and cortex but not the mesencephalon.^{20,21} It is important to note, however, that several studies have contested this hypothesis, finding no marked changes in extracellular 5-HT levels (either increase or decrease) in the corticolimbic structures of conscious rats.^{22,23} This pharmacology is in stark contrast to other antidepressants, which usually elicit their function through inhibition of biogenic amine transporters (specifically dopamine transporter, DAT; serotonin transporter, SERT; noradrenergic transporter, NET).⁶ In fact, several studies have shown that tianeptine has no affinity for many obvious targets in the central nervous system. In particular, tianeptine has no affinity for adrenergic receptors (α_{1A} , α_{1B} , α_{2A} , α_{2B} , α_{2C} , β_1 , β_2), serotonin receptors (5-HT₁, 5-HT₂, 5-HT₃, 5-HT₄, 5-HT_{5A}, 5-HT₆, 5-HT₇), benzodiazepine receptors, gamma-aminobutyric acid receptors (GABA-B), and dopamine receptors (D₁, D₂, D₃, D₄, D₅).²⁴ Further, tianeptine does not inhibit monoamine oxidases (MAOa and MAOb), another common mechanism for antidepressants.²⁵

In addition to modulating serotonin levels *in vivo*, tianeptine is also known to modulate the glutamatergic system. For instance, tianeptine has been shown to inhibit pathological changes in glutamatergic neurotransmission in the hippocampus and amygdala of various animal models in response to stress.^{26,27} Further, chronic and acute treatment with tianeptine increased phosphorylation of the CaMKII-PKC (protein kinase C) site (serine 831) on the GluR1 subunit

of AMPA receptors in the hippocampus and frontal cortex of both mice and rats.^{24,28} Given the plentiful examples of tianeptine's modulation of the glutamatergic system, many researchers have come to accept that tianeptine, like other fast-acting antidepressants (see ketamine, Introductory Chapter 1), exerts its antidepressant and neurorestorative effects through this system. Interestingly, however, tianeptine has no measurable affinity for these receptors or kainate receptors.^{6,24}

There are an increasing number of examples that indirectly connect the actions of tianeptine with the opioid system. Although tianeptine has no known affinity or modulatory properties at the dopamine receptors, systemic administration of tianeptine is reported to increase mesolimbic release of dopamine.²⁹ This observation is of particular interest since mu-opioid receptor (MOR) agonists are reported to activate the mesolimbic rewards pathway, leading to the addictive properties of opioids.^{30,31} Further, in a case study involving a woman suffering from tianeptine and amitriptyline poisoning, administration of naloxone, an MOR antagonist, resulted in a rapid, full recovery of the patient, suggesting that either one of both of the antidepressants involved is functioning through the opioid system.³² Consequently, there is reason to study tianeptine further in the context of the opioid receptor system.

Motivated by the impressive and wide-reaching biological effects of tianeptine, we became interested in elucidating its primary molecular target. This chapter will discuss the identification of tianeptine as an efficacious MOR and delta-opioid receptor (DOR) agonist *in vitro*. A full account of this work can be found in our published report.³³ Further, we explore the functional activity of known metabolites of tianeptine. Finally, preliminary *in vivo* studies suggest that MOR agonism underlies the clinical, preclinical, and *in vitro* effects of tianeptine. Through this collection of new data on the functions of tianeptine, we suggest a new mode of

action for treating depression and discuss how to move forward in the development of new therapeutics.

Results

Identifying the Molecular Target of Tianeptine

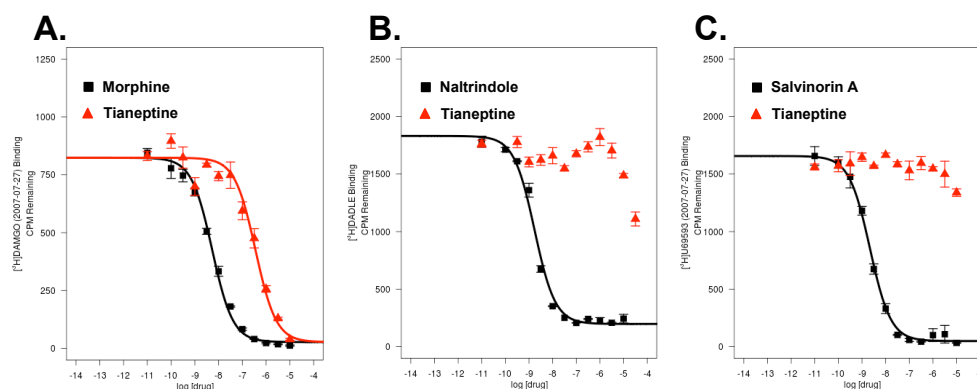


Figure 2. Tianeptine Binds to the Opioid Receptors. A. Radioligand (³H]DAMGO) displacement assay on human MOR using morphine as a control. Tianeptine has a binding affinity of 382.7 ± 183.3 nM for MOR. B. Radioligand (³H]DADLE) displacement assay on human DOR using naltrindole as a control. Tianeptine has a binding affinity of > 10 μ M for DOR. C. Radioligand (³H]U-69,593) displacement assay on human KOR using salvinator A as a control. Tianeptine shows no binding affinity for KOR. Data represent mean \pm SEM of a representative experiment of $n = 3$ (MOR), $n = 4$ (DOR), $n = 4$ (KOR) independent experiments performed by PDSP.

Tianeptine Binds to the Opioid Receptors. In collaboration with the Psychoactive Drug Screening Program (PDSP), a much more extensive evaluation of tianeptine binding to human CNS targets was conducted. In addition to the receptors tested by Svenningsson and coworkers²⁴, tianeptine was measured for its ability to bind to nicotinic acetylcholine receptors ($\alpha_2\beta_2$, $\alpha_3\beta_2$, $\alpha_3\beta_4$, $\alpha_4\beta_2$, $\alpha_4\beta_4$, α_7), cannabinoid receptors (CB1, 2), histamine receptors (H1, 3, 4), muscarinic acetylcholine receptors (M1-5), peripheral benzodiazepine receptors (PBR), sigma receptors (1, 2), metabotropic glutamate receptors (mGluR1a, 2, 4, 5, 6, 8), and opioid receptors (MOR, DOR, and kappa-opioid receptor, KOR) using traditional radioligand binding assays in overexpressed cellular systems. As was observed before, tianeptine had no measurable affinity for most of these targets. The only exception was the opioid receptor family. Tianeptine bound to the MOR with a

$K_i = 383 \pm 183$ nM (**Figure 2A**). Tianeptine also showed some affinity for the DOR, however it

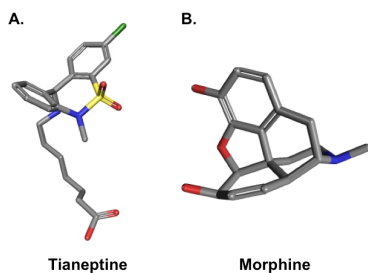


Figure 3. Three-Dimensional representation of tianeptine (A) and morphine (B) reveal similar bent conformation. Minimized structures generated through PubChem3D.⁷⁶

was much weaker in comparison to that observed for the MOR ($K_i > 10$ μ M, **Figure 2B**). There was no binding affinity of tianeptine at the KOR (**Figure 2C**). This separate measure of tianeptine's binding affinity highlights again how clean the pharmacological profile is in comparison to other tricyclic antidepressants. In fact, the apparent selectivity of binding to only the opioid receptors may explain the improved side effect profile of tianeptine. Although the

binding results of tianeptine to the opioid receptors may be surprising at first, its similarly bent structure in comparison to the classical opioid morphine does reveal indirectly that the two compounds could in theory have the same molecular target (**Figure 3**). A summary of binding affinities at the MOR and DOR can be found in **Table 1**.

Tianeptine is an Agonist at the MOR. To complement the binding studies of tianeptine,

Table 1. Tianeptine Affinity at Opioid Receptors

hMOR	K_i (μ M)	
	hDOR	hKOR
0.38 ± 0.18	> 10	X

Data represent mean \pm SEM (μ M) of $n \geq 3$ independent trials. "X" indicates not active. Data obtained by PDSP.

the functional activity at the opioid receptors was measured utilizing bioluminescent resonance energy transfer (BRET) assays (see Chapter 1). Tianeptine was first characterized

for its functional activity at the rodent isoforms of the receptors. In a BRET G protein activation assay, tianeptine was able to activate the mouse MOR (mMOR) with an EC_{50} of 641 ± 120 nM (**Figure 4A**). Additionally, tianeptine showed full agonism at the mouse DOR (mDOR) with an EC_{50} of 14.5 ± 6.6 μ M (**Figure 4B**) and showed no agonism at the rat KOR (rKOR, **Figure 4C**).

These data represent the first example of opioid receptor activity from tianeptine and could explain some of the preclinical effects observed. To confirm these results, tianeptine was

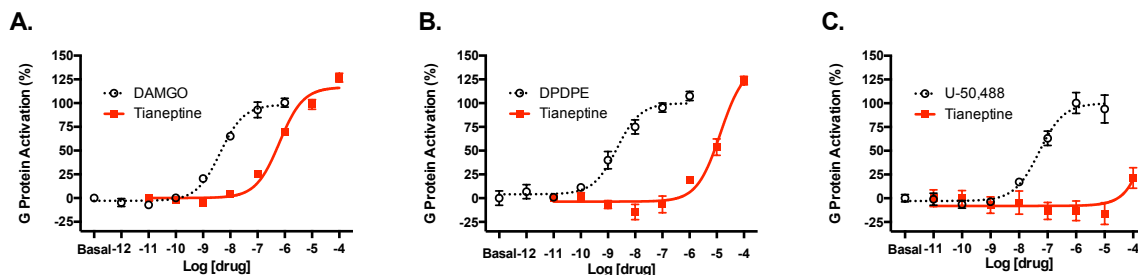


Figure 4. Tianeptine is a Full Agonist at the Rodent Opioid Receptors. mMOR (A), mDOR (B), or rKOR (C) were co-expressed with $G\alpha_B$ -RLuc8, β_1 , and mVenus- γ_2 to assay G protein activation. Curves represent the average of $n \geq 3$, with error bars representing \pm SEM.

measured in a separate assay for cAMP inhibition. As a $G_{i/o}$ -coupled G Protein Coupled Receptor (GPCR), the functional activity of MOR can be correlated to cAMP levels (see Introductory Chapter 1). Similarly to the G protein activation assay, tianeptine showed full agonism at the mMOR with an EC_{50} of $1.03 \pm 0.10 \mu\text{M}$ (**Figure 5A**), as well as at the mDOR with an EC_{50} of $9.46 \pm 1.34 \mu\text{M}$ (**Figure 5B**). Again, there was no agonist activity at the rKOR (**Figure 5C**). As a further measure of opioid activity, naltrexone (an MOR antagonist) dose-

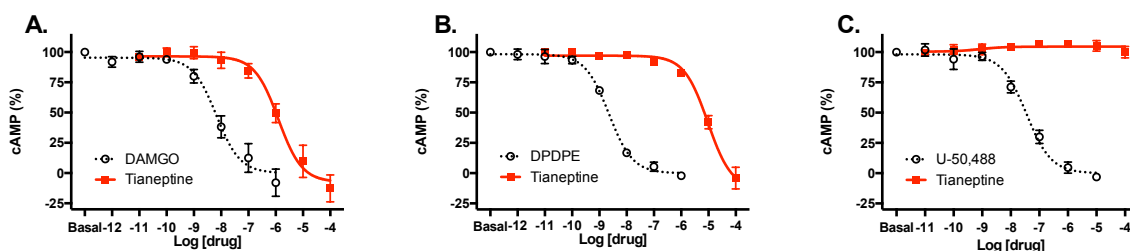


Figure 5. Tianeptine is a Full Agonist at the Rodent Opioid Receptors. mMOR (A), mDOR (B), or rKOR (C) were co-expressed with $G\alpha_B$, β_1 , γ_2 , and CAMYEL (cAMP sensor using YFP-Epac-RLuc) to assay cAMP inhibition. Curves represent the average of $n \geq 3$, with error bars representing \pm SEM.

independently inhibited the agonist signal from tianeptine, showing the specificity of the signal measured in the cells as belonging to mMOR (**Figure 6A**). A similar experiment was performed for mDOR, and TIPP-psi (a DOR antagonist) dose-dependently inhibited the agonist signal from tianeptine (**Figure 6B**). There are numerous reports from preclinical models that KOR

antagonists show antidepressant actions.^{34,35} In order to rule out that the antidepressant effects of tianeptine are not in fact mediated through KOR antagonism, tianeptine was measured for its ability to dose-dependently inhibit the signal from KOR agonist U-50,488 (**Figure 6C**). Tianeptine was unable to inhibit the agonist signal from U-50,488, showing that tianeptine neither binds nor has any functional activity at this receptor through traditional mechanisms.

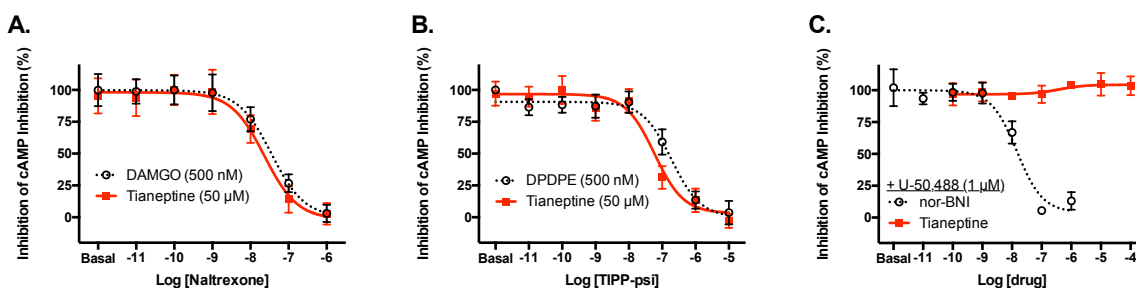


Figure 6. Antagonist Profiles of Tianeptine at the Rodent Opioid Receptors. mMOR (A), mDOR (B), or rKOR (C) were co-expressed with $G\alpha_B$, β_1 , γ_2 , and CAMYEL to assay inhibition of cAMP inhibition. Naltrexone (A) or TIPP-psi (B) dose-dependently inhibit the cAMP inhibition of both tianeptine and the respective control. C. Tianeptine is unable to dose-dependently inhibit the signal from control U-50,488. Curves represent the average of $n \geq 3$, with error bars representing \pm SEM.

Although the *in vitro* results from the rodent receptors was promising, it was also important to study the effects of tianeptine at human receptors, not only for comparison with the human binding data obtained but also because of its use in humans currently. At the human MOR (hMOR), tianeptine again showed full agonism with an $EC_{50} = 194 \pm 70$ nM for G protein activation (**Figure 7A**). This value very closely matches the binding affinity measured at the hMOR, suggesting high internal correlation between the different data sets. While tianeptine was also a full agonist at the human DOR (hDOR) for G protein activation, it showed much weaker potency ($EC_{50} = 37.4 \pm 11.2$ μ M, **Figure 7B**) in comparison to the mouse isoform. Therefore, although the selectivity for MOR in mouse is only 20-fold over DOR, it is close to 200-fold in humans. Given the low potency of tianeptine at hDOR, it seems unlikely to play a large role in its antidepressant and neurorestorative actions, though this might not be the case in mouse. Not surprisingly, tianeptine showed no agonist activity at the human KOR (hKOR, **Figure 7C**). As

before, tianeptine was measured for its agonist activity in the cAMP inhibition assay. At the hMOR, tianeptine showed full agonism with similar potency to that observed in the G protein activation assay ($EC_{50} = 151 \pm 45$ nM, **Figure 8A**). Tianeptine also showed full agonism at the hDOR ($EC_{50} = 12.2 \pm 5.3$ μ M, **Figure 8B**). There was also no agonist activity at the hKOR in this assay (**Figure 8C**). A summary of the functional potencies of tianeptine at the opioid receptors can be found in **Table 2**.

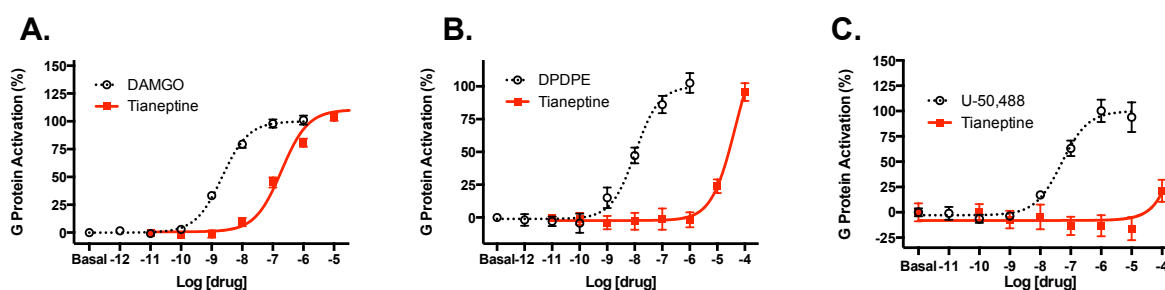


Figure 7. Tianeptine is a Full Agonist at the Human Opioid Receptors. hMOR (A), hDOR (B), or hKOR (C) were co-expressed with $G\alpha_B$ -RLuc8, β_1 , and mVenus- γ_2 to assay G protein activation. Curves represent the average of $n \geq 3$, with error bars representing \pm SEM.

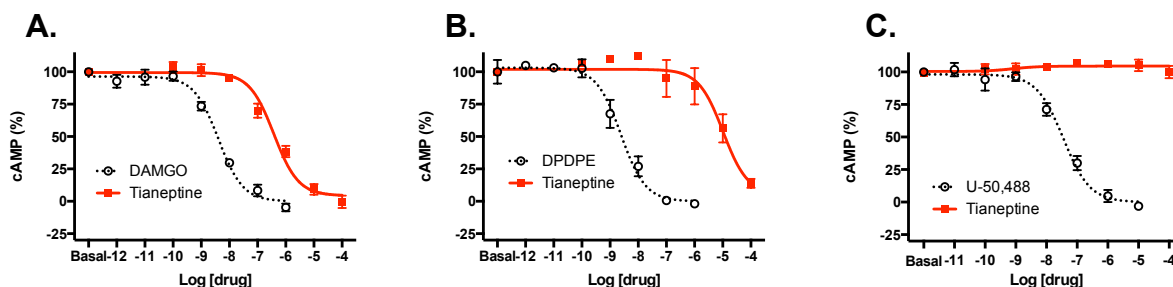


Figure 8. Tianeptine is a Full Agonist at the Human Opioid Receptors. hMOR (A), hDOR (B), or hKOR (C) were co-expressed with $G\alpha_B$, β_1 , γ_2 , and CAMYEL to assay cAMP inhibition. Curves represent the average of $n \geq 3$, with error bars representing \pm SEM.

Table 2. Tianeptine Functional Activity at Opioid Receptors

Assay	EC_{50} (μ M)					
	mMOR	hMOR	mDOR	hDOR	rKOR	hKOR
G Protein	0.64 ± 0.12	0.19 ± 0.07	14.5 ± 6.6	37.4 ± 11.2	X	X
cAMP	1.0 ± 0.1	0.15 ± 0.05	9.5 ± 1.3	12.2 ± 5.3	X	X

Data represent mean \pm SEM (nM) of $n \geq 3$ independent trials. "X" indicates not active.

In a study on pentylenetetrazole-induced seizure in mice, tianeptine was found to delay

Table 3. Tianeptine Activity at the Adenosine A1 Receptor

Tianeptine	A1 Receptor
% Activation (10 μ M)	-0.9 ± 0.7
% Activation (1 μ M)	-0.7 ± 2.2
% Inhibition (10 μ M)	1.0 ± 1.4
% Inhibition (1 μ M)	-13.6 ± 2.4

Data represent mean \pm SEM (%) of $n = 2$ independent experiments. Data obtained by GenScript USA Inc.

the onset time of seizures, purportedly through the adenosine A1 receptor (A1R).³⁶ To rule out this functional activity, we had tianeptine measured for functional activity using the FLIPR[®]

calcium assay. We found no direct agonist or antagonist activity of tianeptine on this receptor

(Table 3).

Functional Activity of Tianeptine Metabolites. Tianeptine readily undergoes β -oxidation

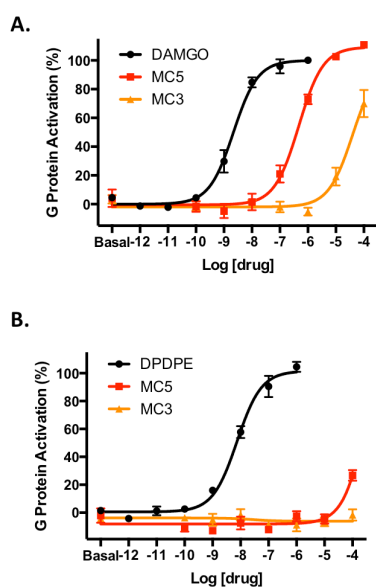


Figure 9. Agonist Activity of Tianeptine Metabolites at the Human Opioid Receptors. hMOR (A) or hDOR (B) were co-expressed with $G\alpha_B$ -RLuc8, β_1 , and mVenus- γ_2 to assay G protein activation. Curves represent the average of $n \geq 3$, with error bars representing \pm SEM.

to provide metabolites MC5 (aminopentanoic acid side chain) and MC3 (aminopropanoic acid side chain). This metabolism results in tianeptine having a reported half-life of about only 15 minutes, and dosing is required three times a day for effect.^{37,38} Interestingly, MC5 does retain most agonist activity at hMOR ($EC_{50} = 454 \pm 174$ nM, **Figure 9A**) when measured for G protein activation, however there is no measurable activity at hDOR. MC3, on the other hand, shows only minimal agonist activity at hMOR ($EC_{50} = 24.9 \pm 12.6$ μ M, **Figure 9A**) and no activity at hDOR. These results suggest that when tianeptine is metabolized to MC5, there may still be some effects exerted on hMOR and that these effects are likely

not modulated by the actions of the next metabolite, MC3. As expected, neither compound showed any activity at hKOR (data not shown).

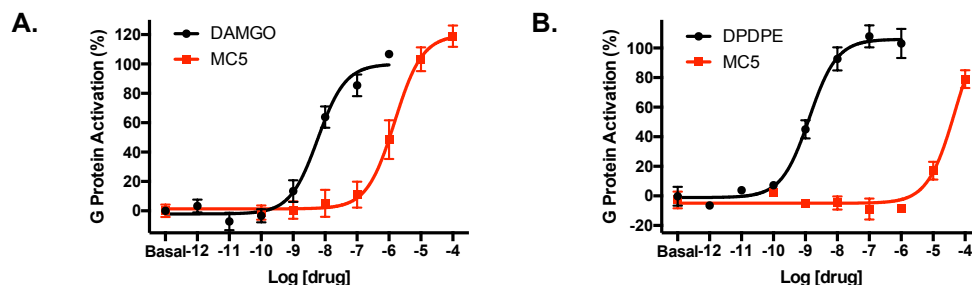


Figure 10. Agonist Activity of Tianeptide Metabolite MC5 at the Mouse Opioid Receptors. mMOR (A) or mDOR (B) were co-expressed with $G\alpha_B$ -RLuc8, β_1 , and mVenus- γ_2 to assay G protein activation. Curves represent the average of $n = 3$, with error bars representing \pm SEM.

MC5 was measured also for functional activity in the G protein activation assay at mouse MOR (mMOR). These measures will undoubtedly correlate more accurately with the future *in vivo* data than will the human *in vitro* data measured above. MC5 was active at the mMOR with an $EC_{50} = 1.7 \pm 0.9 \mu\text{M}$ (**Figure 10A**) and at the mDOR though with much weaker potency ($EC_{50} > 20 \mu\text{M}$, **Figure 10B**) in comparison to tianeptine.

Measuring Other Signaling Pathways. Given the *in vitro* pharmacology results at the

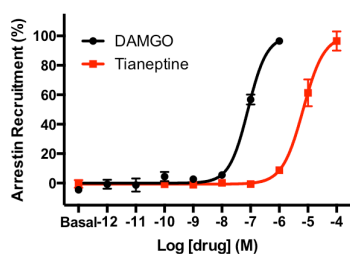


Figure 11. Tianeptine Fully Recruits Arrestin. hMOR was co-expressed with RLuc8-arrestin3-Sp1, mem-linker-citrine-SH3, and GRK2. Data represent mean \pm SEM of $n = 3$. BRET GAP43 translocation assay used.

MOR, we were interested in studying other signaling pathways further. In particular, GPCRs signal through G protein-dependent pathways (i.e. G protein activation and cAMP inhibition), as well as G protein-independent pathways (i.e. arrestin). There are an increasing number of reports suggesting that G protein biased agonists may avoid some unwanted side effects from opioid signaling. In particular at the MOR, a G protein biased agonist may have

analgesic properties without respiratory depression or constipation (see Chapter 1 for further

discussion),³⁹ while compounds with balanced signaling may have lower tolerance build-up and abuse potential.^{40,41} As an atypical antidepressant, it is possible that the unique actions of tianeptine are due to the fact that it is a G protein biased MOR agonist. In fact, in combination with morphine, tianeptine has been shown to reduce tolerance and physical dependence⁴² while also preventing respiratory depression⁴³, suggesting the possibility of functional selectivity. To measure the arrestin recruitment from tianeptine, the BRET GAP43 translocation assay was used (see Chapter 1 for further discussion).⁴⁴ Interestingly, in this assay, tianeptine was able to recruit arrestin fully, suggesting that it is an unbiased ligand (**Figure 11**).

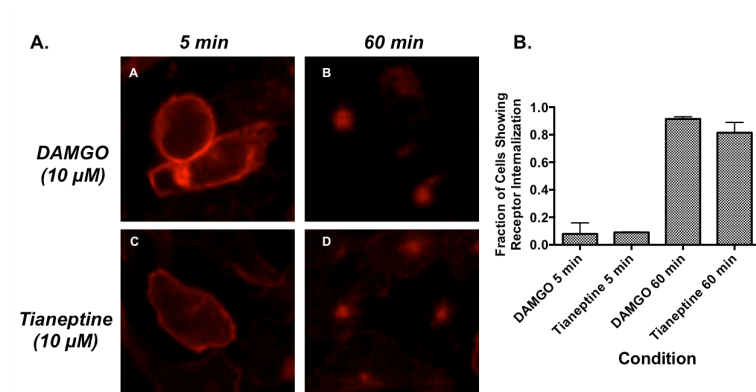


Figure 12. Tianeptine Causes Receptor Internalization. A. Tianeptine shows similar levels of receptor internalization when compared to control DAMGO in mMOR-CHO cells. Representative immunofluorescence images shown. B. Quantification of A. Compounds were used at 10 μM. On average, 30-60 cells were analyzed for each treatment per experiment. Data represent mean ± SEM of n = 3 independent experiments.

To confirm these arrestin results, tianeptine was measured for its ability to cause receptor internalization. Recruitment of arrestin typically leads to receptor internalization⁴⁵, so in this way receptor internalization can act as a

“downstream” measure of arrestin activity. Using immunofluorescence as a qualitative measure of receptor internalization, tianeptine was found to internalize the MOR to the same extent as unbiased control ligand DAMGO (10 μM treatments, **Figure 12A**). Quantification of the population of cells internalizing receptors for a given field of view confirms that tianeptine shows high receptor internalization (**Figure 12D**), similarly to DAMGO (**Figure 12B**). The combined arrestin activity and receptor internalization measured for tianeptine does suggest that

a more complex mechanism may be working to provide the unique behavioral effects known for this drug.

In Vitro Pharmacokinetic Data on Tianeptine and MC5. Pharmacokinetic studies were performed with MC5 in the plasma (**Figure 13C**) and the brain (**Figure 13D**) in C57BL/6 mice alongside tianeptine at 30 mg/kg (intraperitoneal administration, i.p.). Tianeptine quickly peaked within five minutes and was nearly eliminated after 1 hour. In contrast, MC5 gradually reached a higher peak concentration than tianeptine and had a significantly longer half-life in comparison to tianeptine; it was detectable in the brain tissue for at least 8 hours, leading to a higher overall exposure (quantified by area under the curve). Therefore, given the short half-life of tianeptine, it seems likely that the metabolite MC5 might play a role in the behavioral effects observed for tianeptine.

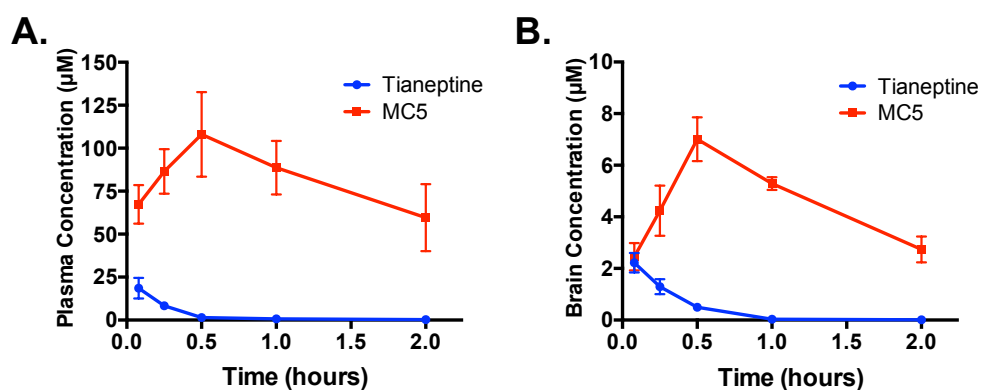


Figure 13. Pharmacokinetic Effects of Tianeptine and MC5 Metabolite. Plasma (A) and brain (B) concentrations \pm SD of tianeptine and MC5 in C57BL/6 mice following a single administration of tianeptine (30 mg/kg ip).

Discussion

Mechanism of Action. These results describe the first identification of the primary molecular target of the antidepressant tianeptine as the MOR (and possibly the DOR). Given the heavy focus on the glutamatergic modulation of tianeptine in understanding its mechanism of action, the observed MOR agonism was surprising. Through our studies, we confirmed that

tianeptine has no affinity for NMDA, AMPA, or kainate receptors, as well as the metabotropic glutamate receptors (mGluR1a, 2, 4, 5, 6, 8). It seems more likely, therefore, that tianeptine's modulation of the glutamatergic system is indirect, at least in the concentration range measured (< 10 μ M). Current dosing of tianeptine in humans (12.5 mg) or in rodents (10 mg/kg/day) leads to a 1 μ M or 10 μ M plasma concentration, respectively^{37,38}, which does suggest that the concentration range of tianeptine is sufficient enough to activate the receptor system since potencies at the MOR were \sim 0.2-1 μ M and at the DOR were \sim 12-34 μ M. Based on this evidence, it is possible that MOR activation is the primary molecular event leading to tianeptine's modulation of the glutamatergic system and subsequent antidepressant/anxiolytic effects.

In order to understand better how tianeptine modulates the glutamatergic system via MOR, it is helpful to look to its actions in specific populations of neurons and synapses. MOR is widely expressed in the hippocampus, particularly on interneurons⁴⁶, and is already recognized to modulate glutamatergic neurons.³¹ For example, MOR activation is known to decrease protein kinase A activity in dentate granule cells (rat), which leads to decreased NMDA receptor phosphorylation and activity, which could account for the corrective effects of tianeptine on stress-induced increases in NMDA receptor signaling.⁴⁷ Additionally, one study suggests that acute morphine treatment activates CaMKII in the rat hippocampus⁴⁸, which agrees with several other reports connecting the importance of the AMPA receptor subunit GluR1 phosphorylation (Ser831) in mediating the antidepressant effects of tianeptine. Therefore, activation of MORs (or DORs) in a hippocampal inhibitory interneuron would likely decrease their activity (GABA release) through hyperpolarization, leading to disinhibition of the CA1 glutamatergic neurons and enhanced excitability and synaptic plasticity (**Figure 14**), consistent with reports on

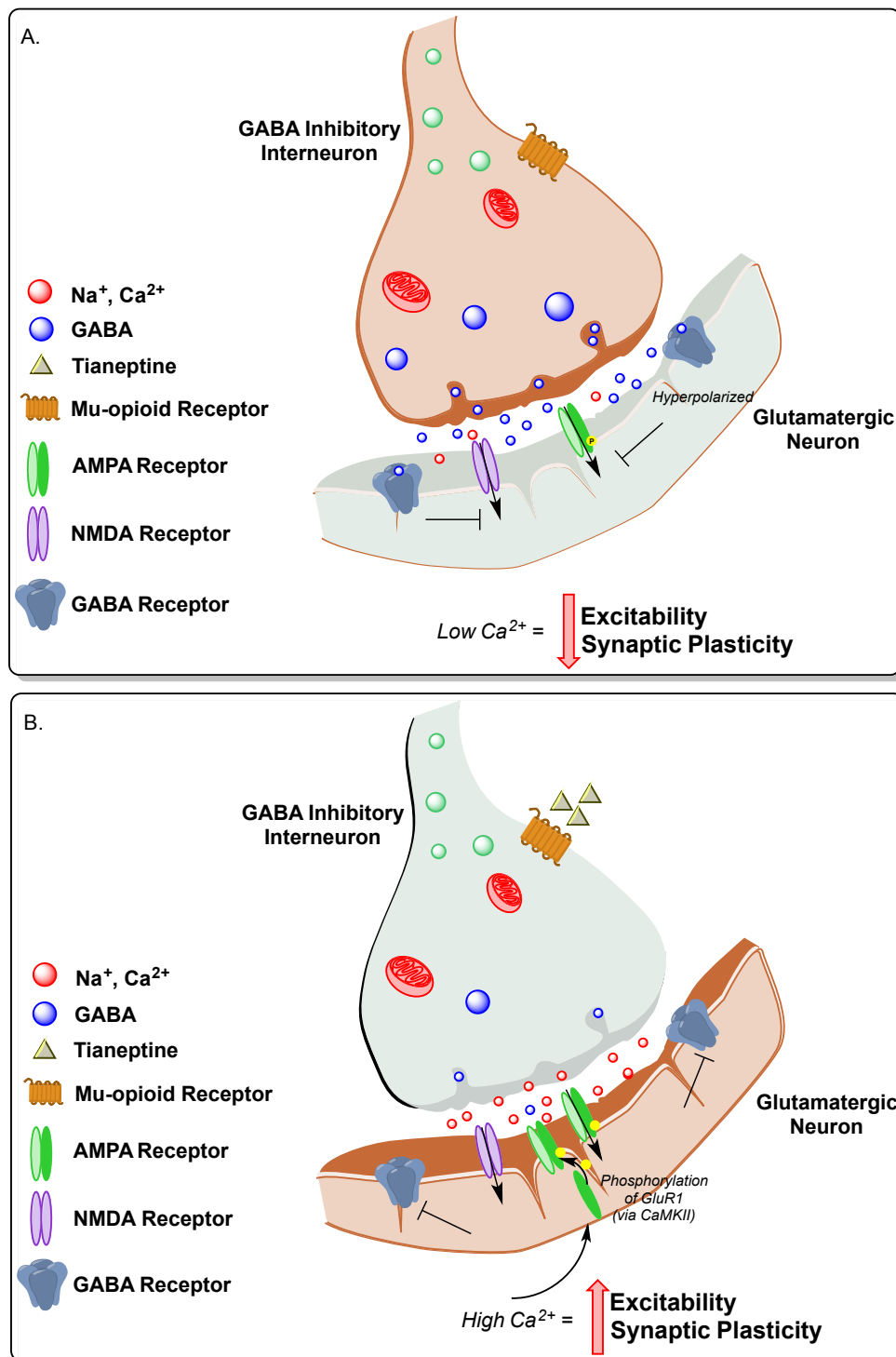


Figure 14. Potential Modulation of the Glutamatergic System by Tianeptine in the Hippocampus. A. GABAergic interneurons exert an inhibitory signal on neighboring glutamatergic neurons through activation of GABA receptors in a drug naïve state. B. In the presence of tianeptine, activation of MOR hyperpolarizes the interneuron, causing a reduction of GABA release, and disinhibiting the glutamate signaling. This disinhibition increases Ca^{2+} influx through NMDA receptors, activating CaMKII and increasing phosphorylation of AMPA receptor GluR1 subunits.

tianeptine's effects in the CA1.⁶ These effects make sense, as the disinhibited glutamate signaling increases Ca^{2+} influx through NMDA receptors, activating CaMKII and increasing phosphorylation of AMPA receptor GluR1 subunits (**Figure 14**). Interestingly, chronic exposure to morphine leads to decreased CaMKII activity in the hippocampus⁴⁶, as well as induced dephosphorylation-dependent internalization of AMPA receptors.⁴⁹ These effects are in contrast to tianeptine, which retains enhanced AMPA receptor-mediated excitatory post-synaptic currents (ESPCs) and phosphorylation of GluR1 subunits even after chronic treatments.^{24,27} Therefore, the long-term effects in the hippocampus of tianeptine in comparison to classical opioids like morphine appear to be distinct, suggesting that there may be some divisions between the different classes of opioids. Although it is still unclear how these distinctions emerge, tianeptine's unique long-term effects may explain its reduced tolerance development in depressed human patients.⁵⁰

As an opioid agonist, it is also important to understand how tianeptine might modulate the dopamine rewards pathway. It is well-known that activation of opioid receptors in the ventral tegmental area (VTA) and nucleus accumbens (NAc) can lead to increased dopamine signaling, which mediates reward responses to positive stimuli such as food or drugs of abuse. It makes sense then that dysregulation of these systems might play a role in mediating depressive states. This hypothesis is supported by reports of decreased NAc activity in depressed individuals.^{51,52} Further, acute and chronic treatment of tianeptine elevates extracellular dopamine levels in both the NAc and prefrontal cortex.^{29,53} Tianeptine's MOR (or DOR) activity combined with its lack of affinity for dopamine transporters or receptors suggests a more remote disinhibition of VTA-NAc dopaminergic projections via MOR-mediated inhibition of GABAergic inhibitory interneurons in the VTA, just like classical opioids (**Figure 15A**). The increased inhibitory

activity of D2 receptors on the GABAergic neuron in the NAc decreases intracellular Ca^{2+} levels, leading to lessened CaMKII and PKC activity and ultimately decreased phosphorylation of AMPA receptor subunits GluR1 and GluR2. These subunits, however, appear to be differentially regulated by phosphorylation, where decreased phosphorylation increases trafficking of synaptic GluR2 and decreases GluR1 on the cell surface.^{24,54,55} This modulation of calcium levels in the NAc helps to normalize AMPA receptor signaling, which initiates long-lasting antidepressant effects and the reward response. Interestingly, NMDA antagonists like ketamine act similarly in the NAc.⁵⁶ This disinhibition of dopaminergic neurons in the VTA may

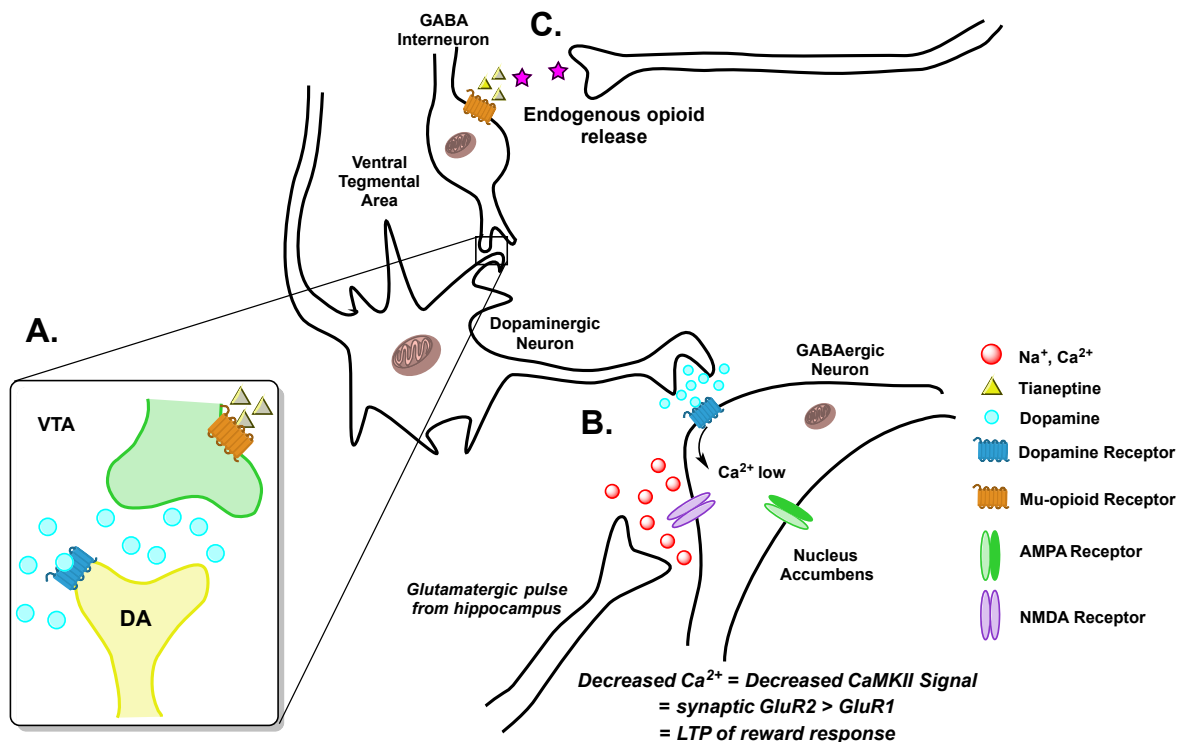


Figure 15. Potential Modulation of the Mesolimbic Rewards Pathway by Tianeptine. A. Activation of MOR on GABAergic interneurons in the VTA by tianeptine causes increased release of dopamine in the ventral tegmental area. B. Dopamine release is also possible more remotely in the nucleus accumbens. Activation of inhibitory D₂ receptors (or activation of MORs directly) leads to decreased Ca^{2+} signaling (via glutamate signaling or NMDA receptor activity) via hyperpolarization, leading to a reward response. Reduced Ca^{2+} signaling also decreases CaMKII activity on phosphorylation of AMPA receptor subunits, resulting in enriched synaptic GluR2 and depleted synaptic GluR1, inducing LTP of the reward response. It is unclear whether these effects modulate other neighboring glutamatergic neurons or if this is a circuit effect only. C. Endogenous opioid release is also occurring simultaneously.

also activate neighboring GABAergic neurons in the NAc, thus further modulating AMPA receptor activity in an area of the brain distinct from the hippocampus (**Figure 15B**). These effects are also competing with excitatory glutamateric inputs from other regions of the brain, like the hippocampus, and implicate the NAc as an important hub for mediating the mood-related signaling from various pathways. Therefore, the opioid-mediated glutamate receptor signaling in this region is likely connected with reward and antidepressant responses.^{31,57,58} The rewarding effects of tianeptine and other opioids are further confounded by the endogenous opioid release taking place simultaneously (**Figure 15C**). Exogenously administered opioids are known to have antidepressant effects, such as β -endorphin, which rapidly improved the depressive symptoms of MDD in the clinic.⁵⁹ Additionally, untreated patients with MDD were shown to have decreased endogenous opioid release in response to social rejection and after the rewarding stimulus of social acceptance⁶⁰, implicating an important role of opioids in modulating mood disorders. The therapeutic effects of tianeptine and other antidepressants may be compensating for reduced signaling of the endogenous opioid system and diminished natural reward response.

Preliminary In Vivo Results Implicate MOR in Behavioral Effects of Tianeptine and MC5. *In vivo* characterization of both tianeptine and its metabolite MC5 are currently being pursued in the laboratory of Professor Rene Hen at Columbia University using both wildtype and MOR deficient mice. Our studies are utilizing the forced swim test for depression, where a decrease in immobility is correlated to antidepressant function,⁶¹ and the elevated plus maze (EPM) is being used to assess the anxiolytic effects of tianeptine. In this assay, anxious mice will be less likely to explore the open arms of an elevated plus; therefore, a reduction in anxiety can be correlated with more exploration of the open arms.⁶² In preliminary experiments, tianeptine is ineffective at decreasing immobility in MOR-deficient littermates in comparison to wildtype

mice, indicating that the antidepressant effects of tianeptine are dependent upon MOR. Analogous results are being found in the EPM, suggesting an MOR dependence in the anxiolytic effects of tianeptine, as well. Tianeptine is also showing positive effects in assays indicative of MOR agonist activity⁶³⁻⁶⁷, including hypophagia (reduced intake of food), analgesia, and hyperactivity, which are all reduced in MOR-deficient mice. These preliminary results indicate that both the antidepressant and opioid-like behaviors of tianeptine are likely mediated by MOR. As a first measure of target-specific behaviors from tianeptine, there is further evidence that MOR should be explored as a serious lead for new antidepressants.

We are also studying the behavioral effects of MC5 in both wildtype and MOR deficient mice. Similar to tianeptine, MC5 is showing antidepressant effects in the forced swim test that seem to be absent in the MOR deficient littermates, suggesting that the effects of the forced swim test are likely mediated by MOR for both tianeptine and MC5. Although initially puzzled by how a drug with such a short half-life can cause remarkable effects in preclinical and clinical models, the observation of antidepressant effects from MC5, which has a much longer half-life and duration in the plasma and brain, indicates an important role in the mechanism of action of tianeptine. In the forced swim test for instance, which is performed 60 minutes after drug administration, antidepressant effects are evident from both tianeptine and MC5. Given the PK results from tianeptine, however, it seems unlikely that any tianeptine is present at this time, indicating that MC5 is likely mediating the behavioral effects at these later time points. Tianeptine dosing can thus provide acute effects while MC5 continues signaling through the same receptor target, thus allowing antidepressant effects to continue.

Goals for Structure Activity Relationship (SAR) Studies. Through modifications of the tianeptine scaffold, two main goals can be addressed regarding the functional activity. First, with

a potency of approximately 200 nM at MOR, tianeptine is not a particularly potent compound, and therefore new analogs should be identified with superior potency at MOR. Second, as a therapeutic, tianeptine does not have ideal pharmacokinetic properties (see PK results above). Therefore, in theory, an analog that is similarly potent to tianeptine but is less susceptible to metabolism may be a superior therapeutic that would only require a once-daily dose. Using a streamlined synthetic strategy, with the help of Andrew Kruegel and Dr. Adam Henke, over 100 tianeptine analogs have been synthesized to date that explore the regions in the scaffold that are important for MOR and DOR activity. A full study of the analogs synthesized and their relationship to our synthetic goals has been reported.⁶⁸

Abuse Potential of Tianeptine. Although the evidence is clear that tianeptine acts as an MOR agonist, there are some obvious concerns with developing a drug with opioid properties for treating depression. Opioids, such as morphine and oxycodone, are prescribed everyday to treat pain, but the medications also have extremely high abuse potential. It is estimated that in 2012, upwards of 12.5 million Americans abused prescription opioids⁶⁹, and recent tragedies like the death of pop star Prince make consumers and drug developers alike hesitant to support the expansion of the opioid market. Tianeptine, however, has been widely used in Europe, Asia, and Latin America for decades now, so there is strong evidence to suggest that the abuse potential is low. In fact, after decades of usage, there are only a few isolated case studies on addiction or withdrawal symptoms associated with tianeptine.^{32,70-74} Further, in comparison to opioids of high abuse potential, like morphine, oxycodone, and fentanyl, tianeptine is orders of magnitude less potent. Therefore, the likelihood of tianeptine being abused is low, as evidence indicates that therapeutic effects on depression do not require high potency activity at MOR. There is also reason to believe that not all opioids are signaling in the same way (i.e. tianeptine versus

morphine), so it is possible that something special about tianeptine's signaling provides antidepressant effects with lower risk of addiction.

Conclusions

Herein we describe for the first time a distinct molecular target accounting for the numerous and unique properties of the atypical antidepressant tianeptine. Given the known modulation of MOR activation in several areas of the brain in a manner consistent with beneficial effects on mood, it is completely plausible that MOR represents the initial molecular signaling event for tianeptine. Through careful *in vitro* experimentation, tianeptine was found to be a full agonist at the MOR (and DOR), which are being further supported through *in vivo* studies. These studies provide the first true indication of MOR as a real target for treating depression, and the new tools developed here will allow further study into this new mechanism. Given the high complexity with which tianeptine modulates signaling in the brain (broad expression of opioid receptors in distinct brain regions, some opposing effects in different regions/cell types, interconnection of brain signaling through direct and indirect pathways that are not fully understood), future studies will aim to identify the particular circuits in the brain responsible for tianeptine's effects, which will hopefully further distinguish this opioid from others and allow the development of safe and effective therapeutics.

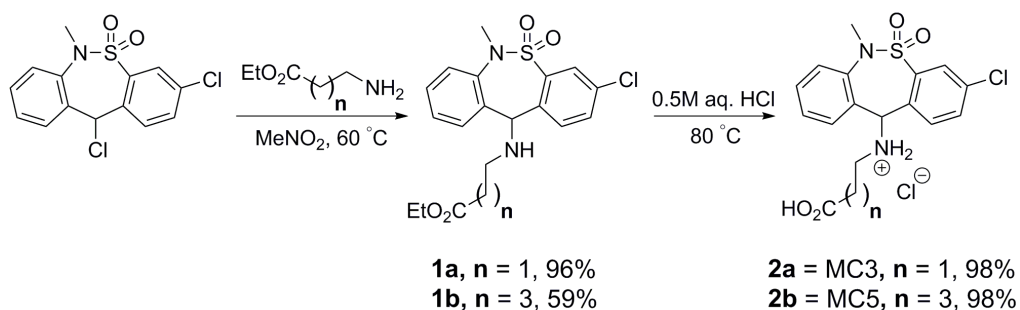
Experimental

Preparation of MC3 and MC5 Metabolites (performed by Andrew Kruegel)

General Considerations. Reagents and solvents were obtained from commercial sources and were used without further purification unless otherwise stated (including anhydrous

solvents). All reactions were performed in flame-dried glassware under an argon atmosphere unless otherwise stated and monitored by TLC using solvent mixtures appropriate to each reaction. All column chromatography was performed on silica gel (40-63 μ m). Nuclear magnetic resonance spectra were recorded on Bruker 400 or 500 MHz instruments as indicated. Chemical shifts are reported as δ values in ppm referenced to CDCl₃ (¹H NMR = 7.26 and ¹³C NMR = 77.16) or CD₃OD (¹H NMR = 3.31 and ¹³C NMR = 49.00). Multiplicity is indicated as follows: s (singlet); d (doublet); t (triplet); q (quartet); dd (doublet of doublets); ddd (doublet of doublet of doublets); td (triplet of doublets); m (multiplet); br (broad). All carbon peaks are rounded to one decimal place.

ethyl 3-((3-chloro-6-methyl-5,5-dioxido-6,11-dihydrodibenzo[c,f][1,2]thiazepin-11-yl)amino)propanoate (1a). To a mixture of 3,11-dichloro-6-methyl-6,11-



dihydrodibenzo[c,f][1,2]thiazepine 5,5-dioxide (328 mg, 1.00 mmol) and β -alanine ethyl ester hydrochloride (184 mg, 1.20 mmol) was added nitromethane (2.0 mL) followed by triethylamine (335 μ L, 243 mg, 2.40 mmol). The resulting mixture was warmed to 60 $^{\circ}$ C, stirred for 1 h, and then concentrated to give a sticky, colorless solid. This material was purified directly by column chromatography (20:1 CH₂Cl₂:Et₂O, 3 column volumes \rightarrow 7:3 CH₂Cl₂:Et₂O, 3 column volumes) to provide the pure ester **1a** as an extremely viscous, colorless oil (393 mg, 96%). ¹H NMR (400 MHz, CDCl₃) δ 7.96 – 7.94 (m, 1H), 7.49 – 7.43 (m, 2H), 7.41 – 7.33 (m, 3H), 7.32 – 7.26 (m,

1H), 5.05 (s, 1H), 4.12 (q, $J = 7.1$ Hz, 2H), 3.39 (s, 3H), 2.82 – 2.69 (m, 2H), 2.60 – 2.40 (m, 3H), 1.24 (t, $J = 7.1$ Hz, 3H); ^{13}C NMR (101 MHz, CDCl_3) δ 172.7, 140.6, 138.8, 138.6, 136.9, 134.5, 132.4, 131.1, 129.9, 129.5, 128.5, 128.3, 128.1, 65.9, 60.7, 43.6, 38.6, 34.9, 14.3.

ethyl 5-((3-chloro-6-methyl-5,5-dioxido-6,11-dihydrodibenzo[*c,f*][1,2]thiazepin-11-yl)amino)pentanoate (1b). To a mixture of 3,11-dichloro-6-methyl-6,11-dihydrodibenzo[*c,f*][1,2]thiazepine 5,5-dioxide (328 mg, 1.00 mmol) and ethyl 5-aminovalerate hydrochloride (218 mg, 1.20 mmol) was added nitromethane (2.0 mL) followed by triethylamine (335 μL , 243 mg, 2.40 mmol). The resulting mixture was warmed to 60 °C, stirred for 1 h, and then concentrated to give a sticky, colorless solid. To this material was added water (20 mL) and the mixture was extracted with Et_2O (2 x 20 mL). The combined organics were washed with water (10 mL) and 10% NH_4OH (10 mL), dried over Na_2SO_4 , and concentrated to give a viscous, pale-yellow oil. This material was purified by column chromatography (40:1 CH_2Cl_2 : Et_2O , 4 column volumes \rightarrow 20:1 CH_2Cl_2 : Et_2O , 2 column volumes \rightarrow 7:3 CH_2Cl_2 : Et_2O , 2 column volumes) to provide the pure ester **1b** as an extremely viscous, nearly colorless oil (256 mg, 59%). ^1H NMR (400 MHz, CDCl_3) δ 7.96 (d, $J = 2.1$ Hz, 1H), 7.48 – 7.33 (m, 5H), 7.32 – 7.27 (m, 1H), 5.00 (s, 1H), 4.11 (q, $J = 7.1$ Hz, 2H), 3.36 (s, 3H), 2.48 (t, $J = 7.0$ Hz, 2H), 2.27 (t, $J = 7.3$ Hz, 2H), 2.08 (br s, 1H), 1.70 – 1.58 (m, 2H), 1.58 – 1.44 (m, 2H), 1.24 (t, $J = 7.1$ Hz, 3H); ^{13}C NMR (101 MHz, CDCl_3) δ 173.6, 140.5, 138.7, 137.0, 134.4, 132.3, 131.3, 130.3, 129.5, 128.6, 128.2, 128.1, 66.3, 60.4, 47.8, 38.8, 34.2, 29.6, 22.8, 14.4.

3-((3-chloro-6-methyl-5,5-dioxido-6,11-dihydrodibenzo[*c,f*][1,2]thiazepin-11-yl)amino)propanoic acid hydrochloride (2a = MC3). To ester **1a** (364 mg, 0.890 mmol) was added 0.5 M aqueous HCl (20 mL), and the mixture was stirred vigorously for 4.5 h at 80 °C. The solution was then concentrated *in vacuo* with heating to provide a foamy, colorless glass. In

order to remove residual HCl (causes esterification during NMR in CD₃OD), this residue was re-dissolved in a small quantity of water and concentrated again *in vacuo* with heating. This procedure was repeated once more to provide the pure hydrochloride salt **2a**, free from residual HCl, as a foamy, colorless glass (364 mg, 98%, white solid when crushed). **¹H NMR (400 MHz, CD₃OD)** δ 8.09 (d, *J* = 2.2 Hz, 1H), 7.94 (d, *J* = 8.3 Hz, 1H), 7.87 (dd, *J* = 8.2, 2.2 Hz, 1H), 7.77 (dd, *J* = 7.8, 1.4 Hz, 1H), 7.68 – 7.63 (m, 1H), 7.60 (dd, *J* = 8.1, 1.3 Hz, 1H), 7.49 (td, *J* = 7.6, 1.4 Hz, 1H), 6.02 (s, 1H), 3.33 – 3.26 (m, 1H), 3.28 (s, 3H), 3.17 – 3.06 (m, 1H), 2.83 – 2.68 (m, 2H); **¹³C NMR (101 MHz, CD₃OD)** δ 174.2, 142.3, 142.1, 139.0, 137.1, 135.1, 134.7, 133.6, 129.5, 129.3, 128.3, 127.8, 127.4, 68.1, 44.3, 39.4, 30.7.

5-((3-chloro-6-methyl-5,5-dioxido-6,11-dihydrodibenzo[*c,f*][1,2]thiazepin-11-yl)amino)pentanoic acid hydrochloride (2b = MC5). To ester **1b** (243 mg, 0.556 mmol) was added 0.5 M aqueous HCl (13 mL), and the mixture was stirred vigorously for 3 h at 80 °C. The solution was then concentrated *in vacuo* with heating to provide a foamy, nearly colorless glass. In order to remove residual HCl (causes esterification during NMR in CD₃OD), this residue was re-dissolved in a small quantity of water and concentrated again *in vacuo* with heating. This procedure was repeated once more to provide the pure hydrochloride salt **2b**, free from residual HCl, as a foamy, nearly colorless glass (243 mg, 98%, off-white solid when crushed). **¹H NMR (400 MHz, CD₃OD)** δ 8.09 (d, *J* = 2.1 Hz, 1H), 7.92 (d, *J* = 8.2 Hz, 1H), 7.87 (dd, *J* = 8.2, 2.2 Hz, 1H), 7.74 (dd, *J* = 7.8, 1.4 Hz, 1H), 7.68 – 7.62 (m, 1H), 7.58 (dd, *J* = 8.1, 1.3 Hz, 1H), 7.49 (td, *J* = 7.6, 1.4 Hz, 1H), 5.98 (s, 1H), 3.24 (s, 3H), 3.00 (ddd, *J* = 12.3, 9.6, 5.9 Hz, 1H), 2.86 (ddd, *J* = 12.3, 9.6, 6.3 Hz, 1H), 2.31 (t, *J* = 7.0 Hz, 2H), 1.82 – 1.64 (m, 2H), 1.64 – 1.54 (m, 2H); **¹³C NMR (101 MHz, CD₃OD)** δ 176.7, 142.5, 141.9, 138.8, 137.1, 135.2, 134.8, 133.5, 129.4, 129.2, 128.5, 127.9, 127.1, 67.6, 48.1, 39.7, 33.8, 26.4, 22.7.

Biology

Materials: BRET. HEK-293T cells were obtained from the American Type Culture Collection (Rockville, MD) and were cultured in a 5% CO₂ atmosphere at 37 °C in Dulbecco's Modified Eagle Medium (high glucose #11965; Life Technologies Corp.; Grand Island, NY) supplemented with 10% FBS (Premium Select, Atlanta Biologicals; Atlanta, GA) and 100 U/mL penicillin and 100 µg/mL streptomycin (#15140, Life Technologies).

DNA Constructs. The mouse MOR (mMOR), the mouse DOR (mDOR), and the rat KOR (rKOR) were provided by Dr. Lakshmi Devi at Mount Sinai Hospital. The hMOR, hDOR, hKOR, hα_{2A}R, hα_{2B}R, hα_{2C}R and GRK2 were obtained from the Missouri S&T Resource Center. The human G protein constructs used here have been previously described and were provided by C. Galés or were obtained from the Missouri S&T Resource Center unless otherwise noted.^{12,13} The G proteins used included untagged Gα_{oB} (Gα_{oB}); Gα_{oB} with Renilla luciferase 8 (RLuc8) inserted at position 91 (Gα_{oB}-RLuc8); Gβ₁ (β₁); untagged Gγ₂ (γ₂); Gγ₂ which we fused to the full-length mVenus at its *N*-terminus via the amino acid linker GSAGT (mVenus-γ₂). The plasmids employed in the arrestin recruitment assay, RLuc8-arrestin3-Sp1 and mem-linker-citrine-SH3, were synthesized in-house as previously described.⁴⁴ YFP-Epac-RLuc (CAMYEL) was obtained from ATCC (no. MBA-277).⁷⁵ All constructs were sequence-confirmed prior to use in experiments.

Transfection. The following cDNA amounts were transfected into HEK-293T cells (5 x 10⁶ cells/plate) in 10-cm dishes using polyethylenimine (PEI) in a 1:1 ratio (diluted in Opti-MEM, Life Technologies): **G protein activation:** 2.5 µg MOR/DOR/KOR, 0.125 µg Gα_{oB}-RLuc8, 6.25 µg β₁, 6.25 µg mVenus-γ₂; **cAMP Inhibition:** 1.25 µg MOR/DOR/KOR, 1.25 µg Gα_{oB}, 1.25 µg β₁, 1.25 µg γ₂, 10 µg CAMYEL; **BRET GAP43 Translocation:** 2 µg hMOR, 0.25

μg Rluc8-arrestin3-Sp1, 5 μg mem-linker-citrine-SH3, 5 μg GRK2. Cells were maintained in the HEK-293T media described above. After 24 hours the media was changed, and the experiment was performed 24 hours later (48 hours after transfection).

BRET. Transfected cells were dissociated and re-suspended in phosphate-buffered saline (PBS). Approximately 200,000 cells/well were added to a black-framed, white well 96-well plate (#60050; Perkin Elmer; Waltham, MA). The microplate was centrifuged and the cells were re-suspended in PBS. For agonist experiments, after 5 minutes, 5 μM of the luciferase substrate coelenterazine H was added to each well. After 5 minutes, ligands were added and the BRET signal was measured 5 minutes later on a PHERAstar FS plate reader. For cAMP, cells were first incubated with forskolin (1 μM) for 5 minutes prior to coelenterazine h addition. For antagonist competition experiments, cells were pre-incubated with the antagonist at varying concentrations for 30 minutes. Coelenterazine H (5 μM) was then added to each well for 5 minutes. Following coelenterazine H incubation, a fixed concentration of the reference agonist (5x EC_{50}) was added, and the BRET signal was measured at 30 minutes on a PHERAstar FS plate reader. The BRET signal was quantified by calculating the ratio of the light emitted by the energy acceptor, mVenus (510-540 nm) or citrine (510-540 nm), over the light emitted by the energy donor, RLuc8 (485 nm). This drug-induced BRET signal was normalized using the E_{max} of [D-Ala², N-Me-Phe⁴, Gly-ol⁵]-enkephalin (DAMGO), [D-Pen(2,5)]enkephalin (DPDPE), or U-50,488 as the maximal response at MOR, DOR, and KOR respectively. Dose response curves were fit using a three-parameter logistic equation in GraphPad Prism 6.

Human K_i Determination. Binding constants (K_i) at the human opioid receptors were generously determined using radioligand displacement experiments by the National Institute of Mental Health's Psychoactive Drug Screening Program, Contract #HHSN-271-2008-00025-C

(NIMH PDSP). The NIMH PDSP is Directed by Bryan L. Roth MD, PhD at the University of North Carolina at Chapel Hill and Project Officer Jamie Driscoll at NIMH, Bethesda, MD, USA. For experimental details please refer to the PDSP website (<https://pdspdb.unc.edu/pdspWeb/>). In all cases, the reported K_i values are the average of 3 or more independent experiments, each run with triplicate wells for each ligand concentration.

Immunofluorescence. mMOR-CHO cells were grown in Ham's F-12 supplemented with 10% FBS, 100 U/mL penicillin and 100 μ g/mL streptomycin, and 200 μ g/mL hygromycin B prior to the experiment. The cells were starved with serum free media for 3-5 hours before treatment with drugs (10 μ M) for 5 min or 1 hr. Cells were then fixed with 4% formaldehyde in PBS, washed with PBS, permeabilized (0.25% Triton X-100 in PBS), washed, blocked (2% glycine, 2% bovine serum albumin in 50 mM NH_4Cl) for 30 min at 37 °C and incubated overnight with anti-MOR antibodies (1:200 in blocking solution; Abcam #ab134054) at 4 °C. Cells were then washed 5X with PBS, blocked again for 30 min at 37 °C, and incubated with a mixture of anti-rabbit Alexa Fluor[®] 594 secondary antibody (1:1000 in blocking solution; Cell Signaling #8889) and Hoechst stain (1:10,000). The cells were then washed 5X in PBS and imaged on a Leica DMI4000B microscope.

Pharmacokinetics. The pharmacokinetic study of tianeptine was conducted by Sai Life Sciences Limited (Hinjewadi, India). A group of 24 male C57BL/6 mice was administered tianeptine as a solution formulation in normal saline intraperitoneally at a dose of 30 mg/kg. Blood samples (approximately 60 μ L) were collected under light isoflurane anesthesia from the retro-orbital plexus at 0.08, 0.25, 0.5, 1, 2, 4, 8 and 24 h. Plasma samples were separated by centrifugation of whole blood and stored below -70 °C until analysis. Immediately after collection of blood, brain samples were collected from each mouse at 0.08, 0.25, 0.5, 1, 2, 4, 8

and 24 h (3 mice per time point). Brain samples were homogenized using ice-cold phosphate-buffered saline (pH 7.4), and homogenates were stored below -70 °C until analysis. Total brain homogenate volume was three times the tissue weight. All samples were processed for analysis by protein precipitation using acetonitrile and analyzed to determine the concentrations of both tianeptine and MC5 by a fit-for-purpose LC/MS/MS method (lower limit of quantification = 2.02 ng/mL in plasma and 1.01 ng/mL in brain). Pharmacokinetic parameters were calculated using the non-compartmental analysis tool of Phoenix WinNonlin® (Version 6.3).

References

- (1) Micoulaud, F. G. Neuroenhancement in Healthy Adults, Part I: Pharmaceutical Cognitive Enhancement: A Systematic Review. *J. Clin. Res. Bioeth.* **2015**, *06*.
- (2) Defrance, R.; Marey, C.; Kamoun, A. Antidepressant and Anxiolytic Activities of Tianeptine: An Overview of Clinical Trials. *Clin. Neuropharmacol.* **1988**, *11 Suppl 2*, S74–S82.
- (3) Wagstaff, A. J.; Ormrod, D.; Spencer, C. M. Tianeptine: A Review of Its Use in Depressive Disorders. *CNS Drugs* **2001**, *15*, 231–259.
- (4) Mitchell, P. B. Novel French Antidepressants Not Available in the United States. *Psychopharmacol. Bull.* **1995**, *31*, 509–519.
- (5) Martinowich, K.; Jimenez, D. V.; Zarate, C. A.; Manji, H. K. Rapid Antidepressant Effects: Moving Right Along. *Mol. Psychiatry* **2013**, *18*, 856–863.
- (6) McEwen, B. S.; Chattarji, S.; Diamond, D. M.; Jay, T. M.; Reagan, L. P.; Svenningsson, P.; Fuchs, E. The Neurobiological Properties of Tianeptine (Stablon): From Monoamine Hypothesis to Glutamatergic Modulation. *Mol. Psychiatry* **2010**, *15*, 237–249.
- (7) Invernizzi, G.; Aguglia, E.; Bertolino, A.; Casacchia, M.; Ciani, N.; Marchesi, G. F.; Nardini, M.; Rapisarda, V. The Efficacy and Safety of Tianeptine in the Treatment of Depressive Disorder: Results of a Controlled Double-Blind Multicentre Study vs. Amitriptyline. *Neuropsychobiology* **1994**, *30*, 85–93.
- (8) Woo, Y. S.; Bahk, W. M.; Jeong, J. H.; Lee, S. H.; Sung, H. M.; Pae, C. U.; Koo, B. H.; Kim, W. Tianeptine Combination for Partial or Non-Response to Selective Serotonin Re-Uptake Inhibitor Monotherapy. *Psychiatry Clin. Neurosci.* **2013**, *67*, 219–227.
- (9) Ridout, F.; Hindmarch, I. Effects of Tianeptine and Mianserin on Car Driving Skills. *Psychopharmacology (Berl)*. **2001**, *154*, 356–361.
- (10) Wilde, M. I.; Benfield, P. Tianeptine. A Review of Its Pharmacodynamic and Pharmacokinetic Properties, and Therapeutic Efficacy in Depression and Coexisting Anxiety and Depression. *Drugs* **1995**, *49*, 411–439.
- (11) Atmaca, M.; Kuloglu, M.; Tezcan, E.; Buyukbayram, A. Switching to Tianeptine in Patients with Antidepressant-Induced Sexual Dysfunction. *Hum. Psychopharmacol.* **2003**,

- 18, 277–280.
- (12) Bonierbale, M.; Lan, C.; Tignol, J. The ELIXIR Study : Evaluation of Sexual Dysfunction in 4557 Depressed Patients in France. *Curr. Med. Res. Opin.* **2003**, *19*, 114–124.
 - (13) Zoladz, P. R.; Fleshner, M.; Diamond, D. M. Differential Effectiveness of Tianeptine, Clonidine and Amitriptyline in Blocking Traumatic Memory Expression, Anxiety and Hypertension in an Animal Model of PTSD. *Prog. Neuropsychopharmacol. Biol. Psychiatry* **2013**, *44*, 1–16.
 - (14) Sheline, Y. I. Neuroimaging Studies of Mood Disorder Effects on the Brain. *Biol. Psychiatry* **2003**, *54*, 338–352.
 - (15) MacQueen, G. M.; Campbell, S.; McEwen, B. S.; Macdonald, K.; Amano, S.; Joffe, R. T.; Nahmias, C.; Young, L. T. Course of Illness, Hippocampal Function, and Hippocampal Volume in Major Depression. *Proc. Natl. Acad. Sci. U. S. A.* **2003**, *100*, 1387–1392.
 - (16) Rajkowska, G. Cell Pathology in Mood Disorders. *Semin. Clin. Neuropsychiatry* **2002**, *7*, 281–292.
 - (17) Czéh, B.; Michaelis, T.; Watanabe, T.; Frahm, J.; de Biurrun, G.; van Kampen, M.; Bartolomucci, A.; Fuchs, E. Stress-Induced Changes in Cerebral Metabolites, Hippocampal Volume, and Cell Proliferation Are Prevented by Antidepressant Treatment with Tianeptine. *Proc. Natl. Acad. Sci.* **2001**, *98*, 12796–12801.
 - (18) Alfonso, J.; Frick, L. R.; Silberman, D. M.; Palumbo, M. L.; Genaro, A. M.; Frasch, A. C. Regulation of Hippocampal Gene Expression Is Conserved in Two Species Subjected to Different Stressors and Antidepressant Treatments. *Biol. Psychiatry* **2006**, *59*, 244–251.
 - (19) Reagan, L. P.; Hendry, R. M.; Reznikov, L. R.; Piroli, G. G.; Wood, G. E.; McEwen, B. S.; Grillo, C. a. Tianeptine Increases Brain-Derived Neurotrophic Factor Expression in the Rat Amygdala. *Eur. J. Pharmacol.* **2007**, *565*, 68–75.
 - (20) Mennini, T.; Mocaer, E.; Garattini, S. Tianeptine, a Selective Enhancer of Serotonin Uptake in Rat Brain. *Naunyn. Schmiedebergs. Arch. Pharmacol.* **1987**, *336*, 478–482.
 - (21) Fattaccini, C. M.; Bolaños-Jimenez, F.; Gozlan, H.; Hamon, M. Tianeptine Stimulates Uptake of 5-Hydroxytryptamine in Vivo in the Rat Brain. *Neuropharmacology* **1990**, *29*, 1–8.
 - (22) Piñeyro, G.; Deveault, L.; de Montigny, C.; Blier, P. Effect of Prolonged Administration of Tianeptine on 5-HT Neurotransmission: An Electrophysiological Study in the Rat Hippocampus and Dorsal Raphe. *Naunyn. Schmiedebergs. Arch. Pharmacol.* **1995**, *351*, 119–125.
 - (23) Malagié, I.; Deslandes, A.; Gardier, A. M. Effects of Acute and Chronic Tianeptine Administration on Serotonin Outflow in Rats: Comparison with Paroxetine by Using in Vivo Microdialysis. *Eur. J. Pharmacol.* **2000**, *403*, 55–65.
 - (24) Svenningsson, P.; Bateup, H.; Qi, H.; Takamiya, K.; Huganir, R. L.; Spedding, M.; Roth, B. L.; McEwen, B. S.; Greengard, P. Involvement of AMPA Receptor Phosphorylation in Antidepressant Actions with Special Reference to Tianeptine. *Eur. J. Neurosci.* **2007**, *26*, 3509–3517.
 - (25) Kato, G.; Weitsch, A. F. Neurochemical Profile of Tianeptine, a New Antidepressant Drug. *Clin. Neuropharmacol.* **1988**, *11 Suppl 2*, S43–S50.
 - (26) Reznikov, L. R.; Grillo, C. A.; Piroli, G. G.; Pasumarthi, R. K.; Reagan, L. P.; Fadel, J. Acute Stress-Mediated Increases in Extracellular Glutamate Levels in the Rat Amygdala: Differential Effects of Antidepressant Treatment. *Eur. J. Neurosci.* **2007**, *25*, 3109–3114.
 - (27) Kole, M. H. P.; Swan, L.; Fuchs, E. The Antidepressant Tianeptine Persistently Modulates

- Glutamate Receptor Currents of the Hippocampal CA3 Commissural Associational Synapse in Chronically Stressed Rats. *Eur. J. Neurosci.* **2002**, *16*, 807–816.
- (28) Qi, H.; Mailliet, F.; Spedding, M.; Rocher, C.; Zhang, X.; Delagrange, P.; McEwen, B.; Jay, T. M.; Svenningsson, P. Antidepressants Reverse the Attenuation of the Neurotrophic MEK/MAPK Cascade in Frontal Cortex by Elevated Platform Stress; Reversal of Effects on LTP Is Associated with GluA1 Phosphorylation. *Neuropharmacology* **2009**, *56*, 37–46.
- (29) Invernizzi, R.; Pozzi, L.; Garattini, S.; Samanin, R. Tianeptine Increases the Extracellular Concentrations of Dopamine in the Nucleus Accumbens by a Serotonin-Independent Mechanism. *Neuropharmacology* **1992**, *31*, 221–227.
- (30) Adinoff, B. Neurobiologic Processes in Drug Reward and Addiction. *Harv. Rev. Psychiatry* **2004**, *12*, 305–320.
- (31) Chartoff, E. H.; Connery, H. S. It's MORE Exciting than Mu: Crosstalk between Mu Opioid Receptors and Glutamatergic Transmission in the Mesolimbic Dopamine System. *Front. Pharmacol.* **2014**, *5 MAY*, 1–21.
- (32) Ari, M.; Oktar, S.; Duru, M. Amitriptyline and Tianeptine Poisoning Treated by Naloxone. *Hum. Exp. Toxicol.* **2010**, *29*, 793–795.
- (33) Gassaway, M. M.; Rives, M.-L.; Kruegel, A. C.; Javitch, J. A.; Sames, D. The Atypical Antidepressant and Neurorestorative Agent Tianeptine Is a μ -Opioid Receptor Agonist. *Transl. Psychiatry* **2014**, *4*, e411.
- (34) Li, W.; Sun, H.; Chen, H.; Yang, X.; Xiao, L.; Liu, R.; Shao, L.; Qiu, Z. Major Depressive Disorder and Kappa Opioid Receptor Antagonists. *Transl. Perioper. pain Med.* **2015**, *1*, 4–16.
- (35) Beardsley, P. M.; Howard, J. L.; Shelton, K. L.; Carroll, F. I. Differential Effects of the Novel Kappa Opioid Receptor Antagonist, JD1c, on Reinstatement of Cocaine-Seeking Induced by Footshock Stressors vs Cocaine Primes and Its Antidepressant-like Effects in Rats. *Psychopharmacology (Berl.)* **2005**, *183*, 118–126.
- (36) Uzbay, T. I.; Kayir, H.; Ceyhan, M. Effects of Tianeptine on Onset Time of Pentylentetrazole-Induced Seizures in Mice: Possible Role of Adenosine A1 Receptors. *Neuropsychopharmacology* **2007**, *32*, 412–416.
- (37) Couet, W.; Girault, J.; Latrille, F.; Salvadori, C.; Fourtillan, J. B. Kinetic Profiles of Tianeptine and Its MC5 Metabolite in Plasma, Blood and Brain after Single and Chronic Intraperitoneal Administration in the Rat. *Eur. J. Drug Metab. Pharmacokinet.* **1990**, *15*, 69–74.
- (38) Grislain, L.; Gele, P.; Bertrand, M.; Luijten, W.; Bromet, N.; Salvadori, C.; Kamoun, A. The Metabolic Pathways of Tianeptine, a New Antidepressant, in Healthy Volunteers. *Drug Metab. Dispos.* **1990**, *18*, 804–808.
- (39) DeWire, S. M.; Yamashita, D. S.; Rominger, D. H.; Liu, G.; Cowan, C. L.; Graczyk, T. M.; Chen, X.-T.; Pitis, P. M.; Gotchev, D.; Yuan, C.; Koblish, M.; Lark, M. W.; Violin, J. D. A G Protein-Biased Ligand at the μ -Opioid Receptor Is Potently Analgesic with Reduced Gastrointestinal and Respiratory Dysfunction Compared with Morphine. *J. Pharmacol. Exp. Ther.* **2013**, *344*, 708–717.
- (40) Kim, J. A.; Bartlett, S.; He, L.; Nielsen, C. K.; Chang, A. M.; Kharazia, V.; Waldhoer, M.; Ou, C. J.; Taylor, S.; Ferwerda, M.; Cado, D.; Whistler, J. L. Morphine-Induced Receptor Endocytosis in a Novel Knockin Mouse Reduces Tolerance and Dependence. *Curr. Biol.* **2008**, *18*, 129–135.
- (41) Berger, A. C.; Whistler, J. L. Morphine-Induced Mu Opioid Receptor Trafficking

- Enhances Reward yet Prevents Compulsive Drug Use. *EMBO Mol. Med.* **2011**, *3*, 385–397.
- (42) Chu, C.-C.; Shieh, J.-P.; Shui, H.-A.; Chen, J.-Y.; Hsing, C.-H.; Tzeng, J.-I.; Wang, J.-J.; Ho, S.-T. Tianeptine Reduces Morphine Antinociceptive Tolerance and Physical Dependence. *Behav. Pharmacol.* **2010**, *21*, 523–529.
- (43) Cavalla, D.; Chianelli, F.; Korsak, A.; Hosford, P. S.; Gourine, A. V.; Marina, N. Tianeptine Prevents Respiratory Depression without Affecting Analgesic Effect of Opiates in Conscious Rats. *Eur. J. Pharmacol.* **2015**, *761*, 268–272.
- (44) Clayton, C. C.; Donthamsetti, P.; Lambert, N. A.; Javitch, J. A.; Neve, K. A. Mutation of Three Residues in the Third Intracellular Loop of the Dopamine D2 Receptor Creates an Internalization-Defective Receptor. *J. Biol. Chem.* **2014**, *289*, 33663–33675.
- (45) Williams, J. T.; Ingram, S. L.; Henderson, G.; Chavkin, C.; von Zastrow, M.; Schulz, S.; Koch, T.; Evans, C. J.; Christie, M. J.; Zastrow, M. Von; Schulz, S.; Koch, T.; Evans, C. J.; Christie, M. J. Regulation of μ -Opioid Receptors: Desensitization, Phosphorylation, Internalization, and Tolerance. *Pharmacol. Rev.* **2013**, *65*, 223–254.
- (46) Drake, C. T.; Milner, T. A. Mu Opioid Receptors Are in Discrete Hippocampal Interneuron Subpopulations. *Hippocampus* **2002**, *12*, 119–136.
- (47) Xie, C. W.; Lewis, D. V. Involvement of cAMP-Dependent Protein Kinase in Mu-Opioid Modulation of NMDA-Mediated Synaptic Currents. *J. Neurophysiol.* **1997**, *78*, 759–766.
- (48) Lou, L.; Zhou, T.; Wang, P.; Pei, G. Modulation of Ca²⁺/calmodulin-Dependent Protein Kinase II Activity by Acute and Chronic Morphine Administration in Rat Hippocampus: Differential Regulation of Alpha and Beta Isoforms. *Mol. Pharmacol.* **1999**, *55*, 557–563.
- (49) Kam, A. Y. F.; Liao, D.; Loh, H. H.; Law, P.-Y. Morphine Induces AMPA Receptor Internalization in Primary Hippocampal Neurons via Calcineurin-Dependent Dephosphorylation of GluR1 Subunits. *J. Neurosci.* **2010**, *30*, 15304–15316.
- (50) Dalery, J.; Dagens-Lafont, V.; De Bodinat, C. Efficacy of Tianeptine vs Placebo in the Long-Term Treatment (16.5 Months) of Unipolar Major Recurrent Depression. *Hum. Psychopharmacol.* **2001**, *16*.
- (51) Mayberg, H. S.; Brannan, S. K.; Tekell, J. L.; Silva, J. A.; Mahurin, R. K.; McGinnis, S.; Jerabek, P. A. Regional Metabolic Effects of Fluoxetine in Major Depression: Serial Changes and Relationship to Clinical Response. *Biol. Psychiatry* **2000**, *48*, 830–843.
- (52) Sheline, Y. I.; Barch, D. M.; Donnelly, J. M.; Ollinger, J. M.; Snyder, A. Z.; Mintun, M. A. Increased Amygdala Response to Masked Emotional Faces in Depressed Subjects Resolves with Antidepressant Treatment: An fMRI Study. *Biol. Psychiatry* **2001**, *50*, 651–658.
- (53) Sacchetti, G.; Bonini, I.; Cools Waeterloos, G.; Samanin, R. Tianeptine Raises Dopamine and Blocks Stress-Induced Noradrenaline Release in the Rat Frontal Cortex. *Eur. J. Pharmacol.* **1993**, *236*, 171–175.
- (54) Szegedi, V.; Juhász, G.; Zhang, X.; Barkóczi, B.; Qi, H.; Madeira, A.; Kapus, G.; Svenningsson, P.; Spedding, M.; Penke, B. Tianeptine Potentiates AMPA Receptors by Activating CaMKII and PKA via the p38, p42/44 MAPK and JNK Pathways. *Neurochem. Int.* **2011**, *59*, 1109–1122.
- (55) Zhang, H.; Etherington, L.-A.; Hafner, A.-S.; Belelli, D.; Coussen, F.; Delagrange, P.; Chaouloff, F.; Spedding, M.; Lambert, J. J.; Choquet, D.; Groc, L. Regulation of AMPA Receptor Surface Trafficking and Synaptic Plasticity by a Cognitive Enhancer and Antidepressant Molecule. *Mol. Psychiatry* **2013**, *18*, 471–484.

- (56) Duman, R. S.; Li, N.; Liu, R.-J.; Duric, V.; Aghajanian, G. Signaling Pathways Underlying the Rapid Antidepressant Actions of Ketamine. *Neuropharmacology* **2012**, *62*, 35–41.
- (57) Shirayama, Y.; Chaki, S. Neurochemistry of the Nucleus Accumbens and Its Relevance to Depression and Antidepressant Action in Rodents. *Curr. Neuropharmacol.* **2006**, *4*, 277–291.
- (58) Carlezon, W. A.; Thomas, M. J. Biological Substrates of Reward and Aversion: A Nucleus Accumbens Activity Hypothesis. *Neuropharmacology* **2009**, *56*, 122–132.
- (59) Gerner, R. H.; Catlin, D. H.; Gorelick, D. A.; Hui, K. K.; Li, C. H. Beta-Endorphin. Intravenous Infusion Causes Behavioral Change in Psychiatric Inpatients. *Arch. Gen. Psychiatry* **1980**, *37*, 642–647.
- (60) Hsu, D. T.; Sanford, B. J.; Meyers, K. K.; Love, T. M.; Hazlett, K. E.; Walker, S. J.; Mickey, B. J.; Koeppe, R. A.; Langenecker, S. A.; Zubieta, J. It Still Hurts: Altered Endogenous Opioid Activity in the Brain during Social Rejection and Acceptance in Major Depressive Disorder. *Mol. Psychiatry* **2015**, *20*, 193–200.
- (61) Porsolt, R. D.; Bertin, A.; Jalfre, M. Behavioral Despair in Mice: A Primary Screening Test for Antidepressants. *Arch. Int. Pharmacodyn. therapie* **1977**, *229*, 327–336.
- (62) Lister, R. G. The Use of a plus-Maze to Measure Anxiety in the Mouse. *Psychopharmacology (Berl)*. **1987**, *92*, 180–185.
- (63) Belknap, J. K.; Noordewier, B.; Lamé, M. Genetic Dissociation of Multiple Morphine Effects among C57BL/6J, DBA/2J and C3H/HeJ Inbred Mouse Strains. *Physiol. Behav.* **1989**, *46*, 69–74.
- (64) Belknap, J. K.; Riggan, J.; Cross, S.; Young, E. R.; Gallaher, E. J.; Crabbe, J. C. Genetic Determinants of Morphine Activity and Thermal Responses in 15 Inbred Mouse Strains. *Pharmacol. Biochem. Behav.* **1998**, *59*, 353–360.
- (65) Levine, A. S.; Morley, J. E.; Gosnell, B. A.; Billington, C. J.; Bartness, T. J. Opioids and Consummatory Behavior. *Brain Res. Bull.* **1985**, *14*, 663–672.
- (66) Oliverio, A.; Castellano, C. Experience Modifies Morphine-Induced Behavioral Excitation of Mice. *Nature* **1974**, *252*, 229–230.
- (67) Wenger, G. R. The Role of Control Activity Levels in the Reported Strain Differences to the Behavioral Effects of Drugs in Mice. *Pharmacol. Biochem. Behav.* **1989**, *32*, 241–247.
- (68) Kruegel, A. C. Chemical and Biological Explorations of Novel Opioid Receptor Modulators, Columbia University, 2015.
- (69) Brady, K. T.; McCauley, J. L.; Back, S. E. Prescription Opioid Misuse, Abuse, and Treatment in the United States: An Update. *Am. J. Psychiatry* **2016**, *173*, 18–26.
- (70) Guillem, E.; Lépine, J.-P. [Does Addiction to Antidepressants Exist? About a Case of One Addiction to Tianeptine]. *L'Encéphale* **29**, 456–459.
- (71) Leterme, L.; Singlan, Y.-S.; Auclair, V.; Le Boisselier, R.; Frimas, V. [Misuse of Tianeptine: Five Cases of Abuse]. *Ann. médecine interne* **2003**, *154 Spec N*, S58–S63.
- (72) Saatçioğlu, O.; Erim, R.; Cakmak, D. [A Case of Tianeptine Abuse]. *Türk Psikiyatr. Derg. = Turkish J. psychiatry* **2006**, *17*, 72–75.
- (73) Vadachkoria, D.; Gabunia, L.; Gambashidze, K.; Pkhaladze, N.; Kuridze, N. Addictive Potential of Tianeptine - the Threatening Reality. *Georgian Med. News* **2009**, 92–94.
- (74) Vandel, P.; Regina, W.; Bonin, B.; Sechter, D.; Bizouard, P. [Abuse of Tianeptine. A Case Report]. *L'Encéphale* **25**, 672–673.
- (75) Jiang, L. I.; Collins, J.; Davis, R.; Lin, K.-M.; DeCamp, D.; Roach, T.; Hsueh, R.; Rebres,

- R. A.; Ross, E. M.; Taussig, R.; Fraser, I.; Sternweis, P. C. Use of a cAMP BRET Sensor to Characterize a Novel Regulation of cAMP by the Sphingosine 1-phosphate/G13 Pathway. *J. Biol. Chem.* **2007**, *282*, 10576–10584.
- (76) Bolton, E. E.; Chen, J.; Kim, S.; Han, L.; He, S.; Shi, W.; Simonyan, V.; Sun, Y.; Thiessen, P. A.; Wang, J.; Yu, B.; Zhang, J.; Bryant, S. H. PubChem3D: A New Resource for Scientists. *J. Cheminform.* **2011**, *3*, 1–15.

Chapter 3 – Exploring the Biological Activity of the *Mitragyna speciosa* Alkaloids at the Opioid Receptors

Introduction

Mitragyna speciosa (**Figure 1**) is a psychoactive plant known as “kratom” in Thailand or “biak biak” in Malaysia. It has been widely used by humans in Southeast Asia for many centuries to treat a variety of ailments, particularly among farm populations where it is used traditionally to combat fatigue and increase productivity.¹ Kratom has additionally been used for centuries in socioreligious ceremonies, lending its name potentially from “Mithraic cults,” an ancient source

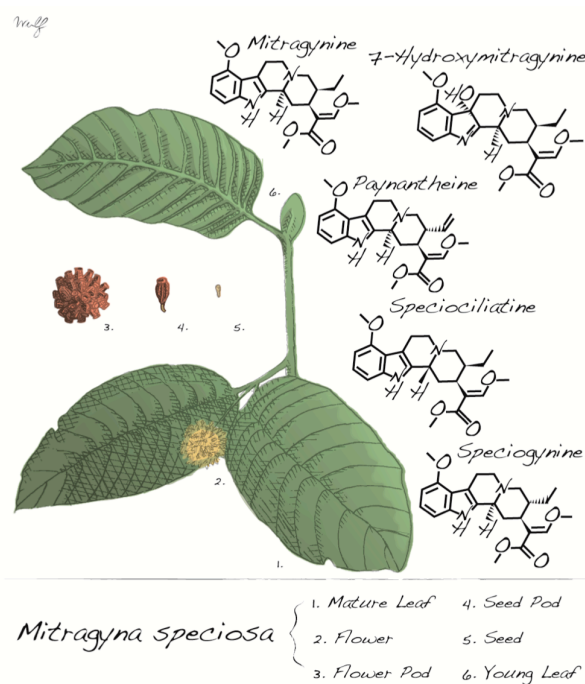


Figure 1. Leaves and fruiting bodies of *Mitragyna speciosa* and chemical structures of notable alkaloids.¹⁷

of spiritual transcendence.² The plant material is typically consumed as a tea, chewed directly, or smoked. The effects of kratom can vary depending on the amount consumed. The stimulating effects of kratom can be achieved at low doses, while more opioid-like effects predominate at higher doses. The plant, therefore, has been used as a general analgesic as well as a substitute for opium due to its euphoric and sedative effects. It is even used as a method to treat opioid withdrawal. Further, kratom has been used

in the treatment of other conditions, such as fever, cough, diarrhea, and depression. Additionally, there is a precedent for recreational use and abuse of the plant, which has likely contributed to legal control of *Mitragyna speciosa* in both Thailand and Malaysia today. Interestingly, however,

the origins of this kratom ban might not be as straightforward. “The Kratom Act” banned kratom use in Thailand in 1943 not due to its psychoactive properties (that would come later in the “Thai Narcotics Act” of 1979) but because the general population preferred cheaper kratom over heavily taxed opium, which was negatively impacting the government’s income.³ The plant does, however, remain uncontrolled outside its native regions.^{1,4-7}

Given the extensive medicinal use of *Mitragyna speciosa*, there has been much study on the molecular constituents responsible for its psychoactive effects, and to date more than 40 unique indole alkaloids having been identified in the plant.^{1,4,5,8} Mitragynine (**Figure 1**) has been generally acknowledged as the primary indole alkaloid constituent of *Mitragyna speciosa*, which accounts for up to 66% by mass of crude alkaloid extracts.⁴ Paynantheine, speciogynine, and speciociliatine have been identified as the other major alkaloids in the plant (**Figure 1**).⁴ Among the many different regional varieties of *Mitragyna speciosa*, the quantities of these major alkaloids, along with a wide variety of minor alkaloids, are considerably varied and can also vary depending on plant age. In interpreting the psychoactive effects of the plant, these considerations greatly complicate our understanding of which alkaloids are most important.^{1,4,5,8} Amongst the minor alkaloids, the oxidized mitragynine derivative 7-hydroxymitragynine (7-OH)⁹ (**Figure 1**) is most interesting due to its reported analgesic effects mediated through agonist activity at the mu-opioid receptor (MOR), which are known to exceed in potency those of the prototypical opioid agonist morphine.^{7,10}

The mechanism of action of *Mitragyna* alkaloids has been studied both *in vitro* and *in vivo*. Takayama and coworkers, in particular, have published several studies indicating that the opioid receptor system is the primary mechanism for the psychoactive effects of these alkaloids. For instance, mitragynine and 7-OH both show nanomolar binding affinities for the MOR and

demonstrate functional activity in both *ex vivo* and *in vivo* studies.^{7,10} Guinea pig ileum, which is rich with MORs, was used to assess *ex vivo* functional activity of *Mitragyna* alkaloids, whereby MOR agonists can inhibit electrically induced twitching in the tissue. The alkaloids showed agonist properties in this assay.^{7,10} The antinociceptive effects (measured via the tail flick assay) of mitragynine and 7-OH have additionally been shown to be inhibited by the opioid antagonist naloxone in several rodent models, an indication of their agonist activity at the MOR.^{7,10,11} Although there is evidence implicating the opioid receptor system in the analgesic effects of the *Mitragyna* alkaloids, specifically MOR, reports in the literature are conflicting. In a prominent study from the 1970s, mitragynine was found to induce behavioral effects in cats, and analgesic effects in rats, that were not reversed by treatment with nalorphine, an opioid antagonist.¹² Additionally, this study also found mitragynine to produce markedly less respiratory depression than the opium poppy-derived alkaloid codeine. Further, the biological activity of mitragynine is not exclusive to the opioid receptors. One report has shown mitragynine to bind to several non-opioid CNS receptors, including the alpha-2 adrenergic receptor (α_2R), adenosine A_{2a}, dopamine D₂, and the serotonin receptors 5-HT_{2C} and 5-HT₇, but no binding affinities were reported.¹³ The analgesic effects of mitragynine have also been shown to be inhibited not only by the α_2R antagonist idazoxan, but also by the non-specific serotonin antagonist cyproheptadine, indicating that the notable biological activity of this alkaloid may be complex.¹⁴

Although the physiological *in vivo* and *ex vivo* tissue experiments (such as the *ex vivo* assay described above) are the only currently accessible methods to probe system level effects from compounds such as the *Mitragyna* alkaloids, these methods cannot provide molecular analysis of receptor activation and signaling. Given what the considerable number of conflicting reports suggests on the activity of *Mitragyna* alkaloids, it seems that such *in vivo* and *ex vivo*

assays still cannot solely substitute for studying receptor-level functionality *in vitro*. There have been recent studies on receptor-level functional activity for several synthetic oxidized mitragynine analogs in [³⁵S]GTPγS binding assays using overexpressed cellular systems¹⁵, but no similar functional studies have been reported for mitragynine or for the other alkaloids in *Mitragyna speciosa*.¹⁶ This chapter will explore a systematic study of the *Mitragyna* alkaloids at the opioid receptors, assessing not only binding affinities but also receptor activation and other fundamental intracellular signaling pathways. Through thoughtful examination of the functional activity of these compounds, we bring a new perspective to the psychoactive properties of these compounds and highlight their further potential as novel therapeutics for pain and depression. Some of this work has been described in a recent publication.¹⁷

Results

Biological Activity of *Mitragyna* Alkaloids at Rodent Opioid Receptors

Isolation of the Alkaloids From the Plant Material. The four major alkaloids of *Mitragyna speciosa* were isolated directly from the Thai strain of the plant, and 7-OH was

Table 1. Binding Affinity of *Mitragyna* Alkaloids at Mouse Receptors.
K_i (μM)

Compound	mMOR	mKOR	mDOR
mitragynine	0.230 ± 0.047	0.231 ± 0.021	1.01 ± 0.05
paynantheine	0.666 ± 0.083	0.888 ± 0.294	4.25 ± 0.73
speciociliatine	0.0786 ± 0.0109	0.649 ± 0.169	1.16 ± 0.23
speciogynine	0.578 ± 0.064	2.90 ± 0.49	7.95 ± 0.95
7-OH	0.0366 ± 0.0041	0.132 ± 0.007	0.0906 ± 0.0085

Data represent mean ± SEM (μM) of n ≥ 3. Data collected by Dr. Susruta Majumdar.

prepared via photochemical oxidation of the major alkaloid mitragynine (performed by Andrew Kruegel).¹⁷ Only trace amounts of 7-OH could be

detected in the extractions of the plant material (as observed by mass spectroscopy), and we were unable to isolate any of this alkaloid directly. Given these findings, it is unlikely that 7-OH is

found as a major alkaloid from extractions of *Mitragyna speciosa* (although certainly amounts may vary between strains and batches), and it may therefore be inferred that it is not responsible for the psychoactive properties of the plant. Interestingly, we were able to convert a small amount of mitragynine into 7-OH simply using oxidation from the air in the presence of rose bengal (singlet oxygen generator), so it is possible that leaf batches exposed to sunlight for long periods of time may be able to produce measurable quantities of 7-OH *in situ* from mitragynine.

Binding Affinity. In an attempt to determine the functional activity of the *Mitragyna* alkaloids at the opioid receptors, we first looked to study these natural products at the rodent receptors, as all previous studies were reported in animal tissues or cells. Using radioligand binding assays in chinese hamster ovary (CHO) cells stably expressing the murine MOR, DOR, or KOR, our collaborator Dr. Susruta Majumdar determined the binding affinity of all five *Mitragyna* alkaloids. All compounds bound to each opioid receptor to some degree, however 7-OH showed the highest binding affinity for the opioid receptors with approximately 2.5- to 4-

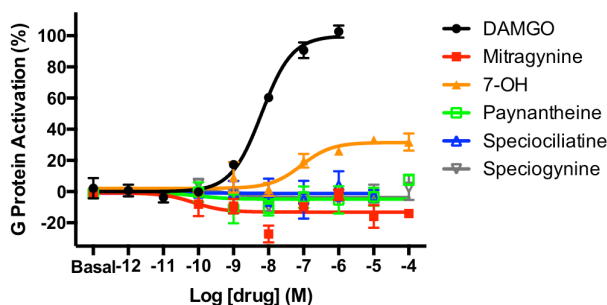


Figure 2. Agonist Activity of *Mitragyna* alkaloids and 7-hydroxymitragynine (7-OH) at the mouse mu-opioid receptor (mMOR). mMOR was co-expressed with $G_{\alpha_{\text{O}}\text{B}}$ -RLuc8, $\beta 1$, and mVenus- $\gamma 2$ to assay G protein activation. 7-OH shows an $EC_{50} = 38.3 \pm 24.7$ nM and $E_{\text{Max}} = 23\%$ at mMOR. Curves represent the average of $n \geq 3$, with error bars representing \pm SEM. Positive control = [D-Ala², N-Me-Phe⁴, Gly-ol³]-enkephalin (DAMGO).

fold selectivity for MOR over KOR and DOR (**Table 1**). These results were comparable with those reported in literature for 7-OH, but our affinities were much weaker for mitragynine at MOR and DOR^{7,10}. We were therefore interested in measuring the functional activity of these alkaloids in cell-based assays.

Functional Activity. Using BRET assays for G protein activation (see Chapter 1), we measured the agonist activity of all five *Mitragyna* alkaloids at the three opioid receptors. Interestingly, we found no measurable agonist activity of any of the five alkaloids at the three opioid receptors, with the exception of 7-OH, which showed partial agonism at both MOR and DOR (**Figure 2** and **Table 2**, $EC_{50\text{ mMOR}} = 0.038 \pm 0.025 \mu\text{M}$ ($E_{\text{Max}} = 23\%$); $EC_{50\text{ mMOR}} = 0.66 \pm 0.44 \mu\text{M}$ ($E_{\text{Max}} = 16\%$)). Given the known analgesic effects of mitragynine in animal models (mouse tail flick assay), we were surprised to observe no agonist activity from mitragynine itself.

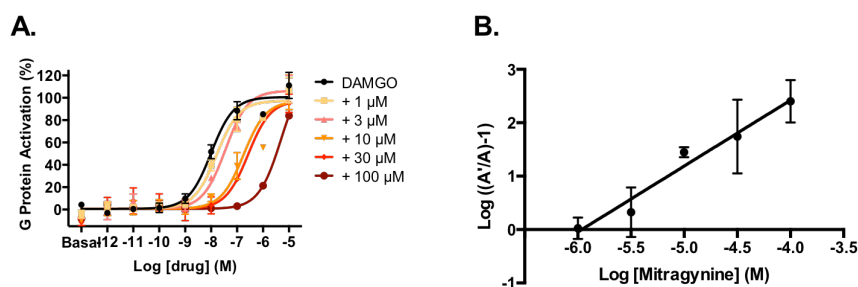


Figure 3. Mitragynine is an antagonist at mMOR. mMOR was co-expressed with G_{α_B} -RLuc8, β_1 , and mVenus- γ_2 to assay G protein activation. Curves represent the average of $n \geq 3$, with error bars representing \pm SEM. A. Control agonist DAMGO was incubated with increasing concentrations of mitragynine. B. Schild plot of (A) reveals a competitive antagonist mode of action.

We next sought to measure the antagonist activity of these compounds at the rodent opioid receptors since we were unable to match the binding

affinity of most alkaloids with agonist activity. Again the alkaloids paynantheine, speciociliatine, and speciogynine showed no antagonist activity at any of the opioid receptors (**Table 2**). When we measured the antagonism of mitragynine and 7-OH, however, we found that mitragynine was an antagonist at mMOR, while both mitragynine and 7-OH were antagonists at rKOR (**Table 2**). To further quantify the antagonism of mitragynine at MOR, we used Schild analysis to determine an $A_2 = 0.807 \pm 0.573 \mu\text{M}$ (where $\log(K_d) = -pA_2$, an approximation of binding affinity, K_d) and a competitive mode of action based on the slope of the plot (**Figure 3**, slope = 1.23). While mitragynine may be a true antagonist at the mouse MOR, it is also possible that mitragynine

shows partial agonism that is below the detection limit of our functional assays. In this case, the

Table 2. Functional Activity of *Mitragyna* Alkaloids at Mouse Receptors.
EC₅₀ (E_{Max}) or [IC₅₀] (μM)

Compound	mMOR	mKOR	mDOR
mitragynine	$A_2 = 0.81$	[> 10]	X
paynantheine	X	X	X
speciociliatine	X	X	X
speciogynine	X	X	X
7-OH	0.0383 ± 0.0247 (23%)	[> 10]	0.664 ± 0.435 (16%)

Data represent mean ± SEM (μM) of n ≥ 3 from G protein activation assays. A₂ value determined through Schild analysis. "X" indicates not active in agonist or antagonist mode.

possible that low efficacy functional activity from the other three alkaloids, paynantheine, speciociliatine, and speciogynine, may be undetected in our assays and could therefore explain why the compounds bind the receptors but do not exhibit functional activity.

We were particularly excited by the antagonism seen at rKOR by mitragynine and 7-OH.

Table 3. Binding Affinity of *Mitragyna* Alkaloids at Human Receptors.
K_i (μM)

Compound	hMOR	hKOR	hDOR
mitragynine	0.233 ± 0.048	0.772 ± 0.207	> 10
paynantheine	0.410 ± 0.152	2.56 ± 0.37	> 10
speciociliatine	0.560 ± 0.168	0.329 ± 0.112	> 10
speciogynine	0.728 ± 0.061	3.20 ± 0.36	> 10
7-OH	0.047 ± 0.018	0.188 ± 0.038	0.219 ± 0.041

Data represent mean ± SEM (μM) of n ≥ 3. Data collected by the Psychoactive Drug Screening Program (PDSP).

have not only analgesic properties but also antidepressant effects, as well. To date, *Mitragyna* alkaloids had only been reported as KOR agonists²¹, based on assumptions from the *in vivo* data. These results represent the first study demonstrating functional activity at the KOR.

Biological Activity of *Mitragyna* Alkaloids at Human Opioid Receptors

antagonism of this very weak partial agonist could be detected at mMOR, as shown. This hypothesis also better explains the analgesic effects reported for mitragynine. Similarly, it is

KOR antagonists are reported in animal models to have antidepressant effects and clinical trials are in the early stages for some known compounds.¹⁸⁻²⁰ Therefore, mitragynine and 7-OH might

Binding Affinity. Given the interesting therapeutic potential for these compounds and the heavy use of the plant material worldwide, it was important for us to explore the signaling at human receptors further. Up until our laboratory's recent report on the functional activity of *Mitragyna* alkaloids¹⁷, there were no reports presenting data at the human variant of the receptors. In collaboration with the Psychoactive Drug Screening Program (PDSP, University of

Table 4. Functional Activity of *Mitragyna* Alkaloids at Human Receptors.
EC₅₀ (E_{Max}) or IC₅₀ (μM)

Compound	hMOR	hKOR	hDOR
mitragynine	0.339 ± 0.178 (34%)	[8.5 ± 7.6] A ₂ = 1.4	[> 10]
paynantheine	[2.2 ± 10]	[> 10]	[> 10]
speciociliatine	[4.2 ± 1.6]	[> 10]	[> 10]
speciogynine	[5.7 ± 2.8]	[> 10]	[> 10]
7-OH	0.0345 ± 0.0045 (47%)	[7.9 ± 3.7] pA ₂ = 0.49	[> 10]

Data represent mean ± SEM (μM) of n ≥ 3 from G protein activation assays. A₂ value determined through Schild analysis.

North Carolina, Chapel

Hill), we measured the binding affinity of the five *Mitragyna* alkaloids at the human opioid receptors (Table 3). Interestingly, the affinities of the five

alkaloids for the opioid receptors were similar between the two species, with the exception of those for DOR, which were markedly weaker at hDOR. Often there can be large discrepancies in data between different variants of receptors, as reported previously for chymases and toll-like receptors^{22,23}; in fact, computational modeling of the two receptor variants may reveal key residues that impart species specificity for ligand binding. Nonetheless, the similar binding observed at the human receptors in comparison to the rodent receptors was encouraging.

Functional Activity. When measured for G protein activation using BRET assays, mitragynine showed partial agonism at the human MOR (Figure 4B) with an EC₅₀ hMOR = 0.34 ± 0.18 μM and E_{Max} = 34%. In contrast, mitragynine showed antagonism at both KOR (Figure 5A, IC₅₀ hKOR = 8.5 ± 7.6 μM) and DOR (Figure 5C, IC₅₀ hDOR > 10 μM). Further Schild analysis showed an A₂ of 1.4 ± 0.4 μM for hKOR antagonism and a competitive mode of action (Figure

6B, slope = 1.3). The KOR antagonism is similar to what was observed at the rat KOR. Mitragynine was also able to inhibit the agonism from control DAMGO, even as a partial

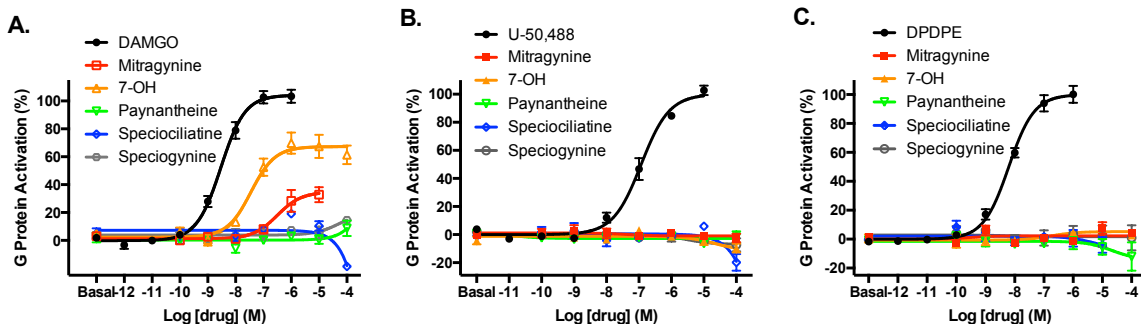


Figure 4. Agonist Activity of *Mitragyna* alkaloids and 7-OH at the human opioid receptors. hMOR (A), hKOR (B), or hDOR (C) were co-expressed with $G\alpha_B$ -RLuc8, β_1 , and mVenus- γ 2 to assay G protein activation. Mitragynine shows an $EC_{50} = 339 \pm 178$ nM and $E_{Max} = 34\%$ at hMOR. 7-OH shows an $EC_{50} = 34.5 \pm 4.5$ nM and $E_{Max} = 47\%$ at hMOR. Curves represent the average of $n \geq 3$, with error bars representing \pm SEM. B. Positive control = U-50,488. C. Positive control = positive control = [D-Pen(2,5)]enkephalin (DPDPE).

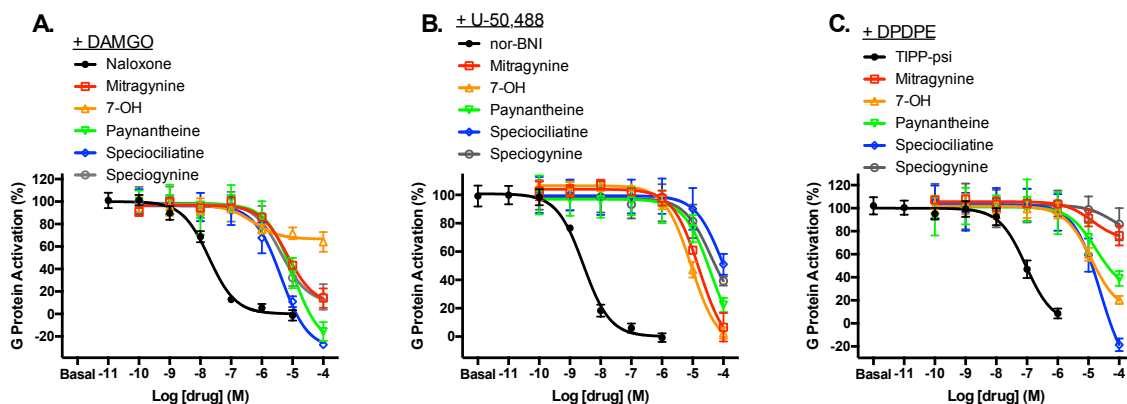


Figure 5. Antagonist Activity of *Mitragyna* alkaloids and 7-OH at the human opioid receptors. hMOR (A), hKOR (B), or hDOR (C) were co-expressed with $G\alpha_B$ -RLuc8, β_1 , and mVenus- γ 2 to assay G protein activation. Curves represent the average of $n \geq 3$, with error bars representing \pm SEM. A. Inhibition of DAMGO, positive control = naloxone. B. Inhibition of U-50,488, positive control = nor-binaltorphimine (nor-BNI). C. Inhibition of DPDPE, positive control = TIPP-psi. In antagonist experiments, the agonist was used at 5x its EC_{50} concentration.

agonist, and support the idea that low efficacy partial agonism at the mouse MOR may be too weak to detect in the assays and instead appears as antagonism. However, the other natural alkaloids paynantheine, speciociliatine, and speciogyne showed no agonist activity at concentrations up to 100 μ M and only weak antagonist effects (Figures 4 and 5). These results

were comparable to the lack of agonist or antagonist activity at the rodent receptors. 7-OH was found to be a potent, partial agonist at the human MOR with $EC_{50\text{ hMOR}} = 34.5 \pm 4.5\text{ nM}$ and $E_{\text{Max}} = 47\%$ (**Figure 4B**), which was similar in potency to the activity at mMOR, but more efficacious. Again, 7-OH was measured as a competitive antagonist at both hKOR (**Figure 5A**, $IC_{50\text{ hKOR}} = 7.9 \pm 3.7\text{ }\mu\text{M}$) and hDOR (**Figure C**, $IC_{50\text{ hDOR}} = 15.6 \pm 9.1\text{ }\mu\text{M}$). In Schild analysis for hKOR antagonism, 7-OH showed an $A_2 = 490 \pm 131\text{ nM}$ and a slope of 1.1 (**Figure 6B**). Similar to mitragynine, 7-OH was able to partially inhibit the response from control agonist DAMGO at hMOR. The functional activity of the *Mitragyna* alkaloids at the human opioid receptors is summarized in **Table 4**.

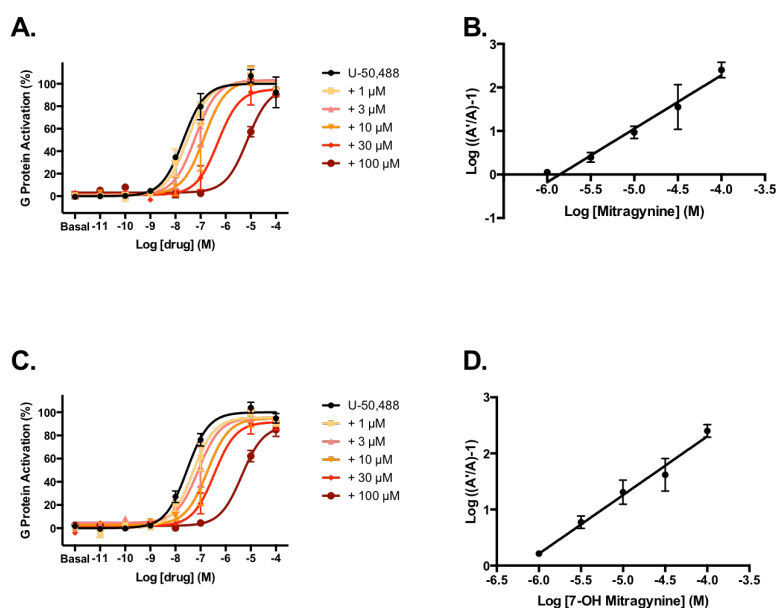


Figure 6. Mitragynine and 7-OH are antagonists at hKOR. hKOR was co-expressed with $G\alpha_B$ -RLuc8, β_1 , and mVenus- γ_2 to assay G protein activation. Curves represent the average of $n \geq 3$, with error bars representing \pm SEM. A. Control agonist U-50,488 was incubated with increasing concentrations of mitragynine. B. Schild plot of (A) reveals a competitive antagonist mode of action. C. Control agonist U-50,488 was incubated with increasing concentrations of 7-OH. D. Schild plot of (C) reveals a competitive antagonist mode of action.

To confirm the agonist activity observed at the human opioid receptors, mitragynine and 7-OH were measured for their ability to inhibit cAMP production in an independent BRET assay. This assay uses CAMYEL, a BRET sensor that undergoes a conformational change in the presence of cAMP,

which in turn alters the induced BRET signal (see **Figure 15** in Chapter 1). Similar to the G

protein activation results, both mitragynine and 7-OH were found to be partial agonists at the human MOR (**Figure 7**). Interestingly, 7-OH showed partial agonism at hDOR in this assay. Given the effects of downstream amplification and therefore greater sensitivity of cAMP inhibition in comparison to G protein activation, it is possible that the low efficacy agonism at hDOR was undetected in the G protein readout and thus only registered in antagonist mode. These results were also in line with the mouse data, where 7-OH induced low efficacy partial activation of mDOR.

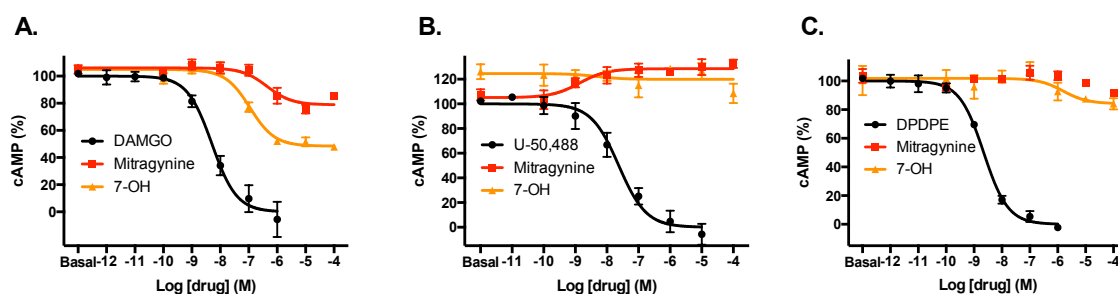


Figure 7. Agonist Activity of Mitragynine and 7-OH at the Human Opioid Receptors in the cAMP Inhibition Assay. hMOR (A), hKOR (B), or hDOR (C) were co-expressed with $G\alpha_{OB}$, $\beta 1$, $\gamma 2$, and CAMYEL to assay inhibition of forskolin-induced cAMP production. Mitragynine shows an $EC_{50} = 259 \pm 119$ nM and $E_{Max} = 25\%$ at hMOR. 7-OH shows an $EC_{50} = 95 \pm 27$ nM and $E_{Max} = 52\%$ at hMOR and weak partial agonism at hDOR. Curves represent the average of $n \geq 3$, with error bars representing \pm SEM.

Overall the functional activity and binding affinity observed for the five *Mitragyna* alkaloids at the opioid receptors is internally consistent, both in rodent and human species. This is further supported when the functional data (EC_{50} or IC_{50}) are corrected by the Cheng-Prusoff equation.²⁴ The pA_2 values and slope measured via Schild analysis provide an additional favorable comparison to the binding data and is perhaps more rigorous than the Cheng-Prusoff correction. Again though the affinities for mitragynine at MOR and DOR appear much weaker than reported^{7,10}, the similarities between our *in vitro* data and the reported relative *in vivo* potencies of either mitragynine or 7-OH lead us to conclude that the new functional data may be more reliable.

Exploring Other Isomers of Mitragynine

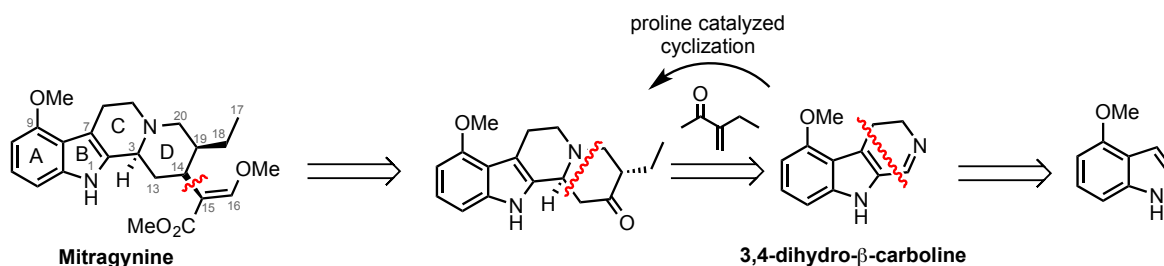


Figure 8. Retrosynthesis of Mitragynine for Access to Unnatural Isomers.

Synthesis of Mitragynine Isomers. In order to access the functional activity of some unnatural isomers of mitragynine, a total synthesis was employed that would allow modification of the A-D rings, if desired (**Figure 8**). Starting from 4-methoxyindole, the C ring was installed via a Bischler-Napieralski reaction to give a 3,4-dihydro-β-carboline. This intermediate was then subjected to an enantioselective, proline-catalyzed Mannich-Michael-type cyclization to install ring D and set the stereocenter at position 3. This step provided either the *S* enantiomer, ultimately leading to (-)-mitragynine (the natural isomer), or the *R* enantiomer, leading to the unnatural (+)-enantiomer. The ketone intermediates were then subjected to a Horner-Wadsworth-Emmons reaction, followed by reduction, formylation, and methylation to give (-)-mitragynine, (*Z*)-mitragynine, or (+)-mitragynine. A full discussion of the synthesis (performed by Andrew Kruegel) was reported by our group in the literature.¹⁷

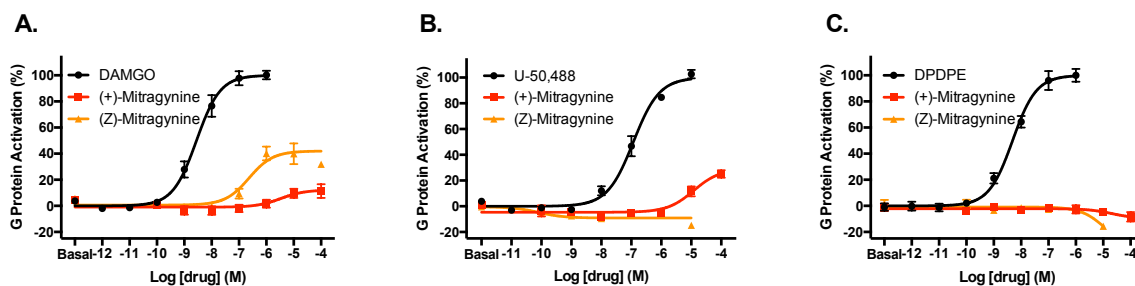


Figure 9. Agonist Activity of Unnatural Mitragynine Isomers at the Human Opioid Receptors. hMOR (A), hKOR (B), or hDOR (C) were co-expressed with G_{α_B} -RLuc8, β_1 , and mVenus- γ_2 to assay G protein activation. (*Z*)-mitragynine shows an $EC_{50} = 219 \pm 71$ nM and $E_{Max} = 38\%$ at hMOR. (+)-mitragynine shows weak partial agonism at hMOR and hKOR. Curves represent the average of $n \geq 3$, with error bars representing \pm SEM.

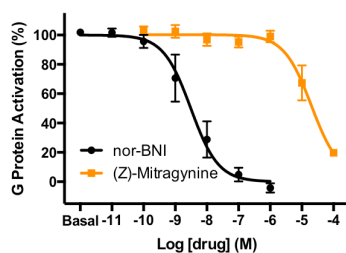


Figure 10. (Z)-Mitragynine is a Competitive Antagonist at hKOR. hKOR was co-expressed with $G\alpha_B$ -RLuc8, $\beta 1$, and mVenus- $\gamma 2$ to assay G protein activation. Curves represent the average of $n \geq 3$, with error bars representing \pm SEM.

data highlight that MOR appears more tolerant to changes in stereochemistry at the acrylate position than does KOR, as demonstrated by the identical potency at hMOR and weaker potency at hKOR for the Z-isomer. In contrast, (+)-mitragynine exhibited drastically different functional activity in comparison to the natural isomer (-)-mitragynine. While it was also a partial agonist at

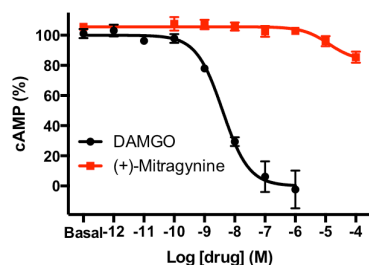


Figure 11. (+)-Mitragynine is a Partial Agonist at hKOR in the cAMP Inhibition Assay. hKOR was co-expressed with $G\alpha_B$, $\beta 1$, $\gamma 2$, and CAMYEL to assay forskolin-induced cAMP inhibition. Curves represent the average of $n \geq 3$, with error bars representing \pm SEM.

Functional Activity of Mitragynine Isomers. When measured for functional activity in the BRET-based assays for G protein activation, (Z)-mitragynine showed nearly identical activity at hMOR to (-)-mitragynine. Again, we observed partial agonism with an $EC_{50} \text{ hMOR} = 220 \pm 71 \text{ nM}$ and an $E_{\text{Max}} = 38\%$ (**Figure 9**). Also, similarly to (-)-mitragynine, (Z)-mitragynine was a weak KOR antagonist with $IC_{50} \text{ hKOR} = 42 \pm 15 \mu\text{M}$ (**Figure 10**). (Z)-Mitragynine showed no agonist or antagonist activity at hDOR (**Figure 9** and **Table 5**). These

data highlight that MOR appears more tolerant to changes in stereochemistry at the acrylate position than does KOR, as demonstrated by the identical potency at hMOR and weaker potency at hKOR for the Z-isomer. In contrast, (+)-mitragynine exhibited drastically different functional activity in comparison to the natural isomer (-)-mitragynine. While it was also a partial agonist at hMOR, it was an order of magnitude weaker in potency (**Figure 9**, $EC_{50} \text{ hMOR} = 3.3 \pm 1.1 \mu\text{M}$, $E_{\text{Max}} = 18\%$). This result makes sense as the active isomer (-)-mitragynine should be significantly more potent than the less active (+)-isomer. The agonist activity of (+)-mitragynine was confirmed in the cAMP inhibition assay (**Figure 11**). Interestingly, (+)-mitragynine showed weak partial agonism at KOR (**Figure 9**, $EC_{50} \text{ hKOR} = 9.1 \pm 4.3 \mu\text{M}$, $E_{\text{Max}} = 31\%$), which represents the first example of such activity amongst

the *Mitragyna* alkaloids. (+)-Mitragnine showed no agonist or antagonist activity at hDOR. It is

Table 5. Functional Activity of Mitragnine Isomers and Mitragnine Pseudoindoxyl (MP).

Compound	EC ₅₀ (E _{Max}) or [IC ₅₀] (μM)				
	hMOR	mMOR	hDOR	mDOR	hKOR
(+)-mitragnine	3.34 ± 1.1 (18%)	-	[>10]	-	9.1 ± 4.3 (31%)
(Z)-mitragnine	0.219 ± 0.071 (38%)	-	[>10]	-	[>10]
MP	0.0084 ± 0.0059 (52%)	0.0088 ± 0.0073 (23%)	0.029 ± 0.014 (15%)	0.01 ± 0.002 (50%)	[4.8 ± 2.3] A ₂ = 0.078 ± 0.031

Data represent mean ± SEM (μM) of n ≥ 3 from G protein activation assays. A₂ value determined through Schild analysis. “-“ represents not tested.

possible that isolating the (+)-isomer of 7-OH might have the same effect on functional activity and provide another KOR agonist while retaining better MOR potency than mitragnine itself. A *Mitragyna* alkaloid that is both a partial KOR and MOR agonist may have both antidepressant effects from MOR and non-addictive analgesic effects from KOR. A summary of functional activity of mitragnine isomers can be found in **Table 5**.

Mitragnine Pseudoindoxyl is an Interesting Pharmacological Tool

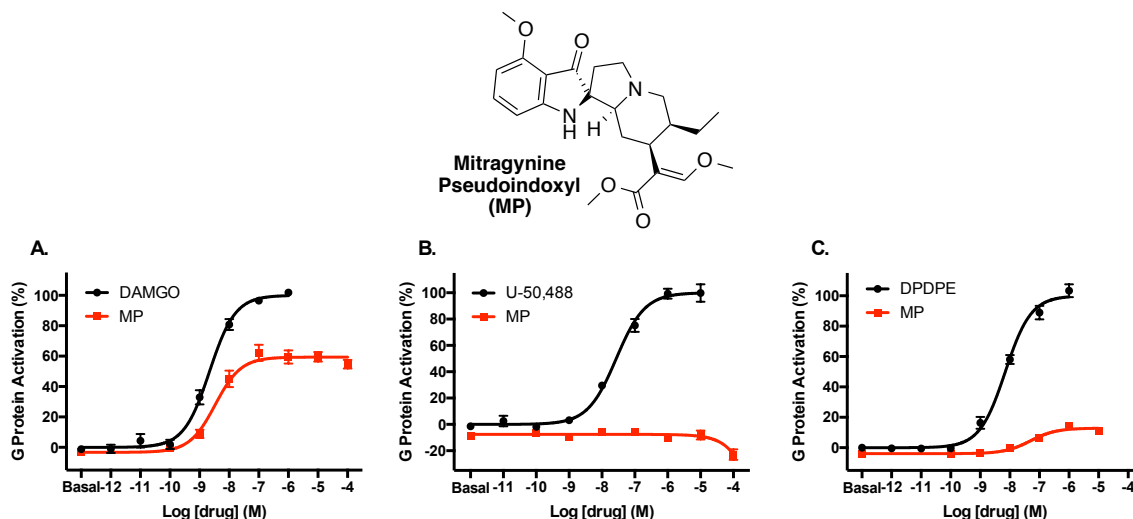


Figure 12. Agonist Activity of Mitragnine Pseudoindoxyl at the Human Opioid Receptors. hMOR (A), hKOR (B), or hDOR (C) were co-expressed with Gα_B-RLuc8, β1, and mVenus-γ2 to assay G protein activation. MP shows an EC₅₀ = 8.4 ± 5.9 nM (E_{Max} = 52%) at hMOR and an EC₅₀ = 29 ± 14 nM (E_{Max} = 15%) at hDOR. Curves represent the average of n ≥ 4, with error bars representing ± SEM.

Synthesis of Mitragynine Pseudoindoxyl. The rearrangement of 7-OH can lead to the formation of mitragynine pseudoindoxyl (MP), an alkaloid metabolite with a spiroketone moiety between rings B and C. Much like the other *Mitragyna* alkaloids, MP has been studied in terms of binding affinity at the opioid receptors (guinea pig brain) and analgesic properties, but no functional activity has been recorded to date.⁷ In fact, MP has been reported as a microbial metabolite of mitragynine.²⁵ MP can be prepared synthetically from 7-OH under refluxing basic conditions (performed by Andrew Kruegel, see **Experimental**). Although the yield is quite low, we were able to isolate enough material for use in the functional assays.

Functional Activity of Mitragynine Pseudoindoxyl. MP showed partial agonist activity at MOR in both human (**Figure 12**, $EC_{50 \text{ hMOR}} = 8.4 \pm 5.9 \text{ nM}$, $E_{\text{Max}} = 52\%$) and mouse (**Figure 13**, $EC_{50 \text{ mMOR}} = 8.8 \pm 7.3 \text{ nM}$, $E_{\text{Max}} = 23\%$) species with higher potency than 7-OH. In fact, this *Mitragyna* alkaloid derivative represents the most potent compound at the MOR tested in this series so far. Additionally, MP showed potent partial agonism at DOR in both human (**Figure 12**, $EC_{50 \text{ hDOR}} = 28.9 \pm 14 \text{ nM}$, $E_{\text{Max}} = 15\%$) and mouse species (**Figure 13**, $EC_{50 \text{ mDOR}} = 10.1 \pm$

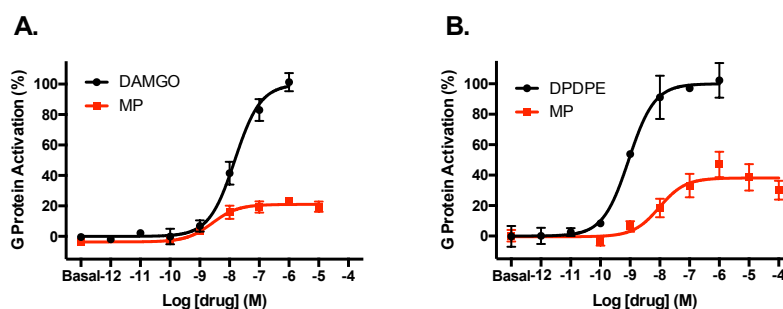


Figure 13. Agonist Activity of Mitragynine Pseudoindoxyl at the Mouse Opioid Receptors. mMOR (A) or mDOR (B) were co-expressed with $G\alpha_B$ -RLuc8, $\beta 1$, and mVenus- $\gamma 2$ to assay G protein activation. MP shows an $EC_{50} = 8.8 \pm 7.3 \text{ nM}$ ($E_{\text{Max}} = 23\%$) at mMOR and an $EC_{50} = 10 \pm 2 \text{ nM}$ ($E_{\text{Max}} = 50\%$) at mDOR. Curves represent the average of $n = 3$ with error bars representing \pm SEM.

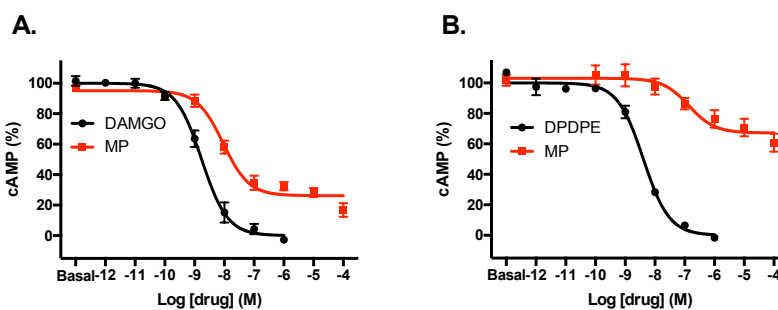


Figure 14. Agonist Activity of MP at the Human Opioid Receptors in the cAMP Inhibition Assay. hMOR (A) or hDOR (B) were co-expressed with $G\alpha_{OB}$, $\beta 1$, $\gamma 2$, and CAMYEL to assay inhibition of forskolin-induced cAMP production. Curves represent the average of $n \geq 3$, with error bars representing \pm SEM. $EC_{50}^{hMOR\ cAMP} = 8.7 \pm 3.6$ nM, $E_{Max} = 79\%$; $EC_{50}^{hDOR\ cAMP} = 65 \pm 11$ nM, $E_{Max} = 41\%$.

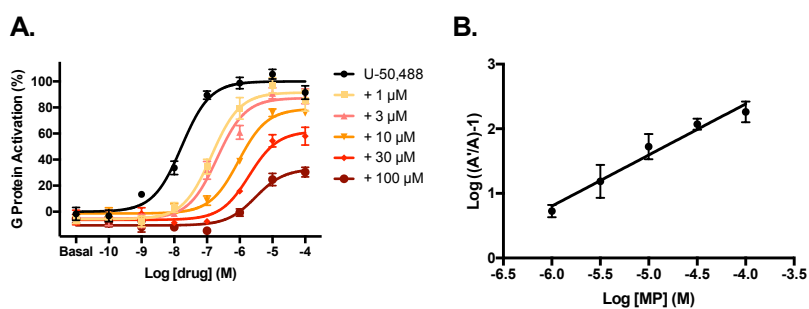


Figure 15. MP is an antagonist at hKOR. hKOR was co-expressed with $G\alpha_{OB}$ -RLuc8, $\beta 1$, and mVenus- $\gamma 2$ to assay G protein activation. Curves represent the average of $n = 4$, with error bars representing \pm SEM. A. Control agonist U-50,488 was incubated with increasing concentrations of MP. B. Schild plot of (A) reveals a competitive antagonist mode of action.

1.9 nM, $E_{Max} = 50\%$). The agonism was also confirmed in the cAMP inhibition assay (**Figure 14**). MP also acts as a KOR antagonist (**Table 5**, $IC_{50}^{hKOR} = 4.8 \pm 2.3$ μ M). This KOR antagonism was further quantified via Schild analysis, which revealed an A_2 of 77.6 ± 30.9 nM and slope of 0.84 (**Figure 15**). Interestingly, the E_{Max} of U-50,488 does seem to decrease with increasing concentrations of MP, which would indicate some complex inhibition (either non-competitive or uncompetitive). Given the increased potency observed at all three receptors by MP, it may represent an even more promising therapeutic lead in comparison to mitragynine itself, since a smaller dose should provide similar clinical effects. A summary of functional activity of mitragynine pseudoindoxyl can be found in **Table 5**.

Exploring G Protein Independent Signaling Pathways of *Mitragyna* Alkaloids

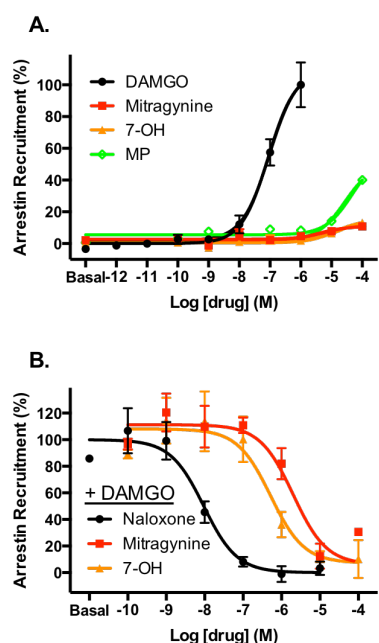


Figure 16. *Mitragyna* Alkaloids Are G Protein Biased. hMOR was co-expressed with Rluc8-arrestin3-Sp1, mem-linker-citrine-SH3, and GRK2. *Mitragyna* alkaloids were measured for their ability to recruit arrestin in the standard method (A) or the competitive method³³ (B). Data represent mean \pm SEM of $n \geq 3$. BRET GAP43 translocation assay used.

Mitragyna Alkaloids do not Signal Through

Arrestin. There is some evidence that functionally selective (or biased) agonists at the opioid receptors may offer promising analgesic or antidepressant effects without unwanted side effects from opioid signaling. It is not surprising to find that the search for functionally selective ligands is currently an active area of research.^{26–29}

Specifically there are reports that MOR agonists that signal exclusively through the G protein pathway and not the arrestin pathway (or a G protein biased agonist) avoid side effects such as constipation and respiratory depression, both thought to be mediated through arrestin signaling.³⁰

The benefit of G protein biased agonists is, however, not fully understood, as reports of reduced tolerance and addiction potential from unbiased MOR signaling are also

plentiful.^{31,32} (See Introductory Chapter 1 for further discussion). Given the need to understand the therapeutic potential of both G protein and arrestin signaling better, we were interested in testing the active *Mitragyna* alkaloids for their ability to recruit arrestin. We used our BRET GAP43 translocation assay to measure the levels of arrestin recruitment. In this assay (see **Figure 18** in Chapter 1), unmodified receptor is transfected along with arrestin-3 fused with luciferase and the SH3 binding domain, Sp1, along with the membrane protein GAP43 fused with the fluorescent protein citrine and an SH3 domain. Presumably, following receptor

activation and arrestin recruitment to the receptor, Sp1 and the SH3 domain will be in close enough proximity for binding, stabilizing a protein complex that allows BRET to occur between the luciferase and citrine molecules. When mitragynine, 7-OH, and MP were tested for arrestin recruitment, mitragynine and 7-OH showed little measurable arrestin activity, while MP showed 1-point activity (**Figure 16A**). These results were intriguing as it suggested that perhaps these *Mitragyna* alkaloids could in fact be G protein biased and offer beneficial therapeutic potential by eliminating some unwanted side effects in comparison to traditional opioids like morphine.

Calculating the Bias Factors of Mitragyna Alkaloids. In order to quantify the level of bias towards G protein for the *Mitragyna* alkaloids, it was necessary to fit the data using the Black-Leff operational model to get $\log(\tau/K_A)$, a measure of ligand bias (see Chapter 1 for further discussion). In performing these calculations, 7-OH and MP show a significant bias for G protein over arrestin, while mitragynine is closer to a neutral, unbiased ligand (**Table 6**). Given

Table 6. Calculated Bias Factors of *Mitragyna* Alkaloids.

Compound	Standard Method	Competitive Method
mitragynine	-0.066	1.3
7-OH	84	3.6
MP	321	-

Data represent mean \pm SEM (μ M) of $n \geq 3$ from arrestin translocation assays. Bias factors were calculated using the Black-Leff operational model. “-“ indicates not calculated.

the lower efficacy and potency of mitragynine in comparison to 7-OH for G protein activation, the calculated bias for mitragynine seems

reasonable. One issue with these calculations, however, is the obvious problem that there are no real curves for the compounds in the arrestin assay given the very low efficacy. In this case, the quantifications provided by the operational model may not be the most accurate, which ultimately obscures our understanding of the signaling. Laura Bohn has suggested a competitive method for analyzing functional selectivity, such that low efficacy compounds may be able to

inhibit the arrestin signal from a full, unbiased agonist, thus providing a full curve with which to use in the operational model calculations.³³ When mitragynine and 7-OH were utilized in antagonist mode for arrestin recruitment, they were both able to inhibit the arrestin recruitment from the control agonist DAMGO (**Figure 16B**). If these data are then fit with the operational model, the bias factors are much smaller than before (**Table 6**). Although both compounds do show a G protein bias when fit with the competitive mode, these changes are not significantly greater than the neutral control ligand. Given the large discrepancy in bias factors calculated in the two different methods, there is a greater need to study these ligands *in vivo* to measure their signaling in relevant cells for each physiological/behavioral effect (e.g., constipation, respiratory

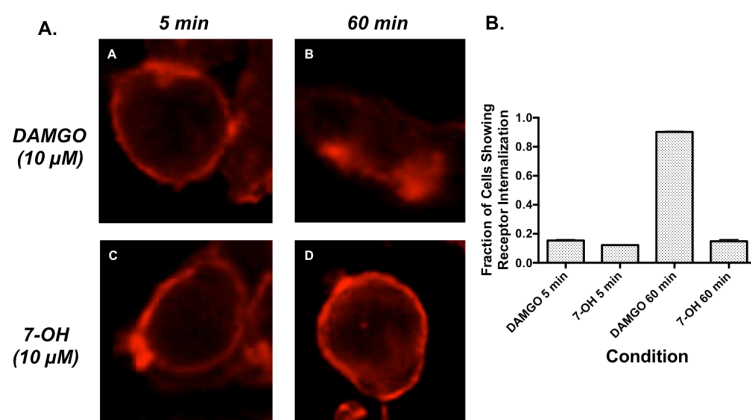


Figure 17. 7-OH Shows Less Receptor Internalization than DAMGO. The MOR internalization was imaged (A) using immunofluorescence and quantified (B). Compounds were used at 10 μM. Data represent one representative image of multiple independent experiments. On average, 30-60 cells were analyzed for each treatment per experiment (n = 2).

depression, tolerance development, dependence liability). Only with further testing will we understand how the different levels of bias in these compounds correlates to *in vivo* effects. As additional evidence to support the G protein bias of the compounds, 7-OH was assessed for its ability to cause receptor internalization in CHO cells stably expressing mMOR. Receptor internalization is mediated by arrestin signaling, therefore, a ligand that is G protein biased should, in theory, be unable to cause receptor internalization.^{34,35} Therefore, observing receptor internalization can be an indirect measure of arrestin signaling

from a ligand. Using immunofluorescence, 7-OH (10 μM) showed significantly less receptor internalization in comparison to DAMGO (10 μM) at 60 minutes (**Figure 17**). These receptor internalization measurements are in accord with the arrestin recruitment functional data and further support 7-OH as a G protein biased agonist.

Mitragynine Pseudoindoxyl is a Potential Imaging Agent

Mitragynine Pseudoindoxyl as an Imaging Agent. Interestingly, MP is a fluorescent

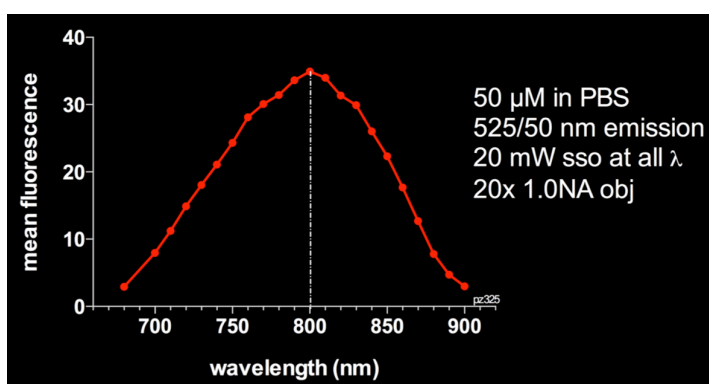


Figure 18. Two-photon Excitation Spectrum for MP. The maximum excitation peak for MP is 800 nm. Data obtained by Dr. Mark Sonders.

compound, and we hoped to utilize it as a tool to image opioid receptors *in vitro* or *in vivo*. Using two-photon microscopy, we first characterized the spectral properties of MP and found it to have a maximum excitation

peak at 800 nm (**Figure 18**). Unfortunately in solution, MP was not as brightly fluorescent as we had hoped, and high concentrations of the compound were necessary for experiments in cells.

In initial experiments in HEK cells transiently expressing the hMOR, there was significant background fluorescence coming from the cells. Looking to the media formulations used, it was determined that small amounts of riboflavin contained in all medias and produced endogenously by cells may have contributed to this observed autofluorescence as riboflavin's excitation and emission peaks overlap with that of MP (Emission = 525 nm). Instead of using normal Dulbecco's modified eagle media, Hank's Balanced Salt Solution was incubated with cells for the duration of imaging experiments to ensure that riboflavin would be minimized in

cells. Using this set-up, MP quickly labeled structures within all cells (**Figure 19A**). This staining, unfortunately, was not blocked by addition of the MOR antagonist naloxone. Further analysis of the cell culture being used revealed that only a small percentage of cells present actually expressed the receptor (**Figure 19B-C**). Therefore, it is unlikely that the compound is staining the cells in an MOR-dependent manner.

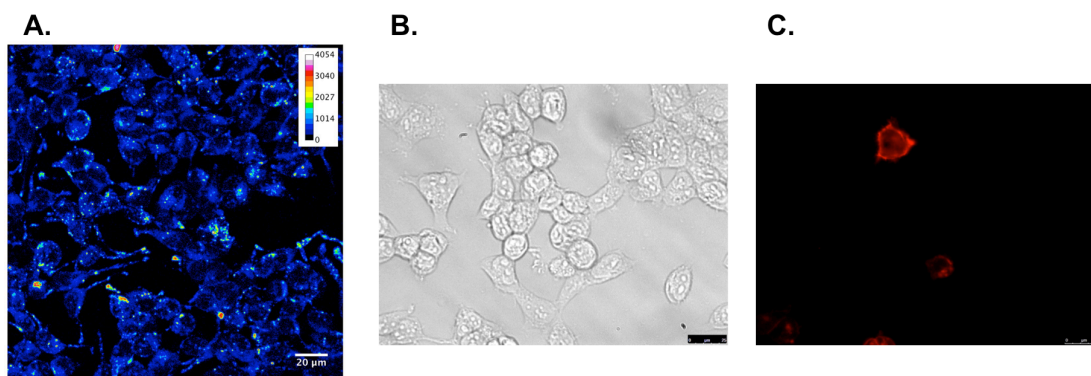


Figure 19. Two-Photon Imaging with MP. A. MP (10 μM) was bath applied to HEK cells transiently expressing hMOR and imaged (Ex 800 nm/Em 525 nm). Data obtained by Dr. Mark Sonders. The same cells were then fixed and immunostained for MOR. Brightfield (B) and MOR (red, C) images reveal low transfection efficiency. Data represent one representative image of multiple independent experiments.

However, we were quite intrigued by the rapid staining of cellular structures and looked to the fluorescence lifetime of the compound for explanation. The fluorescence lifetime of MP was different in phosphate buffered saline (3.5 ns) versus chloroform (4.7 ns). Given the greater fluorescence lifetime in an organic solvent (chloroform) versus an aqueous solvent (phosphate buffered saline), it is not surprising that MP might be able to quickly stain lipid rich, nonpolar membrane structures within the cells. In terms of the labeling, the staining pattern seemed most similar to that of a dye for the Golgi apparatus. To test his hypothesis, we co-localized MP with a spectrally separated sphingolipid dye known to stain the Golgi. After pretreating with the sphingolipid dye, MP rapidly stained what appeared to be the same, small intracellular structures but not the plasma membrane, showing some overlap with the sphingolipid dye (**Figure 20**).

While further experiments are required to better explain the biological mechanism of this staining, it is possible that MP does label the Golgi apparatus, as hypothesized. Interestingly, the sphingolipid dye required more than 30 minutes to selectively stain the golgi, while staining with MP required less than 1 minute, indicating a potential use for MP as a fast stain of cellular structures (the identity of which is currently being determined). It seems likely that these two dyes either stain the Golgi via distinct mechanisms or MP is staining a different cellular structure that overlaps well with the Golgi. Unfortunately the brightness of MP is relatively low, and high concentrations of the drug (~ 3 orders of magnitude higher than the EC_{50} at MOR) were necessary to obtain images. Therefore, the overall potential of MP as an MOR imaging agent is limited.

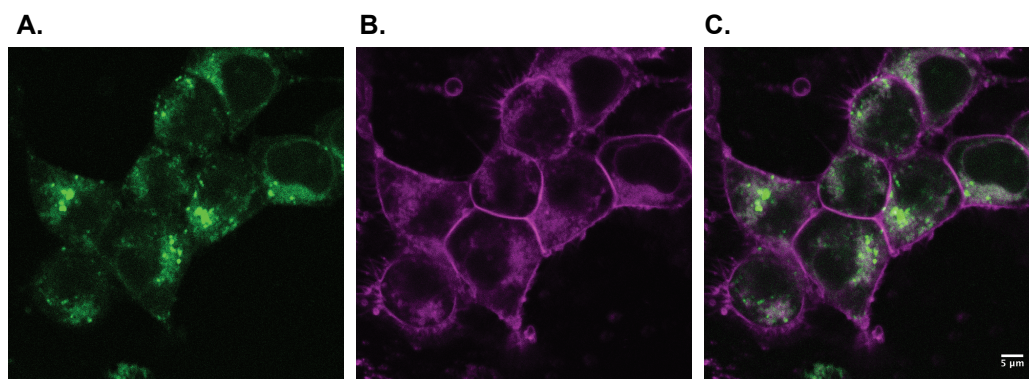


Figure 20. MP Co-localizes with Sphingolipid Golgi Stain. HEK cells expressing hMOR were incubated with MP (10 μ M) (A) before staining with Ceramide-bodipyTR sphingolipid golgi stain (B). C. Merge of the two images. Data represent one representative image of multiple experiments.

Molecular Docking of *Mitragyna* Alkaloids at the MOR

Mitragynine Scaffold has Unique Binding Pose at MOR. In order to better understand the unique biological activity and SAR of the *Mitragyna* alkaloids, preliminary docking studies can be reviewed that describe the alkaloids in the binding pocket of the agonist-bound X-ray crystal structure of mMOR (PDBID = 5C1M)³⁶ (**Figure 21**).¹⁷ The top-scored binding pose of orthosterically bound (-)-mitragynine partially overlapped with the binding pose of the co-

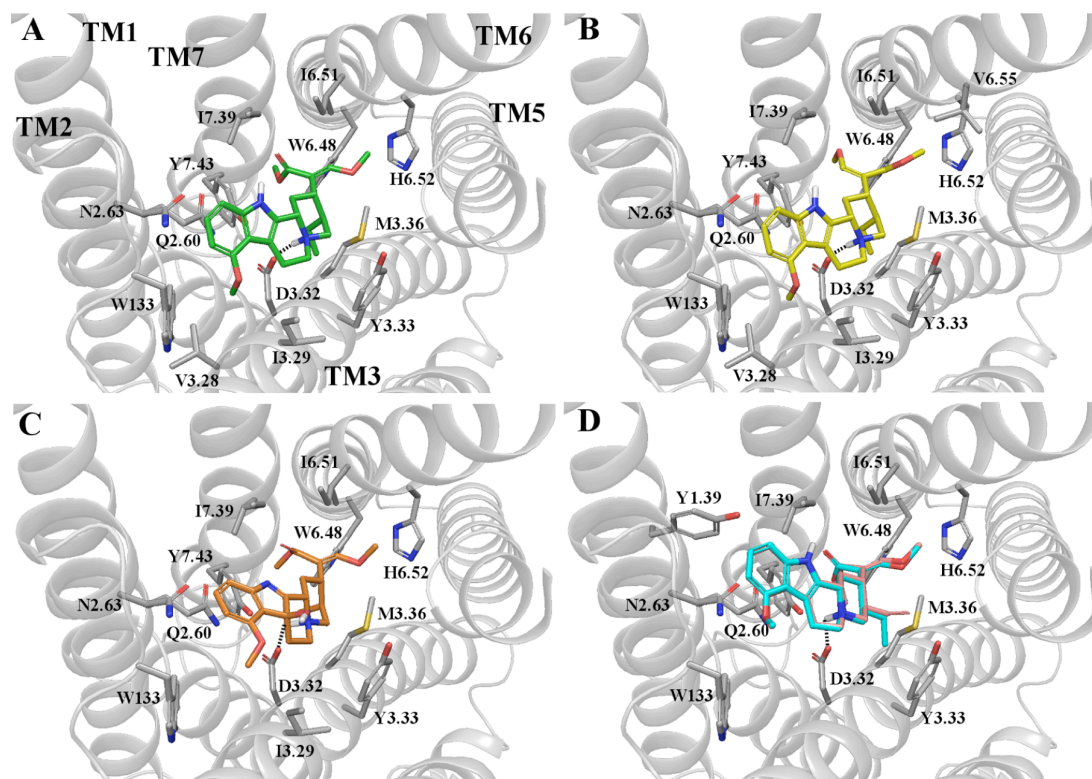


Figure 21. Docking of (-)-mitragynine and other analogs to the active μ -opioid receptor crystal structure. Top-scoring binding poses of (A) (-)-mitragynine, (B) (Z)-mitragynine, (C) 7-hydroxymitragynine, and (D) antagonists paynantheine (pink) and speciogynine (cyan). Only residue sidechains within 4 Å of the ligand are reported. Polar interactions are shown as dotted lines. TM helices are shown in cartoon representation (in gray). ECL2 and part of TM5 have been omitted for clarity. Residues are labeled using one-letter amino acid code and Ballesteros and Weinstein's generic numbering scheme. Data obtained by Dr. Marta Filizola.

crystallized morphinan derivative BU72, with some important exceptions (compare **Figure 21** to **Figure 22**). Even though there is a common polar interaction between the protonated amines in (-)-mitragynine and BU72 and D147^{3,32}, which is known to be required for binding of classical opioid agonists and antagonists^{36,37}, there are significant differences between other important ligand-receptor contacts. For example, in BU72 (**Figure 22**), the phenol occupies a hydrophobic pocket formed by TM5 and TM6 and also forms a water-mediated hydrogen bonding network with H297^{6,52}. This interaction is common to opioid ligands in the morphinan class.^{16,37,38} Our docking studies, however, suggest that the methoxyindole portion of (-)-mitragynine is

preferentially directed toward a different hydrophobic pocket formed by the residues of TM2 and TM3 (**Figure 21A**), which apparently has no way of forming an analogous hydrogen bonding network. Instead, the enol ether part of the β -methoxyacrylate of mitragynine appears to be directed into the same region as the phenol of BU72 (toward TM5 and TM6). Therefore, it seems that this functional group has a similar hydrogen bonding network with H297^{6,52}.

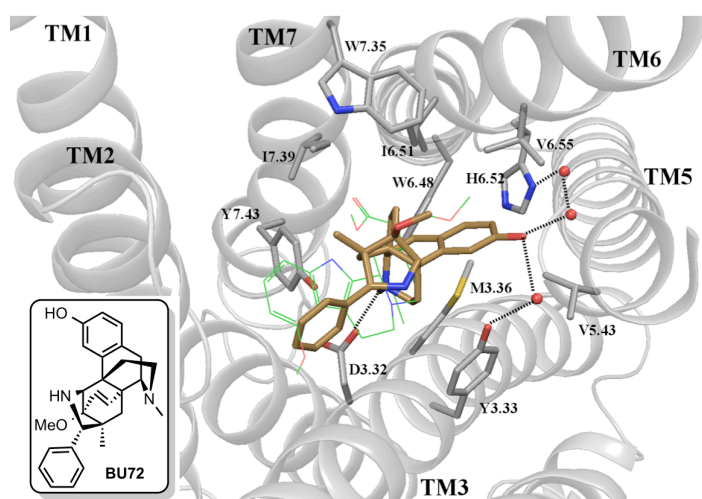


Figure 22. Top-scored docking pose of (-)-mitragynine (green) compared with agonist BU72 (brown) bound to active MOR crystal structure. Only residue sidechains within 4 Å of BU72 are reported. Polar interactions are depicted as dotted lines. Crystal waters are shown as red sphere. TM helices are shown in cartoon representation (in gray). ECL2 and part of TM5 have been omitted for clarity. Residues are labeled using one-letter amino acid code and Ballesteros and Weinstein's generic numbering scheme.⁸³ Data obtained by Dr. Marta Filizola. Inset: structure of BU72.

Docking of the other mitragynine isomers described above also produced results that were in agreement with the *in vitro* activity data. For instance, (-)-mitragynine and (Z)-mitragynine adopted a nearly identical binding pose, which is in accordance with the similar activities seen *in vitro* (**Figure 21**). Similarly, the predicted low-energy binding pose of 7-OH

was also comparable, with all key functionalities, including the acrylate, ethyl group, tertiary amine, and indole, occupying similar positions (**Figure 21C**). Remarkably, the hydroxy group in the 7-position does not appear to make close contacts with the surface of the receptor, and therefore, any potential hydrogen bonding interactions do not seem to be the cause of the significant increase in potency seen by 7-OH in comparison to mitragynine. Rather, there is a slight bend introduced to the core structure by this modification, which perhaps is more

important. Notably, 7-OH interacts with W293^{6,48} through both the ethyl and acrylate groups, while (-)-mitragynine interacts with this residue through its acrylate group only. While many different stereochemical configurations in the *Mitragyna* alkaloids studied appear to be sufficient to retain binding at hMOR, the absolute stereochemistry found in mitragynine is necessary for activation of the receptor. A full discussion on the binding poses of the natural and unnatural *Mitragyna* alkaloids can be found in our publication.¹⁷

Biological Activity of *Mitragyna* Alkaloids at Non-Opioid Receptors

Binding Affinity at Human α_2R . Given the reported binding of mitragynine at α_2Rs ¹³ (see **Introduction**), we were interested in exploring the pharmacology of *Mitragyna* alkaloids at other receptors in the CNS. Additionally the adrenergic receptors are known to mediate analgesic properties, particularly the receptors in the spinal cord³⁹, and therefore it was important to assess whether the *Mitragyna* alkaloids may impart some of their analgesic effects through the α_2R . Again in collaboration with PDSP, mitragynine and the other *Mitragyna* alkaloids were measured for their binding affinity at the human $\alpha_{2A}R$, $\alpha_{2B}R$, and $\alpha_{2C}R$ receptors using a

Table 7. Binding Affinity of *Mitragyna* Alkaloids at Adrenergic Receptors.

Compound	K_i (μM)		
	h α_{2A}	h α_{2B}	h α_{2C}
mitragynine	0.839 \pm 0.193	2.26 \pm 0.49	1.47 \pm 0.42
paynantheine	0.131 \pm 0.022	0.947 \pm 0.09	0.191 \pm 0.04
speciociliatine	1.54 \pm 0.15	2.74 \pm 0.66	1.68 \pm 0.42
speciogyne	0.119 \pm 0.031	1.21 \pm 0.11	0.288 \pm 0.107
7-OH	> 10	> 10	> 10

Data represent mean \pm SEM (μM) of $n \geq 3$. Data collected by the Psychoactive Drug Screening Program (PDSP).

radioligand binding assay. Mitragynine showed similar affinity for all three α_2Rs , while interestingly, 7-OH did not bind to any of the

them (**Table 7**). When assessing the three other natural *Mitragyna* alkaloids, paynantheine, speciociliatine, and speciogyne, there were notable differences in the binding affinities when compared to mitragynine or 7-OH (**Table 7**). Paynantheine and speciogyne showed much

tighter binding to the α_{2A} and the α_{2C} receptors in comparison to mitragynine (approximately 8-fold higher affinity at both receptors), with weaker binding at the α_{2B} receptor. In contrast, speciociliatine showed binding affinities similar to mitragynine at all three receptors (**Table 7**), suggesting perhaps that the stereoconfiguration at position 19 shared between the two compounds (see **Figure 8** above) could reduce affinity for binding at these adrenergic receptors.

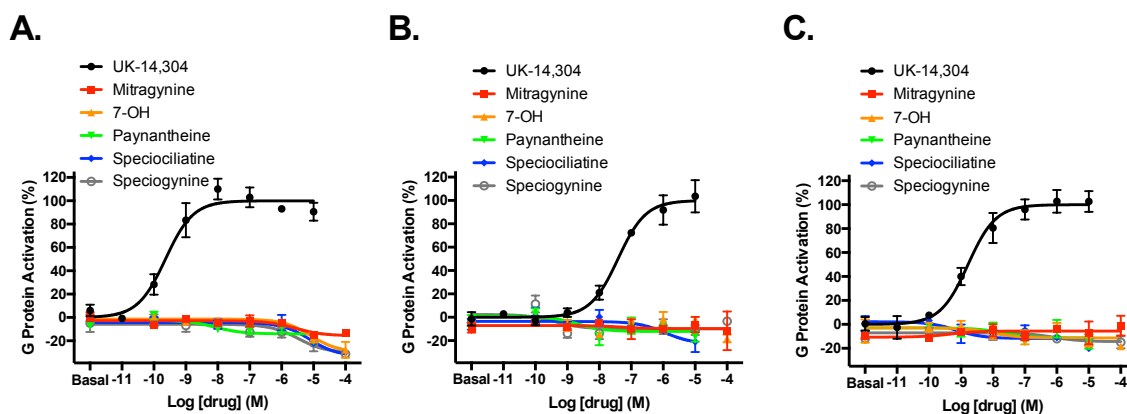


Figure 23. Agonist Activity of *Mitragyna* Alkaloids and 7-OH at the Human Adrenergic α_2 Receptors. $h\alpha_{2A}$ (A), $h\alpha_{2B}$ (B), or $h\alpha_{2C}$ (C) were co-expressed with $G\alpha_B$ -RLuc8, β_1 , and mVenus- γ_2 to assay G protein activation. Curves represent the average of $n = 3$, with error bars representing \pm SEM. Control agonist = UK-14,304.

Functional Activity at Human α_2R . The *Mitragyna* alkaloids were first assessed for their agonist activity at each of the three adrenergic receptors (**Figure 23**) using the BRET assay for G protein activation. Interestingly, none of the five compounds displayed any agonist activity at the three adrenergic α_2 receptors at concentrations up to 100 μ M. In contrast, when the *Mitragyna* alkaloids were tested for their ability to inhibit the signal of full agonist UK-14,304, interesting results emerged. At the α_{2A} receptor, mitragynine and speciociliatine were able to only weakly inhibit the agonist activity of UK-14,304 at the highest concentration tested (100 μ M), while paynantheine and speciogynine showed full inhibition (**Figure 24**). Paynantheine and speciogynine again showed antagonism at the adrenergic α_{2B} and α_{2C} receptors, though with weakest inhibition of the α_{2B} receptor. Mitragynine and speciociliatine showed inhibition only at

the 100 μM concentration at the adrenergic α_{2B} and α_{2C} receptors, and 7-OH was generally inactive at all three.

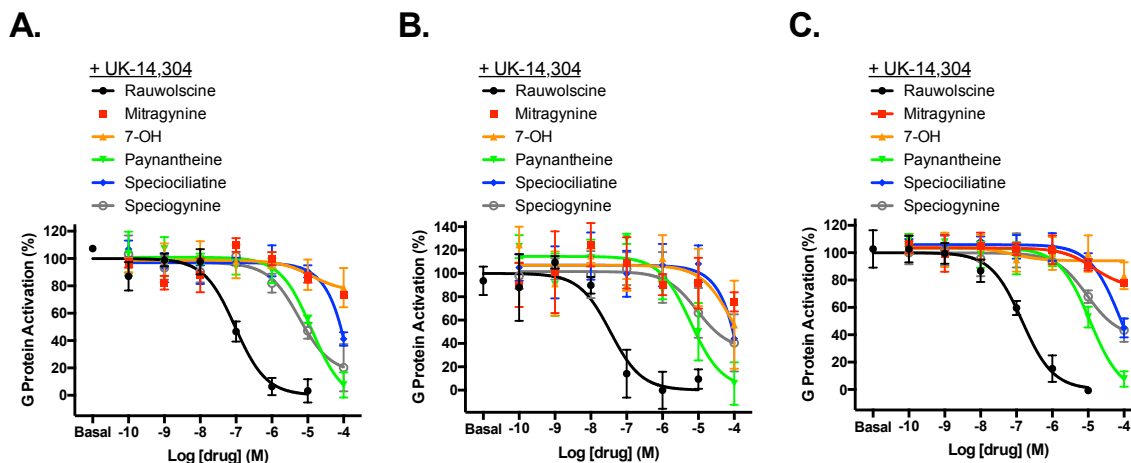


Figure 24. Antagonist Activity of *Mitragyna* Alkaloids and 7-OH at the Human Adrenergic α_2 Receptors. $h\alpha_{2A}$ (A), $h\alpha_{2B}$ (B), or $h\alpha_{2C}$ (C) were co-expressed with $G\alpha_{\text{B}}\text{-RLuc8}$, β_1 , and $m\text{Venus-}\gamma_2$ to assay G protein activation. Curves represent the average of $n \geq 3$, with error bars representing \pm SEM. Competitive inhibition of UK-14,304, positive control = Rauwolscine.

These results are in line with the binding affinities measured for the three receptors. Mitragynine and speciociliatine generally showed minimal antagonism, supporting their weak

binding affinities in

Table 4. Functional Activity of *Mitragyna* Alkaloids at Adrenergic Receptors.

Compound	IC_{50} (μM)		
	$h \alpha_{2A}$	$h \alpha_{2B}$	$h \alpha_{2C}$
mitragynine	> 10	> 10	> 10
paynantheine	> 10	> 10	6.3 ± 1.4
speciociliatine	> 10	> 10	> 10
speciogynine	> 10	> 10	4.5 ± 1.9
7-OH	X	X	X

Data represent mean \pm SEM (μM) of $n \geq 3$ from G protein activation assays. "X" indicates not active.

comparison to the other

alkaloids, and

paynantheine and

speciogynine (with

tighter binding affinity),

in contrast, showed

measurable inhibition at the three adrenergic α_2 receptors. The functional data at these receptors

match quite well with the binding affinities measured and do suggest that some effects in the

plant material itself may be mediated through the adrenergic effects of the less prevalent alkaloids (**Table 8**).

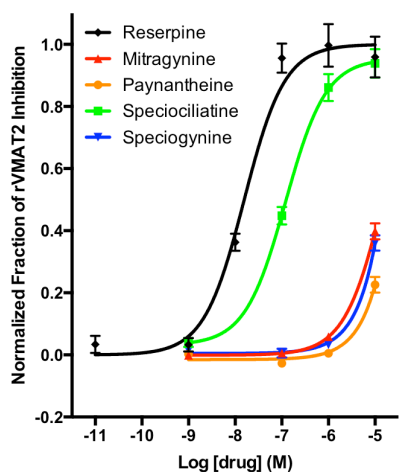


Figure 25. Speciociliatine is a Rat VMAT2 Inhibitor. The *Mitragyna* alkaloids were measured for their ability to inhibit specific uptake of FFN206 at rat VMAT2 in HEK-293 cells. Data represent mean \pm SEM of $n > 4$ independent experiments. Data obtained by Yekaterina Kovalyova.

Functional Activity at Vesicular Monoamine

Transporter 2 (VMAT2). We also wanted to assess the functional activity of the *Mitragyna* alkaloids at the monoamine transporters, given their connection to mechanisms of depression (see **Introductory Chapter 1** or **Discussion** below). All *Mitragyna* alkaloids except speciociliatine were unable to inhibit rat VMAT2 at concentrations less than 100 μ M (**Figure 25**).

Speciociliatine was able to inhibit VMAT2 with an $IC_{50} = 121 \pm 28$ nM, consistent with its structural similarity to reserpine (stereoconfiguration of the rings C and D are identical), a typical VMAT2 inhibitor. All of the *Mitragyna*

alkaloids were inactive at the human dopamine transporter (DAT), human serotonin transporter (SERT), and human norepinephrine transporter (NET) (data not shown).

Discussion

Opioid Activity of Mitragyna Alkaloids. These studies represent the first thorough examination of the *Mitragyna* alkaloids at the opioid receptors. Previous reports relied heavily on binding affinities, as well as *ex vivo* effects in guinea pig ileum, an anatomical area rich with opioid receptors, and *in vivo* analgesic effects in the tail flick assay.⁷ By simply assuming the agonist activity of the alkaloids as fact, much of the subtle signaling nuances were missed.

Takayama and co-workers recently collaborated with researchers at Mount Sinai to develop functional assays for their mitragynine analogs.¹⁵ Using the [³⁵S]GTP γ S binding assay (see Chapter 1 for more detail), they were able to measure the functional activity of a few semi-synthetic mitragynine analogs, however even with the technology available, the researchers chose not to confirm the functional activity of the parent *Mitragyna* alkaloids. Thus, the functional activity of the *Mitragyna* alkaloids has not been examined in detail to date. In this study, mitragynine and 7-OH were found to be partial agonists at the human MOR and antagonists at the human KOR. As partial agonists, the compounds are able to elicit analgesic effects perhaps without the need to fully activate the receptor. This functional activity could potentially offer a way to safely consume the plant material with a lesser risk of overdosing.^{3,40-42} For example, the partial MOR agonist buprenorphine is an effective analgesic that has a ceiling (maximum effect) in respiratory depression and is therefore perhaps a safer pain therapeutic in comparison to classical opioids morphine or fentanyl (see Chapter 4 for further discussion of buprenorphine).⁴³ Additionally the KOR antagonism was both surprising and intriguing as a therapeutic option for depression. The *in vivo* reports on KOR antagonists^{18,44} suggest they may provide some antidepressant activity, which is only beginning to be studied in clinical trials.²⁰ As dual MOR agonists/KOR antagonists, both mitragynine and 7-OH may be able to combat pain and depression simultaneously (again see buprenorphine), offering a promising lead for the development of new therapeutics. Often times, those suffering from chronic pain succumb to feelings of depression, making pharmacological management difficult.⁴⁵ Therefore these types of dual therapeutics could find use in a diverse subset of patients. There were also similar activities measured with (Z)-mitragynine, as well as MP, which may both be additional leads to explore further. The other natural alkaloids, paynantheine, speciociliatine, and speciogynine, on the other

hand, showed only competitive antagonism at the human opioid receptors. As the first study on the functional activity of these alkaloids at human receptors, this work provides a better insight into the physiological effects of kratom and how these compounds might be translated into meaningful therapeutics for human use.

G Protein Bias of Three Alkaloids. Interestingly, both mitragynine, 7-OH, and MP showed no apparent ability to recruit arrestin. As more examples of G protein-biased agonists continue to emerge at the opioid receptors, there is a need to better understand their signaling in relevant cells. As Laura Bohn highlights in a recent paper, there is not yet a clear connection between how *in vitro* bias results translate *in vivo* (see Chapter 5 for further discussion).²⁶ If the G protein biased MOR agonists hold the answer to offering analgesic relief without respiratory depression, constipation, or tolerance development⁴⁶, then we may be emerging into a new age of opioid therapeutics where they can be used clinically with less concern for serious side effects. Trevena has developed one such drug, TRV130, developed as a G protein-biased MOR agonist, that is showing promising results in the clinic,^{30,47} (see Chapter 4 for further discussion on this compound). Rigorous analysis of the data using the operational model in two different experimental set-ups showed 7-OH mitragynine to exhibit bias for the G protein pathway over the arrestin pathway, suggesting that even partial agonists, which may not be detected in the less sensitive arrestin assay, can still be identified as biased. However, it remains to be demonstrated that the pharmacological functional selectivity observed for this compound may translate to measurable physiological effects *in vivo*.

Mitragyna Alkaloids Have a Unique Binding Pose at MOR. In furthering our study of the *Mitragyna* alkaloids, we looked to find a structural basis for the unique biological activity observed *in vitro*. Computational models, while not as definitive as an x-ray crystal structure

obtained with bound ligand, offer an important insight into drug-receptor interactions. If computational results are reliable, then binding poses might help to explain pharmacological activity from drugs and even allow the design of new analogs for synthesis (when methods come to a point where the connections between the receptor and the physiology can be made through the many levels of complexity). In comparing the top-scored pose of mitragynine with morphinoid BU72 (**Figure 22**), it was clear that the two compounds do not adopt the same binding position within the MOR, indicating that it is possible the two compounds may stabilize different features of the binding pocket, which ultimately lead to distinct signaling cascades. These differences in binding pose may lead to insights in terms of the links between the binding and the receptor activation and signaling (e.g., explain why mitragynine has only partial agonism at MOR and is G protein biased). Additionally, 7-OH had a slightly altered binding pose even compared to mitragynine. Again, this may explain the increased potency observed *in vitro* for 7-OH and the G protein bias. Given the level to which the computational docking confirms much of the *in vitro* results observed, it is possible that better analogs might be virtually designed that can target the various signaling pathways of interest. Additionally, given the unexpected KOR antagonism, it may be worth exploring computational modeling at this receptor, as well, which may provide a means to tune functional activities in both receptors with future analogs.

Variation Between Rodent and Human Data. It has been widely accepted that mitragynine acts as an MOR agonist. However, given the variable results obtained here in regards to mitragynine at the mouse and human MOR, there is some uncertainty in interpreting the literature on the analgesic properties of *Mitragyna* alkaloids using animal models. The partial hMOR agonist activity of mitragynine can likely explain its analgesic effects in humans, but the interpretation of literature reports on analgesic effects elicited by this compound in rodent

models is now unclear, given the observation here of purely antagonistic effects from mitragynine at rodent opioid receptors *in vitro*. Another possibility is that the functional assays utilized here are not sensitive enough to detect very low efficacy partial agonist activity (on the order of <10% E_{Max}). With downstream signaling amplification, these compounds could have a larger effect *in vivo*. As a very low efficacy partial agonist, mitragynine would still largely inhibit the activation by DAMGO, making its functional activity appear to be that of an antagonist.

7-OH as a Natural Alkaloid of Mitragyna speciosa. Although it has been published that 7-OH is an isolatable alkaloid from the plant material, we found no evidence to support this claim, other than trace amounts measurable by mass spectrometry. Given the apparent lack of 7-OH measurable in the different strains of kratom leaves tested, it seems unlikely that 7-OH is a major constituent in the effects of the plant material in humans. A few possibilities may help to explain the inconsistencies, however. As discussed in the **Results**, 7-OH might just be present only in particular strains of kratom or oxidized from mitragynine directly in the presence of sunlight and atmospheric oxygen. These hypotheses are more likely than one where mitragynine is metabolized directly to 7-OH. Mitragynine has some metabolic stability *in vitro* (liver microsomes, simulated intestinal fluid), and in fact there is evidence suggesting that 7-OH can actually metabolize back into mitragynine.⁴⁸ Therefore it seems likely that mitragynine is the main alkaloid responsible for the effects of kratom.

Pharmacological Consequences of Adrenergic Activity. To understand the non-opioid biological activity of the *Mitragyna* alkaloids, it is helpful to revisit some closely related indole alkaloids that are structurally similar. Yohimbine (**Figure 26**), for instance, isolated from the bark of *Pausinystalia johimbe* and *Rauvolfia* evergreen trees, was first extracted in 1896 and has

been the focus of many total syntheses and is used in a veterinary setting to reverse anesthetic sedation, among many other uses.^{49–52} Known as one of the yohimban alkaloids, yohimbine is reported to bind to the adrenergic receptors (both α_1 and α_2), as well as serotonin receptors and

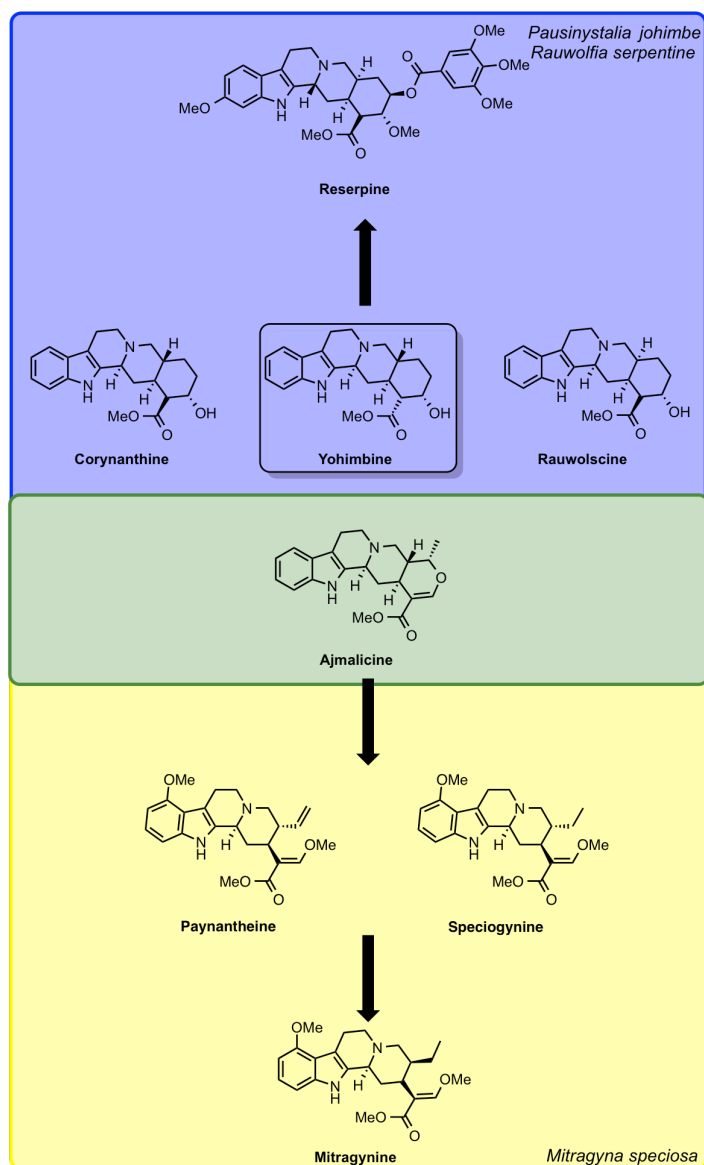


Figure 26. Structures of Indole Alkaloids Closely Related to Mitragynine. Classical yohimban alkaloids share some structural features with the *Mitragyna* alkaloids. Yohimban alkaloid ajmalicine is shared by both *Rauwolfia* and *Mitragyna* plants.

dopamine receptors.^{53,54} Other diastereomers of yohimbine include corynanthine and rauwolscine (**Figure 26**), both of which bind to similar biological targets. If the E ring of yohimbine is further elaborated, with cis stereoconfiguration between the D and E rings as well as the opposite stereoconfiguration at position 3, the structure of reserpine (**Figure 26**) emerges, which was also isolated from the roots of *Rauwolfia serpentine* in 1952⁵⁵ and then synthesized by R.B. Woodward in 1958.⁵⁶ Reserpine has been used in India to treat insanity and snakebites for centuries and was an influential

player in the biogenic amine hypothesis for treating depression due to its inhibition of the vesicular monoamine transporter (VMAT)⁵⁷; in the early days of use, reserpine treatment in some patients and animals caused depressive-like symptoms, which was later correlated to decreased stores of presynaptic norepinephrine, serotonin, and dopamine leading to the biogenic amine hypothesis (see Introductory Chapter 1 for further discussion).⁵⁸ Functionally speaking, this structure is also moving away from adrenergic receptor activity. With the cis stereoconfiguration between the D and E rings, mitragynine has the stereoconfiguration of isoreserpine (epimer of reserpine with inverted C-3 center) at the C-D rings. This difference could explain why mitragynine is not an inhibitor of VMAT (see **Figure 26** above). When the E ring of yohimbine is instead opened, the structure of the *Mitragyna* alkaloids emerge, first with the structures of paynantheine and speciogynine, which share the same trans configuration between rings D and E as yohimbine (**Figure 26**), and then with the opposite stereochemistry at position 19 to provide the structure of mitragynine. The stereocenter of the tetrahydrocarboline (position 3) remains the same in comparison to yohimbine. Indeed, the connection between yohimban alkaloids and *Mitragyna* alkaloids is clear, as the two plants even share alkaloids in common, such as ajmalicine (**Figure 26**).^{1,59} Although their biological activity is varied and diverse, these indole alkaloids share structural features that can be traced back to their biosynthesis in the plants. The *Mitragyna* alkaloids are unique in their functional activity at the opioid receptors, but perhaps it is their structural similarity to the yohimban alkaloids that accounts for some of their non-opioid activity. In particular, the stereochemical similarity of yohimbine with paynantheine and speciogynine at position 3 could explain these alkaloids' increased potency at the α_2 Rs.

It has been widely reported that α_2 R agonists have therapeutic potential in pain management.⁶⁰ Since many of the *Mitragyna* alkaloids tested here were found to bind to these α_2 adrenergic receptors, their functional activity was explored further. Interestingly, no agonist activity was found for the compounds at any of the α_2 Rs, which indicates that the analgesic properties of the kratom plant are likely mediated through the MOR, as the functional data shows. Some of the alkaloids, however, exhibited antagonism at the α_2 Rs, specifically paynantheine and speciogynine. Clinically, there are studies of α_2 R antagonists having antidepressant effects⁶¹⁻⁶⁴, suggesting that perhaps the reported antidepressant effects of the kratom plant⁶⁵ may be mediated through the alkaloids' modulation of both the opioid receptors and the α_2 Rs. However other conflicting reports conclude that in fact, α_2 R agonists have antidepressant effects^{66,67}, which implicates an unclear therapeutic role for these receptors in depression. There are additional reports of α_2 R antagonist effects on precipitated withdrawal. For example, yohimbine has been shown both clinically and in animal models to reduce the effects of precipitated withdrawal from opioid dependence and the addictive potential of MOR agonists in mice.⁶⁸⁻⁷⁰ Unfortunately, there are some conflicting reports. For instance, in mice, while one study reports that yohimbine reduces the symptoms of opioid withdrawal and dependence without effects on analgesia⁷⁰, a second report finds yohimbine co-treatment with morphine to eliminate antinociceptive effects.⁷¹ In a separate study, yohimbine treatment in opioid-dependent patients elicited withdrawal symptoms and an increase in cravings for opioids (methadone)⁷², while α_2 R agonists have separately been reported to precipitate and shorten withdrawal symptoms in comparison to methadone administration.⁷³ Although the results vary, there still does seem to be more indication in literature of benefit from α_2 R antagonists in treating opioid addiction, which could have important implications in the context of the *Mitragyna* alkaloids. A

recent study in humans noted that daily doses of kratom (tea consumption) for 7 days resulted in a maximum plasma concentration of mitragynine around 250 nM.⁷⁴ Therefore, the combined α_2 R antagonistic effects of mitragynine, paynantheine, and speciogynine in a sample of kratom may be enough to elicit some effects on withdrawal. In fact, kratom has been widely used for treating opioid withdrawal¹, which may be due in part to the α_2 R antagonists effects of some of the alkaloids. It is important to note, however, that a plasma concentration of 250 nM is quite low and is likely at a lower concentration in the brain. Additionally, given the low potency of mitragynine at the α_2 Rs and the even lower concentration of the alkaloids paynantheine and speciogynine in samples of kratom, it is unclear how much the adrenergic receptors are actually being modulated by these alkaloids through kratom consumption. Nonetheless the polypharmacology of these compounds is rich and interesting: agonism at MOR can provide both analgesic relief and antidepressant effects, while the partial efficacy at MOR and α_2 R antagonism may simultaneously offer a safer withdrawal from opioid addiction. Certainly, more conclusive studies should be published, however some *Mitragyna* alkaloids in the kratom plant may perhaps be useful tools to study these receptor effects. For instance, behavioral studies *in vivo* in mice lacking either the MOR or individual α_2 adrenergic receptors may shed light on the pharmacological profile of the *Mitragyna* alkaloids in depression and addiction. Given these findings, the effects of raw *Mitragyna* alkaloid extracts in humans may be quite complex. However, if individual alkaloids are instead isolated for therapeutics, they are likely to have more selective effects.

Conclusions

In this chapter, we characterized for the first time the *Mitragyna* alkaloids at the human opioid receptors and found surprisingly that mitragynine and 7-OH mitragynine were partial MOR agonists and KOR antagonists with weak antagonist effects at DOR. Additionally some isomers of mitragynine as well as MP were characterized in functional assays and helped to reveal important areas of the scaffold that appear to be tolerant to changes in stereochemistry. These studies will aid in future structure activity relationship explorations. Given the biological activity of these alkaloids, they hold great promise therapeutically, either isolated or together in the kratom plant material. As a first report of human functional activity of the *Mitragyna* alkaloids, this work will better inform both users of the plant material and medical professionals regarding the risks and potential benefits of kratom consumption.

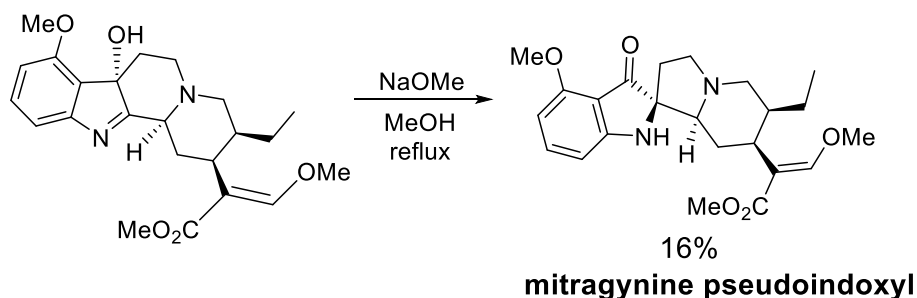
Experimental

Chemistry

General Considerations. Reagents and solvents were obtained from commercial sources and were used without further purification unless otherwise stated (including anhydrous solvents). All reactions were performed in flame-dried glassware under an argon atmosphere unless otherwise stated, and monitored by TLC using solvent mixtures appropriate to each reaction. All column chromatography was performed on silica gel (40-63 μ m). For compounds containing a basic nitrogen, Et₃N was often used in the mobile phase in order to provide better resolution. In these cases, TLC plates were pre-soaked in the Et₃N-containing solvent and then allowed to dry briefly before use in analysis, such that an accurate representation of R_f was obtained. Nuclear magnetic resonance spectra were recorded on 400 or 500 MHz instruments as indicated. Chemical shifts are reported as δ values in ppm referenced to CDCl₃ (¹H NMR = 7.26

and ^{13}C NMR = 77.16) or $(\text{CD}_3)_2\text{SO}$ (^1H NMR = 2.50 and ^{13}C NMR = 39.52). Multiplicity is indicated as follows: s (singlet); d (doublet); t (triplet); q (quartet); dd (doublet of doublets); dt (doublet of triplets); td (triplet of doublets); m (multiplet); br (broad). In some cases, spectra are complicated by the presence of multiple conformers, resulting in peak broadening or additional splitting. As a result of these effects, multiple peaks may correspond to the same proton group or carbon atom. When possible, this is indicated by an "and" joining two listed peaks or spectral regions. All carbon peaks are rounded to one decimal place unless such rounding would cause two close peaks to become identical. In these cases, two decimal places are retained. Low-resolution mass spectra (LRMS) were recorded on a quadrupole mass spectrometer (ionization mode: APCI+ or ESI+). High-resolution mass spectra (HRMS) were recorded on a quadrupole time-of-flight mass spectrometer (ionization mode: ESI+).

Scheme 1. Synthesis of mitragynine pseudoindoxyl (MP).



Mitragynine pseudoindoxyl (MP) = methyl (*E*)-2-((2*S*,6'*S*,7'*S*,8*a*'*S*)-6'-ethyl-4-methoxy-3-oxo-2',3',6',7',8',8*a*'-hexahydro-5'*H*-spiro[indoline-2,1'-indolizin]-7'-yl)-3-methoxyacrylate. A fresh solution of sodium methoxide was prepared by dissolving Na metal (7.6 mg, 0.330 mmol) in anhydrous MeOH (5.6 mL) at room temperature. To this solution was then added 7-hydroxymitragynine (62.2 mg, 0.150 mmol) and the yellow solution was refluxed for 4.5 h (incomplete conversion). After cooling to room temperature, the reaction was diluted

with water (20 mL) and extracted with Et₂O (3 x 20 mL). The combined organics were washed with water (10 mL) and brine (10 mL), dried over Na₂SO₄, and concentrated to provide a brown foam (60 mg). This material was purified by repeated preparative TLC (1 mm silica layer, 20 x 20 cm plates; **Plate 1:** Et₂O + 2% Et₃N; **Plate 2:** 7:3 CH₂Cl₂:Et₂O; **Plate 3:** Et₂O + 2% Et₃N) to provide spirocyclic product **5** as a foamy yellow solid (9.9 mg, 16%). Spectral properties matched those previously reported.^{9,75} **¹H NMR (500 MHz, CDCl₃)** δ 7.31 (t, *J* = 8.1 Hz, 1H), 7.28 (s, 1H), 6.40 (d, *J* = 8.1 Hz, 1H), 6.13 (d, *J* = 8.1 Hz, 1H), 5.11 (br s, 1H), 3.89 (s, 3H), 3.66 (s, 3H), 3.62 (s, 3H), 3.12 (br s, 2H), 2.77 (d, *J* = 12.1 Hz, 1H), 2.41 – 2.28 (m, 2H), 2.28 – 2.08 (m, 3H), 1.90 (br s, 1H), 1.64 (br s, 1H), 1.51 (br s, 1H), 1.23 – 1.16 (m, 1H), 1.16 – 1.08 (m, 1H), 0.85 (t, *J* = 7.4 Hz, 3H); **¹³C NMR (126 MHz, CDCl₃)** δ 199.6, 169.0, 162.2, 160.4, 158.7, 138.8, 125.7, 111.8, 103.9, 99.2, 75.3, 73.4, 61.6, 55.8, 54.9, 53.3, 51.3, 40.2, 38.5, 35.2, 23.9, 19.4, 13.0; **LR-MS** calcd. for C₂₃H₃₁N₂O₅⁺ [M+H]⁺ 415.22, found 416.36.

Biological Procedures

Materials: BRET. HEK-293T cells were obtained from the American Type Culture Collection (Rockville, MD) and were cultured in a 5% CO₂ atmosphere at 37 °C in Dulbecco's Modified Eagle Medium (high glucose #11965; Life Technologies Corp.; Grand Island, NY) supplemented with 10% FBS (Premium Select, Atlanta Biologicals; Atlanta, GA) and 100 U/mL penicillin and 100 µg/mL streptomycin (#15140, Life Technologies).

DNA Constructs. The mouse MOR (mMOR), the mouse DOR (mDOR), and the rat KOR (rKOR) were provided by Dr. Lakshmi Devi at Mount Sinai Hospital. The hMOR, hDOR, hKOR, hα_{2A}R, hα_{2B}R, hα_{2C}R and GRK2 were obtained from the Missouri S&T Resource Center. The human G protein constructs used here have been previously described and were provided by C. Galés or were obtained from the Missouri S&T Resource Center unless otherwise

noted.^{12,13} The G proteins used included untagged $G\alpha_{oB}$ ($G\alpha_{oB}$); $G\alpha_{oB}$ with Renilla luciferase 8 (RLuc8) inserted at position 91 ($G\alpha_{oB}$ -RLuc8); $G\beta_1$ (β_1); untagged $G\gamma_2$ (γ_2); $G\gamma_2$ which we fused to the full-length mVenus at its N-terminus via the amino acid linker GSAGT (mVenus- γ_2). The plasmids employed in the arrestin recruitment assay, RLuc8-arrestin3-Sp1 and mem-linker-citrine-SH3, were synthesized in-house as previously described.⁷⁶ YFP-Epac-RLuc (CAMYEL) was obtained from ATCC (no. MBA-277).⁷⁷ All constructs were sequence-confirmed prior to use in experiments.

Transfection. The following cDNA amounts were transfected into HEK-293T cells (5×10^6 cells/plate) in 10-cm dishes using polyethylenimine (PEI) in a 1:1 ratio (diluted in Opti-MEM, Life Technologies): **G protein activation:** 2.5 μ g MOR/DOR/KOR, 0.125 μ g $G\alpha_{oB}$ -RLuc8, 6.25 μ g β_1 , 6.25 μ g mVenus- γ_2 ; **cAMP Inhibition:** 1.25 μ g MOR/DOR/KOR, 1.25 μ g $G\alpha_{oB}$, 1.25 μ g β_1 , 1.25 μ g γ_2 , 10 μ g CAMYEL; **BRET GAP43 translocation:** 2 μ g hMOR, 0.25 μ g RLuc8-arrestin3-Sp1, 5 μ g mem-linker-citrine-SH3, 5 μ g GRK2. Cells were maintained in the HEK-293T media described above. After 24 hours the media was changed, and the experiment was performed 24 hours later (48 hours after transfection).

BRET. Transfected cells were dissociated and re-suspended in phosphate-buffered saline (PBS). Approximately 200,000 cells/well were added to a black-framed, white well 96-well plate (#60050; Perkin Elmer; Waltham, MA). The microplate was centrifuged and the cells were re-suspended in PBS. For agonist experiments, after 5 minutes, 5 μ M of the luciferase substrate coelenterazine H was added to each well. After 5 minutes, ligands were added and the BRET signal was measured 5 minutes later on a PHERAstar FS plate reader. For cAMP, cells were first incubated with forskolin (1 μ M) for 5 minutes prior to coelenterazine h addition. For antagonist competition experiments, cells were pre-incubated with the antagonist at varying concentrations

for 30 minutes. Coelenterazine H (5 μ M) was then added to each well for 5 minutes. Following coelenterazine H incubation, a fixed concentration of the reference agonist (5x EC₅₀) was added, and the BRET signal was measured at 30 minutes on a PHERAstar FS plate reader. The BRET signal was quantified by calculating the ratio of the light emitted by the energy acceptor, mVenus (510-540 nm) or citrine (510-540 nm), over the light emitted by the energy donor, RLuc8 (485 nm). This drug-induced BRET signal was normalized using the E_{max} of [D-Ala², N-Me-Phe⁴, Gly-ol⁵]-enkephalin (DAMGO), [D-Pen(2,5)]enkephalin (DPDPE), or U-50,488 as the maximal response at MOR, DOR, and KOR respectively. Dose response curves were fit using a three-parameter logistic equation in GraphPad Prism 6.

Materials: Mouse K_i Determination. IBNtxA and [¹²⁵I]BNtxA were synthesized at MSKCC as previously described.⁷⁸⁻⁸⁰ Na¹²⁵I was purchased from Perkin-Elmer (Waltham, MA).

Radioligand Competition Binding Assays with Mouse Receptors (performed at Memorial Sloan Kettering Cancer Center by Dr Susruta Majumdar). [¹²⁵I]BNtxA binding was carried out in membranes prepared from Chinese Hamster Ovary (CHO) cells stably expressing murine clones of MOR, DOR, and KOR, as previously described.^{78,80,81} Assays were performed at 25 °C for 90 min in 50 mM potassium phosphate buffer, pH 7.4, containing 5 mM magnesium sulfate. After the incubation, the reaction was filtered through glass-fiber filters (Whatman Schleicher & Schuell, Keene, NH) and washed three times with 3 mL of ice-cold 50 mM Tris-HCl, pH 7.4, on a semiautomatic cell harvester. Nonspecific binding was defined by addition of levallorphan (8 μ M) to matching samples and was subtracted from total binding to yield specific binding. K_i values were calculated by nonlinear regression analysis (GraphPad Prism, San Diego, CA). Protein concentrations were determined using the Lowry method with BSA as the standard.⁸²

Human K_i Determination. Binding constants (K_i) at the human opioid receptors were generously determined using radioligand displacement experiments by the National Institute of Mental Health's Psychoactive Drug Screening Program, Contract #HHSN-271-2008-00025-C (NIMH PDSP). The NIMH PDSP is Directed by Bryan L. Roth MD, PhD at the University of North Carolina at Chapel Hill and Project Officer Jamie Driscoll at NIMH, Bethesda, MD, USA. For experimental details please refer to the PDSP website (<https://pdspdb.unc.edu/pdspWeb/>). In all cases, the reported K_i values are the average of 3 or more independent experiments, each run with triplicate wells for each ligand concentration.

Imaging. 2P or confocal imaging with MP was performed on a Prairie Ultima or Leica SP5 upright microscopes equipped with either the Coherent Chameleon or MaiTai laser, respectively. Images were obtained using a 20x objective at 800 nm excitation wavelength. A 525/50 nm emission filter was used. Drugs were applied via bath application. The BODIPY Tr Ceramide dye was purchased from Thermo Fisher Scientific (#D7540).

Immunofluorescence. mMOR-CHO cells were grown in Ham's F-12 supplemented with 10% FBS, 100 U/mL penicillin and 100 μ g/mL streptomycin, and 200 μ g/mL hygromycin B prior to the experiment. The cells were starved with serum free media for 3-5 hours before treatment with drugs (10 μ M) for 5 min or 1 hr. Cells were then fixed with 4% formaldehyde in PBS, washed with PBS, permeabilized (0.25% Triton X-100 in PBS), washed, blocked (2% glycine, 2% bovine serum albumin in 50 mM NH_4Cl) for 30 min at 37 °C and incubated overnight with anti-MOR antibodies (1:200 in blocking solution; Abcam #ab134054) at 4 °C. Cells were then washed 5X with PBS, blocked again for 30 min at 37 °C, and incubated with a mixture of anti-rabbit Alexa Fluor[®] 594 secondary antibody (1:1000 in blocking solution; Cell

Signaling #8889) and Hoechst stain (1:10,000). The cells were then washed 5X in PBS and imaged on a Leica DMI400B microscope.

Inhibition of VMAT2. A HEK cell line stably expressing rVMAT2 (VMAT2-HEK) was kindly provided by Professor Robert Edwards of the Department of Neurology at the University of California San Francisco (UCSF). Cells were cultured in a 5% CO₂ atmosphere at 37 °C in DMEM + GlutaMAX (Invitrogen #10569) supplemented with 10% FBS (Atlanta Biologicals) and 100 U/mL penicillin and 100 µg/mL streptomycin.

rVMAT2-HEK cells were seeded at a density of 0.04-0.05 x 10⁶ cells per well in black flat-bottom 96-well plates and incubated in growth medium at 37 °C for approximately 3 days to reach confluence. On the day of the experiment, the complete growth medium was aspirated, wells were washed with 200 µL PBS, and treated with 100 µL/well experimental medium (DMEM without phenol red containing 25 mM HEPES and 1% FBS) with DMSO (vehicle), the control inhibitor reserpine of varying concentrations, or experimental compound of varying concentrations. The cells were incubated for 30 min at 37 °C. FFN206 (100 µL/well of 1.5 µM solution in experimental medium) was added to each well and incubated for 60 min at 37 °C. The experimental medium was aspirated, 120 µL of PBS was added to each well, and the cells were incubated for another 20 min at 37 °C. The experiment was terminated by replacement with 120 µL fresh PBS into each well. The fluorescence uptake in cells was immediately recorded using a BioTek H1MF plate reader (3x3 area scan, bottom read mode) with excitation and emission wavelengths set at 368 nm and 464 nm, respectively. Extent of inhibition was determined as the difference between signal and basal measurements: mean fluorescence uptake of FFN206 (with DMSO vehicle) minus that in the presence of the experimental compound. These values were

normalized to reserpine (100% inhibition) to yield a normalized fraction of inhibition. Dose response curves were fit using a three-parameter logistic equation in GraphPad Prism 6.

Calculations

Operational Model Ligand Bias Calculations. $\text{Log}(\tau/K_A)$ for individual data sets was estimated using a GraphPad Prism program developed by Robert Lane. For full agonists, the $\text{Log}K_A$ values were set to zero. E_{Max} , n (Hill slope), and basal values were shared across all data sets. It was important to use the calculated $\text{Log}K_A$ (functional affinity) from the data sets, since experimental binding affinity may not account for multiple active receptor conformations. The calculated $\text{Log}(\tau/K_A)$ were then converted into bias factors as shown in the Chapter 1 (Equations 2 and 3).

References

- (1) Adkins, J. E.; Boyer, E. W.; McCurdy, C. R. *Mitragyna Speciosa*, a Psychoactive Tree from Southeast Asia with Opioid Activity. *Curr. Top. Med. Chem.* **2011**, *11*, 1165–1175.
- (2) Cinosi, E.; Martinotti, G.; Simonato, P.; Singh, D.; Demetrovics, Z.; Roman-Urrestarazu, A.; Bersani, F. S.; Vicknasingam, B.; Piazzon, G.; Li, J. H.; Yu, W. J.; Kapitány-Fövényi, M.; Farkas, J.; Di Giannantonio, M.; Corazza, O. Following “the Roots” of Kratom (*Mitragyna Speciosa*): The Evolution of an Enhancer from a Traditional Use to Increase Work and Productivity in Southeast Asia to a Recreational Psychoactive Drug in Western Countries. *Biomed Res. Int.* **2015**, *2015*.
- (3) Tanguay, P. Kratom in Thailand: Decriminalisation and Community Control? *Legis. Reform Drug Policies* **2011**, 16pp.
- (4) Takayama, H. Chemistry and Pharmacology of Analgesic Indole Alkaloids from the Rubiaceae Plant, *Mitragyna Speciosa*. *Chem. Pharm. Bull.* **2004**, *52*, 916–928.
- (5) Raffa, R. B.; Beckett, J. R.; Brahmabhatt, V. N.; Ebinger, T. M.; Fabian, C. A.; Nixon, J. R.; Orlando, S. T.; Rana, C. A.; Tejani, A. H.; Tomazic, R. J. Orally Active Opioid Compounds from a Non-Poppy Source. *J. Med. Chem.* **2013**.
- (6) Matsumoto, K. Pharmacological Studies on 7-Hydroxymitragynine, Isolated from the Thai Herbal Medicine *Mitragyna Speciosa*: Discovery of an Orally Active Opioid Analgesic, Chiba University, 2006.
- (7) Takayama, H.; Ishikawa, H.; Kurihara, M.; Kitajima, M.; Aimi, N.; Ponglux, D.; Koyama, F.; Matsumoto, K.; Moriyama, T.; Yamamoto, L. T.; Watanabe, K.; Murayama, T.; Horie, S. Studies on the Synthesis and Opioid Agonistic Activities of Mitragynine-Related Indole Alkaloids: Discovery of Opioid Agonists Structurally Different from Other Opioid

- Ligands. *J. Med. Chem.* **2002**, *45*, 1949–1956.
- (8) Léon, F.; Habib, E.; Adkins, J. E.; Furr, E.; McCurdy, C. R.; Cutler, S. Phytochemical Characterization of the Leaves of *Mitragyna Speciosa* Grown in U.S.A. *Nat. Prod. Communications* **2009**, *4*, 907–910.
 - (9) Ponglux, D.; Wongseripipatana, S.; Takayama, H.; Kikuchi, M.; Kurihara, M.; Kitajima, M.; Aimi, N.; Sakai, S. A New Indole Alkaloid, 7 α -Hydroxy-7H-Mitragynine, from *Mitragyna Speciosa* in Thailand. *Planta Med.* **1994**, *60*, 580–581.
 - (10) Matsumoto, K.; Horie, S.; Ishikawa, H.; Takayama, H.; Aimi, N.; Ponglux, D.; Watanabe, K. Antinociceptive Effect of 7-Hydroxymitragynine in Mice: Discovery of an Orally Active Opioid Analgesic from the Thai Medicinal Herb *Mitragyna Speciosa*. *Life Sci.* **2004**, *74*, 2143–2155.
 - (11) Matsumoto, K.; Mizowaki, M.; Suchitra, T.; Takayama, H.; Sakai, S.; Aimi, N.; Watanabe, H. Antinociceptive Action of Mitragynine in Mice: Evidence for the Involvement of Supraspinal Opioid Receptors. *Life Sci.* **1996**, *59*, 1149–1155.
 - (12) Macko, E.; Weisbach, J. A.; Douglas, B. Some Observations on the Pharmacology of Mitragynine. *Arch. Int. Pharmacodyn. Thérapie* **1972**, *198*, 145–161.
 - (13) Boyer, E. W.; Babu, K. M.; Adkins, J. E.; McCurdy, C. R.; Halpern, J. H. Self-Treatment of Opioid Withdrawal Using Kratom (*Mitragynia Speciosa* Korth). *Addiction* **2008**, *103*, 1048–1050.
 - (14) Matsumoto, K.; Mizowaki, M.; Suchitra, T.; Murakami, Y.; Takayama, H.; Sakai, S.; Aimi, N.; Watanabe, H. Central Antinociceptive Effects of Mitragynine in Mice: Contribution of Descending Noradrenergic and Serotonergic Systems. *Eur. J. Pharmacol.* **1996**, *317*, 75–81.
 - (15) Matsumoto, K.; Narita, M.; Muramatsu, N.; Nakayama, T.; Misawa, K.; Kitajima, M.; Tashima, K.; Devi, L. A.; Suzuki, T.; Takayama, H.; Horie, S. Orally Active Opioid M/ δ Dual Agonist MGM-16, a Derivative of the Indole Alkaloid Mitragynine, Exhibits Potent Antiallodynic Effect on Neuropathic Pain in Mice. *J. Pharmacol. Exp. Ther.* **2014**, *348*, 383–392.
 - (16) Dale, O.; Ma, G.; Gemelli, C.; Husni, A.; McCurdy, C.; Avery, B.; Leon, J.; Furr, E.; Manly, S.; Cutler, S. Effects of Mitragynine and Its Derivatives on Human Opioid Receptors (Delta, Kappa, and Mu). *Planta Med.* **2012**, *78*, P_91.
 - (17) Kruegel, A. C.; Gassaway, M. M.; Kapoor, A.; Váradi, A.; Majumdar, S.; Filizola, M.; Javitch, J. A.; Sames, D. Synthetic and Receptor Signaling Explorations of the *Mitragyna* Alkaloids: Mitragynine as an Atypical Molecular Framework for Opioid Receptor Modulators. *J. Am. Chem. Soc.* **2016**, *138*, 6754–6764.
 - (18) Li, W.; Sun, H.; Chen, H.; Yang, X.; Xiao, L.; Liu, R.; Shao, L.; Qiu, Z. Major Depressive Disorder and Kappa Opioid Receptor Antagonists. *Transl. Perioper. pain Med.* **2015**, *1*, 4–16.
 - (19) Mague, S. D.; Pliakas, A. M.; Todtenkopf, M. S.; Tomasiewicz, H. C.; Zhang, Y.; Stevens, W. C.; Jones, R. M.; Portoghese, P. S.; Carlezon, W. A. Antidepressant-like Effects of Kappa-Opioid Receptor Antagonists in the Forced Swim Test in Rats. *J. Pharmacol. Exp. Ther.* **2003**, *305*, 323–330.
 - (20) Buda KJ, Carroll FI, Kosten TR, D. S. D. W. B. A Double-Blind, Placebo-Controlled Study to Evaluate the Safety, Tolerability, and Pharmacokinetics of Single, Escalating Oral Doses of JD_Tic in Healthy Male Subjects. *Neuropsychopharmacology* **2015**, *40*, 1–7.
 - (21) Thongpradichote, S.; Matsumoto, K.; Tohda, M.; Takayama, H.; Aimi, N.; Sakai, S.;

- Watanabe, H. Identification of Opioid Receptor Subtypes in Antinociceptive Actions of Supraspinally-Administered Mitragynine in Mice. *Life Sci.* **1998**, *62*, 1371–1378.
- (22) Kervinen, J.; Crysler, C.; Bayoumy, S.; Abad, M. C.; Spurlino, J.; Deckman, I.; Greco, M. N.; Maryanoff, B. E.; de Garavilla, L. Potency Variation of Small-Molecule Chymase Inhibitors across Species. *Biochem. Pharmacol.* **2010**, *80*, 1033–1041.
- (23) Govindaraj, R. G.; Manavalan, B.; Basith, S.; Choi, S. Comparative Analysis of Species-Specific Ligand Recognition in Toll-like Receptor 8 Signaling: A Hypothesis. *PLoS One* **2011**, *6*.
- (24) Burlingham, B. T.; Widlanski, T. S. An Intuitive Look at the Relationship of K_i and IC_{50} : A More General Use for the Dixon Plot. *J. Chem. Educ.* **2003**, *80*, 214.
- (25) Zarembo, J. E.; Douglas, B.; Valenta, J.; Weisbach, J. A. Metabolites of Mitragynine. *J. Pharm. Sci.* **1974**, *63*, 1407–1415.
- (26) Luttrell, L. M.; Maudsley, S.; Bohn, L. M. Fulfilling the Promise of “Biased” G Protein-Coupled Receptor Agonism. *Mol. Pharmacol.* **2015**, *88*, 579–588.
- (27) Kyle, D. J. Functionally Biased Agonism of Mu and Kappa Opioid Receptors. *ACS Symp. Ser.* **2013**, *1131*, 177–197.
- (28) Pradhan, A. A.; Smith, M. L.; Kieffer, B. L.; Evans, C. J. Ligand-Directed Signalling within the Opioid Receptor Family. *Br. J. Pharmacol.* **2012**, *167*, 960–969.
- (29) Raehal, K. M.; Schmid, C. L.; Groer, C. E.; Bohn, L. M. Functional Selectivity at the Mu-Opioid Receptor: Implications for Understanding Opioid Analgesia. *Pharmacol. Rev.* **2011**, *63*, 1001–1019.
- (30) DeWire, S. M.; Yamashita, D. S.; Rominger, D. H.; Liu, G.; Cowan, C. L.; Graczyk, T. M.; Chen, X.-T.; Pitis, P. M.; Gotchev, D.; Yuan, C.; Koblish, M.; Lark, M. W.; Violin, J. D. A G Protein-Biased Ligand at the μ -Opioid Receptor Is Potently Analgesic with Reduced Gastrointestinal and Respiratory Dysfunction Compared with Morphine. *J. Pharmacol. Exp. Ther.* **2013**, *344*, 708–717.
- (31) Finn, A. K.; Whistler, J. L. Endocytosis of the Mu Opioid Receptor Reduces Tolerance and a Cellular Hallmark of Opiate Withdrawal. *Neuron* **2001**, *32*, 829–839.
- (32) Berger, A. C.; Whistler, J. L. Morphine-Induced Mu Opioid Receptor Trafficking Enhances Reward yet Prevents Compulsive Drug Use. *EMBO Mol. Med.* **2011**, *3*, 385–397.
- (33) Stahl, E. L.; Zhou, L.; Ehlert, F. J.; Bohn, L. M. A Novel Method for Analyzing Extremely Biased Agonism at G Protein-Coupled Receptors. *Mol. Pharmacol.* **2015**, *87*, 866–877.
- (34) Groer, C. E.; Tidgewell, K.; Moyer, R. a; Harding, W. W.; Rothman, R. B.; Prisinzano, T. E.; Bohn, L. M. An Opioid Agonist That Does Not Induce M-Opioid Receptor--Arrestin Interactions or Receptor Internalization. *Mol. Pharmacol.* **2007**, *71*, 549–557.
- (35) Groarke, D. A.; Wilson, S.; Krasell, C.; Milligan, G. Visualization of Agonist-Induced Association and Trafficking of Green Fluorescent Protein-Tagged Forms of Both β -Arrestin-1 and the Thyrotropin- Releasing Hormone Receptor-1. *J. Biol. Chem.* **1999**, *274*, 23263–23269.
- (36) Huang, W.; Manglik, A.; Venkatakrishnan, A. J.; Laeremans, T.; Feinberg, E. N.; Sanborn, A. L.; Kato, H. E.; Livingston, K. E.; Thorsen, T. S.; Kling, R. C.; Granier, S.; Gmeiner, P.; Husbands, S. M.; Traynor, J. R.; Weis, W. I.; Steyaert, J.; Dror, R. O.; Kobilka, B. K. Structural Insights into M-Opioid Receptor Activation. *Nature* **2015**, *524*, 315–321.

- (37) Manglik, A.; Kruse, A. C.; Kobilka, T. S.; Thian, F. S.; Mathiesen, J. M.; Sunahara, R. K.; Pardo, L.; Weis, W. I.; Kobilka, B. K.; Granier, S. Crystal Structure of the M-Opioid Receptor Bound to a Morphinan Antagonist. *Nature* **2012**, *485*, 321–326.
- (38) Hedberg, M. H.; Johansson, A. M.; Fowler, C. J.; Terenius, L.; Hacksell, U. Palladium-Catalyzed Synthesis of C3-Substituted 3-Deoxymorphines. *Bioorg. Med. Chem. Lett.* **1994**, *4*, 2527–2532.
- (39) Fairbanks, C. A.; Stone, L. S.; Wilcox, G. L. Pharmacological Profiles of Alpha 2 Adrenergic Receptor Agonists Identified Using Genetically Altered Mice and Isobolographic Analysis. *Pharmacol. Ther.* **2009**, *123*, 224–238.
- (40) Rech, M. A.; Donahey, E.; Cappiello Dziedzic, J. M.; Oh, L.; Greenhalgh, E. New Drugs of Abuse. *Pharmacotherapy* **2015**, *35*, 189–197.
- (41) Babu, K. M.; McCurdy, C. R.; Boyer, E. W. Opioid Receptors and Legal Highs: Salvia Divinorum and Kratom. *Clin Toxicol* **2008**, *46*, 146–152.
- (42) Trakulsrichai, S.; Tongpo, A.; Sriapha, C.; Wongvisawakorn, S.; Rittilert, P.; Kaojarern, S.; Wananukul, W. Kratom Abuse in Ramathibodi Poison Center, Thailand: A Five-Year Experience. *J. Psychoactive Drugs* **2013**, *45*, 404–408.
- (43) Dahan, A.; Yassen, A.; Romberg, R.; Sarton, E.; Teppema, L.; Olofsen, E.; Danhof, M. Buprenorphine Induces Ceiling in Respiratory Depression but Not in Analgesia. *Br. J. Anaesth.* **2006**, *96*, 627–632.
- (44) Bruchas, M. R.; Yang, T.; Schreiber, S.; Defino, M.; Kwan, S. C.; Li, S.; Chavkin, C. Long-Acting Kappa Opioid Antagonists Disrupt Receptor Signaling and Produce Noncompetitive Effects by Activating c-Jun N-Terminal Kinase. *J. Biol. Chem.* **2007**, *282*, 29803–29811.
- (45) Hooten, W. M. Chronic Pain and Mental Health Disorders: Shared Neural Mechanisms, Epidemiology, and Treatment. *Mayo Clin. Proc.* **2016**, *91*, 955–970.
- (46) Violin, J. D.; Crombie, A. L.; Soergel, D. G.; Lark, M. W. Biased Ligands at G-Protein-Coupled Receptors: Promise and Progress. *Trends Pharmacol. Sci.* **2014**, *35*, 308–316.
- (47) Viscusi, E. R.; Webster, L.; Kuss, M.; Daniels, S.; Bolognese, J. A.; Zuckerman, S.; Soergel, D. G.; Subach, R. A.; Cook, E.; Skobieranda, F. A Randomized, Phase 2 Study Investigating TRV130, a Biased Ligand of the Mu-Opioid Receptor, for the Intravenous Treatment of Acute Pain. *Pain* **2016**, *157*, 264–272.
- (48) Manda, V. K.; Avula, B.; Ali, Z.; Khan, I. A.; Walker, L. A.; Khan, S. I. Evaluation of in Vitro Absorption, Distribution, Metabolism, and Excretion (ADME) Properties of Mitragynine, 7-Hydroxymitragynine, and Mitraphylline. *Planta Med.* **2014**, *80*, 568–576.
- (49) Ishidate, M.; Okada, M.; Saito, K. Isolation of Alkaloids from *Rauwolfia* Spp. *Pharm. Bull.* **1955**, *3*, 319–320.
- (50) Van Tamelen, E. E.; Shamma, M.; Burgstahler, A. W.; Wolinsky, J.; Tamm, R.; Aldrich, P. E. Total Synthesis of Yohimbine. *J. Am. Chem. Soc.* **1969**, *91*, 7315–7333.
- (51) Van Wyk, B. E. A Review of Commercially Important African Medicinal Plants. *J. Ethnopharmacol.* **2015**, *176*, 118–134.
- (52) Wong, A. H.; Smith, M.; Boon, H. S. Herbal Remedies in Psychiatric Practice. *Arch. Gen. Psychiatry* **1998**, *55*, 1033–1044.
- (53) Petrash, A. C.; Bylund, D. B. Alpha-2 Adrenergic Receptor Subtypes Indicated by [³H]yohimbine Binding in Human Brain. *Life Sci.* **1986**, *38*, 2129–2137.
- (54) Winter, J. C.; Rabin, R. A. Yohimbine as a Serotonergic Agent: Evidence from Receptor Binding and Drug Discrimination. *J. Pharmacol. Exp. Ther.* **1992**, *263*, 682–689.

- (55) Poisson, J.; Le Hir, A.; Goutarel, R.; Janot, M. [Isolation of Reserpine from Roots of *Rauwolfia Vomitoria* Afz]. *Comptes rendus Hebd. des séances l'Académie des Sci.* **1954**, *238*, 1607–1609.
- (56) Woodward, R. B.; Bader, F. E.; Bickel, H.; Frey, A. J.; Kierstead, R. W. The Total Synthesis of Reserpine. *Tetrahedron* **1958**, *2*, 1–57.
- (57) Schildkraut, J. J.; Kety, S. S. Biogenic Amines and Emotion. *Science* **1967**, *156*, 21–37.
- (58) Barchas, J. D.; Altemus, M. Monoamine Hypotheses of Mood Disorders. In *Basic neurochemistry: Molecular, Cellular, and Medical Aspects*; Lippincott-Raven: Philadelphia, 1999.
- (59) Klohs, M. W.; Draper, M. D.; Keller, F.; Malesh, W.; Petracek, F. J. Alkaloids of *Rauwolfia Serpentina* Benth. II. 1 The Isolation of Naturally Occurring Py-Tetrahydroserpentine (Ajmalicine) and a Contribution Toward Its Structure. *J. Am. Chem. Soc.* **1954**, *76*, 1332–1334.
- (60) Smith, H.; Elliott, J. Alpha(2) Receptors and Agonists in Pain Management. *Curr. Opin. Anaesthesiol.* **2001**, *14*, 513–518.
- (61) Dwyer, J. M.; Platt, B. J.; Rizzo, S. J.; Pulicicchio, C. M.; Wantuch, C.; Zhang, M. Y.; Cummons, T.; Leventhal, L.; Bender, C. N.; Zhang, J.; Kowal, D.; Lu, S.; Rajarao, S. J.; Smith, D. L.; Shilling, A. D.; Wang, J.; Butera, J.; Resnick, L.; Rosenzweig-Lipson, S.; Schechter, L. E.; Beyer, C. E. Preclinical Characterization of BRL 44408: Antidepressant- and Analgesic-like Activity through Selective alpha2A-Adrenoceptor Antagonism. *Int J Neuropsychopharmacol* **2010**, *13*, 1193–1205.
- (62) Muguruza, C.; Rodríguez, F.; Rozas, I.; Meana, J. J.; Urigüen, L.; Callado, L. F. Antidepressant-like Properties of Three New α 2-Adrenoceptor Antagonists. *Neuropharmacology* **2013**, *65*, 13–19.
- (63) Sallinen, J.; Holappa, J.; Koivisto, A.; Kuokkanen, K.; Chapman, H.; Lehtimäki, J.; Piepponen, P.; Mijatovic, J.; Tanila, H.; Virtanen, R.; Sirviö, J.; Haapalinna, A. Pharmacological Characterisation of a Structurally Novel α 2C -Adrenoceptor Antagonist ORM-10921 and Its Effects in Neuropsychiatric Models. *Basic Clin. Pharmacol. Toxicol.* **2013**, *113*, 239–249.
- (64) Osman, O. T.; Rudorfer, M. V.; Potter, W. Z. Idazoxan: A Selective Alpha 2-Antagonist and Effective Sustained Antidepressant in Two Bipolar Depressed Patients. *Arch. Gen. Psychiatry* **1989**, *46*, 958–959.
- (65) Idayu, N. F.; Hidayat, M. T.; Moklas, M. A. M.; Sharida, F.; Raudzah, A. R. N.; Shamima, A. R.; Apyani, E. Antidepressant-like Effect of Mitragynine Isolated from *Mitragyna Speciosa* Korth in Mice Model of Depression. *Phytomedicine* **2011**, *18*, 402–407.
- (66) Stone, E. A.; Lin, Y.; Sarfraz, Y.; Quartermain, D. Antidepressant-like Action of Intracerebral 6-Fluoronorepinephrine, a Selective Full α -Adrenoceptor Agonist. *Int. J. Neuropsychopharmacol.* **2011**, *14*, 319–331.
- (67) Schramm, N. L.; McDonald, M. P.; Limbird, L. E. The alpha(2a)-Adrenergic Receptor Plays a Protective Role in Mouse Behavioral Models of Depression and Anxiety. *J. Neurosci.* **2001**, *21*, 4875–4882.
- (68) Hameedi, F. A.; Woods, S. W.; Rosen, M. I.; Pearsall, H. R.; Kosten, T. R. Dose Dependent Effects of Yohimbine on Methadone Maintained Patients. *Am. J. Drug Alcohol Abuse* **1997**, *23*, 327–333.
- (69) Taylor, J. R.; Lewis, V. O.; Elsworth, J. D.; Pivrotto, P.; Roth, R. H.; Redmond, D. E.

- Yohimbine Co-Treatment during Chronic Morphine Administration Attenuates Naloxone-Precipitated Withdrawal without Diminishing Tail-Flick Analgesia in Rats. *Psychopharmacology (Berl)*. **1991**, *103*, 407–414.
- (70) Iglesias, V.; Alamo, C.; Cuenca, E.; Morales, L.; Perez-Garcia, C.; Alguacil, L. F. Effect of Oral Yohimbine on Withdrawal Jumping Behaviour of Morphine-Dependent Mice. *Addict. Biol.* **1998**, *3*, 459–463.
- (71) Morales, L.; Perez-Garcia, C.; Alguacil, L. F. Effects of Yohimbine on the Antinociceptive and Place Conditioning Effects of Opioid Agonists in Rodents. *Br. J. Pharmacol.* **2001**, *133*, 172–178.
- (72) Stine, S. M.; Southwick, S. M.; Petrakis, I. L.; Kosten, T. R.; Charney, D. S.; Krystal, J. H. Yohimbine-Induced Withdrawal and Anxiety Symptoms in Opioid-Dependent Patients. *Biol. Psychiatry* **2002**, *51*, 642–651.
- (73) Gowing, L. R.; Farrell, M.; Ali, R. L.; White, J. M. Alpha2-Adrenergic Agonists in Opioid Withdrawal. *Addiction* **2002**, *97*, 49–58.
- (74) Trakulsrichai, S.; Sathirakul, K.; Auparakkitanon, S.; Krongvorakul, J.; Sueajai, J.; Noumjad, N.; Sukasem, C.; Wananukul, W. Pharmacokinetics of Mitragynine in Man. *Drug Des. Devel. Ther.* **2015**, *9*, 2421–2429.
- (75) Takayama, H.; Kurihara, M.; Subhadhirasakul, S.; Kitajima, M.; Aimi, N.; Sakai, S. Stereochemical Assignment of Pseudoindoxyl Alkaloids. *Heterocycles* **1996**, *42*, 87–92.
- (76) Clayton, C. C.; Donthamsetti, P.; Lambert, N. A.; Javitch, J. A.; Neve, K. A. Mutation of Three Residues in the Third Intracellular Loop of the Dopamine D2 Receptor Creates an Internalization-Defective Receptor. *J. Biol. Chem.* **2014**, *289*, 33663–33675.
- (77) Jiang, L. I.; Collins, J.; Davis, R.; Lin, K.-M.; DeCamp, D.; Roach, T.; Hsueh, R.; Rebres, R. A.; Ross, E. M.; Taussig, R.; Fraser, I.; Sternweis, P. C. Use of a cAMP BRET Sensor to Characterize a Novel Regulation of cAMP by the Sphingosine 1-phosphate/G13 Pathway. *J. Biol. Chem.* **2007**, *282*, 10576–10584.
- (78) Majumdar, S.; Burgman, M.; Haselton, N.; Grinnell, S.; Ocampo, J.; Pasternak, A. R.; Pasternak, G. W. Generation of Novel Radiolabeled Opiates through Site-Selective Iodination. *Bioorganic Med. Chem. Lett.* **2011**, *21*, 4001–4004.
- (79) Majumdar, S.; Grinnell, S.; Le Rouzic, V.; Burgman, M.; Polikar, L.; Ansonoff, M.; Pintar, J.; Pan, Y.-X.; Pasternak, G. W. Truncated G Protein-Coupled Mu Opioid Receptor MOR-1 Splice Variants Are Targets for Highly Potent Opioid Analgesics Lacking Side Effects. *Proc. Natl. Acad. Sci.* **2011**, *108*, 19778–19783.
- (80) Pickett, J. E.; Váradi, A.; Palmer, T. C.; Grinnell, S. G.; Schrock, J. M.; Pasternak, G. W.; Karimov, R. R.; Majumdar, S. Mild, Pd-Catalyzed Stannylation of Radioiodination Targets. *Bioorg. Med. Chem. Lett.* **2015**, *25*, 1761–1764.
- (81) Pan, Y.-X.; Xu, J.; Bolan, E.; Abbadie, C.; Chang, a; Zuckerman, a; Rossi, G.; Pasternak, G. W. Identification and Characterization of Three New Alternatively Spliced Mu-Opioid Receptor Isoforms. *Mol. Pharmacol.* **1999**, *56*, 396–403.
- (82) Lowry, O.; Rosebrough, N.; Farr, A. L.; Randall, R. Protein Measurement with the Folin Phenol Reagent. *J. Biol. Chem.* **1951**, *193*, 265–275.
- (83) Ballesteros, J. A.; Weinstein, H. Integrated Methods for the Construction of Three-Dimensional Models and Computational Probing of Structure-Function Relations in G Protein-Coupled Receptors. *Methods Neurosci.* **1995**, *25*, 366–428.

Chapter 4 – 12-Hydroxy-Oxaibogamine as a Novel Scaffold for Opioid Receptor Modulation

Introduction

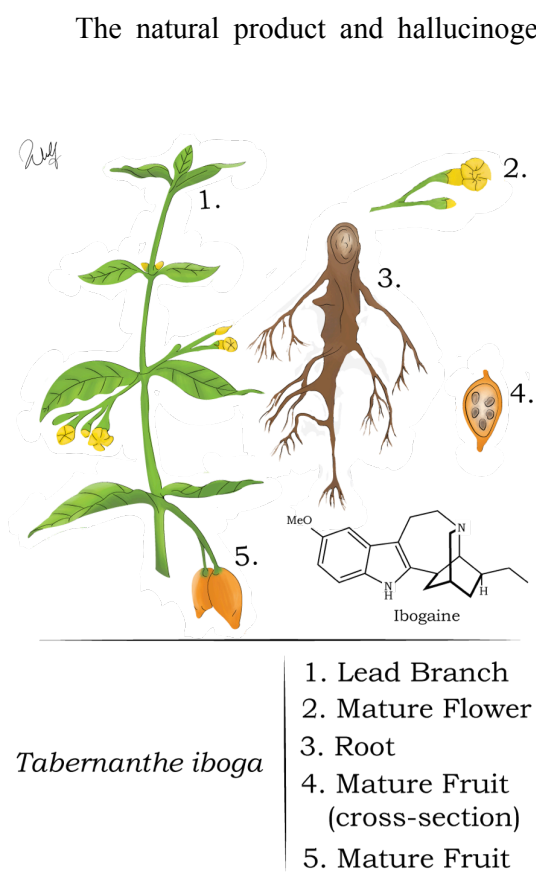


Figure 1. Leaves and fruiting bodies of *Tabernanthe iboga* and chemical structure of the notable alkaloid ibogaine.

The natural product and hallucinogen ibogaine, isolated from the shrub *Tabernanthe iboga*, together with other members of the *iboga* alkaloid family, including ibogamine, continue to be used in ritualistic ceremonies by shamans of a West African (Gabon) spiritual practice known as Bwiti (Figure 1).¹⁻³ More interestingly, in the past few decades ibogaine has been shown to hold real promise for treating substance use disorders (SUDs) by affecting not only craving and self-administration of many drugs of abuse, including alcohol, opioids, and cocaine, but also symptoms of acute opioid withdrawal, such as mydriasis, sweating, elevated pulse rate, shivering, piloerection, diarrhea, or prolonged vomiting.⁴ These remarkable effects from ibogaine can be sustained for longer periods of time, as well (weeks to even months).⁵ While the clinical data represent a collection of uncontrolled studies and anecdotal reports⁵, these effects have also been observed in animal models.⁶⁻⁸ For instance ibogaine elicits dose-dependent decreases of morphine self-administration in rats, which lasts in some rats for several days or weeks after a single dose.⁶

Additionally, a single administration of ibogaine has been shown to dose-dependently decrease intake of both alcohol and cocaine in rats.^{7,8}

Although studied for many years, the mechanism of action explaining ibogaine's unique properties is still unclear. Numerous reports show that ibogaine binds to and/or shows functional activity at many targets in the central nervous system (CNS) with modest micromolar affinity and/or potency, including the N-methyl-D-aspartate receptor (NMDAR), the dopamine and serotonin transporters (DAT and SERT, respectively), mu-opioid receptor (MOR), sigma 2 receptor, 5-HT_{2a} receptor, acetylcholine receptors, and others⁹⁻¹², which makes ibogaine a controversial and potentially dangerous therapeutic. Additionally, ibogaine has been reported to cause heart arrhythmias¹², which may be due to the inhibition of human ERG channels (potency near 4 μ M).^{12,13} Studies on the pharmacology of both ibogaine and its metabolite noribogaine are ongoing.^{14,15} For instance, although ibogaine has been shown to be an NDMAR antagonist in tissue from different brain regions (potency of <10 μ M)¹⁶⁻¹⁸, the activity at the MOR has not yet been confirmed, which does suggest an alternative mechanism by which ibogaine may ameliorate opioid withdrawal.¹⁹ Interestingly, a recent report by Mash and coworkers discusses the opioid activity of noribogaine (EC₅₀ = 9 μ M at the human kappa-opioid receptor, KOR)²⁰, so it is possible that ibogaine's effects on opioid withdrawal might in fact be mediated through its metabolite.¹⁵

Given ibogaine's polypharmacological actions and potentially dangerous side effects²¹, there is a great need to isolate the therapeutic mechanisms by studying alternative *iboga* analogs that may be more selective for the beneficial effects.²² Several research groups have been pursuing this course of action. Deborah Mash, for instance, has spent several decades exploring the clinical use of ibogaine, opening the first medically-based ibogaine clinic (Clear Sky

Recovery in Cancún, Mexico). Stanley Glick first identified the active metabolite noribogaine²³, which has since demonstrated many promising effects *in vivo*²⁴ and is now entering clinical trials in New Zealand.²⁵ Additionally the *iboga* analog 18-methoxycoronaridine (18-MC) is effective at reducing self-administration of morphine, cocaine, ethanol, and nicotine in rodent models for addiction.²⁶ As an antagonist of the $\alpha 3\beta 4$ nicotinic receptor with greater selectivity in the CNS compared to ibogaine, 18-MC may be a suitable alternative to ibogaine. More exotic hypotheses connect ibogaine's effects on alcohol addiction and cravings to the modulation of growth factor glial cell line-derived neurotrophic disorder (GDNF, see Chapter 6).²⁷⁻³⁰ There has also been a push to develop completely novel modifications to the ibogaine structure in the hopes of having more selective pharmacology within the CNS. Such compounds have been reported, which bind to dopamine and serotonin transporters, the KOR, and the NMDAR, but no follow-up on these studies have yet been reported.³¹ Given our ongoing interest in studying opioid receptor modulators^{32,33}, we decided to utilize the latter approach in order to identify novel *iboga* alkaloid analogs that would show increased selectivity for the opioid receptors, which ultimately could provide beneficial therapeutics for pain, mood disorders, and substance mood disorders.

This chapter will describe the synthesis and biological activity of a novel class of *iboga* alkaloid analogs. Utilizing the structure of the active metabolite noribogaine, we found that 12-hydroxy-oxaibogamine analogs showed promising activity at the opioid receptors, increasing the potency compared to noribogaine up to 280-, 6.5-, and greater than 300-fold at KOR, MOR, and delta-opioid receptor (DOR), respectively. We also found that one compound in particular, **36c**, shows apparent biased activation of KOR and therefore represents an interesting lead in the pursuit of non-addictive, non-dysphoric alternatives to morphine (see Introductory Chapter 1).

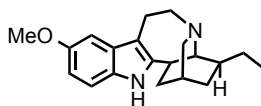
Results

Biological Activity of Noribogaine at the Opioid Receptors

Ibogaine is reported to bind quite promiscuously to receptors and transporters in the CNS (see **Introduction**), including many studies that show binding by both ibogaine and its active metabolite noribogaine to the opioid receptors with modest affinity.^{15,23,34–36} Additionally, Mash

Table 1. Reported Binding Affinities of Ibogaine (A) and its Metabolite Noribogaine (B) at the Opioid Receptors.

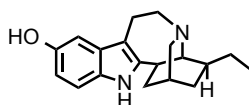
A.



Ibogaine

Tissue	KOR	MOR	DOR
<i>Bovine Cortex</i> ³⁴	2.08 ± 0.23	> 100	> 100
<i>Calf Brain</i> ²³	3.77 ± 0.81	11.04 ± 0.66	> 100
<i>Calf Brain</i> ¹⁵	2.2 ± 0.10	2.0 ± 0.15	> 10
<i>Rat Thalamus</i> ³⁷	-	3.76 ± 0.223	-
<i>Rat Forebrain</i> ³⁶	29.8 ± 8.3	-	-
<i>Mouse Forebrain</i> ³⁶	13.8 ± 0.60	-	-
<i>Not specified</i> ³⁵	3.16	-	-

B.



Noribogaine

Tissue	KOR	MOR	DOR
<i>Calf Brain</i> ²³	0.96 ± 0.080	2.66 ± 0.62	24.72 ± 2.26
<i>Calf Cortex</i> ¹⁵	0.61 ± 0.015	0.68 ± 0.016	5.2 ± 0.64
<i>Rat Thalamus</i> ³⁷	-	0.16 ± 0.012	-
<i>Rat Forebrain</i> ³⁶	0.28 ± 0.11	-	-
<i>Mouse Forebrain</i> ³⁶	1.2 ± 0.10	-	-

Data represent mean ± SEM of various replicates (μM) from indicated membranes.

receptor activation accounts for the unique biological effects observed from ibogaine administration. However it is possible that noribogaine, which binds in the submicromolar range

and co-workers showed that noribogaine stimulated [³⁵S]GTPγS binding to rat thalamic membranes with an EC₅₀ of 324 nM (E_{Max} = 100%), activity which could be competitively inhibited by the MOR antagonist naloxone. Ibogaine showed weak stimulation of [³⁵S]GTPγS binding with a theoretical EC₅₀ > 100 mM.³⁷ Given the low affinity with which ibogaine binds to the opioid receptors, it is unlikely that opioid

(approximately 10 fold greater affinity than ibogaine at MOR), may elicit some signaling through the opioid receptors if high enough concentrations are reached in the brain – highly likely in the situation of an “ibogaine reset” where multigram doses are taken (**Table 1**). Therefore it is plausible that noribogaine may act as a substitute for an abused opioid at opioid receptors and help to alleviate withdrawal symptoms. This hypothesis is in line with reported pharmacokinetic studies on ibogaine, which reveal micromolar concentrations reached in the brain.^{2,38–42} Additionally noribogaine has been reported to show binding at some of the monoamine transporters, specifically the dopamine transporter (DAT, $IC_{50} = 3 \mu\text{M}$), the vesicular monoamine transporter (VMAT, unspecified isoform, $IC_{50} = 29 \mu\text{M}$), and the serotonin transporter (SERT, $IC_{50} = 0.04 \mu\text{M}$).⁴⁰ We also found noribogaine to inhibit human DAT, human SERT, and human NET with $IC_{50} = 10.1 \pm 6.6$, 0.52 ± 0.07 , and $43 \pm 9.3 \mu\text{M}$, respectively (**Figure 2**).

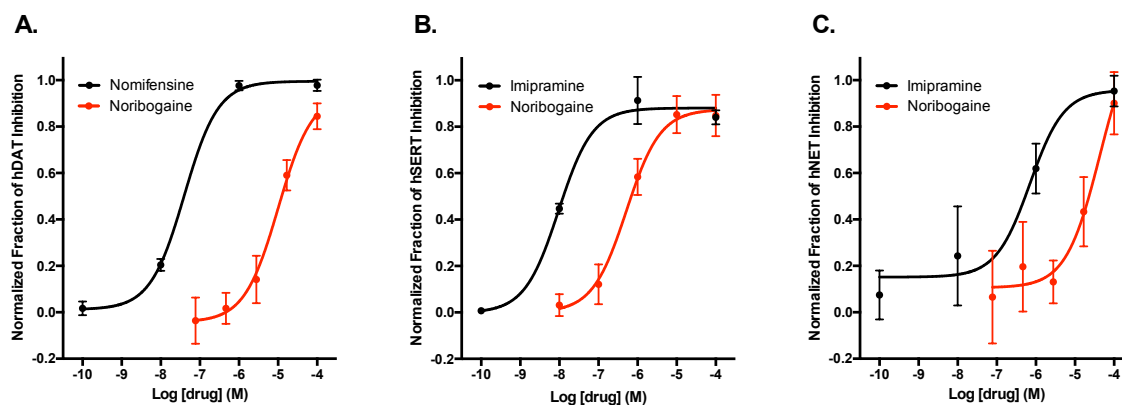


Figure 2. Noribogaine Inhibits Human Monoamine Transporters. In overexpressed cells (EM4 or HEK-293), noribogaine inhibits the specific uptake of acridone dye NG54 at human DAT (A), SERT (B), and NET (C) with an $IC_{50} = 10.1 \pm 6.6$, 0.52 ± 0.07 , and $43 \pm 9.3 \mu\text{M}$, respectively. Data represent mean \pm SD of $n > 2$ independent experiments. Data obtained by Yekaterina Kovalyova.

In order to further characterize the opioid modulating activity of noribogaine, it was important to assess its activity in our own functional assays for G protein activation. Using bioluminescence resonance energy transfer (BRET) assays (see Chapter 1) in HEK cells

transiently expressing either KOR, MOR, or DOR, the agonist and antagonist activity of noribogaine was determined. Noribogaine displayed partial agonist activity at all three opioid receptors, with an EC_{50} of $5.6 \pm 2.6 \mu\text{M}$ ($E_{\text{max}} = 36\%$) at MOR and weaker potency at KOR ($24.6 \pm 8.8 \mu\text{M}$, $E_{\text{max}} = 43\%$) and DOR ($>50 \mu\text{M}$) (**Figure 3**). In comparison to previous literature

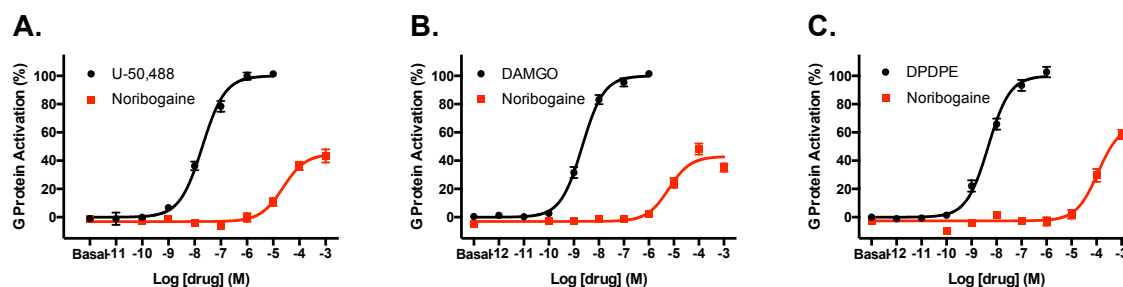


Figure 3. Agonist Activity of Noribogaine at the Human Opioid Receptors. hKOR (A), hMOR (B), or hDOR (C) were co-expressed with $G\alpha_B$ -RLuc8, $\beta 1$, and mVenus- $\gamma 2$ to assay G protein activation. Curves represent the average of $n \geq 6$, with error bars representing \pm SEM. A. Positive control = U-50,488. Noribogaine showed an $EC_{50} = 24.6 \pm 8.8 \mu\text{M}$ and $E_{\text{Max}} = 43\%$. B. Positive control = [D-Ala², N-Me-Phe⁴, Gly-ol⁵]-enkephalin (DAMGO). Noribogaine showed an $EC_{50} = 5.6 \pm 2.6 \mu\text{M}$ and $E_{\text{Max}} = 36\%$. C. Positive control = [D-Pen(2,5)]enkephalin (DPDPE). Noribogaine showed an $EC_{50} > 50 \mu\text{M}$.

reports of functional activity ($EC_{50} = 324 \text{ nM}$, $E_{\text{Max}} = 100\%$ at rat MOR and $EC_{50} = 9 \mu\text{M}$, $E_{\text{Max}} = 72\%$ at human KOR) these data are comparable though somewhat weaker. Given the different species of MOR (rat versus humans) and assay ($[^{35}\text{S}]\text{GTP}\gamma\text{S}$ binding for both versus BRET) tested previously, the potencies reported here do seem reasonable. Despite the noted differences between data sets generated by independent researchers, the data in aggregate support the hypothesis that high enough concentrations of noribogaine (produced by metabolism of ibogaine) could elicit physiologically relevant signaling through the opioid receptors. This hypothesis is supported by pharmacokinetic profiles of ibogaine in human (20 mg/kg oral dose) and monkey (25 mg/kg oral dose), where noribogaine can be detected (from ibogaine dose) in plasma at concentrations of $\sim 2 \mu\text{M}$ and $\sim 1 \mu\text{M}$, respectively.^{38,39} Several separate studies found that the ibogaine concentration in rat brain following a single dose was higher than those found in plasma,^{41,43} suggesting that noribogaine might also exist at higher levels than those found in

the plasma. A large, multi-gram dose of ibogaine (as used in the “reset”), therefore, is likely to result in significant amounts of noribogaine in plasma and brain.

Discovery and Biological Activity of Novel Oxaibogamine Analogs

Initial Structure Activity Relationships (SAR) Reveal Alternate Scaffold. Inspired by the preliminary findings, we set out to explore the SAR of novel analogs that would improve the opioid activity. In preliminary studies, the opioid activity of three *iboga* alkaloid analogs

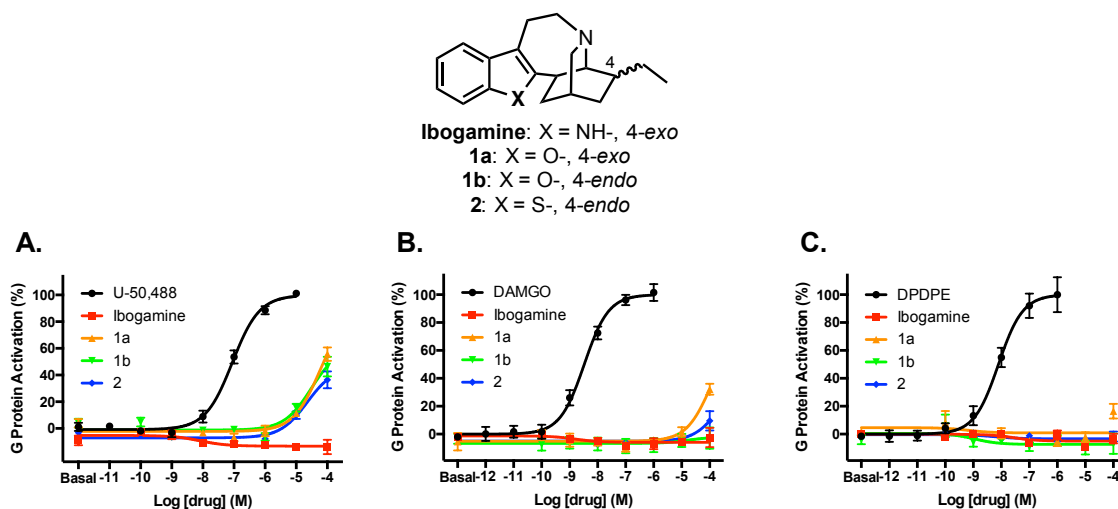


Figure 4. Initial Structure Activity Relationships in the *Iboga* Alkaloid Scaffold. hKOR (A), hMOR (B), or hDOR (C) were co-expressed with G_{α_B} -RLuc8, β_1 , and mVenus- γ_2 to assay G protein activation. Curves represent the average of $n \geq 3$, with error bars representing \pm SEM. Modification of the heteroarene moiety in structures 1-2 reveals enhanced efficacy at hKOR (A).

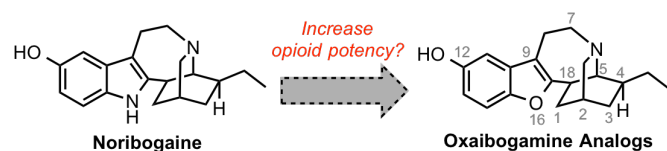


Figure 5. Design of 12-hydroxy-16-oxaibogamines as new opioid receptor modulators based on preliminary SAR studies.

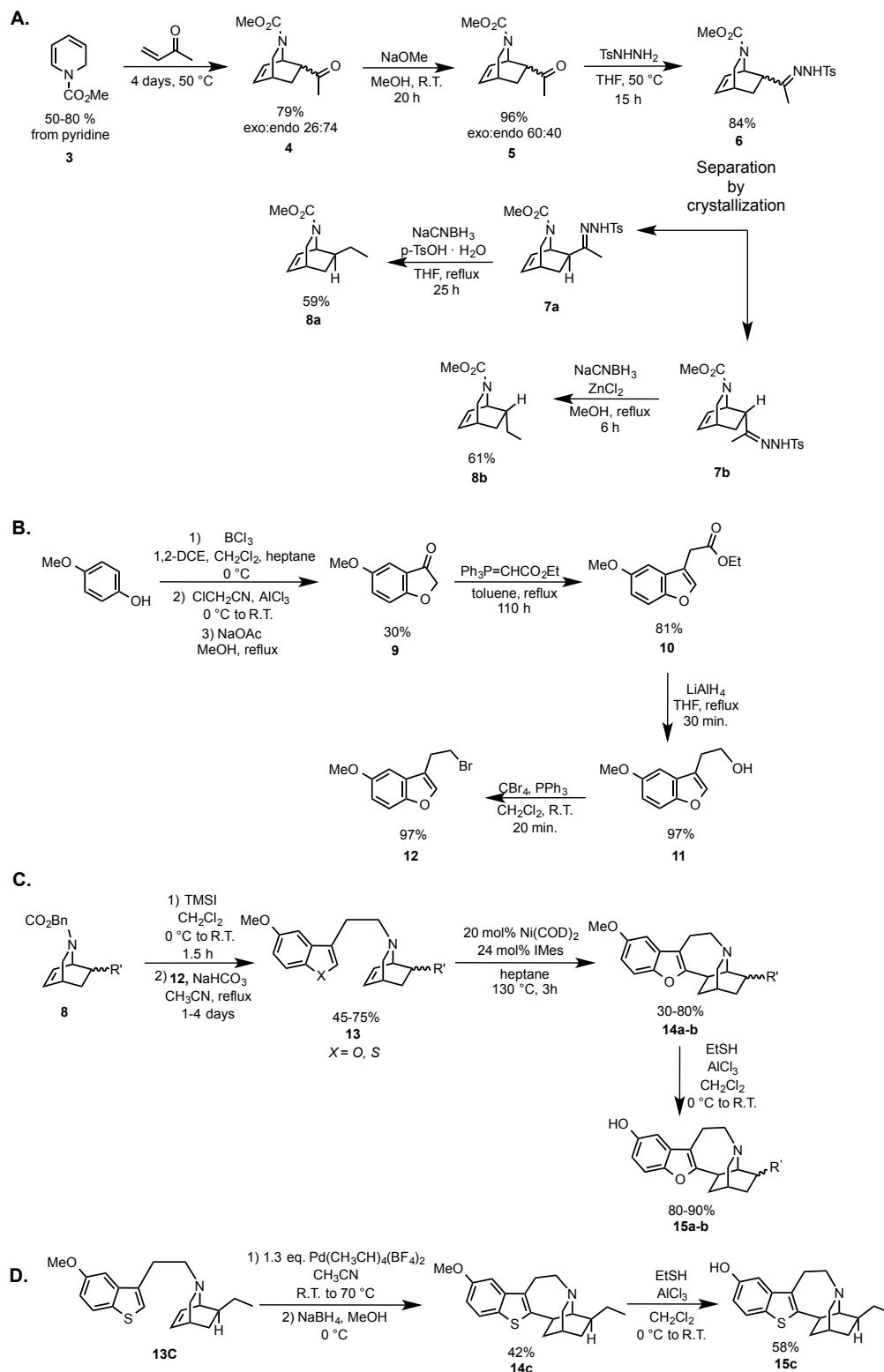
varied at the heteroatom (denoted X in **Figure 5**), including one known compound, ibogamine, was assessed. It was found that compared to ibogamine, which had no measurable

activity at any of the three receptors, the benzofuran analogs (**1a** and **1b**) showed a notable

increase in efficacy at KOR, although still exhibiting a weak activity (**Figure 4**). Both compounds showed no measurable activity at MOR or DOR. The lack of activity from ibogamine suggested that the 12-hydroxy functionality be wholly necessary (for the scaffold numbering, see **Figure 5**). This hypothesis is further supported when comparing the structures of ibogaine and noribogaine where there is a clear necessity for a metabolism of the methyl ether into the phenol functionality on the indole system in order to increase functional activity at the opioid receptors. Similar trends can be found in the classical opium-derived opioids. For instance, codeine is a weak analgesic that binds to the MOR with 300 times lower affinity than morphine and can be readily metabolized to morphine through a demethylation reaction, much like in ibogaine.^{44,45} It was therefore hypothesized that *iboga* analogs, containing both the 12-hydroxy substitution and the benzofuran heteroarene, would impart a greater potency at the opioid receptors (**Figure 5**).

Synthesis of 12-Hydroxy-Oxaibogamine Analogs. Employing methods previously developed in our group^{46,47}, the isoquinuclidine portion of the molecule was synthesized through a Diels-Alder reaction and subsequent tosylhydrazone formation to separate *exo*- and *endo*-isomers (**Scheme 1A**). After tosyl hydrazone reduction and carbamate deprotection the secondary amines were coupled with the 5-methoxy benzofuran intermediate **12** via amine alkylation (**Scheme 1B**). These advanced intermediates were cyclized using the Ni-catalyzed C-H functionalization reaction developed in our group to provide 12-methoxy-oxaibogamine analogs.⁴⁶ A final demethylation with ethanethiol and aluminum chloride yielded the 12-hydroxy-oxaibogamine analogs (**Scheme 1C**). For the benzothiophene intermediate **13c**, electrophilic palladation conditions were necessary to complete the cyclization reaction (**Scheme 1D**). This chemistry was optimized and completed by Andrew Kruegel. A summary list of the

Scheme 1. Synthesis of Key Isoquinuclidine and Heteroarene Fragments of 12-Oxaibogamine Analogs.



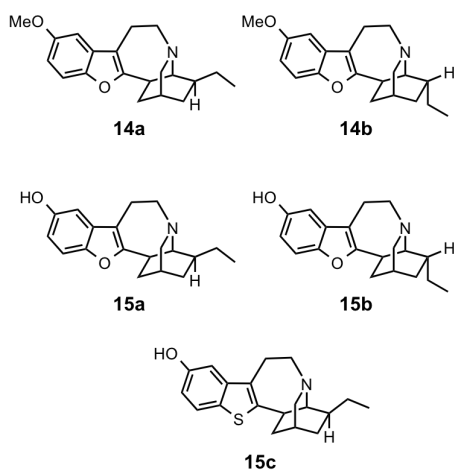


Figure 6. First Generation Oxa- and Thia-ibogamine Analog.

first generation 12-hydroxy-oxaibogamine analogs can be found in **Figure 6**.

Functional Activity of Novel 12-Hydroxy-Oxaibogamine Analogs. The combination of both the benzofuran functionality with the 12-hydroxy substituent analogous to noribogaine proved to greatly increase both potency and efficacy in comparison to noribogaine itself. The *exo*-ethyl

analog (**15a**) showed full agonism at all three opioid receptor subtypes (**Figure 7**, $EC_{50\text{ KOR}} = 0.66 \pm 0.13 \mu\text{M}$; $EC_{50\text{ MOR}} = 0.98 \pm 0.14 \mu\text{M}$; $EC_{50\text{ DOR}} = 4.5 \pm 1.2 \mu\text{M}$), representing a major improvement in functional activity. The *endo*-ethyl analog (**15b**) interestingly showed differences in both potency and efficacy at the three receptors compared to the *exo*-isomers (**Figure 7**, $EC_{50\text{ KOR}} = 0.16 \pm 0.09 \mu\text{M}$ ($E_{\text{Max}} = 100\%$); $EC_{50\text{ MOR}} = 0.83 \pm 0.28 \mu\text{M}$ ($E_{\text{Max}} = 78\%$); $EC_{50\text{ DOR}} = 2.8 \pm 1.6 \mu\text{M}$ ($E_{\text{Max}} = 29\%$)). Consequently, the 12-hydroxy substitution in these analogs proved to be crucial, while the *exo*- and *endo*-stereochemistry conveyed some control

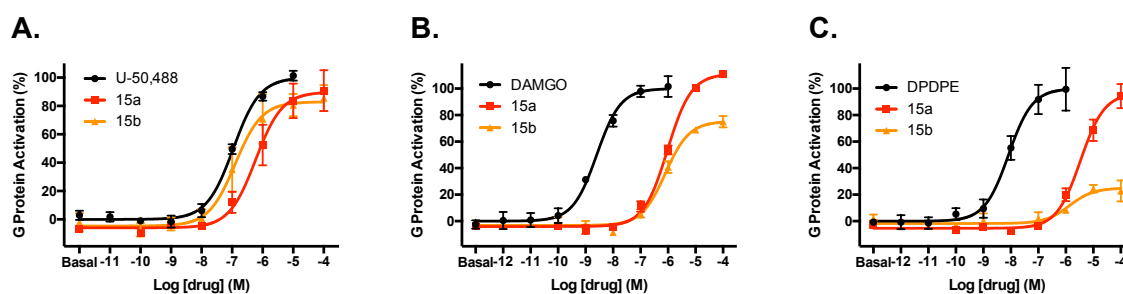


Figure 7. Agonist Activity of the First Generation 12-Hydroxy-Oxaibogamine Analogs at the Human Opioid Receptors. hKOR (A), hMOR (B), or hDOR (C) were co-expressed with $G\alpha_{\text{O}}\beta$ -RLuc8, $\beta 1$, and mVenus- $\gamma 2$ to assay G protein activation. Curves represent the average of $n=3$, with error bars representing \pm SEM. Analog **15a** shows $EC_{50\text{ KOR}} = 0.66 \pm 0.13 \mu\text{M}$ ($E_{\text{Max}} = 100\%$), $EC_{50\text{ MOR}} = 0.98 \pm 0.14 \mu\text{M}$ ($E_{\text{Max}} = 100\%$), and $EC_{50\text{ DOR}} = 4.5 \pm 1.2 \mu\text{M}$. Analog **15b** shows $EC_{50\text{ KOR}} = 0.16 \pm 0.09 \mu\text{M}$ ($E_{\text{Max}} = 100\%$), $EC_{50\text{ MOR}} = 0.83 \pm 0.28 \mu\text{M}$ ($E_{\text{Max}} = 78\%$), and $EC_{50\text{ DOR}} = 2.8 \pm 1.6 \mu\text{M}$ ($E_{\text{Max}} = 29\%$).

over efficacy and subtype selectivity. Analogs with the 12-methoxy substitution instead (analogous to ibogaine) showed much weaker potency and efficacy by orders of magnitude (**14a** and **14b**, **Table 2**). Such SAR highlights the importance of the phenolic substitution for activation of the opioid receptors. The implications of such biological activity are quite intriguing. The idea of polypharmacology as a way to treat different diseases has been reported

Table 2. Summary of Functional Activity of *Iboga* Alkaloid Analogs at the Human Opioid Receptors.

Compound	KOR	MOR	DOR
<i>Noribogaine</i>	24.6 ± 8.8 (43%)	5.6 ± 2.6 (36%)	>50
<i>Ibogamine</i>	X	X	X
<i>1b</i>	27.5 ± 2.4 (43%)	X	X
<i>1a</i>	56.5 ± 11.2 (60%)	X	X
<i>2</i>	21.0 ± 3.8 (50%)	X	X
<i>14a</i>	23.9 ± 2.8 (62%)	38.6 ± 2.0 (50%)	X
<i>14b</i>	25.0 ± 17.1 (43%)	X	X
<i>15a</i>	0.66 ± 0.13 (100%)	0.98 ± 0.14 (100%)	4.5 ± 1.2 (100%)
<i>15b</i>	0.16 ± 0.09 (100%)	0.83 ± 0.28 (78%)	2.8 ± 1.6 (29%)
<i>15c</i>	4.5 ± 3.4 (70%)	7.2 ± 4.2 (46%)	>50
<i>30a</i>	0.46 ± 0.27 (85%)	0.52 ± 0.16 (100%)	1.9 ± 1.5 (100%)
<i>30b</i>	0.24 ± 0.06 (41%)	0.49 ± 0.2 (85%)	1.9 ± 0.8 (64%)
<i>30c</i>	10.5 ± 1.1 (16%)	2.8 ± 0.1 (86%)	7.6 ± 1.6 (58%)
<i>32a</i>	1.3 ± 0.3 (87%)	12.2 ± 6.5 (62%)	25.2 ± 4.7 (28%)
<i>32b</i>	27 ± 5.9 (20%)	> 50	> 50
<i>36a</i>	1.7 ± 1.1 (26%)	4.7 ± 3.6 (24%)	X
<i>36b</i>	0.44 ± 0.06 (88%)	0.40 ± 0.06 (98%)	4.2 ± 0.7 (98%)
<i>36c</i>	0.12 ± 0.01 (47%)	X	X
<i>36d</i>	0.14 ± 0.006 (72%)	0.37 ± 0.24 (50%)	5.1 ± 2.2 (24%)
<i>36e</i>	0.09 ± 0.02 (81%)	0.86 ± 0.02 (30%)	0.31 ± 0.0003 (20%)
<i>36f</i>	IC ₅₀ = 8.2 ± 0.5 <i>0.43 ± 0.23</i>	X	X
<i>(5S)-46</i>	1.4 ± 1.2 (41%)	4.2 ± 2.0 (61%)	10 ± 10 (20%)

EC₅₀ values are shown in μM with E_{Max} relative to control shown in parentheses. Value in italics represents the pA₂ determined through Schild analysis. “X” means inactive. Data shown represent mean ± SD of various replicates (μM).

in the literature previously. A

compound that activates both KOR and MOR offers a potentially improved physiological efficacy for treating pain.

Additionally, mood-enhancing effects could result from combined modulation of the three opioid receptors. For example, the mood enhancement from MOR signaling

combating the aversive effects of KOR activation, and KOR activation providing non-addictive pain relief (see Introductory Chapter 1 for further discussion), it is possible that this opioid

polypharmacology may help to balance out the negative effects of signaling through each opioid receptor individually. It is unclear at this point what levels of activation from each receptor are necessary to provide the ideal “chord,” however compounds such as these offer a promising possibility for an all-in-one drug for treating pain and or depression. Further studying the SAR of this scaffold may reveal what tuning is necessary to provide the ideal combination of pharmacology. Similar analogs were also synthesized utilizing the benzothiophene core, which in the initial SAR studies showed improvement over the indole substitution, but while active at the opioid receptors, this heteroarene substitution was inferior when compared to benzofuran

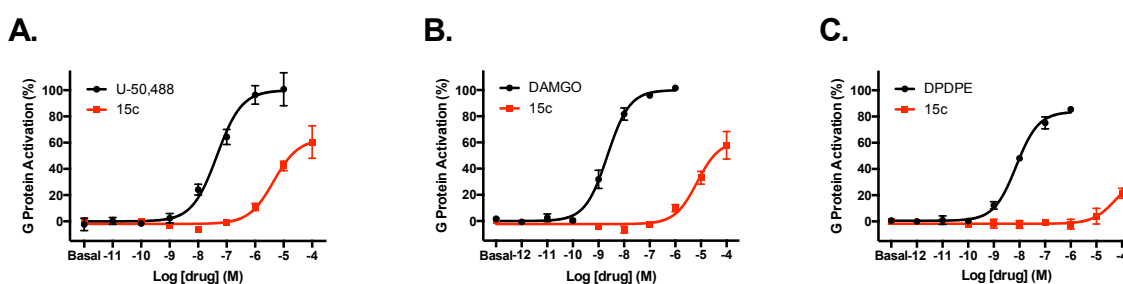


Figure 8. Benzothiophene **15c** Shows Weaker Activity at the Opioid Receptors Compared to the Benzofuran Analog. hKOR (A), hMOR (B), or hDOR (C) were co-expressed with G α_{OB} -RLuc8, β 1, and mVenus- γ 2 to assay G protein activation. Analog **15c** shows EC_{50 KOR} = 4.5 \pm 3.4 μ M (E_{Max} = 70%), EC_{50 MOR} = 7.2 \pm 4.2 μ M (E_{Max} = 46%), and EC_{50 DOR} > 50 μ M. Curves represent the average of n=3, with error bars representing \pm SEM.

(**Compound 15c**, **Figure 8**, EC_{50 KOR} = 4.5 \pm 3.4 μ M (E_{Max} = 70%); EC_{50 MOR} = 7.2 \pm 4.2 μ M (E_{Max} = 46%); EC_{50 DOR} > 50 μ M).

Analog **15a** and **15c** were also measured for their ability to inhibit monoamine transporters. At human DAT, **15a** and **15c** showed an IC₅₀ = 8.4 \pm 3.9 and 0.69 \pm 0.16 μ M, respectively (**Figure 9a**). At human SERT, **15a** and **15c** showed an IC₅₀ = 2.6 \pm 1.2 and 0.06 \pm 0.01 μ M, respectively (**Figure 9b**). At human NET, **15a** and **15c** showed an IC₅₀ = 14.9 \pm 8.1 and 7.0 \pm 7.0 μ M, respectively (**Figure 9c**). Based on these data, it appears that the benzothiophene moiety of analog **15c** imparts a much stronger potency for inhibition of these

monoamine transporters than does the benzofuran functionality. It also appears that these analogs, in general, have increased selectivity for SERT over DAT and NET.

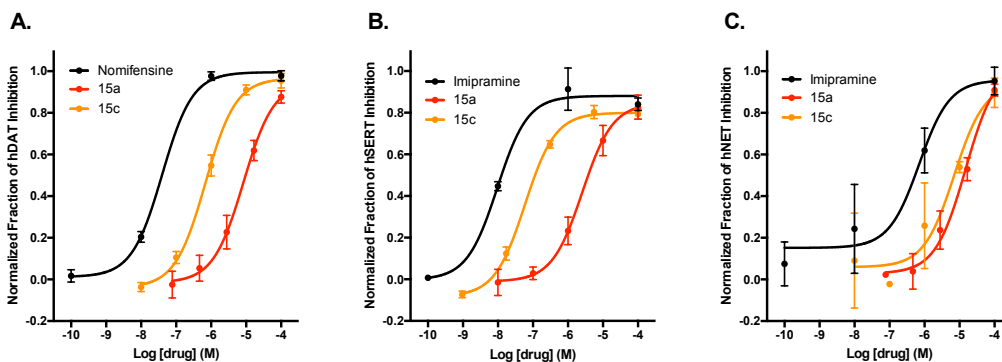
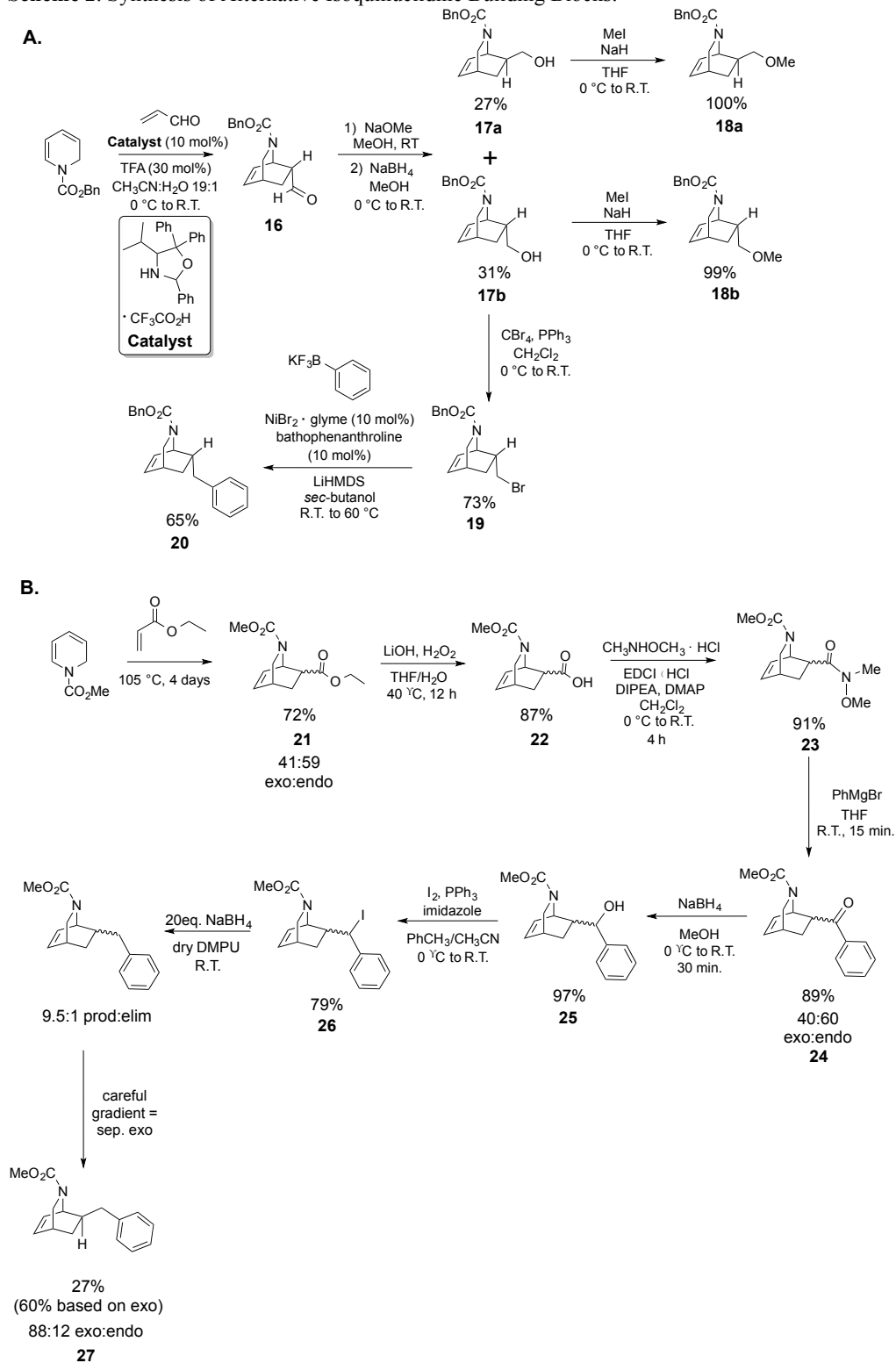


Figure 9. Oxa- and Thia-ibogamine Analogs Inhibit Human Monoamine Transporters. In overexpressed cells (EM4 or HEK-293), analogs **15a** and **15c** inhibit the specific uptake of acridone dye NG54 at DAT (A), SERT (B), and NET (C). **15a** showed an $IC_{50} = 8.4 \pm 3.9$, 2.6 ± 1.2 , and 14.9 ± 8.1 μM at DAT, SERT, and NET, respectively. **15c** showed an $IC_{50} = 0.69 \pm 0.16$, 0.06 ± 0.01 , and 7.0 ± 7.0 μM at DAT, SERT, and NET, respectively. Data represent mean \pm SD of $n > 2$ independent experiments. Data obtained by Yekaterina Kovalyova.

Exploring the SAR of *Exo*- and *Endo*-Substituents Within the Oxaibogamine Scaffold

Synthesis of Analogs Beyond the Ethyl Substituent. In an effort to understand the SAR surrounding the *exo*- and *endo*-substituents at position 4 (see **Figure 5** above), a few key analogs were designed and synthesized. Looking to our exploration within the tianeptine scaffold (see Chapter 2), we wanted to synthesize compounds that contained a methoxy methyl ether at position 4. We were also interested in understanding how much space was available in the putative receptor binding pocket for both *exo*- and *endo*-substituents. Consequently, we chose to synthesize analogs with a bulky benzyl substituent in the *exo*- and *endo*-position. In order to study these compounds, a different synthetic route was needed to gain access to these novel isoquinuclidines. In contrast to the racemic route to the isoquinuclidine that utilized vinylmethylketone as the dienophile, we instead employed acrolein and an oxazolidine organocatalyst in the Diels- Alder reaction, followed by epimerization and reduction, to synthesize isoquinuclidine alcohol **17**. These intermediates were then either be O-methylated to

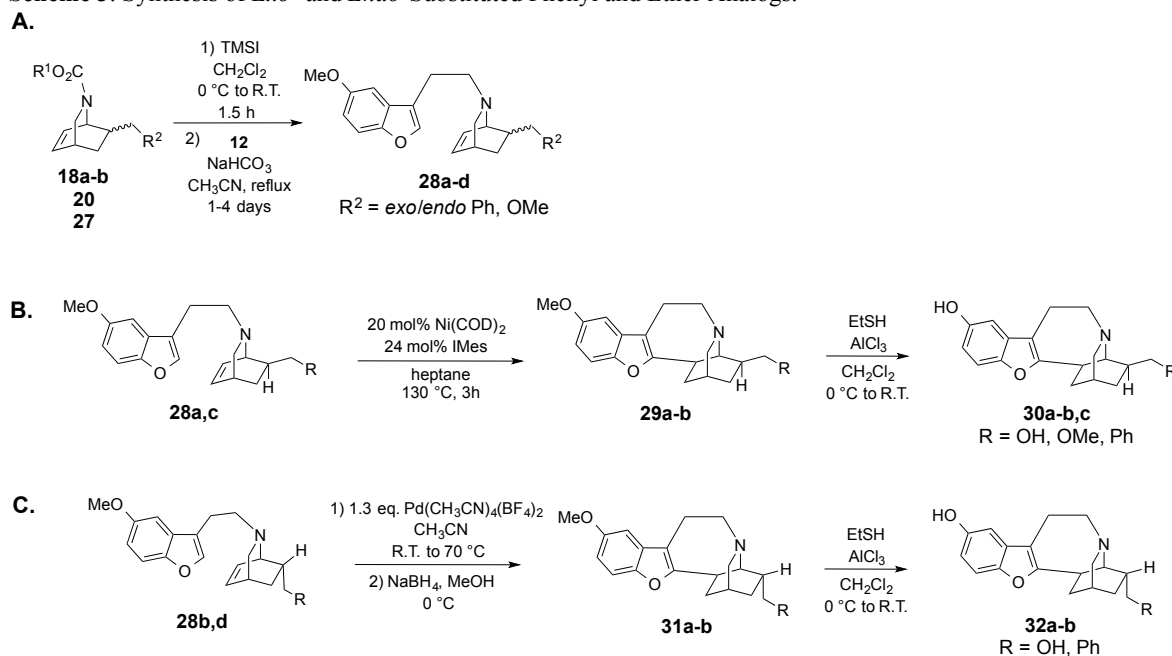
Scheme 2. Synthesis of Alternative Isoquinuclidine Building Blocks.



intermediates **18a** and **18b**, or brominated and subjected to Suzuki conditions to obtain the *endo*-benzyl isoquinuclidine **20** (**Scheme 2A**). This chemistry was optimized and completed with Andrew Kruegel and Dr. Souvik Rakshit.

Due to limited amounts of intermediates, a separate synthetic scheme was devised for the *exo*-benzyl isoquinuclidine, which utilized more readily available materials. Dihydropyridine was reacted in a Diels-Alder reaction to yield the ethyl ester substituted isoquinuclidine **21**, which was then hydrolyzed and converted into the Weinreb amide **23**. This isoquinuclidine was then converted to phenyl ketone **24**, reduced, iodinated, and reduced again before carefully isolating the *exo*-intermediate **27**. These isoquinuclidines could then be reacted as before with heteroarene **12** followed by cyclization and demethylation to provide analogs **30**. For *endo*-

Scheme 3. Synthesis of *Exo*- and *Endo*-Substituted Phenyl and Ether Analogs.



intermediates **28b** and **28d**, the substrates were apparently unreactive to the Ni-catalyzed cyclization conditions (**Scheme 3A-B**). The *exo*-phenyl analog **30c** was synthesized by Andrew Kruegel. Presumably in the *endo*-configuration, the nitrogen at position 6 is more exposed due to

the farther positioning of the ethyl substituent, which makes it substantially more basic. It is likely that the increased basicity provides a means to interfere with the catalytic species in the reaction, thus greatly reducing the reactivity of the substrate. For this reason, intermediates **28b** and **28d** had to be cyclized using traditional electrophilic palladation conditions (**Scheme 3C**). In

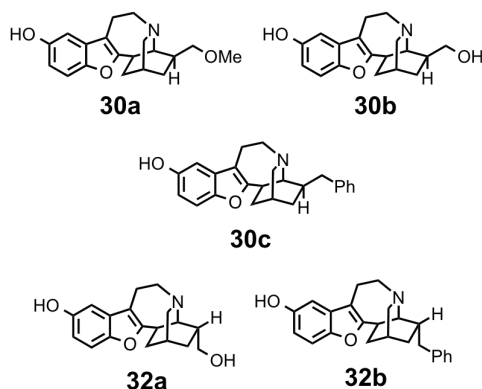


Figure 10. Second Generation 12-Hydroxy-Oxaibogamine Analogs **30** and **32**.

the demethylation of *exo*-intermediate **29a**, we were able to isolate both the singly (**30a**) and doubly (**30b**) demethylated analogs. Interestingly, in the demethylation of the *endo*-intermediate **31a**, we were only able to isolate the doubly demethylated analog. This intermediate was found to be more reactive to demethylation conditions than the *exo*-analog, leading to rapid conversion to the doubly

demethylated analog **32a**. A summary of this second generation of 12-hydroxy-oxaibogamine analogs is listed in **Figure 10**.

Functional Activity of Second Generation 12-Hydroxy-Oxaibogamine Analogs at the Opioid Receptors. The second generation oxaibogamine analogs **30** and **32** revealed interesting SAR at the opioid receptors. Analog **30a**, for example, was in a similar potency range to the ethyl analogs **15a-b**, showing tolerance in the *exo*-position for an ether substituent (**Figure 11**, $EC_{50\text{ KOR}} = 0.46 \pm 0.27 \mu\text{M}$ ($E_{\text{Max}} = 85\%$); $EC_{50\text{ MOR}} = 0.52 \pm 0.16 \mu\text{M}$ ($E_{\text{Max}} = 100\%$); $EC_{50\text{ DOR}} = 1.9 \pm 1.5 \mu\text{M}$ ($E_{\text{Max}} = 100\%$)). In the doubly demethylated analog **30b**, the first example of partial agonism at KOR was observed with similar potency compared to the corresponding ethyl analogs (**Figure 11**, $EC_{50\text{ KOR}} = 0.24 \pm 0.06 \mu\text{M}$ ($E_{\text{Max}} = 41\%$); $EC_{50\text{ MOR}} = 0.49 \pm 0.2 \mu\text{M}$ ($E_{\text{Max}} = 85\%$); $EC_{50\text{ DOR}} = 1.9 \pm 0.8 \mu\text{M}$ ($E_{\text{Max}} = 64\%$)). We were pleased to see the modulation of opioid

agonism to different levels of efficacy in this series of analogs, which indicated that tuning opioid potency and efficacy might be possible by alteration of this specific position. The doubly demethylated *endo*-alcohol **32a**, showed similar potency compared to analogs **30a-b** (Figure 11, $EC_{50\text{ KOR}} = 1.3 \pm 0.3 \mu\text{M}$ ($E_{\text{Max}} = 87\%$); $EC_{50\text{ MOR}} = 12.2 \pm 6.5 \mu\text{M}$ ($E_{\text{Max}} = 62\%$); $EC_{50\text{ DOR}} = 25 \pm 5$ ($E_{\text{Max}} = 28\%$)).

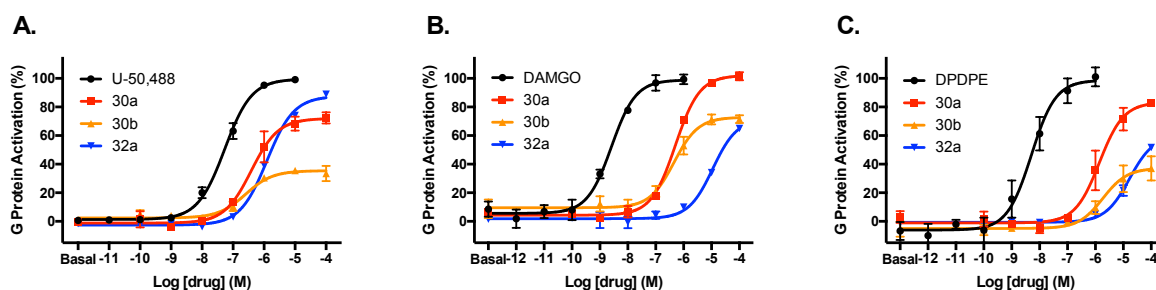


Figure 11. Agonist Activity of the Second Generation 12-Hydroxy-Oxaibogamine Analogs at the Human Opioid Receptors Highlighting Ether and Alcohol Substituents. hKOR (A), hMOR (B), or hDOR (C) were co-expressed with $G\alpha_{\text{O}}$ -RLuc8, $\beta 1$, and mVenus- $\gamma 2$ to assay G protein activation. Analog **30a** shows $EC_{50\text{ KOR}} = 0.46 \pm 0.27 \mu\text{M}$ ($E_{\text{Max}} = 85\%$), $EC_{50\text{ MOR}} = 0.52 \pm 0.16 \mu\text{M}$ ($E_{\text{Max}} = 100\%$), and $EC_{50\text{ DOR}} = 1.9 \pm 1.5 \mu\text{M}$ ($E_{\text{Max}} = 100\%$). Analog **30b** shows $EC_{50\text{ KOR}} = 0.24 \pm 0.06 \mu\text{M}$ ($E_{\text{Max}} = 41\%$), $EC_{50\text{ MOR}} = 0.49 \pm 0.2 \mu\text{M}$ ($E_{\text{Max}} = 85\%$), and $EC_{50\text{ DOR}} = 1.9 \pm 0.8 \mu\text{M}$ ($E_{\text{Max}} = 64\%$). Analog **32** shows $EC_{50\text{ KOR}} = 1.3 \pm 0.3 \mu\text{M}$ ($E_{\text{Max}} = 87\%$), $EC_{50\text{ MOR}} = 12.2 \pm 6.5 \mu\text{M}$ ($E_{\text{Max}} = 62\%$), and $EC_{50\text{ DOR}} = 25 \pm 5$ ($E_{\text{Max}} = 28\%$). Curves represent the average of $n > 2$, with error bars representing \pm SEM.

The benzyl-substituted analogs **30c** and **32b** (Figure 12) were helpful in furthering our understanding of SAR in terms of the configuration at this position. While *exo*-analog **30c** showed minimal activity at the opioid receptors (Figure 12, $EC_{50\text{ KOR}} = 10 \pm 1 \mu\text{M}$ ($E_{\text{Max}} = 16\%$);

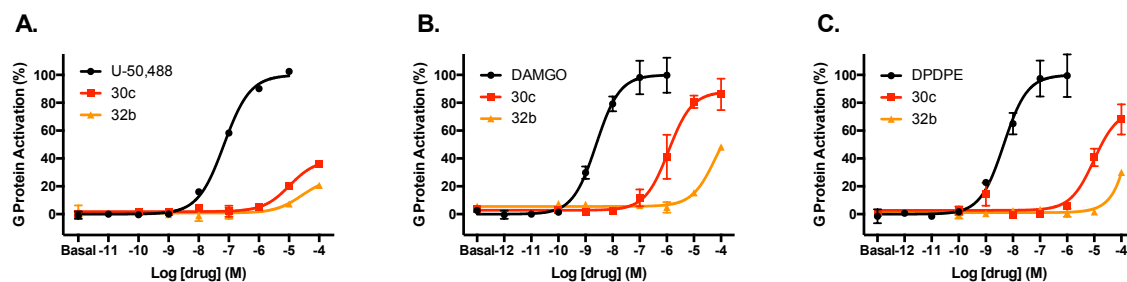
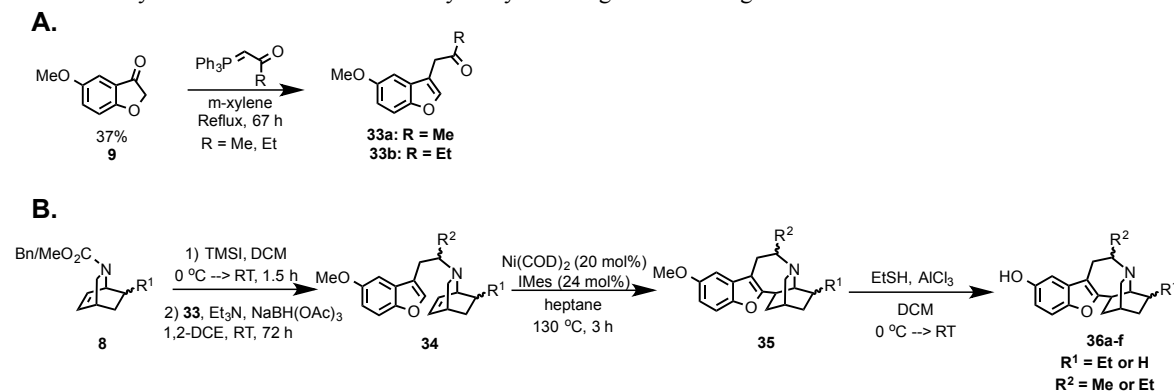


Figure 12. Agonist Activity of the Second Generation 12-Hydroxy-Oxaibogamine Analogs at the Human Opioid Receptors Highlighting Benzyl Substituents. hKOR (A), hMOR (B), or hDOR (C) were co-expressed with $G\alpha_{\text{O}}$ -RLuc8, $\beta 1$, and mVenus- $\gamma 2$ to assay G protein activation. Analog **30c** shows $EC_{50\text{ KOR}} = 10 \pm 1 \mu\text{M}$ ($E_{\text{Max}} = 16\%$), $EC_{50\text{ MOR}} = 2.8 \pm 0.1 \mu\text{M}$ ($E_{\text{Max}} = 86\%$), and $EC_{50\text{ DOR}} = 7.6 \pm 1.6$ ($E_{\text{Max}} = 58\%$). Analog **32b** shows $EC_{50\text{ KOR}} = 27 \pm 6 \mu\text{M}$ ($E_{\text{Max}} = 20\%$), $EC_{50\text{ MOR}} > 50 \mu\text{M}$, and $EC_{50\text{ DOR}} > 50 \mu\text{M}$. Curves represent the average of $n = 2$, with error bars representing \pm SEM.

$EC_{50\text{ MOR}} = 2.8 \pm 0.1 \mu\text{M}$ ($E_{\text{Max}} = 86\%$); $EC_{50\text{ DOR}} = 7.6 \pm 1.6$ ($E_{\text{Max}} = 58\%$)), the *endo*-benzyl analog **32b** had even weaker activity (**Figure 12**, $EC_{50\text{ KOR}} = 27 \pm 6 \mu\text{M}$ ($E_{\text{Max}} = 20\%$); $EC_{50\text{ MOR}} > 50 \mu\text{M}$; $EC_{50\text{ DOR}} > 50 \mu\text{M}$). The differences seen in *endo*- versus *exo*-substitutions in the ether and alcohol analogs were mirrored in the benzyl analogs, with *exo*-substituents being somewhat more potent. Indeed, given the steric bulk of the phenyl analogs, it is possible that there is less space in the binding pocket of the opioid receptors to accommodate such a large functional group in the *endo*-position.

Synthesis and SAR of Oxaibogamines Leads to Novel Analogs with Biased Receptor Signaling

Scheme 4. Synthesis of 7-Substituted 12-Hydroxy-Oxaibogamine Analogs.



Synthesis of Bridgehead-Substituted Analogs. In exploring the SAR of this scaffold further, we found that introduction of a new chiral center at position 7 in the bridgehead imparted promising biological activity. The required ketone intermediates **33** (**Scheme 4A**, **33a-b**) were synthesized from benzofuranone **9** via a Wittig reaction. The deprotected isoquinuclidine was then coupled via a reductive amination with ketones **33** to provide a mixture of methyl- or ethyl-substituted diastereomers (at the position 7). These diastereomers could be separated after the Ni-catalyzed C-H activation reaction and then demethylated as described above (**Scheme 4B**). Interestingly, in the cyclization towards analog **36f**, only one isomer could be isolated. The other

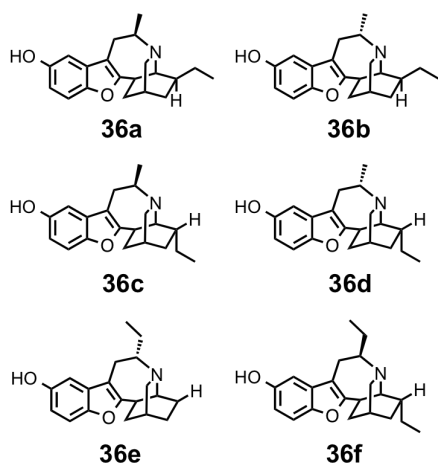


Figure 13. Third Generation 12-Hydroxy-Oxaibogamine Analogs **36a-f**.

hydroxy-oxaibogamine analogs can be found in **Figure 13**.

Functional Activity of Bridgehead-Substituted Analogs. Substitution of a methyl group on carbon 7 (see **Figure 5** for numbering) proved to offer new opportunities for modulating opioid receptor activity. The *endo*- and *exo*-7 substituted *exo*-ethyl analogs showed modest potency at all three opioid receptors (**Table 2**). With the single switch to the *endo*-ethyl analogs (at the position 4), the two compounds showed a minor increase in potency at KOR and compound **36d** showed partial agonism at all three receptors (**Figure 14**, $EC_{50\text{ KOR}} = 0.14 \pm 0.006 \mu\text{M}$ ($E_{\text{Max}} = 72\%$); $EC_{50\text{ MOR}} = 0.37 \pm 0.24 \mu\text{M}$ ($E_{\text{Max}} = 50\%$); $EC_{50\text{ DOR}} = 5.1 \pm 2.2 \mu\text{M}$ ($E_{\text{Max}} = 24\%$)), and

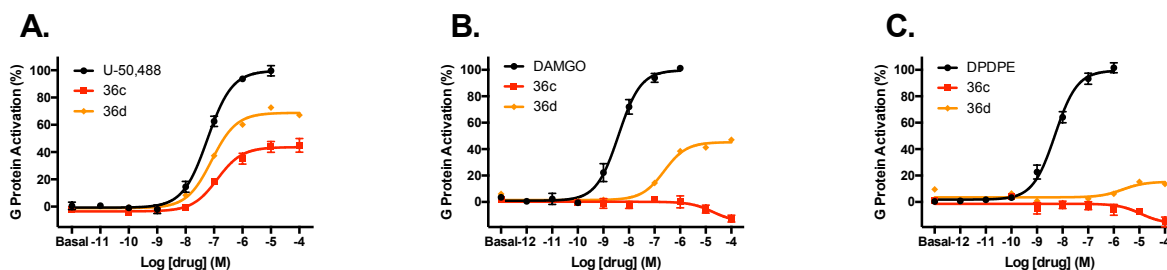


Figure 14. Agonist Activity of Third Generation 12-Hydroxy-Oxaibogamine Analogs **36c-d**. hKOR (A), hMOR (B), or hDOR (C) were co-expressed with $G_{\alpha\text{O}_B}$ -RLuc8, $\beta 1$, and mVenus- $\gamma 2$ to assay G protein activation. Analog **36c** shows $EC_{50\text{ KOR}} = 0.12 \pm 0.01 \mu\text{M}$ ($E_{\text{Max}} = 47\%$). Analog **36d** shows $EC_{50\text{ KOR}} = 0.14 \pm 0.006 \mu\text{M}$ ($E_{\text{Max}} = 72\%$), $EC_{50\text{ MOR}} = 0.37 \pm 0.24 \mu\text{M}$ ($E_{\text{Max}} = 50\%$), and $EC_{50\text{ DOR}} = 5.1 \pm 2.2 \mu\text{M}$ ($E_{\text{Max}} = 24\%$). Curves represent the average of $n \geq 3$, with error bars representing \pm SEM.

remained unreactive, even when subjected to the electrophilic palladation conditions shown in **Schemes 1D** and **3C**. This is in contrast to analog **36e** where the opposite bridgehead stereochemistry was able to be isolated, suggesting some difference in reactivity imparted by the 4 position. Chemistry was optimized and completed by Andrew Kruegel with the help of Elizaveta Kulko. A summary of the third generation 12-

compound **36e** showed selective partial agonism at KOR (**Figure 14**, $EC_{50\text{ KOR}} = 0.12 \pm 0.01 \mu\text{M}$ ($E_{\text{Max}} = 47\%$)). While there is currently limited evidence, it is possible that a potent, partial agonist may avoid some of the unwanted side effects from opioid signaling (such as hallucinations at KOR or constipation at MOR) by not activating the receptor to its fullest, thus curbing the signaling in comparison to a fully efficacious drug. For example, the partial MOR agonist buprenorphine (see **Discussion** below) was shown to cause less respiratory depression in comparison to other opioids like levorphanol and methadone in rhesus monkeys, thus highlighting this principle.⁴⁸ Drawing similarity from this example at MOR, as a selective partial KOR agonist, **36e** may be less dysphoric than classical KOR agonists like salvinorin A and is likely to have low abuse potential. Ethyl substitutions on the bridgehead carbon also showed interesting activity at the opioid receptors. The compound **36e** (“*iso*-ethyl” with respect to **15b**) represents the most potent compound in the series at KOR and shows selectivity for KOR over MOR and DOR (**Figure 15**, $EC_{50\text{ KOR}} = 0.09 \pm 0.02 \mu\text{M}$ ($E_{\text{Max}} = 81\%$); $EC_{50\text{ MOR}} = 0.86 \pm 0.02 \mu\text{M}$ ($E_{\text{Max}} = 30\%$); $EC_{50\text{ DOR}} = 0.31 \pm 0.0003 \mu\text{M}$ ($E_{\text{Max}} = 20\%$)). The *endo*-ethyl analog (**36f**)

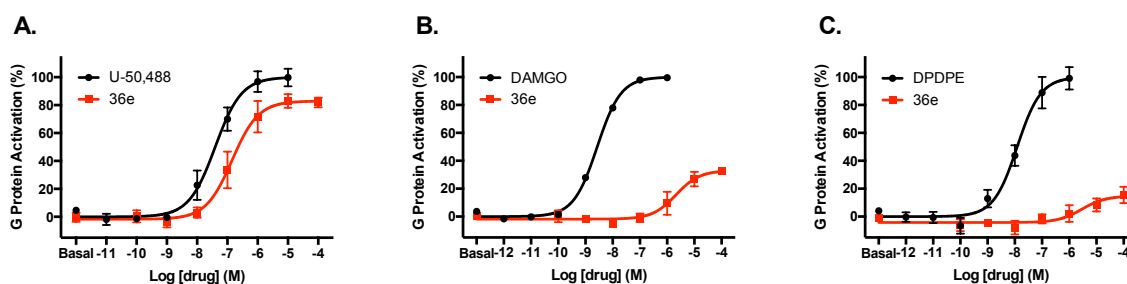


Figure 15. Third Generation 12-Hydroxy-Oxaibogamine Analog **36e** is a Potent and Selective KOR Agonist. hKOR (A), hMOR (B), or hDOR (C) were co-expressed with $G\alpha_{\text{OB-RLuc8}}$, $\beta 1$, and mVenus- $\gamma 2$ to assay G protein activation. Analog **36e** shows $EC_{50\text{ KOR}} = 0.09 \pm 0.02 \mu\text{M}$ ($E_{\text{Max}} = 81\%$), $EC_{50\text{ MOR}} = 0.86 \pm 0.02 \mu\text{M}$ ($E_{\text{Max}} = 30\%$), and $EC_{50\text{ DOR}} = 0.31 \pm 0.0003 \mu\text{M}$ ($E_{\text{Max}} = 20\%$). Curves represent the average of $n = 3$, with error bars representing \pm SEM.

was unique in this series in that it shows antagonism at KOR (**Figure 16**, $IC_{50\text{ KOR}} = 8.2 \pm 0.5 \mu\text{M}$), the only compound in this scaffold showing such biological activity. Additionally, Schild analysis of **36f** revealed an A_2 of $0.43 \pm 0.23 \mu\text{M}$ and slope of 0.9 ± 0.03 , indicating a

competitive mode of action (**Figure 16**). While KOR antagonists have little therapeutic potential

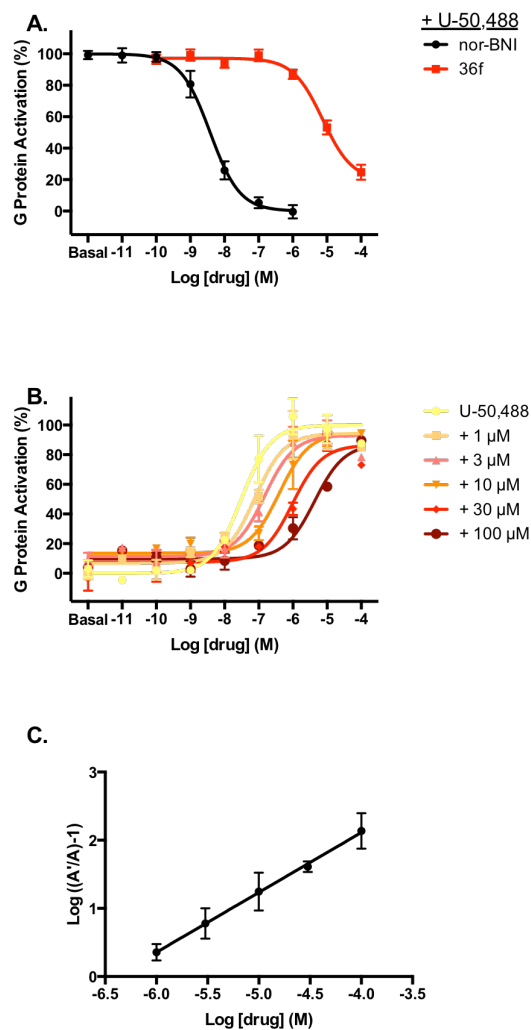


Figure 16. Third Generation 12-Hydroxy-Oxaibogamine Analog **36f** is a KOR Antagonist. hKOR was co-expressed with $G\alpha_B$ -RLuc8, $\beta 1$, and mVenus- $\gamma 2$ to assay G protein activation. **A.** **36f** was tested for KOR antagonism. Control antagonist = nor-BNI, and agonist U-50,488 was used at 5x its EC_{50} concentration. **B.** Control agonist U-50,488 was incubated with increasing concentrations of **36f**. **C.** Schild plot of (B) reveals a competitive antagonist mode of action. Curves represent the average of $n = 3$, with error bars representing \pm SEM.

for pain, they are widely reported to have antidepressant effects in several animal models.^{49–51} Therefore additional testing on this compound is necessary to assess its potential for antidepressant therapy. Clinical trials with KOR antagonists are only just beginning.⁵² A phase I trial with selective KOR antagonist JDtic has concluded, but the compound caused tachycardia in some subjects and thus will not be continuing in additional trials aimed at assessing behavioral effects.⁵³

New Analog Shows G Protein Biased Signaling. In order to better understand the biological activity within this scaffold, compound **36c** was chosen as the most promising lead to move forward in more complex signaling studies. As a selective KOR agonist, compound **36c** represents an alternative to MOR agonists, like morphine, for pain relief since KOR agonists do not activate the dopamine reward pathway (in fact,

KOR agonists negatively control the release and extracellular concentration of dopamine).^{54,55} As such, KOR agonists are a non-addictive therapeutic for pain. They do, however, have their own unwanted side effects, like dysphoria (see Introductory Chapter 1). While compound **36c** may avoid some of these effects due its partial activation of the receptor, a more suitable alternative would be to avoid the unwanted side effects altogether. It is hypothesized that such unwanted side effects are mediated through the arrestin signaling associated with GPCR activation. Therefore, if a compound could selectively activate the G protein signaling cascade over the arrestin signaling, then this biased signaling could provide the analgesic benefits of receptor activation while avoiding the aversive side effects (again see Chapter 1).^{56,57}

In order to assess whether compound **36c** showed any arrestin recruitment, a different BRET assay was utilized. Using KOR tagged with RLuc8 (BRET donor) and Arrestin-3 tagged with the yellow fluorescent protein variant mVenus (BRET acceptor), a positive BRET signal can be correlated with arrestin recruitment. When compound **36c** was tested in this BRET

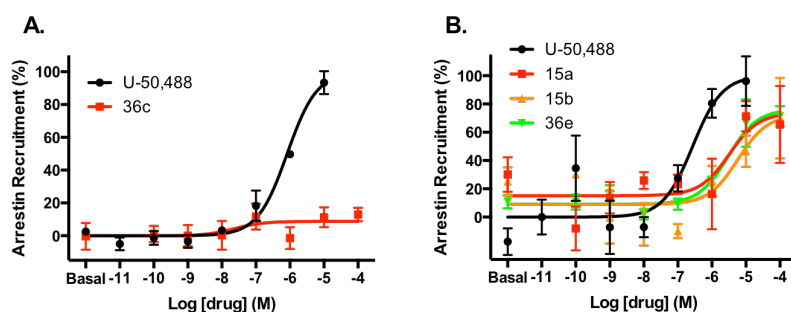


Figure 17. 12-Hydroxy-Oxaibogamine Analog **36c** Shows No Measureable Arrestin Recruitment. hKOR-RLuc8 was transfected with Arr3-Venus and GRK3. A. **36c** shows an apparent bias towards G protein signaling with no obvious arrestin recruitment detected. B. Other 12-hydroxy-oxaibogamine analogs show arrestin recruitment similar to the control compound U-50,488. Curves represent the average of $n \geq 3$, with error bars representing \pm SEM. BRET recruitment assay used.

recruitment assay (see Introductory Chapter 1 for more detail), there was no measurable recruitment of arrestin when compared to either the control U-50,488 or other oxaibogamine analogs **15a** and **15b**

(**Figure 17**), thus indicating an extreme efficacy bias for G protein activation. Therefore, further

testing of **36c** is warranted to determine if the unique biological activity observed *in vitro* translates into distinct behavioral effects *in vivo*, including for example, a lack of aversive side effects.

Enantioselective Synthesis of Oxaibogamine Analog (5S)-46. In an attempt to better understand the biology of these new compounds, we decided to undertake an enantioselective synthesis of select analogs. In the current synthetic route described above, all compounds are synthesized in racemic form. Since the natural product ibogaine itself (and consequently its metabolite, noribogaine) are optically pure, there was interest in comparing the activity of our racemically prepared compounds with their active enantiomers (defined at carbon 5, see **Figure 5** above). Utilizing a previously described method for preparing enantiomerically enriched isoquinuclidines⁵⁸, the required chiral oxazolidine catalyst **38** was synthesized from the corresponding amino alcohol and benzaldehyde (**Scheme 5A**). This organocatalyst was then utilized in a Diels-Alder reaction similar to that seen in **Scheme 2A** with dihydropyridine and acrolein to provide the *endo*-isoquinuclidine (**Scheme 5B, (IR)-16**). This material was then epimerized and reduced to provide

both the *exo*- and *endo*- alcohols ((**IR**)-17a and (**IR**)-17b) as the *IR*-enantiomer in ~85 and > 95% ee, respectively, determined on chiral HPLC. Due to the large bulk from the phenyl groups on the oxazolidine catalyst, control over the equilibrium

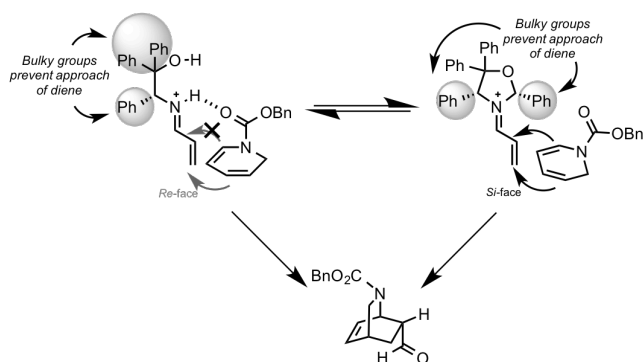
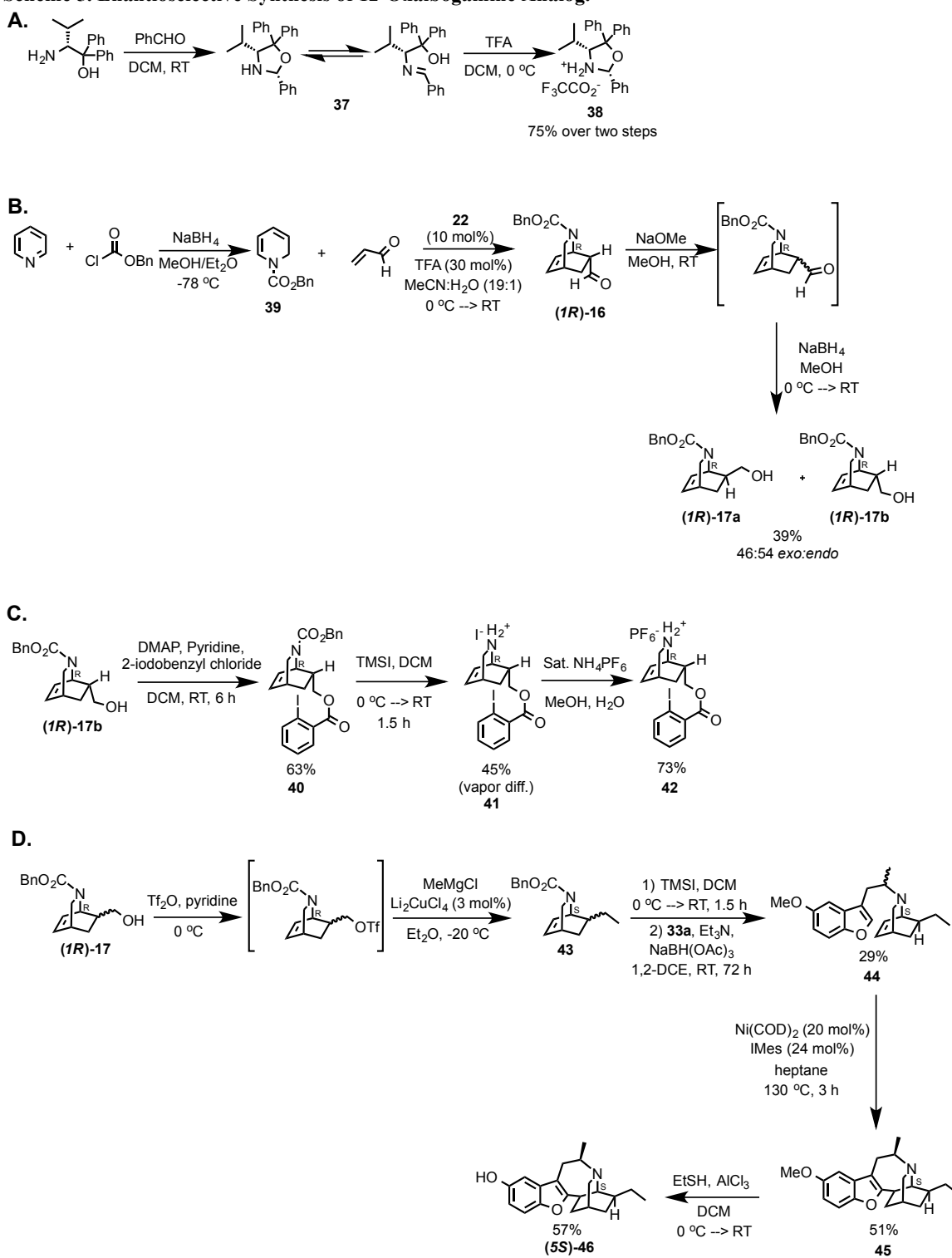


Figure 18. Oxazolidine Organocatalyst Leads to High Enantioselectivity and Exclusive Formation of the *Endo*-Isoquinuclidine.

between iminium intermediates from the dienophile is obtained, which effectively blocks one

Scheme 5. Enantioselective Synthesis of 12-Oxaibogamine Analog.



iminium face from attack by the diene, leading to high enantioselectivity (**Figure 18**). The *si*-face attack allows for greater frontier orbital overlap between diene and dienophile, which

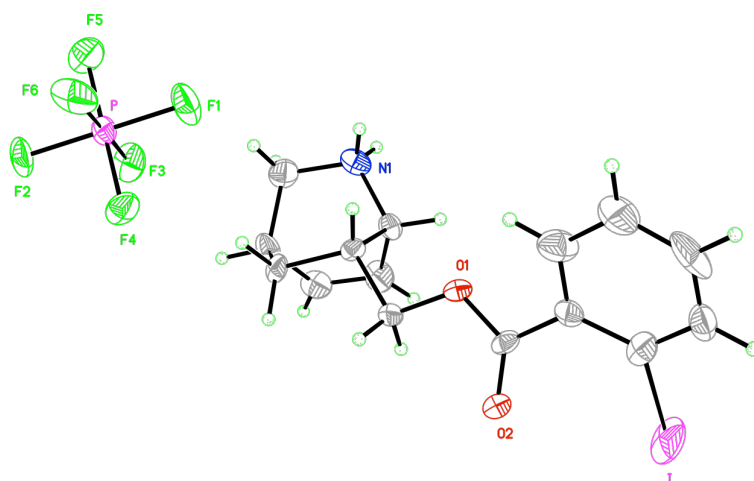


Figure 19. X-Ray Crystal Structure of Isoquinuclidine **42** Confirms Relative and Absolute Configuration.

ultimately enhances the enantioselectivity. We

chose the enantiomer to synthesize based on the absolute configuration of ibogaine. In order to confirm the absolute stereochemistry of

isoquinuclidines (**IR**)-**17**, a crystal structure was

needed. Because (**IR**)-**17** is isolated as an oil, it was necessary to convert it to a compound that not only could be crystallized, but also contained a heavy atom near the stereocenter in question. Based on these criteria, compound **42** was prepared (**Scheme 5C**), crystallized and the X-ray structure analysis obtained (the structure was solved by Serge Ruccolo in the Parkin laboratory); the absolute geometry was thus independently confirmed (**Figure 19**).

Next, isoquinuclidines (**IR**)-**17** were subjected to a copper-catalyzed cross-coupling reaction⁵⁹ to transform the alcohol into a methyl group, thus providing the desired enantiomerically enriched isoquinuclidines (**Scheme 5D**). Given the diverse scope of triflates and reaction conditions reported for this reaction, much optimization was required to obtain satisfying yields on our substrate (not included in this report). After converting the alcohol (**IR**)-**17** to a triflate, this material was used directly in the copper-catalyzed cross-coupling reaction

utilizing dilithium tetrachlorocuprate (II) and methyl magnesium bromide. Exploring various temperatures, reaction times, and reagent order, optimal conditions were determined (**Table 3**), which provided yields consistently >60% (highest yield obtained at 96%).

Table 3. Optimization of Copper-Catalyzed Cross-Coupling Reaction to Isoquinuclidine 29

Entry	Li ₂ CuCl ₄ (mol%)	Order of Addition	Temp (°C)	Time (h)	Conversion (Yield)
1	3%	1. Li ₂ CuCl ₄ , MeMgBr	-15	2 h → O/N	Incomplete (<10%)
2	3% → 9%	1. MeMgBr, Li ₂ CuCl ₄	-15 → RT	2 h	Complete (10%)
3	20%	1. MeMgBr, Li ₂ CuCl ₄	-15	1 h	Complete (30%)
4	20%	1. Li ₂ CuCl ₄ , MeMgBr	-80 → -15	2 h	Complete (43%)
5	50%	1. Li ₂ CuCl ₄ , MeMgBr	-45	30 m	Complete (96%)

Once intermediates **43** were synthesized, the same synthetic route described in **Scheme 4** could be utilized. Given the consistently higher yields seen for *exo*-isomers both in the reductive amination and the nickel-catalyzed C-H activation reaction, it was decided that *exo*-intermediate **43a** should be carried forward through the rest of the synthesis and tested in our biological assays. Isoquinuclidine **43a** was thus reacted with ketone **33a**, cyclized, and demethylated as before to provide enantiomerically enriched (**5S**)-**46** (>85% ee from (*1R*)-**17a**, **Scheme 5D**).

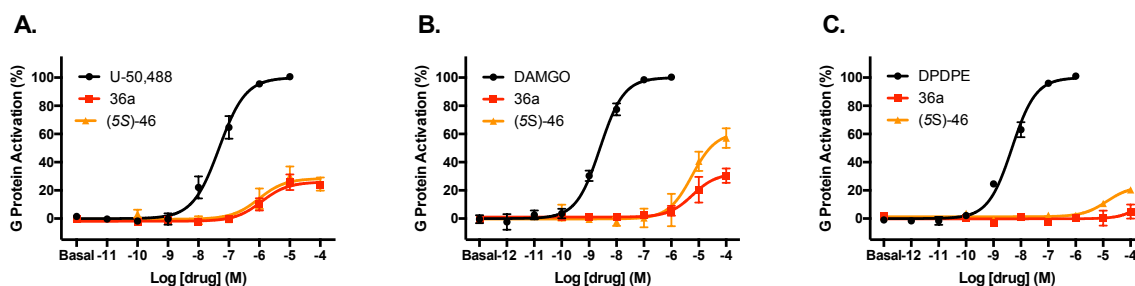


Figure 20. Enantiomerically Enriched 12-Hydroxy-Oxaibogamine Analog Shows Similar Biological Activity to Its Racemic Form. hKOR (A), hMOR (B), or hDOR (C) were co-expressed with Gao_B-RLuc8, β1, and mVenus-γ2 to assay G protein activation. Analog **36a** shows EC₅₀_{KOR} = 1.7 ± 1.1 μM (E_{Max} = 26%) and EC₅₀_{MOR} = 4.7 ± 3.6 μM (E_{Max} = 24%). Analog (**5S**)-**46** shows EC₅₀_{KOR} = 1.4 ± 1.2 μM (E_{Max} = 24%), EC₅₀_{MOR} = 4.2 ± 2.0 μM (E_{Max} = 61%), and EC₅₀_{DOR} = 10 ± 10 μM (E_{Max} = 20%). Curves represent the average of n = 3, with error bars representing ± SEM.

Oxaibogamine Enantiomer Has Similar Functional Activity to its Racemic Analog. Next, we aimed to assess the biological activity of enantiomer (**5S**)-**46** alongside the parent racemic

analog **36a** (Figure 20). Interestingly, we found that their biological activities were similar across all three opioid receptors; racemic **36a** showed weak activity at the KOR and MOR opioid receptors ($EC_{50\text{ KOR}} = 1.7 \pm 1.1 \mu\text{M}$ ($E_{\text{Max}} = 26\%$); $EC_{50\text{ MOR}} = 4.7 \pm 3.6 \mu\text{M}$ ($E_{\text{Max}} = 24\%$) and no activity at DOR in this concentration range; enantiomer (**5S**)-**46** shows essentially the same activity at KOR ($EC_{50\text{ KOR}} = 1.4 \pm 1.2 \mu\text{M}$, $E_{\text{Max}} = 24\%$), while improved efficacy at MOR ($EC_{50\text{ MOR}} = 4.2 \pm 2.0 \mu\text{M}$, $E_{\text{Max}} = 61\%$), and marginal but detectable activity at DOR ($EC_{50\text{ DOR}} = 10 \pm 10 \mu\text{M}$, $E_{\text{Max}} = 20\%$). Given the nearly identical potency and efficacy between racemic **36a** and its enantiomer **46**, it seems that the (*5S*)- and (*5R*)-enantiomer (untested) impart similar biological activity at KOR. At MOR it is plausible that weak partial agonism from the less active *5R* enantiomer may inhibit the activity of the more active *5S* enantiomer in the racemic mixture. In order to confirm these findings, the (*5R*)-enantiomer of the compound should be synthesized for comparison. Since the biological activity of **36a** and (**5S**)-**46** were so similar, we decided against synthesizing other enantiomerically pure compounds at this time and will continue with the racemic forms in future *in vivo* studies.

Discussion

Mechanism of Action of Ibogaine. The non-selective nature of ibogaine's binding within the CNS has led to a much-contested debate about its ultimate mechanism of action. Although ibogaine is reported to bind to many targets with only relatively weak affinities, the large dose of the drug administered during an "ibogaine reset" implies that high enough concentrations of the drug may be reached in the brain to make these weak targets relevant (see **Introduction**).^{2,41,42} Given the known acute effects of the ibogaine treatment (severe hallucinations, nausea, vomiting, headaches)⁵ and binding affinities of ibogaine to CNS targets, a likely starting point in the

biological activity of ibogaine is NMDAR antagonism. NMDAR antagonists are well known to have dissociative effects and several of these compounds have been reported to attenuate the acquisition and/or expression of drug dependence (e.g., drug self administration and other aspects of drug dependence states).^{60,61} Further, ibogaine is well known to be a noncompetitive inhibitor of SERT (both in our laboratory and others), regulating the dissociation of serotonin into the cytoplasm, as well as at DAT.^{62,63} The effects of dual SERT-DAT inhibition in several animal models are known to reduce cocaine self-administration, which could additionally contribute to the unique properties of ibogaine on drug dependence. It is interesting that as a natural product, ibogaine is modulating the function of many CNS targets that are key players in psychiatry – namely selective serotonin reuptake inhibitors for depression and mood disorders and NMDAR antagonists for depression (see Introductory Chapter 1 for further discussion). In this regard, NMDAR antagonism can lead to increased brain-derived neurotrophic factor (BDNF) release and remodeling of brain circuitry⁶⁴, perhaps in response to damage caused from drug dependence. In a similar manner, the known release of GDNF following ibogaine administration in rats may also act to reset the dopaminergic reward system resulting in decreased alcohol self-administration.²⁷

Upon first-pass metabolism of ibogaine to noribogaine, opioid activity may then play a role in the known effects of ibogaine. KOR activation by noribogaine may also contribute to the hallucinations, however with the added MOR activation may lead mood enhancement (after the dissociative effects subside). NMDAR is also known to potentiate MOR signaling and thus there is a possibility for additive or synergistic effects. In terms of reported side effects, there are reported cases of cardiac arrhythmia following ibogaine consumption. It is likely that these effects are caused by hERG channel blockade.¹² This brief analysis leads to a reasonable

pharmacological hypothesis for both the acute and long-term effects of ibogaine reset, where the users emerge feeling hopeful and apparently free from addiction.

Important SAR of Iboga Scaffold. In order to enhance the opioid activity in this scaffold, SAR was explored to find more potent compounds. Using a systematic approach, simple changes to the core *iboga* structure were made in order to understand what key features of the scaffold were necessary for opioid activity. This method of SAR exploration revealed the importance of benzofuran substitution within the *iboga* scaffold over the parent indole structure. When combined with the 12-hydroxy substitution of noribogaine, novel analogs were identified with greatly increased potency and efficacy when compared to noribogaine. Deborah Mash and colleagues are actively pursuing noribogaine itself in controlled clinical trials for opioid substance abuse, suggesting that both ibogaine and noribogaine are bioavailable compounds with proven clinical efficacy. In this regard, compounds such as those described here, being distinct yet closely related to ibogaine itself, will likely retain many of the favorable properties of this natural product, including blood brain barrier penetration, favorable pharmacokinetics and metabolism, and safety in human usage (noribogaine specifically)²⁵, which highlights the therapeutic potential for these analogs.

Implications of Polypharmacology. Successful drug candidates are often praised for their selectivity for one biological target over another. In fact, off target activity is a common downfall of lead candidates before reaching the clinical stage of development. If a drug binds to many targets at therapeutic doses, this can lead to unwanted side effects and muddle the beneficial signaling imparted by the main mechanism of action. Polypharmacology, however, is currently being utilized in the context of many diseases, including Alzheimer's disease⁶⁵, cancer⁶⁶, viruses⁶⁷, and anti-inflammatory diseases⁶⁸. The idea of polypharmacology is interesting in the

context of opioid signaling as well. Buprenorphine, for instance, has mixed KOR antagonism and MOR partial agonism.⁶⁹ Used clinically for treating both pain and substance abuse disorders, buprenorphine is as efficacious as morphine for analgesia but has a lower risk of respiratory depression.⁷⁰ It has additionally been found in multiple clinical trials to have antidepressant effects, not surprising given its dual opioid activity.^{71–73} While some report the antidepressant effects of buprenorphine to be mediated solely through its KOR antagonism⁷⁴, there is a likely contribution from MOR agonism, as well (see tianeptine Chapter 2). There are various other examples of mixed opioids: MP1104, an IBNtxA analog, is a KOR and DOR agonist with potent analgesic effects that does not cause aversion, preference, or rewarding behavior⁷⁵; MGM-16 is a mitragynine alkaloid analog (see Chapter 3) that is 240 times more potent than morphine in the mouse tail-flick test and shows promise for treating neuropathic pain⁷⁶; and a DOR antagonist/MOR agonist is being pursued in the clinic for the treatment of irritable bowel syndrome.⁷⁷ Interestingly there is a report exploring the synthesis and characterization of *iboga* analogs with proposed activity at the opioid receptors. The study looks promising in that compounds tested show comparable analgesia to morphine in mice, however with nothing but binding data provided at the opioid receptors, it is difficult to appreciate the extent to which each opioid receptor plays a role in these *in vivo* results.⁷⁸ Finally, selective targeting of MOR/DOR heteromers (See Introductory Chapter 1) represents a novel (yet controversial) form of polypharmacology.⁷⁹

With the three opioid receptors containing a high level of homology⁸⁰, it is not surprising that they share some pharmacology. When activated, all three opioid receptors are known to have analgesic properties, however each holds unique cellular and physiological effects, as well. We have reported MOR agonists to also have antidepressant and anxiolytic effects³², while KOR

antagonists and DOR agonists have been shown to have antidepressant-like effects in rodents. One can imagine that finding the right combination of receptor activity may allow the tuning of desired effects while mitigating those that are undesired. In many ways, this concept is still in its infancy for therapeutic purposes, but it does expand the possibilities for finding the most effective treatments for patients, especially as we begin to understand on the molecular level what causes disease in any one individual.

Biased Signaling as a Path to Better Therapeutics? It is widely reported that opioid activation can lead to many unwanted side effects.⁸¹ For instance, KOR activation, while offering a non-addictive alternative to morphine, is known to cause dysphoria and hallucinations.⁸² MOR activation may lead to addiction and also causes respiratory depression, constipation, and tolerance to therapeutic effects.⁸³ Finally, DOR activation can lead to seizures in animals,^{84–88} albeit with limited known adverse effects in humans to date (see also Clinical Trial NCT00759395, unpublished).⁸⁹ Considering these potentially dangerous side effects, it is not surprising that serious reservations cloud the development of new opioid therapeutics. However a new age of opioid usage is coming as scientists explore the idea of biased agonism suggested first by Laura Bohn⁹⁰ for MOR and by Charles Chavkin⁵⁶ for KOR (see Introductory Chapter 1 for further background). It is hypothesized that if compounds can be identified with functional bias for G protein signaling over arrestin recruitment, then there is possibility for opioid therapeutics that will avoid deleterious effects altogether. Several examples are already showing promise both in literature and in the clinic. The KOR partial agonist 6'-guanidinonaltrindole (6'-GNTI) has been reported by several groups to be G protein biased, acting as an antagonist of arrestin signaling and blocking receptor internalization.^{91,92} Although this compound shows real promise in the *in vitro* setting, its alleged inability to cross the blood brain barrier (BBB) has

halted the progress of study *in vivo* and in the clinic, highlighting the need for novel biased KOR agonists with improved brain penetration. Laura Bohn and coworkers have developed several brain-penetrant, functionally selective KOR agonists, however further exploration of these interesting compounds *in vivo* is unclear at this point.⁵⁷ Additionally, Trevena has developed an MOR agonist, TRV130, that shows clear G protein bias *in vitro*, as well as potent analgesia with decreased respiratory suppression and gastrointestinal dysfunction.⁹³ Currently TRV130 is in multiple clinical trials for post-operation (acute) pain, and thus scientists should observe direct evidence soon about how *in vitro* bias translates into human therapeutics. There is still an evident disconnect between what G protein bias actually means when applied to real therapeutic potential⁹⁴, and therefore a greater effort needs to begin to move such studies to relevant circuits and cell types, and connect these findings with *in vivo* results. Compound **36c**, reported here, stands out when compared to another G protein biased KOR agonist, like 6'-GNTI, for its improved physicochemical properties and potential BBB penetration and warrants further study *in vivo*.

Arrestin does, however, regulate many important cellular functions, including receptor internalization and recycling (see Introductory Chapter 1 for more detail), making the benefit of developing G protein biased compounds unclear. For instance, morphine suffers from respiratory depression and tolerance development, but does not cause receptor internalization in every cell type, suggesting some level of G protein bias without beneficial effects.⁹⁵ Further, Whistler and colleagues have found that MOR endocytosis actually reduces tolerance and dependence, suggesting that the mechanisms controlling some undesired opioid effects may be more complex than just biased versus unbiased signaling.⁹⁶⁻⁹⁸ One hypothesis suggests that prolonged MOR signaling could instead lead to the development of adverse effects rather than receptor

desensitization and endocytosis. In light of this evidence, exploring G protein biased compounds further *in vivo* may reveal how *in vitro* signaling translates into beneficial behavioral effects, if any.

Conclusions

Here we report on a new class of *iboga* alkaloid analogs that show much improved activation of the opioid receptors when compared to the ibogaine metabolite noribogaine. Through a targeted SAR exploration, we identified the necessity of the 12-oxaibogamine structure for opioid activity. Utilizing both organic chemistry to synthesize new analogs in this scaffold as well as *in vitro* pharmacology to measure the functional activity of these compounds, several analogs were identified with varying degrees of potency and efficacy at the KOR, MOR, and DOR. In particular, compound **36c** shows apparent bias for G protein signaling over arrestin signaling in these assays. This compound and its close derivatives represent new leads for study *in vivo*. This G protein biased KOR agonist offers new hope for improved analgesic therapeutics and may finally overcome the many shortcomings of traditional MOR analgesics.

Experimental

Chemistry

General Considerations. Reagents and solvents (including anhydrous solvents) were obtained from commercial sources and were used without further purification unless otherwise stated. All compounds were prepared in racemic form. All reactions were performed in flame-dried glassware under argon atmosphere unless otherwise stated and monitored by TLC using solvent mixtures appropriate to each reaction. All column chromatography was performed on

silica gel (40-63 μm) and preparative TLC on 20 x 20 cm plates coated in a 1 mm silica layer. Nuclear magnetic resonance spectra were recorded on Bruker 300, 400, or 500 MHz instruments as indicated. Chemical shifts are reported as δ values in ppm referenced to CDCl_3 (^1H NMR = 7.26 and ^{13}C NMR = 77.16) or Methanol- d_4 (^1H NMR = 3.31 and ^{13}C NMR = 49.00). Multiplicity is indicated as follows: s (singlet); d (doublet); t (triplet); q (quartet); p (pentet); h (heptet); dd (doublet of doublets); ddd (doublet of doublet of doublets); dt (doublet of triplets); td (triplet of doublets); dtd (doublet of triplet of doublets); ddt (double of doublet of triplets); m (multiplet); br (broad). For those described compounds containing a carbamate group, complex spectra with split peaks are observed. This effect can be ascribed to the presence of conformers about the carbamate group. Furthermore, compounds containing fluorine are subject to F-C coupling, resulting in splitting of some carbon peaks. As a result of these effects, multiple peaks may correspond to the same proton group or carbon atom. In some cases, this is indicated by an "and" joining two peaks or spectral regions. Alternatively, certain carbon peaks overlap and thus represent two carbons (indicated by (2C) designation). In all cases the assignments of these complex peaks were determined by COSY, HSQC, and/or DEPT-135 experiments. All carbon peaks are rounded to one decimal place unless such rounding would cause two close peaks to become identical. In these cases, two decimal places are retained. Low-resolution mass spectra (LR-MS) were recorded on a JEOL LCmate (ionization mode: APCI+). High-resolution mass spectra (HRMS) were acquired on a high-resolution sector-type double-focusing mass spectrometer (ionization mode: FAB+). In calculated high-resolution masses, the mass difference for loss of one electron has been taken into account for positive ions.

Compounds 3-19. The synthesis of compounds **3-19** was carried out as previously reported in our group.^{46,47}

endo-benzyl 7-benzyl-2-azabicyclo[2.2.2]oct-5-ene-2-carboxylate (20). Potassium phenyltrifluoroborate (139 mg, 0.75 mmol) and bathophenanthroline (24 mg, 0.072 mmol) were combined with LiHMDS (376 mg, 2.25 mmol), NiBr₂•glyme (23 mg, 0.075 mmol), and sec-butanol (1.5 ml) in a glovebox. The reaction was stirred at room temperature for 30 min. outside the glovebox followed by addition of bromide **19** (250 mg, 0.74 mmol). The reaction was then warmed to 60 °C and stirred for 21 h after which time it was cooled to room temperature and run through a short silica column with EtOAc (40 mL). The organics were concentrated to give a yellow oil, which was purified by column chromatography (6:1 hexanes:EtOAc) to give the pure product as a yellow oil (160.1 mg, 65%). **¹H NMR (400 MHz, CDCl₃)** (spectrum complicated by conformers). δ 7.51 – 7.27 (m, 7H), 7.26 – 7.13 (m, 3H), 6.59 – 6.43 (m, 1.5H), 6.43 – 6.29 (m, 0.5H), 5.18 (dd, J = 13.6, 6.4 Hz, 2H), 4.71 (dq, J = 4.9, 2.5 Hz, 0.5H), 4.54 (d, J = 6.2 Hz, 0.5H), 3.31 (ddd, J = 10.1, 4.7, 2.4 Hz, 1H), 3.12 – 2.98 (m, 1H), 2.83 – 2.71 (m, 1H), 2.62 – 2.32 (m, 3H), 1.99 – 1.85 (m, 0.6H), 1.79 (dt, J = 13.6, 4.9 Hz, 0.4H), 1.10 – 0.95 (m, 1H). **¹³C NMR (101 MHz, CDCl₃)** (spectrum complicated by conformers and some minor impurities). δ 155.43, 154.89, 140.08, 139.90, 137.42, 137.28, 135.42, 134.81, 131.14, 130.28, 129.17, 129.01, 128.74, 128.12, 128.03, 127.61, 126.39, 77.80, 77.48, 77.16, 66.94, 49.36, 49.13, 47.48, 47.16, 41.92, 40.80, 40.46, 31.57, 31.40, 30.41, 30.11. **LR-MS** calcd. for C₂₂H₂₄NO₂⁺ [M+H]⁺ 334.18, found 334.35.

Compounds 21-27. The synthesis of compounds **21-27** was carried out as previously reported in our group.⁴⁷

General Procedure for Preparation of N-arylalkylisoquinuclidines (28a-d). To a solution of a carbamate protected isoquinuclidine **18a-b** or **20** or **27** (1 equivalent) in anhydrous CH₂Cl₂ (0.125 M, based on isoquinuclidine) at 0 °C was added iodotrimethylsilane (4

equivalents), and the resulting mixture was stirred for 10 min. at 0 °C and then at room temp. until TLC indicated that no isoquinuclidine remained (typically ~1 h). The reaction mixture was then concentrated to yield the deprotected isoquinuclidine hydroiodide salt in quantitative yield (for benzyl carbamate protected isoquinuclidines, the resulting salt was washed several times with hexanes to remove the benzyl iodide byproduct). To this material was added to **12** (1 equivalent) and NaHCO₃ (4 equivalents) followed by anhydrous CH₃CN (0.208 M, based on isoquinuclidine), and the resulting mixture was refluxed until TLC indicated the disappearance of the bromide (typically >24 h). The reaction was then diluted with H₂O, made strongly basic with aqueous NaOH, and extracted with CHCl₃ (3x). The combined organics were washed with H₂O, dried over Na₂SO₄, and concentrated to provide the crude product, which was purified by column chromatography with an appropriate solvent mixture (as described below for each compound).

***exo*-2-(2-(5-methoxybenzofuran-3-yl)ethyl)-7-(methoxymethyl)-2-azabicyclo[2.2.2]oct-5-ene (28a)**. The product **28a** was prepared according to the general procedure and was purified by column chromatography (15:1 hexanes:EtOAc, 2 column volumes → 15:1 hexanes:EtOAc + 2% Et₃N) and obtained as a light-brown oil (76.1 mg, 58%). ¹H NMR (400 MHz, CDCl₃) δ 7.46 (d, J = 1.2 Hz, 1H), 7.33 (d, J = 8.9 Hz, 1H), 6.97 (d, J = 2.6 Hz, 1H), 6.87 (dd, J = 8.9, 2.6 Hz, 1H), 6.38 (ddd, J = 8.0, 6.4, 1.5 Hz, 1H), 6.30 (ddd, J = 8.1, 5.4, 1.4 Hz, 1H), 3.86 (s, 3H), 3.54 (t, J = 9.0 Hz, 1H), 3.43 (dt, J = 5.4, 1.8 Hz, 1H), 3.33 (dd, J = 8.8, 5.7 Hz, 1H), 3.27 (s, 3H), 3.06 (dd, J = 9.1, 2.4 Hz, 1H), 2.87 - 2.79 (m, 1H), 2.78 - 2.63 (m, 2H), 2.53 (ddd, J = 11.2, 6.4, 2.6 Hz, 1H), 2.47 (ddd, J = 6.3, 4.6, 3.0 Hz, 1H), 1.93 (dt, J = 9.1, 2.6 Hz, 1H), 1.74 (ddd, J = 5.5, 3.4, 2.0 Hz, 1H), 1.46 - 1.37 (m, 1H), 0.84 (ddd, J = 12.4, 5.2, 2.2 Hz, 1H). ¹³C NMR (101 MHz, CDCl₃) δ 155.8, 150.3, 142.7, 133.6, 132.2, 129.2, 119.2, 112.6,

111.8, 102.5, 75.4, 58.8, 57.5, 56.2, 56.1, 53.8, 39.5, 31.4, 26.3, 22.9; **LR-MS** calcd. for $C_{20}H_{26}NO_3^+$ $[M+H]^+$ 328.19, found 328.42.

***endo*-2-(2-(5-methoxybenzofuran-3-yl)ethyl)-7-(methoxymethyl)-2-azabicyclo[2.2.2]oct-5-ene (28b)**. The product **28b** was prepared according to the general procedure and was purified by column chromatography (5:1 hexanes:EtOAc with 2% Et₃N) and obtained as a light-brown oil (173.1 mg, 50%). **¹H NMR (400 MHz, CDCl₃)** δ 7.42 (d, J = 1.1 Hz, 1H), 7.32 (d, J = 8.9 Hz, 1H), 6.99 (d, J = 2.6 Hz, 1H), 6.87 (dd, J = 8.9, 2.6 Hz, 1H), 6.41 (ddd, J = 8.1, 6.5, 1.4 Hz, 1H), 6.21 - 6.14 (m, 1H), 3.85 (s, 3H), 3.57 (ddd, J = 5.4, 2.9, 1.5 Hz, 1H), 3.30 (s, 3H), 3.07 (dd, J = 9.5, 2.1 Hz, 1H), 3.01 - 2.97 (m, 2H), 2.89 - 2.72 (m, 3H), 2.59 - 2.49 (m, 3H), 2.07 (dt, J = 9.6, 2.7 Hz, 1H), 1.72 (ddd, J = 12.3, 9.5, 2.8 Hz, 1H), 0.66 (ddt, J = 12.5, 4.7, 2.8 Hz, 1H); **¹³C NMR (101 MHz, CDCl₃)** δ 156.1, 150.6, 142.7, 134.2, 130.2, 129.3, 119.1, 113.1, 112.2, 102.7, 76.5, 59.0, 58.0, 56.4, 54.9, 54.9, 39.0, 31.4, 26.9, 23.4; **LR-MS** calcd. for $C_{20}H_{26}NO_3^+$ $[M+H]^+$ 328.19, found 327.79.

***exo*-7-benzyl-2-(2-(5-methoxybenzofuran-3-yl)ethyl)-2-azabicyclo[2.2.2] oct-5-ene (28c)**. The product **28c** was prepared according to the general procedure and was purified by column chromatography (20:1 hexanes:Et₂O, 4 column volumes → 20:1 hexanes:Et₂O + 2% Et₃N, 4 column volumes) and obtained as a pale-yellow oil (41.9 mg, 60%) as previously described.⁴⁷

***endo*-7-benzyl-2-(2-(5-methoxybenzofuran-3-yl)ethyl)-2-azabicyclo [2.2.2]oct-5-ene (28d)**. The product **28d** was prepared according to the general procedure and was purified by column chromatography (15:1 hexanes:EtOAc + 2% Et₃N) and obtained as a pale-yellow oil (95.8 mg, 54%). **¹H NMR (400 MHz, CDCl₃)** δ 7.41 (d, J = 1.1 Hz, 1H), 7.38 (d, J = 8.9 Hz, 1H), 7.34 - 7.31 (m, 2H), 7.26 - 7.21 (m, 3H), 7.02 (d, J = 2.6 Hz, 1H), 6.93 (dd, J = 8.9, 2.6 Hz,

1H), 6.53 (ddd, J = 7.9, 6.4, 1.4 Hz, 1H), 6.28 (ddd, J = 8.2, 5.4, 1.4 Hz, 1H), 3.90 (s, 3H), 3.32 (ddd, J = 5.3, 2.7, 1.4 Hz, 1H), 3.10 (dd, J = 9.6, 2.1 Hz, 1H), 2.89 - 2.81 (m, 1H), 2.80 - 2.73 (m, 2H), 2.62 - 2.54 (m, 3H), 2.45 (dd, J = 8.1, 6.7 Hz, 2H), 2.12 (d, J = 9.5 Hz, 1H), 1.83 (ddd, J = 12.2, 9.1, 2.8 Hz, 1H), 0.98 - 0.93 (m, 1H); ^{13}C NMR (101 MHz, CDCl_3) δ 156.1, 150.6, 142.7, 140.9, 134.4, 130.2, 129.4, 129.2, 128.7, 126.3, 119.1, 113.0, 112.2, 102.8, 58.0, 57.1, 56.5, 54.7, 42.4, 40.6, 31.9, 30.7, 23.3; **LR-MS** calcd. for $\text{C}_{25}\text{H}_{28}\text{NO}_2^+$ $[\text{M}+\text{H}]^+$ 374.21, found 374.07.

General Procedure for Preparation of Heteroarylazepines by Ni(0) C-H Insertion (29a-b). In a glovebox, a vial was charged with $\text{Ni}(\text{COD})_2$ (0.20 equivalents) and 1,3-bis(2,4,6-trimethylphenyl)-1,3-dihydro-2H-imidazol-2-ylidene (IMes, 0.24 equivalents) followed by anhydrous heptane (0.100 M based on $\text{Ni}(\text{COD})_2$), and the resulting black solution was stirred at room temp. for 30 min. To this mixture was then added a solution of the *N*-arylalkylisoquinclidine substrate **28a-b** (1 equivalent) in anhydrous heptane (0.333 M based on **28**), and the reaction vessel was sealed, removed from the glovebox, and heated at 130 °C for 3 h. After cooling to room temperature the reaction mixture was purified directly by a combination of column chromatography and/or preparative TLC as described below for each substrate. (*Note: For substrates that are insoluble in heptane, the catalyst solution is instead added into the heterogeneous mixture of the substrate and heptane.)

Heteroarylazepine 29a. The crude reaction mixture was purified directly by column chromatography (20:1 hexanes:EtOAc + 2% Et_3N) to yield the pure product **29a** as a beige oil (27.1 mg, 55%). A few fractions contaminated with a co-eluting spot were further purified by preparative TLC using the same solvent system to yield additional product (9.3 mg, 19%). ^1H NMR (400 MHz, CDCl_3) δ 7.28 - 7.21 (m, 1H), 6.87 (d, J = 2.6 Hz, 1H), 6.81 (dd, J = 8.8, 2.6 Hz, 1H), 3.85 (s, 3H), 3.57 (t, J = 8.9 Hz, 1H), 3.42 - 3.38 (m, 2H), 3.37 (s, 3H), 3.31 (dd, J =

9.0, 5.5 Hz, 1H), 3.24 - 3.14 (m, 3H), 3.00 (dt, J = 11.6, 1.9 Hz, 2H), 2.96 - 2.89 (m, 1H), 2.55 - 2.44 (m, 1H), 2.13 - 1.96 (m, 2H), 1.88 (dq, J = 4.1, 2.0 Hz, 1H), 1.79 - 1.62 (m, 2H), 1.18 - 1.08 (m, 1H); ^{13}C NMR (101 MHz, CDCl_3) δ 160.7, 155.7, 148.6, 131.4, 111.7, 111.4, 110.9, 101.8, 75.2, 58.9, 56.1, 54.4, 52.9, 49.5, 40.5, 39.4, 33.2, 28.3, 26.1, 19.5; LR-MS calcd. for $\text{C}_{20}\text{H}_{26}\text{NO}_3^+$ $[\text{M}+\text{H}]^+$ 328.19, found 327.79.

Heteroarylazepine 29b. The crude reaction mixture was purified directly by column chromatography (30:1 hexanes:EtOAc + 1% Et_3N) to yield the crude product as a yellow-orange oil. This material was further purified by preparative TLC (30:1 hexanes:EtOAc + 2% Et_3N) to provide the pure product **29b** as a nearly colorless glass (26.0 mg, 62%) as previously described.⁴⁷

General Procedure for Preparation of Hydroxyheteroarylazepines by Demethylation (30a-c). To a solution of the methoxyheteroarylazepine **29** (1 equivalent) in dry dichloromethane (0.125 M, based on **29**) at 0 °C was added aluminum chloride (6 equivalents) followed by ethanethiol (18 equivalents), and the resulting mixture was allowed to warm to room temperature and stirred until TLC indicated the complete consumption of starting material (typically <1.5 h). The reaction was then quenched with saturated aqueous NaHCO_3 (10 mL per mmol **29**) and extracted with CH_2Cl_2 (4x-6x, until no further extraction by TLC). The combined organic layers were dried over Na_2SO_4 and concentrated to provide the crude product. This material was purified by column chromatography with an appropriate solvent mixture as described below for each substrate.

Hydroxyheteroarylazepines 30a and 30b. The crude product was prepared according to the general procedure and purified by column chromatography (1:2 hexanes:EtOAc) to give both the ether (**30a**) and alcohol (**30b**) analogs.

30a. Ether **30a** was prepared and separated as described above and obtained as a beige oil (10.3 mg, 41%). **¹H NMR (400 MHz, CDCl₃)** δ 7.17 (d, J = 8.6 Hz, 1H), 6.76 (d, J = 2.5 Hz, 1H), 6.71 (dd, J = 8.6, 2.6 Hz, 1H), 4.00 (br s, 1H), 3.61 (t, J = 9.2 Hz, 1H), 3.39 (s, 3H), 3.38 - 3.28 (m, 2H), 3.16 - 3.07 (m, 2H), 3.04 (dd, J = 11.4, 2.8 Hz, 1H), 2.99 (t, J = 1.7 Hz, 1H), 2.92 (d, J = 2.1 Hz, 2H), 2.43 - 2.35 (m, 1H), 2.03 - 1.96 (m, 2H), 1.85 (dp, J = 4.2, 2.2 Hz, 1H), 1.71 (ddd, J = 14.1, 10.4, 4.1 Hz, 1H), 1.62 (dq, J = 10.2, 3.3 Hz, 1H), 1.15 - 1.07 (m, 1H); **¹³C NMR (101 MHz, CDCl₃)** δ 160.4, 151.6, 148.5, 131.5, 111.8, 111.2, 110.9, 104.2, 75.0, 58.9, 54.4, 53.0, 49.4, 40.1, 39.3, 32.9, 28.0, 25.9, 19.4; **LR-MS** calcd. for C₁₉H₂₄NO₃⁺ [M+H]⁺ 314.18, found 314.47.

30b. Alcohol **30b** was prepared and separated as described above and obtained as a white solid (3.2 mg, 13%). **¹H NMR (500 MHz, MeOD)** δ 7.12 (d, J = 8.6 Hz, 1H), 6.77 (d, J = 2.5 Hz, 1H), 6.67 (dd, J = 8.7, 2.5 Hz, 1H), 3.69 (d, J = 5.4 Hz, 2H), 3.39 - 3.34 (m, 1H), 3.22 (d, J = 3.5 Hz, 1H), 3.19 (s, 1H), 3.17 (d, J = 2.8 Hz, 1H), 3.13 (t, J = 1.9 Hz, 1H), 3.09 - 3.05 (m, 1H), 2.95 (d, J = 9.4 Hz, 1H), 2.54 - 2.49 (m, 1H), 2.15 - 2.07 (m, 1H), 1.95 - 1.88 (m, 2H), 1.80 (ddd, J = 12.9, 4.1, 2.1 Hz, 1H), 1.69 - 1.62 (m, 1H), 1.41 (ddt, J = 12.9, 6.8, 2.4 Hz, 1H), 1.29 (s, 1H); **¹³C NMR (126 MHz, MeOD)** δ 161.2, 153.9, 149.5, 132.6, 112.8, 112.3, 111.4, 104.6, 66.3, 57.2, 53.7, 50.2, 41.25, 41.22, 33.9, 28.4, 27.4, 19.9; **LR-MS** calcd. for C₁₈H₂₂NO₃⁺ [M+H]⁺ 300.16, found 300.44.

Hydroxyheteroarylazepine 30c. The product **30c** was prepared according to the general procedure and was purified by column chromatography (7:3 hexanes:EtOAc) and obtained as a white foamy solid (14.2 mg, 79%) as previously described.⁴⁷

Heteroarylazepine 31a. In a glovebox, a Schlenk flask was charged with Pd(CH₃CN)₄(BF₄)₂ (1.3 equivalents). It was then sealed and removed from the glovebox and

anhydrous CH_3CN (0.093 M, based on $\text{Pd}(\text{CH}_3\text{CN})_4(\text{BF}_4)_2$) was added to form a yellow solution. To this solution was added a solution of the substrate **28b** (1 equivalent) in anhydrous CH_3CN (0.028 M based on **28b**) resulting in a color change (yellow to orange/orange-red). The reaction mixture was stirred for 2 h at room temperature and then warmed to 70 °C and stirred for a further 16 h. At this time, the reaction was cooled to 0 °C, and anhydrous MeOH (9 mL per mmol of **28b**) was added followed by NaBH_4 (3.2 equivalents), causing the immediate precipitation of palladium black. The resulting black mixture was stirred for 20 min. at 0 °C, then diluted with Et_2O , filtered through celite, and the filter cake washed with additional Et_2O (4x). The combined filtrate and washings were concentrated to afford the crude product. The product **31c** was purified by column chromatography (6:1 hexanes:EtOAc + 2% Et_3N , 2 column volumes \rightarrow 4:1 hexanes:EtOAc + 2% Et_3N , 2 column volumes \rightarrow 2:1 hexanes:EtOAc + 2% Et_3N , 3 column volumes) to provide a colorless oil (23.2 mg, 24%). $^1\text{H NMR}$ (400 MHz, CDCl_3) δ 7.28 (s, 1H), 6.90 (d, $J = 2.6$ Hz, 1H), 6.84 (dd, $J = 8.8, 2.6$ Hz, 1H), 3.88 (s, 3H), 3.47 (dd, $J = 5.2, 2.4$ Hz, 1H), 3.44 (dd, $J = 5.2, 2.1$ Hz, 1H), 3.39 (s, 3H), 3.35 (d, $J = 2.0$ Hz, 1H), 3.34 – 3.31 (m, 1H), 3.29 – 3.27 (m, 1H), 3.26 – 3.23 (m, 1H), 3.13 (dt, $J = 9.5, 2.9$ Hz, 1H), 3.09 (m, 2H), 2.57 – 2.48 (m, 2H), 2.02 (ddt, $J = 22.6, 10.9, 2.8$ Hz, 1H), 1.97 – 1.90 (m, 1H), 1.68 (dq, $J = 13.4, 3.5$ Hz, 1H), 1.13 – 1.06 (m, 1H), 0.96 – 0.87 (m, 1H).; $^{13}\text{C NMR}$ (101 MHz, CDCl_3) δ 161.4, 156.2, 148.7, 131.6, 112.6, 111.9, 111.3, 102.2, 76.0, 59.3, 56.5, 54.5, 53.6, 49.4, 39.8, 35.1, 34.4, 28.1, 26.3, 19.4.; **LR-MS** calcd. for $\text{C}_{20}\text{H}_{26}\text{NO}_3^+$ $[\text{M}+\text{H}]^+$ 328.19, found 328.19.

Heteroarylazepine 31b. The product **31b** was prepared according to the general procedure (see compound **31a** above) was purified by column chromatography (10:1 hexanes:EtOAc + 2% Et_3N , 2 column volumes \rightarrow 6:1 hexanes:EtOAc + 2% Et_3N , 2 column volumes \rightarrow 2:1 hexanes:EtOAc + 2% Et_3N , 3 column volumes) followed by preparative TLC

(2:1 hexanes:EtOAc + 2% Et₃N) and obtained as a yellow oil (20.5 mg, 20%). **¹H NMR (400 MHz, CDCl₃)** δ 7.32 – 7.24 (m, 5H), 7.23 – 7.18 (m, 1H), 6.89 (d, J = 2.5 Hz, 1H), 6.85 (ddd, J = 8.8, 2.6, 0.9 Hz, 1H), 3.88 (s, 3H), 3.52 – 3.47 (m, 1H), 3.43 – 3.37 (m, 1H), 3.27 – 3.19 (m, 2H), 3.13 – 3.08 (m, 2H), 2.82 (dd, J = 3.3, 1.8 Hz, 1H), 2.76 – 2.72 (m, 2H), 2.54 (dtd, J = 10.6, 5.9, 5.2, 3.1 Hz, 1H), 2.50 – 2.43 (m, 1H), 2.17 (ddt, J = 14.2, 11.9, 2.6 Hz, 1H), 2.03 – 1.94 (m, 2H), 1.71 (dq, J = 13.3, 3.5 Hz, 1H), 0.95 – 0.87 (m, 1H); **¹³C NMR (101 MHz, CDCl₃)** δ 161.8, 156.2, 148.7, 145.4, 140.8, 131.6, 129.3, 128.9, 126.4, 112.7, 111.9, 111.5, 111.4, 102.1, 56.5, 56.3, 53.8, 49.4, 41.8, 41.7, 34.9, 34.6, 31.8, 26.8, 19.3; **LR-MS** calcd. for C₂₅H₂₈NO₂⁺ [M+H]⁺ 374.21, found 374.31.

Hydroxyheteroarylazepine 32a. The product **32a** was prepared according to the general procedure (see compound **30** above) and purified by column chromatography (5% MeOH in CH₂Cl₂, 2 column volumes → 10% MeOH in CH₂Cl₂, 2 column volumes → 20% MeOH in CH₂Cl₂, 2 column volumes) to provide an off-white solid (5 mg, 28%). **¹H NMR (500 MHz, MeOD)** δ 7.13 (d, J = 8.7 Hz, 1H), 6.79 (d, J = 2.5 Hz, 1H), 6.67 (dd, J = 8.7, 2.5 Hz, 1H), 3.58 (dd, J = 11.2, 6.4 Hz, 1H), 3.50 (dd, J = 11.2, 9.8 Hz, 1H), 3.41 – 3.35 (m, 2H), 3.17 – 3.11 (m, 2H), 3.07 – 3.03 (m, 1H), 2.55 (dt, J = 16.8, 3.2 Hz, 1H), 2.38 (td, J = 9.0, 8.6, 4.1 Hz, 1H), 2.06 (ddt, J = 14.3, 12.0, 2.7 Hz, 1H), 1.91 (h, J = 3.1 Hz, 1H), 1.89 – 1.84 (m, 1H), 1.63 (dq, J = 13.4, 3.6 Hz, 1H), 1.11 (ddt, J = 13.0, 4.7, 2.5 Hz, 1H), 0.89 (m, 2H); **¹³C NMR (126 MHz, CDCl₃)** δ 161.6, 154.0, 149.4, 132.3, 112.9, 111.5, 111.0, 104.5, 65.3, 55.3, 54.7, 49.9, 42.3, 34.7, 34.5, 28.1, 26.9, 19.4; **LR-MS** calcd. for C₁₈H₂₂NO₃⁺ [M+H]⁺ 300.16, found 300.27.

Hydroxyheteroarylazepine 32b. The product **32b** was prepared according to the general procedure (see compound **30** above) and purified by column chromatography (10:1 hexanes:EtOAc, 2 column volumes → 5:1 hexanes:EtOAc, 2 column volumes → 2:1

hexanes:EtOAc, 2 column volumes) to provide an off-white solid (2 mg, 11%). **¹H NMR (500 MHz, CDCl₃)** δ 7.22 (m, 5H), 7.20 (m, 1H), 6.82 – 6.78 (m, 1H), 6.72 – 6.68 (m, 1H), 3.87 – 3.83 (m, 1H), 3.48 – 3.43 (m, 1H), 3.40 – 3.33 (m, 2H), 3.27 – 3.19 (m, 2H), 3.05 (s, 1H), 2.78 (s, 1H), 2.72 – 2.67 (m, 2H), 2.50 (s, 1H), 2.41 – 2.36 (m, 1H), 2.17 – 2.11 (m, 1H), 2.05 – 1.99 (m, 1H), 1.92 (s, 1H), 0.72 (t, J = 7.7 Hz, 2H); **LR-MS** calcd. for C₂₄H₂₆NO₂⁺ [M+H]⁺ 360.20, found 360.38.

Compounds 33-36. The synthesis of compounds **21-27** was carried out as previously reported in our group.⁴⁷

4-isopropyl-2,5,5-triphenyloxazolidine 2,2,2-trifluoroacetate (38). Oxazolidine catalyst **38** was prepared according to the procedures described previously⁴⁷ and obtained as white solids.⁵⁸

N-(benzyloxycarbonyl)-1,2-dihydropyridine (39). Dihydropyridine **39** was prepared according to the procedures described and obtained as a pale yellow oil.⁹⁹

(1R)-exo-benzyl 7-(hydroxymethyl)-2-azabicyclo[2.2.2]oct-5-ene-2-carboxylate ((1R)-17a) and (1R)-endo-benzyl 7-(hydroxymethyl)-2-azabicyclo[2.2.2]oct-5-ene-2-carboxylate ((1R)-17b). To a CH₃CN (106 mL) solution of catalyst **38** (511 mg, 1.12 mmol), cold water (5.6 mL), trifluoroacetic acid (0.25 mL, 3.26 mmol), and freshly distilled acrolein (0.75 mL, 11.2 mmol) were added at 0 °C, and the solution was stirred. After 1 min., **39** (4.84 g, 22.4 mmol, freshly purified) was added, and the solution was stirred at 0 °C for 24 h. The reaction was quenched with water (500 mL) and extracted with Et₂O (3 x 200 mL). The combined organic extracts were washed with water and brine (100 mL), dried over Na₂SO₄, and concentrated under reduced pressure to give the crude *endo*-aldehyde **(1R)-16** (5.7 g), which was used in the next reaction without further purification.

To a stirred solution of crude *endo*-aldehyde (**IR**-16 (5.7 g) in anhydrous MeOH (30 mL), NaOMe (3.0 g) was added, and the mixture was stirred at room temperature for 12 h. The reaction was quenched with water (500 mL), extracted with EtOAc (3 x 200 mL), dried over Na₂SO₄, and concentrated under reduced pressure to give the crude *exo/endo* mixture of aldehyde (4.5 g), which was used in the next reaction without further purification.

To a stirred solution of the crude *exo/endo*-aldehyde (4.5 g) in ethanol (20 mL), NaBH₄ (488 mg, 12.9 mmol) was added, and the mixture was stirred at room temperature for 1 h. The solvent was evaporated under reduced pressure, and the residue was diluted with water (200 mL) and extracted with EtOAc (3 x 200 mL). The combined organic extracts were washed with brine (100 mL), dried over Na₂SO₄, and concentrated under reduced pressure. The epimers were separated by column chromatography (7:3 hexanes:EtOAc → 5:1 DCM:EtOAc) to give 18% (*IR*)-*exo*-alcohol (**IR**-17a) and 21% (*IR*)-*endo*-alcohol (**IR**-17b) over three steps.

(IR)-17a. (*IR*)-*exo*-alcohol (**IR**-17a) was prepared and separated as described above and obtained as a colorless oil (560 mg, 18%). ¹H NMR (400 MHz, CDCl₃) δ 7.40 – 7.27 (m, 5H), 6.52 – 6.38 (m, 2H), 5.27 – 5.04 (m, 3H), 4.81 (dt, J = 6.2, 1.7 Hz, 1H), 3.67 (dd, J = 11.7, 5.4 Hz, 1H), 3.37 (d, J = 10.4 Hz, 1H), 3.28 – 3.17 (m, 2H), 3.03 (dt, J = 10.2, 2.5 Hz, 1H), 2.68 (tt, J = 3.7, 2.0 Hz, 1H), 1.97 – 1.78 (m, 1H), 1.62 – 1.49 (m, 1H), 0.85 (ddd, J = 12.9, 4.5, 2.2 Hz, 1H), [OH not seen]. ¹³C NMR (101 MHz, CDCl₃) (spectrum complicated by conformers) δ 156.7, 155.5, 136.7, 134.6, 134.4, 132.5, 132.4, 128.5, 128.4, 128.4, 128.3, 127.9, 127.8, 127.6, 127.6, 66.9, 66.8, 64.5, 53.5, 48.5, 48.3, 46.9, 46.3, 41.2, 41.1, 30.4, 30.2, 26.0, 25.7, 14.1. LR-MS calcd. for C₁₆H₁₉NNaO₃⁺ [M+Na]⁺ 296.32, found 296.24. [α]_D²³ = -52.1 (CHCl₃). The enantiomeric excess was determined by chiral HPLC: t_R = 20.3 min (Daicel Chiralcel OD column, Gradient 2% to 8% iPrOH in Hexanes, 0.3%/min, 1.2 mL/min), %ee = 85%.

(1R)-17b. (*1R*)-endo-alcohol **(1R)-17b** was prepared and separated as described above and obtained as a colorless oil (640 mg, 21%). $^1\text{H NMR}$ (400 MHz, CDCl_3) (spectrum complicated by conformers) δ 7.41 – 7.27 (m, 5H), 6.47 – 6.27 (m, 2H), 5.24 – 5.07 (m, 2H), 4.95 – 4.81 (m, 1H), 3.33 – 3.23 (m, 2H), 3.17 (dd, $J = 10.6, 8.9$ Hz, 1H), 3.03 (m, 1H), 2.78 – 2.68 (m, 1H), 2.37 (tt, $J = 9.4, 5.2$ Hz, 1H), 1.76 (ddd, $J = 12.3, 7.9, 2.8$ Hz, 1H), 0.87 – 0.79 (m, 1H) [OH not seen]; $^{13}\text{C NMR}$ (101 MHz, CDCl_3) (spectrum complicated by conformers) δ 155.1, 154.8, 136.6, 134.6, 134.4, 130.2, 129.9, 128.3, 128.3, 128.2, 127.7, 127.6, 127.4, 127.4, 66.6, 66.5, 65.1, 64.9, 50.0, 47.2, 47.1, 46.8, 46.8, 41.3, 41.3, 30.6, 30.4, 25.9, 25.9. **LR-MS** calcd. for $\text{C}_{16}\text{H}_{19}\text{NNaO}_3^+$ $[\text{M}+\text{Na}]^+$ 296.32, found 296.31. $[\alpha]_D^{25} = -73.2$ (CHCl_3); The enantiomeric excess was determined by chiral HPLC: $t_R = 22.1$ min (Daicel Chiralcel OD column, Gradient 2% to 8% iPrOH in Hexanes, 0.3%/min, 1.2 mL/min), %ee > 95%.

Isoquinuclidine 40. To a solution of pyridine (0.12 mL, 1.48 mmol), (*1R*)-endo-alcohol **(1R)-17b** (180 mg, 0.66 mmol), 4-dimethylaminopyridine (DMAP, 4 mg, 0.03 mmol) in dry dichloromethane (5 mL) was added 2-iodobenzoylchloride (194.5 mg, 0.73 mmol) in 1 mL of dichloromethane. An additional 1 mL of dichloromethane was used to wash out the syringe. The reaction was stirred at room temperature for 45 h, after which time the reaction had gone to completion. The reaction was poured into 5% HCl (50 mL) and washed with additional 5% HCl (20 mL) and saturated NaHCO_3 (20 mL). The organic layer was dried over MgSO_4 and concentrated. The crude material was purified by column chromatography (1:9 MeOH:DCM) to give the product as a tan oil (210.5 mg, 65%). $^1\text{H NMR}$ (400 MHz, CDCl_3) δ 7.90 (dd, $J = 8.0, 3.0$ Hz, 1H), 7.74 (dd, $J = 7.8, 1.8$ Hz, 1H), 7.63 (dd, $J = 7.7, 1.8$ Hz, 1H), 7.37 – 7.15 (m, 7H), 7.07 (td, $J = 7.7, 1.8$ Hz, 1H), 6.47 – 6.25 (m, 2H), 5.06 (d, $J = 12.0$ Hz, 2H), 4.88 (ddd, $J = 33.9, 6.2, 2.8$ Hz, 1H), 3.97 (dt, $J = 10.7, 5.3$ Hz, 1H), 3.77 (q, $J = 11.0$ Hz, 1H), 3.26 (dd, $J = 10.3, 2.1$

Hz, 1H), 2.97 (dq, $J = 9.5, 3.0, 2.5$ Hz, 1H), 2.79 – 2.67 (m, 1H), 2.66 – 2.53 (m, 1H), 1.81 (ddd, $J = 12.2, 9.2, 2.8$ Hz, 1H), 0.89 (ddd, $J = 13.5, 6.8, 3.7$ Hz, 1H). ^{13}C NMR (101 MHz, CDCl_3) δ 166.8, 155.6, 155.2, 141.7, 137.3, 135.8, 135.7, 135.3, 133.0, 131.5, 131.3, 130.9, 130.3, 128.9, 128.4, 128.3, 128.2, 110.4, 94.5, 67.9, 67.8, 67.3, 67.2, 47.7, 47.6, 47.3, 38.6, 38.3, 31.2, 31.0, 26.7, 26.6. LR-MS calcd. for $\text{C}_{23}\text{H}_{23}\text{INO}_4^+$ $[\text{M}+\text{H}]^+$ 504.34, found 504.23.

Isoquinuclidine 41. Isoquinuclidine **40** was deprotected as described above (see compound **13**). Briefly, isoquinuclidine **40** was dissolved in dichloromethane (3 mL) at 0 °C, and TMSI (0.24 mL, 1.62 mmol) was added. The reaction was stirred for 10 min. before warming to room temperature for 1 hr. The reaction was quenched with MeOH (3 mL) and concentrated to a crude brown oil that was washed with hexanes (5 X 1 mL). This crude oil was dried *in vacuo* before being dissolved in a minimal amount of MeOH and recrystallized overnight by vapor diffusion with diethyl ether. A first crop of **41** was isolated as a white solid (3.6 mg), and the mother liquors were concentrated and recrystallized in the same manner to yield a second crop (89 mg, 45% combined). ^1H NMR (400 MHz, MeOD) δ 8.10 (dd, $J = 8.0, 1.1$ Hz, 1H), 7.85 (dd, $J = 7.7, 1.7$ Hz, 1H), 7.57 (td, $J = 7.6, 1.2$ Hz, 1H), 7.32 (td, $J = 7.7, 1.7$ Hz, 1H), 6.91 (ddd, $J = 8.3, 6.9, 1.5$ Hz, 1H), 6.53 – 6.46 (m, 1H), 4.51 (ddd, $J = 6.0, 2.6, 1.3$ Hz, 1H), 4.22 (dd, $J = 11.3, 5.6$ Hz, 1H), 4.00 (dd, $J = 11.3, 9.6$ Hz, 1H), 3.29 (dd, $J = 11.4, 1.7$ Hz, 1H), 3.12 (ddt, $J = 5.8, 2.9, 1.5$ Hz, 1H), 2.86 (dt, $J = 11.7, 3.0$ Hz, 2H), 2.17 (ddd, $J = 12.7, 9.3, 2.9$ Hz, 1H), 1.20 – 1.12 (m, 1H). ^{13}C NMR (101 MHz, MeOD) δ 166.7, 140.8, 138.9, 135.8, 134.5, 132.54, 130.4, 127.9, 125.9, 92.9, 66.1, 42.4, 33.6, 28.1, 24.9. LR-MS calcd. for $\text{C}_{15}\text{H}_{17}\text{INO}_2^+$ $[\text{M}+\text{H}]^+$ 370.21, found 370.14.

Isoquinuclidine 42. Isoquinuclidine **41** (89 mg, 0.18 mmol) was dissolved in water (2.5 mL), MeOH (2.5 mL), and saturated NH_4PF_6 (2.5 mL) and allowed to sit overnight at room

temperature. The product **42** was isolated as shiny beige crystals (66.9 mg, 73%). **¹H NMR (400 MHz, MeOD)** δ 8.10 (d, $J = 7.9$ Hz, 1H), 7.86 (dd, $J = 7.7, 1.7$ Hz, 1H), 7.57 (t, $J = 7.5$ Hz, 1H), 7.32 (td, $J = 7.7, 1.7$ Hz, 1H), 6.91 (t, $J = 7.5$ Hz, 1H), 6.53 – 6.41 (m, 1H), 4.53 – 4.45 (m, 1H), 4.22 (dd, $J = 11.3, 5.7$ Hz, 1H), 4.00 (dd, $J = 11.3, 9.5$ Hz, 1H), 3.40 (p, $J = 1.6$ Hz, 1H), 3.27 (dd, $J = 11.4, 1.8$ Hz, 1H), 3.14 – 3.07 (m, 1H), 2.84 (ddt, $J = 15.2, 9.0, 2.9$ Hz, 2H), 2.16 (ddd, $J = 12.7, 9.3, 3.0$ Hz, 1H), 1.16 (ddd, $J = 10.3, 5.7, 2.8$ Hz, 1H). **¹³C NMR (101 MHz, MeOD)** δ 168.0, 142.7, 140.7, 137.5, 134.4, 132.2, 129.7, 127.6, 126.7, 94.4, 67.9, 44.2, 35.4, 29.8, 26.6. **LR-MS** calcd. for $C_{15}H_{17}INO_2^+$ $[M+H]^+$ 370.21, found 370.06.

General Procedure for Preparation of Heteroarylazepines (*IS*)-*exo*-benzyl 7-ethyl-2-azabicyclo[2.2.2]oct-5-ene-2-carboxylate (43a) and (*IS*)-*endo*-benzyl 7-butyl-2-azabicyclo[2.2.2]oct-5-ene-2-carboxylate (43b) by Copper-Catalyzed Cross Coupling. A solution of trifluoromethanesulfonic anhydride (1.5 equivalents relative to alcohol (*IR*)-17) in anhydrous CH_2Cl_2 (to make 0.5 M solution) was added dropwise to a solution of alcohol (*IR*)-17 (1 equivalent) and pyridine (11 equivalents) in anhydrous CH_2Cl_2 (0.18 M relative to (*IR*)-17) at 0 °C over a period of 10 min. The resulting mixture was stirred for 45 min. at 0 °C and then diluted with CH_2Cl_2 (10 mL per 0.2 mmol of (*IR*)-17), washed with 10% aqueous HCl (2X), water (1X) and 5% aqueous $NaHCO_3$ (2X), and dried over Na_2SO_4 . The solvent was removed under reduced pressure to afford essentially pure triflate product, which was used in the next step without further purification.

Next, to a solution of freshly prepared crude triflate (1 equivalent) in anhydrous Et_2O (0.18 M relative to (*IR*)-17) was added Li_2CuCl_4 (50 mol% from 0.1 M solution in THF) and then $MeMgBr$ (3 equivalents, from 3.0 M solution in Et_2O) slowly at -50 °C over 10 min, and the reaction mixture was stirred for 30 min at -50 °C. The reaction was quenched with saturated

NH₄Cl (10 mL per 0.18 mmol of (*IR*)-**17**) and warmed to room temperature. The organic layer was separated, and the aqueous layer was extracted with diethyl ether (3 x 10 mL), dried over Na₂SO₄, and concentrated to afford the crude product. This material was purified by column chromatography (20:1 DCM:EtOAc) to provide pure isoquinuclidines.

(1*S*)-exo-benzyl 7-ethyl-2-azabicyclo[2.2.2]oct-5-ene-2-carboxylate (43a). The compound was isolated according to the general procedure to give a pale yellow oil with minor impurities (0.91 g, 44%). ¹H NMR (400 MHz, CDCl₃) δ 7.42 – 7.27 (m, 5H), 6.53 – 6.21 (m, 2H), 5.20 – 5.06 (m, 2H), 4.71 – 4.49 (m, 1H), 3.26 (m, 1H), 3.01 (m, 1H), 2.75 – 2.60 (m, 1H), 2.00 (d, J = 7.3 Hz, 1H), 1.87 – 1.75 (m, 0.7H), 1.70 – 1.60 (m, 0.3H), 1.50 – 1.32 (m, 1H), 1.29 – 1.12 (m, 1H), 1.05 – 0.92 (m, 2H), 0.86 (tt, J = 7.3, 5.0 Hz, 3H).

(1*S*)-endo-benzyl 7-butyl-2-azabicyclo[2.2.2]oct-5-ene-2-carboxylate (43b). The compound was isolated according to the general procedure to give a pale yellow oil (47.6 mg, 96%). ¹H NMR (500 MHz, CDCl₃) (partial integrals due to conformers) δ 7.40 – 7.28 (m, 5H), 6.43 – 6.29 (m, 1.6H), 6.25 (m, 0.4H), 5.19 – 5.09 (m, 2H), 4.69 (m, 0.6H), 4.58 (m, 0.4H), 3.25 (m, 1H), 3.03 – 2.95 (m, 1H), 2.76 – 2.63 (m, 1H), 1.98 (m, 1H), 1.82 (m, 1H), 1.36 – 1.11 (m, 2H), 1.04 – 0.94 (m, 1H), 0.87 (m, 3H). ¹³C NMR (126 MHz, CDCl₃) δ 155.6, 137.5, 135.1, 134.6, 131.2, 130.5, 128.8, 128.8, 128.2, 128.1, 128.0, 67.0, 67.0, 50.0, 49.5, 47.6, 47.2, 41.4, 41.1, 32.0, 31.6, 31.4, 30.6, 28.7, 28.8, 23.1, 14.5, 11.8, 11.8. LR-MS calcd. for C₁₇H₂₁NNaO₂⁺ [M+Na]⁺ 294.35, found 294.29. [α]_D²⁵ = -114.1 (CHCl₃).

(5*S*)-exo-7-Ethyl-2-(α-endo-1-(5-methoxybenzofuran-3-yl)propan-2-yl)-2-azabicyclo[2.2.2]oct-5-ene and (5*S*)-exo-7-ethyl-2-(α-exo-1-(5-methoxybenzofuran-3-yl)propan-2-yl)-2-azabicyclo[2.2.2]oct-5-ene (44). To a solution of isoquinuclidine **43a** (744 mg, 2.7 mmol) in anhydrous CH₂Cl₂ (20 mL) at 0 °C was added iodotrimethylsilane (1.6 mL,

11.2 mmol), and the orange solution was allowed to warm to room temperature and stirred for 1 h. The reaction was then quenched with MeOH (20 mL) and concentrated to provide the isoquinuclidine HI salt as an orange-brown oil. This oil was washed with hexanes (5 X 5 mL) and then dried again *in vacuo*. This material was dissolved in anhydrous 1,2-dichloroethane (17 mL), Et₃N (772 μL, 5.5 mmol), ketone **33a** (560 mg, 2.7 mmol), and NaBH(OAc)₃ (1.2 mg, 5.7 mmol) were added, and the pale-orange mixture was stirred at room temperature. After 26 h, an additional portion of NaBH(OAc)₃ (1.2 mg, 5.7 mmol) was added. At 48 h, acetic acid (0.3 mL, 5.4 mmol) was added. After 65 h, the reaction was diluted with water (100 mL), basified with concentrated aqueous NaOH, and extracted with CH₂Cl₂ (3 x 50 mL). The combined organics were washed with water (50 mL), dried over Na₂SO₄, and concentrated to provide a red-brown oil. This material was purified by repeated column chromatography (Column 1: 7:3 hexanes:EtOAc → 7:3 hexanes:EtOAc + 2% Et₃N; Column 2: 9:1 hexanes:EtOAc + 2% Et₃N; Column 3: 30:1 hexanes:EtOAc + 2% Et₃N) to provide a mixture of the two diastereomers **44** as a yellow-orange oil (254.3 mg, 29%, 68:32 *α-endo:α-exo*) with some minor impurities. ¹H NMR (400 MHz, CDCl₃) (Partial integrals due to 68:32 mixture of two diastereomers and some minor impurities) δ 7.55 – 7.53 (m, 0.5H), 7.47 (s, 0.2H), 7.46 – 7.44 (m, 1H), 7.38 (d, J = 2.7 Hz, 1H), 7.35 (d, J = 8.9 Hz, 1H), 7.09 – 7.06 (m, 1H), 7.02 (dd, J = 8.9, 2.7 Hz, 1H), 6.98 (dd, J = 7.7, 2.6 Hz, 1H), 6.89 (dd, J = 8.9, 2.6 Hz, 1H), 6.33 – 6.27 (m, 2H), 3.91 (s, 0.96H), 3.87 (d, J = 1.7 Hz, 2.04H), 3.34 (dt, J = 5.6, 2.2 Hz, 1H), 3.10 (dd, J = 8.6, 2.6 Hz, 1H), 2.97 – 2.86 (m, 0.25H), 2.81 – 2.75 (m, 0.75H), 2.76 – 2.68 (m, 1H), 2.55 (d, J = 6.0 Hz, 1H), 2.51 (dd, J = 6.1, 0.9 Hz, 0.52H), 2.50 – 2.45 (m, 3H), 2.35 (m, 0.46H), 2.24 (dt, J = 8.5, 2.4 Hz, 1H), 1.64 – 1.42 (m, 2H), 1.35 – 1.24 (m, 1H), 1.02 – 0.93 (m, 3H), 0.89 (t, J = 7.4 Hz, 2H), 0.83 (t, J = 7.4 Hz, 1H). ¹³C NMR (101 MHz, CDCl₃) (Additional peaks due to 68:32 mixture of two diastereomers and

some minor impurities) δ 156.1, 156.1, 150.6, 143.4, 133.9, 133.1, 132.5, 129.8, 129.1, 128.4, 121.8, 119.0, 118.3, 115.2, 112.8, 112.7, 112.5, 112.1, 104.2, 103.2, 59.0, 56.7, 56.5, 55.3, 54.9, 53.7, 51.7, 51.1, 43.0, 42.4, 41.8, 32.3, 32.2, 30.5, 30.4, 30.3, 29.9, 29.6, 27.4, 27.2, 18.4, 17.9, 12.9, 12.8. **LR-MS** calcd. for $C_{21}H_{28}NO_2^+$ $[M+H]^+$ 326.21, found 326.49.

(5S)-12-Methoxy-7- α -endo-methyl-16-oxaibogamine (45). The product **45** was prepared according to the general procedure (see compound **14** above), starting from the mixed diastereomers **44**, and obtained as a mixture with the α -*exo*-epimer. It was separated by repeated column chromatography (Column 1: 30:1 hexanes:EtOAc + 1% Et₃N \rightarrow 9:1 hexanes:EtOAc + 2% Et₃N \rightarrow 7:3 hexanes:EtOAc + 2% Et₃N; Column 2: 40:1 hexanes:EtOAc + 1% Et₃N \rightarrow 20:1 hexanes:EtOAc + 1% Et₃N) to provide a very pale-brown oil (68.8 mg, 51%, 76% based on quantity of α -*endo* in starting material). **¹H NMR (400 MHz, CDCl₃)** δ 7.24 (d, J = 8.7 Hz, 1H), 6.87 (d, J = 2.5 Hz, 1H), 6.80 (dd, J = 8.8, 2.6 Hz, 1H), 3.85 (s, 3H), 3.27 (m, 1H), 3.13 (dt, J = 11.5, 2.7 Hz, 1H), 2.99 – 2.88 (m, 2H), 2.84 (dt, J = 8.7, 2.0 Hz, 1H), 2.78 (d, J = 2.3 Hz, 1H), 2.54 (dd, J = 16.7, 4.1 Hz, 1H), 2.03 (m, 1H), 1.85 – 1.81 (m, 1H), 1.79 – 1.74 (m, 1H) (1.66 – 1.59 (m, 1H), 1.52 (m, 3H), 1.24 (d, J = 6.7 Hz, 3H), 1.18 (m, 1H), 0.91 (t, J = 7.1 Hz, 3H). **¹³C NMR (101 MHz, CDCl₃)** δ 161.0, 155.8, 148.4, 131.5, 111.5, 110.9, 110.9, 101.8, 58.7, 58.3, 56.1, 46.2, 41.4, 40.8, 33.8, 32.7, 27.5, 26.5, 26.4, 21.5, 11.9. **LR-MS** calcd. for $C_{21}H_{28}NO_2^+$ $[M+H]^+$ 326.21, found 326.6. $[\alpha]_D^{20} = -26.9$ (CHCl₃).

(5S)-12-Hydroxy-7- α -endo-methyl-16-oxaibogamine ((5S)-46). The product **(5S)-46** was prepared according to the general procedure (see compound **15** above) and purified by column chromatography (20:1 DCM:MeOH \rightarrow 20:1 Acetone: MeOH) to provide a beige, foamy solid (24.7 mg, 57%). **¹H NMR (400 MHz, CDCl₃)** δ 7.18 (d, J = 8.6 Hz, 1H), 6.81 (d, J = 2.5 Hz, 1H), 6.71 (dd, J = 8.6, 2.6 Hz, 1H), 5.13 (s, 1H), 3.23 (m, 1H), 3.10 (dt, J = 11.5, 2.7 Hz,

1H), 2.89 (td, $J = 8.7, 4.5$ Hz, 2H), 2.82 (dt, $J = 8.8, 2.0$ Hz, 1H), 2.77 – 2.72 (m, 1H), 2.47 (dd, $J = 16.8, 4.1$ Hz, 1H), 2.01 (m, 1H), 1.82 (m, 1H), 1.76 (m, 1H), 1.61 (m, 1H), 1.51-1.25 (m, 3H), 1.21 (m, 3H), 1.14 (d, $J = 6.9$ Hz, 1H), 0.89 (t, $J = 7.0$ Hz, 3H). ^{13}C NMR (101 MHz, CDCl_3) δ 161.2, 151.3, 148.5, 131.9, 111.5, 110.8, 110.7, 104.2, 58.7, 58.3, 46.2, 41.4, 40.8, 33.8, 32.7, 27.5, 26.5, 26.3, 21.4, 11.9. LR-MS calcd. for $\text{C}_{20}\text{H}_{26}\text{NO}_2^+$ $[\text{M}+\text{H}]^+$ 312.20, found 312.27. $[\alpha]_D^{19} = -13.8$ (CHCl_3).

X-ray Structure Determinations

X-ray diffraction data were collected on a Bruker Apex II diffractometer. Crystal data, data collection and refinement parameters are summarized in **Table 4**. The structures were solved using direct methods and standard difference map techniques, and were refined by full matrix least squares procedures on F2 with SHELXTL (Version 2014/7).¹⁰⁰⁻¹⁰²

Property	Isoquinuclidine 28
lattice	Monoclinic
formula	$\text{C}_{30}\text{H}_{34}\text{F}_{12}\text{I}_2\text{N}_2\text{O}_4\text{P}_2$
formula weight	1030.33
space group	$P2_1$
$a/\text{\AA}$	7.031(4)
$b/\text{\AA}$	8.593(5)
$c/\text{\AA}$	15.567(10)
$\alpha/^\circ$	90
$\beta/^\circ$	102.861(9)
$\gamma/^\circ$	90
$V/\text{\AA}^3$	917.0(10)
Z	1
temperature (K)	130(2)
radiation (λ , \AA)	0.71073
ρ (calcd.) g cm^{-3}	1.866
μ (Mo $K\alpha$), mm^{-1}	1.901
θ max, deg.	30.751
no. of data collected	13912
no. of data	5600
no. of parameters	238

$R_I [I > 2s(I)]$	0.0627
$wR_2 [I > 2s(I)]$	0.1492
R_I [all data]	0.0904
wR_2 [all data]	0.1635
GOF	1.028

Biological Procedures

Materials: BRET. HEK-293T cells were obtained from the American Type Culture Collection (Rockville, MD) and were cultured in a 5% CO₂ atmosphere at 37 °C in Dulbecco's Modified Eagle Medium (high glucose #11965; Life Technologies Corp.; Grand Island, NY) supplemented with 10% Fetal Bovine Serum (FBS, Premium Select, Atlanta Biologicals; Atlanta, GA) and 100 U/mL penicillin and 100 µg/mL streptomycin (#15140, Life Technologies).

DNA Constructs. The human MOR (hMOR), human DOR (hDOR), human KOR (hKOR), and GRK3 were obtained from the Missouri S&T Resource Center. The human G protein constructs used here have been previously described and were provided by C. Galés or were obtained from the Missouri S&T Resource Center unless otherwise noted.^{91,103} The G proteins used included untagged G α_{oB} (G α_{oB}); G α_{oB} with Renilla luciferase 8 (RLuc8) inserted at position 91 (G α_{oB} -RLuc8); G β_1 (β_1); untagged G γ_2 (γ_2); G γ_2 , which we fused to the full-length mVenus at its *N*-terminus via the amino acid linker GSAGT (mVenus- γ_2). The plasmids employed in the arrestin recruitment assay, hKOR-RLuc8 and Arr3-mVenus, were synthesized in-house as previously described.⁹¹ All constructs were sequence-confirmed prior to use in experiments.

Transfection. The following cDNA amounts were transfected into HEK-293T cells (5 x 10⁶ cells/plate) in 10-cm dishes using polyethylenimine (PEI) in a 1:1 ratio (diluted in Opti-MEM, Life Technologies): ***G protein activation:*** 2.5 µg MOR/DOR/KOR, 0.125 µg G α_{oB} -RLuc8, 6.25 µg β_1 , 6.25 µg mVenus- γ_2 ; ***BRET recruitment:*** 0.2 µg hKOR-RLuc8, 15 µg Arr3-

mVenus, 5 μ g GRK3. Cells were maintained in the HEK-293T media described above. After 24 hours the media was changed, and the experiment was performed 24 hours later (48 hours after transfection).

BRET. Transfected cells were dissociated and re-suspended in phosphate-buffered saline (PBS). Approximately 200,000 cells/well were added to a black-framed, white well 96-well plate (#60050; Perkin Elmer; Waltham, MA). The microplate was centrifuged and the cells were re-suspended in PBS. For agonist experiments, after 5 minutes, 5 μ M of the luciferase substrate coelenterazine H was added to each well. After 5 minutes, ligands were added and the BRET signal was measured 5 minutes later on a PHERAstar FS plate reader. For antagonist competition experiments, cells were pre-incubated with the antagonist at varying concentrations for 30 minutes. Coelenterazine H (5 μ M) was then added to each well for 5 minutes. Following coelenterazine H incubation, a fixed concentration of the reference agonist (5x EC_{50}) was added, and the BRET signal was measured at 30 minutes on a PHERAstar FS plate reader. The BRET signal was quantified by calculating the ratio of the light emitted by the energy acceptor, mVenus (510-540 nm), over the light emitted by the energy donor, RLuc8 (485 nm). This drug-induced BRET signal was normalized using the E_{max} of [D-Ala², N-Me-Phe⁴, Gly-ol⁵]-enkephalin (DAMGO), [D-Pen(2,5)]enkephalin (DPDPE), or U-50,488 as the maximal response at MOR, DOR, and KOR respectively. Dose response curves were fit using a three-parameter logistic equation in GraphPad Prism 6.

Inhibition of Monoamine Transporters. An EM4 cell line stably expressing hDAT (hDAT-EM4) was kindly provided by Drs. Jonathan Javitch and Mark Sonders of the Department of Psychiatry at Columbia University Medical Center. Cells were cultured in a 5% CO₂ atmosphere at 37 °C in DMEM + GlutaMAX (Invitrogen #10569) supplemented with 10%

FBS (Atlanta Biologicals) and 100 U/mL penicillin and 100 µg/mL streptomycin. HEK-293 cell lines stably expressing hNET or hSERT were obtained from the laboratory of Professor Bryan Roth (University of North Carolina at Chapel Hill). hNET-HEK and hSERT-HEK cells were cultured as above with additional 500 µg/mL G418 (Calbiochem).

Cells were seeded at a density of $0.08\text{-}0.09 \times 10^6$ cells per well in black flat-bottom 96-well plates and incubated in growth medium at 37 °C for approximately 2 days to reach confluence. On the day of the experiment, the complete growth medium was aspirated, and wells were washed with 200 µL PBS and treated with 100 µL/well experimental medium (DMEM without phenol red containing 25 mM HEPES and 1% FBS) containing DMSO (vehicle), control inhibitor of varying concentrations (nomifensine for hDAT-EM4 and hNET-HEK cells, imipramine for hSERT-HEK cells) or experimental compound of varying concentrations. The cells were incubated for 60 min at 37 °C. Then 100 µL/well of NG54 (5 µM solution for hSERT-HEK, 8.2 µM solution for hDAT-HEK, or 10.4 µM solution for hNET-HEK to keep the Cheng Prusoff equation consistent – i.e. $0.65 \cdot K_m$) was added to each well in experimental medium and incubated for 30 min at 37 °C. The experiment was terminated by one rapid PBS wash (200 µL/well) followed by addition of fresh PBS buffer (120 µL/well). The fluorescence uptake in cells was immediately recorded using a BioTek H1MF plate reader (3x3 area scan, bottom read mode) with excitation and emission wavelengths set at 389 nm and 442 nm, respectively. The extent of inhibition was determined as the difference between signal and basal measurements: mean fluorescence uptake of NG54 (with DMSO vehicle) minus that in the presence of the experimental compound. These values were normalized to the control inhibitor (100% inhibition) to yield a normalized fraction of inhibition. Dose response curves were fit using a three-parameter logistic equation in GraphPad Prism 6.

References

- (1) Alper, K. R. Ibogaine: A Review. *Alkaloids Chem. Biol.* **2001**, *56*, 1–38.
- (2) Mash, D. C.; Kovera, C. A.; Pablo, J.; Tyndale, R. F.; Ervin, F. D.; Williams, I. C.; Singleton, E. G.; Mayor, M. Ibogaine: Complex Pharmacokinetics, Concerns for Safety, and Preliminary Efficacy Measures. *Ann. N. Y. Acad. Sci.* **2000**, *914*, 394–401.
- (3) Metzner, R. Hallucinogenic Drugs and Plants in Psychotherapy and Shamanism. *J. Psychoactive Drugs* **1998**, *30*, 333–341.
- (4) Alper, K. R.; Lotsof, H. S.; Frenken, G. M.; Luciano, D. J.; Bastiaans, J. Treatment of Acute Opioid Withdrawal with Ibogaine. *Am. J. Addict.* **1999**, *8*, 234–242.
- (5) Schenberg, E. E.; de Castro Comis, M. A.; Chaves, B. R.; da Silveira, D. X. Treating Drug Dependence with the Aid of Ibogaine: A Retrospective Study. *J. Psychopharmacol.* **2014**, *28*, 993–1000.
- (6) Glick, S. D.; Rossman, K.; Steindorf, S.; Maisonneuve, I. M.; Carlson, J. N. Effects and Aftereffects of Ibogaine on Morphine Self-Administration in Rats. *Eur. J. Pharmacol.* **1991**, *195*, 341–345.
- (7) Rezvani, A. H.; Overstreet, D. H.; Lee, Y. W. Attenuation of Alcohol Intake by Ibogaine in Three Strains of Alcohol-Preferring Rats. *Pharmacol. Biochem. Behav.* **1995**, *52*, 615–620.
- (8) Cappendijk, S. L.; Dzoljic, M. R. Inhibitory Effects of Ibogaine on Cocaine Self-Administration in Rats. *Eur. J. Pharmacol.* **1993**, *241*, 261–265.
- (9) Popik, P.; Layer, R. T.; Skolnick, P. 100 Years of Ibogaine: Neurochemical and Pharmacological Actions of a Putative Anti-Addictive Drug. *Pharmacol. Rev.* **1995**, *47*, 235–253.
- (10) Sershen, H.; Hashim, A.; Lajtha, A. Characterization of Multiple Sites of Action of Ibogaine. *Alkaloids. Chem. Biol.* **2001**, *56*, 115–133.
- (11) Bowen, W. D. Sigma Receptors and Iboga Alkaloids. *Alkaloids. Chem. Biol.* **2001**, *56*, 173–191.
- (12) Alper, K.; Bai, R.; Liu, N.; Fowler, S. J.; Huang, X.-P.; Priori, S. G.; Ruan, Y. hERG Blockade by Iboga Alkaloids. *Cardiovasc. Toxicol.* **2016**, *16*, 14–22.
- (13) Koenig, X.; Kovar, M.; Rubi, L.; Mike, A. K.; Lukacs, P.; Gawali, V. S.; Todt, H.; Hilber, K.; Sandtner, W. Anti-Addiction Drug Ibogaine Inhibits Voltage-Gated Ionic Currents: A Study to Assess the Drug's Cardiac Ion Channel Profile. *Toxicol. Appl. Pharmacol.* **2013**, *273*, 259–268.
- (14) Baumann, M. H.; Pablo, J.; Ali, S. F.; Rothman, R. B.; Mash, D. C. Comparative Neuropharmacology of Ibogaine and Its O-Desmethyl Metabolite, Noribogaine. *Alkaloids. Chem. Biol.* **2001**, *56*, 79–113.
- (15) Glick, S. D.; Maisonneuve, I. M.; Szumlinski, K. K. Mechanisms of Action of Ibogaine: Relevance to Putative Therapeutic Effects and Development of a Safer Iboga Alkaloid Congener. *Alkaloids. Chem. Biol.* **2001**, *56*, 39–53.
- (16) Sweetnam, P. M.; Lancaster, J.; Snowman, A.; Collins, J. L.; Perschke, S.; Bauer, C.; Ferkany, J. Receptor Binding Profile Suggests Multiple Mechanisms of Action Are Responsible for Ibogaine's Putative Anti-Addictive Activity. *Psychopharmacology (Berl.)* **1995**, *118*, 369–376.
- (17) Chen, K.; Kokate, T. G.; Donevan, S. D.; Carroll, F. I.; Rogawski, M. A. Ibogaine Block of the NMDA Receptor: In Vitro and in Vivo Studies. *Neuropharmacology* **1996**, *35*,

- 423–431.
- (18) Popik, P.; Layer, R. T.; Fossom, L. H.; Benveniste, M.; Geter-Douglass, B.; Witkin, J. M.; Skolnick, P. NMDA Antagonist Properties of the Putative Antiaddictive Drug, Ibogaine. *J. Pharmacol. Exp. Ther.* **1995**, *275*, 753–760.
 - (19) Antonio, T.; Childers, S. R.; Rothman, R. B.; Dersch, C. M.; King, C.; Kuehne, M.; Bornmann, W. G.; Eshleman, A. J.; Janowsky, A.; Simon, E. R.; Reith, M. E. A.; Alper, K. Effect of Iboga Alkaloids on μ -Opioid Receptor-Coupled G Protein Activation. *PLoS One* **2013**, *8*, 1–18.
 - (20) Maillet, E. L.; Milon, N.; Heghinian, M. D.; Fishback, J.; Schürer, S. C.; Garamszegi, N.; Mash, D. C. Noribogaine Is a G-Protein Biased κ -Opioid Receptor Agonist. *Neuropharmacology* **2015**, *99*, 675–688.
 - (21) Paling, F. P.; Andrews, L. M.; Valk, G. D.; Blom, H. J. Life-Threatening Complications of Ibogaine: Three Case Reports. *Neth. J. Med.* **2012**, *70*, 422–424.
 - (22) Vlaanderen, L.; Martial, L. C.; Franssen, E. J. F.; van der Voort, P. H. J.; Oosterwerff, E.; Somsen, G. A. Cardiac Arrest after Ibogaine Ingestion. *Clin. Toxicol.* **2014**, *52*, 642–643.
 - (23) Pearl, S. M.; Herrick-Davis, K.; Teitler, M.; Glick, S. D. Radioligand-Binding Study of Noribogaine, a Likely Metabolite of Ibogaine. *Brain Res.* **1995**, *675*, 342–344.
 - (24) Chang, Q.; Hanania, T.; Mash, D. C.; Maillet, E. L. Noribogaine Reduces Nicotine Self-Administration in Rats. *J. Psychopharmacol.* **2015**, *29*, 704–711.
 - (25) Glue, P.; Lockhart, M.; Lam, F.; Hung, N.; Hung, C. T.; Friedhoff, L. Ascending-Dose Study of Noribogaine in Healthy Volunteers: Pharmacokinetics, Pharmacodynamics, Safety, and Tolerability. *J. Clin. Pharmacol.* **2015**, *55*, 189–194.
 - (26) Glick, S. D.; Maisonneuve, I. M.; Szumlinski, K. K. 18-Methoxycoronaridine (18-MC) and Ibogaine: Comparison of Antiaddictive Efficacy, Toxicity, and Mechanisms of Action. *Ann. N. Y. Acad. Sci.* **2000**, *914*, 369–386.
 - (27) He, D.-Y.; McGough, N. N. H.; Ravindranathan, A.; Jeanblanc, J.; Logrip, M. L.; Phamluong, K.; Janak, P. H.; Ron, D. Glial Cell Line-Derived Neurotrophic Factor Mediates the Desirable Actions of the Anti-Addiction Drug Ibogaine against Alcohol Consumption. *J. Neurosci.* **2005**, *25*, 619–628.
 - (28) Lu, L.; Wang, X.; Wu, P.; Xu, C.; Zhao, M.; Morales, M.; Harvey, B. K.; Hoffer, B. J.; Shaham, Y. Role of Ventral Tegmental Area Glial Cell Line-Derived Neurotrophic Factor in Incubation of Cocaine Craving. *Biol. Psychiatry* **2009**, *66*, 137–145.
 - (29) Green-Sadan, T.; Kinor, N.; Roth-Deri, I.; Geffen-Aricha, R.; Schindler, C. J.; Yadid, G. Transplantation of Glial Cell Line-Derived Neurotrophic Factor-Expressing Cells into the Striatum and Nucleus Accumbens Attenuates Acquisition of Cocaine Self-Administration in Rats. *Eur. J. Neurosci.* **2003**, *18*, 2093–2098.
 - (30) Green-Sadan, T.; Kuttner, Y.; Lublin-Tennenbaum, T.; Kinor, N.; Boguslavsky, Y.; Margel, S.; Yadid, G. Glial Cell Line-Derived Neurotrophic Factor-Conjugated Nanoparticles Suppress Acquisition of Cocaine Self-Administration in Rats. *Exp. Neurol.* **2005**, *194*, 97–105.
 - (31) Passarella, D.; Favia, R.; Giardini, A.; Lesma, G.; Martinelli, M.; Silvani, A.; Danieli, B.; Efange, S. M. N.; Mash, D. C. Ibogaine Analogues. Synthesis and Preliminary Pharmacological Evaluation of 7-Heteroaryl-2-azabicyclo[2.2.2]oct-7-Enes. *Bioorganic Med. Chem.* **2003**, *11*, 1007–1014.
 - (32) Gassaway, M. M.; Rives, M.-L.; Kruegel, A. C.; Javitch, J. A.; Sames, D. The Atypical Antidepressant and Neurorestorative Agent Tianeptine Is a μ -Opioid Receptor Agonist.

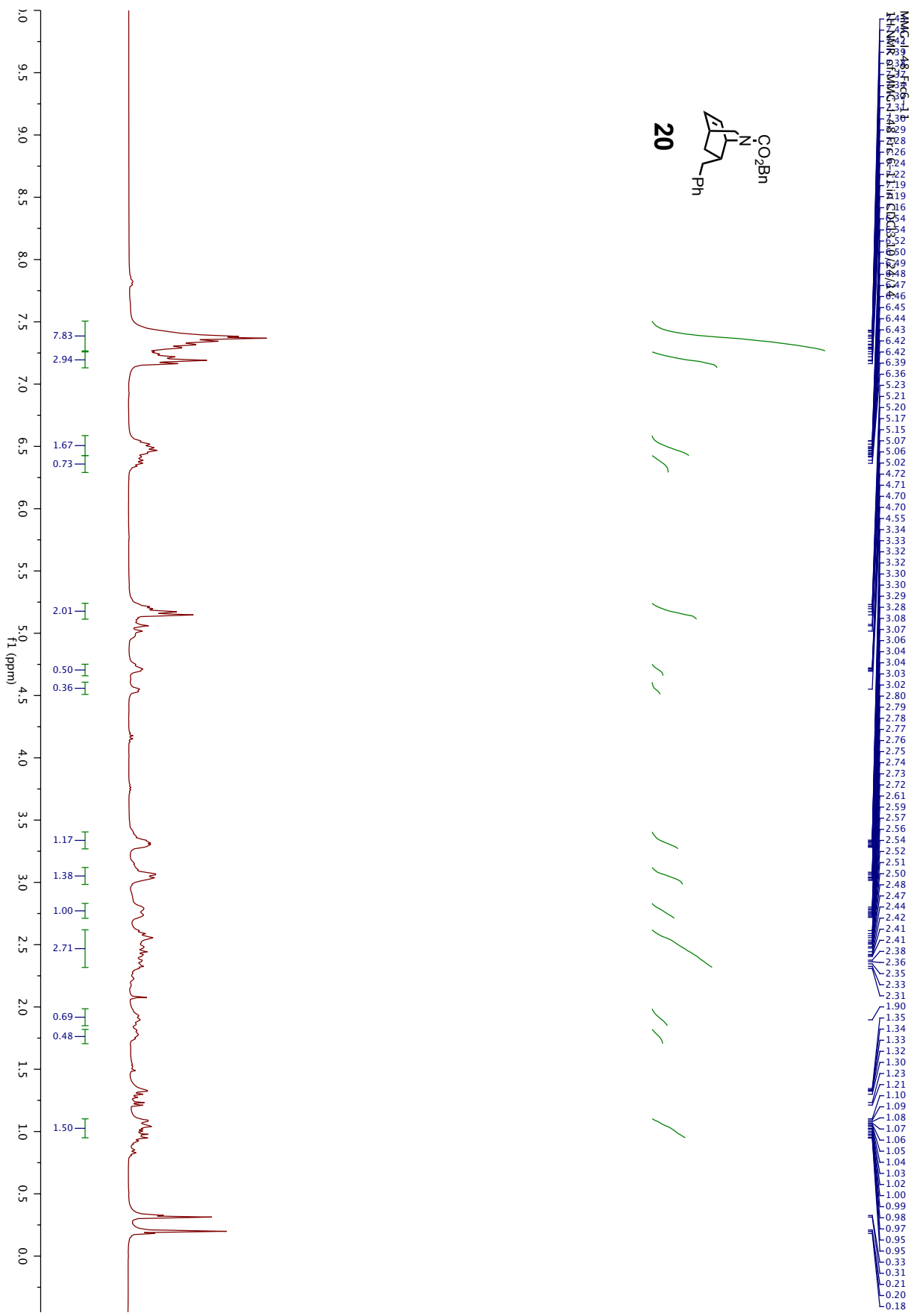
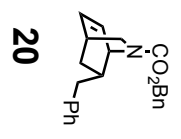
- Transl. Psychiatry* **2014**, *4*, e411.
- (33) Kruegel, A. C.; Gassaway, M. M.; Kapoor, A.; Váradi, A.; Majumdar, S.; Filizola, M.; Javitch, J. A.; Sames, D. Synthetic and Receptor Signaling Explorations of the Mitragyna Alkaloids: Mitragynine as an Atypical Molecular Framework for Opioid Receptor Modulators. *J. Am. Chem. Soc.* **2016**, *138*, 6754–6764.
- (34) Deecher, D. C.; Teitler, M.; Soderlund, D. M.; Bornmann, W. G.; Kuehne, M. E.; Glick, S. D. Mechanisms of Action of Ibogaine and Harmaline Congeners Based on Radioligand Binding Studies. *Brain Res.* **1992**, *571*, 242–247.
- (35) Repke, D. B.; Artis, D. R.; Nelson, J. T.; Wong, E. H. F. Abbreviated Ibogaine Congeners. Synthesis and Reactions of Tropan-3-Yl-2 and -3-Indoles. Investigation of an Unusual Isomerization of 2-Substituted Indoles Using Computational and Spectroscopic Techniques. *J. Org. Chem.* **1994**, *59*, 2164–2171.
- (36) Layer, R. T.; Skolnick, P.; Bertha, C. M.; Bandarage, U. K.; Kuehne, M. E.; Popik, P. Structurally Modified Ibogaine Analogs Exhibit Differing Affinities for NMDA Receptors. *Eur. J. Pharmacol.* **1996**, *309*, 159–165.
- (37) Pablo, J. P.; Mash, D. C. Noribogaine Stimulates Naloxone-Sensitive [35S]GTP γ S Binding. *Neuroreport* **1998**, *9*, 109–114.
- (38) Mash, D. C.; Staley, J. K.; Baumann, M. H.; Rothman, R. B.; Lee Hearn, W. Identification of a Primary Metabolite of Ibogaine That Targets Serotonin Transporters and Elevates Serotonin. *Life Sci.* **1995**, *57*, 45–50.
- (39) Hearn, W. L.; Pablo, J.; Hime, G. W.; Mash, D. C. Identification and Quantitation of Ibogaine and an O-Demethylated Metabolite in Brain and Biological Fluids Using Gas Chromatography-Mass Spectrometry. *J. Anal. Toxicol.* **1995**, *19*, 427–434.
- (40) Staley, J. K.; Ouyang, Q.; Pablo, J.; Hearn, W. L.; Flynn, D. D.; Rothman, R. B.; Rice, K. C.; Mash, D. C. Pharmacological Screen for Activities of 12-Hydroxyibogamine: A Primary Metabolite of the Indole Alkaloid Ibogaine. *Psychopharmacology (Berl.)* **1996**, *127*, 10–18.
- (41) Hough, L. B.; Pearl, S. M.; Glick, S. D. Tissue Distribution of Ibogaine After Intraperitoneal and Subcutaneous Administration. *Life Sci.* **1996**, *58*, 119–122.
- (42) Baumann, M. H.; Rothman, R. B.; Pablo, J. P.; Mash, D. C. In Vivo Neurobiological Effects of Ibogaine and Its O-Desmethyl Metabolite, 12-Hydroxyibogamine (Noribogaine), in Rats. *J. Pharmacol. Exp. Ther.* **2001**, *297*, 531–539.
- (43) Hough, L. B.; Bagal, A. A.; Glick, S. D. Pharmacokinetic Characterization of the Indole Alkaloid Ibogaine in Rats. *Methods Find. Exp. Clin. Pharmacol.* **2000**, *22*, 77–81.
- (44) Mannering, G. J.; Dixon, A. C.; Baker, E. M.; Asami, T. The in Vivo Liberation of Morphine from Codeine in Man. *J. Pharmacol. Exp. Ther.* **1954**, *111*, 142–146.
- (45) Armstrong, S. C.; Cozza, K. L. Pharmacokinetic Drug Interactions of Morphine, Codeine, and Their Derivatives: Theory and Clinical Reality, Part II. *Psychosomatics* **2003**, *44*, 515–520.
- (46) Kruegel, A. C.; Rakshit, S.; Li, X.; Sames, D. Constructing Iboga Alkaloids via C–H Bond Functionalization: Examination of the Direct and Catalytic Union of Heteroarenes and Isoquinuclidine Alkenes. *J. Org. Chem.* **2015**, *80*, 2062–2071.
- (47) Kruegel, A. C. Chemical and Biological Explorations of Novel Opioid Receptor Modulators, Columbia University, 2015.
- (48) Liguori, A.; Morse, W. H.; Bergman, J. Respiratory Effects of Opioid Full and Partial Agonists in Rhesus Monkeys. *J. Pharmacol. Exp. Ther.* **1996**, *277*, 462–472.

- (49) Beardsley, P. M.; Howard, J. L.; Shelton, K. L.; Carroll, F. I. Differential Effects of the Novel Kappa Opioid Receptor Antagonist, JD1c, on Reinstatement of Cocaine-Seeking Induced by Footshock Stressors vs Cocaine Primes and Its Antidepressant-like Effects in Rats. *Psychopharmacology (Berl)*. **2005**, *183*, 118–126.
- (50) Mague, S. D.; Pliakas, A. M.; Todtenkopf, M. S.; Tomaszewicz, H. C.; Zhang, Y.; Stevens, W. C.; Jones, R. M.; Portoghese, P. S.; Carlezon, W. A. Antidepressant-like Effects of Kappa-Opioid Receptor Antagonists in the Forced Swim Test in Rats. *J. Pharmacol. Exp. Ther.* **2003**, *305*, 323–330.
- (51) Carr, G. V.; Bangasser, D. A.; Bethea, T.; Young, M.; Valentino, R. J.; Lucki, I. Antidepressant-Like Effects of κ -Opioid Receptor Antagonists in Wistar Kyoto Rats. *Neuropsychopharmacology* **2009**, *35*, 752–763.
- (52) Li, W.; Sun, H.; Chen, H.; Yang, X.; Xiao, L.; Liu, R.; Shao, L.; Qiu, Z. Major Depressive Disorder and Kappa Opioid Receptor Antagonists. *Transl. Perioper. pain Med.* **2015**, *1*, 4–16.
- (53) Buda KJ, Carroll FI, Kosten TR, D. S. D. W. B. A Double-Blind, Placebo-Controlled Study to Evaluate the Safety, Tolerability, and Pharmacokinetics of Single, Escalating Oral Doses of JD1c in Healthy Male Subjects. *Neuropsychopharmacology* **2015**, *40*, 1–7.
- (54) Spanagel, R.; Herz, A.; Shippenberg, T. S. Opposing Tonically Active Endogenous Opioid Systems Modulate the Mesolimbic Dopaminergic Pathway. *Proc. Natl. Acad. Sci. U. S. A.* **1992**, *89*, 2046–2050.
- (55) Margolis, E. B.; Hjelmstad, G. O.; Bonci, A.; Fields, H. L. Kappa-Opioid Agonists Directly Inhibit Midbrain Dopaminergic Neurons. *J. Neurosci.* **2003**, *23*, 9981–9986.
- (56) Bruchas, M. R.; Land, B. B.; Aita, M.; Xu, M.; Barot, S. K.; Li, S.; Chavkin, C. Stress-Induced p38 Mitogen-Activated Protein Kinase Activation Mediates Kappa-Opioid-Dependent Dysphoria. *J. Neurosci.* **2007**, *27*, 11614–11623.
- (57) Zhou, L.; Lovell, K. M.; Frankowski, K. J.; Slauson, S. R.; Phillips, A. M.; Streicher, J. M.; Stahl, E.; Schmid, C. L.; Hodde, P.; Madoux, F.; Cameron, M. D.; Priszano, T. E.; Aubé, J.; Bohn, L. M. Development of Functionally Selective, Small Molecule Agonists at Kappa Opioid Receptors. *J. Biol. Chem.* **2013**, *288*, 36703–36716.
- (58) Nakano, H.; Osone, K.; Takeshita, M.; Kwon, E.; Seki, C.; Matsuyama, H.; Takano, N.; Kohari, Y. A Novel Chiral Oxazolidine Organocatalyst for the Synthesis of an Oseltamivir Intermediate Using a Highly Enantioselective Diels-Alder Reaction of 1,2-Dihydropyridine. *Chem. Commun. (Camb)*. **2010**, *46*, 4827–4829.
- (59) Wang, S.; Zhang, A. An Improved Copper-Catalyzed Cross-Coupling Reaction of Alkyl Triflates With Primary Alkyl Grignard Reagents. *Org. Prep. Proced. Int.* **2008**, *40*, 293–301.
- (60) Schenk, S.; Valadez, A.; Worley, C. M.; McNamara, C. Blockade of the Acquisition of Cocaine Self-Administration by the NMDA Antagonist MK-801 (Dizocilpine). *Behavioural pharmacology*, 1993, *4*, 652–659.
- (61) Popik, P.; Skolnick, P. The NMDA Antagonist Memantine Blocks the Expression and Maintenance of Morphine Dependence. *Pharmacol. Biochem. Behav.* **1996**, *53*, 791–797.
- (62) Jacobs, M. T.; Zhang, Y. W.; Campbell, S. D.; Rudnick, G. Ibogaine, a Noncompetitive Inhibitor of Serotonin Transport, Acts by Stabilizing the Cytoplasm-Facing State of the Transporter. *J. Biol. Chem.* **2007**, *282*, 29441–29447.
- (63) Bulling, S.; Schicker, K.; Zhang, Y. W.; Steinkellner, T.; Stockner, T.; Gruber, C. W.; Boehm, S.; Freissmuth, M.; Rudnick, G.; Sitte, H. H.; Sandtner, W. The Mechanistic

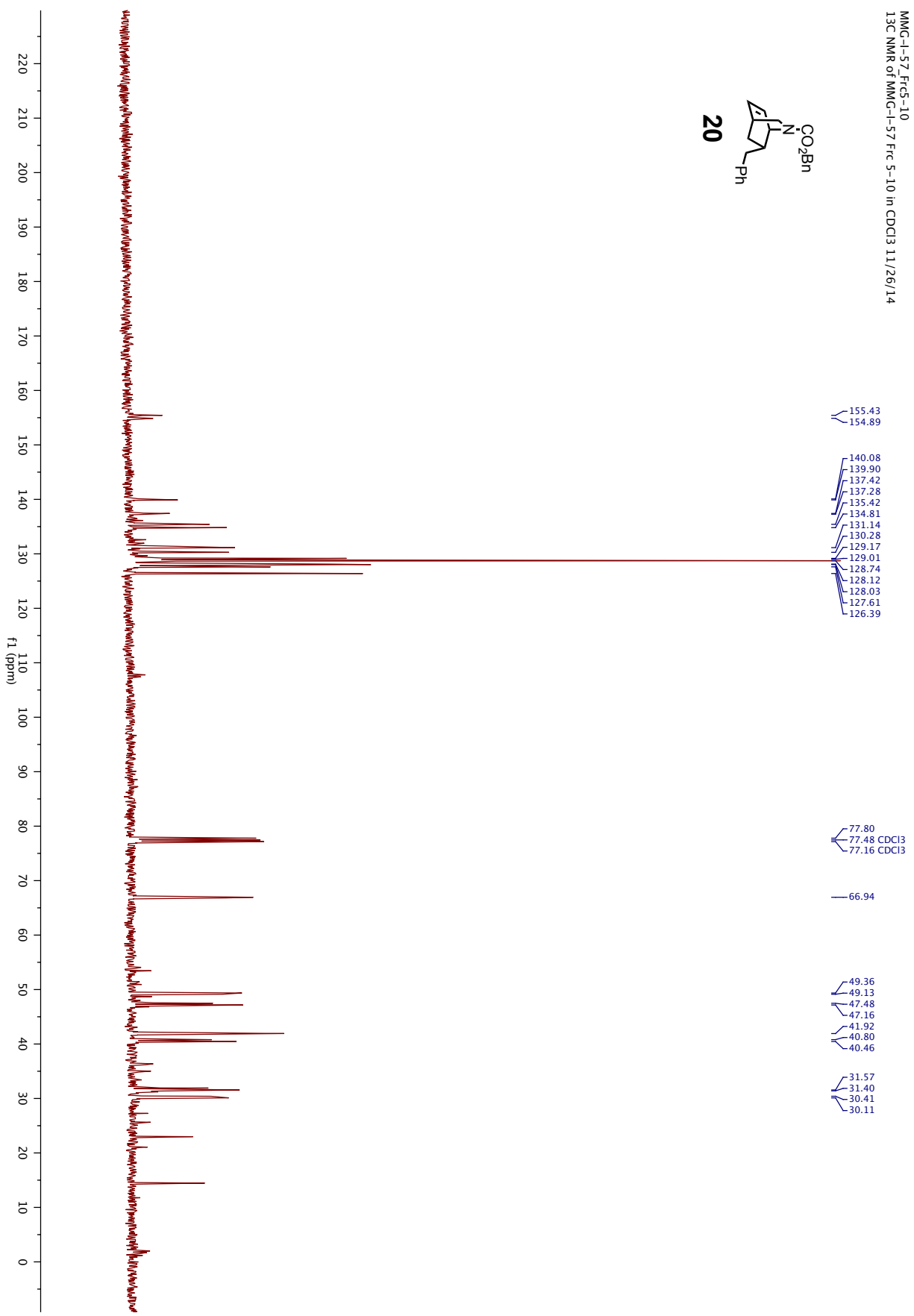
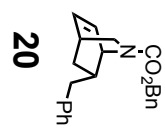
- Basis for Noncompetitive Ibogaine Inhibition of Serotonin and Dopamine Transporters. *J. Biol. Chem.* **2012**, *287*, 18524–18534.
- (64) Liu, R. J.; Lee, F. S.; Li, X. Y.; Bambico, F.; Duman, R. S.; Aghajanian, G. K. Brain-Derived Neurotrophic Factor Val66Met Allele Impairs Basal and Ketamine-Stimulated Synaptogenesis in Prefrontal Cortex. *Biol. Psychiatry* **2012**, *71*, 996–1005.
- (65) Youdim, M. B. H. Multi Target Neuroprotective and Neurorestorative Anti-Parkinson and Anti-Alzheimer Drugs Ladostigil and m30 Derived from Rasagiline. *Exp. Neurobiol.* **2013**, *22*, 1–10.
- (66) Jansson, P. J.; Kalinowski, D. S.; Lane, D. J. R.; Kovacevic, Z.; Seebacher, N. A.; Fouani, L.; Sahni, S.; Merlot, A. M.; Richardson, D. R. The Renaissance of Polypharmacology in the Development of Anti-Cancer Therapeutics: Inhibition of The “triad of Death” in Cancer by Di-2-Pyridylketone Thiosemicarbazones. *Pharmacol. Res.* **2015**, *100*, 255–260.
- (67) Liu, H.; Wang, J.; Zhou, W.; Wang, Y.; Yang, L. Systems Approaches and Polypharmacology for Drug Discovery from Herbal Medicines: An Example Using Licorice. *J. Ethnopharmacol.* **2013**, *146*, 773–793.
- (68) Scarpelli, R.; Sasso, O.; Piomelli, D. A Double Whammy: Targeting Both Fatty Acid Amide Hydrolase (FAAH) and Cyclooxygenase (COX) To Treat Pain and Inflammation. *ChemMedChem* **2015**, *4625*, 1–11.
- (69) Lutfy, K.; Cowan, A. Buprenorphine: A Unique Drug with Complex Pharmacology. *Curr. Neuropharmacol.* **2004**, *2*, 395–402.
- (70) Pergolizzi, J.; Aloisi, A. M.; Dahan, A.; Filitz, J.; Langford, R.; Likar, R.; Mercadante, S.; Morlion, B.; Raffa, R. B.; Sabatowski, R.; Sacerdote, P.; Torres, L. M.; Weinbroum, A. A. Current Knowledge of Buprenorphine and Its Unique Pharmacological Profile. *Pain Pract.* **2010**, *10*, 428–450.
- (71) Emrich, H. M.; Vogt, P.; Herz, A. Possible Antidepressive Effects of Opioids: Action of Buprenorphine. *Ann. N. Y. Acad. Sci.* **1982**, *398*, 108–112.
- (72) Bodkin, J. A.; Zornberg, G. L.; Lukas, S. E.; Cole, J. O. Buprenorphine Treatment of Refractory Depression. *J. Clin. Psychopharmacol.* **1995**, *15*, 49–57.
- (73) Nyhuis, P. W.; Gastpar, M.; Scherbaum, N. *Opiate Treatment in Depression Refractory to Antidepressants and Electroconvulsive Therapy*; 2008; Vol. 28.
- (74) Falcon, E.; Browne, C. A.; Leon, R. M.; Fleites, V. C.; Sweeney, R.; Kirby, L. G.; Lucki, I. Antidepressant-like Effects of Buprenorphine Are Mediated by Kappa Opioid Receptors. *Neuropsychopharmacology* **2016**, *41*, 2344–2351.
- (75) Váradi, A.; Marrone, G. F.; Eans, S. O.; Ganno, M. L.; Subrath, J. J.; Le Rouzic, V.; Hunkele, A.; Pasternak, G. W.; McLaughlin, J. P.; Majumdar, S. Synthesis and Characterization of a Dual Kappa-Delta Opioid Receptor Agonist Analgesic Blocking Cocaine Reward Behavior. *ACS Chem. Neurosci.* **2015**, *6*, 1813–1824.
- (76) Matsumoto, K.; Narita, M.; Muramatsu, N.; Nakayama, T.; Misawa, K.; Kitajima, M.; Tashima, K.; Devi, L. A.; Suzuki, T.; Takayama, H.; Horie, S. Orally Active Opioid M/δ Dual Agonist MGM-16, a Derivative of the Indole Alkaloid Mitragynine, Exhibits Potent Antiallodynic Effect on Neuropathic Pain in Mice. *J. Pharmacol. Exp. Ther.* **2014**, *348*, 383–392.
- (77) Breslin, H. J.; Diamond, C. J.; Kavash, R. W.; Cai, C.; Dyatkin, A. B.; Miskowski, T. A.; Zhang, S.-P.; Wade, P. R.; Hornby, P. J.; He, W. Identification of a Dual δ OR Antagonist/μ OR Agonist as a Potential Therapeutic for Diarrhea-Predominant Irritable Bowel Syndrome (IBS-D). *Bioorganic Med. Chem. Lett.* **2012**, *22*, 4869–4872.

- (78) Banerjee, T. S.; Paul, S.; Sinha, S.; Das, S. Synthesis of Iboga-like Isoquinuclidines: Dual Opioid Receptors Agonists Having Antinociceptive Properties. *Bioorg. Med. Chem.* **2014**, *22*, 6062–6070.
- (79) Fujita, W.; Gomes, I.; Dove, L. S.; Prohaska, D.; McIntyre, G.; Devi, L. A. Molecular Characterization of Eluxadoline as a Potential Ligand Targeting Mu-Delta Opioid Receptor Heteromers. *Biochem. Pharmacol.* **2014**, *92*, 448–456.
- (80) Chen, Y.; Mestek, A.; Liu, J.; Yu, L. Molecular Cloning of a Rat Kappa Opioid Receptor Reveals Sequence Similarities to the Mu and Delta Opioid Receptors. *Biochem. J.* **1993**, *295*, 625–628.
- (81) Benyamin, R.; Trescot, A. M.; Datta, S.; Buenaventura, R.; Adlaka, R.; Sehgal, N.; Glaser, S. E.; Vallejo, R. Opioid Complications and Side Effects. *Pain Physician* **2008**, *Opioid Spe*, S105–S120.
- (82) Díaz, J. L. Salvia Divinorum: A Psychopharmacological Riddle and a Mind-Body Prospect. *Curr. Drug Abuse Rev.* **2013**, *6*, 43–53.
- (83) Trang, T.; Al-Hasani, R.; Salvemini, D.; Salter, M. W.; Gutstein, H.; Cahill, C. M. Pain and Poppies: The Good, the Bad, and the Ugly of Opioid Analgesics. *J. Neurosci.* **2015**, *35*, 13879–13888.
- (84) Broom, D. C.; Jutkiewicz, E. M.; Folk, J. E.; Traynor, J. R.; Rice, K. C.; Woods, J. H. Convulsant Activity of a Non-Peptidic δ -Opioid Receptor Agonist Is Not Required for Its Antidepressant-like Effects in Sprague-Dawley Rats. *Psychopharmacology (Berl.)* **2002**, *164*, 42–48.
- (85) Comer, S. D.; Hoenicke, E. M.; Sable, A. I.; McNutt, R. W.; Chang, K. J.; Decosta, B. R.; Mosberg, H. I.; Woods, J. H. Convulsive Effects of Systemic Administration of the Delta-Opioid Agonist Bw373U86 in Mice. *J. Pharmacol. Exp. Ther.* **1993**, *267*, 888–895.
- (86) Negus, S. S.; Butelman, E. R.; Chang, K. J.; DeCosta, B.; Winger, G.; Woods, J. H. Behavioral Effects of the Systemically Active Delta Opioid Agonist BW373U86 in Rhesus Monkeys. *J. Pharmacol. Exp. Ther.* **1994**, *270*, 1025–1034.
- (87) Jutkiewicz, E. M.; Eller, E. B.; Folk, J. E.; Rice, K. C.; Traynor, J. R.; Woods, J. H. Delta-Opioid Agonists: Differential Efficacy and Potency of SNC80, Its 3-OH (SNC86) and 3-Desoxy (SNC162) Derivatives in Sprague-Dawley Rats. *J. Pharmacol. Exp. Ther.* **2004**, *309*, 173–181.
- (88) Saitoh, A.; Sugiyama, A.; Nemoto, T.; Fujii, H.; Wada, K.; Oka, J.-I.; Nagase, H.; Yamada, M. The Novel δ Opioid Receptor Agonist KNT-127 Produces Antidepressant-like and Antinociceptive Effects in Mice without Producing Convulsions. *Behav. Brain Res.* **2011**, *223*, 271–279.
- (89) Pasanisi, F.; Sloan, L.; Rubin, P. C. Cardiovascular Properties of Metkephamid, a δ Opioid Receptor Agonist, in Man. *Clin. Sci.* **1985**, *68*, 209–213.
- (90) Bohn, L. M.; Lefkowitz, R. J.; Gainetdinov, R. R.; Peppel, K.; Caron, M. G.; Lin, F. T. Enhanced Morphine Analgesia in Mice Lacking Beta-Arrestin 2. *Science* **1999**, *286*, 2495–2498.
- (91) Rives, M.-L.; Rossillo, M.; Liu-Chen, L.-Y.; Javitch, J. A. 6'-Guanidinonaltrindole (6'-GNTI) Is a G Protein-Biased κ -Opioid Receptor Agonist That Inhibits Arrestin Recruitment. *J. Biol. Chem.* **2012**, *287*, 27050–27054.
- (92) Schmid, C. L.; Streicher, J. M.; Groer, C. E.; Munro, T. A.; Zhou, L.; Bohn, L. M. Functional Selectivity of 6'-guanidinonaltrindole (6'-GNTI) at κ -Opioid Receptors in Striatal Neurons. *J. Biol. Chem.* **2013**, *288*, 22387–22398.

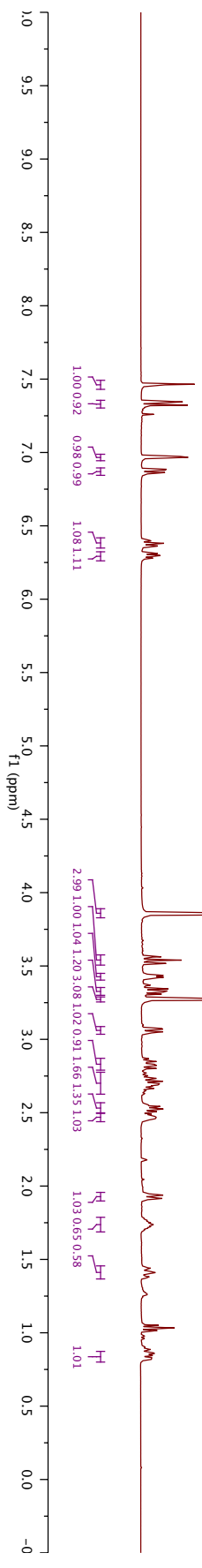
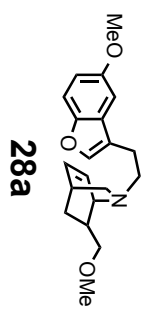
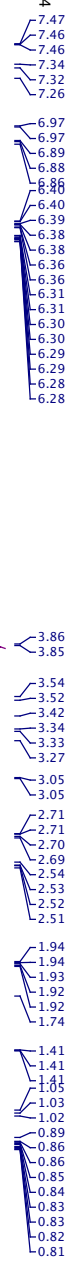
- (93) DeWire, S. M.; Yamashita, D. S.; Rominger, D. H.; Liu, G.; Cowan, C. L.; Graczyk, T. M.; Chen, X.-T.; Pitis, P. M.; Gotchev, D.; Yuan, C.; Koblish, M.; Lark, M. W.; Violin, J. D. A G Protein-Biased Ligand at the μ -Opioid Receptor Is Potently Analgesic with Reduced Gastrointestinal and Respiratory Dysfunction Compared with Morphine. *J. Pharmacol. Exp. Ther.* **2013**, *344*, 708–717.
- (94) Luttrell, L. M.; Maudsley, S.; Bohn, L. M. Fulfilling the Promise of “Biased” G Protein-Coupled Receptor Agonism. *Mol. Pharmacol.* **2015**, *88*, 579–588.
- (95) Beaulieu, J. M. Morphine-Induced Mu-Opioid Receptor Internalization: A Paradox Solved in Neurons. *J. Neurosci.* **2005**, *25*, 10061–10063.
- (96) Finn, A. K.; Whistler, J. L. Endocytosis of the Mu Opioid Receptor Reduces Tolerance and a Cellular Hallmark of Opiate Withdrawal. *Neuron* **2001**, *32*, 829–839.
- (97) Kim, J. A.; Bartlett, S.; He, L.; Nielsen, C. K.; Chang, A. M.; Kharazia, V.; Waldhoer, M.; Ou, C. J.; Taylor, S.; Ferwerda, M.; Cado, D.; Whistler, J. L. Morphine-Induced Receptor Endocytosis in a Novel Knockin Mouse Reduces Tolerance and Dependence. *Curr. Biol.* **2008**, *18*, 129–135.
- (98) Berger, A. C.; Whistler, J. L. Morphine-Induced Mu Opioid Receptor Trafficking Enhances Reward yet Prevents Compulsive Drug Use. *EMBO Mol. Med.* **2011**, *3*, 385–397.
- (99) Satoh, N.; Akiba, T.; Yokoshima, S.; Fukuyama, T. A Practical Synthesis of (–)-Oseltamivir. *Angew. Chemie Int. Ed.* **2007**, *46*, 5734–5736.
- (100) Sheldrick, G. M. *SHELXTL, An Integrated System for Solving, Refining and Displaying Crystal Structures from Diffraction Data*; University of Göttingen: Göttingen, Federal Republic of Germany, 1981.
- (101) Sheldrick, G. M. A Short History of SHELX. *Acta Crystallogr. Sect. A Found. Crystallogr.* **2007**, *64*, 112–122.
- (102) Sheldrick, G. M. SHELXT - Integrated Space-Group and Crystal-Structure Determination. *Acta Crystallogr. Sect. A Found. Crystallogr.* **2015**, *71*, 3–8.
- (103) Negri, A.; Rives, M.-L.; Caspers, M. J.; Prisinzano, T. E.; Javitch, J. A.; Filizola, M. Discovery of a Novel Selective Kappa-Opioid Receptor Agonist Using Crystal Structure-Based Virtual Screening. *J. Chem. Inf. Model.* **2013**, *53*, 521–526.



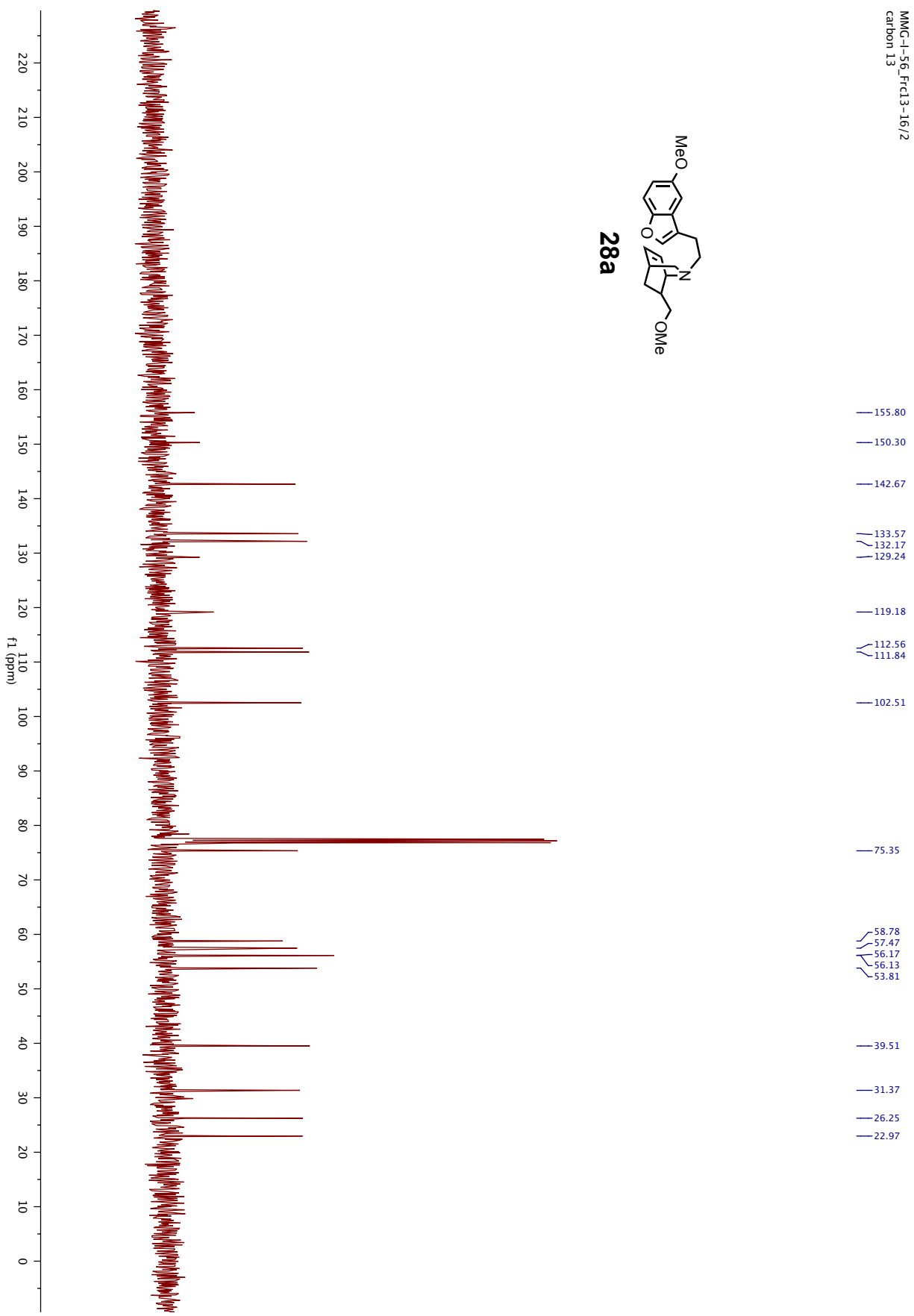
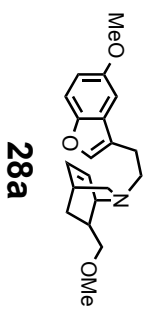
MMG-I-57_Frc5-10
13C NMR of MMG-I-57_Frc 5-10 in CDCl3 11/26/14



MMG-1-43 Frc25-30
1H NMR of MMG-1-43 Frc 25-30 in CDCl3 10/4/14



MMG-1-56, FeCl3-16/2
carbon 13



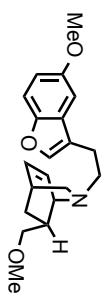
MMG-I-53 F1629-55
1H NMR of MMG-I-53 F1629-55 (recovered MMG-47)

7.42
7.42
7.44
7.11
7.09
6.99
6.99
6.99
6.88
6.86
6.41
6.41
6.39
6.19
6.19
6.18
6.17
6.17
6.17
6.15
6.15

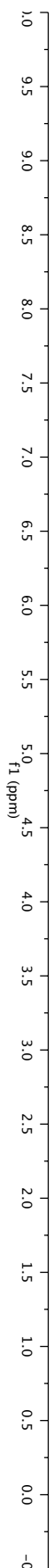
3.85
3.58
3.58
3.57
3.57
3.57

3.01
3.00
2.98
2.85
2.84
2.53
2.52
2.52
2.51
2.51
2.08
2.08
2.07
2.06
1.75
1.73
1.72
1.72
1.70
1.69

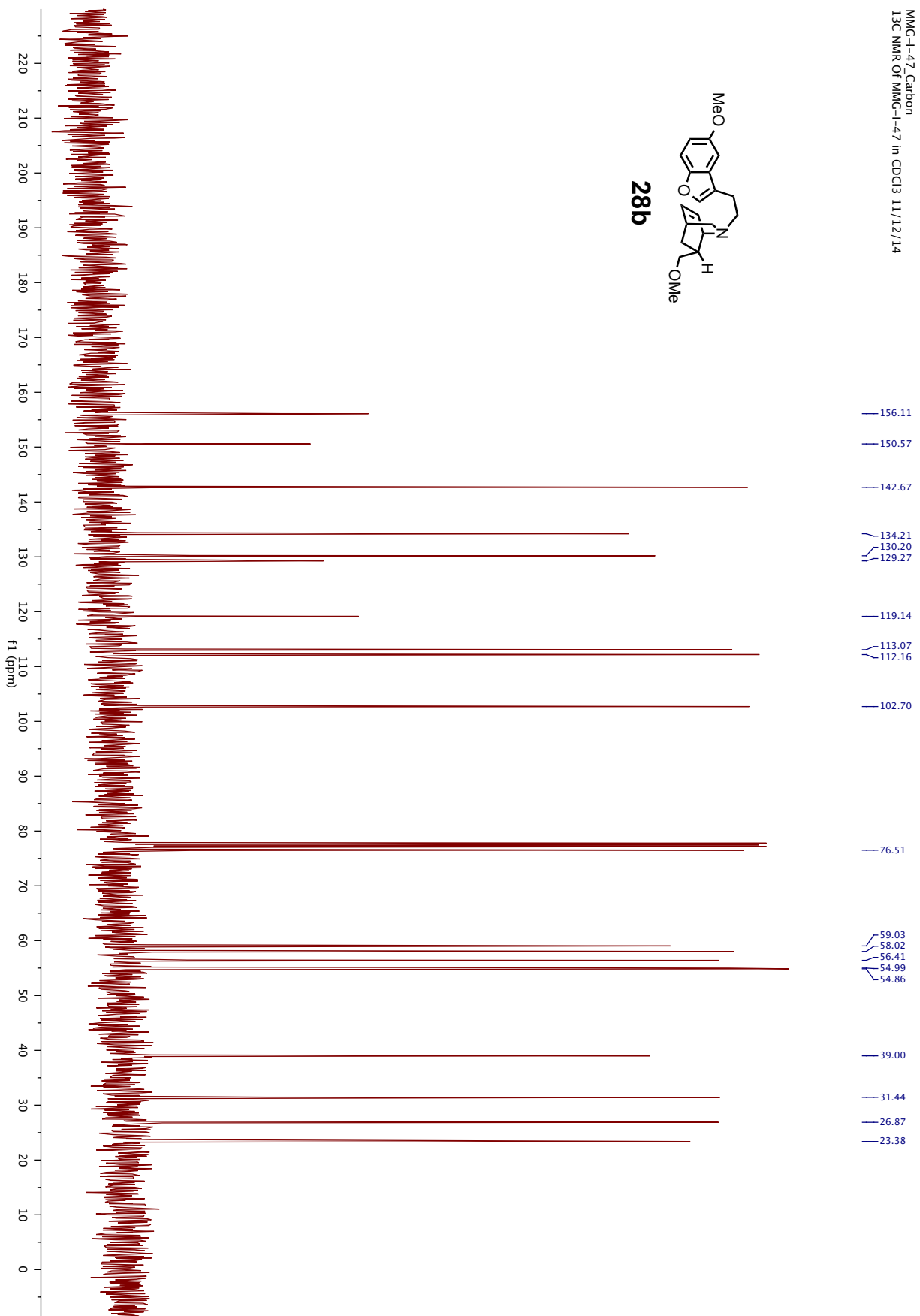
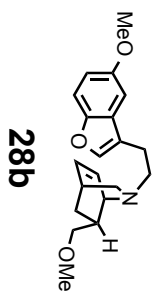
0.69
0.69
0.68
0.68
0.67
0.67
0.66
0.65
0.65
0.64
0.64



28b



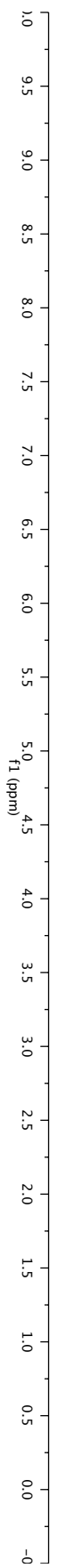
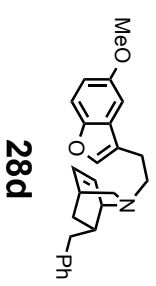
MMG-1-47 Carbon
13C NMR OF MMG-1-47 in CDCl3 11/12/14



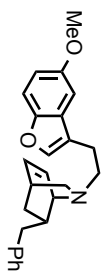
MMG-1-52 PrepTLC_Higher
1H NMR of MMG-1-52 Prep TLC_Higher Spot (recovered MMG-49)

7.51
7.49
7.47
7.35
7.33
7.33
7.22
7.22
7.24
7.26
7.24
7.23
7.22
7.21
7.11
7.02
7.01
6.94
6.92
6.83
6.83
6.72
6.70
6.69
6.53
6.53
6.51
6.50
6.49
6.28
6.28
6.27
6.26
6.26

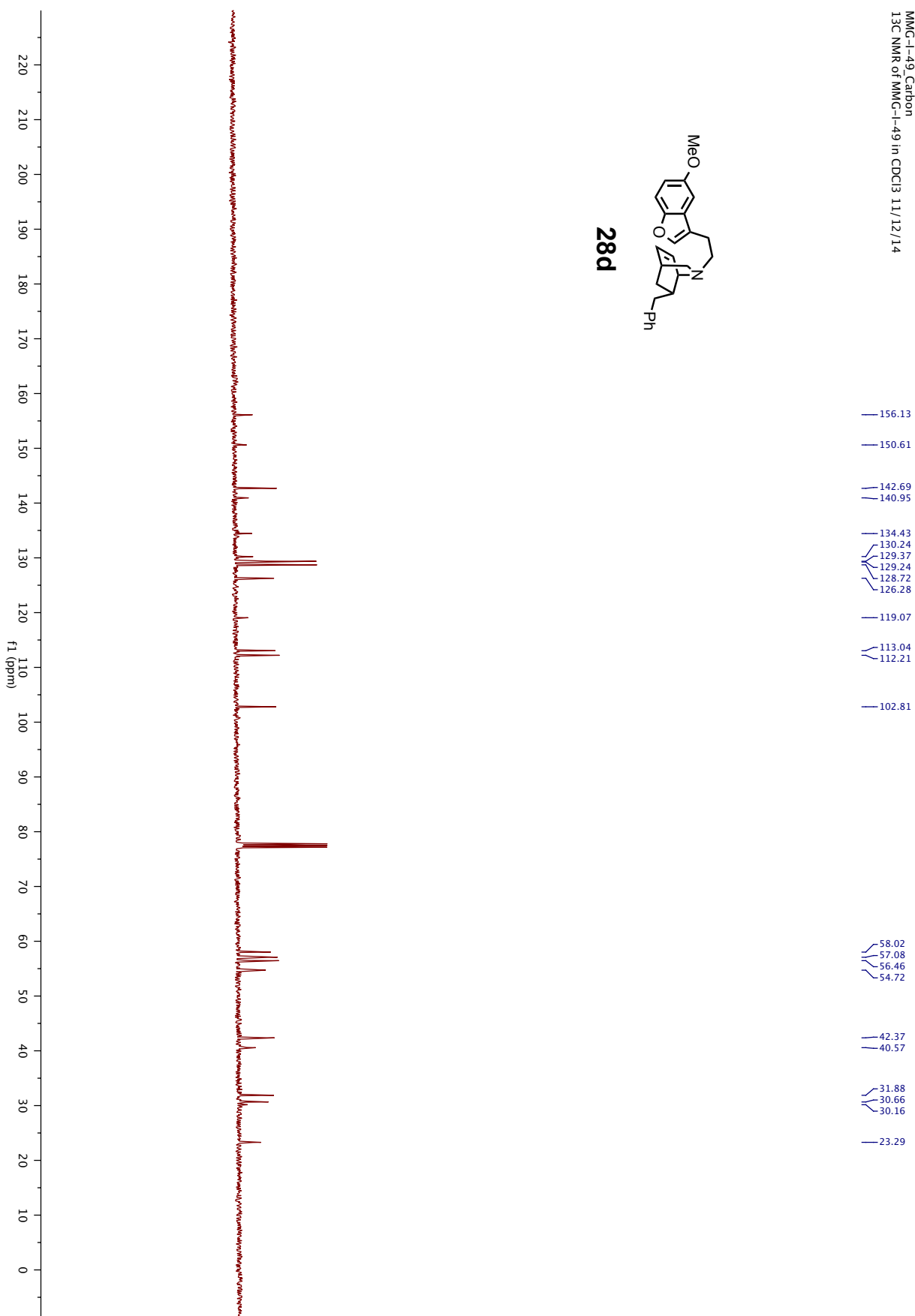
3.90
3.33
3.32
3.32
3.32
3.31
3.31
3.31
3.09
3.08
2.59
2.59
2.58
2.57
2.47
2.45
2.14
2.11
2.11
1.86
1.86
1.83
1.82
1.34
1.33
1.32
1.31
1.12
1.10
1.08
0.98
0.98
0.97
0.96
0.95
0.94
0.94
0.93
0.93



MMG-1-49 Carbon
13C NMR of MMG-1-49 in CDCl3 11/12/14



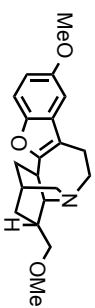
28d



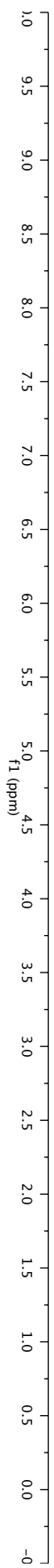
MMG-1-45_Frc7-11
1H NMR of MMG-1-45 Frc 7-11 in CDCl3 10/9/14

7.27
7.26
7.24
6.87
6.86
6.83
6.82
6.80
6.80

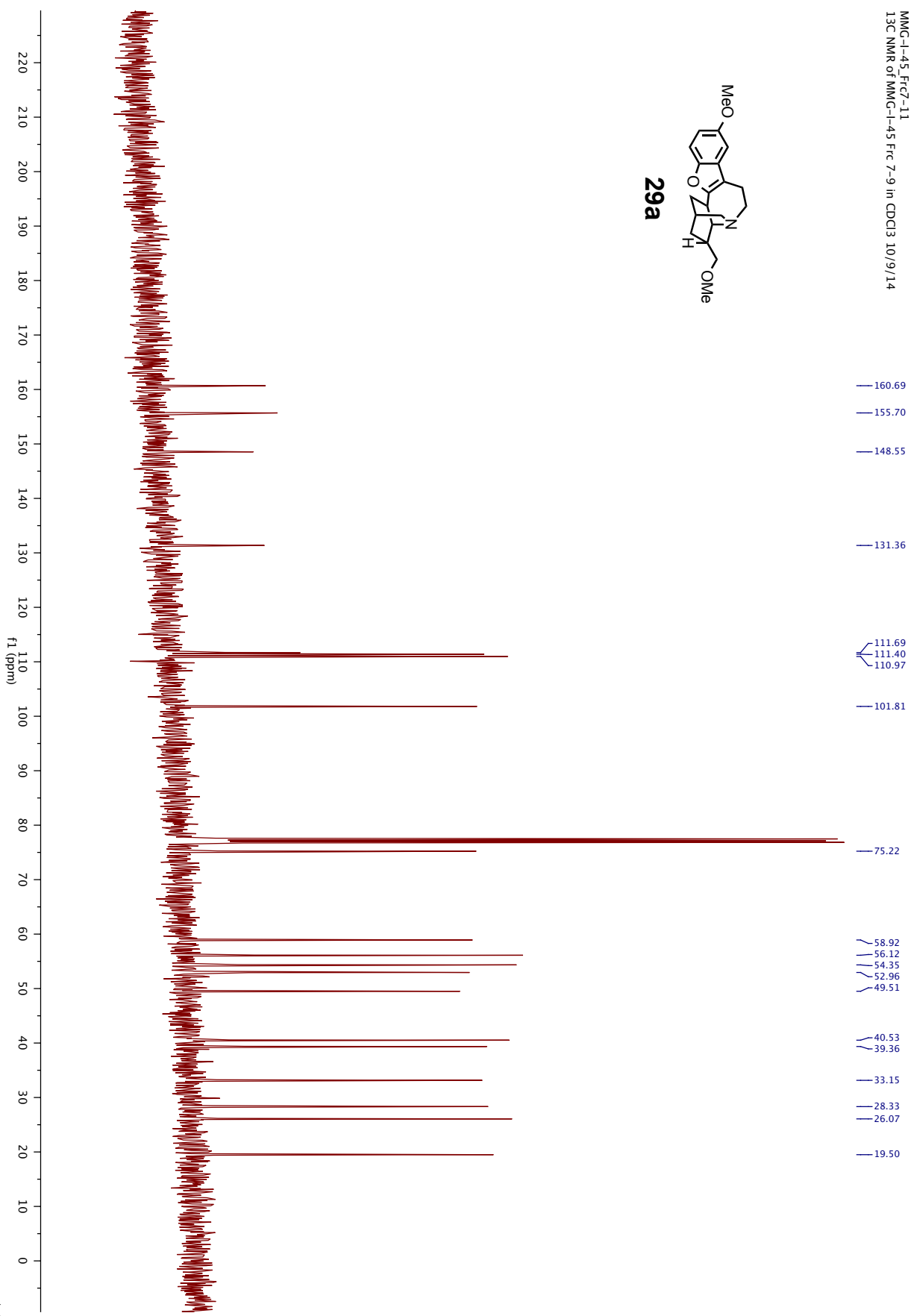
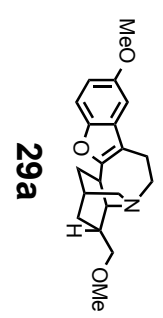
3.85
3.84
3.57
3.37
3.36
3.31
3.21
3.20
3.18
3.02
3.01
3.01
2.98
2.52
2.48
2.48
2.48
2.07
2.06
2.03
2.03
1.88
1.88
1.87
1.87
1.69
1.16
1.15
1.15
1.14
1.13
1.13
1.13
1.11



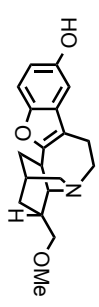
29a



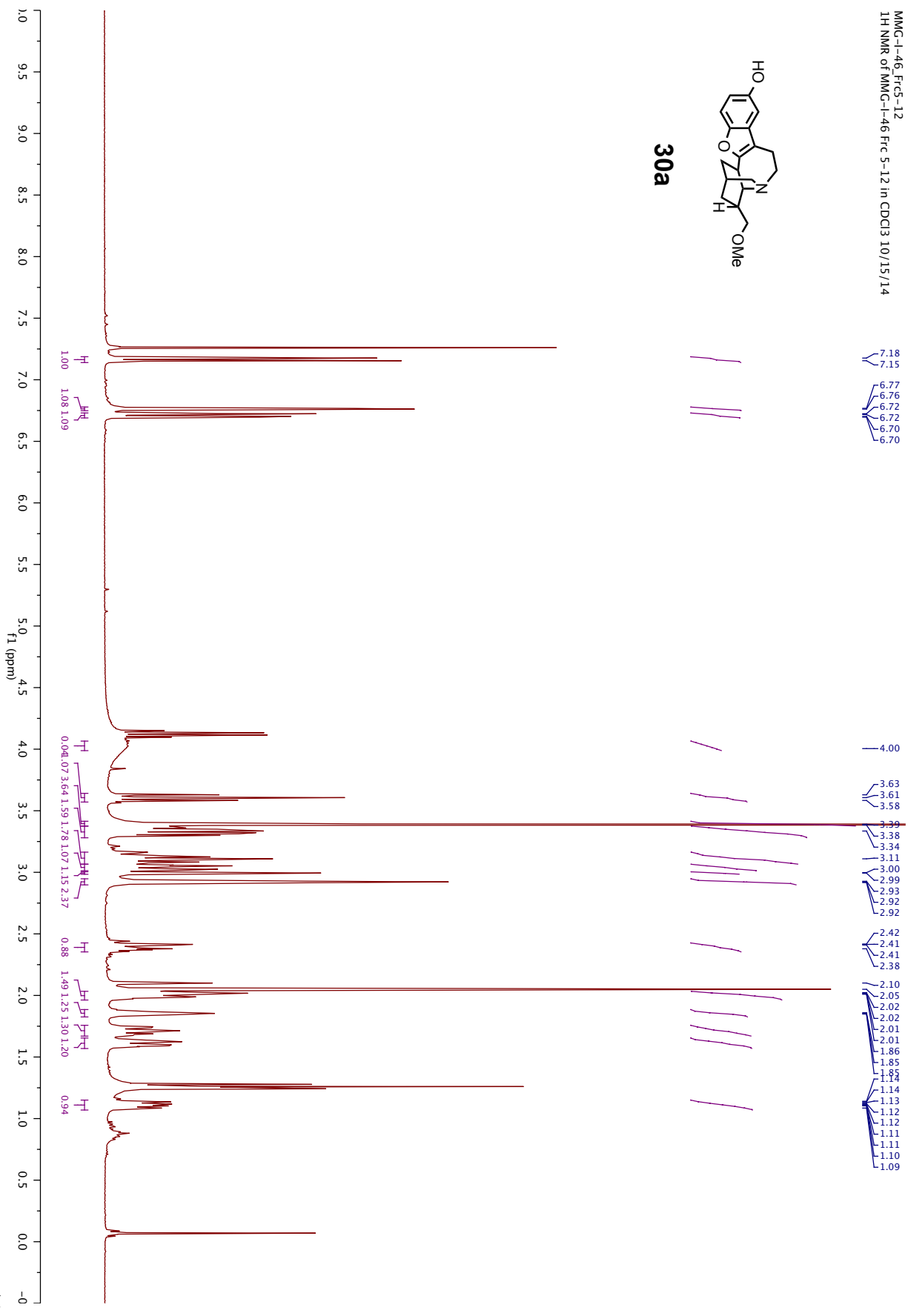
MMG-1-45_Fc7-11
13C NMR of MMG-1-45 Frc 7-9 in CDCl3 10/9/14



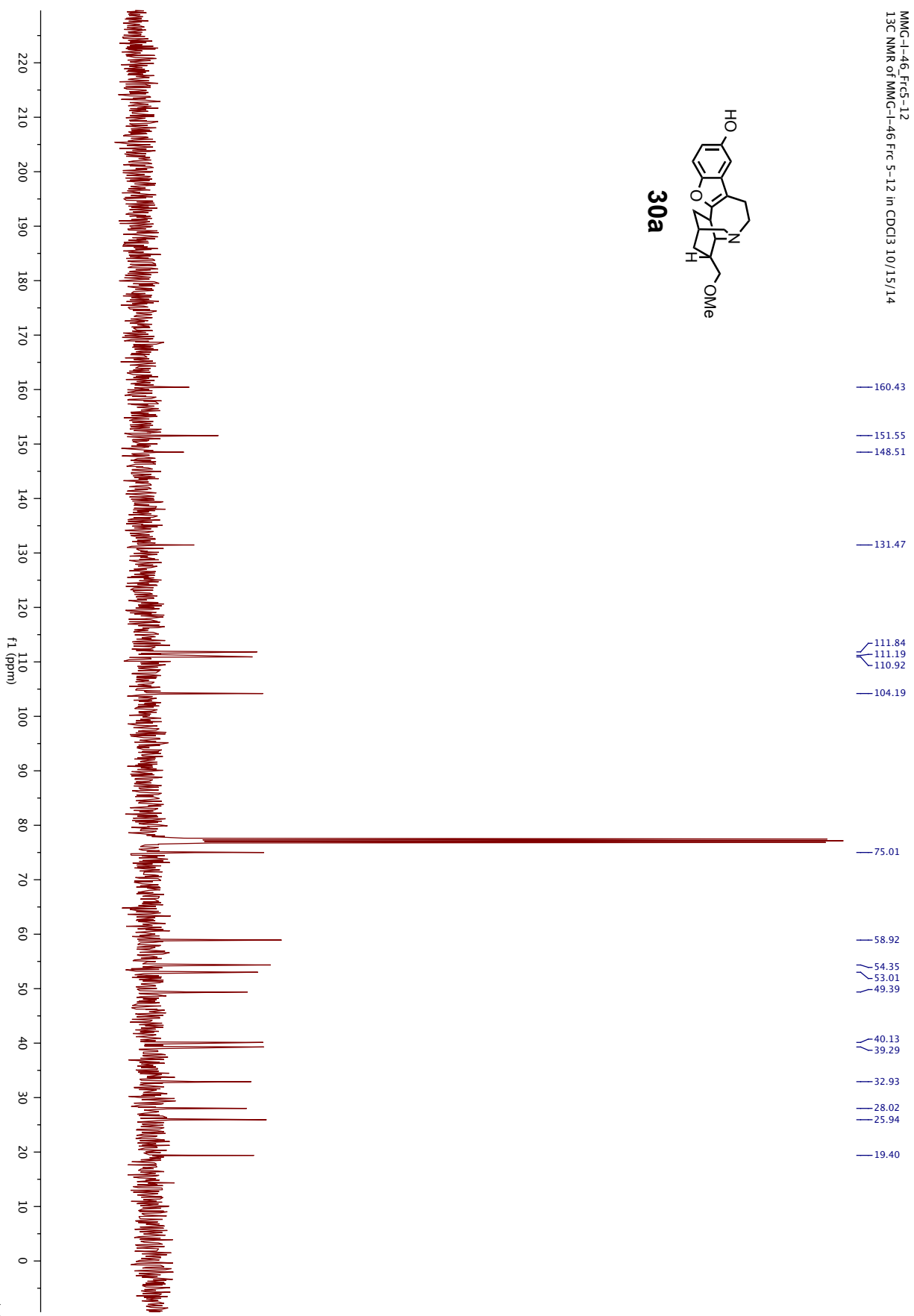
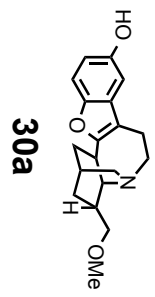
MMG-1-46_Frc5-12
1H NMR of MMG-1-46 Frc 5-12 in CDCl3 10/15/14



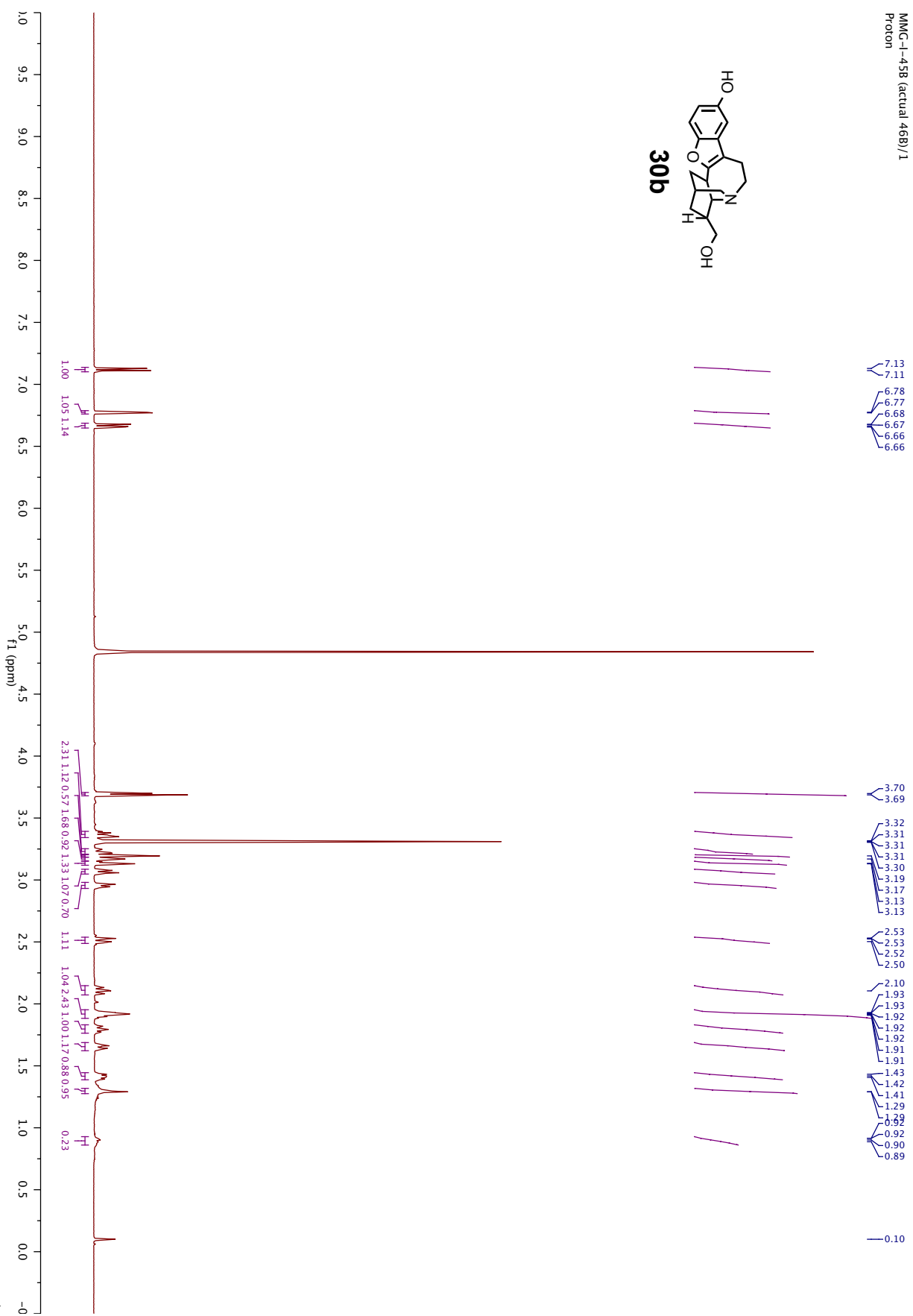
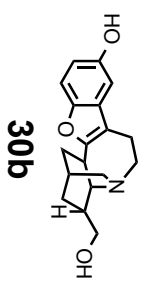
30a



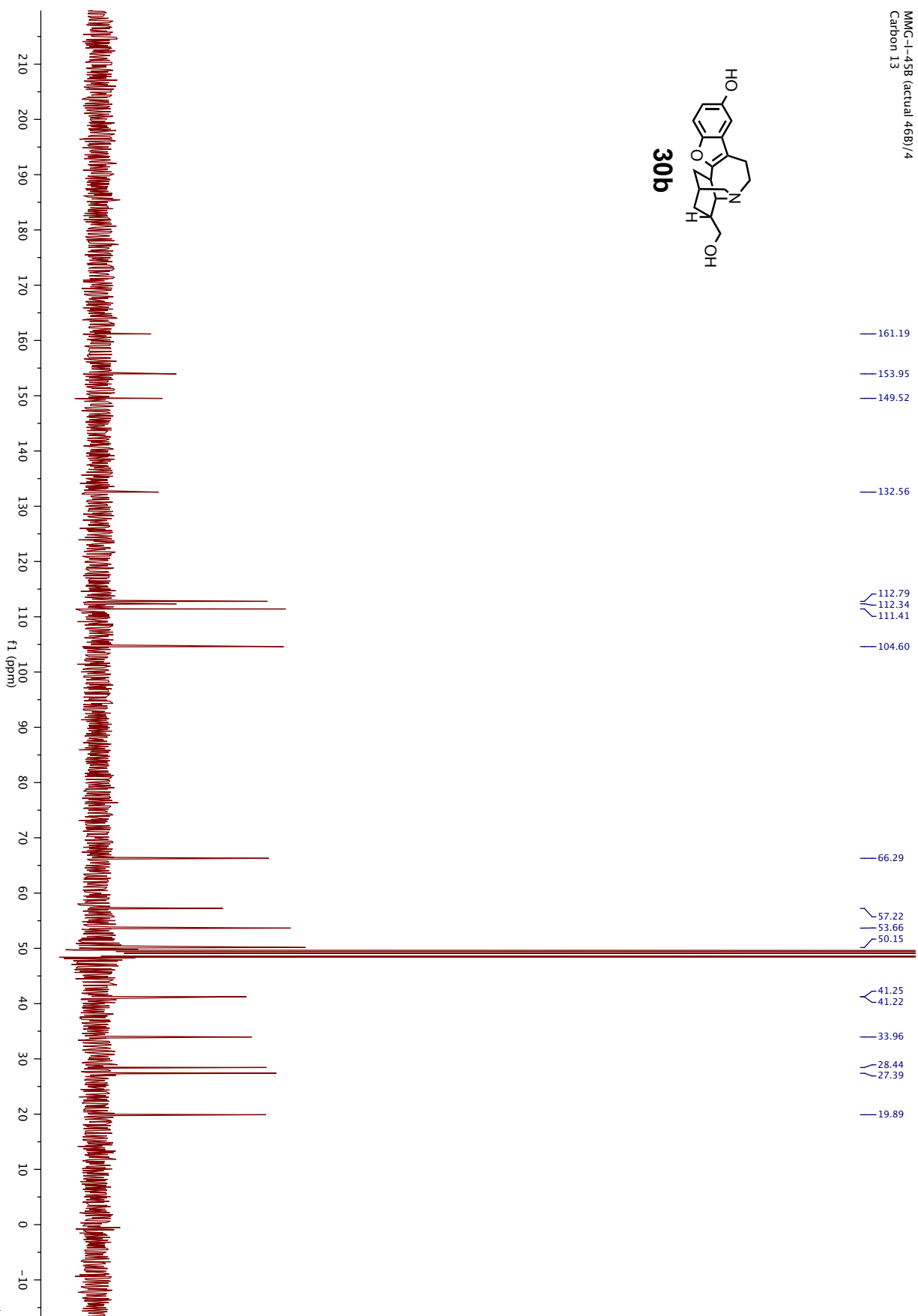
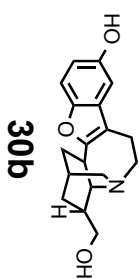
MMG-1-46_Frc5-12
13C NMR of MMG-1-46 Frc 5-12 in CDCl3 10/15/14

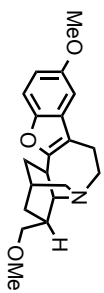
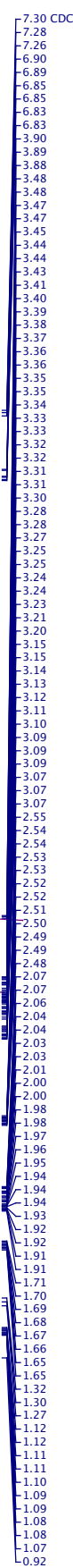


MMG-1-458 (actual 468)/1
Proton

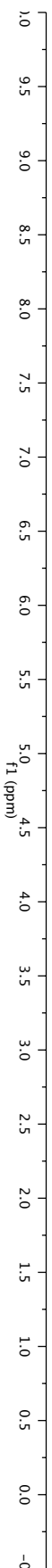


MMG-I-458 (actual 468)/4
Carbon 13

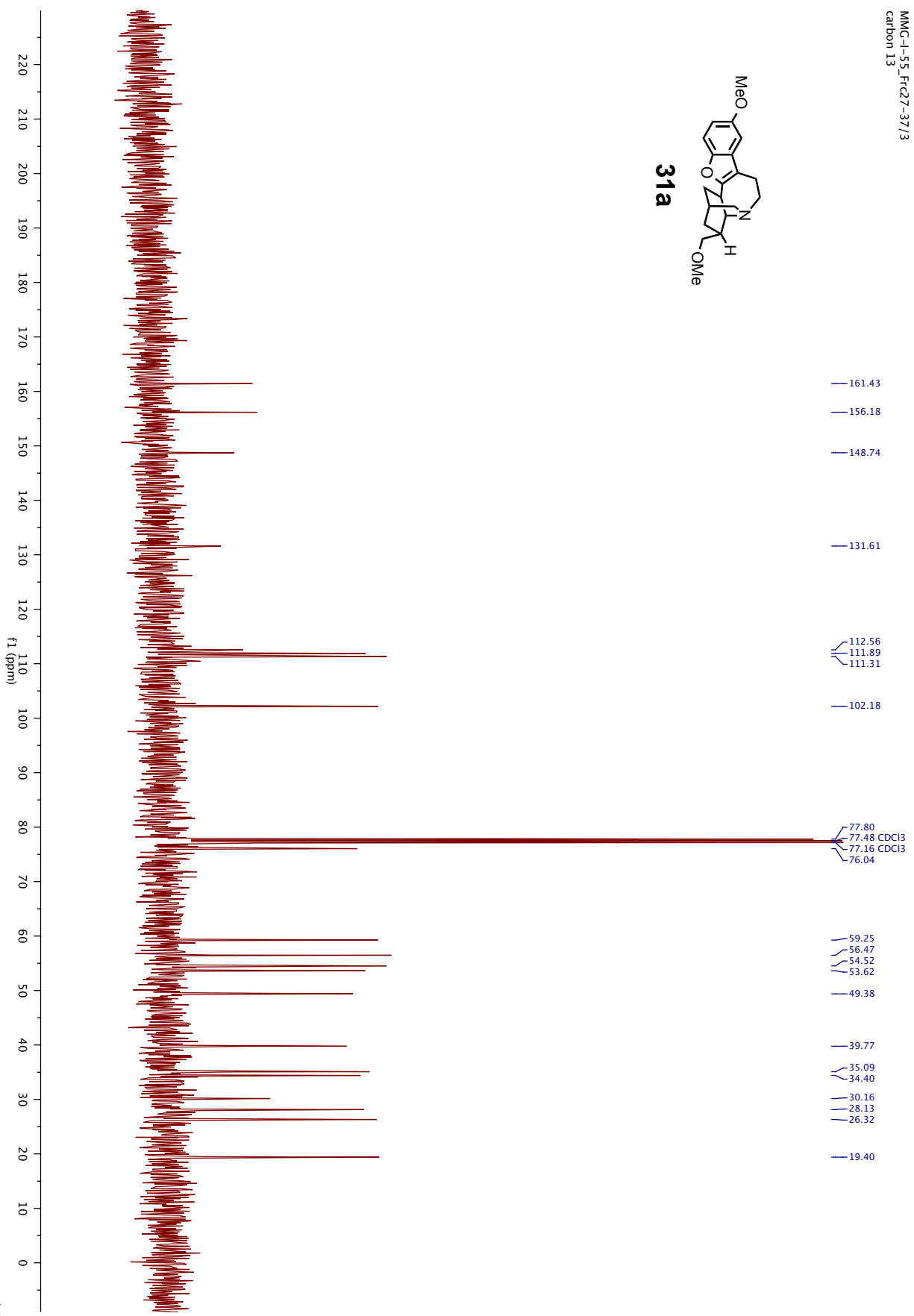
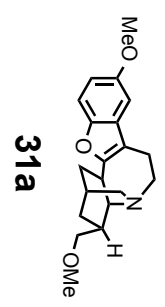




31a

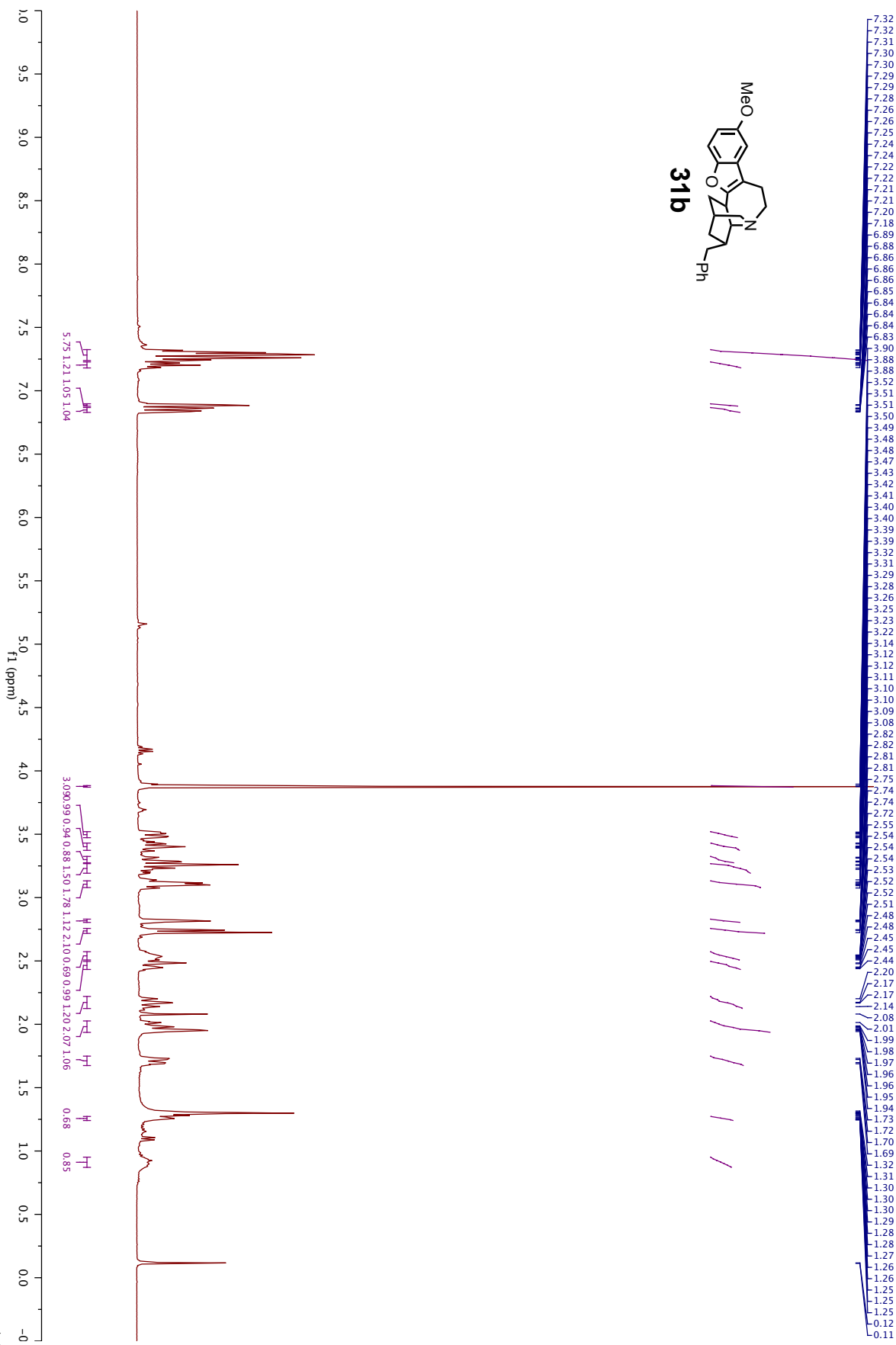
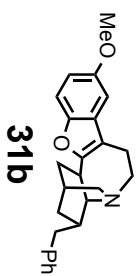


MMG-I-55_Fc27-37/3
Carbon 13

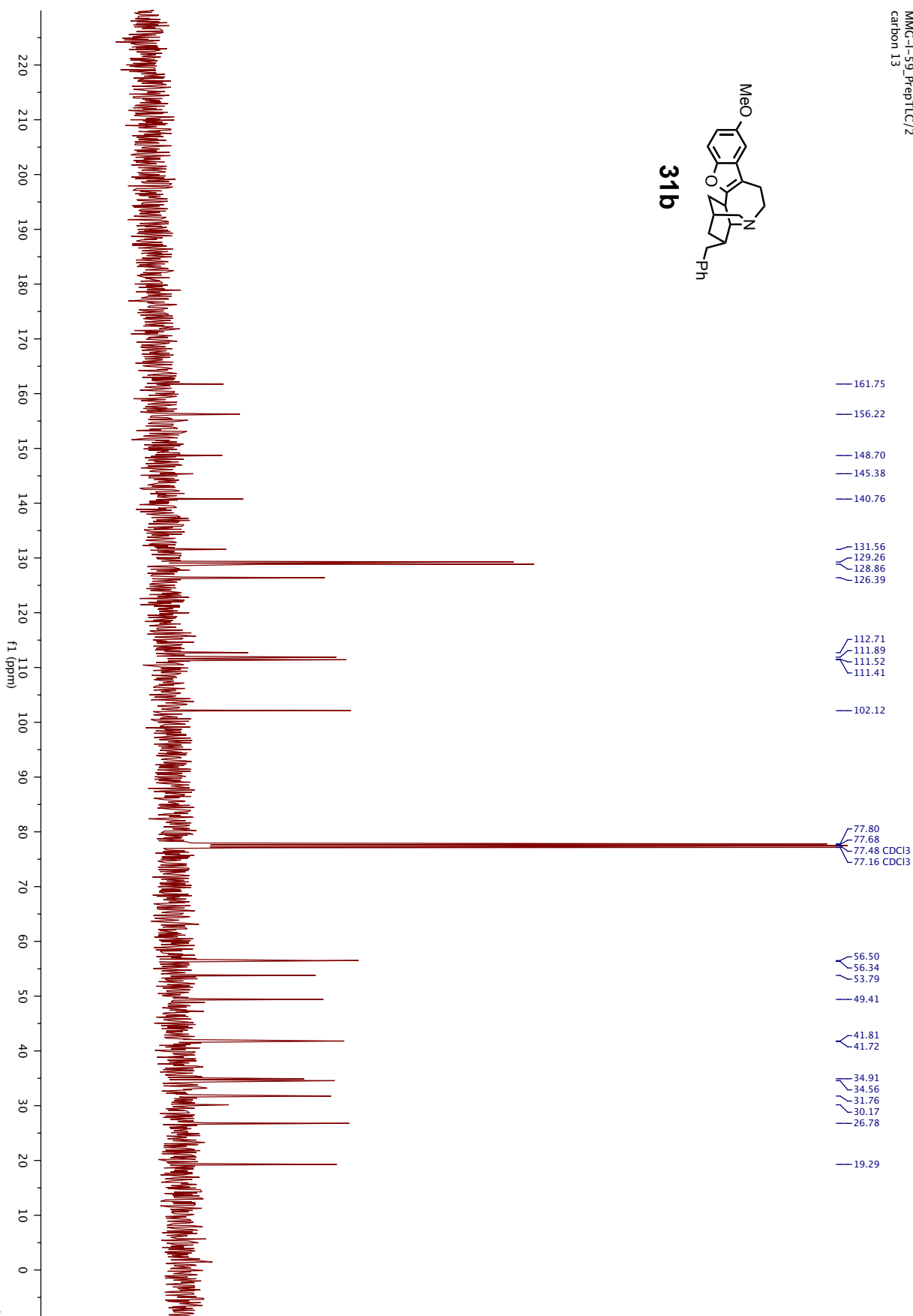
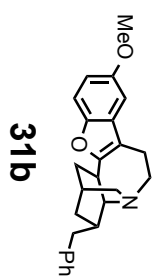


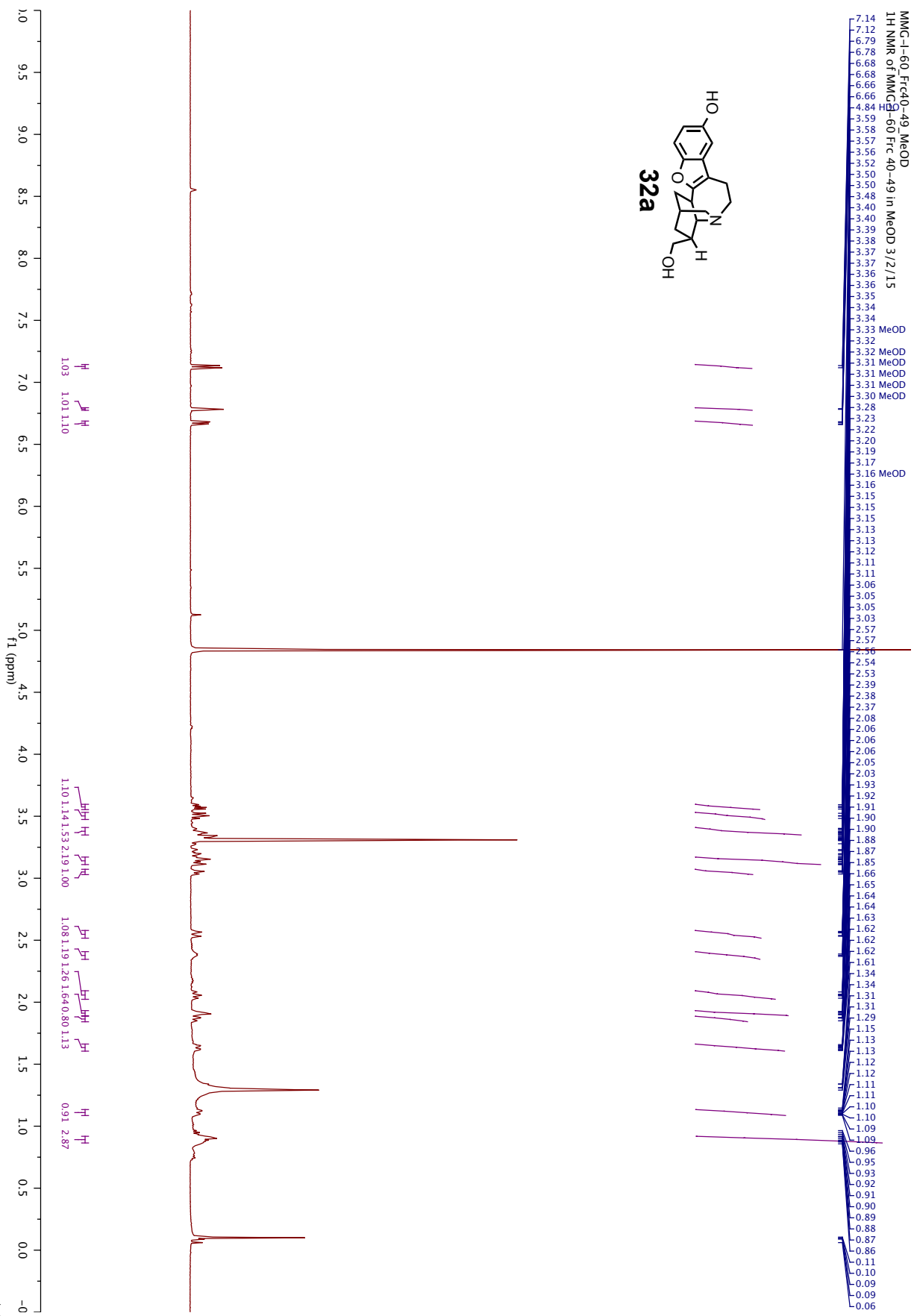
MMG-1-59-PrepTLC/1

CDCl₃

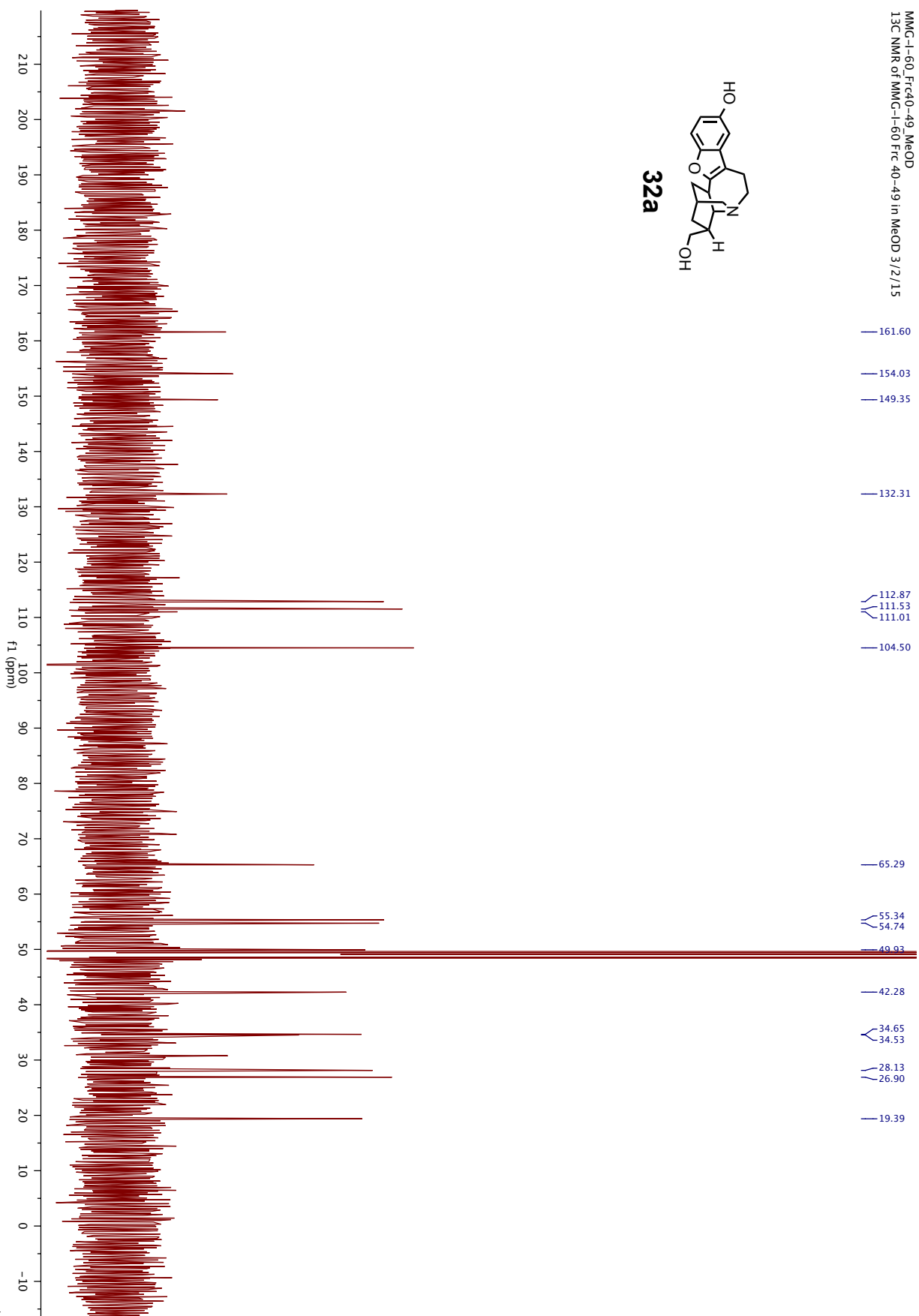
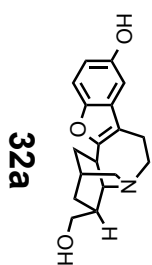


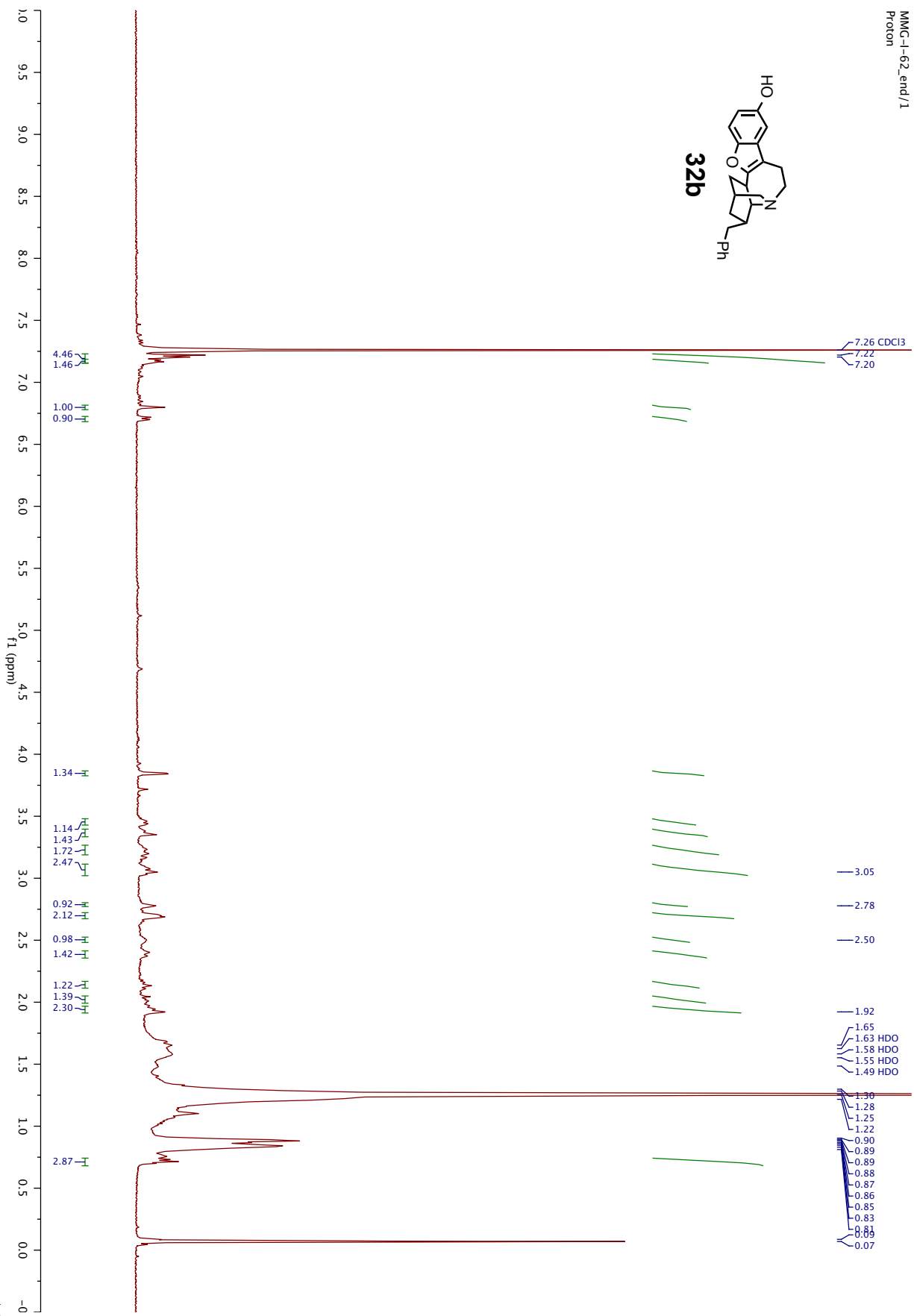
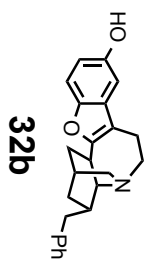
MMG-1-59 PrePTLC/2
carbon 13

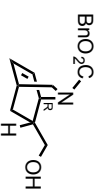
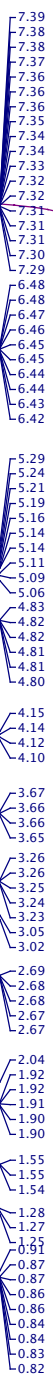
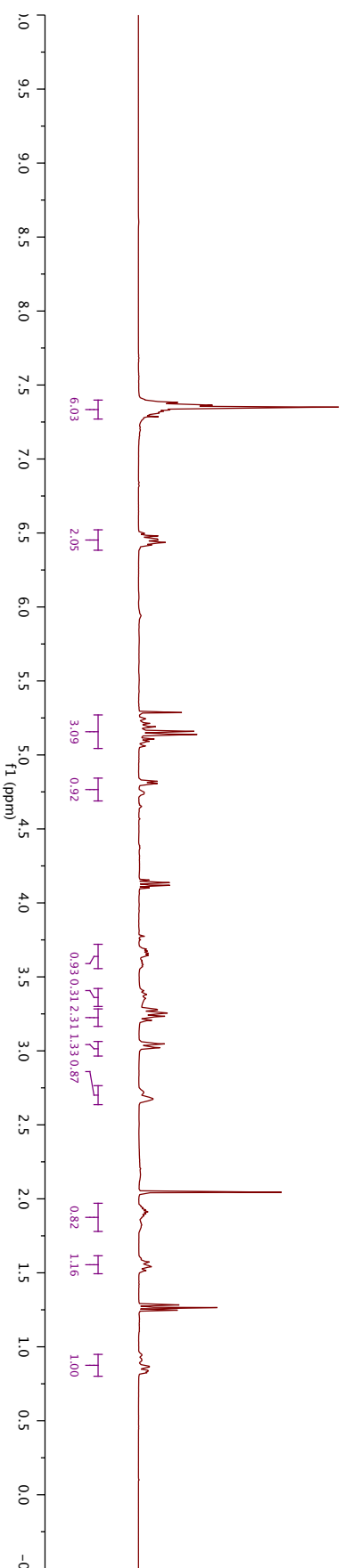




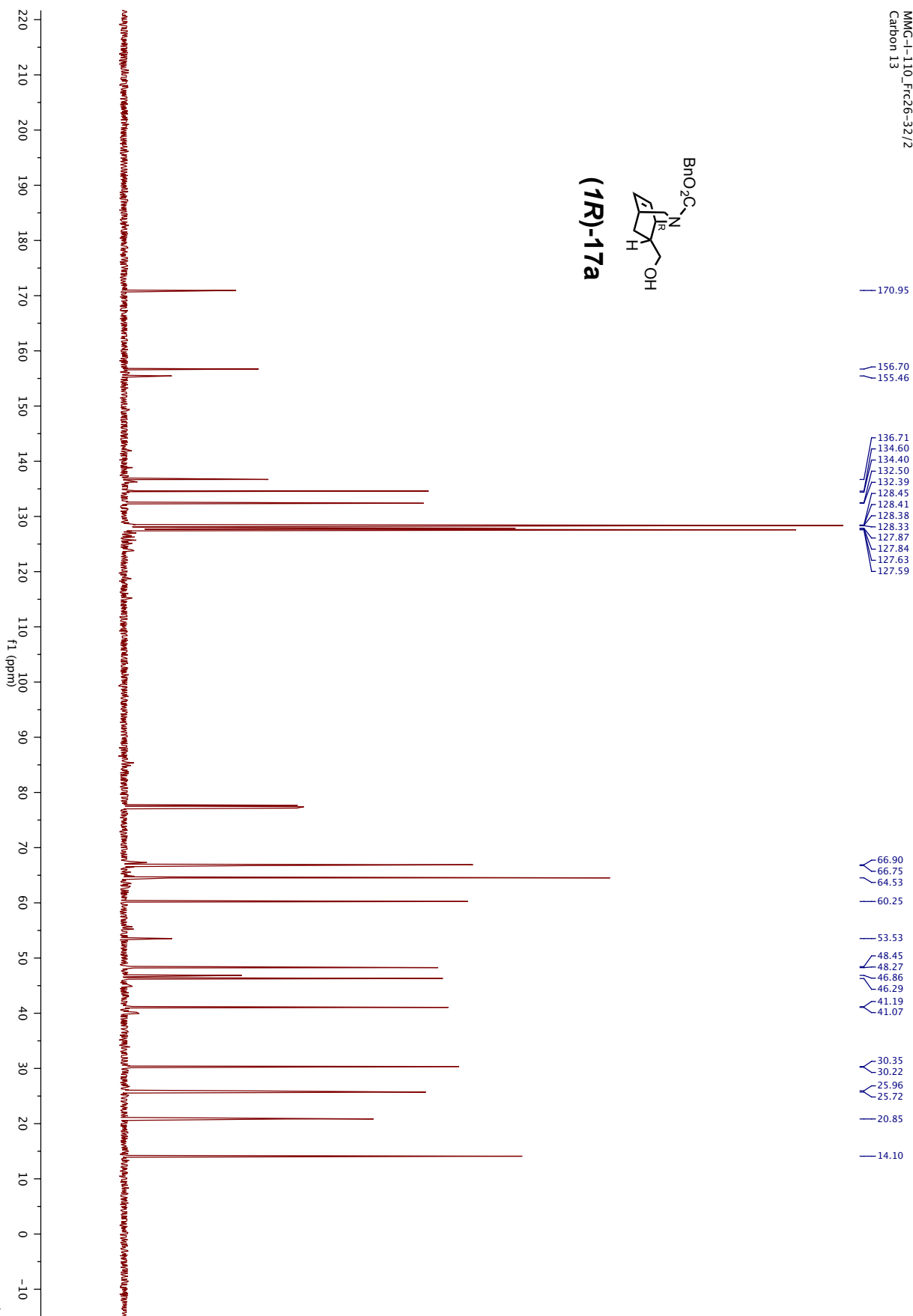
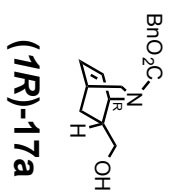
MMG-1-60_Frc40-49_MeOD
13C NMR of MMG-1-60_Frc 40-49 in MeOD 3/2/15

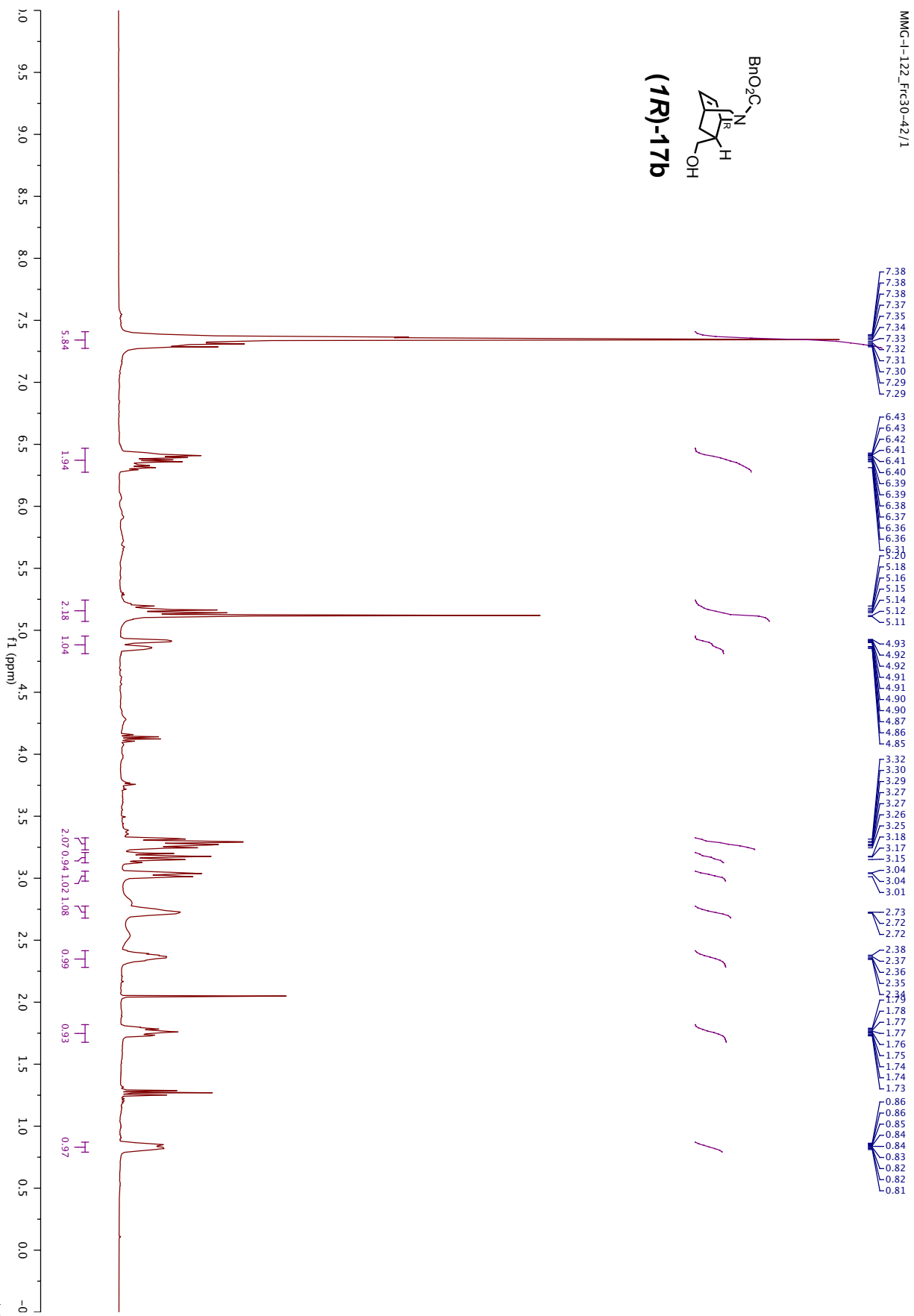
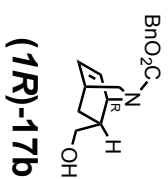




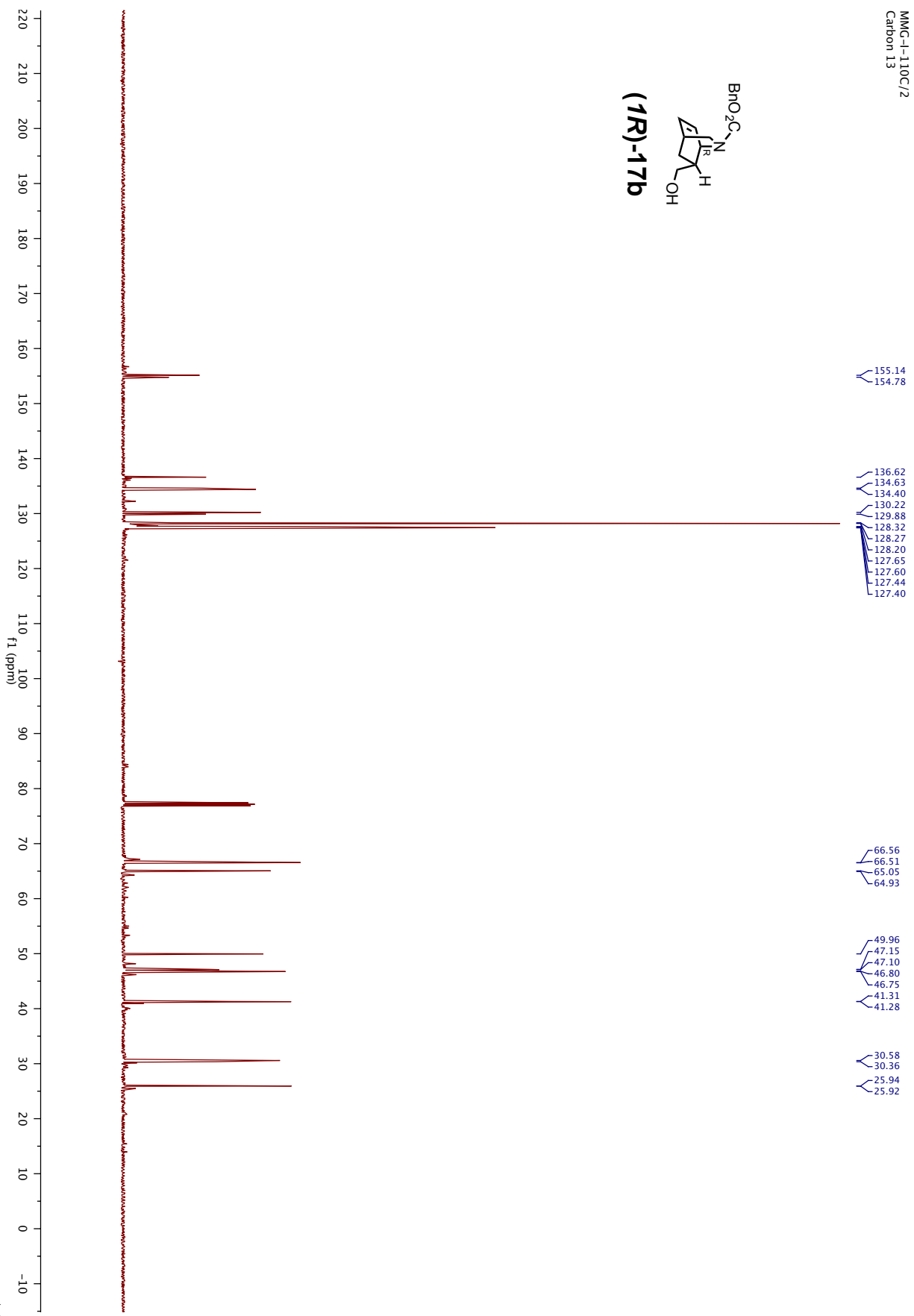
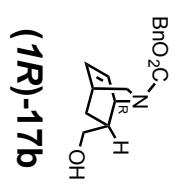
**(1R)-17a**

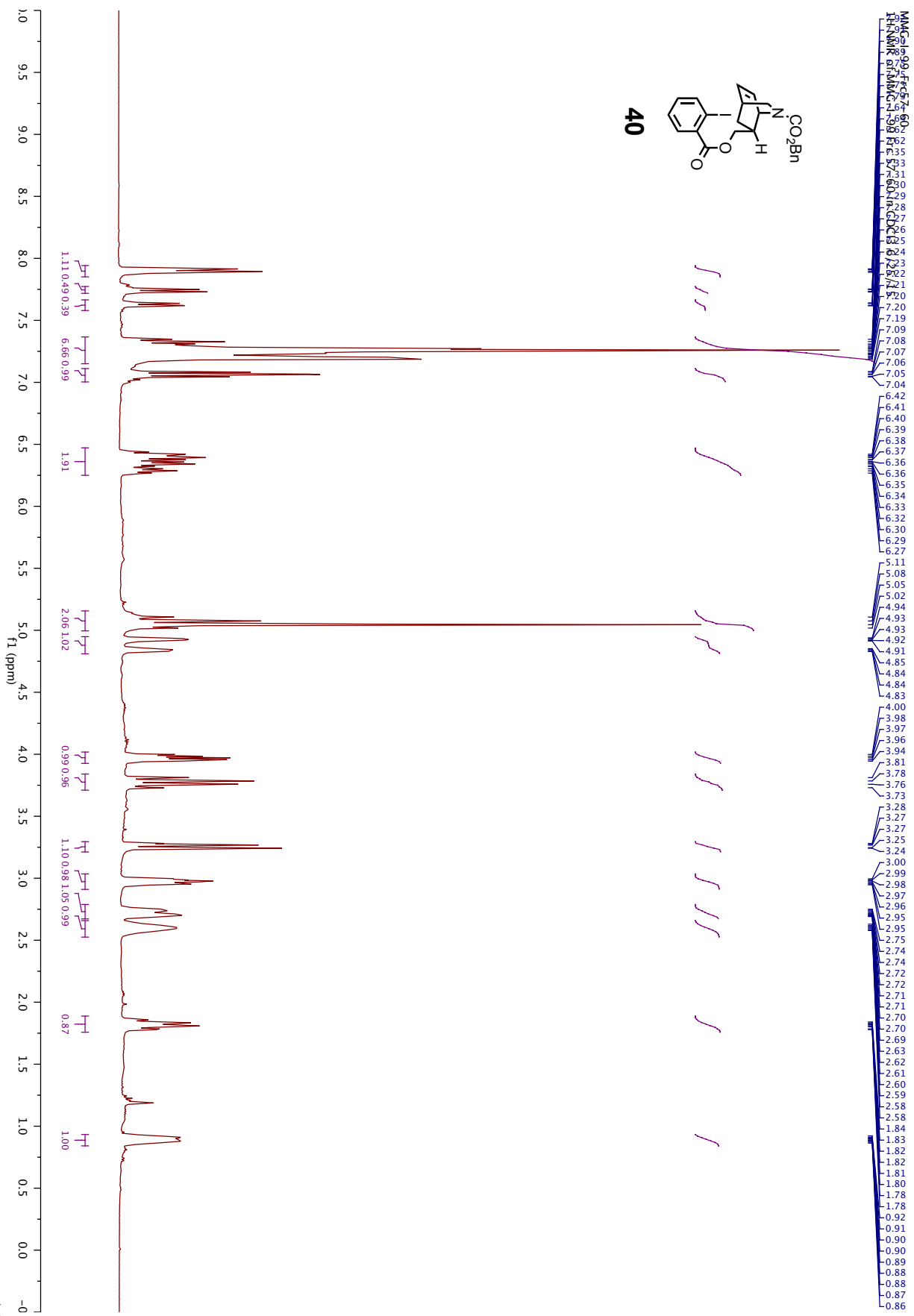
MMG-I-110_Frc26-32/2
Carbon 13



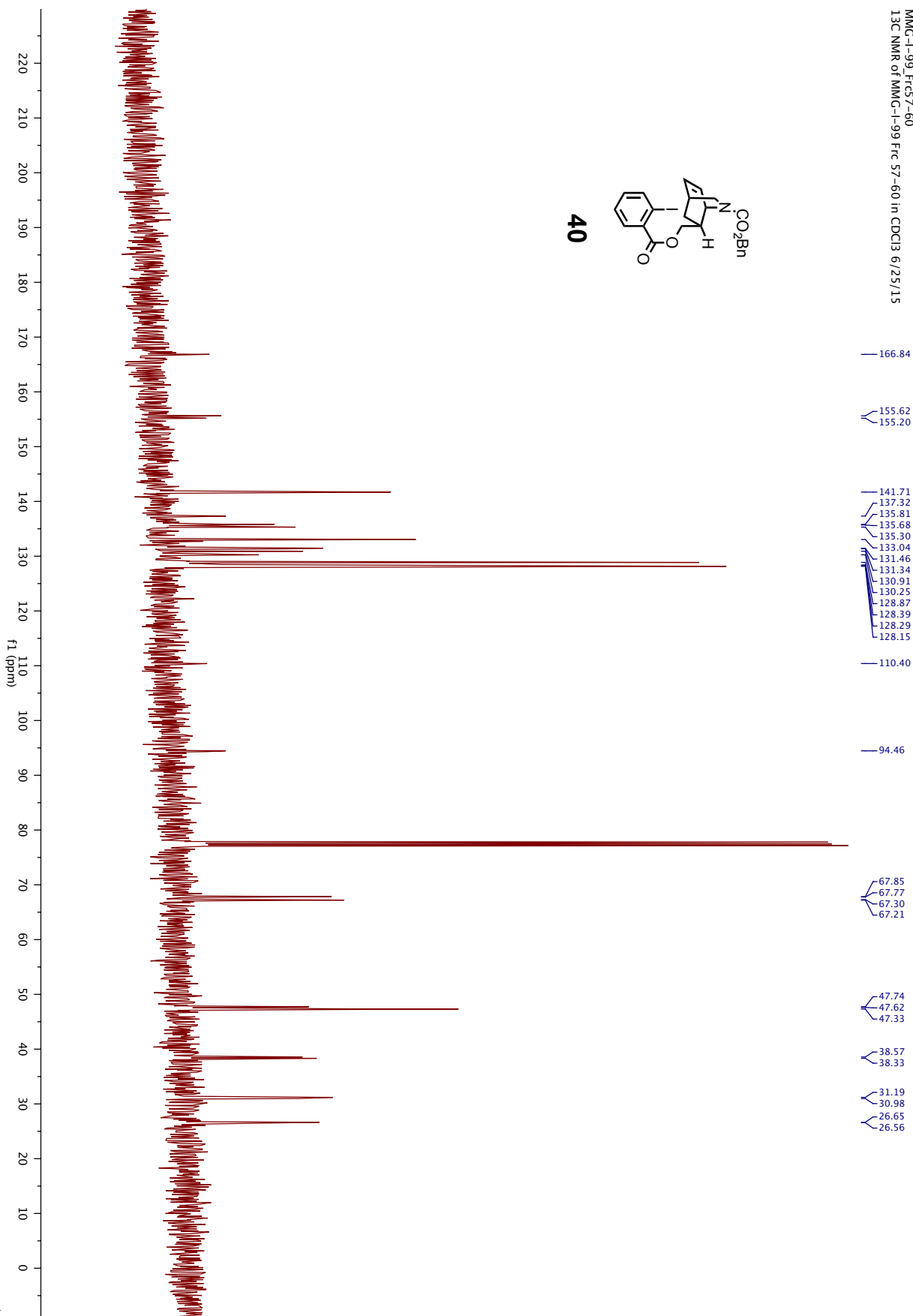
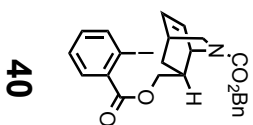


MMG-I-110C/2
Carbon 13

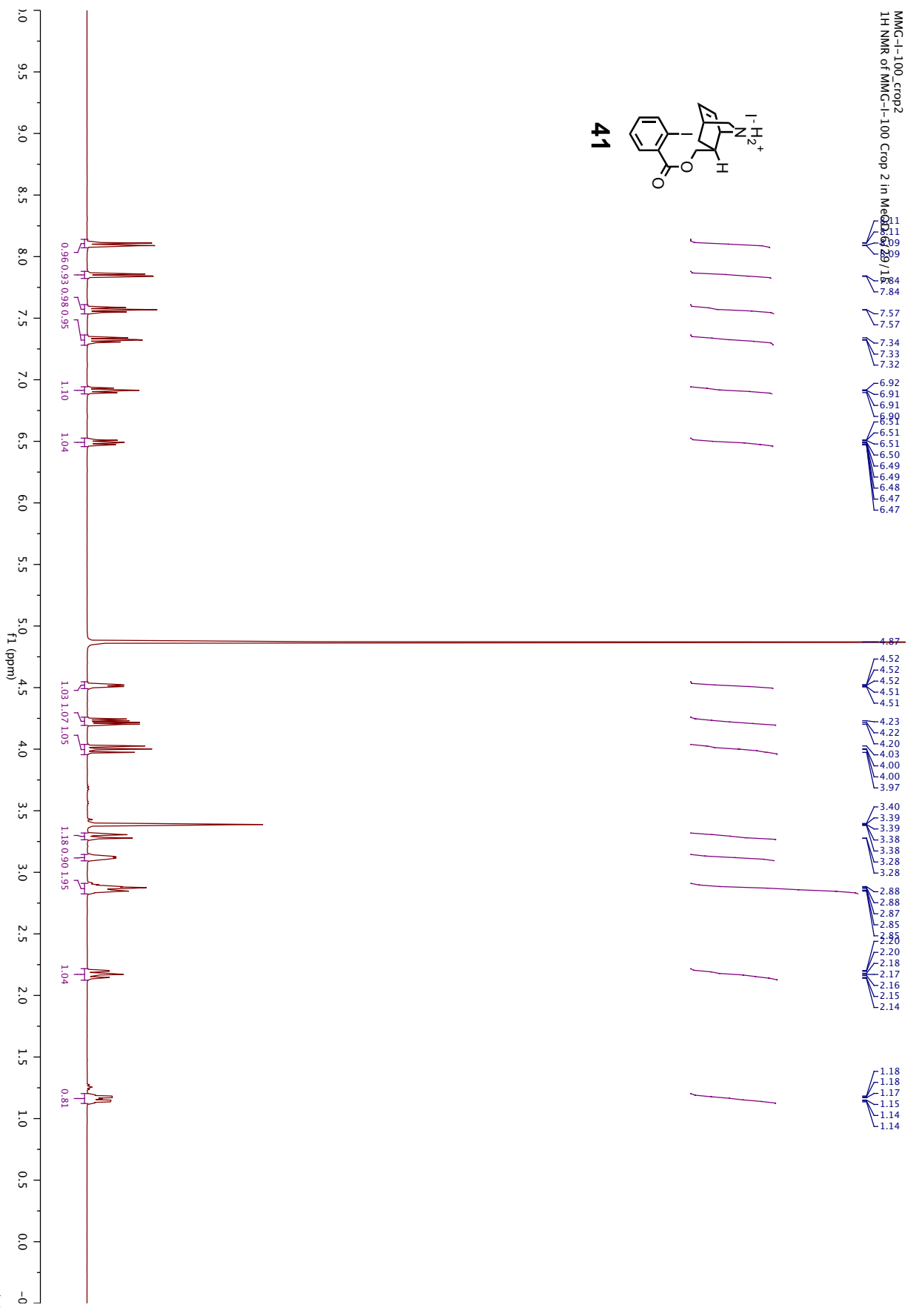
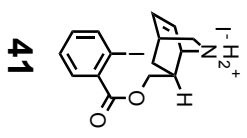




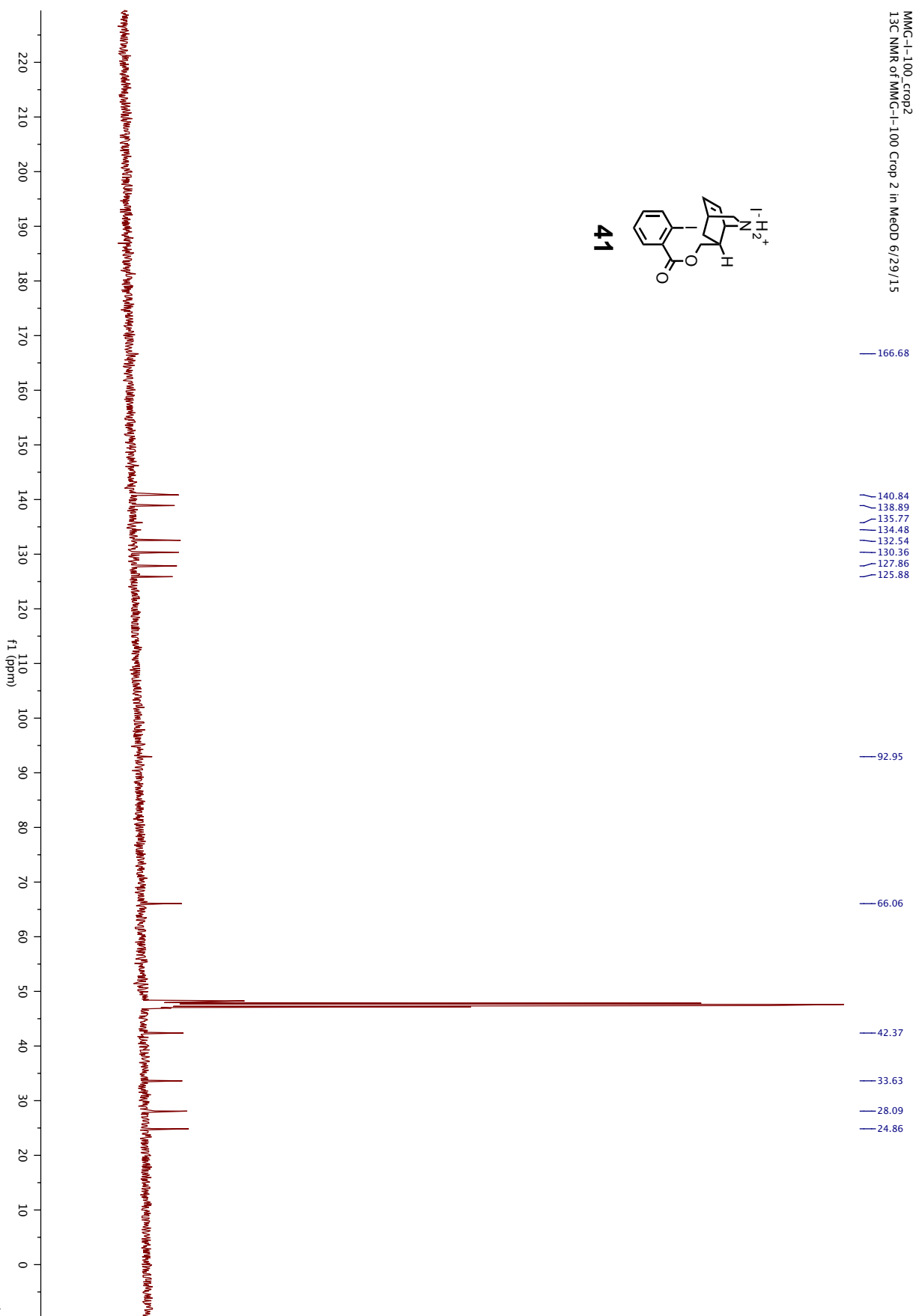
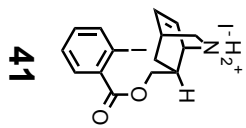
MMG-1-99_Frc57-60
13C NMR of MMG-1-99 Frc 57-60 in CDCl3 6/25/15

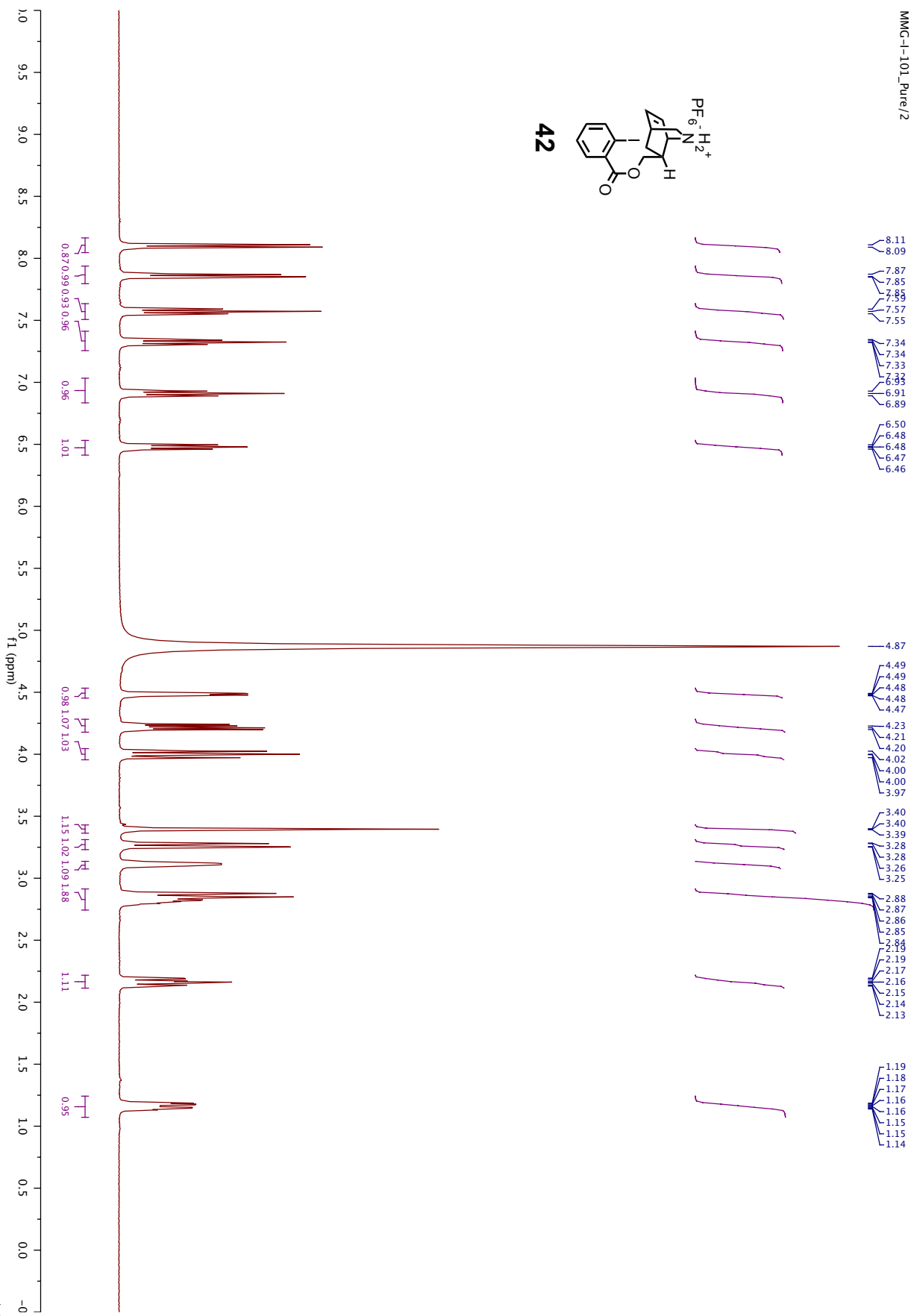
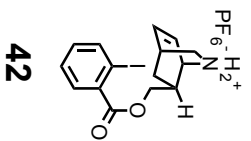


MMG-1-100_crop2
1H NMR of MMG-1-100 Crop 2 in Me2SO-d6

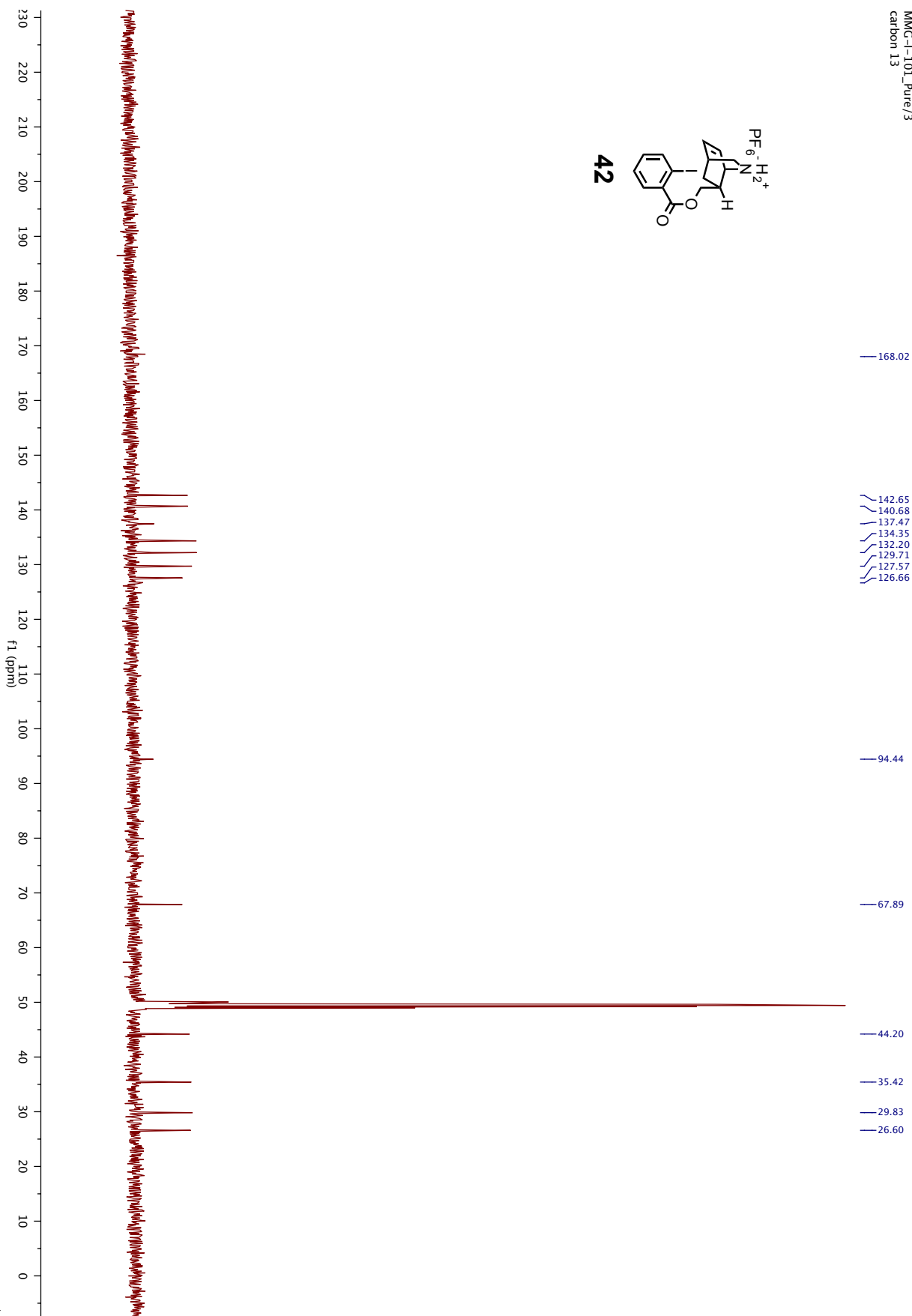
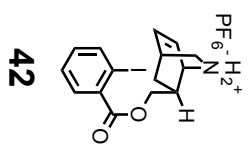


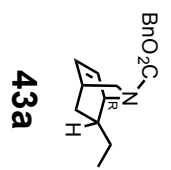
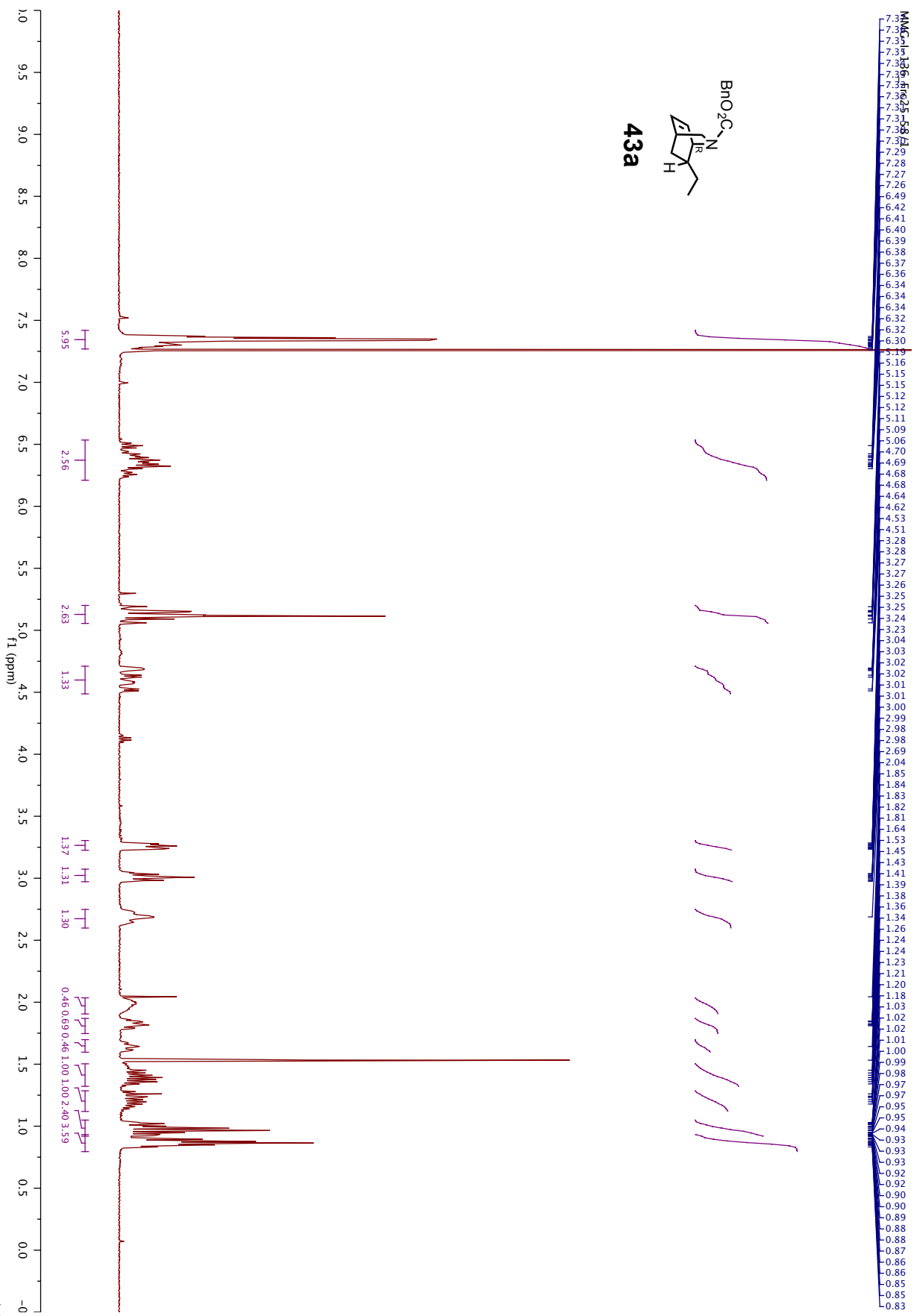
MMG-1-100_crop2
13C NMR of MMG-1-100 Crop 2 in MeOD 6/29/15



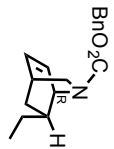


MMG-I-101_Pure/3
carbon 13

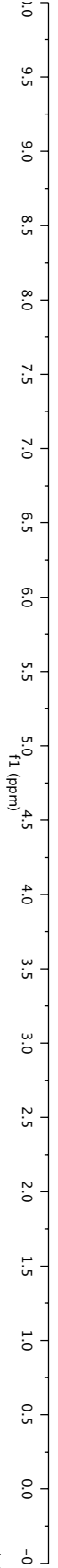




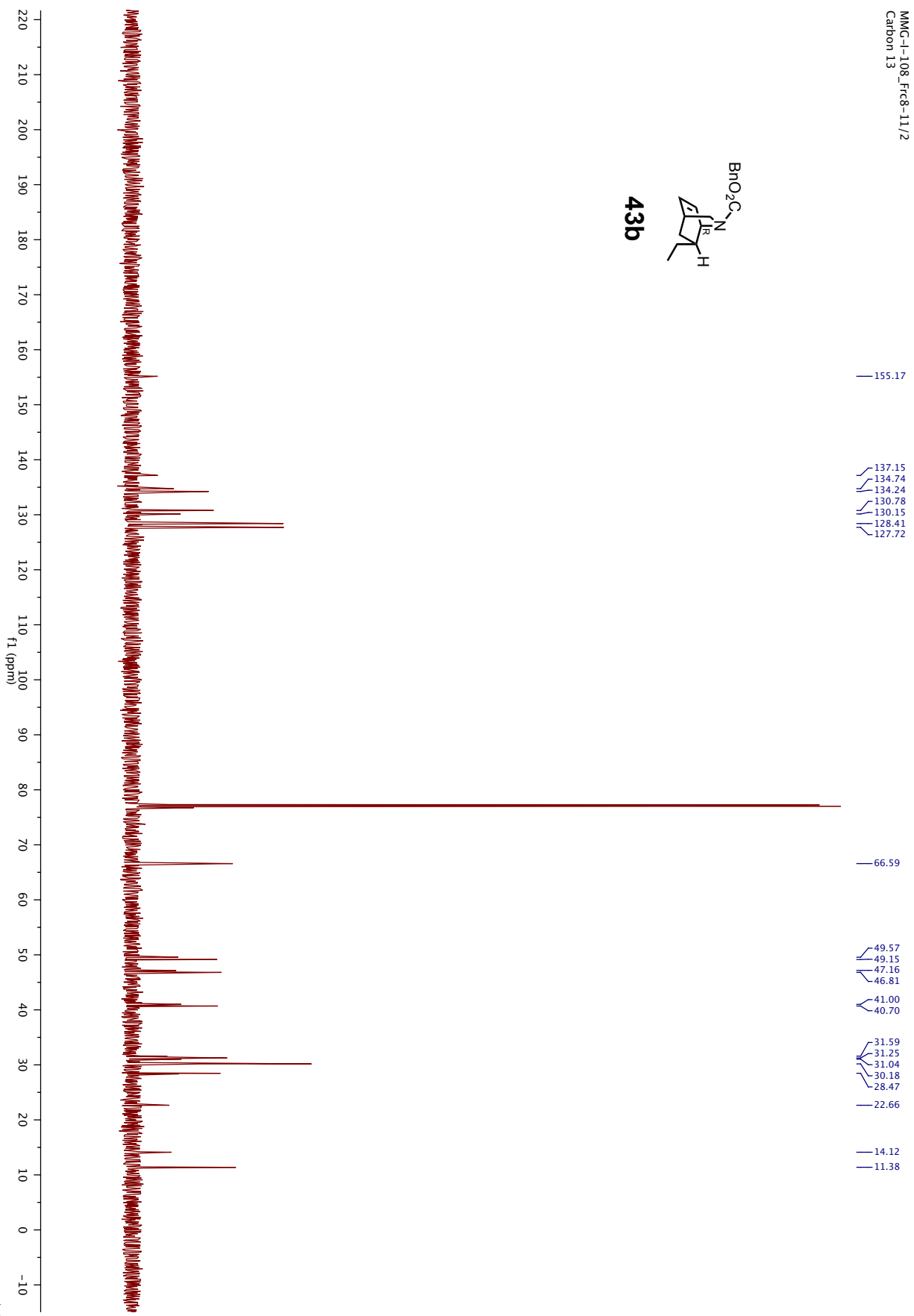
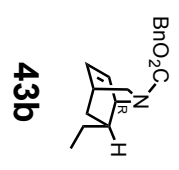
MMG-111_Fc31-35
1H NMR of MMG-111 Fc 31-35 in CDCl3 9/14/15

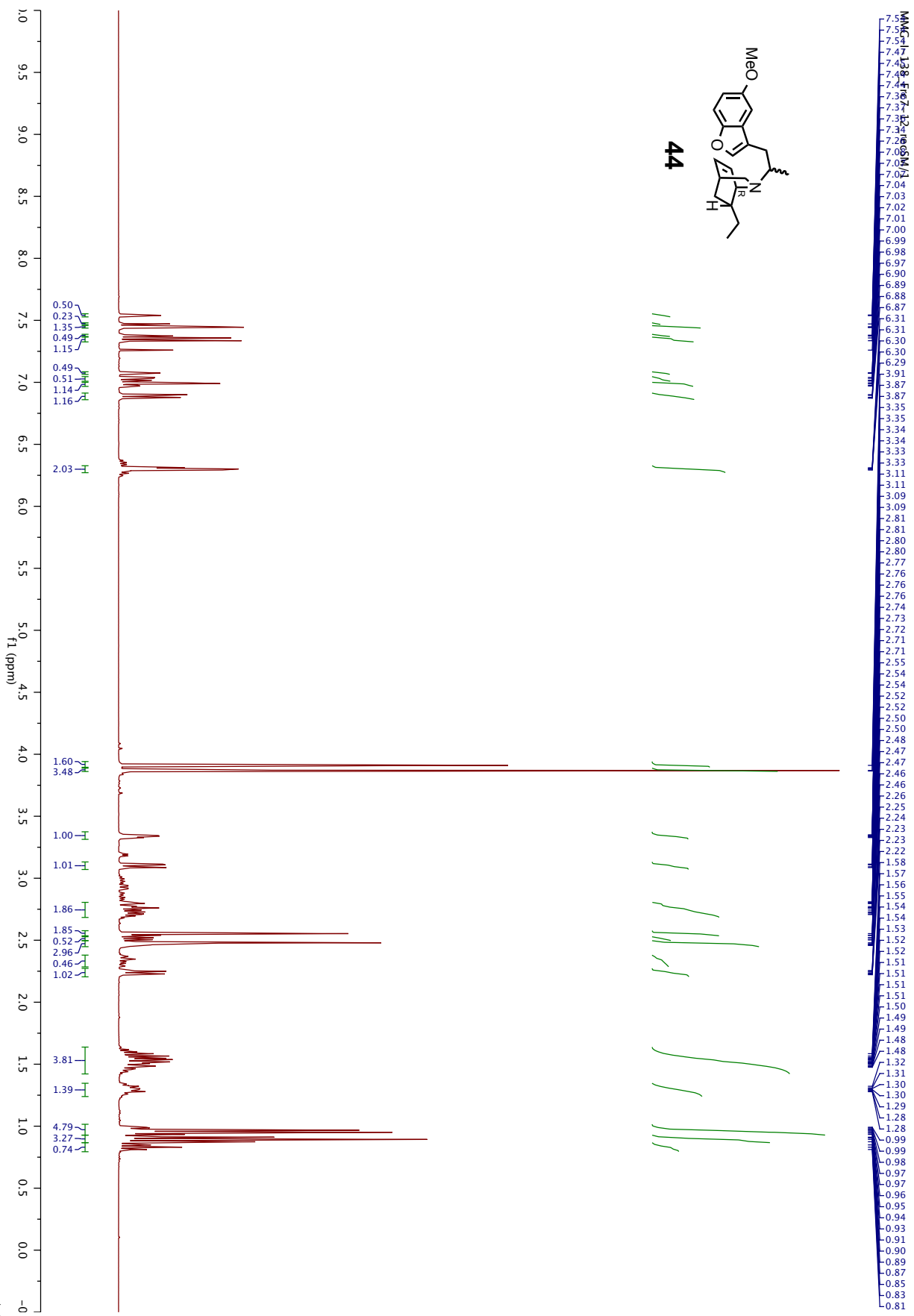


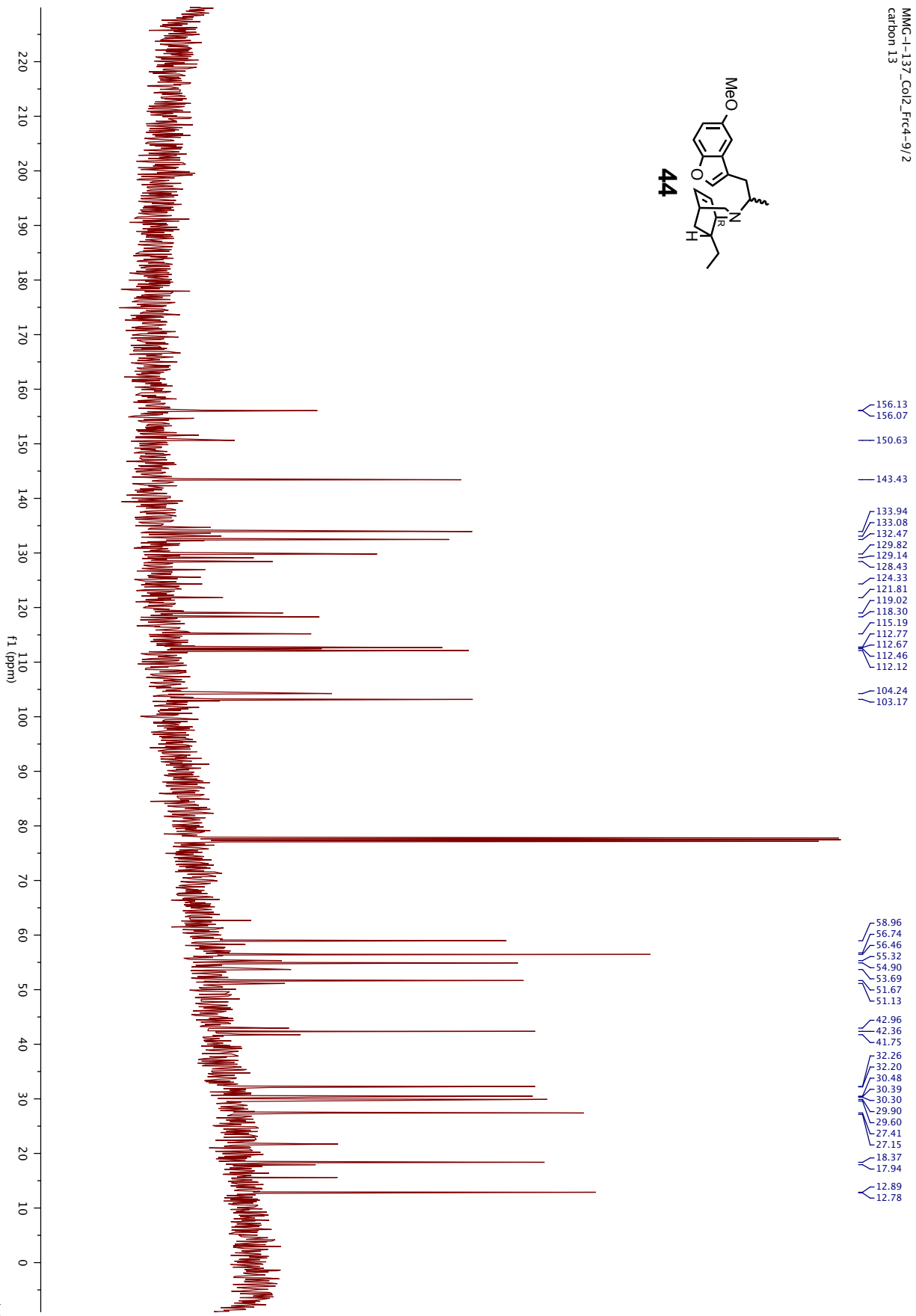
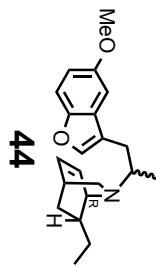
43b



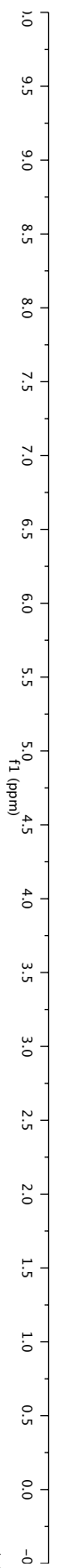
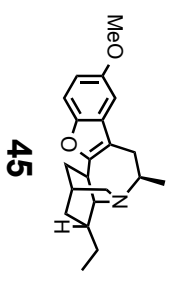
MMG-I-108_Frc8-11/2
Carbon 13

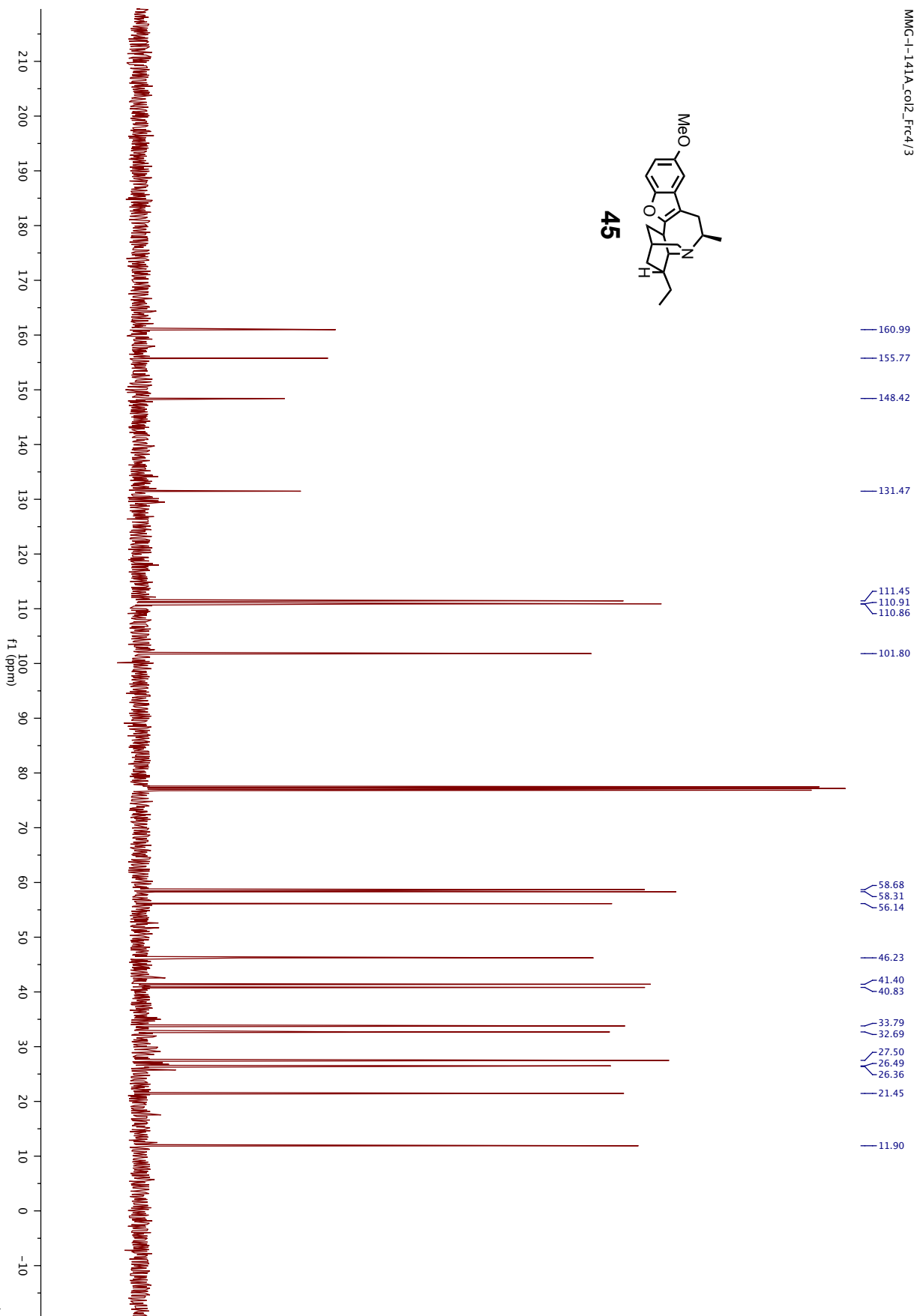
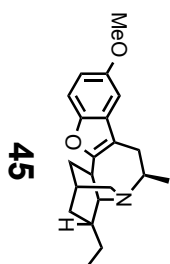


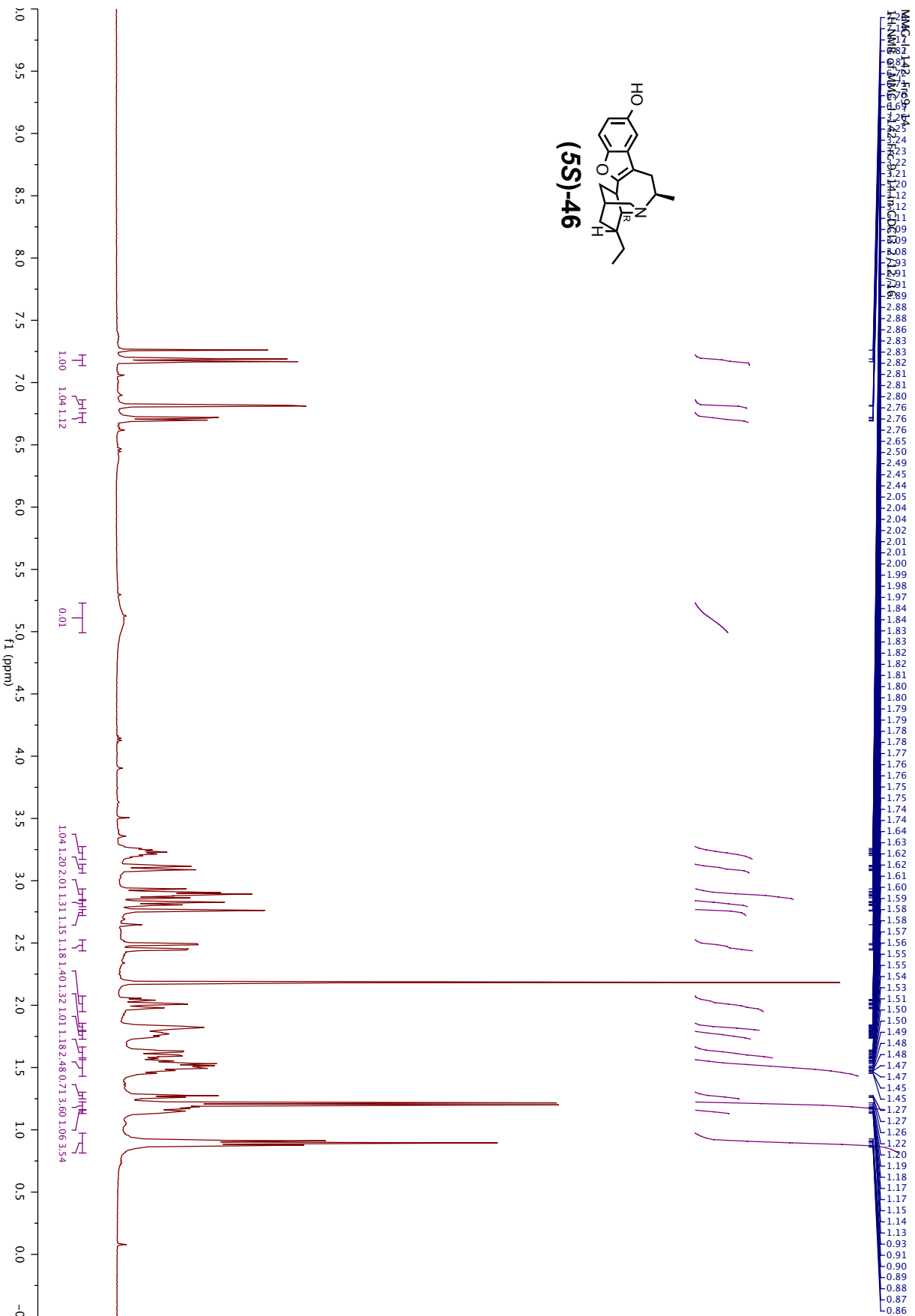
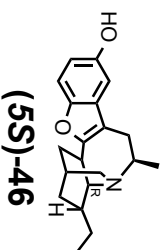


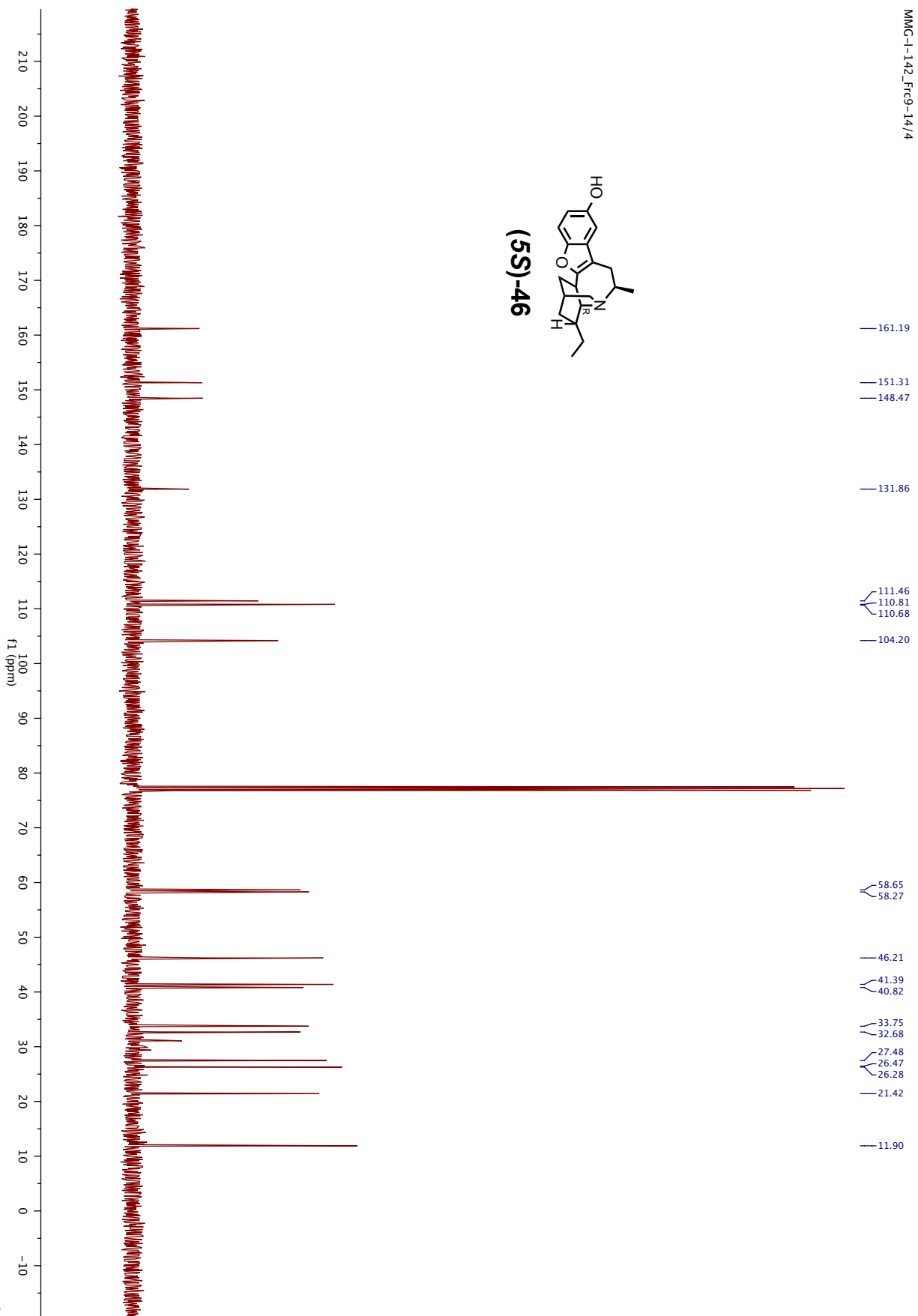
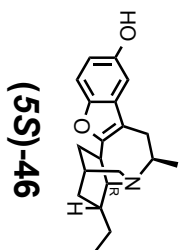


6.87
6.86
6.85
6.84
6.83
6.82
6.81
6.80
6.79
6.78
6.77
6.76
6.75
6.74
6.73
6.72
6.71
6.70
6.69
6.68
6.67
6.66
6.65
6.64
6.63
6.62
6.61
6.60
6.59
6.58
6.57
6.56
6.55
6.54
6.53
6.52
6.51
6.50
6.49
6.48
6.47
6.46
6.45
6.44
6.43
6.42
6.41
6.40
6.39
6.38
6.37
6.36
6.35
6.34
6.33
6.32
6.31
6.30
6.29
6.28
6.27
6.26
6.25
6.24
6.23
6.22
6.21
6.20
6.19
6.18
6.17
6.16
6.15
6.14
6.13
6.12
6.11
6.10
6.09
6.08
6.07
6.06
6.05
6.04
6.03
6.02
6.01
6.00
5.99
5.98
5.97
5.96
5.95
5.94
5.93
5.92
5.91
5.90
5.89
5.88
5.87
5.86
5.85
5.84
5.83
5.82
5.81
5.80
5.79
5.78
5.77
5.76
5.75
5.74
5.73
5.72
5.71
5.70
5.69
5.68
5.67
5.66
5.65
5.64
5.63
5.62
5.61
5.60
5.59
5.58
5.57
5.56
5.55
5.54
5.53
5.52
5.51
5.50
5.49
5.48
5.47
5.46
5.45
5.44
5.43
5.42
5.41
5.40
5.39
5.38
5.37
5.36
5.35
5.34
5.33
5.32
5.31
5.30
5.29
5.28
5.27
5.26
5.25
5.24
5.23
5.22
5.21
5.20
5.19
5.18
5.17
5.16
5.15
5.14
5.13
5.12
5.11
5.10
5.09
5.08
5.07
5.06
5.05
5.04
5.03
5.02
5.01
5.00
4.99
4.98
4.97
4.96
4.95
4.94
4.93
4.92
4.91
4.90
4.89
4.88
4.87
4.86
4.85
4.84
4.83
4.82
4.81
4.80
4.79
4.78
4.77
4.76
4.75
4.74
4.73
4.72
4.71
4.70
4.69
4.68
4.67
4.66
4.65
4.64
4.63
4.62
4.61
4.60
4.59
4.58
4.57
4.56
4.55
4.54
4.53
4.52
4.51
4.50
4.49
4.48
4.47
4.46
4.45
4.44
4.43
4.42
4.41
4.40
4.39
4.38
4.37
4.36
4.35
4.34
4.33
4.32
4.31
4.30
4.29
4.28
4.27
4.26
4.25
4.24
4.23
4.22
4.21
4.20
4.19
4.18
4.17
4.16
4.15
4.14
4.13
4.12
4.11
4.10
4.09
4.08
4.07
4.06
4.05
4.04
4.03
4.02
4.01
4.00
3.99
3.98
3.97
3.96
3.95
3.94
3.93
3.92
3.91
3.90
3.89
3.88
3.87
3.86
3.85
3.84
3.83
3.82
3.81
3.80
3.79
3.78
3.77
3.76
3.75
3.74
3.73
3.72
3.71
3.70
3.69
3.68
3.67
3.66
3.65
3.64
3.63
3.62
3.61
3.60
3.59
3.58
3.57
3.56
3.55
3.54
3.53
3.52
3.51
3.50
3.49
3.48
3.47
3.46
3.45
3.44
3.43
3.42
3.41
3.40
3.39
3.38
3.37
3.36
3.35
3.34
3.33
3.32
3.31
3.30
3.29
3.28
3.27
3.26
3.25
3.24
3.23
3.22
3.21
3.20
3.19
3.18
3.17
3.16
3.15
3.14
3.13
3.12
3.11
3.10
3.09
3.08
3.07
3.06
3.05
3.04
3.03
3.02
3.01
3.00
2.99
2.98
2.97
2.96
2.95
2.94
2.93
2.92
2.91
2.90
2.89
2.88
2.87
2.86
2.85
2.84
2.83
2.82
2.81
2.80
2.79
2.78
2.77
2.76
2.75
2.74
2.73
2.72
2.71
2.70
2.69
2.68
2.67
2.66
2.65
2.64
2.63
2.62
2.61
2.60
2.59
2.58
2.57
2.56
2.55
2.54
2.53
2.52
2.51
2.50
2.49
2.48
2.47
2.46
2.45
2.44
2.43
2.42
2.41
2.40
2.39
2.38
2.37
2.36
2.35
2.34
2.33
2.32
2.31
2.30
2.29
2.28
2.27
2.26
2.25
2.24
2.23
2.22
2.21
2.20
2.19
2.18
2.17
2.16
2.15
2.14
2.13
2.12
2.11
2.10
2.09
2.08
2.07
2.06
2.05
2.04
2.03
2.02
2.01
2.00
1.99
1.98
1.97
1.96
1.95
1.94
1.93
1.92
1.91
1.90
1.89
1.88
1.87
1.86
1.85
1.84
1.83
1.82
1.81
1.80
1.79
1.78
1.77
1.76
1.75
1.74
1.73
1.72
1.71
1.70
1.69
1.68
1.67
1.66
1.65
1.64
1.63
1.62
1.61
1.60
1.59
1.58
1.57
1.56
1.55
1.54
1.53
1.52
1.51
1.50
1.49
1.48
1.47
1.46
1.45
1.44
1.43
1.42
1.41
1.40
1.39
1.38
1.37
1.36
1.35
1.34
1.33
1.32
1.31
1.30
1.29
1.28
1.27
1.26
1.25
1.24
1.23
1.22
1.21
1.20
1.19
1.18
1.17
1.16
1.15
1.14
1.13
1.12
1.11
1.10
1.09
1.08
1.07
1.06
1.05
1.04
1.03
1.02
1.01
1.00
0.99
0.98
0.97
0.96
0.95
0.94
0.93
0.92
0.91
0.90
0.89
0.88
0.87
0.86
0.85
0.84
0.83
0.82
0.81
0.80
0.79
0.78
0.77
0.76
0.75
0.74
0.73
0.72
0.71
0.70
0.69
0.68
0.67
0.66
0.65
0.64
0.63
0.62
0.61
0.60
0.59
0.58
0.57
0.56
0.55
0.54
0.53
0.52
0.51
0.50
0.49
0.48
0.47
0.46
0.45
0.44
0.43
0.42
0.41
0.40
0.39
0.38
0.37
0.36
0.35
0.34
0.33
0.32
0.31
0.30
0.29
0.28
0.27
0.26
0.25
0.24
0.23
0.22
0.21
0.20
0.19
0.18
0.17
0.16
0.15
0.14
0.13
0.12
0.11
0.10
0.09
0.08
0.07
0.06
0.05
0.04
0.03
0.02
0.01
0.00
-0.01
-0.02
-0.03
-0.04
-0.05
-0.06
-0.07
-0.08
-0.09
-0.10









Chapter 5 – A Tale of a Tail: Understanding the Tools Available to Measure Ligand Bias

Introduction

The PRESTO-Tango™ assay (Tango assay) is a useful tool developed by Bryan Roth and marketed by Invitrogen.¹ In this reporter gene assay, the GPCR is C-terminally tagged with a portion of the vasopressin 2 receptor tail (V₂ tail), followed by a TEV (tobacco etch virus)

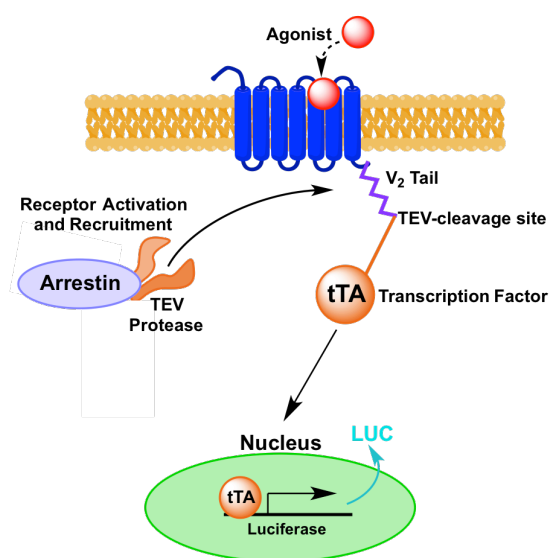


Figure 1. Mechanism of the Tango Assay. A TEV protease tagged-arrestin molecule cleaves and releases the tTA transcription factor upon recruitment to the receptor. The tTA then turns on expression of the luciferase reporter gene.

protease cleavage site and then a transcription factor, tTA (tetracycline controlled transcription activator). Also expressed in the cells is arrestin-3 tagged with the TEV protease. Upon receptor activation and arrestin recruitment, the protease is in close enough proximity to the protease cleavage site to release the transcription factor into the cytosol, which can then enter the nucleus and turn on reporter gene expression (**Figure 1**).

While this assay is highly effective at measuring arrestin recruitment and many

researchers have taken advantage of the technology (close to 150 citations to date), a closer look at the receptor construct leads to puzzlement. The V₂ tail has been reported previously to enhance recruitment of arrestin to receptors, both in BRET-based contexts² and others.^{3,4} There are independent reports that in the context of the Tango assay, the V₂ tail had little effect on the signaling of certain receptors.⁵ However the authors who developed the Tango assays themselves find great variability among receptors in the presence or absence of the V₂ tail: the LTBR4

leukotriene receptor showed no differences to removing the V₂ tail, while the CMKLR1 chemerin receptor had increased signal without the V₂ tail and the FFAR2 free-fatty-acid receptor had decreased signal without the V₂ tail.¹ Such variability in the assay between different receptors, brings into question its validity as a mainstream platform for measuring arrestin recruitment, as it is difficult to know whether the V₂ tail is an innocent bystander in the Tango assay, simply providing the necessary dynamic range to make the assay more robust, or whether instead the V₂ tail is artificially affecting arrestin recruitment and thus making any bias calculations based this assay debatable.

This chapter will explore the Tango assay and others in a systematic search to understand the best way to study and identify biased ligands in the context of opioid receptors, particularly the KOR. Through analysis and deconstruction of many assays, we ultimately verify the validity of many cell-based assays for arrestin recruitment and highlight the importance of choosing an appropriate assay for each particular drug in question.

Results

Uncovering the “Bias” of Endogenous KOR Agonist Dynorphin A

Initial Findings in the Tango Assay. When first utilizing the Tango assay in experiments for measuring arrestin recruitment by the KOR, it was important to test various control ligands and compare those results to published potencies in the same cellular system and assay. For KOR, we initially chose to study dynorphin A (DYN)^{6,7}, the endogenous neuropeptide for KOR, U-50,488⁸ (U-50), a synthetic compound widely used as a KOR agonist, salvinorin A⁹ (SALV), a naturally occurring terpenoid with potent KOR agonist activity, and 6'-guanidinonaltrindole (6'-GNTI), an example of a partial G protein biased agonist.^{10,11} When tested in the Tango assay

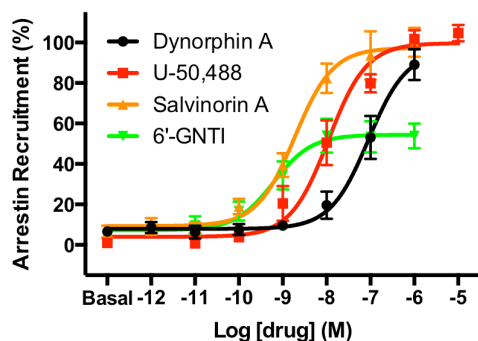


Figure 2. Arrestin-3 Recruitment as Measured in the Tango Assay. A Tango construct for hKOR was transfected into HTLA cells expressing a TEV-tagged arrestin-3. After overnight incubation with the drugs, the luciferase signal was measured through a luminescence readout. Data represent mean \pm SEM of $n \geq 6$.

first because endogenous agonists are usually balanced through G protein and arrestin pathways, and 6'-GNTI has previously been reported to have low arrestin signaling (see Introductory Chapter 1).

Researching Dynorphin Results Further. Despite the initial surprise of the apparent weak

Table 1. Summary of Experimental and Published Tango Assay Results.

Compound	Experimental EC_{50} (E_{Max})	Published ¹² EC_{50} (E_{Max})
<i>Dynorphin A</i>	247 \pm 192 nM (100%)	268 nM (74.8%)
(\pm)- <i>U-50,488</i>	15 \pm 12 nM (100%)	0.822 nM (94.6%) [§]
<i>Salvinorin A</i>	2.6 \pm 1.3 nM (100%)	5.6 nM (97.2%)
6'- <i>GNTI</i>	0.3 \pm 0.2 nM (63%)	7.38 nM (34.7%)

[§]Reported with (-)-*U-50,488* enantiomer. (+)-*U-50,488* is given an EC_{50} of 959 nM (92.3%). Data represent mean \pm SEM of various independent trials.

= 268 nM, **Table 1**)¹², the results are nearly identical – not surprising given that both measures were performed in the same cellular system (Tango Assay). Accordingly these results could indicate an example of “endogenous bias,” as suggested by White¹², but overall it would

at KOR the compounds showed varying degrees of potency and efficacy for arrestin recruitment (**Figure 2** and **Table 1**: $EC_{50}^{DYN} = 247 \pm 192$ nM, $E_{Max} = 100\%$; $EC_{50}^{U-50} = 15 \pm 12$ nM, $E_{Max} = 100\%$; $EC_{50}^{SALV} = 2.6 \pm 1.3$ nM, $E_{Max} = 100\%$; $EC_{50}^{6'-GNTI} = 0.3 \pm 0.2$ nM, $E_{Max} = 71\%$). Although our data compared nicely with those reported (**Table 1**), we were generally skeptical of the results with both dynorphin A and 6'-GNTI,

potency for arrestin recruitment of dynorphin A (compared to the other KOR control ligands), there is precedent for dynorphins to show a G protein bias.¹² In comparing the arrestin recruitment of dynorphin A we measured to those found by White and co-workers (published EC_{50}

represent a unique phenomena. Therefore, although our Tango arrestin results with dynorphin A were supported by an independent report that used the same assay format, we were skeptical about the prospect of dynorphin A, an endogenous KOR ligand, being G protein biased, especially when the experimental set-up for the Tango assay is taken into consideration (see below).

Assessing the Stability of Dynorphin A in the Tango Assay Set-up. In order to perform the Tango assay, five days of experimental set-up is required. First the cells must be transfected with the fusion construct of the receptor of choice, and 24 hours later these cells are transferred to a 96-well plate. Following an additional 24 hours, cells can be treated with drugs and allowed to incubate overnight at 37 °C. The long incubation step is critical to the success of the assay – based on a reporter gene mechanism, enough time must be allotted to not only activate the receptor but also to recruit arrestin and then turn on expression of the reporter gene (usually hours). With an extended incubation, there is ample time to allow for sufficient protein production from the reporter gene, luciferase in this case, such to provide a meaningful signal-to-background ratio upon detection. For many small molecules, stability is not an issue, and an overnight incubation would not cause concern. There are several reports on the *in vitro* stability of dynorphins^{13,14}, namely that several proteases can cleave the peptide bonds, making dynorphins especially susceptible to metabolism. Therefore as neuropeptides, they are likely unstable in an overnight incubation in cells, where various proteases and other factors are present that can cause peptide degradation.

In order to assess the stability of dynorphin A in the Tango assay, an experiment was devised that would not only determine whether dynorphin A was present in cellular supernatant after overnight incubation with cells, but also whether this supernatant contained factors that

might degrade dynorphin in solution. The experiment set-up utilized our BRET assay for G protein activation as a method independent from the Tango assay to measure whether or not drugs were still viable after overnight treatment with the Tango cells. Experimental medium was changed to Hank's Balanced Salt Solution (HBSS) since DMEM can contain luciferase inhibitors, such as phenol red and others, that might interfere with the BRET signal.

The layout of these experiments is depicted in **Figure 3**. Three sets of drugs were tested

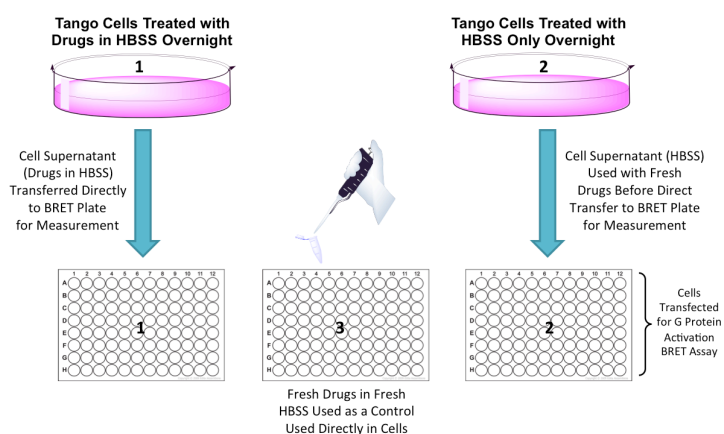


Figure 3. Schematic Diagram of Experimental Set-up to Measure Dynorphin A's Stability in Cells After Overnight Incubation.

in the G protein activation BRET assay: 1) drugs that were incubated overnight in HBSS in Tango cells; 2) drugs that were freshly prepared in HBSS that was incubated overnight in Tango cells; and 3) drugs that were freshly prepared in fresh HBSS (control). These three

HBSS treatments were then added directly to cells transfected to measure G protein activation using BRET (**Figure 3**). By utilizing the three drug treatments, we could determine whether drugs degraded overnight in Tango cells or whether factors released into the media by cells overnight could degrade fresh stocks of drugs, all of which were compared to control treatments.

As anticipated, when drugs incubated overnight on Tango cells were used in a separate BRET assay, all drugs activated the receptor normally except for dynorphin A (**Figure 4**). Dynorphin A under these conditions only showed one-point activity in the dose response curve with partial efficacy. Given this result, it is unlikely that an appreciable amount of dynorphin A

exists in solution after overnight treatment. Interestingly, when new stock solutions were prepared with conditioned HBSS (i.e. HBSS that was incubated overnight with the Tango cells)

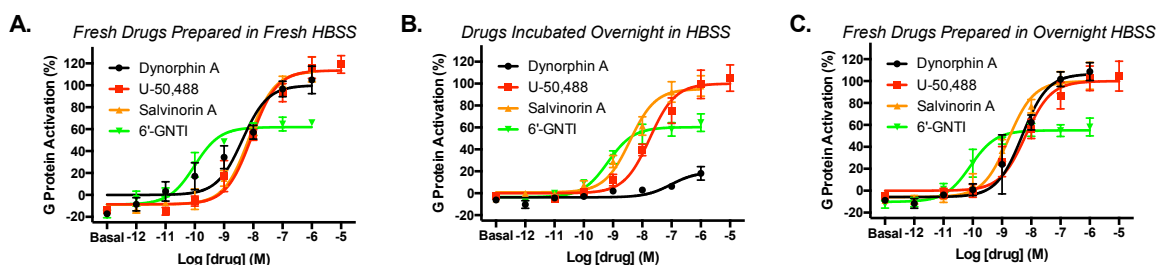


Figure 4. Dynorphin A Stability After Overnight Incubation Differs from Other Drugs. hKOR was co-expressed with $G\alpha_B$ -RLuc8, $\beta 1$, and mVenus- $\gamma 2$ to assay G protein activation. Curves represent the average of $n = 3$, with error bars representing \pm SEM. A. Control experiment showing functional activity of compounds using freshly prepared dose response curves in HBSS. B. When drugs are treated first overnight on Tango cells, most of the activity from dynorphin A is gone, suggesting it has degraded. The other drugs are stable after overnight treatment. C. When drugs are prepared fresh in HBSS that was incubated with Tango cells overnight, all functional responses are normal.

for use in the BRET assay, dynorphin A showed potency and efficacy in the normal ranges for G protein activation, suggesting that factors released into the media by cells overnight either do not interfere with the functional activity of dynorphin A or require a longer incubation time for effect (Figure 4C).

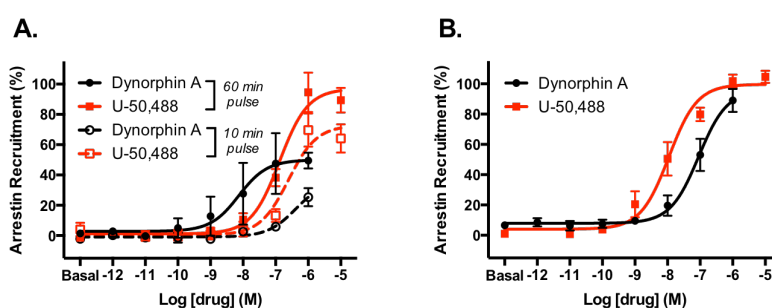


Figure 5. Pulse Experiment in the Tango Assay shows Arrestin Recruitment Can be Measured But With Much Weaker Potency. A Tango construct for hKOR was transfected into HTLA cells expressing a TEV-tagged arrestin-3. A. Pulse experiment with U-50,488 and Dynorphin A at two different pulse time points. B. Comparison to overnight treatment (reproduced from Figure 2). Data represent mean \pm SEM of $n = 4$.

To explore the timing with which receptor activation is required to observe sufficient signal in the Tango assay, a pulse experiment was designed. The idea

behind this experiment was to determine whether a short “pulse” of receptor activation from the

compound would be sufficient to start the reporter gene activation and subsequent protein production overnight, in the absence of drug, thus allowing use of dynorphin A in the Tango assay. When either dynorphin A or U-50,488 were added on the Tango cells for 10 minutes or 1 hour prior to drug removal and overnight incubation in fresh media, some arrestin recruitment was observed (**Figure 5**). The 10-minute pulse with drugs was only enough time to see the early signs of arrestin recruitment, as the efficacy and potency for these treatments, while visible, was quite weak in comparison to overnight treatments ($EC_{50 \text{ DYN}} \sim 402 \pm 268 \text{ nM}$, $E_{\text{Max}} = 36\%$; $EC_{50 \text{ U-50}} = 273 \pm 95 \text{ nM}$, $E_{\text{Max}} = 73\%$). In contrast, the 60-minute pulse showed much more promise, activating the receptor recruitment mechanism with increased potency and efficacy when compared to the 10-minute pulsed treatment ($EC_{50 \text{ DYN}} = 10 \pm 8 \text{ nM}$, $E_{\text{Max}} = 50\%$; $EC_{50 \text{ U-50}} = 184 \pm 75 \text{ nM}$, $E_{\text{Max}} = 100\%$). While dynorphin A led to arrestin recruitment in 60-minutes, the efficacy was much lower in comparison to that seen in overnight treatments while the potency was similar (more potent, in fact). The higher potency of dynorphin A in the 60-minute pulse indicates that the time domain of the receptor activation is very important as reported in this assay. At 60 minutes, U-50,488 was significantly less potent than the overnight incubation though with full efficacy, indicating that a longer pulse time may be necessary to illicit maximal potency for arrestin recruitment when compared to the usual overnight treatment (see **Table 1** for comparison). Unfortunately, a longer pulse time still might not solve the issue of dynorphin A stability in the cells. In all likelihood, the longer dynorphin A is incubated in the

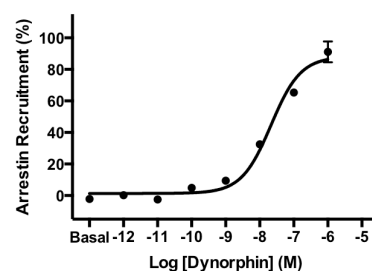


Figure 6. Dynorphin A Recruits Arrestin in an Independent Assay for Arrestin Recruitment (BRET GAP43 Translocation Assay). A Tango construct for hKOR was co-expressed with Rluc8-arrestin3-Sp1, mem-linker-citrine-SH3, and GRK3. Dynorphin A showed an $EC_{50} = 16 \pm 5 \text{ nM}$ ($E_{\text{Max}} = 100\%$). Data represent mean \pm SEM of $n = 7$.

cells, even without the need of overnight treatment times, the more chance of it degrading and thus clouding the true nature of the arrestin recruitment.

Finally, to truly understand whether dynorphin A is capable of recruiting arrestin after receptor activation, dynorphin was tested in an alternate assay for arrestin recruitment, the BRET GAP43 translocation assay (see Introductory Chapter 1). The same DNA construct for KOR was used in this assay as in the Tango assay to account for any sequence variation. Interestingly, we found that dynorphin A was able to recruit arrestin with full efficacy (compared to both U-50 and salvinorin A, see **Figure 10** below) in this independent assay, and highlights that perhaps

dynorphin A is not G protein biased after all (**Figure 6**). More importantly, these results prove that since dynorphin A can recruit arrestin in a separate assay, the Tango assay should be revisited as a tool for measuring the functional activity of peptides and other sensitive compounds.

Dissecting the Role of the V₂ Tail in Arrestin Recruitment

Removing the V₂ Tail From the Tango

Construct. When analyzing the initial Tango results (see **Figure 2**), we were also concerned by the fact that 6'-GNTI was both potent and

efficacious in arrestin recruitment – something that has not yet been observed in the context of this compound, a reported G protein biased ligand.^{10,11,15} We suspected that perhaps again the V₂

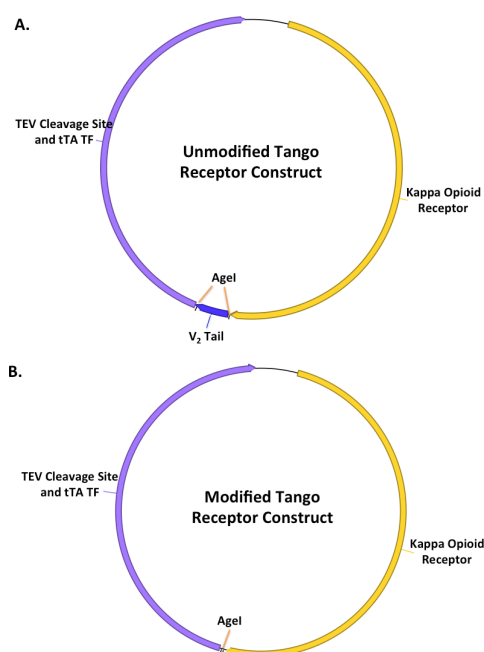


Figure 7. Schematic DNA Map Shows Easy Manipulation of Tango Construct. Digestion of (A) with AgeI restriction enzyme allows removal of the V₂ Tail to get the construct shown in B.

tail was increasing sensitivity to arrestin recruitment measurements, which could make 6'-GNTI seem unbiased and simultaneously make dynorphin A seem more biased. While it is also possible that the unique *in vitro* results reported for 6'-GNTI are an outcome of unidentified, independent signaling pathways and not from being G protein biased, we still wanted to understand better the role of the V₂ tail in arrestin signaling. The cDNA construct for the receptors used in the Tango assay are cleverly constructed to allow easy manipulation of the individual components. As such, the V₂ tail is flanked

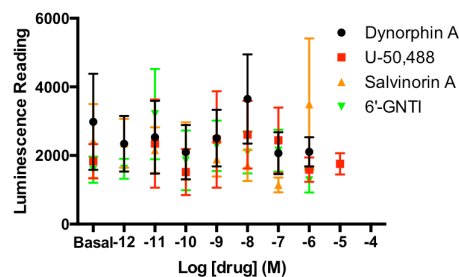


Figure 8. Removal of the V₂ Tail from the hKOR Tango Construct Makes It Ineffective at Arrestin Recruitment. The modified Tango construct for hKOR was transfected into HTLA cells expressing a TEV-tagged arrestin-3. Data represent mean \pm SEM of n = 4.

by AgeI restriction sites in the sequence, thus making its removal a straightforward experiment (**Figure 7**). When the modified receptor construct was used in the Tango assay, we found that no measureable signal could be detected, even when following identical experimental conditions (**Figure 8**). Given the known effects of the V₂ tail on enhancing arrestin recruitment and signal-to-background ratios (see **Introduction**), we were not surprised to find that the entire assay

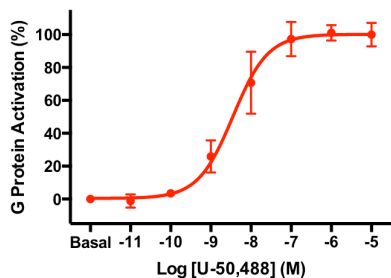


Figure 9. Modified Tango Construct is a Functional Receptor. The modified Tango hKOR was co-expressed with G α_B -RLuc8, β 1, and mVenus- γ 2 to assay G protein activation. Curves represent the average of n = 2, with error bars representing \pm SEM.

required this integral receptor modification. As the researchers who developed the Tango assay have acknowledged¹, the V₂ tail does not affect all receptors in the same way, so it is possible that the opioid receptors are more susceptible to the effects the V₂ tail has on arrestin recruitment.

As a control, we tested this modified Tango construct for its ability to function in the G protein

activation BRET assay. Although the sequence was confirmed, it was important to make sure that the receptor could still properly signal as that could be an alternative explanation for the construct's inability to work in the Tango assay. Even without the V₂ tail, the modified Tango construct was able to function normally in the G protein activation assay, verifying the influence of the V₂ tail on the Tango assay (**Figure 9**). Given the dramatic changes observed in arrestin recruitment between the two constructs in the Tango assay, we were even more interested in understanding the role of the V₂ tail in these assays and sought to explore it further in the context of other assays.

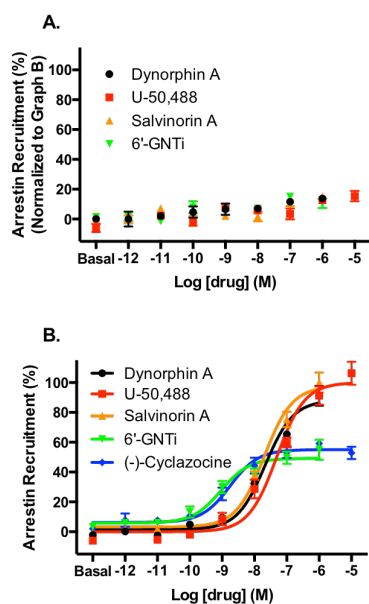


Figure 10. V₂ Tail Enhances Dynamic Range of Independent BRET GAP43 Translocation Assay for Arrestin Recruitment. Unmodified hKOR (A) or Tango construct for hKOR (B) were co-expressed with Rluc8-arrestin3-Sp1, mem-linker-citrine-SH3, and GRK3. For the assay design, see **Figure 18** in Chapter 1. Data represent mean \pm SEM of $n \geq 4$.

Utilizing the Tango Construct in Another Arrestin

Assay. To further explore the role of the V₂ tail in arrestin recruitment, the construct needed to be used in an alternate assay. In our BRET GAP43 translocation assay (see **Figure 18** in Chapter 1), the normal unmodified KOR construct is unable to show any appreciable amount of arrestin recruitment (**Figure 10A**). While various transfection and reaction conditions were attempted to make the assay work with the unmodified construct, ultimately the signals were too weak to be meaningful. In contrast, when the Tango construct (with V₂ tail) was used in the same assay (as in **Figure 6** above), an excellent dynamic and potency range was obtained for the drugs tested. These results again highlight the ability of the V₂ tail to enhance arrestin

recruitment, especially in an assay that did not work with a different construct of the same

receptor. Interestingly, even in an alternate assay, the G protein biased agonist 6'-GNTI showed measurable recruitment of arrestin, indicating that either the V₂ tail is artificially enhancing the arrestin recruitment (thus making a G protein biased ligand seem unbiased) or that 6'-GNTI has a lower degree of G protein bias than published previously. We also added an additional ligand, (-)-cyclazocine¹⁶, a partial agonist at KOR, as a control for efficacy effects on arrestin recruitment, and it also recruited arrestin similarly to 6'-GNTI. In order to further assess the role of the V₂ tail in arrestin signaling, there was a need to expand these studies further into even

more arrestin assays.

Bringing the V₂ Tail into a Different KOR

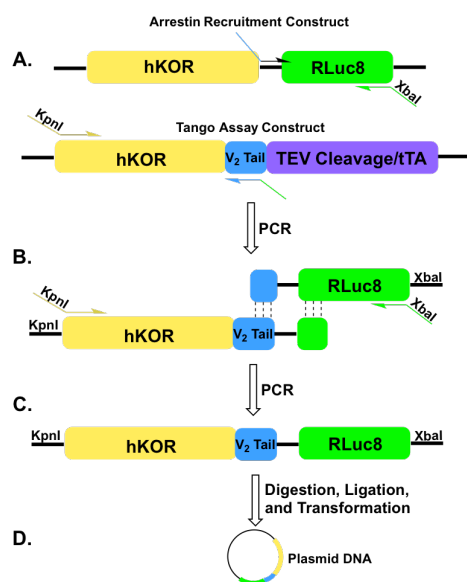


Figure 11. Molecular Biology Strategy for Synthesis of hKOR-V₂ Tail-RLuc8 DNA Construct. An initial PCR reaction (A) provides two products that when run through a second PCR reaction (B) yield a single product that is digested and ligated (C) before transformation into *E. coli* (D).

Construct. In addition to the BRET GAP43 translocation assay, there is an additional BRET assay that uses a luciferase tagged receptor and mVenus tagged arrestin (BRET recruitment assay, see Introductory Chapter 1). We hypothesized that inserting the V₂ tail between the receptor and RLuc8 in the receptor construct for this assay might have similar effects on potency and efficacy as seen in the arrestin assays already explored (Tango and translocation assays specifically). In order to make

this hypothetical construct, a molecular cloning strategy was designed and implemented (**Figure 11**, also see more details in **Experimental**). In this strategy, primers were designed for separate PCR reactions with the KOR Tango construct and the KOR-RLuc8 construct. This reaction would yield two overlapping products, the first that contained the receptor and part of the V₂ tail

and the second that contained the remainder of the V₂ tail and RLuc8. A second PCR reaction allowed elongation from the overlapping base pairs, providing a single product that could be digested with appropriate restriction enzymes and ligated into a new vector for transformation.

With the new KOR-V₂ Tail-RLuc8 construct synthesized, arrestin recruitment could be analyzed. In comparison to the parent KOR-RLuc8 construct (**Table 2** and **Figure 12A**, EC₅₀ DYN = 12.1 ± 8.2 nM, E_{Max} = 100%; EC₅₀ U-50 = 200 ± 78 nM, E_{Max} = 100%; EC₅₀ SALV = 55 ± 39 nM, E_{Max} = 100%; EC₅₀ 6'-GNTI = 0.3 ± 0.1 nM, E_{Max} = 37%; EC₅₀ CYC = 2.7 ± 1.8 nM, E_{Max} = 34%), the V₂ tail enhanced the dynamic range of the assay (by about 3X), as well as the potency of all the compounds (**Table 2** and **Figure 12B**, EC₅₀ DYN = 4.1 ± 3.9 nM, E_{Max} = 49%; EC₅₀ U-50 = 17 ± 5.6 nM, E_{Max} = 100%; EC₅₀ SALV = 7.3 ± 2.4 nM, E_{Max} = 100%; EC₅₀ 6'-GNTI = 0.5 ± 0.4 nM, E_{Max} = 36%; EC₅₀ CYC = 1.7 ± 1.1 nM, E_{Max} = 68%). While it is clear the unmodified KOR-RLuc8

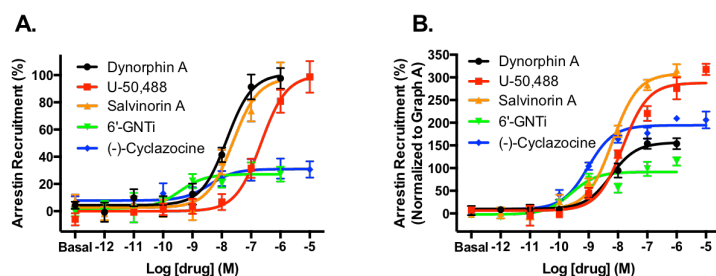


Figure 12. Addition of the V₂ Tail into an Independent Receptor Construct for Arrestin Recruitment Increases the Dynamic Range. hKOR-RLuc8 (A) or hKOR-V₂ Tail-RLuc8 (B) were co-transfected with Arrestin3-mVenus and GRK3 in the BRET recruitment assay. Data represent mean ± SEM of n ≥ 4.

assay is less sensitive than any arrestin assay tested, some compounds are not greatly affected by the addition of the V₂ tail. For instance, the partial agonists 6'-GNTI and cyclazocine did not show significant changes

in potency between the two constructs, although cyclazocine seemed much more efficacious in the presence of the V₂ tail – not surprising given results in the Tango assay and the BRET GAP43 translocation assay. However all three of the full agonists showed significant increases in potency with the addition of the V₂ tail. Interestingly, dynorphin A consistently showed partial

agonism in the presence of the V₂ tail even though the potency increased somewhat. There is not yet any satisfying explanation for this observation. It is possible that dynorphin A does have special signaling properties in comparison to the other ligands tested. As such, perhaps the addition of the V₂ tail changes the conformation of the receptor in a way that makes KOR more sensitive to dynorphin A, thus changing how much it activates arrestin recruitment. Another possibility is that dynorphin A really does have some bias for the G protein pathway, just not to

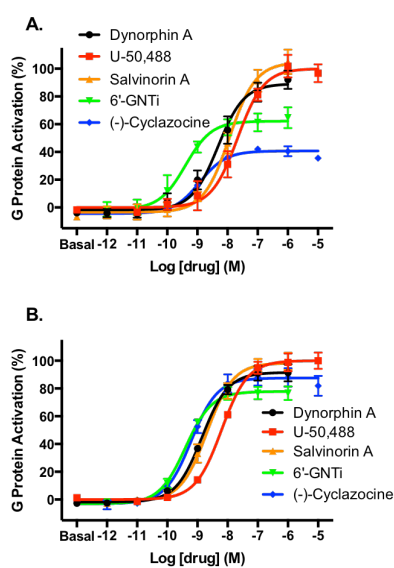


Figure 13. Unmodified and Tango hKOR Constructs Function Normally in G Protein Activation Signaling. hKOR (A) or Tango hKOR (B) were co-expressed with $G\alpha_B$ -RLuc8, $\beta 1$, and mVenus- $\gamma 2$ to assay G protein activation. Data represent mean \pm SEM of $n \geq 3$.

the extent that was suggested by the Tango assay. The data is summarized in **Table 2**.

Interpreting the Data in Terms of Bias Factors

G Protein Activation Data Provides Comparison for Bias Factor Calculations. As described in the Introductory Chapter 1, bias calculations cannot be made unless there are dose response curves for compounds along two or more different signaling pathways. By definition a compound can only be biased to one pathway over another – otherwise just observations about potency and efficacy can be made along a single signaling pathway. The control ligands were tested for their ability to activate KOR in the G protein Activation BRET assays

in the presence (Tango construct) or absence (unmodified receptor) of the V₂ tail (**Figure 13**). In general, all agonists seemed to be slightly more potent in the presence of the V₂ tail for G protein activation. While the potencies of U-50,488 and salvinorin A show the greatest differences in potency between the two constructs, the differences were within an order of magnitude and can

thus be considered reasonable. There are also noticeable (though minor) differences in efficacy for 6'-GNTI and cyclazocine between the two constructs, indicating a potential role of the V₂ tail enhancing the efficacy of partial agonists. These data are also provided in **Table 2**.

Table 2. Summary of Potencies and Efficacies of Drugs Measured.

Compound	G Protein	G Protein	Arrestin	Arrestin	Arrestin
	EC ₅₀ (E _{Max})	EC ₅₀ (E _{Max})	EC ₅₀ (E _{Max})	EC ₅₀ (E _{Max})	EC ₅₀ (E _{Max})
V ₂ Tail?	-	✓	-	✓	✓
Assay	Activation	Activation	hKOR-Luc	hKOR-Luc	Translocation
<i>Dynorphin A</i>	2.9 ± 0.5 nM (100%)	1.4 ± 0.4 nM (100%)	12 ± 8.2 nM (100%)	4.1 ± 3.9 nM (49%)	16 ± 5 nM (100%)
<i>U-50,488</i>	26 ± 6.0 nM (100%)	6.3 ± 2.6 nM (100%)	200 ± 78 nM (100 nM)	17 ± 5.6 nM (100%)	49 ± 15 nM (100%)
<i>Salvinorin A</i>	16 ± 9.2 nM (100%)	2.5 ± 1.5 nM (100%)	55 ± 39 nM (100%)	7.3 ± 2.4 nM (100%)	21 ± 9 nM (100%)
<i>6'-GNTI</i>	0.6 ± 0.05 nM (63%)	0.4 ± 0.1 nM (78%)	0.3 ± 0.1 nM (37%)	0.5 ± 0.4 nM (36%)	0.7 ± 0.3 nM (47%)
<i>(-)-Cyclazocine</i>	1.2 ± 0.2 nM (63%)	0.7 ± 0.1 nM (89%)	2.7 ± 1.8 nM (65%)	1.7 ± 1.1 nM (68%)	1.2 ± 0.1 nM (63%)

Data represent mean ± SEM of various independent trials.

Calculating Ligand Bias From the Data. With a GraphPad Prism program developed by Professor J. Robert Lane (Pharmacy and Pharmaceutical Sciences, Monash University), the data could be fit using the operational model to provide estimates for $\log(\tau/K_A)$. Given the many ways in which ligand bias can be calculated, it seemed that utilizing the operational model as a way to estimate $\log(\tau/K_A)$ from actual data would be the most accurate way to represent bias factors between the two signaling pathways. In doing so, we would be able to compare bias factors between the different assays and interpret the effects of the V₂ tail with confidence. Additionally, given the large fluctuation that was observed with U-50,488 across multiple arrestin assays, as well as literature precedent on what unbiased ligand to choose, we used salvinorin A as the reference unbiased ligand in all our bias calculations shown below.

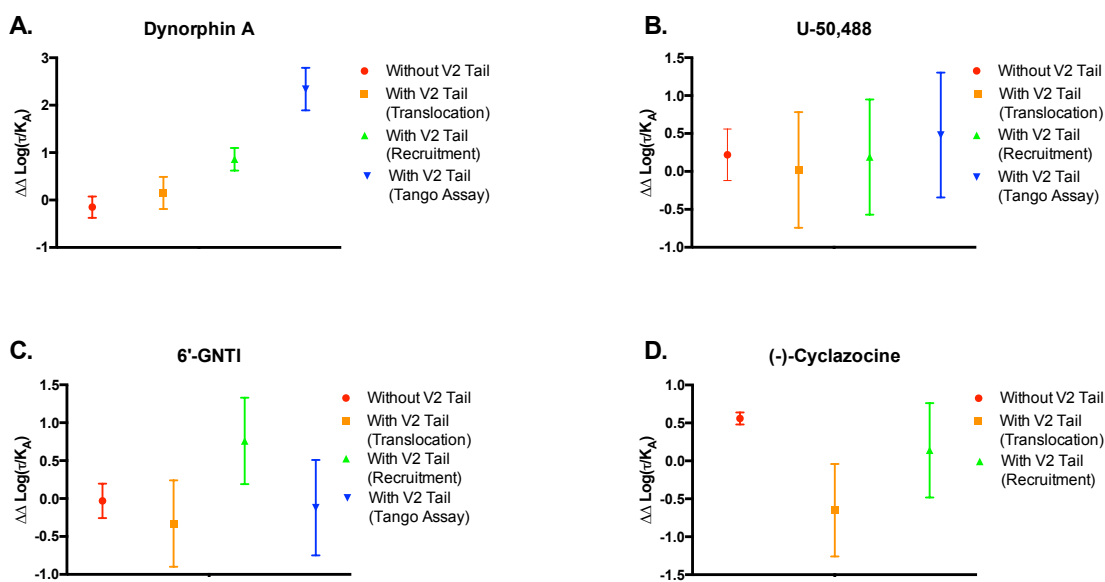


Figure 14. $\Delta\Delta\log(\tau/K_A)$ Values Calculated Using the Data in **Table 2** for Each Individual Compound. Measurements without the V_2 tail (red circle) and with the V_2 tail (BRET GAP43 translocation assay shown with orange squares, BRET recruitment assay is shown with green triangles, and the Tango assay is shown with blue triangles) for dynorphin A (A), U-50,488 (B), 6'-GNTI (C), and (-)-cyclazocine (D) are shown. Data represent mean \pm SEM of $n \geq 4$. Note: Salvinorin A was used as the unbiased agonist with $\Delta\Delta\log(\tau/K_A) = 0$ and is therefore not shown.

Summary of Bias Factor Calculations. **Table 3** summarizes the bias factors calculated from the G protein activation and arrestin data among all the different assays. **Figure 14** shows a graphical representation of the $\log(\text{bias factor})$ calculated for each compound in the different assays. Although there was much variation in potency between the different assays for U-50,488, the overall effect is that the calculated $\Delta\Delta\log(\tau/K_A)$ (aka $\log(\text{bias})$) is relatively constant over all the different assays. Excluding the Tango results for dynorphin A, which are likely false given the low amounts of dynorphin A present in Tango cells after overnight incubation and the peculiar potency increase observed in the pulse experiment of the Tango assay (see **Figure 4**), dynorphin A also showed fairly consistent $\Delta\Delta\log(\tau/K_A)$ over the different assays, even with the V_2 tail. The only other exception, of course, is the interesting partial agonism in the KOR-Luc assay with the construct containing the V_2 tail. However even so this difference in the bias factor

is not significant. The partial agonists, on the other hand, were much more susceptible to

Table 3. Summary of Calculated Bias Factors.

Compound	Arrestin Recruitment	Arrestin Translocation	Arrestin Recruitment	Tango
V ₂ Tail?	-	✓	✓	✓
<i>Dynorphin A</i>	0.7	1.42	7.31	221
<i>U-50,488</i>	1.65	1.04	1.54	3
<i>Salvinorin A</i>	1	1	1	1
<i>6'-GNTI</i>	0.93	0.47	5.79	0.75
<i>(-)-Cyclazocine</i>	3.65	0.22	1.38	-

Bias factors were calculated using the Black-Leff operational model and are in the direction of G protein (i.e. Arrestin Bias < 1 < G Protein Bias). A bias factor of 1 (Salvinorin A) indicates a balanced/unbiased ligand.

variation between the assays, with some set-ups showing a G protein bias (positive $\Delta\Delta\log(\tau/K_A)$) and others showing an arrestin bias (negative $\Delta\Delta\log(\tau/K_A)$).

While there were no obvious patterns concerning the V₂ tail in the calculated $\Delta\Delta\log(\tau/K_A)$ for these partial agonists and the variation is not always dramatic, it does suggest that calculating and understanding ligand bias for a partial agonist might be more complicated than expected. Indeed it does seem that the V₂ tail may actually play little role in artificially enhancing arrestin signaling and just act to provide a better cellular read-out.

Discussion

Interpreting the Variation of Arrestin Recruitment by Dynorphin Between Assays. While dynorphin A showed comparable arrestin recruitment to control ligands U-50,488 and salvinorin A in the BRET GAP43 translocation assay, two separate assays for arrestin recruitment showed distinct results. In the Tango assay, overnight incubation with dynorphin A (as described for the optimized assay protocol) resulted in low potency arrestin recruitment. These results would indicate a G protein bias for dynorphin A, as reported previously.¹² Given our studies (see **Figure 4** above), however, it is unlikely that dynorphin is stable overnight and therefore cannot accurately be defined as G protein biased, since this interpretation is based on the Tango assay

results that rely upon signaling from a metabolically unstable compound. In contrast, the increased potency from the 60-minute pulse with dynorphin A in the Tango assay indicates that two competing factors may be at play – both the instability of dynorphin A as well as potentially unique signaling observed in the presence of the V₂ tail. These results are further supported by the BRET recruitment assay results, where the V₂ tail consistently led to partial efficacy from dynorphin A. As indicated by the creators of the Tango assay (see **Introduction**), the V₂ tail can either enhance or depress arrestin signaling depending on the receptor – though no clear trends have been identified. It therefore seems possible that the V₂ reduces the arrestin recruitment of dynorphin A in certain assays. To be certain of the role of the V₂ tail in dynorphin A's arrestin recruitment, more assays should be studied. The phenomena does not seem universal over all assays (see BRET GAP43 translocation assay), and so certainly more data will be necessary to make firm conclusions. It therefore seems possible that under certain assay conditions with the V₂ tail, dynorphin A might appear G protein biased.

Uncovering True Examples of Biased Ligands. While the best way to determine ligand bias is still debatable, there continue to appear numerous examples of compounds in the literature with alleged bias for one signaling pathway over another. The more biased ligands that are uncovered, the better the understanding of what causes these phenomena at the receptor level. Interestingly there are numerous examples of supposedly biased ligands at KOR (see Introductory Chapter 1), which does bring into question whether some receptors are more capable of ligand bias over another. As more examples of potentially bias compounds are identified, especially specific to certain receptors, hopefully structural features of the receptor will allow ligand bias to be predicted or even designed into new molecules.

Applying Assay Principles to Specific Ligands. With so many assays available today for measuring signaling from receptor activation, it can be a daunting task to correctly identify what assay is the best for the ligand in question. Each assay has its own set of benefits and disadvantages, however ultimately a few key facts need to be decided upon. Will the ligand be stable under the prescribed assay conditions? As we found with dynorphin A in the Tango assay, overnight incubation of the peptide ligand with the cells greatly decreased its viability in the assay, which complicated the results and lead to interpretation difficulties. When utilized in several alternate assays for arrestin recruitment, we were able to show that dynorphin A is able to recruit arrestin without much issue, leading us to conclude that the ligand is probably not G protein biased after all. Another consideration to take into account is the cellular background of the assay. While overexpressed systems can be a helpful first pass at uncovering the signaling mechanisms of a ligand, utilizing endogenous systems and relevant cells may provide a better insight into how a novel ligand might behave *in vivo*. For example, morphine is unable to cause receptor internalization in overexpressed HEK cells, leading to the conclusion that morphine might be G protein biased. However morphine is able to induce receptor internalization in striatal neurons, indicating differential effects from two different cellular systems and opposite interpretations of arrestin signaling.¹⁷ As Terry Kenakin states in his textbook *Principles of Pharmacology*, it is always important to look ahead to the ultimate goal in understanding the pharmacology (**Figure 15**). If the end result is clinical work, then aim to utilize assays with human receptors before moving into endogenous systems. This concept applies well the example of 6'-GNTI, where testing in assays from multiple cellular backgrounds revealed a lack of activity in neurons, highlighting that overexpressed *in vitro* results may not translate well into natural systems.

Correctly Interpreting Results for a Meaningful Bias Factor. Not only are there many assays to measure receptor signaling, but also there is an increasing number of ways in which bias factors can be calculated. In order to obtain the most accurate results, it is important to utilize the operational model, which takes into

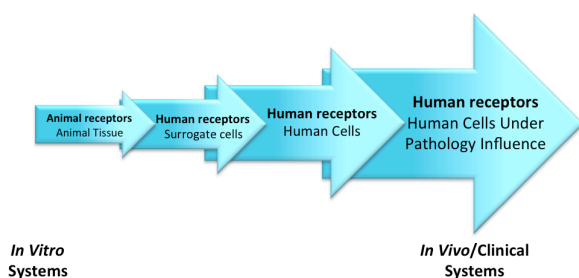


Figure 15. Flow of the State of the Art of Pharmacology. Early studies often start in *in vitro* systems, but the ultimate goal should always be in mind towards *in vivo* and clinical studies if relevant. Adapted from *A Pharmacology Primer* (Figure 1.4, 3rd ed.).²⁷

account both the efficacy, potency, and affinity of the ligand for the receptor, as used in the bias calculations shown in this chapter. Without the affinity, even calculated from a data set of concentration-response curves, an integral piece of information will be missing that affects understanding of the ligand bias. Methods that use only the potency and efficacy to calculate bias are fine for a cursory overview of the data but should be avoided in place of the more rigorous operational model. Additionally, data can be difficult to interpret for low efficacy compounds. All compounds analyzed in this chapter showed meaningful dose response curves that allowed use of standard operational model calculations. However ligand bias is near impossible to calculate if there is not a full curve of the ligand for each signaling pathway. Laura Bohn discusses this extensively in a recent study.¹⁸ Rather than fitting curves on data sets that show little to no efficacy, Bohn suggests instead to use a competitive method to obtain the data. In this way, low efficacy compounds might be able to instead show inhibition of a full agonist, thus providing a full curve that can be used in the operational model.¹⁸ A most important point is to view data with some level of skepticism and be convinced of results only after multiple assays and cellular systems have been used. Criticism of results we obtained in the Tango assay allowed

further study of the signaling of dynorphin A and led us to uncover an unexpected activity for recruiting arrestin of dynorphin A in an artificial, reconstructed system. Further study of dynorphin A's signaling in endogenous systems or *in vivo* may provide more information about the true level of bias from this compound.

Moving Assays Closer to In Vivo. One solution to the issue of highly modified, overexpressed cellular systems, like those studied in this chapter, is to bring some functional assays into an *in vivo* setting. While this is certainly an ambitious goal, some researchers are making attempts to start this process. In one example, researchers used fluorescein arsenical hairpin binder (FAsH) technology in combination with fluorescence resonance energy transfer (FRET) to measure GPCR activation in live HeLa cells.¹⁹ Cyan fluorescence protein (CFP) and yellow fluorescent protein (YFP) were inserted into the human adenosine A_{2A} receptor, which allowed FRET monitoring of receptor activation and kinetics. FAsH technology has been utilized *in vivo*²⁰, and thus if translated into the study of GPCRs there would be a method to image G protein activation signaling cascades live rather than just interpreting through plate reader-based assays currently utilized heavily. FAsH technology is unfortunately another highly modified system and may not be able to measure bias of GPCRs. Another technology being utilized to measure GPCR activation *in vivo* is Designer Receptors Exclusively Activated by designer Drugs (DREADDs). Developed by Bryan Roth, this system utilized a specially engineered GPCR that is only activated by a synthetic ligand (usually clozapine N-oxide, CNO), not likely to hit any other receptors/targets.²¹ Once genetically encoded into animal models (mice mostly), receptors can be activated by addition of CNO. Updated versions of the technology utilizing channelrhodopsins allow receptors to be activated (and imaged) by certain wavelengths of light in the brain.²² Unfortunately, these methods require heavy genetic manipulation, and

while they can be performed *in vivo*, the results in some ways are no better than *in vitro* assays. Perhaps in the most relevant attempt, researchers have utilized positron emission tomography (PET) technology to measure the activation of MOR in the brain of subjects undergoing “social pain.”²³ Using the MOR radioligand [¹¹C]carfentanil, researchers showed that subjects with major depressive disorder (MDD) had reduced levels of endogenous opioid release in the brain in response to social rejection. Although this study could not show receptor activation on the cellular level, it does highlight the possibility to image opioid receptors *in vivo* (and in humans). In the advent of better technology for measuring G protein activation and arrestin recruitment, the results of ligands described in this chapter and others will be more reliable and hopefully translate well into more complex systems.

It should be noted, however, that there are no methods for studying GPCR signaling or even bias directly *in vivo*. This lack of technology is seriously impeding further progress on understanding the implications of biased signaling on behavioral responses. Researchers are left trying to draw comparisons between *in vitro* signaling results and *in vivo* behavioral effects, which in all likelihood may not be comparable at all. While some assays can be applied to *ex vivo* analysis of excised tissue or dissociated cells (most commonly used are the [³⁵S]GTPγS binding assay and western blotting, see Introductory Chapter 1 for more detail), they still cannot provide the complete picture of how biased signaling might affect the processes and function of living *in vivo* systems.

Testing Ligands In Vivo. Laura Bohn accurately describes the predicament with biased ligands in a recent report.²⁴ Although an increasing number of biased ligands are being discovered each year, the evidence of what it means to be biased *in vivo* is quite limited. Bohn notes that ideally biased calculations between two pathways should be performed using the same

cellular readout, thus eliminating any cellular discrepancies that may arise. Additionally, it is important to test lead compounds in an *in vivo* setting. Without analyzing the behavioral effects a biased ligand might have on an animal, then the whole concept of functional selectivity is limited to a cellular context only. There is also the added caveat that animal models for certain behaviors are not always a true depiction of how they will react in humans. However, hopefully in studying an increasing number of biased ligands both *in vitro* and *in vivo*, scientists will be better equipped to interpret results as those leads move into the clinic. There are still no true methods to study biased signaling *in vivo*, however (see above), so researchers must draw conclusions on functional selectivity with caution.

Conclusions

We have shown, through a rigorous dissection and analysis of many assays for arrestin recruitment, that caution should be taken when choosing the appropriate assay for studying a particular ligand of GPCRs. After confirming dynorphin A bias in the Tango assay, we determined that conditions required for the Tango assay were not conducive to neuropeptides, leading to a potentially misleading conclusion of ligand bias. In studying the Tango assay further, we scrutinized the role of the V₂ tail in the context of arrestin recruitment by both removing it from the Tango assay itself and applying it to other BRET-based arrestin assays. We found that while the V₂ tail seems crucial for success of the Tango assay, its use in other arrestin assays did not alter bias calculations to a significant extent (although it did affect potency and efficacy parameters of some compounds). Therefore, although the V₂ tail may enhance (or otherwise affect) recruitment of arrestin to GPCRs, it does not appear to artificially enhance arrestin levels to an extent that would significantly affect bias factor calculations. Through this

exercise, we have come to appreciate the importance of testing novel ligands in multiple assays as a way to understand the complex molecular signaling with the utmost accuracy.

Experimental

Cell Culture. HEK-293T cells were obtained from the American Type Culture Collection (Rockville, MD) and were cultured in a 5% CO₂ atmosphere at 37 °C in Dulbecco's Modified Eagle Medium (high glucose #11965; Life Technologies Corp.; Grand Island, NY) supplemented with 10% FBS (Premium Select, Atlanta Biologicals; Atlanta, GA) and 100 U/mL penicillin and 100 µg/mL streptomycin (#15140, Life Technologies). HTLA cells (HEK293 cells stably transfected with tTA-dependent luciferase reporter and β-arrestin2-TEV fusion gene) were a gift from Bryan Roth and were culture in a 5% CO₂ atmosphere at 37 °C in Dulbecco's Modified Eagle Medium supplemented with 10% FBS, 100 U/mL penicillin and 100 µg/mL streptomycin, 100 µg/mL streptomycin, 2 µg/mL puromycin, and 100 µg/mL hygromycin B.

DNA Constructs. The human MOR (hMOR), human DOR (hDOR), human KOR (hKOR), and GRK3 were obtained from the Missouri S&T Resource Center. The human KOR Tango construct was generously provided by Bryan Roth. The human G protein constructs used here have been previously described and were provided by C. Galés or were obtained from the Missouri S&T Resource Center unless otherwise noted.^{10,25} The G proteins used included untagged G_{α_{oB}} (G_{α_{oB}}); G_{α_{oB}} with Renilla luciferase 8 (RLuc8) inserted at position 91 (G_{α_{oB}}-RLuc8); Gβ₁ (β₁); untagged Gγ₂ (γ₂); Gγ₂, which we fused to the full-length mVenus at its *N*-terminus via the amino acid linker GSAGT (mVenus-γ₂). The plasmids employed in the arrestin recruitment assay, hKOR-RLuc8 and Arr3-mVenus, were synthesized in-house as previously described.¹⁰ All constructs were sequence-confirmed prior to use in experiments.

Tango Assay. HTLA cells were added to a 10-cm plate at 5×10^6 cells/plate (day 1). On the next day (day 2), cells were transfected with 8 μg of receptor using the calcium phosphate method.²⁶ After 24 hours (day 3), cells were transferred to a poly-D-lysine coated 96-well white, clear-bottomed plate at 40,000 cells/well. After another 24 hours (day 4), media was refreshed to 100 μL /well, and ligands were added at 5X concentrated stocks in 25 μL of HBSS with 20 mM HEPES (assay buffer). Cells were incubated overnight at 37 °C. After 18-24 hours (day 5), cells were equilibrated to room temperature after which time the media was removed and replaced with 100 μL /well of Promega Bright-Glo (#E2610) solution (diluted 1:10 in assay buffer) in the absence of light. Luminescence was measured on a standard plate reader after 15 minutes.

BRET

Transfection. The following cDNA amounts were transfected into HEK-293T cells (5×10^6 cells/plate) in 10-cm dishes using polyethylenimine (PEI) in a 1:1 ratio (diluted in Opti-MEM, Life Technologies): ***G protein activation:*** 2.5 μg MOR/DOR/KOR, 0.125 μg $G\alpha_{\text{OB}}$ -RLuc8, 6.25 μg β_1 , 6.25 μg mVenus- $\gamma 2$; ***BRET GAP43 translocation:*** 2 μg hKOR, 0.25 μg RLuc8-arrestin3-Sp1, 5 μg mem-linker-citrine-SH3, 5 μg GRK3; ***BRET recruitment:*** 0.2 μg hKOR-RLuc8, 15 μg Arr3-mVenus, 5 μg GRK3. Cells were maintained in the HEK-293T media described above. After 24 hours the media was changed, and the experiment was performed 24 hours later (48 hours after transfection).

BRET. Transfected cells were dissociated and re-suspended in phosphate-buffered saline (PBS). Approximately 200,000 cells/well were added to a black-framed, white well 96-well plate (#60050; Perkin Elmer; Waltham, MA). The microplate was centrifuged and the cells were re-suspended in PBS. For agonist experiments, after 5 minutes, 5 μM of the luciferase substrate coelenterazine H was added to each well. After 5 minutes, ligands were added and the BRET

signal was measured 5 minutes later on a PHERAstar FS plate reader. For antagonist competition experiments, cells were pre-incubated with the antagonist at varying concentrations for 30 minutes. Coelenterazine H (5 μ M) was then added to each well for 5 minutes. Following coelenterazine H incubation, a fixed concentration of the reference agonist (5x EC₅₀) was added, and the BRET signal was measured at 30 minutes on a PHERAstar FS plate reader. The BRET signal was quantified by calculating the ratio of the light emitted by the energy acceptor, mVenus (510-540 nm) or citrine (510-540 nm), over the light emitted by the energy donor, RLuc8 (485 nm). This drug-induced BRET signal was normalized using the E_{max} of [D-Ala², N-Me-Phe⁴, Gly-ol⁵]-enkephalin (DAMGO), [D-Pen(2,5)]enkephalin (DPDPE), or U-50,488 as the maximal response at MOR, DOR, and KOR respectively. Dose response curves were fit using a three-parameter logistic equation in GraphPad Prism 6.

Cloning

Synthesis of Tango hKOR without V₂ Tail. The hKOR Tango construct was digested with AgeI-HF[®] (#R3552L; New England Biolabs, Ipswich, MA) according to the manufacturer's protocol in CutSmart[®] Buffer (#B7204S; New England Biolabs) at 37 °C for 1.5 hours. A small portion of the reaction (10 μ L) was loaded onto an agarose gel, and the correct band was cut out and purified using the QIAquick Gel Extraction kit (#28704; Qiagen Inc, Valencia, CA). Next, this cut vector (3 μ L) was ligated according to the manufacturer's protocol using T4 DNA ligase (#M0202, New England Biolabs) in T4 DNA ligase reaction buffer (#B0202S, New England Biolabs) overnight at 4 °C. The ligation reaction was transformed into *E. coli* and then amplified before using.

Synthesis of hKOR-V₂ Tail-RLuc8. A PCR reaction was run with the hKOR Tango construct (Forward Primer = CTTGGTACCATGAAGACGAT; Reverse Primer =

GAAGCCATCCCCCTCTTGACGATGAAGTGCCTTGGC) and the hKOR-RLuc8 construct (Forward Primer = GCCAAGGACACTTCATCGTCAAGAGGGGGGATGGCTTC; Reverse Primer = GCCCTCTAGATTACTGCTCGTTCTTCAGC) described previously.¹⁰ The PCR reactions were loaded onto an agarose gel, and the correct bands were cut out and purified using the QIAquick Gel Extraction Kit. These two PCR products were combined in a new PCR reaction (Forward Primer = CTTGGTACCATGAAGACGAT; Reverse Primer = GCCCTCTAGATTACTGCTCGTTCTTCAGC), which was then loaded onto an agarose gel and isolated again using the QIAquick Gel Extraction Kit. The second PCR product was digested with KpnI-HF[®] (#R3142, New England Biolabs) and XbaI (#R0145, New England Biolabs) for 1 hour at 37 °C. The digestion was loaded onto an agarose gel and isolated again using the QIAquick Gel Extraction Kit. The purified cut PCR product was ligated with cut vector (digested in the presence of calf intestinal alkaline phosphatase, #M0290, New England Biolabs) (1 µg) with T4 DNA ligase (#M0202, New England Biolabs) in T4 DNA ligase reaction buffer (#B0202S, New England Biolabs) for 10 minutes at room temperature. This ligation product was immediately transformed into *E. coli* and then amplified before using.

Calculations

Operational Model Ligand Bias Calculations. $\text{Log}(\tau/K_A)$ for individual data sets was estimated using a GraphPad Prism program developed by Professor L. Robert Lane (Monash University). For full agonists, the $\text{Log}K_A$ values were set to zero. E_{Max} , n (Hill slope), and basal values were shared across all data sets. It was important to use the calculated $\text{Log}K_A$ (functional affinity) from the data sets, since experimental binding affinity may not account for multiple active receptor conformations. The calculated $\text{Log}(\tau/K_A)$ were then converted into bias factors as shown in the Introductory Chapter 1 (Equations 2 and 3).

References

- (1) Kroeze, W. K.; Sassano, M. F.; Huang, X.-P.; Lansu, K.; McCorvy, J. D.; Giguère, P. M.; Sciaky, N.; Roth, B. L. PRESTO-Tango as an Open-Source Resource for Interrogation of the Druggable Human GPCRome. *Nat. Struct. Mol. Biol.* **2015**.
- (2) Vrecl, M.; Nørregaard, P. K.; Almholt, D. L. C.; Elster, L.; Pogacnik, A.; Heding, A. Beta-Arrestin-Based Bret2 Screening Assay for The “non”-Beta-Arrestin Binding CB1 Receptor. *J. Biomol. Screen. Off. J. Soc. Biomol. Screen.* **2009**, *14*, 371–380.
- (3) Charest, P. G.; Bouvier, M. Palmitoylation of the V2 Vasopressin Receptor Carboxyl Tail Enhances β -Arrestin Recruitment Leading to Efficient Receptor Endocytosis and ERK1/2 Activation. *J. Biol. Chem.* **2003**, *278*, 41541–41551.
- (4) Tohgo, A.; Choy, E. W.; Gesty-Palmer, D.; Pierce, K. L.; Laporte, S.; Oakley, R. H.; Caron, M. G.; Lefkowitz, R. J.; Luttrell, L. M. The Stability of the G Protein-Coupled Receptor-Beta-Arrestin Interaction Determines the Mechanism and Functional Consequence of ERK Activation. *J. Biol. Chem.* **2003**, *278*, 6258–6267.
- (5) Hanson, B. J.; Wetter, J.; Bercher, M. R.; Kopp, L.; Fuerstenau-Sharp, M.; Vedvik, K. L.; Zielinski, T.; Doucette, C.; Whitney, P. J.; Revankar, C. A Homogeneous Fluorescent Live-Cell Assay for Measuring 7-Transmembrane Receptor Activity and Agonist Functional Selectivity Through Beta-Arrestin Recruitment. *J. Biomol. Screen.* **2009**, *14*, 798–810.
- (6) Wüster, M.; Schulz, R.; Herz, A. Opiate Activity and Receptor Selectivity of Dynorphin1-13 and Related Peptides. *Neurosci. Lett.* **1980**, *20*, 79–83.
- (7) Chavkin, C.; James, I. F.; Goldstein, A. Dynorphin Is a Specific Endogenous Ligand of the Kappa Opioid Receptor. *Science* **1982**, *215*, 413–415.
- (8) Von Voigtlander, P. F.; Lewis, R. A. U-50,488, a Selective Kappa Opioid Agonist: Comparison to Other Reputed Kappa Agonists. *Prog. Neuropsychopharmacol. Biol. Psychiatry* **1982**, *6*, 467–470.
- (9) Yan, F.; Roth, B. L. Salvinorin A: A Novel and Highly Selective κ -Opioid Receptor Agonist. *Life Sci.* **2004**, *75*, 2615–2619.
- (10) Rives, M.-L.; Rossillo, M.; Liu-Chen, L.-Y.; Javitch, J. A. 6'-Guanidinonaltrindole (6'-GNTI) Is a G Protein-Biased κ -Opioid Receptor Agonist That Inhibits Arrestin Recruitment. *J. Biol. Chem.* **2012**, *287*, 27050–27054.
- (11) Schmid, C. L.; Streicher, J. M.; Groer, C. E.; Munro, T. A.; Zhou, L.; Bohn, L. M. Functional Selectivity of 6'-guanidinonaltrindole (6'-GNTI) at κ -Opioid Receptors in Striatal Neurons. *J. Biol. Chem.* **2013**, *288*, 22387–22398.
- (12) White, K. L.; Scopton, A. P.; Rives, M.-L.; Bikbulatov, R. V.; Polepally, P. R.; Brown, P. J.; Kenakin, T.; Javitch, J. A.; Zjawiony, J. K.; Roth, B. L. Identification of Novel Functionally Selective κ -Opioid Receptor Scaffolds. *Mol. Pharmacol.* **2014**, *85*, 83–90.
- (13) Meyer, J. P.; Gillespie, T. J.; Hom, S.; Hruby, V. J.; Davis, T. P. In Vitro Stability of Some Reduced Peptide Bond Pseudopeptide Analogues of Dynorphin A. *Peptides* **1995**, *16*, 1215–1219.
- (14) Bell, K. M.; Traynor, J. R. Dynorphin A(1-8): Stability and Implications for in Vitro Opioid Activity. *Can. J. Physiol. Pharmacol.* **1998**, *76*, 325–333.
- (15) Zangrandi, L.; Burtcher, J.; MacKay, J. P.; Colmers, W. F.; Schwarzer, C. The G-Protein Biased Partial κ Opioid Receptor Agonist 6'-GNTI Blocks Hippocampal Paroxysmal Discharges without Inducing Aversion. *Br. J. Pharmacol.* **2016**, *173*, 1756–1767.

- (16) Archer, S.; Glick, S. D.; Bidlack, J. M. Cyclazocine Revisited. *Neurochem Res* **1996**, *21*, 1369–1373.
- (17) Beaulieu, J. M. Morphine-Induced Mu-Opioid Receptor Internalization: A Paradox Solved in Neurons. *J. Neurosci.* **2005**, *25*, 10061–10063.
- (18) Stahl, E. L.; Zhou, L.; Ehlert, F. J.; Bohn, L. M. A Novel Method for Analyzing Extremely Biased Agonism at G Protein-Coupled Receptors. *Mol. Pharmacol.* **2015**, *87*, 866–877.
- (19) Hoffmann, C.; Gaietta, G.; Bünemann, M.; Adams, S. R.; Oberdorff-Maass, S.; Behr, B.; Vilardaga, J.-P.; Tsien, R. Y.; Ellisman, M. H.; Lohse, M. J. A FIAsh-Based FRET Approach to Determine G Protein-Coupled Receptor Activation in Living Cells. *Nat. Methods* **2005**, *2*, 171–176.
- (20) Venken, K. J. T.; Kasprowitz, J.; Kuenen, S.; Yan, J.; Hassan, B. B.; Verstreken, P. Recombineering-Mediated Tagging of Drosophila Genomic Constructs for in Vivo Localization and Acute Protein Inactivation. *Nucleic Acids Res.* **2008**, *36*, 1–9.
- (21) Urban, D. J.; Roth, B. L. DREADDs (Designer Receptors Exclusively Activated by Designer Drugs): Chemogenetic Tools with Therapeutic Utility. *Annu. Rev. Pharmacol. Toxicol.* **2014**, 1–19.
- (22) Nair, S. G.; Strand, N. S.; Neumaier, J. F. DREADDing the Lateral Habenula: A Review of Methodological Approaches for Studying Lateral Habenula Function. *Brain Res.* **2013**, *1511*, 93–101.
- (23) Hsu, D. T.; Sanford, B. J.; Meyers, K. K.; Love, T. M.; Hazlett, K. E.; Walker, S. J.; Mickey, B. J.; Koeppe, R. A.; Langenecker, S. A.; Zubieta, J. It Still Hurts: Altered Endogenous Opioid Activity in the Brain during Social Rejection and Acceptance in Major Depressive Disorder. *Mol. Psychiatry* **2015**, *20*, 193–200.
- (24) Luttrell, L. M.; Maudsley, S.; Bohn, L. M. Fulfilling the Promise of “Biased” G Protein-Coupled Receptor Agonism. *Mol. Pharmacol.* **2015**, *88*, 579–588.
- (25) Negri, A.; Rives, M.-L.; Caspers, M. J.; Prisinzano, T. E.; Javitch, J. A.; Filizola, M. Discovery of a Novel Selective Kappa-Opioid Receptor Agonist Using Crystal Structure-Based Virtual Screening. *J. Chem. Inf. Model.* **2013**, *53*, 521–526.
- (26) Jordan, M.; Schallhorn, A.; Wurm, F. M. Transfecting Mammalian Cells: Optimization of Critical Parameters Affecting Calcium-Phosphate Precipitate Formation. *Nucleic Acids Res.* **1996**, *24*, 596–601.
- (27) Kenakin, T. *A Pharmacology Primer: Theory, Applications, and Methods*; 3rd Editio.; Elsevier Academic Press: Burlington, MA, 2009.

Part II – The Growth Factor Signaling System

Chapter 6 – Potentiation of FGF2-Induced Glial Cell Line-Derived Neurotrophic Factor Release by a Novel Deconstructed *Iboga* Alkaloid Analog

Introduction

Glial cell line-derived neurotrophic factor (GDNF) is an important signaling protein in the central nervous system (CNS)¹⁻⁵ that belongs to the GDNF-family of ligands (GFL), which together includes other members neurturin,⁶ persephin,⁷ and artemin.⁸ GDNF signals through the transmembrane receptor tyrosine kinase (RTK), which is known as rearranged during transfection receptor (Ret). Upon activation of Ret by GDNF, a tetrameric complex containing two molecules of Ret and two molecules of GDNF family receptor α (GFR α 1 in particular for GDNF) forms.⁹ This activated Ret/GFR α complex can then trigger intracellular signaling through the MEK, PI3K, and PLC γ pathways, which leads to a variety of cellular effects including modulation of differentiation, survival, proliferation, and plasticity of neurons.¹⁰

GDNF and other neurotrophic factors such as brain-derived neurotrophic factor (BDNF), fibroblast growth factors (FGFs), and vascular endothelial growth factor (VEGF) are gaining popularity for their important role in mood disorders and addiction.¹¹⁻¹⁴ Recent studies have found that there is cross-talk between different neurotrophins and growth factors. For instance, the fibroblast growth factor 2 (FGF2) induces GDNF release in both C6 glioma cells and in human neuroblastoma and glioblastoma cell lines through activation of the FGF receptor 1 (FGFR1).^{15,16} The fibroblast growth factor system, currently comprised of 4 fibroblast growth factor receptors (FGFRs) and 18 fibroblast growth factors (FGFs), is a fundamental cellular system that plays critical roles in the development, maintenance, and regeneration of CNS tissues.^{11,17-19} Also, evidence suggests that the FGF system may play a direct role in neuropsychiatric disorders such as depression and anxiety (for further discussion on the FGF

system, see Chapter 7). Proteins such as GDNF and FGF2 are not typically able to cross the blood-brain barrier, so small molecule modulators of neurotrophic factor signaling *in situ* represent a novel approach to treat complex neuropsychiatric diseases.^{20–25}

One such reported small molecule modulator of GDNF is the natural product ibogaine, from the *Tabernanthe iboga* plant. Among the many hypotheses on the mechanism of action of ibogaine (see Chapter 4), one intriguing suggestion that stands out links *iboga* alkaloids to the modulation of neurotrophic factor signaling systems. Namely, reports show that ibogaine can induce GDNF expression in the ventral tegmental area (VTA) of rats, suggesting that perhaps GDNF activates an autocrine loop, which in turn increases the long-term synthesis and release of GDNF (**Figure 1A**). These increased levels of GDNF could repair damage in the VTA-ventral striatum reward system and perhaps explain the long-lasting effects of ibogaine usage.²⁶ Additionally, GDNF infusion to the VTA also reduces self-administration of alcohol and cocaine in rats.^{26–29} It should be noted, however, that the role of GDNF in addiction may be more complex, as GDNF enhances the incubation of cocaine cravings during the first few weeks of withdrawal.^{27–29} Although this hypothesis does not provide a primary molecular target for the mechanism of ibogaine, it offers a larger physiological picture and a foundation for understanding the long-term effects of *iboga* alkaloids.

Therefore, we chose to explore novel analogs of *iboga* alkaloids in order to discover superior releasers of GDNF that were also structurally distinct from ibogaine, which could provide a drug-like alternative to direct GDNF administration or viral gene delivery in the treatment of neuropsychiatric disorders. One can envision, therefore, that ibogaine analogs that more robustly increase GDNF production may in fact be superior therapeutics to ibogaine itself.

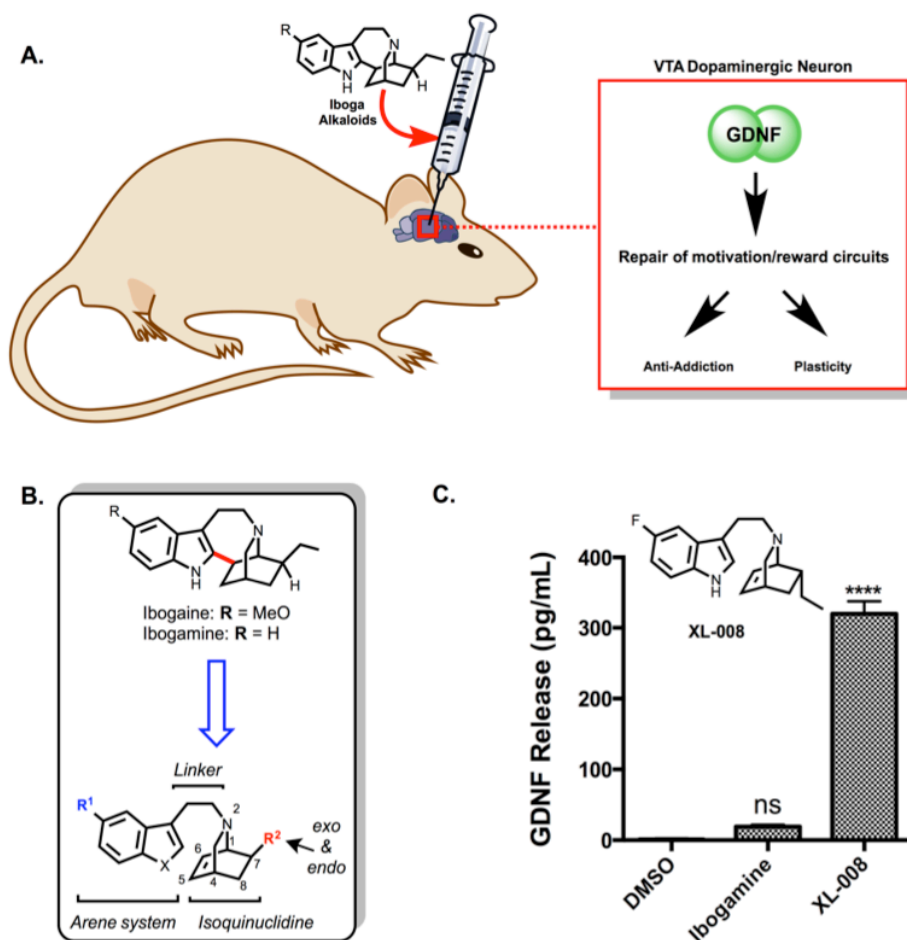


Figure 1. GDNF Release and Addiction. A. Glial-cell line derived neurotrophic factor (GDNF) is a small protein that is synthesized and secreted in glial and neuronal cells. It has been shown to protect dopaminergic neurons in the brain and is linked to many brain disorders. Ibogaine, an alkaloid natural product isolated from *Tabernanthe iboga* has shown anti-addictive properties, possibly mediated through the induction of GDNF release in the reward circuits of the brain. It was suggested that the GDNF release repairs neuronal circuits altered by the development of the drug-dependent state (supported by reduction of alcohol consumption in rodents). B. Disconnection of the heteroarene and isoquinuclidine systems of the *iboga* skeleton reveals a novel class of *iboga* analogs. C. One such analog, XL-008, is a superior releaser of GDNF in comparison to the *iboga* alkaloid ibogamine, when tested at a 10 μM concentration after 24 hours in C6 cells, an established secondary glial cell model. Data represent mean \pm SD of biological replicates in one experiment from $n = 4$ independent experiments. One-way ANOVA followed by Dunnett's Multiple Comparisons Test is shown (** $p < 0.01$).

In this chapter, the novel *iboga* analog XL-008 is described, including its synthesis and ability to induce GDNF release from C6 glioma cells. A full account of this work can be found in our published report.³⁰ Not only does XL-008 induce GDNF release on its own, but it also greatly potentiates the GDNF release by FGF2. Additionally, the GDNF release by FGF2 and

afforded the selective bromination at the indole 2-position. This crude arylbromide intermediate was then cyclized under reductive Heck conditions to provide *rac*-ibogamine. XL-008 could further be cyclized utilizing an electrophilic palladation-type cyclization to provide cyclic XL-008 (CY-XL-008).

GDNF Release From C6 Glioma Cells. It is well-recognized that GDNF release can be measured in the growth medium of conditioned C6 rat glioma cells using conventional ELISA with basal levels between 6 and 81 pg/mL.³² C6 glioma cells are a model for astrocytes and are

known to express the mRNA of GDNF, as well as that of Ret and GFR α 1. Therefore, the cells

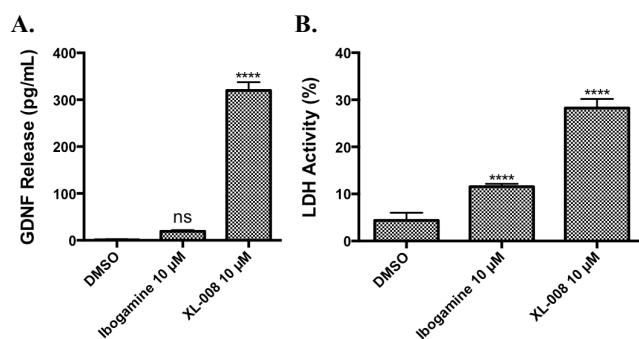


Figure 3. GDNF Release at 48 Hours is Cytotoxic. A. GDNF release from ibogamine and XL-008 at 48 hours. B. LDH release from C6 (P41) in 96-well plates after 48 hours. Conditions were performed in quadruplicate and measured in singlet. Error bars represent SD of a representative experiment of $n = 3$ independent experiments. One-way ANOVA with Dunnett's Multiple Comparisons Test are shown (**** $p < 0.0001$).

can be utilized for measuring GDNF release induced by different compounds *in vitro*.³³ In order to assay the GDNF release induced by novel compounds, C6 cells were incubated with test compounds for 24–48 hours, and GDNF levels were then detected in the conditioned media with picogram sensitivity using a commercially available standard sandwich-style ELISA. The assay required extensive optimization of cell culture and release conditions, which allowed reproducible experiments to

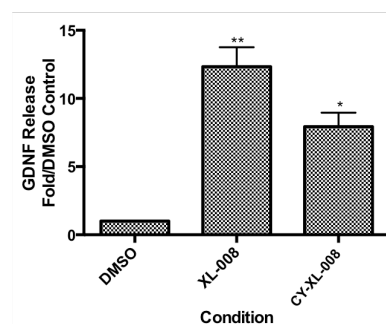


Figure 2. GDNF Release from XL-008 and CY-XL-008 Derivatives. A. GDNF release from *iboga* alkaloid analog XL-008 and cyclic derivative CY-XL-008 after 48 hours. Error bars represent SD of biological replicates. Conditions were performed in duplicate and measured in triplicate. One-way ANOVA with Dunnett's Multiple Comparisons Test are shown (* $p < 0.05$, ** $p < 0.01$). Data obtained by Rich Karpowicz.

can be utilized for measuring GDNF release induced by different compounds *in vitro*.³³ In order to assay the GDNF release induced by novel compounds, C6 cells were incubated with test compounds for 24–48 hours, and GDNF levels were then detected in the conditioned media with picogram sensitivity

be obtained (see **Experimental** below). In early experiments, XL-008 was identified as a superior releaser of GDNF in a screen of ibogamine analogs. In particular, its GDNF release was far greater than that of ibogamine (**Figure 1C**), which revealed the importance of the key disconnection in the *iboga* skeleton between the isoquinuclidine and indole 2-position to form "acyclic" analogs. This hypothesis was further supported when the GDNF release by CY-XL-008 was measured, which showed a significant but lesser release than XL-008 when compared to DMSO (**Figure 2**). In the 48-hour experiments, substantial production of GDNF was noted (**Figures 2** and **3A**); however, it became clear that such release was stressful to the cells and resulted in marked cytotoxicity, as visualized by changes in cell morphology (**Figures 3B** and **4**). Rather than showing a healthy, flat monolayer of cells (**Figure 4A**), the addition of XL-008 after

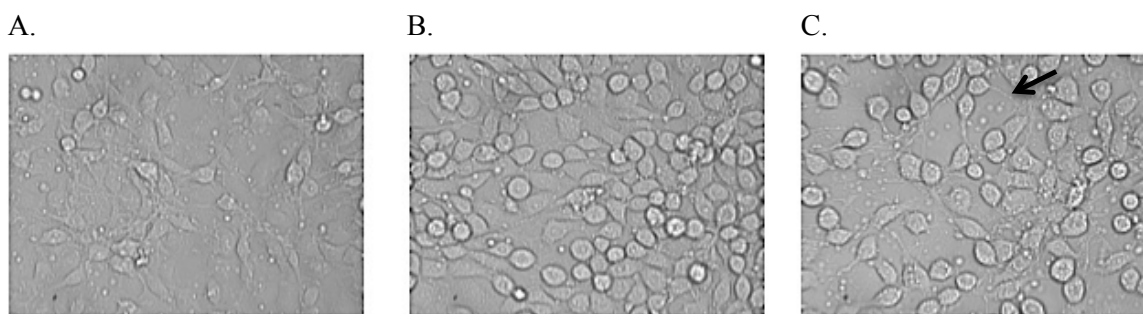


Figure 4. Brightfield images (400X) of C6 morphology in response to 48-hour treatment with XL-008 at (A) 0.1% DMSO control, showing normal, flat, fibroblastic morphology, (B) 10 μ M, and (C) 40 μ M. An example process induced by XL-008 is indicated with an arrow. Data obtained by Rich Karpowicz.

48 hours caused rounding of cells (**Figure 4B**) and the formation of processes (**Figure 4C**).^{34,35}

Therefore, all GDNF release experiments were conducted using a 24-hour treatment. Even though the GDNF release at 24 hours was not as robust in comparison to 48 hours, the measures were statistically significant while minimizing cytotoxic effects.

XL-008 Potentiation of FGF2-Induced GDNF Release

XL-008 Induces Potentiation of GDNF Release From FGF2. In addition to studying the effects of XL-008 on GDNF release from C6 cells, we were also interested in exploring whether there was any potential GDNF release caused by growth factors, FGF2 in particular (see **Introduction** for the rationale). Similar to previous reports, FGF2 afforded measurable GDNF release in our assays, and so we aimed to explore further the potential interactions of XL-008 and FGF2 on GDNF release.^{15,36} In a competition experiment where XL-008 and FGF2 were co-incubated to determine if their GDNF releasing effects were additive, interesting results were obtained. The GDNF release induced by FGF2 (25 ng/mL) was greatly increased in the presence of 10 μ M XL-008 (**Figure 5A**). In contrast, the effect of ibogamine on the GDNF release induced by FGF2 was only additive (**Figure 5B**). XL-008, therefore, not only induces release of GDNF independently but also potentiates the GDNF release by FGF2, another pharmacologically relevant target. In fact, the effects of FGF2 and XL-008 together on GDNF release are almost two-fold higher than the additive effects of their individual GDNF releases.

Interested by the observed potentiation, it was necessary to study the effect of FGF2 (25 ng/mL) on the GDNF release elicited by varying concentrations of XL-008. When the GDNF release was measured for FGF2 on a dose response curve of XL-008, we found that FGF2 both increases the efficacy of GDNF release by XL-008 in C6 glioma cells and potentiates the dose response curve, shifting the EC_{50} from more than 15 μ M to 6.17 ± 2.40 μ M, a greater than two-fold increase in potency (**Figure 5C**). Since higher concentrations of XL-008 caused cytotoxic effects in the C6 cells, a full dose response curve for XL-008 alone was not obtained. Typically, when concentrations greater than 30 μ M were measured, they were found to be highly toxic even in the 24-hour treatment, as determined by visual observation, lactate dehydrogenase (LDH) assay, and water-soluble tetrazolium (WST-1) assay. Consequently, **Figure 5C** shows only an

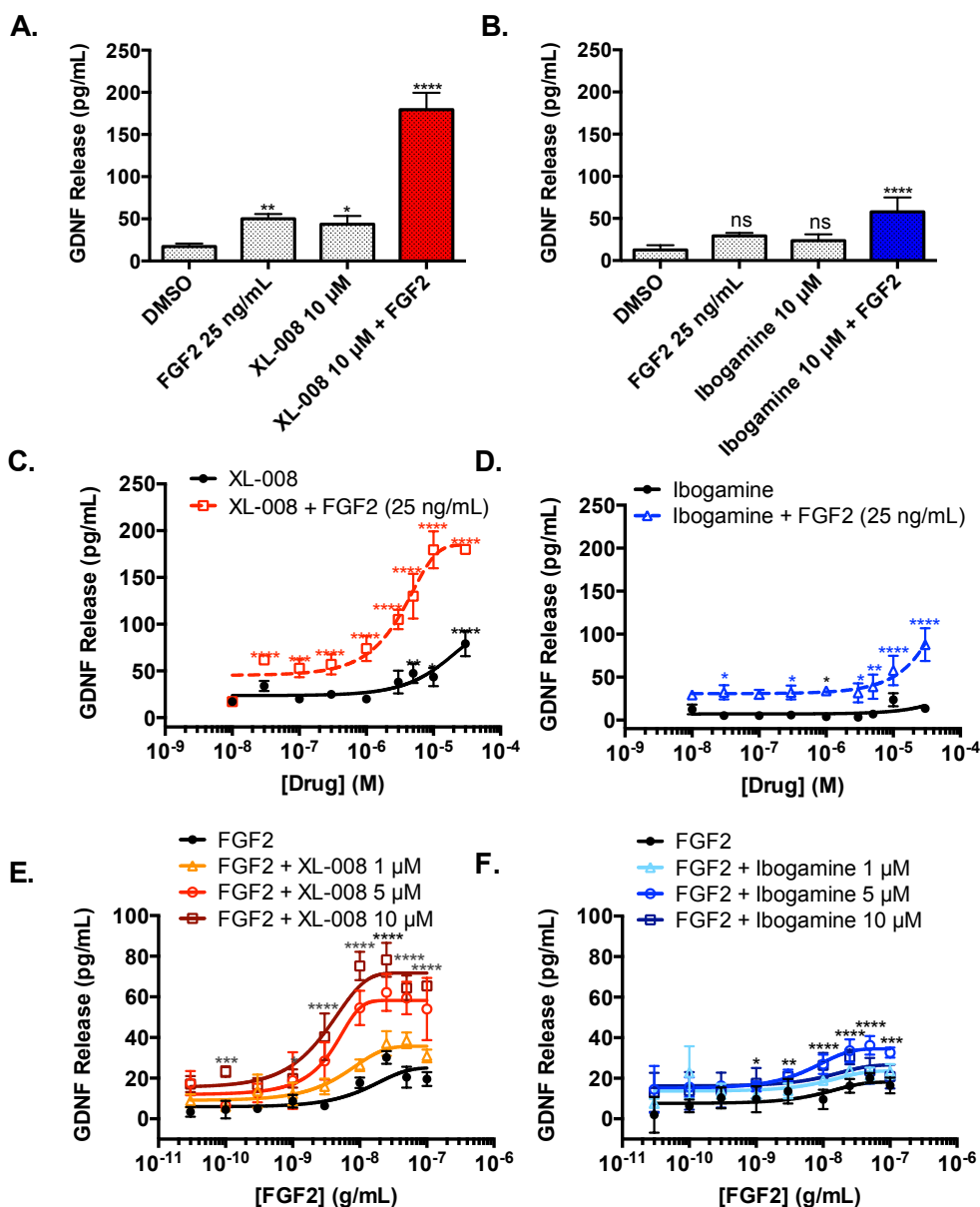


Figure 5. FGF2-Induced GDNF Release in C6 Cells is Potentiated by *Iboga* Analog XL-008. A. Fibroblast growth factor 2 (FGF2)-induced GDNF release is greatly enhanced by XL-008 in C6 cells after a 24-hour treatment time. B. Ibogamine gives much smaller induction effect in comparison to XL-008. C. FGF2 (25 ng/mL) potentiates the dose response of XL-008 from an EC₅₀ > 15 μ M to $6.17 \pm 2.40 \mu$ M ($n=4$). D. This effect is only additive on the dose response of ibogamine. E. The dose response curve of FGF2 is potentiated by XL-008 in a dose-dependent manner. F. The effect on FGF2 curve is less pronounced in the presence of ibogamine. Data represent mean \pm SD of biological replicates in one experiment from $n > 4$ independent experiments. One-way ANOVA with Dunnett's Multiple Comparisons Test are shown (* $p < 0.05$, ** $p < 0.01$, *** $p < 0.001$, **** $p < 0.0001$).

approximate EC₅₀ that has been used for comparative purposes. Interestingly, FGF2's effects on the GDNF release from ibogamine were subtler. In contrast to XL-008, ibogamine trends towards GDNF release but does not reach statistical significance. However, in the presence of FGF2, the GDNF release from ibogamine did increase in a statistical manner, but these effects only added to the efficacy of this release rather than potentiating it, as in the case of XL-008 (**Figure 5D**).

Table 1. Summary of GDNF Release Data

Treatment	EC ₅₀
Ibogamine	NS
Ibogamine + FGF2 (25 ng/mL)	>15 μM
XL-008	>15 μM
XL-008 + FGF2 (25 ng/mL)	6.17 ± 2.40 μM
FGF2	7.85 ± 2.59 ng/mL (0.482 ± 0.159 nM)
FGF2 + Ibogamine 1 μM	6.87 ± 2.08 ng/mL (0.422 ± 0.128 nM)
FGF2 + Ibogamine 5 μM	6.24 ± 2.88 ng/mL (0.383 ± 0.177 nM)
FGF2 + Ibogamine 10 μM	4.15 ± 2.22 ng/mL (0.255 ± 0.136 nM)
FGF2 + XL-008 1 μM	6.87 ± 3.00 ng/mL (0.422 ± 0.184 nM)
FGF2 + XL-008 5 μM	4.45 ± 2.68 ng/mL (0.273 ± 0.165 nM)
FGF2 + XL-008 10 μM	3.31 ± 0.98 ng/mL* (0.203 ± 0.060 nM)

*One-way ANOVA with Tukey's Multiple Comparisons Test shows
* p < 0.01 for FGF2 + XL-008 10 μM when compared to FGF2 alone.
NS means "not significant." GDNF, glial cell line-derived neurotrophic factor; FGF2, fibroblast growth factor 2.

To explore this potentiation further, the potency of FGF2-induced GDNF release was then measured in the presence of a range of concentrations of both ibogamine and XL-008. The potency of FGF2-induced GDNF release increased by more than 2-fold when co-incubated with XL-008, from an EC₅₀ of 7.85 ± 2.59 ng/mL to 3.31 ± 0.98 ng/mL with

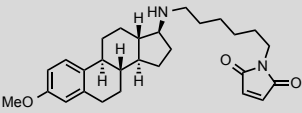
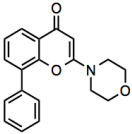
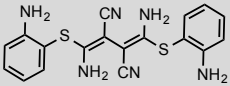
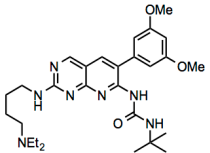
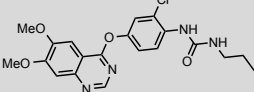
10 μM XL-008 (**Figure 5E**). Statistical analysis with Tukey's multiple comparisons test showed that this change in potency was statistically significant when compared to the EC₅₀ of FGF2 alone (**Table 1**, * p < 0.01). In the presence of lower concentrations of XL-008, the shift in the potency can still be seen; for instance, 5 μM XL-008 shifts the EC₅₀ to 4.45 ± 2.68 ng/mL. Similar to the previous experiments, the effect is much lower with ibogamine. When lower concentrations of ibogamine are tested, such as 1 and 5 μM, there is little effect on the FGF2-

induced GDNF release. Instead, there is a little increase in GDNF release by a 10 μ M co-treatment of ibogamine, which shifts the EC_{50} to 4.15 ± 2.22 ng/mL (**Figure 5F**). Unlike the potency shift with XL-008, this shift in potency is not statistically significant, which is an indication of the superiority of XL-008 as a potentiator of GDNF release by FGF2. The results of **Figure 5** are summarized in **Table 1**.

Understanding the Signaling Pathways Involved in FGF2-Induced GDNF Release. An important next step in studying this novel potentiation of FGF2-induced GDNF release from C6 cells was to explore the mechanism of action. Initially, there was a serious push made to try and study the signal transduction pathways of GDNF release using conventional methods. To start, the ERK1/2 pathway and RET, the kinase involved in GFR α 1 activation, were probed using traditional western blotting techniques. Unfortunately, because this glioma cell line is tumorigenic in nature, it is likely that many of the receptors are overexpressed, which leads to increased basal levels of ERK1/2. Therefore, using a western blot to quantify these critical signaling events remained challenging as the basal levels of ERK1/2 activation in western blotting were high. Furthermore, we observed that the ERK1/2 pathway was extremely sensitive to movement, temperature, and even the vehicle control DMSO, which only further obscured any ERK1/2 or RET activation that might have otherwise been observed using western blot. Taken together, we decided to explore instead more sensitive techniques for measuring signaling pathway activation, including cell-based enzyme-linked immunosorbent assay (ELISA) for measuring both ERK1/2 and AKT phosphorylation. Again, the high levels of basal kinase activation were problematic to our studies, making it impossible to glean meaningful information about the signaling events. Instead the pathway for potentiation had to be studied through more indirect methods.

In an attempt to instead pharmacologically block the signaling pathways involved in the XL-008-induced GDNF release, small molecule inhibitors were utilized. The three major pathways of signal transduction, protein kinase B (PKB or Akt), mitogen-activated protein kinase (MAPK), and protein kinase C (PKC), each have well-studied inhibitors that can be used

Table 2. Pharmacological Inhibitors of GDNF Release

Inhibitor	Structure	Target
U73122 ^{21,37}		PLC γ
LY294002 ^{36,38}		PI3K
U0126 ^{26,37}		MEK-1/2
PD173074 ³⁹⁻⁴¹		FGFR-1, FGFR-3
KRN633 ^{37,42}		VEGFR, PDGFR

for blocking activation through these proteins.⁴³

In order to inhibit the Akt, MAPK, and PKC pathways, the

phosphatidylinositol-4,5-bisphosphate 3-kinase (PI3K) inhibitor

LY294002 (20 μ M),^{36,38}

the mitogen-activated protein kinase kinase

(MEK1/2) inhibitor

U0126 (10 μ M),^{26,37} and

the phospholipase C (PLC- γ) inhibitor U73122 (2 μ M)^{21,37} were used. Additionally, given that the potentiation results require FGF2, it was important to study whether the whole FGF2 family was involved, using the FGFR inhibitor PD173074 (1 μ M)³⁹⁻⁴¹. Further, other growth factor-activated RTKs could be involved in the potentiation effects and were therefore also probed. The inhibitor KRN633 (1 μ M)^{37,42} targets both the platelet-derived growth factor receptor (PDGFR) and the vascular endothelial growth factor receptor (VEGFR) and was used in these experiments

to study the involvement of transactivation in the GDNF signaling. The structures and targets of the inhibitors used are summarized in **Table 2**.

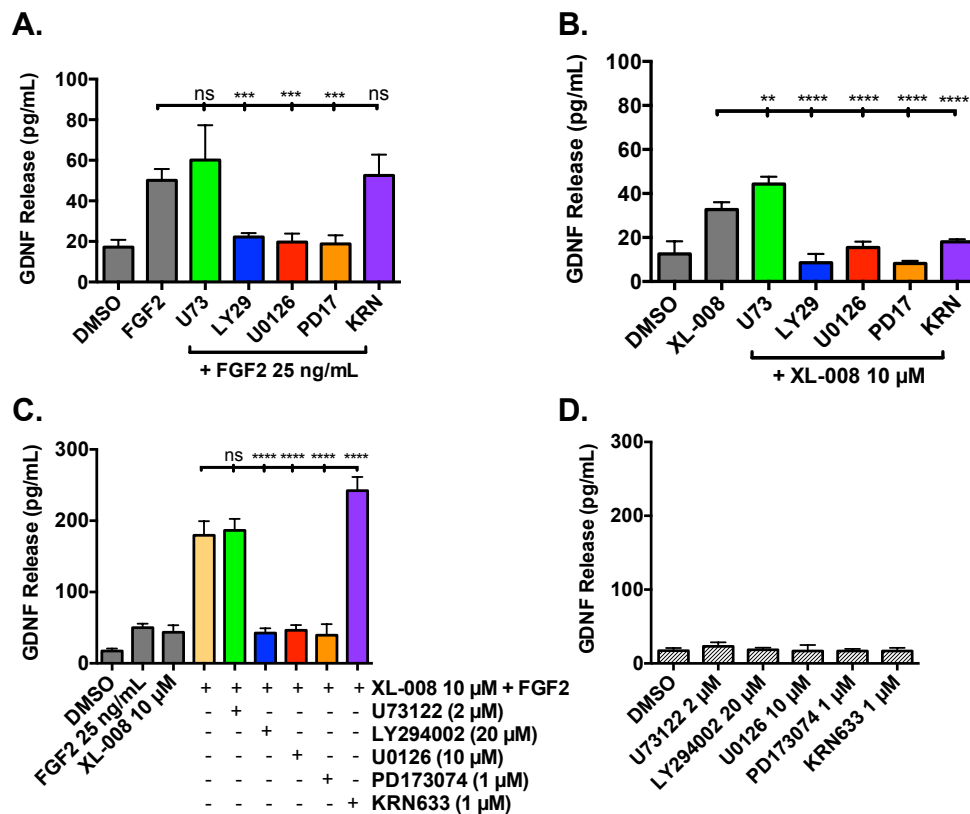


Figure 6. Potentiation of FGF2-Induced GDNF Release by *Iboga* Analogs is Pathway Specific. A. The GDNF release by FGF2 in C6 glioma cells after 24 hours is mediated by the phosphatidylinositol-4,5-bisphosphate 3-kinase (PI3K) and mitogen-activated protein kinase (MAPK) pathways. Pretreatment of cells with inhibitors for 1 hour (30 minutes for U0126, as reported³⁹) indicates involvement of PI3K (LY294002, 20 μM), MAPK (U0126, 10 μM), and fibroblast growth factor receptor (FGFR) (PD173074, 1 μM) pathways but not the phospholipase C (PLCγ) (U73122, 2 μM) and platelet-derived growth factor receptor/vascular endothelial growth factor receptor (PDGFR/VEGFR) (KRN633, 1 μM) pathways. B. The GDNF release by XL-008 in C6 glioma cells after 24 hours shows similar pathway activation as that seen from FGF2 alone with the exception of some inhibition by PDGFR/VEGFR inhibitor KRN633. C. The GDNF release by XL-008/FGF2 in C6 glioma cells after 24 hours shows similar pathway activation to that seen from FGF2 alone. D. No GDNF release is observed in the presence of the inhibitors alone in C6 glioma cells after 24 hours. Data represent mean ± SD of biological replicates in one experiment from n = 9 independent experiments. One-way ANOVA followed by Dunnett's Multiple Comparisons Test is shown (** p < 0.01, *** p < 0.001, **** p < 0.0001).

When these inhibitors were used in the GDNF release experiments, they helped to identify that the FGF2-induced GDNF release alone was dependent on the AKT and MAPK

pathways but not the PKC pathway (**Figure 6A**). These results match with studies that were previously reported.^{22,36,37} In addition, this GDNF release depended upon FGFR but not PDGFR or VEGFR, which did confirm the selectivity of the inhibitors used. The GDNF release from XL-008 alone shows similar trends in comparison to FGF2 with the interesting exception that the GDNF release from XL-008 does show some dependence on the PDGFR and VEGFR pathways (**Figure 6B**). These data do suggest that the mechanism of GDNF release from XL-008 may be unique when compared to that of FGF2. The potentiation of FGF2 by XL-008 was importantly noted to be dependent upon the same pathways as FGF2 alone (**Figure 6C**). Even though the exact target responsible for this XL-008-induced GDNF release is unclear, it is obvious that FGFR is involved in the potentiated GDNF release. To be sure that the inhibitors not were confounding the experiments in any way, the GDNF release induced by the inhibitors alone was measured. None of the inhibitors tested released any statistically significant amount of GDNF when compared to the DMSO vehicle control (**Figure 6D**).

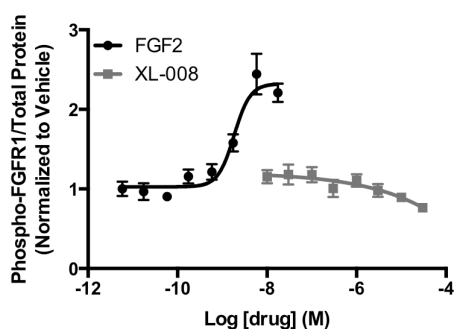


Figure 7. XL-008 Does Not Activate FGFR1 in FGFR1-HEK Cells. FGFR1-HEK were treated with FGF2 or XL-008 for 1 hour. Cell lysate was analyzed using sandwich-style ELISA for detection of phosphorylated receptor. Treatments were normalized to total protein using the BCA assay. Data represent mean \pm SD of biological replicates in one experiment from $n = 3$ independent experiments.

To explore the direct involvement of the FGFR system in this mechanism, the ability of XL-008 to directly activate FGFR1 (fibroblast growth factor receptor 1) was measured. Using a sandwich-style ELISA (see Chapter 7), XL-008 was unable to phosphorylate the FGFR1 (a measure of RTK activation) at any concentration up to 30 μ M (**Figure 7**). Additionally, as a reliable modulator of one growth factor system, it was imperative to determine whether XL-008 was able to cause release of FGF2 in

the same cellular system. Increased levels of FGF2 may be responsible for the potentiation observed as more FGF2 in the system could consequently lead to more GDNF release. XL-008 was unable to cause any measurable release of FGF2 in C6 cells using an ELISA for detecting FGF2 levels (**Figure 8**), indicating that the direct molecular target of the XL-008-induced GDNF may not be FGFR1 itself.

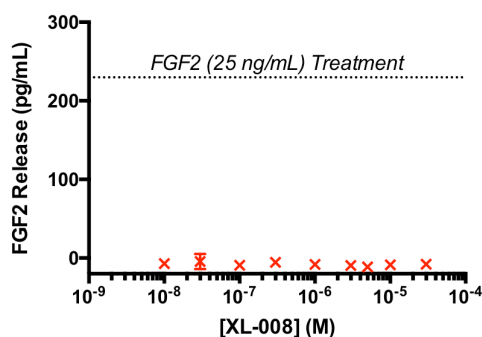


Figure 8. FGF2 Release from XL-008 in C6 Cells. *Iboga* alkaloid analog XL-008 does not cause statistically significant release of FGF2 after 24 hours as measured using an ELISA for FGF2 detection. Data represent mean \pm SD of biological replicates in one experiment from $n = 3$ independent experiments.

Cell Viability and Toxicity Effects From

Treatment with XL-008 and FGF2. Given the known protective and proliferative effects for FGF2 alone, there was motivation to confirm whether the potentiation of FGF2-induced GDNF release also retained some of these same cellular effects. Therefore we carefully analyzed any trends between GDNF release and cytotoxicity in the 24-hour release experiments.

Two different measurements of cell viability were performed to provide a thorough understanding of any possible cytotoxic effects from drug treatments. LDH is an enzyme found in the cytosol of cells that is released upon their lysis, or bursting. Assays available today allow for the simple colorimetric detection for measuring the amount of LDH present in conditioned media, which correlates well with cell membrane integrity and therefore with cell health.⁴⁴ Another assay for the measurement of cell viability is the WST-1 cell assay, which uses a formazan dye to colorimetrically detect intact, metabolizing mitochondria, another indication of cell viability.⁴² Together, these assays were used to identify the cytotoxic effects, if any, occurring either independently or as a result of GDNF release.

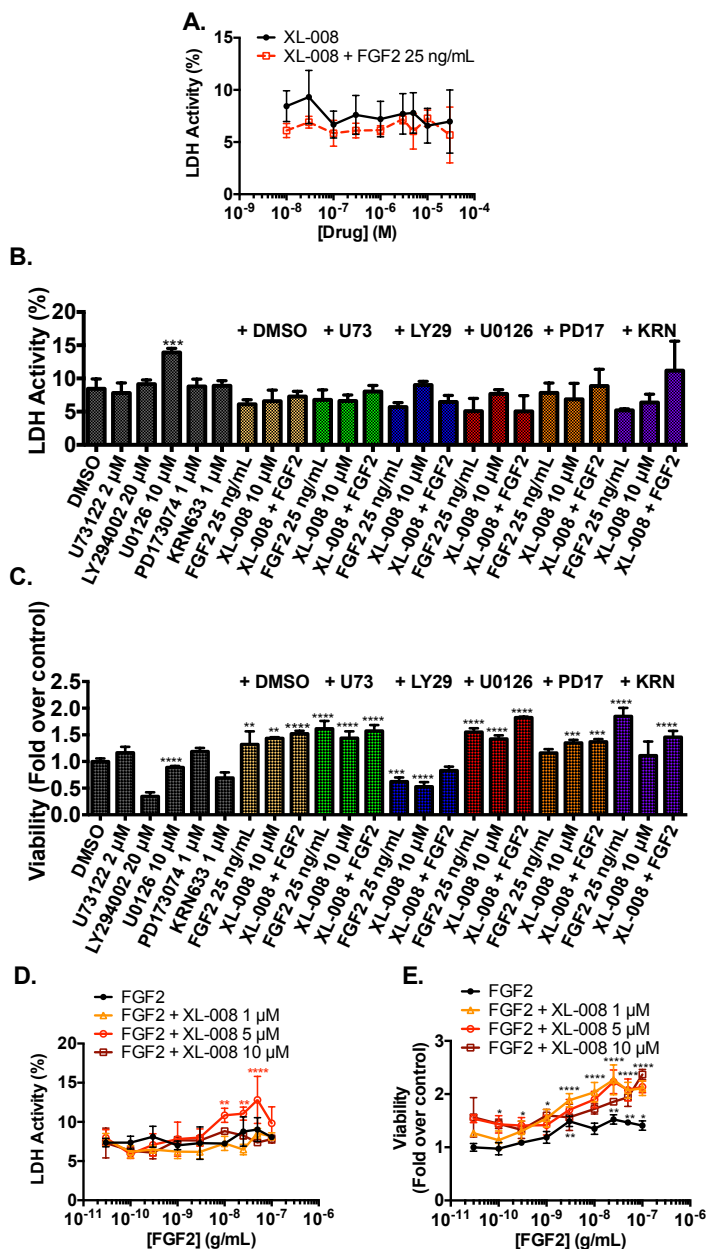


Figure 9. Cell Viability and Cytotoxicity Studies. Potentiation of FGF2-induced GDNF release by XL-008 also shows cell viability enhancing effects and little to no cytotoxicity as measured by lactate dehydrogenase (LDH) release and cell viability assays. A. LDH release after 24 hours of XL-008 in the presence of FGF2 (25 ng/mL) reveals no cytotoxic effects when compared to the DMSO vehicle control. B. LDH release in the presence of XL-008/FGF2 and the kinase inhibitors also indicates no cytotoxic effects, with the exception of a small LDH release in the presence of ERK inhibitor U0126 alone. C. Cell viability measurement by tetrazolium (WST-1) assay shows minor cytotoxic effects in the presence of kinase inhibitors. D. LDH release of varying concentrations of FGF2 in the presence of XL-008 is increased only at higher concentrations of FGF2/XL-008 potentiation mixtures. E. Cell viability as measured by the WST-1 assay reveals no cytotoxic effects from the 24-hour treatment at increasing concentrations of FGF2/XL-008, where cell viability and metabolism is increased (nearly two-fold). Data represent mean \pm SD of biological replicates in one experiment from $n > 4$ independent experiments. One-way ANOVA followed by Dunnett's Multiple Comparisons Test is shown (* $p < 0.05$, ** $p < 0.01$, *** $p < 0.001$, **** $p < 0.0001$).

After a 24-hour treatment in C6 cells, there were no obvious cytotoxic effects from increasing concentrations of XL-008 in the presence or absence of FGF2 (25 ng/mL) as measured by LDH release (**Figure 9A**). Based on these results, there does not appear to be any correlation between GDNF release and cytotoxicity using the 24-hour experimental conditions, in contrast to the 48-hour treatment (see **Figure 3**). Additionally, the use of the selected inhibitors with FGF2, XL-008, or FGF2/XL-008 resulted in no cytotoxicity as measured by LDH

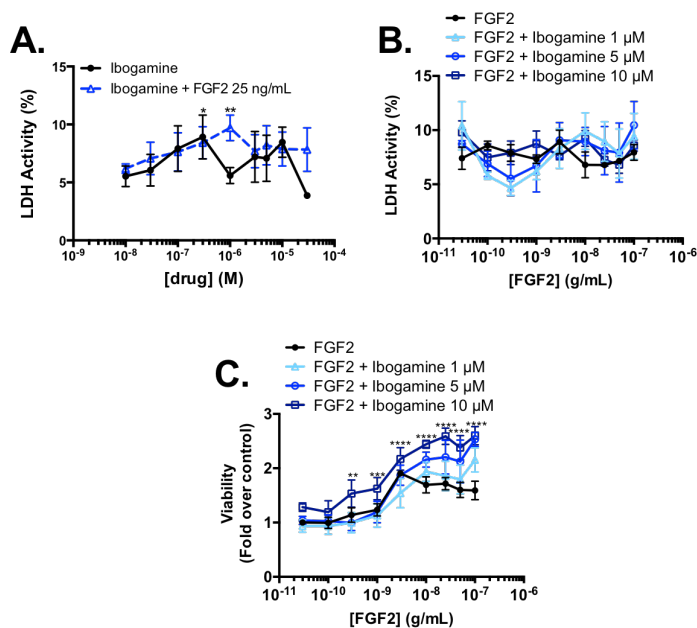


Figure 10. Cytotoxicity Effects From GDNF Release. GDNF release from FGF2 and ibogamine shows little to no effect on cytotoxicity as measured by lactate dehydrogenase (LDH) release and cell viability assays. (A) LDH release after 24 hours of ibogamine in the presence of FGF2 (25 ng/mL) reveals few cytotoxic effects when compared to the DMSO vehicle control. (B) LDH release of varying concentrations of FGF2 in the presence of ibogamine demonstrates no toxicity. (C) Cell proliferation as measured by the WST assay reveals no cytotoxic effects from the 24-hour treatment at increasing concentrations of FGF2/ibogamine, where cell proliferation and metabolism is greatly increased. Data represent mean \pm SD of biological replicates in one experiment from $n = 4$ independent experiments. Results from One-way ANOVA followed by Dunnett's Multiple Comparisons Test are shown (* $p < 0.05$, ** $p < 0.01$, **** $p < 0.0001$).

release (**Figure 9B**). The only treatment to sometimes cause statistically significant release of LDH when compared to DMSO was the addition of inhibitors alone, as seen for inhibitor U0126. This observation highlights the protective effects of FGF2/XL-008 as their addition to cytotoxic inhibitors resulted in reduced toxicity. Similar experiments were performed with the WST-1 assay. The LDH results were supported in the WST-1 assay (**Figure 9C**), which show that, in general, treatments caused

increased metabolism, a measure of cell viability, which was statistically significant when compared to DMSO. This increased metabolism was consistent with increased production of GDNF. The only exception noted was with the PI3K/AKT inhibitor LY294002 pre-treatment, which consistently reduced cell viability. Since this pathway is well-known to mediate cell survival and proliferation,^{45,46} it was not surprising that the inhibitor LY294002 would cause reduced cell viability. Similar results were obtained in the treatments with ibogamine (**Figure 10**).

To explore the mechanism of increased cell viability further, the treatments were measured for their ability to cause cell proliferation using bromodeoxyuridine (BrdU) incorporation. The actual levels of proliferation in the cells for any treatment tested did not increase, which indicates that the increases in cell viability observed were independent of proliferation and likely occur via a metabolism-boosting effect (**Figure 11**). The LDH release and cell viability were additionally measured for the dose response of FGF2 in the absence or presence of increasing concentrations of XL-008. As predicted, the LDH release showed few cytotoxic effects under these treatment conditions (**Figure 9D**). The only exception was the highest concentrations of FGF2 in the presence of XL-008, which only occasionally resulted in elevated LDH levels in some experiments. In comparison to the 48-hour treatments, however, these “toxic” treatments showed a much lower LDH release (~12% LDH activity at 24 hours compared to >30% at 48 hours). The WST-1 assay additionally showed that cell viability was enhanced with increasing concentrations of both FGF2 and XL-008 (**Figure 9E**), suggesting that perhaps the combined treatment of FGF2 with XL-008, in fact, stimulates cell viability and metabolism at every concentration tested. These data indicate that these experimental conditions are likely protective to the cells. XL-008 also enhanced the viability effects of FGF2, even at

concentrations where FGF2 alone had no visible effect (sub-nanomolar concentrations, **Figure 9E**), consistent with the potentiation of GDNF release. From this perspective, XL-008 potentiates not only the release of FGF2-induced GDNF release but also the cell viability as a distinct cellular readout. The viability effects in this assay were dependent on the PI3K/AKT pathway (**Figure 9C**). However, in the 48-hour treatment experiments, the cytotoxic effects correlated closely with trends in GDNF release as measured by LDH release (**Figure 3**), which highlights the use of the 24-hour treatment time in these measurements.

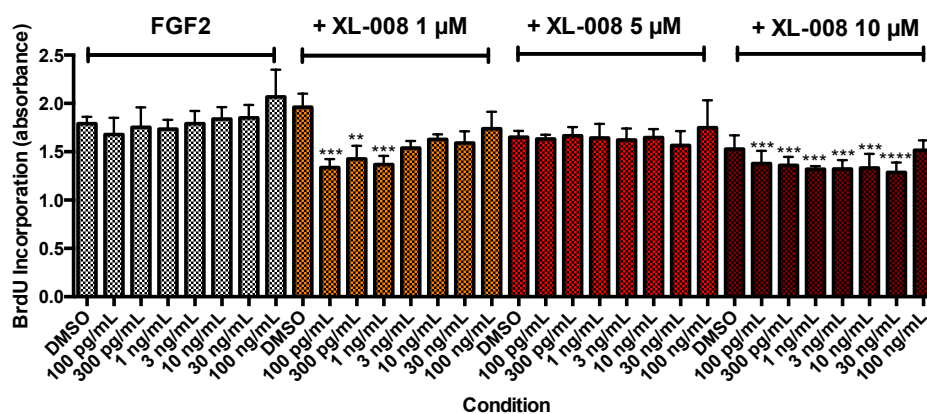


Figure 11. Bromodeoxyuridine (BrdU) Incorporation in C6 Cells. Cell proliferation was assessed by measuring BrdU incorporation in C6 cells after a 24-hour treatment with FGF2 and XL-008 using a commercially available ELISA for detection (Roche #11647229001). The co-treatment of XL-008 with increasing concentrations of FGF2 does not cause increased proliferation during this treatment time. Data represent mean \pm SD of biological replicates in one experiment from $n = 3$ independent experiments. Results from One-way ANOVA followed by Dunnett's Multiple Comparisons Test are shown (** $p < 0.01$, *** $p < 0.001$, **** $p < 0.0001$).

Discussion

Mechanism of Action. A proposed model for the mechanism of FGF2-induced GDNF release from C6 cells is depicted in **Figure 12**. Based on the data, XL-008 likely acts through some target that can either amplify the signaling events of FGF2 directly, which leads to increased GDNF production, or it transactivates FGFRs to increase the GDNF production through the pathways described. There are known examples of transactivation in the context of GDNF signaling. For instance, 5-HT₂R-mediated FGFR2 transactivation as been reported to

induce GDNF mRNA expression in C6 cells, leading to higher levels of GDNF.³⁷ Additional studies have connected a mu-opioid receptor-mediated transactivation of FGFRs in C6 cells, implicating many possibilities for this hypothesis.⁴⁷ Transactivation of FGFRs is a plausible suggestion in understanding this mechanism, based on the evidence provided here. The FGFR

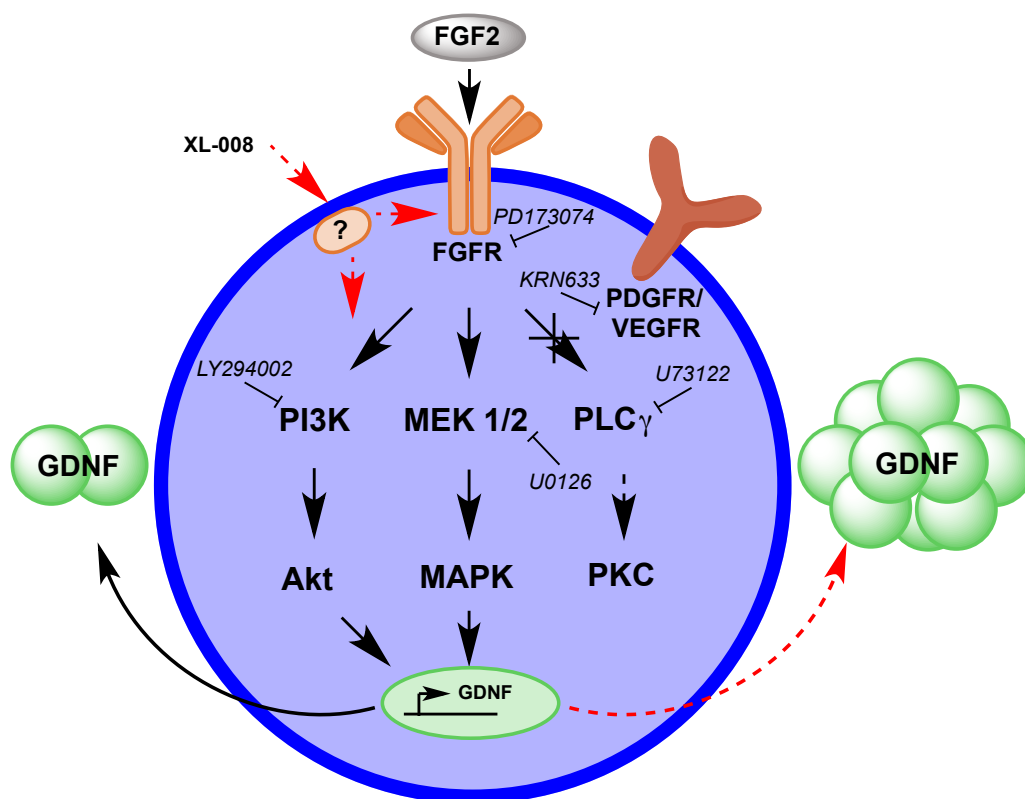


Figure 12. Schematic representation of signaling pathways involved in potentiation of FGF2-induced GDNF release by XL-008. Pharmacological inhibition of XL-008/FGF2 reveals pathway specificity through MAPK and AKT.

inhibitor PD173074 was able to fully block the GDNF release of XL-008 on its own (**Figure 6B**), which ultimately makes transactivation of FGFRs by XL-008 a potential mechanism for the increased production of GDNF. It is also possible that direct activation of FGFRs rather than transactivation leads to the observed changes in GDNF release. Again, the inhibition of XL-008 by PD173074 would support this conclusion. However, as further indication of a direct involvement of FGFR activation, XL-008 was assessed for its ability to phosphorylate FGFR1

(**Figure 7**). Since XL-008 was unable to phosphorylate the RTK at any concentration tested, it therefore is unlikely to be a small molecule agonist of the receptor. Furthermore, as XL-008 did not cause release of FGF2 itself (**Figure 8**), there is little indication that the FGF system plays a significant role in the mechanism of XL-008-induced potentiation of GDNF signaling. Although the direct target of XL-008 is still unclear, the data presented rule out direct action of the FGFRs, indicating that the direct molecular target is most likely downstream of FGFR1.

Difficulty in Working with C6 Cells. C6 glioma cells are a popular *in vitro* model of glial cells that have been used in thousands of publications. In the context of GDNF signaling, C6 cells are often the gold standard for *in vitro* measurements, cited in dozens more studies alone. It was therefore an obvious choice for setting up GDNF detection experiments to evaluate our compounds. With careful experimental optimization, we were able to find reproducible results in the GDNF measurements (see **Experimental**). However, the difficulty encountered in obtaining meaningful signaling results in C6 cells certainly brings into question the use of these cells as a model system. For measuring acute signaling events, we found the C6 cells to be nearly impossible to use, consistently showing high basal levels of the protein targets that obscured important results. Replicating these studies in a better cellular system, such as primary neuronal culture or tissue, would provide more meaning to the results and confirm the findings in a broader context. Certainly measuring the potentiation effects would be fascinating to study *in vivo* and would highlight these targets further for therapeutic use.

Use of Pharmacological Inhibitors. Although more direct signaling studies in the C6 cells were preferable, the small molecule inhibitors used to probe the major signaling pathways of GDNF production provided the necessary insight to uncover a model for the mechanism of XL-008-induced potentiation of GDNF release. In order for these results to be meaningful, it was

necessary to strategically choose pharmacological inhibitors that were selective to each particular pathway at the concentrations employed. It is notoriously difficult to find inhibitors that are truly selective for one pathway/target over another. One recent publication thoroughly examined the selectivity of a large selection of protein kinase inhibitors, including those used in this study.⁴³ Researchers used a panel of 70-80 protein kinase targets to assess inhibitors for their selectivity. U0126, the inhibitor of the MAPK pathway, was confirmed as being selective. LY294002, on the other hand, did have some noticeable off-target activity at some proto-oncogene kinases, including PIM1 and PIM3. Despite this undesired activity, LY294002 still is assessed as the better Akt inhibitor over the widely used small molecule wortmannin, which is unsuitable for longer experiment durations such as those used here. Given the confirmed selectivity of these inhibitors, we are confident of the involvement of the MAPK and AKT pathways in the observed signaling in the GDNF release.

Conclusions

The modulation of growth factor synthesis and release (and/or potentiation of growth factor signaling) by a small molecule presents a novel approach for treating neurological, neurodegenerative and psychiatric disorders.^{24,25} Throughout this chapter, we have shown that the deconstructed *iboga* analog XL-008 is able to increase GDNF release on its own in the well-established glial cell model, as well as potentiate the FGF2-induced GDNF release. In an independent cellular phenotype readout, the potentiation of the FGF2 signaling was also confirmed via increased cell viability. Although the exact molecular target for XL-008 remains unidentified, we were able to isolate the key kinase signaling pathways involved in the potentiation of GDNF release and cellular viability using pharmacological kinase inhibitors. XL-

008 also does not activate FGFR1, as demonstrated through the use of ELISA for receptor phosphorylation and FGFR1 inhibitors, consistent with a mechanistic model where XL-008 acts downstream of FGFR1. The downstream effects of FGF2-induced signaling are well-known to be connected with many desirable physiological, cellular, and behavioral outcomes, including modulating neuronal spiking dynamics, inducing neurogenesis, and exerting antidepressant and anxiolytic effects.^{12,48} Therefore, the identification of a small molecule modulator that potentiates FGF2 signaling is relevant to the search for new therapeutic leads. As we move forward, a full examination will take place of this interesting new *iboga* analog and related compounds in brain tissue and *in vivo*.

Experimental

Chemical synthesis of XL-008, ibogamine, and CY-XL-008 was carried out as reported previously.³¹

Reagents. Recombinant rat fibroblast growth factor basic (FGF2, 400-29) was purchased from Peprotech. Protease inhibitor cocktail (P8340) and phosphatase inhibitor cocktail 2 (P5726) were purchased from Sigma Aldrich. KRN633 was purchased from Selleck Chemicals, LY294002 was purchased from Cayman Chemical Company, PD173074 was purchased from Biotang, Inc, U0126 was purchased from Alfa Aesar, and U73122 was purchased from MP Biomedicals, LLC.

Cell Culture. Rat C6 glioma cells were purchased from the American Type Culture Collection (CC-107) and maintained in Dulbecco's Modified Eagle Medium (Life Technologies; 10569) with 5% (v/v) fetal bovine serum (FBS, Atlanta Biologicals) and 100 U mL⁻¹ of penicillin and streptomycin (Life Technologies). Cells were incubated at 37 °C with 5% CO₂ humidified

atmosphere. The GDNF release in C6 cells is highly variable from one experiment to another and even from one passage to the next. Additionally, as a glioma cell line, C6 cells are highly susceptible to phenotypic drift, which can lead to varying expression levels of receptors and growth factors of interest. For the purposes of these experiments, it was found that if the C6 cells were maintained and used between a strict set of passages, experiments (though variable), provided reliable trends in GDNF release that were highly reproducible. Therefore, all data presented here show a single representative experiment of many independent replicate trials. C6 glioma cells were used between passages 41–42.

GDNF Release Experiments. Into a 96-well plate were added C6 cells at a density of 25,300 cells/well in full growth medium (see above). Cells were allowed to adhere for 24 h at 37 °C. Cells were then serum-starved with media containing 0.5% FBS (low serum) for an additional 24 h. Low serum media was refreshed prior to starting the experiment. Compounds were added in 50 µL of low serum media to obtain a final volume of 200 µL/well. All inhibitors were added for 1 hour in advance with the exception of U0126, which was pretreated for 30 minutes, as reported.³⁹ Treatments were performed in quadruplicate. Cells were incubated at 37 °C for 24 hours. Experiments were terminated by removing the conditioned media from each well and storing at –80 °C until analyzed. GDNF was detected using a standard sandwich-style ELISA kit purchased from Promega Corporation following the manufacturer's instructions. Briefly, monoclonal anti-GDNF antibodies were captured onto a 96-well Nunc Immulon Immunoassay plate at a dilution of 1:1000 in carbonate coating buffer (25 mM sodium bicarbonate, 25 mM sodium carbonate, pH 8.2) overnight at 4 °C. After removing the monoclonal antibody, wells were blocked with 1X Block and Sample Buffer for 1 hour at room temperature (200 µL/well). A GDNF standard curve was created by serially diluting the

recombinant human GDNF standard in 1X Block and Sample Buffer to a concentration range of 0–1000 pg mL⁻¹. To each sample well was added 100 µL of conditioned media from above and the standard curve (in duplicate), and plates were incubated for 6 hours with shaking at room temperature. After washing five times with TBST (150 mM sodium chloride, 10 mM Tris-HCl, 10 mM Tris base, 0.05% Tween 20, pH 7.6), wells were incubated with anti-human polyclonal GDNF antibodies (1:500) in 1X Block and Sample Buffer overnight at 4 °C. Following an additional five washes with TBST, wells were incubated with anti-chicken IgY-HRP conjugate antibody (1:250) for 2 hours with light shaking. After a final five washes, TMB One (100 µL/well) was added to each well and allowed to develop in the absence of light until there were clear differences in color between the highest and lowest concentrations of the standard curve. Wells were then quenched with 1 M HCl (100 µL/well), and the plates were read at an absorbance wavelength of 450 nm using a BioTek Synergy H1 plate reader.

LDH Cytotoxicity Assay. The lactate dehydrogenase cytotoxicity assay (Promega) was performed following the manufacturers instructions. Briefly, following compound treatment, conditioned media was removed, and untreated wells were washed twice with phosphate buffered saline. To untreated wells was added 40 µL of low serum media supplemented with lysis buffer provided in the kit (1:10), protease inhibitor cocktail (1:100), and phosphatase inhibitor cocktail 2 (1:100). Cells were lysed at 37 °C for 1 hour. Cell lysates were diluted with 160 µL of conditioned media and used as 100% cytotoxicity in the LDH standard curve. Lysates were serially diluted down to 6.25% cytotoxicity with low serum media filling the last. The standard curve was added in duplicate to a 96-well plate followed by the conditioned media from each treated well at 50 µL/well. To each well was added 50 µL of the reconstituted Substrate Mix, and the plates were allowed to develop in the dark until differences were seen in the

standard curve. The wells were quenched with 50 μL of Stop Solution, and the plates were read at an absorbance wavelength of 490 nm.

WST-1 Cell Viability Assay. After compound treatment, conditioned media was removed and replaced with 75 μL of warm low-serum media. To each well was added 5 μL of WST-1 Cell Proliferation Reagent (Roche Applied Science), and the cells were incubated at 37 $^{\circ}\text{C}$ for no more than 1 hour. Plates were briefly shaken prior to reading the absorbance at 450 nm. Treatments were compared to vehicle control.

FGFR1 Phosphorylation ELISA. FGFR1-HEK were grown in DMEM supplemented with 10% FBS, 100 U mL^{-1} of penicillin and streptomycin, and 200 $\mu\text{g}/\text{mL}$ G418. Cells were added to a collagen-coated 96-well plate at 40,000 cells/well and allowed to grow for 24 hours. The cells were then starved with low serum media (1% FBS supplement instead) for 5 hours before treatment with drugs for 1 hour. The experiment was stopped on ice by aspirating the cellular supernatant and adding 110 μL of lysis buffer (1% TritonX-100, 10% glycine, and 2 mM EDTA in TBS, pH 8.0 with 1:100 protease inhibitor cocktail and 1:100 phosphatase inhibitor cocktail 2) before storing at -80 $^{\circ}\text{C}$. A separate 96-well plate (Nunc Immulon) was coated with primary FGFR1 antibody (Sigma Aldrich # WH0002260M3) at 1 $\mu\text{g}/\text{mL}$ in PBS and stored overnight at 4 $^{\circ}\text{C}$. The plate was then washed 5X with TBST and blocked (1% BSA in PBS) for 1 hour at room temperature. The plate was washed again 5X with TBST, and 80 μL of the thawed cell lysate was transferred to the 96-well ELISA plate and stored overnight at 4 $^{\circ}\text{C}$. The remaining 20 μL of cell lysate was used for protein quantification in the BCA assay. The plate was then washed again 5X with TBST and incubated with secondary anti-phospho tyrosine-HRP antibody (R&D Systems #HAM1676) at 1:2500 (in 0.05% Tween-20, 0.1% BSA in TBS, pH 7.4). The plate was washed a final 5X with TBST and developed using TMBone (100 $\mu\text{L}/\text{well}$)

for 30 minutes in the absence of light. Wells were then quenched with 1 M HCl (100 μ L/well), and the plates were read at an absorbance wavelength of 450 nm using a BioTek Synergy H1 plate reader. Raw data were quantified as the phospho-FGFR1 signal divided by the total protein content for each well.

FGF2 Release Experiments. Cells were treated according to the same procedure as for measuring GDNF release (see above). FGF2 release was measured using a commercially available ELISA according to the manufacturer's protocol (R&D Systems #DY23305). Briefly, the human FGF2 capture antibody was diluted in PBS (2 μ g/mL) and added to the 96-well plate provided with the kit at 100 μ L/mL. The plate was sealed and stored overnight at 4 °C. The plate was then washed 3X with the wash buffer (0.05% Tween-20 in PBS, pH 7.2-7.4) and blocked at room temperature for 1 hour with 300 μ L/well of reagent diluent (1% BSA in PBS, pH 7.2-7.4). The plate was washed again 3X. A standard curve was made with the human FGF2 standard provided in a concentration range of 15.6 – 1000 pg/mL, diluted in reagent diluent. The standard curve or experimental supernatant were added to the wells (100 μ L) and incubated at room temperature for 2 hours. The wells were then aspirated and washed 3X as before. Next, the detection antibody was diluted in reagent diluent (0.25 μ g/mL) and added to each well (100 μ L/well) for 2 hours at room temperature. The wells were then washed again. The streptavidin-HRP antibody was diluted in reagent diluent (1:40 dilution) and added to each well (100 μ L/well) for 20 minutes at room temperature in the absence of light. The plate was then washed again. Substrate solution (1:1 mixture of Color Reagent A (H_2O_2) and Color Reagent B (tetramethylbenzidine)) was added to each well (100 μ L/well) for 20 minutes at room temperature in the absence of light. The reaction was quenched by adding Stop Solution (2 N

H₂SO₄) to each well (50 µL/well), and the plates were read at an absorbance wavelength of 450 nm using a BioTek Synergy H1 plate reader.

BrdU Incorporation Assay. Cells were treated according to the same procedure as for measuring GDNF release (see above). BrdU incorporation was measured using a commercially available kit according to the manufacturer's protocol (Roche Life Sciences #11647229001). Briefly, after a 24-hour treatment with specified drugs, the BrdU labeling reagent was added to each well (20 µL/well, 10 µM final concentration) for 2 hours at 37 °C. The cell media was then aspirated, and the FixDenat provided was added to the wells (200 µL/well) and incubated at room temperature for 30 minutes. The FixDenat solution was aspirated thoroughly, and anti-BrdU-POD (1:100 in antibody dilution solution provided) was added to the wells (100 µL/mL) for 90 minutes at room temperature. The plate was then thoroughly washed with PBS 3X. Substrate solution was then added to the wells (100 µL/mL) and incubated at room temperature for 5-30 min. The reaction was quenched with 1 N H₂SO₄ (25 µL/well), and the plates were read at an absorbance wavelength of 450 nm using a BioTek Synergy H1 plate reader.

Statistical Analysis. Data analysis was performed using Graphpad Prism 6 Software (San Diego, CA). Conditions are expressed as mean ± SD and were subjected to ANOVA followed by either Dunnett's or Tukey's Multiple Comparisons Test with a significant level of $p < 0.05$. Dose response curves were fit using a four-parameter logistic equation.

References

- (1) Lin, L. F.; Doherty, D. H.; Lile, J. D.; Bektesh, S.; Collins, F. GDNF: A Glial Cell Line-Derived Neurotrophic Factor for Midbrain Dopaminergic Neurons. *Science* **1993**, *260*, 1130–1132.
- (2) Oppenheim, R. W.; Houenou, L. J.; Johnson, J. E.; Lin, L. F.; Li, L.; Lo, A. C.; Newsome, A. L.; Prevet, D. M.; Wang, S. Developing Motor Neurons Rescued from Programmed and Axotomy-Induced Cell Death by GDNF. *Nature* **1995**, *373*, 344–346.
- (3) Hunot, S.; Bernard, V.; Faucheux, B.; Boissière, F.; Leguern, E.; Brana, C.; Gautris, P. P.;

- Guérin, J.; Bloch, B.; Agid, Y.; Hirsch, E. C. Glial Cell Line-Derived Neurotrophic Factor (GDNF) Gene Expression in the Human Brain: A Post Mortem in Situ Hybridization Study with Special Reference to Parkinson's Disease. *J. Neural Transm.* **1996**, *103*, 1043–1052.
- (4) Schaar, D. G.; Sieber, B. A.; Dreyfus, C. F.; Black, I. B. Regional and Cell-Specific Expression of GDNF in Rat Brain. *Exp. Neurol.* **1993**, *124*, 368–371.
- (5) Burazin, T. C. ; Gundlach, A. L. Localization of GDNF/neurturin Receptor (c-Ret, GFRalpha-1 and Alpha-2) mRNAs in Postnatal Rat Brain: Differential Regional and Temporal Expression in Hippocampus, Cortex and Cerebellum. *Brain Res. Mol. Brain Res.* **1999**, *73*, 151–171.
- (6) Kotzbauer, P. T.; Lampe, P. A.; Heuckeroth, R. O.; Golden, J. P.; Creedon, D. J.; Johnson, E. M.; Milbrandt, J. Neurturin, a Relative of Glial-Cell-Line-Derived Neurotrophic Factor. *Nature* **1996**, *384*, 467–470.
- (7) Milbrandt, J.; de Sauvage, F. J.; Fahrner, T. J.; Baloh, R. H.; Leitner, M. L.; Tansey, M. G.; Lampe, P. A.; Heuckeroth, R. O.; Kotzbauer, P. T.; Simburger, K. S.; Golden, J. P.; Davies, J. A.; Vejsada, R.; Kato, A. C.; Hynes, M.; Sherman, D.; Nishimura, M.; Wang, L. C.; Vandlen, R.; Moffat, B.; Klein, R. D.; Poulsen, K.; Gray, C.; Garces, A.; Johnson, E. M. Persephin, a Novel Neurotrophic Factor Related to GDNF and Neurturin. *Neuron* **1998**, *20*, 245–253.
- (8) Baloh, R. H.; Tansey, M. G.; Lampe, P. A.; Fahrner, T. J.; Enomoto, H.; Simburger, K. S.; Leitner, M. L.; Araki, T.; Johnson, E. M.; Milbrandt, J. Artemin, a Novel Member of the GDNF Ligand Family, Supports Peripheral and Central Neurons and Signals through the GFRalpha3-RET Receptor Complex. *Neuron* **1998**, *21*, 1291–1302.
- (9) Paratcha, G.; Ledda, F.; Baars, L.; Couplier, M.; Besset, V.; Anders, J.; Scott, R.; Ibáñez, C. F. Released GFRalpha1 Potentiates Downstream Signaling, Neuronal Survival, and Differentiation via a Novel Mechanism of Recruitment of c-Ret to Lipid Rafts. *Neuron* **2001**, *29*, 171–184.
- (10) Santoro, M.; Melillo, R. M.; Carlomagno, F.; Vecchio, G.; Fusco, A. Minireview: RET: Normal and Abnormal Functions. *Endocrinology* **2004**, *145*, 5448–5451.
- (11) Turner, C. A.; Watson, S. J.; Akil, H. The Fibroblast Growth Factor Family: Neuromodulation of Affective Behavior. *Neuron* **2012**, *76*, 160–174.
- (12) Elsayed, M.; Banasr, M.; Duric, V.; Fournier, N. M.; Licznarski, P.; Duman, R. S. Antidepressant Effects of Fibroblast Growth Factor-2 in Behavioral and Cellular Models of Depression. *Biol. Psychiatry* **2012**, *72*, 258–265.
- (13) Autry, A. E.; Monteggia, L. M. Brain-Derived Neurotrophic Factor and Neuropsychiatric Disorders. *Pharmacol. Rev.* **2012**, *64*, 238–258.
- (14) Lee, B. H.; Kim, Y. K. The Roles of BDNF in the Pathophysiology of Major Depression and in Antidepressant Treatment. *Psychiatry Investig.* **2010**, *7*, 231–235.
- (15) Verity, A. N.; Wyatt, T. L.; Hajos, B.; Eglen, R. M.; Baecker, P. A.; Johnson, R. M. Regulation of Glial Cell Line-Derived Neurotrophic Factor Release from Rat C6 Glioblastoma Cells. *J. Neurochem.* **1998**, *70*, 531–539.
- (16) Verity, A. N.; Wyatt, T. L.; Lee, W.; Hajos, B.; Baecker, P. A.; Eglen, R. M.; Johnson, R.

- M. Differential Regulation of Glial Cell Line-Derived Neurotrophic Factor (GDNF) Expression in Human Neuroblastoma and Glioblastoma Cell Lines. *J. Neurosci. Res.* **1999**, *55*, 187–197.
- (17) Turner, C. A.; Akil, H.; Watson, S. J.; Evans, S. J. The Fibroblast Growth Factor System and Mood Disorders. *Biol. Psychiatry* **2006**, *59*, 1128–1135.
- (18) Suter-Crazzolaro, C.; Unsicker, K. GDNF mRNA Levels Are Induced by FGF-2 in Rat C6 Glioblastoma Cells. *Brain Res. Mol. Brain Res.* **1996**, *41*, 175–182.
- (19) Reuss, B.; von Bohlen und Halbach, O. Fibroblast Growth Factors and Their Receptors in the Central Nervous System. *Cell Tissue Res.* **2003**, *313*, 139–157.
- (20) Sanjo, N.; Owada, K.; Kobayashi, T.; Mizusawa, H.; Awaya, A.; Michikawa, M. A Novel Neurotrophic Pyrimidine Compound MS-818 Enhances Neurotrophic Effects of Basic Fibroblast Growth Factor. *J. Neurosci. Res.* **1998**, *54*, 604–612.
- (21) Yagasaki, Y.; Numakawa, T.; Kumamaru, E.; Hayashi, T.; Su, T.-P.; Kunugi, H. Chronic Antidepressants Potentiate via Sigma-1 Receptors the Brain-Derived Neurotrophic Factor-Induced Signaling for Glutamate Release. *J. Biol. Chem.* **2006**, *281*, 12941–12949.
- (22) Mercier, G.; Lennon, A. M.; Renouf, B.; Dessouroux, A.; Ramaugé, M.; Courtin, F.; Pierre, M. MAP Kinase Activation by Fluoxetine and Its Relation to Gene Expression in Cultured Rat Astrocytes. *J. Mol. Neurosci.* **2004**, *24*, 207–216.
- (23) Duman, R. S.; Monteggia, L. M. A Neurotrophic Model for Stress-Related Mood Disorders. *Biol. Psychiatry* **2006**, *59*, 1116–1127.
- (24) Duman, R. S.; Li, N.; Liu, R.-J.; Duric, V.; Aghajanian, G. Signaling Pathways Underlying the Rapid Antidepressant Actions of Ketamine. *Neuropharmacology* **2012**, *62*, 35–41.
- (25) Liu, R. J.; Lee, F. S.; Li, X. Y.; Bambico, F.; Duman, R. S.; Aghajanian, G. K. Brain-Derived Neurotrophic Factor Val66Met Allele Impairs Basal and Ketamine-Stimulated Synaptogenesis in Prefrontal Cortex. *Biol. Psychiatry* **2012**, *71*, 996–1005.
- (26) He, D.-Y.; McGough, N. N. H.; Ravindranathan, A.; Jeanblanc, J.; Logrip, M. L.; Phamluong, K.; Janak, P. H.; Ron, D. Glial Cell Line-Derived Neurotrophic Factor Mediates the Desirable Actions of the Anti-Addiction Drug Ibogaine against Alcohol Consumption. *J. Neurosci.* **2005**, *25*, 619–628.
- (27) Lu, L.; Wang, X.; Wu, P.; Xu, C.; Zhao, M.; Morales, M.; Harvey, B. K.; Hoffer, B. J.; Shaham, Y. Role of Ventral Tegmental Area Glial Cell Line-Derived Neurotrophic Factor in Incubation of Cocaine Craving. *Biol. Psychiatry* **2009**, *66*, 137–145.
- (28) Green-Sadan, T.; Kinor, N.; Roth-Deri, I.; Geffen-Aricha, R.; Schindler, C. J.; Yadid, G. Transplantation of Glial Cell Line-Derived Neurotrophic Factor-Expressing Cells into the Striatum and Nucleus Accumbens Attenuates Acquisition of Cocaine Self-Administration in Rats. *Eur. J. Neurosci.* **2003**, *18*, 2093–2098.
- (29) Green-Sadan, T.; Kuttner, Y.; Lublin-Tennenbaum, T.; Kinor, N.; Boguslavsky, Y.; Margel, S.; Yadid, G. Glial Cell Line-Derived Neurotrophic Factor-Conjugated Nanoparticles Suppress Acquisition of Cocaine Self-Administration in Rats. *Exp. Neurol.* **2005**, *194*, 97–105.

- (30) Gassaway, M. M.; Jacques, T. L.; Kruegel, A. C.; Karpowicz, R. J.; Li, X.; Li, S.; Myer, Y.; Sames, D. Deconstructing the Iboga Alkaloid Skeleton: Potentiation of FGF2-Induced Glial Cell Line-Derived Neurotrophic Factor Release by a Novel Compound. *ACS Chem. Biol.* **2016**, *11*, 77–87.
- (31) Kruegel, A. C.; Rakshit, S.; Li, X.; Sames, D. Constructing Iboga Alkaloids via C–H Bond Functionalization: Examination of the Direct and Catalytic Union of Heteroarenes and Isoquinuclidine Alkenes. *J. Org. Chem.* **2015**, *80*, 2062–2071.
- (32) Nishiguchi, M.; Tokugawa, K.; Yamamoto, K.; Akama, T.; Nozawa, Y.; Chaki, S.; Ueki, T.; Kameo, K.; Okuyama, S. Increase in Secretion of Glial Cell Line-Derived Neurotrophic Factor from Glial Cell Lines by Inhibitors of Vacuolar ATPase. *Neurochem. Int.* **2003**, *42*, 493–498.
- (33) Wiesenhofer, B.; Stockhammer, G.; Kostron, H.; Maier, H.; Hinterhuber, H.; Humpel, C. Glial Cell Line-Derived Neurotrophic Factor (GDNF) and Its Receptor (GFR-Alpha 1) Are Strongly Expressed in Human Gliomas. *Acta Neuropathol.* **2000**, *99*, 131–137.
- (34) Vilner, B. J.; de Costa, B. R.; Bowen, W. D. Cytotoxic Effects of Sigma Ligands: Sigma Receptor-Mediated Alterations in Cellular Morphology and Viability. *J. Neurosci.* **1995**, *15*, 117–134.
- (35) Kuo, T.; Yang, J.; Lin, M.; Hsu, S.; Lin, J. Emodin Has Cytotoxic and Protective Effects in Rat C6 Glioma Cells: Roles of Mdr1a and Nuclear Factor KB in Cell Survival. *J. Pharmacol. Exp. Ther.* **2009**, *6*, 736–744.
- (36) Tanabe, K.; Matsushima-Nishiwaki, R.; Iida, M.; Kozawa, O.; Iida, H. Involvement of Phosphatidylinositol 3-kinase/Akt on Basic Fibroblast Growth Factor-Induced Glial Cell Line-Derived Neurotrophic Factor Release from Rat Glioma Cells. *Brain Res.* **2012**, *1463*, 21–29.
- (37) Tsuchioka, M.; Takebayashi, M.; Hisaoka, K.; Maeda, N.; Nakata, Y. Serotonin (5-HT) Induces Glial Cell Line-Derived Neurotrophic Factor (GDNF) mRNA Expression via the Transactivation of Fibroblast Growth Factor Receptor 2 (FGFR2) in Rat C6 Glioma Cells. *J. Neurochem.* **2008**, *106*, 244–257.
- (38) Vlahos, C. J.; Matter, W. F.; Hui, K. Y.; Brown, R. F. A Specific Inhibitor of Phosphatidylinositol 3-Kinase, 2-(4-Morpholinyl)-8-Phenyl-4H-1-Benzopyran-4-One (LY294002). *J. Biol. Chem.* **1994**, *269*, 5241–5248.
- (39) Hisaoka, K.; Takebayashi, M.; Tsuchioka, M.; Maeda, N.; Nakata, Y.; Yamawaki, S. Antidepressants Increase Glial Cell Line-Derived Neurotrophic Factor Production through Monoamine-Independent Activation of Protein Tyrosine Kinase and Extracellular Signal-Regulated Kinase in Glial Cells. *J. Pharmacol. Exp. Ther.* **2007**, *321*, 148–157.
- (40) Miyake, M.; Ishii, M.; Koyama, N.; Kawashima, K.; Kodama, T.; Anai, S.; Fujimoto, K.; Hirao, Y.; Sugano, K. 1-Tert-Butyl-3-[6-(3,5-Dimethoxy-Phenyl)-2-(4-Diethylamino-Butylamino)-pyrido[2,3-D]pyrimidin-7-Yl]-Urea (PD173074), a Selective Tyrosine Kinase Inhibitor of Fibroblast Growth Factor Receptor-3 (FGFR3), Inhibits Cell Proliferation of Bladder Cancer Carryi. *J. Pharmacol. Exp. Ther.* **2010**, *332*, 795–802.
- (41) Bansal, R.; Magge, S.; Winkler, S. Specific Inhibitor of FGF Receptor Signaling: FGF-2-Mediated Effects on Proliferation, Differentiation, and MAPK Activation Are Inhibited by

PD173074 in Oligodendrocyte-Lineage Cells. *J. Neurosci. Res.* **2003**, *74*, 486–493.

- (42) Nakamura, K.; Yamamoto, A.; Kamishohara, M.; Takahashi, K.; Taguchi, E.; Miura, T.; Kubo, K.; Shibuya, M.; Isoe, T. KRN633: A Selective Inhibitor of Vascular Endothelial Growth Factor Receptor-2 Tyrosine Kinase That Suppresses Tumor Angiogenesis and Growth. *Mol. Cancer Ther.* **2004**, *3*, 1639–1649.
- (43) Bain, J.; Plater, L.; Elliott, M.; Shpiro, N.; Hastie, C. J.; McLauchlan, H.; Klevernic, I.; Arthur, J. S. C.; Alessi, D. R.; Cohen, P. The Selectivity of Protein Kinase Inhibitors: A Further Update. *Biochem. J.* **2007**, *408*, 297–315.
- (44) Caumont, A.-S.; Octave, J.-N.; Hermans, E. Specific Regulation of Rat Glial Cell Line-Derived Neurotrophic Factor Gene Expression by Riluzole in C6 Glioma Cells. *J. Neurochem.* **2006**, *97*, 128–139.
- (45) Franke, T. F.; Kaplan, D. R.; Cantley, L. C. PI3K: Downstream AKTion Blocks Apoptosis. *Cell* **1997**, *88*, 435–437.
- (46) Krasilnikov, M. A. Phosphatidylinositol-3 Kinase Dependent Pathways: The Role in Control of Cell Growth, Survival, and Malignant Transformation. *Biochem. Biokhimiia* **2000**, *65*, 59–67.
- (47) Belcheva, M. M.; Haas, P. D.; Tan, Y.; Heaton, V. M.; Coscia, C. J. The Fibroblast Growth Factor Receptor Is at the Site of Convergence between Mu-Opioid Receptor and Growth Factor Signaling Pathways in Rat C6 Glioma Cells. *J. Pharmacol. Exp. Ther.* **2002**, *303*, 909–918.
- (48) Zhao, M.; Li, D.; Shimazu, K.; Zhou, Y.-X.; Lu, B.; Deng, C.-X. Fibroblast Growth Factor Receptor-1 Is Required for Long-Term Potentiation, Memory Consolidation, and Neurogenesis. *Biol. Psychiatry* **2007**, *62*, 381–390.

Chapter 7 – Identifying Small Molecule Modulators of the Fibroblast Growth Factor Receptor

Introduction

The fibroblast growth factor family is currently made up of 18 protein ligands, called fibroblast growth factors (FGF1-18 with a few others still being characterized), and 4 fibroblast growth factor receptors (FGFR1-4) that play a critical role in the development, maintenance, and regeneration of numerous tissues throughout the central nervous system and body.^{1,2} FGF2 (also known as basic FGF, FGFb) is notably the most studied member of the FGF family of growth factors, especially in regard to function in the adult brain. FGF2 interacts with all four FGFRs but has the highest affinity for FGFR1, and therefore FGFR1 is often considered the main receptor target of this protein family.¹ As a type of receptor tyrosine kinase (RTK), FGFRs are expressed on the surface of the cell (and along the intracellular protein expression pathways) and become activated by proteinaceous growth and trophic factors (i.e. FGFs).³ In particular, upon receptor dimerization and FGF2 binding, FGFR1 becomes activated, which ultimately leads to receptor autophosphorylation at the intracellular tyrosine kinase domain and subsequent recruitment of adaptor proteins and activation of the mitogen-activated protein kinase/extracellular signal-regulated kinase (MAPK/ERK), phosphatidylinositol-4,5-bisphosphate 3-kinase/protein kinase B (PI3K/Akt), and protein kinase C/phospholipase C (PKC/PLC γ) signaling pathways.⁴ Further, FGFs are heparin-binding proteins, which means that heparan sulfate proteoglycans on the cell surface are essential for bringing FGFs into contact with their receptors (**Figure 1**).⁵⁻⁹ These three pathways are the main mediators of FGFR's trophic activity, which includes neurogenesis, synaptogenesis, and synaptic plasticity (see below).

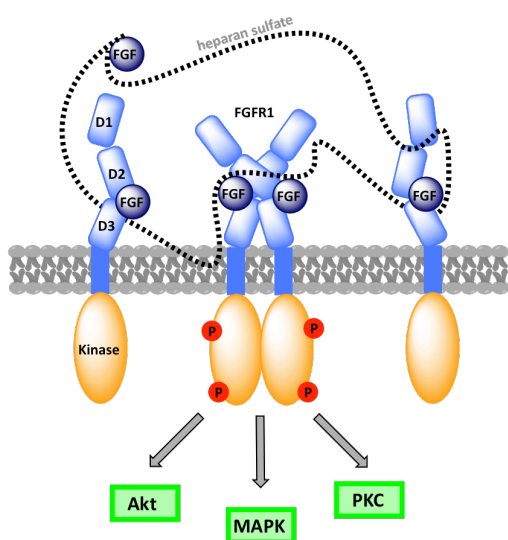


Figure 1. Brief Overview of FGFR1 Signaling. FGFR1 exists in equilibrium between monomeric and dimeric receptor units. The dimeric form is stabilized by binding of two monomeric FGF units, which are brought to the receptor by extracellular heparan sulfate molecules. Receptor dimerization leads to autophosphorylation of the tyrosine kinase domain and subsequent activation of the downstream signaling pathways: Akt (protein kinase B), MAPK (mitogen-activated protein kinase), and PKC (protein kinase C).

The FGF system is of particular interest in regard to depression and anxiety. When postmortem human brains were subjected to a genome-wide gene expression analysis, both FGF2 and FGFR1 were found to be downregulated in patients with major depressive disorder (MDD).¹⁰ In subsequent studies, these initial findings were confirmed by several independent groups and expanded to several specific brain areas.^{11,12} For instance, FGF2 expression was found to be decreased in both the hippocampus and several other cortical regions in patients suffering from MDD. Additionally, some single nucleotide polymorphisms in the *FGF2*

gene, specifically rs1449683 and rs308393, were indicated as strong predictors of antidepressant treatment efficacy and compliance (with selective serotonin reuptake inhibitors), while the rs1048201 SNP was associated with increased side effects and reduced response to antidepressants.¹³ In a rarity among target identification stories, the human data collected ultimately led to successive studies in animal models, where the focus was on the FGF system, most notably FGF2 and FGFR1. Rodents subjected to the social defeat paradigm, a verified model of depression and anxiety *in vivo*, leads to a decrease in the expression of FGF2 and FGFR1 in the hippocampus.¹⁴ When instead FGF2 is infused into the CNS directly, rapid

antidepressant activity is noted for several rodent models, where the behavioral results were additionally linked to increased gliogenesis.^{15,16}

Connections between the FGF system and anxiety have only been made in animal models. For example, FGF2 was able to inhibit anxiety-related behavior in rats bred for increased anxiety and low novelty responsiveness, a measure of anxiety.¹⁷ Additionally the same study found that FGF2 expression in the hippocampus could be modified by environmental stimuli, such as stress, resulting in higher expression of FGF2 that correlates with a stress resistant phenotype. To further support this evidence, the neurogenic and gliogenic effects of FGF2 are most notable in the anxious phenotype and related to enhancing new cell survival. Given the growing evidence on this protein family (both clinical and preclinical), there is a high probability that FGF2 is not only an endogenous antidepressant and anxiolytic factor, but also a biomarker.¹¹ FGF2 is known to exert wide-reaching effects that are acute (e.g., rapid antidepressant activity) and persistent (e.g., resilience to stress), and span the different systems of complexity from behavior (e.g. antidepressant activity) to cells (e.g. neurogenesis and gliogenesis). With an increasing number of patients suffering from MDD today and the lack of treatment options available that are effective for everyone (see Chapter 1)¹⁸, the FGF family represents an intriguing target to explore in the search for novel therapeutics.¹⁹

The FGF2/FGFR1 system is further indicated in the potential treatment of neurodegenerative disorders and brain trauma. For example, in addition to providing antidepressant and anxiolytic effects (see above), infusion of FGF2 into the CNS provided both protective effects in acute stroke models and recovery-enhancing effects in the post-stroke period.²⁰ In fact, in post-stroke recovery of sensory-motor function in adult animals, FGF2 showed dramatic effects through new wiring, synapse formation, and neurogenesis.²⁰

Furthermore, viral delivery and gene expression of FGF2 have shown beneficial effects in rodent models of traumatic brain injury, optic nerve injury, and Alzheimer's disease, specifically through the restoration of spatial learning, hippocampal long-term potentiation (LTP), and neurogenesis.²¹

In addition to the results implicating the FGF system in diseases, many studies have specifically focused on the FGF2 target, FGFR1.²² For example, FGFR1 is required for neurogenesis, or the birth of new neurons from neural stem or progenitor cells. In adult mice containing a conditional knockout of *fgfr1*, there were severe decreases in neurogenesis. Additionally, the LTP of synapses in the hippocampus was impaired, leading to deficits in memory consolidation.²³ It is therefore highly likely that FGFR1 is necessary for neurogenesis, synaptic plasticity, and memory processes. This hypothesis is consistent with evidence showing that over-expression of FGF2 causes increased cell proliferation in the dentate gyrus (DG), while a decrease in the growth factor leads to permanent hippocampal atrophy in neural stem cells.²⁴

Given the vast body of work surrounding the FGF system, FGFR1, as the leading and the most studied member of FGFR family, represents an experimental target of high potential and significance in a number of CNS disorders. FGFR1 is a molecular target capable of not only modulating repair and remodeling of brain tissue on a cellular level via the processes of neurogenesis and synaptogenesis but also controlling acute molecular events necessary for synaptic and neuronal plasticity. In fact, recent evidence suggests that modest synaptic dystrophy may be a cellular biomarker for some neuropsychiatric disorders such as depression¹⁶ even though this pathology is traditionally associated with neurodegenerative disorders.²⁵ Therefore, pharmacological stimulation of neurogenesis and synaptogenesis represents a new mechanistic approach for treating a range of CNS disorders.

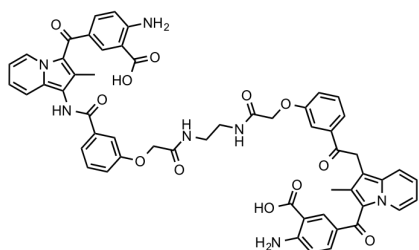


Figure 2. Structure of Reported FGFR Agonist SAR106881.

Currently, there are no reliable small molecule, non-peptidic agonists of FGFR1. Sanofi has recently reported in a patent publication²⁶ that compound SAR106881 is an FGFR agonist (**Figure 2**).

Unfortunately, no data demonstrating activation of FGFR1 (or the other FGFRs) was provided, nor was any data shown for downstream signaling activation. There are, however, numerous reports of peptide agonists of FGFRs that are modeled after the neural cell adhesion molecule (NCAM) contacts made between FGF2 and FGFR1, as well as other extracellular domain contacts.^{27–35} All of these suffer in that their pharmacological characterization relies upon indirect methods, such as downstream signaling events measured through western blot and phenotypic readouts – none of which are shown to be truly receptor-dependent. Given the dearth of convincing examples of true small molecule agonists of FGFR1, we became interested in searching for novel scaffolds that might modulate the system. Small molecules have the advantage over proteins, in the case of direct FGF2 therapy, given their “tuneability” of blood brain barrier (BBB) penetration and other pharmacokinetic properties through synthesis.

In this chapter, cellular assays were developed for the direct measurement of FGFR1 activation and downstream signaling, as well as phenotypic readouts. Using these assays, and in collaboration with the National Center for Advancing Translational Sciences (NCATS), we employed a high-throughput screen (HTS) to find small molecule agonists and modulators of FGFR1. The assay development and initial findings from the HTS are reported here.

Results

Developing Assays for the Measurement of FGFR1 Activation

Stably Expressing FGFR1 Cell Line. As a starting point for developing assays to measure functional activity of FGFR1, it was important to identify an appropriate cellular system in order to perform all the measurements. Although endogenous systems are preferable in order to understand receptor activation in a more natural context, these assays are often not sensitive enough to allow measurement of low efficacy/potency compounds. For this reason, we chose

to create a cell line stably expressing FGFR1. In this overexpressed system, there would be sufficient receptor present to allow for a robust signal activation and signal-to-background ratio (S/B). A commercially available human FGFR1 construct (FGFR1IIIc variant) was chosen that contained the FLAG epitope C-terminally tagged to the receptor to allow for easy detection of the receptor in the cells, as well as a neomycin resistance gene to serve as a selectable marker following transfection. Human embryonic kidney (HEK) cells were transfected with the construct and grown in selective media to create the stably expressing hFGFR1-HEK cells. Western blotting confirmed expression of the receptor (**Figure 3**, see **Experimental** for more details).

Detecting Receptor Phosphorylation. Based on the mechanism of receptor activation (see **Introduction**), it seemed that the best way to detect direct receptor activation would be to probe for autophosphorylation. As receptor phosphorylation is an early event in the receptor activation

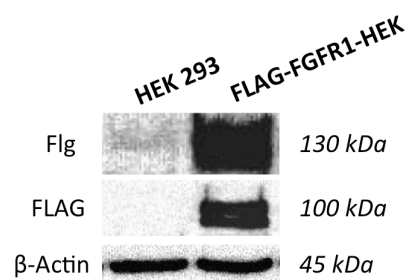


Figure 3. Western blotting enables confirmation of FLAG-tagged FGFR1 expression in stably transfected HEK cells (FGFR1-HEK cells). Cell lysates were probed with the Flg antibody (FGFR1) and the FLAG antibody (DYKDDDDK epitope). Data represent one representative experiment of $n > 3$ independent experiments.

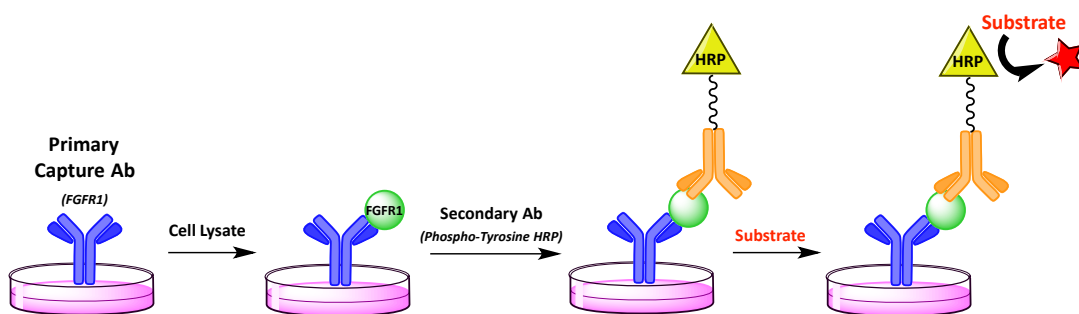


Figure 4. Schematic Depiction of Sandwich-ELISA for FGFR1 Phosphorylation.

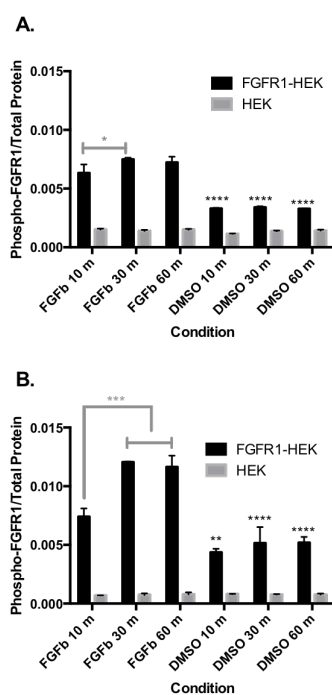


Figure 5. Antibody Screening for Phospho-FGFR1 ELISA. Phosphorylation of FGFR1 was detected using either a Cell Signaling antibody (A; #3476) or a Sigma Aldrich antibody (B; #WH0002260M3). Data represent mean \pm SD of biological replicates in one experiment from $n = 3$ independent experiments. Two-way ANOVA with Tukey's multiple comparisons test shown in gray. Comparison to respective FGF2 treatment shown in black. * $p < 0.05$, ** $p < 0.01$, *** $p < 0.001$, **** $p < 0.0001$.

cascade, this seemed like an appropriate target and the likely earliest point at which we could measure signaling. Inspired by the KIRA-ELISA (enzyme-linked immunosorbent assay) developed by Saddick³⁶, we wanted to develop an antibody-based assay that could be modified to work for multiple targets in various cellular systems. In the sandwich-style ELISA for RTK phosphorylation (**Figure 4**), a capture antibody specific to the receptor (FGFR1 in this case) is used to pull down receptor from cellular lysate. The samples are then probed with an antibody specific for phospho-tyrosine residues and will therefore specifically bind to the phosphorylated receptors that were immunoprecipitated in the first step. While the concept of this ELISA is simple, the task of finding appropriate antibodies suitable for this process is not trivial. In a small screen of four antibodies specific for either FGFR1 or phospho-FGFR1 (both monoclonal and polyclonal), two antibodies were found with a statistically significant increase in phosphorylation in comparison to the vehicle control, as well as untransfected

HEK cells (**Figure 5**). The Cell Signaling antibody detects phospho-FGFR (tyrosines 653 and 654) while the Sigma Aldrich antibody detects total FGFR1. The antibody from Sigma Aldrich

was chosen as the lead for future assays for its increased S/B in comparison to the Cell Signaling antibody and for its ability to measure statistically significant differences in phosphorylation at different treatment times of control. Unfortunately, no antibody was found suitable for the detection of total FGFR1 in the cells, so instead cell signal was normalized to total protein content.

In initial experiments, the ELISA was able to measure phosphorylation of FGFR1 in the presence of increasing concentrations of FGF2 (**Figure 6A**). This receptor activation could be blocked by FGFR inhibitor PD173074 (PD17). These experiments show that the assay can detect acute phosphorylation events that are dependent upon FGFR1. As an additional control, phosphorylation from growth factor FGF1 (or FGFa) could also be detected (**Figure 6B**). A dose response curve was also measured for inhibitor PD17 in the presence of FGF2 (**Figure 6C**). Overall, the assay was able to robustly measure FGFR1 phosphorylation with a typical S/B between 2 and 5 and could be blocked by the presence of inhibitor. Although the assay was not ideal for use in HTS, it would be an

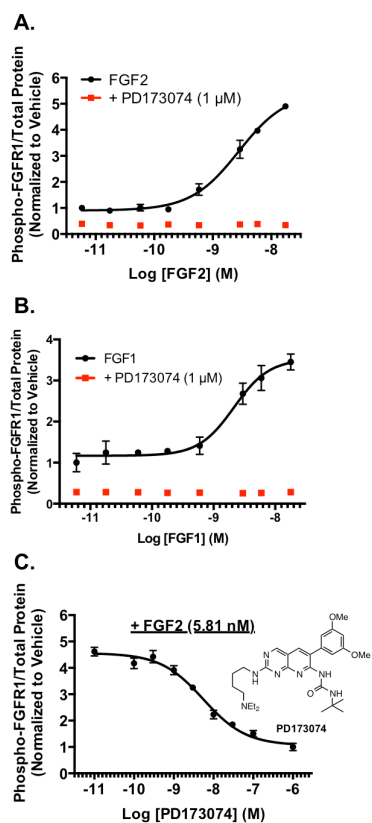


Figure 6. Sandwich-style ELISA Quantitatively Measures the Activation of FGFR1 in FGFR1-HEK Cells. FGF2 (A) or FGF1 (B) activates FGFR1 in a dose-dependent manner with an EC_{50} of 2.9 ± 1.9 nM and S/B of 4.9 or EC_{50} of 1.8 ± 0.9 nM and S/B of 3.5, respectively. FGFR1 activation is blocked by FGFR inhibitor PD173074. C. FGFR inhibitor PD173074 dose-dependently inhibits the signal from FGF2 (5.8 nM, EC_{90}) with an IC_{50} of 8.9 ± 4.7 nM. Data represent mean \pm SD of biological replicates in one experiment from $n > 3$ independent experiments (normalized to DMSO vehicle)

important secondary assay used to rule out initial hits. **Table 1** summarizes the potencies of FGF1 and FGF2 in FGFR1 phosphorylation.

Table 1. Summary of FGFR1 Data

Treatment	EC ₅₀ (IC ₅₀)	Assay
FGF1	1.8 ± 0.9 (3.5)	Phospho-FGFR1
FGF2	2.9 ± 1.9 (4.9)	Phospho-FGFR1
PD173074	[8.9 ± 4.7]	Phospho-FGFR1
FGF2	0.3 ± 0.1 (20)	pERK
FGF2	0.68 ± 0.03 (4.2)	pAkt
FGF1	0.1 ± 0.01 (3.5)	pPLC γ
PD173074	[24.1 ± 6]	pERK
FGF2	0.06 ± 0.003 (5.5)	pERK (PC12)
PD173074	[2.0 ± 0.01]	pERK (PC12)
FGF2	0.59 ± 0.23 (3.5)	PathHunter [®]
Naloxonazine	3300 ± 568	Phospho-FGFR1
PD173074 w/ Naloxonazine	[8.4 ± 3.5]	Phospho-FGFR1

Data represent mean ± SD of various replicates (nM). S/B is shown in parentheses.

A serious attempt was made at translating the assay to endogenous systems, including primary neuronal culture (both rat cortical and rat hippocampal)³⁷ and PC12 cells, a rat pheochromocytoma cell line that expresses FGFR1 endogenously.³⁸ Unfortunately, finding a usable antibody for the assay proved challenging, as the

antibody discussed above was specific to the human isoform of the receptor and was unable to show much signal from the activation of these rat receptors. Given the robustness of the assay already working, we decided to instead focus on developing independent assays that would complement the ELISA already in use.

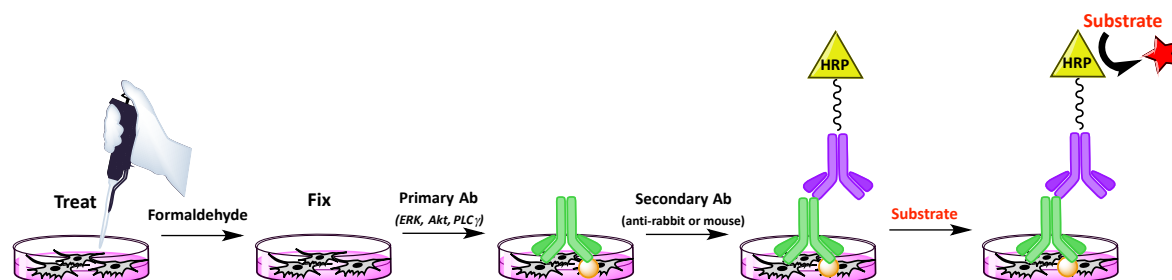


Figure 7. Schematic Depiction of enzyme-linked fixed-cell immunoassay (ELFI) for ERK, Akt, and PLC γ Detection.

Detecting Downstream Signaling Events. Following receptor dimerization and phosphorylation, the downstream MAPK, Akt, and PLC γ signaling pathways become activated. As an indirect measure of receptor activation, we also developed an assay to measure the signaling of these pathways. Rather than using a sandwich-style ELISA, we developed an

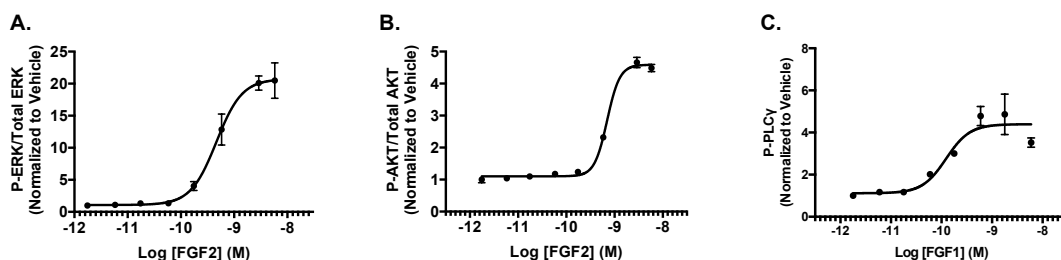


Figure 8. ELFI Enables Measuring of FGFR1's Downstream Signaling Targets. The degree of activation is expressed as the ratio of phosphorylated to total kinase protein (after 5-minute activation pulse). A. FGF2 activates ERK1/2 in FGFR1-HEK cells in a dose-dependent manner with an EC_{50} of 0.3 ± 0.1 nM and S/B of 20. B. FGF2 activates Akt in FGFR1-HEK cells in a dose-dependent manner with an EC_{50} of 0.68 ± 0.03 nM and S/B of 4.2. C. FGF1 activates phospho-PLC γ in FGFR1-HEK cells in a dose-dependent manner with an EC_{50} of 0.1 ± 0.01 nM and S/B of 3.5. No suitable antibody for PLC γ was found, so data are not normalized to total PLC γ levels. Data represent mean \pm SD of biological replicates in one experiment from $n > 3$ independent experiments (normalized to DMSO vehicle control).

enzyme-linked fixed-cell immunoassay (ELFI) that mimics the technique of immunofluorescence. In this assay, cells are fixed immediately following treatment with FGF or test compounds and then probed directly with antibodies for each of the downstream signaling

pathways (Figure 7). Much like western blotting, plates can be stripped and reprobbed with new antibodies, allowing one experiment to provide measurements on multiple downstream signaling pathways.

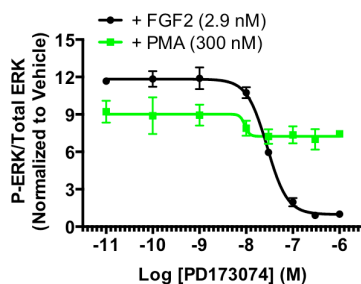


Figure 9. Selectivity of FGFR Inhibitor PD173074 on ERK Activation. FGFR inhibitor PD173074 did not inhibit ERK phosphorylation triggered by an independent pathway (by phorbol-12-myristate-13-acetate, PMA, a PKC activator), while it inhibited ERK phosphorylation induced by FGF2 (2.9 nM) with an IC_{50} of 24.1 ± 6 nM. Data represent mean \pm SD of biological replicates in one experiment from $n = 3$ independent experiments.

in the presence of either FGF2 or PMA, an FGFR-independent stimulator of the MAPK

FGF2 (and FGF1) was able to induce robust phosphorylation of the ERK, Akt, and PLC γ pathways in the hFGFR1-HEK cell line (Figure 8). A relatively high concentration of PD17 was used to inhibit the activation by FGF2 (1 μ M, data not shown), so it was important to confirm that the inhibitor was specific to the FGFR pathway at that concentration. A dose response curve was collected for PD17

pathway³⁹ (and PKC). By comparing the dose response curves, we hoped to identify the concentration window in which PD17 would be selective for the FGFR pathway and not the MAPK pathway. Interestingly, PD17 had little effect on the signal from PMA, indicating that even at higher concentrations, PD17 is selective to FGFR signaling (**Figure 9**). We also noted some time and potency differences in the downstream signaling assays in comparison to the receptor phosphorylation assay. For instance, while the receptor phosphorylation was typically measured at 60 minutes, a time point where the signal was both maximal and stable, the

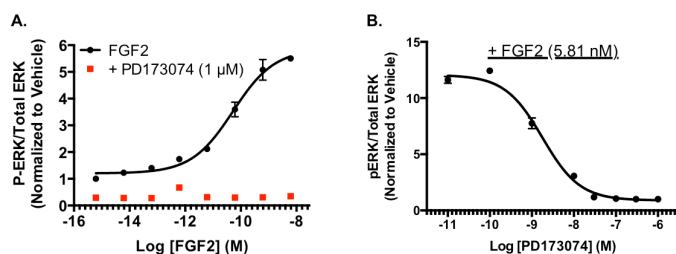


Figure 10. Measuring ERK Activation in PC12 Cells that Endogenously Express FGFR1. A. FGF2 activates ERK1/2 in PC12 cells with an EC₅₀ of 55.1 ± 3.3 pM and S/B of 5.5, which can be blocked by FGFR inhibitor PD173074. B. FGFR inhibitor PD173074 dose-dependently inhibits the signal from FGF2 (5.8 nM, EC₉₀) with an IC₅₀ of 2.0 ± 0.01 nM. Data represent mean ± SD of biological replicates in one experiment from n > 3 independent experiments.

downstream signaling was measured at 5-10 minutes. Since complete RTK phosphorylation is likely slower than the downstream signaling triggered by rapid partial receptor activation^{40,41}, it is not surprising that there a difference in peak activities. RTK phosphorylation might also be sustained in comparison to downstream signaling due to slow dephosphorylation rates. Additionally, the potencies for downstream signaling are markedly greater than those for receptor activation, in line with the idea of downstream signal amplification by which one molecule upstream can trigger the activity of multiple molecules of downstream effectors resulting in an amplified (more potent) signal.

As before, we attempted to utilize this new assay in other cell lines that express FGFR1 endogenously. We were unable to measure a meaningful signal in either primary neuronal cultures tested, which could indicate a lack of FGFR1 in these preparations. However, in PC12

cells, FGF1 and FGF2 robustly activates the ERK signaling pathway and can be blocked by PD17 (FGF2 shown in **Figure 10A**), consistent with previously reported FGFR expression in these cells (also confirmed in this study, see **Figure 11**). No signal was detected for either the Akt or PLC γ pathways. Although we could not measure activation of an endogenously expressed receptor, the ERK assay in PC12 cells at least provided some insight into FGFR1's downstream signaling. The results of the downstream signaling assays are reported in **Table 1**.

Phenotypic Screen for Receptor Activation. As a complement to the ELISAs developed, a

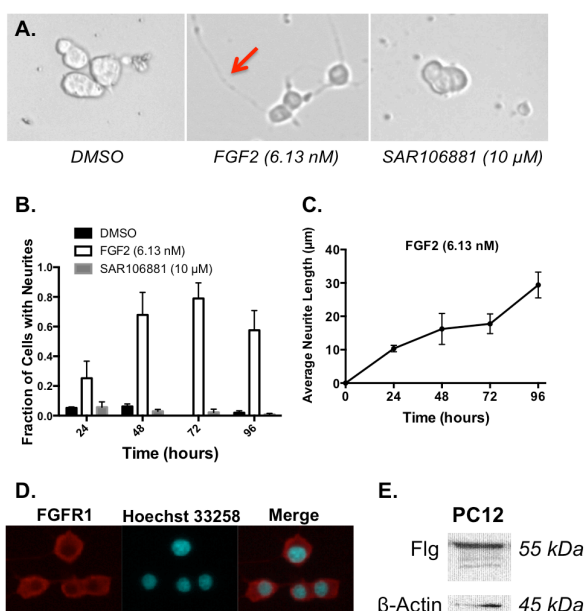


Figure 11. Phenotypic Assay Dependent on Activation of FGFR1. PC12 cells are used to measure neurite outgrowth in response to FGFR1 activation. A,B. FGF2 (6 nM, 100 ng/mL) induces neurite outgrowth in native PC12 cells after 24 hours. Sanofi agonist SAR106881 does not cause neurite outgrowth. C. The length of neurite outgrowth in PC12 cells increased over time when treated with FGF2. D. Immunofluorescence images show expression of FGFR1 in PC12 cells. E. Western blotting of PC12 cells shows expression of FGFR1 (Flg antibody used). Data represent mean \pm SD of biological replicates in one experiment from $n > 3$ independent experiments.

phenotypic screen was developed as an alternate measure of FGFR1 activation. It is well known that PC12 cells are able to undergo differentiation in the form of neurite outgrowth, either in response to nerve growth factor (NGF), acting upon the TrkA receptor⁴², or in response to FGF1 or FGF2, acting upon FGFR1.^{38,43,44}

Utilizing native PC12 cells, we were able to detect neurite outgrowth in response to either FGF1 or FGF2 (FGF2 shown in **Figure 11**). Thus the consequences of receptor signaling can also be assessed via a phenotypic assay.

Reported Small Molecule Agonists

are Inactive in Assays. In a first test, the assays were utilized to measure the response from

reported small molecule agonist SAR106881 (see **Introduction, Figure 2**). Based on the structure of a supposed FGFR antagonist reported in the patent, SAR106881 is dimeric in structure and is supposed to function by favoring the dimeric form of FGFR1, leading to

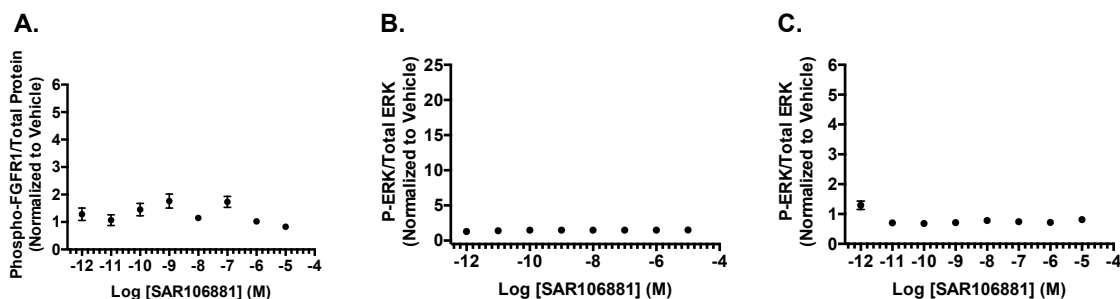


Figure 12. Reported Sanofi FGFR Agonist SAR106881 Does Not Activate FGFR1. A. SAR106881 does not activate FGFR1 in the FGFR1 phosphorylation ELISA. B. SAR106881 does not activate ERK in the ERK ELISA in FGFR1-HEK cells. C. SAR106881 does not activate ERK in the ERK ELISA in PC12 cells. See **Figure 11A** for neurite outgrowth. Data represent mean \pm SD of biological replicates in one experiment from $n = 3$ independent experiments.

activation. SAR106881 was unable to activate FGFR1 in any assay utilized, including receptor

phosphorylation, downstream signaling, or neurite outgrowth (**Figure 11**). However the control endogenous

protein agonists worked well in all assays. In the original patent, no direct evidence was provided on the activity of SAR106881 at FGFRs and presumes the pharmacology based on angiogenesis activity.²⁶ We also tested the

activity of a reported small peptide agonist, FGL monomer (mapped from the FG loop, FGL; sequence:

EVYVVAENQQGKSKA)^{34,35}, for its ability to activate

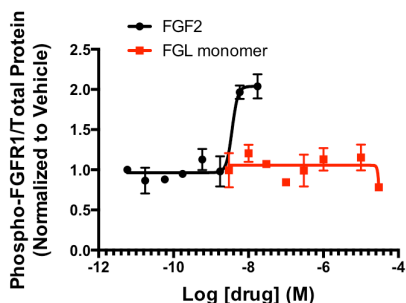


Figure 13. FGL Peptide Monomer is Inactive in Phospho-FGFR1 ELISA in FGFR1-HEK. Data represent mean \pm SD of biological replicates in one experiment from $n = 3$ independent experiments.

FGFR1. Similarly to SAR106881, FGL was unable to activate FGFR1 in any assay tested (phospho-FGFR1 assay shown, **Figure 13**). Given the inability of two different reported agonists

to activate FGFR1, there was even greater necessity of accomplishing a HTS to find true small molecule agonists of this receptor.

Putting Assays in Place for HTS

The Primary Assay for FGFR1 Activation. While the assays developed above were appropriate for validating hits from the HTS (as well as evaluation of reported compounds), they do not offer sufficient throughput for the primary screening assay. For this purpose, a U2OS cell

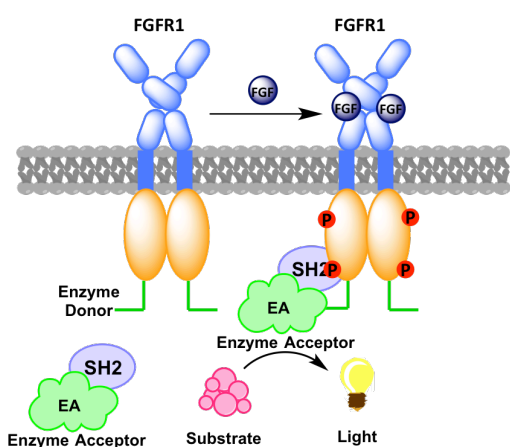


Figure 14. Schematic Depiction of the DiscoverX PathHunter[®] Primary Assay Used for HTS.

line stably transfected with human FGFR1 receptor (hFGFR1-U2OS PathHunter[®] cells, developed by DiscoverX) were used. Similar to the PathHunter[®] assay used to measure arrestin recruitment discussed in Chapter 1, the output signal is generated through the reconstitution of β -galactosidase (β -gal) (**Figure 14**). A small complementary fragment of β -gal is fused to the

FGFR1 C-terminus, while the rest of the enzyme is fused to the SH2 domain of an adaptor/partner protein (DiscoverX proprietary fusion protein). Activation of FGFR1 through autophosphorylation leads to recruitment of the adaptor/partner protein, complementation of the two fragments, and reconstitution of a functional enzyme. Activity of the enzyme is recorded through chemiluminescence.

Adaptation of the Primary Assay to HTS Format. The PathHunter[®] assay with hFGFR1-U2OS cells was adapted to 1536-well format at NCATS with our collaborator Dr. Marc Ferrer. The cells were incubated with varying concentrations of FGF2 and the PathHunter[®] luminescence detection reagent. The luminescence intensity of the assay plates was quantified

using a ViewLux CCD-based plate reader after a one-hour incubation at room temperature. The dose-response curve was obtained for FGF2, and the derived EC_{50} value, a measure of potency, (0.59 ± 0.23 nM, **Figure 15A**) was similar to those reported in the literature (~ 0.5 nM)⁴⁵ and to those obtained in the ELISA developed for hit validation (see above). The Z'-factor, a statistical measure of the quality of a high-throughput assay at a single concentration,^{46,47} was 0.65 ± 0.09 , and the other experimental parameters, namely the S/B (between 3-4) and coefficient of variation (CV<8%), indicated that the assay was suitable for 1536-well format HTS.⁴⁷

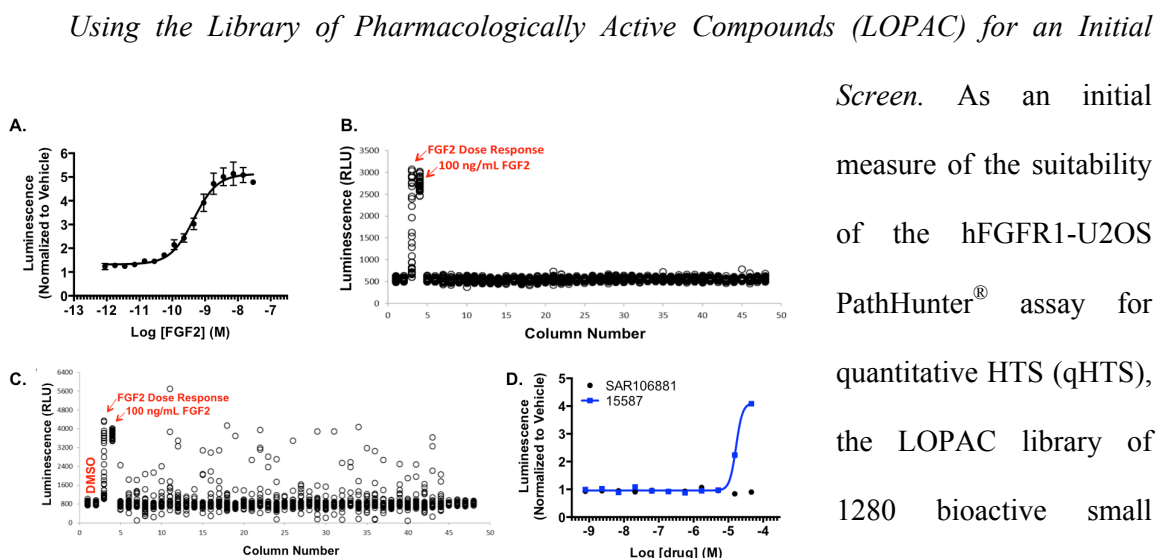


Figure 15. PathHunter[®] Assay Adaptation for HTS of FGFR1 Activation. A. Dose-response curve for FGF2 (EC_{50} of 0.59 ± 0.23 nM). B. This assay was adapted to 1536-well HTS format and afforded adequate statistical parameters. The scatter plot of a plate with DMSO is provided. The y-axis shows luminescence (arbitrary units); the x-axis shows columns on the plate. Columns 1 and 2, DMSO controls (0% control); column 3, a control column with an FGF2 dose response; and column 4, an EC_{100} FGF2 (100% control). C. The 1536-well HTS platform was used to screen a library of 1280 bioactive compounds, shown as a scatter plot with compounds at 46 μ M. D. Five hits were identified. Representative hit compound 15587 is shown alongside SAR106881. Data represent mean \pm SEM of one representative experiment of $n = 3$ independent experiments. Data obtained by Dr. Jennifer Fox (NCATS).

Screen. As an initial measure of the suitability of the hFGFR1-U2OS PathHunter[®] assay for quantitative HTS (qHTS), the LOPAC library of 1280 bioactive small molecules was screened at 4 different concentrations and normalized to FGF2 as 100% efficacy. The data was then corrected by

applying a pattern correction algorithm using compound-free control plates (DMSO plates).⁴⁸

The scatter plots of the assay plate with DMSO (**Figure 15B**), and the assay plate with

compounds at 46 μM (**Figure 15C**) are shown. To rule out any nonselective hits, the LOPAC library was also counter-screened in U2OS cells expressing other receptor targets (GPR40, GPR120, and TSHR-beta-arrestin – data not shown). In this way, any compounds that were active at more than one target could be dismissed from further validation and analysis.

Determining Hit Selection From Screening Results. To gain a handle on the reproducibility of the results, two independent screens of the LOPAC library were performed. These two screens were then compared to the results from three other targets – free fatty acid receptor 1 (GPR40), free fatty acid receptor 4 (GPR120), and thyroid stimulating hormone receptor (TSHR) β -Arrestin (three counter-screens total). From the LOPAC screen, five compounds were selected as active in the primary screen (and inactive in the counter-screens). Activity of representative compound 15587 is shown in **Figure 15D**, alongside the Sanofi compound SAR106881, which was also found to be inactive in this independent assay. The hits were selected using the curve response classification (CRC) algorithms developed at NCATS for hit selection from dose response qHTS.^{48,49} In this method, the data is used to fit dose-response curves, according to a published algorithm⁵⁰ and provide CRC values for each compound. The curves are then classified according to the quality of data (level of curve fitting to the observed data), well-defined upper and lower asymptotes, and efficacy. Curves were categorized as follows: complete response (curve class 1), CRC 1.1, has two well-defined asymptotes, high efficacy (>80%), and good fit ($r^2 \geq 0.9$); partial response, CRC 1.2, is as 1.1 but with efficacy <80%; incomplete curve (curve class 2), CRC 2.1, has one asymptote, high efficacy (>80%), and good fit ($r^2 \geq 0.9$); incomplete partial response, CRC 2.2, has one asymptote and low efficacy (<80%); inconclusive response (curve class 3), CRC 3, shows poor fit and single point activity; and inactive (curve class 4), CRC 4, shows no dose response. All five hits found from the initial

LOPAC screen were categorized as either curve class 1 (1.1 and 1.2) or 2 (2.1 and 2.2) in both trials of the screen. This initial screen highlights the ability of our assay and counter screens to properly identify compounds not in a single concentration format but in a format that instantly provides some information about potency and efficacy in a practice that is not fully utilized in the HTS community.

Validating the Agonist Activity of LOPAC Hit

Small Molecule Hit From LOPAC Screen. The five hits found in the LOPAC screening (Figure 16A) were tested in our secondary assays to validate their activity. Interestingly, only

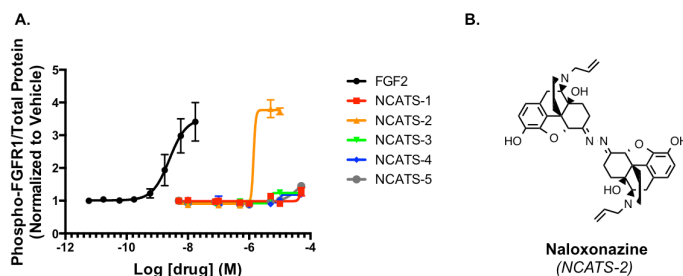


Figure 16. Five Hits from LOPAC Screen Were Measured in FGFR1 Phosphorylation ELISA. A. Five hits from LOPAC screen in PathHunter[®] assay are tested for their ability to phosphorylate FGFR1. B. Naloxonazine (formerly NCATS-2) was found to activate FGFR1. Data represent mean \pm SD of biological replicates in one experiment from $n = 3$ independent experiments.

one compound, NCATS-2 was found to be active in the ELISA for FGFR1 phosphorylation (Figure 16A) while the other four showed no agonist activity in concentrations up to 30 μ M. The identity of NCATS-2 is the small molecule naloxonazine

(Figure 16B). Naloxonazine is a potent antagonist of the mu-opioid receptor (MOR) that allegedly binds irreversibly to its target.^{51–53} Naloxonazine is dimeric in structure, forming in acidic solutions of the antagonist monomer unit naloxazone. Given the dimeric structure of naloxonazine, it is possible that this small molecule fulfills the criteria of bringing together two receptor units for activation. As the other four compounds were unable to cause receptor phosphorylation as measured in the ELISA, they were not pursued further and categorized as false positives. We confirmed the activity of NCATS-2 with a commercially available stock of

naloxonazine in a time course next to FGF2, and a noticeably different activation profile was observed (**Figure 17A**). While FGF2's signal increased and plateaued rather quickly (< 20 min), naloxonazine showed more of a linear activation profile and higher level of receptor phosphorylation. Since the two molecules differ in the kinetics of their receptor phosphorylation, it seemed possible that activation (if confirmed in additional assays) was occurring through

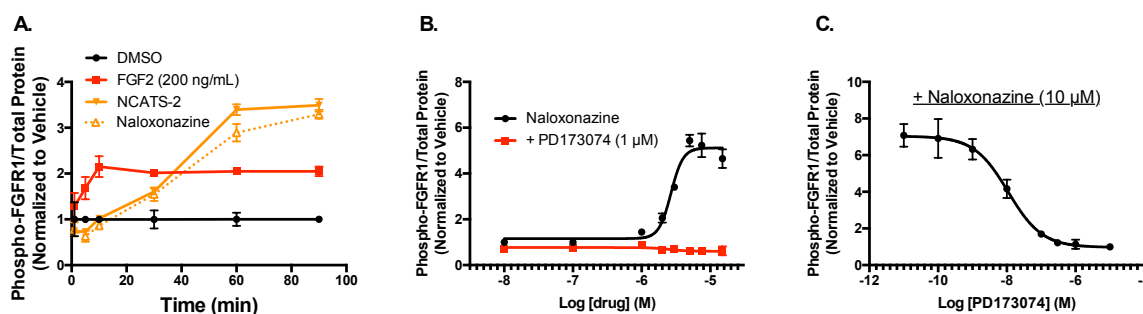


Figure 17. Profile of Naloxonazine in Phospho-FGFR1 ELISA. A time course (A), dose response curve (B), and inhibition curve with PD17 (C) were taken for naloxonazine in the ELISA for measuring phosphorylation of FGFR1. Naloxonazine showed an EC_{50} of $3.3 \pm 0.7 \mu\text{M}$ for FGFR1 phosphorylation. Data represent mean \pm SD of biological replicates in one experiment from $n > 3$ independent experiments.

distinct mechanisms. A full dose response curve for FGFR1 phosphorylation revealed an $EC_{50} = 3.3 \pm 0.6 \mu\text{M}$ that could be blocked by FGFR inhibitor PD17 (**Figure 17B**). Further, PD17 dose dependently inhibits the naloxonazine-induced phosphorylation of FGFR1 (**Figure 17C**),

indicating that the phosphorylation detected seems to be receptor specific.

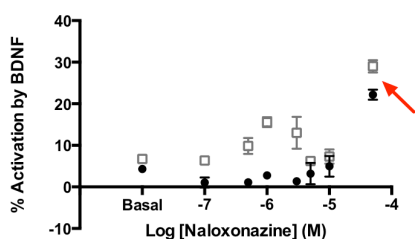


Figure 18. Naloxonazine is Not a TrkB Agonist. TrkB phosphorylation was measured in hTrkB-HEK cells with two stocks of naloxonazine (shown in black and gray) using an analogous ELISA to FGFR1 phosphorylation. Data represent mean \pm SD of biological replicates in one experiment from $n = 3$ independent experiments.

As a measure of selectivity, naloxonazine was tested in a closely related ELISA for TrkB phosphorylation. TrkB is another RTK that together with its growth factor agonist, brain-derived neurotrophic factor (BDNF), is believed to be connected to depression, as well.^{54–56} In contrast to FGFR1 phosphorylation,

naloxonazine was only able to phosphorylate TrkB at the highest concentration tested ($30 \mu\text{M}$)

and only partially at approximately 30% of the maximal BDNF signal (**Figure 18**). These results, in combination with the inhibition data, indicate that there appears to be some measure of selectivity in the actions of naloxonazine on FGFR1 and that likely naloxonazine does not act as a general phosphatase inhibitor.

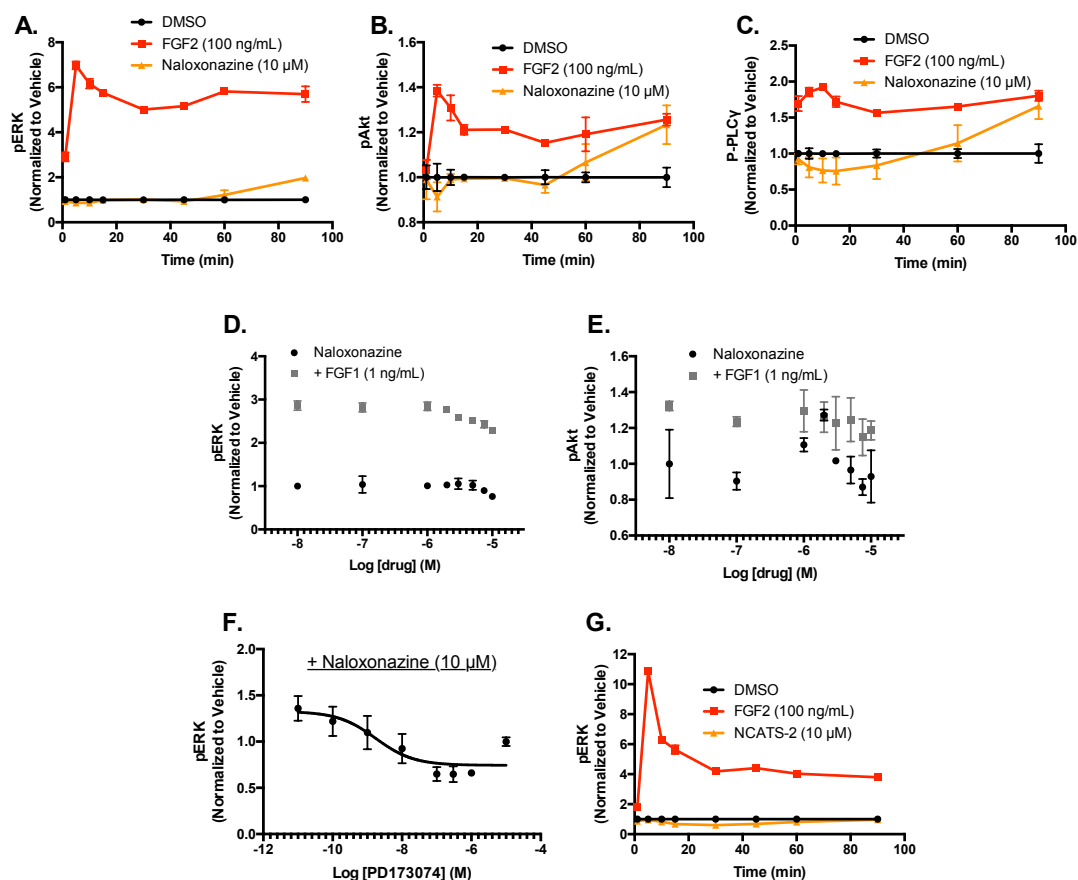


Figure 19. Naloxonazine Does Not Activate Downstream Signaling Cascades. There was minimal activation by naloxonazine at any time tested in the ERK (A), Akt (B), and PLC γ (C) pathways in FGFR1-HEK cells. Naloxonazine also did not activate/inhibit ERK (D) or Akt (E) at any concentration tested either in the presence of absence of FGF1. F. PD17 was able to inhibit the ERK signal from naloxonazine at 90 min, however the S/B is low. G. Naloxonazine could not activate the ERK pathway in PC12 cells. Data represent mean \pm SD of biological replicates in one experiment from $n = 3$ independent experiments.

Measuring Downstream Signaling From Naloxonazine. Next, naloxonazine was measured for its ability to activate the downstream signaling pathways ERK, Akt, and PLC γ . In a time course, naloxonazine was unable to activate any of the downstream signaling pathways (**Figure 19A-C**). Upon closer inspection, there is a slight increase in the signal at the 90-minute

time point in the ERK, Akt, and PLC γ signals, however when a dose response curve of naloxonazine is measured at 90 minutes, rather than the usual 10 minutes, there is still no dose-dependent response to the drug (**Figure 19D-E**). Interestingly, PD17 was able to block the minimal ERK activation of naloxonazine dose-dependently (**Figure 19F**), which does suggest some involvement in signaling, though very minor. Additionally, naloxonazine did not activate the ERK signaling pathway in PC12 cells that natively express FGFR1 (**Figure 19G**). To determine whether naloxonazine acts as an allosteric modulator (i.e. a ligand that acts upon a receptor site distinct from the endogenous ligand) for downstream signaling at FGFR1, the dose response curve of naloxonazine was measured in the presence of a low concentration of FGF1. Even in this setup, no dose response curve was measured from naloxonazine (**Figure 19D-E**), which further indicates that it either indirectly acts upon FGFR1 or has a unique mechanism of action, one that disfavors the activation of downstream signaling cascades.

Neurite Outgrowth From Naloxonazine. To further study the actions of this interesting compound, naloxonazine was assessed in the neurite outgrowth assay. After 4 days, naloxonazine was unable to cause neurite outgrowth in PC12 cells in comparison to FGF2 (**Figure 20**). This result was not surprising when considering the lack of signaling activation found in these cells.

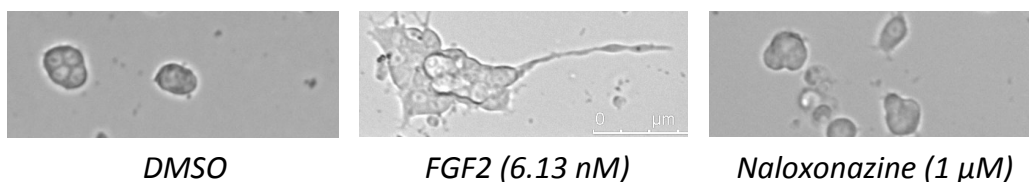


Figure 20. Naloxonazine Does Not Cause Neurite Outgrowth in PC12 Cells. Data represent one representative experiment of $n = 3$ independent experiments.

Exploring the Mechanism of Action of Naloxonazine. As naloxonazine exhibits an

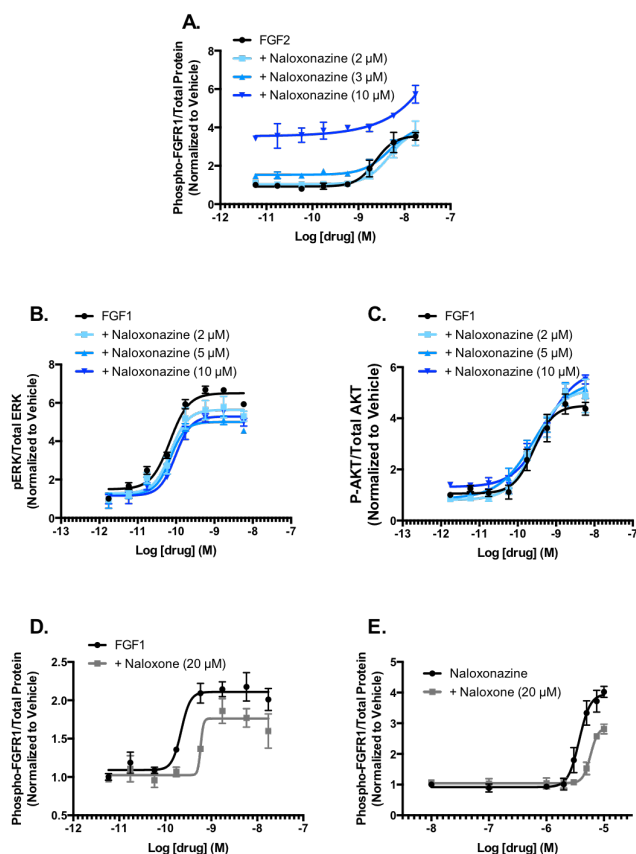


Figure 21. Probing the Mechanism of Naloxonazine Activity at FGFR1. A dose response curve for FGF1 or FGF2 was measured in the presence of increasing concentrations of naloxonazine and measured for FGFR1 phosphorylation at 60 minutes (A), ERK activation (B), or Akt activation (C) at 10 minutes. FGF1 (D) or naloxonazine (E) dose response curves were measured in the presence of naloxone. Data represent mean \pm SD of biological replicates in one experiment from $n = 3$ independent experiments.

unusual pharmacological profile, we were interested in understanding its mechanism of action further. Naloxonazine induces dose-dependently phosphorylation of FGFR1 (as indicated by the ELISAs) but did not induce downstream signaling or neurite outgrowth. Based on these observations, it seemed possible that naloxonazine perhaps was not acting through an orthosteric mechanism but perhaps an allosteric one. Orthosteric agonists bind to the same receptor site as the endogenous ligands, while allosteric bind to and modulate receptors through a separate site. In order to distinguish between these mechanisms in the ELISA, a dose response curve of FGF2 can be measured in the presence of increasing concentrations of naloxonazine. If naloxonazine is an orthosteric agonist, there should be a right shift of the dose response curve of FGF2 (i.e., a shift of EC_{50} to higher concentrations).^{57,58} If naloxonazine instead is an allosteric agonist, the effects can be more complex, the most common effect being a leftward shift in potency and an increase in efficacy.

However, the effects are not limited to this scenario. For instance, if the system already reaches a maximal response from FGF2 alone, then an increase in efficacy by co-treatment with an allosteric agonist may not be observed. In fact, co-treatment with the allosteric agonist may decrease the efficacy of the native ligand. In general, however, because the allosteric agonist activates the receptor on its own, there should be an increase in the basal level of receptor activation as a result of this co-treatment.^{57,58} When naloxonazine was co-incubated with a dose response curve of FGF2, there was no dramatic right shift of the curves, indicating that naloxonazine is likely not an orthosteric ligand – as predicted (**Figure 21A**). In fact, the addition of naloxonazine just seems to increase the basal signal of the curve, ultimately leading to a flat curve as the response from the system is maximal and indicating a likely allosteric mechanism if naloxonazine is an agonist of FGFR1 at all.

To further explore this hypothesis, the same experiment was performed in the ERK and Akt assays. Ideally, the effect of downstream amplification would take part in this experiment to show how naloxonazine might modulate the signaling of FGF even though it had no effect on its own. Interestingly, in the presence of increasing concentrations of naloxonazine, there was no change in the dose response curve from FGF1 at either ERK or Akt (**Figure 21B-C**). This result is not surprising in the context of other experiments, as naloxonazine had little effect on downstream signaling itself. Although naloxonazine may have some allosteric effects on receptor phosphorylation, those effects do not appear to translate into the downstream signaling cascades. Without receptor phosphorylation that leads to a fully functional receptor, the probability of naloxonazine being a true FGFR1 agonist is low.

As an additional measure, a dose response curve of either FGF1 or naloxonazine were measured in the presence of naloxone, a modified monomer unit of naloxonazine. If

naloxonazine is making a physical interaction with FGFR1, leading to receptor phosphorylation, then in all likelihood, a monomer of naloxonazine should act as an inhibitor of this process, much like the rationale behind the design of Sanofi agonist SAR106881. In these experiments, naloxone had some effect on the phosphorylation of FGFR1 induced by FGF1 and did seem to inhibit the dose response curve of naloxonazine (**Figure 21D-E**), indicating that perhaps FGFs and naloxonazine are interacting at the same sites on the FGFR1. Together with the results from **Figure 21A-C**, there still remains some uncertainty about the mechanism of action of naloxonazine in these assays.

Visualizing Receptor Phosphorylation Through Western Blot. Although the ELISA developed is able to detect phosphorylation of the receptor, an independent control is required to

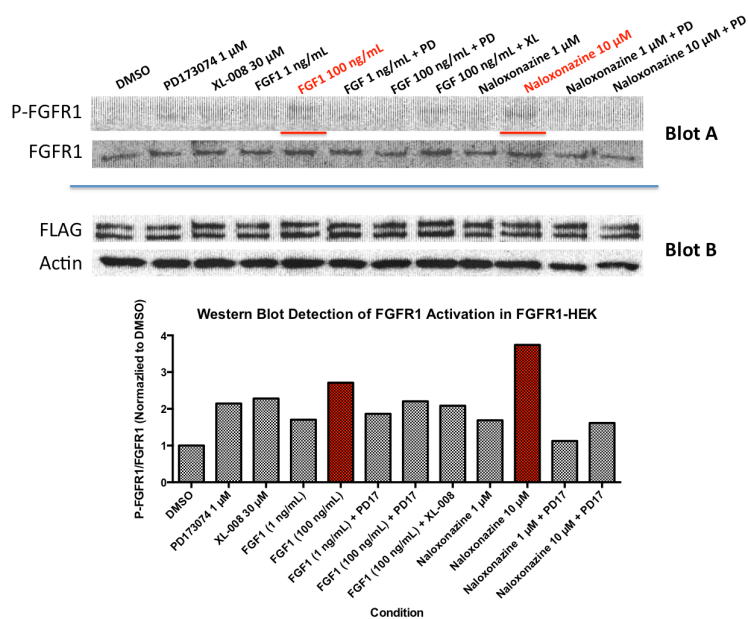


Figure 22. Western Blot of FGFR1 and P-FGFR1 and Controls in FGFR1-HEK Cells Treated with Naloxonazine. The gel was probed for phospho-FGFR1, total FGFR1, the FLAG epitope, and “housekeeping” protein actin. Quantification of the blot reveals increased phosphorylation of FGFR1 by FGF1 and naloxonazine. Data represent one representative experiment of $n = 3$ independent experiments.

confirm that the chosen antibodies pull down the receptor of interest and that the receptor is phosphorylated. Further, it is conceivable that the anti-FGFR1 capturing antibody is not as specific as advertised, in which case the ELISA may be detecting phosphorylation of other proteins (induced by naloxonazine), leading to a false positive signal. The best

way then to visualize the receptor phosphorylation directly is to use western blotting techniques. In this case, even if the receptor is in some complex at the time of the experiment, the denaturing conditions of the electrophoresis will separate the proteins and allow visualization of individual targets.

When receptor phosphorylation was measured in the hFGFR1-HEK cell line as detected with western blot, both FGF1 and naloxonazine were able to phosphorylate the receptor using a phospho-FGFR1 antibody specific to tyrosine residues 653 and 654 (**Figure 22**). These tyrosines are essential for activation of FGFR1's tyrosine kinase domain, as well as downstream ERK and Akt signaling. In contrast, phosphorylation of tyrosine 766 leads to PLC γ signaling.⁵⁹ We were concerned, however, by the relatively low signal visible from the phospho-FGFR1 blot; the bands were visible in both FGF1 (or FGF2 – data not shown) and naloxonazine, but the high background ultimately provided a low quality blot. It seems that perhaps this antibody is not

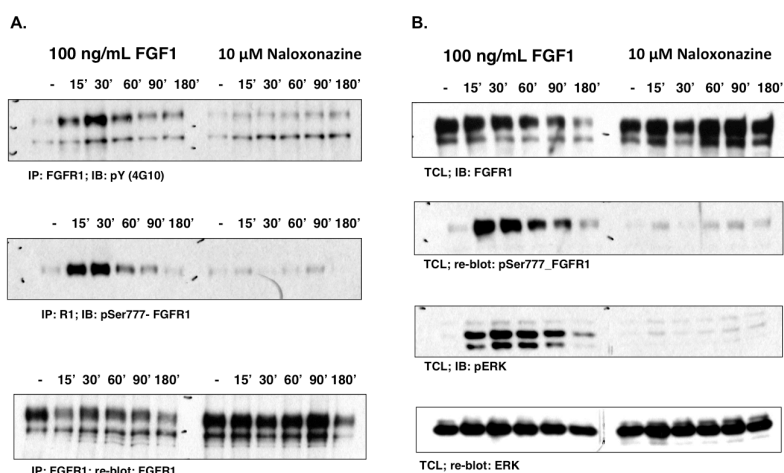


Figure 23. Western Blot of Naloxonazine and Controls in FGFR1-L6 Cells. A. Immunoprecipitation (IP) using two different phospho-antibodies shows no phosphorylation induced by naloxonazine. B. Direct probing of total cell lysates (TCL) at either FGFR1 or ERK shows no activity from naloxonazine. Data represent mean \pm SEM of one representative experiment of $n = 2$ independent experiments. Data obtained by Dr. Leiliane Sousa (Schlessinger Lab, Yale University).

specific enough, leading to a noisy signal that is difficult to quantify.

In a separate blot, our collaborators at Yale University, who have access to more specific FGFR1 antibodies (rat species), tested naloxonazine alongside FGF1 in a time course in

FGFR1-L6 cells, a rat muscle cell line. In these experiments, naloxonazine was unable to phosphorylate the receptor using two different antibodies and was not able to phosphorylate ERK, in-line with the ELISA results (**Figure 23**). In contrast, the FGF1 control worked very well, highlighting the specificity of these in-house antibodies. As western blot analysis with trustworthy antibodies shows no phosphorylation of FGFR1 by naloxonazine, we are confident that this compound is indeed a false positive picked up by the LOPAC screening. This process, while able to correctly identify a false positive, does show the importance of using multiple assays for hit validation. The ELISAs developed for drug pharmacology are an important first step, but given the results with naloxonazine there are some limitations to the assay, and looking at the proteins directly in western blot is an important counter-assay to confirm results.

Continuing Forward with HTS. Currently, a library of 45,000 compounds has been screened for agonism at FGFR1 using the PathHunter[®] assay utilized for the LOPAC screen. Compounds were tested at four different concentrations for agonism and counter screened as described above. After eliminating non-selective hits, 72 hit have been identified that require further testing. These compounds are being retested by our collaborators with fresh powder stocks of each prior to being validated by secondary assays in our laboratory.

Moving forward, we are hopeful that within these 72 hits there will be a true small molecule agonist at FGFR1. However, to prepare for a larger campaign, a larger library of 70,000 is currently being designed for testing in our primary assay. The new library will likely be screened in the presence and absence of a small concentration of FGF2 to test for positive allosteric modulators, or compounds that enhance the signaling of receptor agonist already present. By redoubling our efforts and increasing the scope of our screen, we increase the probability of successfully finding small molecules that will be effective at modulating FGFR1.

Discussion

Mechanism of Action of Naloxonazine. In our pilot screen utilizing the primary PathHunter[®] assay from DiscoverX, naloxonazine was found as a hit among 1280 compounds tested. When naloxonazine was measured in the direct ELISA for FGFR1 phosphorylation, a robust signal was detected that was even more efficacious than the FGF2 control. In early experiments, it was clear that naloxonazine did not activate the receptor in the same way as the native growth factor. For instance, the time profile for activation was strikingly different between FGF2 and naloxonazine. Suspiciously, however, naloxonazine was ineffective at signaling through downstream pathways or at causing neurite outgrowth in PC12 cells. For these reasons, we began to question whether naloxonazine was a true agonist of FGFR1 or just had unique modulatory properties at the receptor. There are known examples of RTK modulation and regulation by tyrosine kinase phosphatases. For example, at the epidermal growth factor receptor (EGFR), inhibition of protein tyrosine phosphatase activity by reactive oxygen species led to increased phosphorylation of the receptor.⁶⁰ In a second study, inhibition of protein tyrosine phosphatase-1B also led to increased phosphorylation of both EGFR and platelet-derived growth factor receptor (PDGFR), however downstream signaling from either ERK or Akt was minimal.⁶¹ Given the similarities between the activities of these phosphatase inhibitors and naloxonazine, it seems plausible that in fact naloxonazine acts as a phosphatase inhibitor. This hypothesis does seem less likely, however, by the observation that naloxonazine was unable to phosphorylate a separate RTK, TrkB, beyond one point activity. As a general phosphatase inhibitor, naloxonazine would in theory be non-selective in its receptor phosphorylation and therefore react similarly with TrkB. It is still possible that naloxonazine is an inhibitor of a more specific phosphatase inhibitor that only acts upon the kinase domain of FGFR1, but such a target

has yet to be identified. Another possibility is that the antibody pair for the phospho-FGFR1 ELISA is not as specific as expected. Although the assay works well with controls, the antibodies being used to capture the receptor could be pulling down proteins other than just FGFR1, as well as bringing FGFR1 complexed with other proteins. The result of such a scenario is that naloxonazine may appear to phosphorylate the receptor when in fact it is acting upon some other target. Testing naloxonazine with much more specific antibodies in a western blot showed no receptor phosphorylation, indicating that either the compound is not a true agonist of the receptor or the phosphorylation detected in our FGFR1-HEK cell line is not robust enough to work in other cells lines or to cause measurable downstream signaling. Working with naloxonazine proved to be an important exercise in understanding the secondary assays. First, the cascade of assays was able to successfully eliminate the compound as a true agonist of the receptor. Second, the use of western blotting was key to the discovery of naloxonazine as a false positive; this fact is important because although western blotting is inferior to ELISA when it comes to measuring quantifiable signaling events, it still plays a complementary role and provides necessary information missing from the ELISA. Finally, the false activity of naloxonazine in the phospho-FGFR1 ELISA suggests that perhaps more specific antibodies should be utilized in this assay. In doing so, we may be able to eliminate false positives earlier in the series of secondary assays or have more sensitive antibodies that can be used in other cellular systems.

Advantages of Using a Small Molecule Modulator. In our search to find true agonists of FGFR1, there are various reasons for pursuing the development of small molecule modulators the receptor (and RTKs in general) rather than endogenous protein agonists. First, as proteins, native growth factors and neurotrophins face many challenges as therapeutics, including limited

ability to cross BBB, short half-life in the bloodstream, and poor oral bioavailability. This concern is supported by the many failed clinical trials performed with growth factors, including BDNF, glial cell line-derived neurotrophic factor (GDNF), and ciliary neurotrophic factor (CNTF), where even with direct infusion the growth factors often suffer from poor penetration.⁶²⁻⁶⁵ Second, the pharmacological and pharmacokinetic properties of small molecules can be readily optimized via the iterative process of medicinal chemistry. Ideally, once a lead compound is identified from HTS, a full SAR exploration will commence to determine important areas of the scaffold for functional activity, as well as the tuning of pharmacokinetic properties. Third, the degree to which an RTK is activated can be achieved by small molecule control of different activation mechanisms. For example, small molecules can act as partial agonists at the RTK, wherein they only achieve partial receptor activation in comparison to the maximal response elicited by native neurotrophins. In particular, partial agonism may be one way to avoid the negative side effects of longer-term FGFR1 activation (see below).¹¹ Finally, a small molecule agonist may be able to bias the signaling to specific pathways in comparison to the native neurotrophins. While there are many studies documenting biased agonism in the context of G-protein coupled receptors (GPCRs),⁶⁶ a few reports also suggest a possibility of biasing RTK-induced signaling with small molecule agonists.^{67,68} A small molecule would allow the fine-tuning of RTK signaling, which would ultimately provide tools to better understand the roles of these receptors in neurogenesis, synaptogenesis, and related processes and ultimately may provide varied therapeutic options in the clinic.

The Difficulty and Likelihood of Developing Small Molecule Agonists for RTKs. Given the high therapeutic value that RTK signaling represents, it is no wonder that the development of RTK small molecule agonists is an active area of research.⁶⁹ Unlike for GPCRs, where small

molecule agonists are plentiful and well studied, there is still limited precedent for the activation of RTKs by small molecules. Additionally, there is increased skepticism in general about the true selectivity of many small molecule probes that perhaps were inadequately characterized at the time of discovery.⁷⁰ RTKs are diverse and activated by many unique protein agonists; some RTKs are activated by receptor dimerization induced by a dimeric protein ligand (e.g., TrkA receptor activation by nerve growth factor), however others are activated by monomeric protein ligands, as shown by FGF2 and FGFR1. There are hypotheses that FGFR1, in fact, exists in a dynamic equilibrium between the monomeric receptor and the dimeric receptor complex, the latter of which is stabilized by two monomeric molecules of FGF2.³ When additional FGF2 binds to the receptor, the receptor is activated (likely due to conformational change of the receptor complex), which then begins the cascade of mutual receptor phosphorylation via the intracellular kinase domains and downstream signaling. Given this rationale, it is not unreasonable to suggest that a small, drug-like molecule could bind to the receptor and favor its dimerization and activation, either as an orthosteric or allosteric agonist. For example, there are reports of small molecule agonists for both the insulin receptor and nerve growth factor receptor (TrkA)^{71,72}, which highlight the feasibility of this approach and the possibility for success in the context of FGFR1.

FGFR1 Activation and Cancer. While the idea of increasing FGFR1/FGF2 signaling makes sense in the context of neuropsychiatric disorders, it is important to consider that FGFR inhibition also has its benefits. Currently, increased expression of FGFR1 alone has been linked to different types of cancer, including breast⁷³, ovarian⁷⁴, bladder⁷⁵, lung⁷⁶, and rhabdomyosarcoma.^{77,78} Consequently, there are many small molecule inhibitors currently in various stages of the clinical trial process that target various FGFR-related tumors.^{77,79} All of

these compounds, however, target multiple RTKs at once as it is notoriously difficult to design a selective RTK inhibitor, suggesting that cancer risk is not necessarily an FGFR specific problem but globally related to RTKs. In any case, this connection to cancer should be taken into account when considering modulating the FGFR system. Presumably patients that require therapeutic FGFR1 intervention will suffer from a deficit in receptor activity, which initially caused the neuropsychiatric disorder. In this sense, the small molecule agonist of FGFR1 would simply be acting to bring FGFR1 signaling up to a higher basal level, repairing any damage caused by the depressed signaling and treating the effects of the mood disorder. A therapeutic dose of agonist, therefore, would likely pose a limited threat of causing cancer.

Conclusions

The recent human and animal data reveal FGFR1 as an important molecular target that modulates neurogenesis, synaptogenesis, and neuronal wiring repair. The application of this receptor to a broad range of CNS disorders, including neurological, neurodegenerative, and psychiatric disorders, is obvious and makes FGFR1 a highly attractive experimental target. Given the lack of true small molecule agonists available today for FGFR1, there is a need to develop novel pharmacological tools and potentially novel therapeutic leads through HTS. Many assays were developed to measure not only receptor activation and downstream signaling but also phenotypic attributes of the cells. Through this battery of secondary assays, a small molecule hit from an initial pilot screen in the primary assay was identified as a false positive, even though two assays found it to be active. A full HTS is now complete, and 72 hits have been identified for validation. The success of correctly eliminating naloxonazine as an FGFR1 agonist proves that lead compounds will be found if they exist. These probes, once identified, will not

only highlight the feasibility of generating small molecule agonists of FGFR1 but will also represent pharmacological validation of FGFR1 as a therapeutic target.

Experimental

Reagents. Recombinant rat or human fibroblast growth factor basic or acidic were purchased from Peprotech. Protease inhibitor cocktail (P8340), phosphatase inhibitor cocktail 2 (P5726), rat tail collagen, poly-D-lysine hydrobromide (30-70 kDa), and PMA were purchased from Sigma Aldrich. PD173074 was purchased from Biotang, Inc. FGL peptide was purchased from Phoenix Pharmaceuticals (#073-36). Naloxonazine hydrochloride was purchased from Tocris.

Cell Culture. hFGFR1-HEK were generated in-house and maintained in Dulbecco's Modified Eagle Medium (Life Technologies; 10569) with 10% (v/v) fetal bovine serum (FBS, Atlanta Biologicals), 100 U mL⁻¹ of penicillin and streptomycin (Life Technologies), and 200 µg/mL G418 (Life Technologies). For stable transfection, HEK-293 were seeded in a 10-cm plate with 1.8 million cells and allowed to grow overnight in media without G418. Then 10 µg of the FGFR1IIIIC cDNA (Origene #RC202080) was transfected using turbofectin (3:1 ratio to cDNA in OptiMEM media, 1 mL). After 24 hours, cells were subcultured into media contained G418 (400 µg/mL). By the second subculture, all cells in a mock transfection plate were dead. Newly transfected cells were then permanently maintained in G418 at a concentration of 200 µg/mL. The transfection was confirmed via western blot. PC12 cells were maintained in RPMI 1640 medium (Life Technologies; 11875085) with 10% horse serum (heat inactivated), 5% FBS, and 100 U mL⁻¹ of penicillin and streptomycin. Cells were incubated at 37 °C with 5% CO₂ humidified atmosphere.

DiscoverX PathHunter[®] assay. PathHunter[®] U2OS FGFR1 cells were detached by detachment reagent (DiscoverX) and resuspended in plating 16 reagent (DiscoverX). Cells (2500 cells/well) were plated into 1536-well plate using a BioRAPTR FRD Microfluidic Workstation. Plates were incubated at 37 °C in 5% CO₂ overnight. Compounds or FGF2 were pin-transferred to the cells. Cells were incubated with compounds for 3 hours at 37 °C. The luminescent detection reagent (DiscoverX) was added for 1 hour at room temperature in the dark. The luminescence was quantified using a ViewLux CCD-based plate reader (PerkinElmer).

FGFR1 Phosphorylation ELISA. FGFR1-HEK were grown in DMEM supplemented with 10% FBS, 100 U mL⁻¹ of penicillin and streptomycin, and 200 µg/mL G418. Cells were added to a collagen-coated 96-well plate at 40,000 cells/well and allowed to grow for 24 hours. The cells were then starved with low serum media (1% FBS supplement instead) for 5 hours before treatment with drugs for 1 hour. The experiment was stopped on ice by aspirating the cellular supernatant and adding 110 µL of lysis buffer (1% TritonX-100, 10% glycine, and 2 mM EDTA in TBS, pH 8.0 with 1:100 protease inhibitor cocktail and 1:100 phosphatase inhibitor cocktail 2) before storing at -80 °C. A separate 96-well plate (Nunc Immulon) was coated with primary FGFR1 antibody (Sigma Aldrich # WH0002260M3) at 1 µg/mL in PBS and stored overnight at 4 °C. The plate was then washed 5X with TBST and blocked (1% BSA in PBS) for 1 hour at room temperature. The plate was washed again 5X with TBST, and 80 µL of the thawed cell lysate was transferred to the 96-well ELISA plate and stored overnight at 4 °C. The remaining 20 µL of cell lysate was used for protein quantification in the BCA assay. The plate was then washed again 5X with TBST and incubated with secondary anti-phospho tyrosine-HRP antibody (R&D Systems #HAM1676) at 1:2500 (in 0.05% Tween-20, 0.1% BSA in TBS, pH 7.4). The plate was washed a final 5X with TBST and developed using TMBone (100 µL/well)

for 30 minutes in the absence of light. Wells were then quenched with 1 M HCl (100 μ L/well), and the plates were read at an absorbance wavelength of 450 nm using a BioTek Synergy H1 plate reader. Raw data were quantified as the phospho-FGFR1 signal divided by the total protein content for each well.

ELFI. Phosphorylation levels of downstream signaling proteins were quantified using enzyme-linked fixed-cell immunoassay (ELFI). Cells were treated similarly as in the phospho-FGFR1 ELISA with a few noted exceptions. FGFR1-HEK cells were seeded at 20,000 cells/well and allowed to grow for 48 hours. Then cells were starved with serum-free media for 30 minutes prior to drug addition. For PC12, cells were seeded at 25,000 cells/well and allowed to grow for 48 hours. The cells were then starved for 48 hours in low serum RPMI (RPMI supplemented with 0.25% horse serum (heat inactivated) and 0.25% fbs) prior to drug addition. Experiments were stopped by fixing the cells in 4% formaldehyde (Sigma, #F8775) for 15 min. Cells were then permeabilized with TBST, blocked in TBST containing 10% BSA, and incubated with detecting antibody for protein of interest for 2 hours at RT or overnight at 4 °C. An appropriate HRP-linked secondary antibody was applied, and luminescence (SuperSignal® ELISA Pico Chemiluminescent Substrate, ThermoScientific #37070) was detected on the plate reader. To quantify different proteins in the same plate, antibodies were stripped using stripping buffer (6M Guanidine•HCl, 0.2% Triton X-100, 20 mM Tris•HCl, pH 7.5)⁸⁰ for 5 min, washed, blocked, and treated with another antibody. Stripping and reprobing cycles were done up to 6 times.

Neurite Outgrowth. PC12 cells were added to a PDL-coated 12-well plate at 50,000 cells/well. After 24 hours, drugs were added to the wells (Day 0). On Day 2, media was aspirated and refreshed with new drug solutions. The experiment was stopped on Day 4. Neurite outgrowth from PC12 cells was measured by light microscopy using a Leica DMI4000B

microscope. Analysis of number and lengths of the neurite outgrowth was quantified using NeuronJ software, where cells having neurites longer than two cell-body lengths were considered differentiated.^{38,81}

Western Blot (FGFR1-HEK). Cells were added to a PDL-coated 12-well plated at 300,000 cell/well. After the experiment, cells were lysed with 100 μ L of lysis buffer (4% SDS, 0.125 M Tris•HCl, 20% glycerol, pH 6.8 with 1:100 protease inhibitor cocktail, phosphatase inhibitor 2 cocktails, and 0.5 M EDTA) and incubated over ice for 15 minutes to an hour, after which cells were scraped and the lysates transferred into microcentrifuge tubes. The tubes were sonicated for 30 s and then centrifuged at 14,500 rpm for 10 minutes. The supernatant was transferred to fresh tubes, and the protein content was measured using the Pierce BCA assay. The lysates were diluted bromophenol for color and β -mercaptoethanol (10% final concentration), and any necessary amount of water. Equal quantities of protein (typically 15-30 μ g/lane) were added to each well of a 10% bis-tris acrylamide gel and were blotted onto Immobilon P PVDF transfer membranes. Blots were blocked in 3% BSA in TBS for at least 1 hour, followed by incubation with the primary antibody overnight (manufacturer recommended dilution and buffer). The blots were washed 3 x 5 minutes with TBST (0.05% Tween20), incubated for 1 hour with secondary antibody (typically 1:1000) in the buffer indicated on the antibody's corresponding data sheet, then washed again for 3 x 5 minutes prior to development with the ECL kit. Chemiluminescence and light absorbance (for protein ladder) was visualized with a Kodak Image Station 440CF imager. Membranes were stripped and reprobbed with the stripping buffer used in the ELFI followed by the same detection procedure for the next target protein. Data were routinely quantified using densitometry by the gel analysis tools in ImageJ (NIH,

Bethesda, MD) following instructions at [http://137.122.232.177/Protocols/ImageJ\(ACM%20revisedv5\).pdf](http://137.122.232.177/Protocols/ImageJ(ACM%20revisedv5).pdf).

Western Blot (FGFR1-L6). After serum starvation, L6 cells stably expressing FGFR1 were stimulated with 100 ng/mL of FGF1 (positive control) or 10 μ M Naloxonazine dihydrochloride (NXZ) at 37 °C for the indicated time points and collected in lysis buffer (50mM HEPES, 150mM NaCl, 1mM EDTA, 1mM EGTA, 10% glycerol, 1% Triton X-100, 25mM NaF, 10 M ZnCl₂, 1mM NaVO₄, and complete protein inhibitor cocktail, Roche). The same amount of total cell lysates (TCL) or lysates subjected to FGFR1 immunoprecipitation (IP) were immunoblotting by standard methods using the following antibodies: ERK and pERK (Santa Cruz); FGFR1, pSer777-FGFR1 and 4G10 anti-phosphotyrosine (Schlessinger's lab). Primary antibodies were detected by anti-mouse HRP and Protein A-HRP (Santa Cruz) and visualized by chemiluminescence kit (Denville, Scientific Inc.) Equal amounts of proteins submitted to WB or IP analysis were also guaranteed by re-probing stripped membranes (0.2 M NaOH, 5 min).

Immunofluorescence. PC12 cells were then fixed with 4% formaldehyde in PBS, washed with PBS, permeabilized (0.25% Triton X-100 in PBS), washed, blocked (2% glycine, 2% bovine serum albumin in 50 mM NH₄Cl) for 30 min at 37 °C and incubated overnight with anti-FGFR1 antibodies (1:200 in blocking solution; #WH0002260M3, Sigma Aldrich) at 4 °C. Cells were then washed 5X with PBS, blocked again for 30 min at 37 °C, and incubated with a mixture of anti-mouse Alexa Fluor[®] 594 secondary antibody (1:1000 in blocking solution; Cell Signaling #8890) and Hoechst 33258 stain (1:10,000). The cells were then washed 5X in PBS and imaged on a Leica DMI4000B microscope.

Statistical Analysis. Data analysis was performed using Graphpad Prism 6 Software (San Diego, CA). Conditions are expressed as mean \pm SD and were subjected to ANOVA

followed by either Dunnett's or Tukey's Multiple Comparisons Test with a significant level of $p < 0.05$. Dose–response curves were fit using a four-parameter logistic equation.

References

- (1) Reuss, B.; von Bohlen und Halbach, O. Fibroblast Growth Factors and Their Receptors in the Central Nervous System. *Cell Tissue Res.* **2003**, *313*, 139–157.
- (2) Goldfarb, M.; Schoorlemmer, J.; Williams, A.; Diwakar, S.; Wang, Q.; Huang, X.; Giza, J.; Tchetchik, D.; Kelley, K.; Vega, A.; Matthews, G.; Rossi, P.; Ornitz, D. M.; D'Angelo, E. Fibroblast Growth Factor Homologous Factors Control Neuronal Excitability through Modulation of Voltage-Gated Sodium Channels. *Neuron* **2007**, *55*, 449–463.
- (3) Lemmon, M. A.; Schlessinger, J. Cell Signaling by Receptor Tyrosine Kinases. *Cell* **2010**, *141*, 1117–1134.
- (4) Huang, E. J.; Reichardt, L. F. Neurotrophins: Roles in Neuronal Development and Function. *Annu. Rev. Neurosci.* **2001**, *24*, 677–736.
- (5) Yayon, A.; Klagsbrun, M.; Esko, J. D.; Leder, P.; Ornitz, D. M. Cell Surface, Heparin-like Molecules Are Required for Binding of Basic Fibroblast Growth Factor to Its High Affinity Receptor. *Cell* **1991**, *64*, 841–848.
- (6) Reiland, J.; Rapraeger, A. C. Heparan Sulfate Proteoglycan and FGF Receptor Target Basic FGF to Different Intracellular Destinations. *J. Cell Sci.* **1993**, *105* (Pt 4), 1085–1093.
- (7) Guimond, S. E.; Turnbull, J. E. Fibroblast Growth Factor Receptor Signalling Is Dictated by Specific Heparan Sulphate Saccharides. *Curr. Biol.* **1999**, *9*, 1343–1346.
- (8) Ornitz, D. M. FGFs, Heparan Sulfate and FGFRs: Complex Interactions Essential for Development. *Bioessays* **2000**, *22*, 108–112.
- (9) Zhu, H.; Duchesne, L.; Rudland, P. S.; Fernig, D. G. The Heparan Sulfate Co-Receptor and the Concentration of Fibroblast Growth Factor-2 Independently Elicit Different Signalling Patterns from the Fibroblast Growth Factor Receptor. *Cell Commun. Signal.* **2010**, *8*, 14.
- (10) Evans, S. J.; Choudary, P. V.; Neal, C. R.; Li, J. Z.; Vawter, M. P.; Tomita, H.; Lopez, J. F.; Thompson, R. C.; Meng, F.; Stead, J. D.; Walsh, D. M.; Myers, R. M.; Bunney, W. E.; Watson, S. J.; Jones, E. G.; Akil, H. Dysregulation of the Fibroblast Growth Factor System in Major Depression. *Proc. Natl. Acad. Sci. U. S. A.* **2004**, *101*, 15506–15511.
- (11) Turner, C. A.; Watson, S. J.; Akil, H. The Fibroblast Growth Factor Family: Neuromodulation of Affective Behavior. *Neuron* **2012**, *76*, 160–174.
- (12) Riva, M. A.; Molteni, R.; Bedogni, F.; Racagni, G.; Fumagalli, F. Emerging Role of the FGF System in Psychiatric Disorders. *Trends Pharmacol. Sci.* **2005**, *26*, 228–231.
- (13) Kato, M.; Okugawa, G.; Wakeno, M.; Takekita, Y.; Nonen, S.; Tetsuo, S.; Nishida, K.; Azuma, J.; Kinoshita, T.; Serretti, A. Effect of Basic Fibroblast Growth Factor (FGF2) Gene Polymorphisms on SSRIs Treatment Response and Side Effects. *Eur. Neuropsychopharmacol.* **2009**, *19*, 718–725.
- (14) Turner, C. A.; Calvo, N.; Frost, D. O.; Akil, H.; Watson, S. J. The Fibroblast Growth Factor System Is Downregulated Following Social Defeat. *Neurosci. Lett.* **2008**, *430*, 147–

- 150.
- (15) Turner, C. A.; Gula, E. L.; Taylor, L. P.; Watson, S. J.; Akil, H. Antidepressant-like Effects of Intracerebroventricular FGF2 in Rats. *Brain Res.* **2008**, *1224*, 63–68.
 - (16) Elsayed, M.; Banasr, M.; Duric, V.; Fournier, N. M.; Licznanski, P.; Duman, R. S. Antidepressant Effects of Fibroblast Growth Factor-2 in Behavioral and Cellular Models of Depression. *Biol. Psychiatry* **2012**, *72*, 258–265.
 - (17) Perez, J. A.; Clinton, S. M.; Turner, C. A.; Watson, S. J.; Akil, H. A New Role for FGF2 as an Endogenous Inhibitor of Anxiety. *J. Neurosci.* **2009**, *29*, 6379–6387.
 - (18) Preston, T. C.; Shelton, R. C. Treatment Resistant Depression: Strategies for Primary Care Topical Collection on Psychiatry in Primary Care. *Curr. Psychiatry Rep.* **2013**, *15*, 13–18.
 - (19) Martinowich, K.; Jimenez, D. V.; Zarate, C. A.; Manji, H. K. Rapid Antidepressant Effects: Moving Right Along. *Mol. Psychiatry* **2013**, *18*, 856–863.
 - (20) Ren, J. M.; Finklestein, S. P. Growth Factor Treatment of Stroke. *Curr. Drug Targets. CNS Neurol. Disord.* **2005**, *4*, 121–125.
 - (21) Woodbury, M. E.; Ikezu, T. Fibroblast Growth Factor-2 Signaling in Neurogenesis and Neurodegeneration. *J. Neuroimmune Pharmacol.* **2014**, *9*, 92–101.
 - (22) Terwisscha van Scheltinga, A. F.; Bakker, S. C.; Kahn, R. S.; Kas, M. J. H. Fibroblast Growth Factors in Neurodevelopment and Psychopathology. *Neuroscientist* **2013**, *19*, 479–494.
 - (23) Zhao, M.; Li, D.; Shimazu, K.; Zhou, Y.-X.; Lu, B.; Deng, C.-X. Fibroblast Growth Factor Receptor-1 Is Required for Long-Term Potentiation, Memory Consolidation, and Neurogenesis. *Biol. Psychiatry* **2007**, *62*, 381–390.
 - (24) Mudò, G.; Bonomo, A.; Di Liberto, V.; Frinchi, M.; Fuxe, K.; Belluardo, N. The FGF-2/FGFRs Neurotrophic System Promotes Neurogenesis in the Adult Brain. *J. Neural Transm.* **2009**, *116*, 995–1005.
 - (25) Terry, R. D.; Masliah, E.; Salmon, D. P.; Butters, N.; DeTeresa, R.; Hill, R.; Hansen, L. A.; Katzman, R. Physical Basis of Cognitive Alterations in Alzheimer’s Disease: Synapse Loss Is the Major Correlate of Cognitive Impairment. *Ann. Neurol.* **1991**, *30*, 572–580.
 - (26) Clary-Ceccato, M.-L.; Guillo, N. FGF Receptor (FGFR) Agonist Dimeric Compounds, Process for the Preparation Thereof and Therapeutic Use Thereof. WO 2013/098764 A1, 2013.
 - (27) Ballinger, M. D.; Shyamala, V.; Forrest, L. D.; Deuter-Reinhard, M.; Doyle, L. V.; Wang, J. X.; Panganiban-Lustan, L.; Stratton, J. R.; Apell, G.; Winter, J. A.; Doyle, M. V.; Rosenberg, S.; Kavanaugh, W. M. Semirational Design of a Potent, Artificial Agonist of Fibroblast Growth Factor Receptors. *Nat. Biotechnol.* **1999**, *17*, 1199–1204.
 - (28) Anderson, A. A.; Kendal, C. E.; Garcia-Maya, M.; Kenny, A. V.; Morris-Triggs, S. A.; Wu, T.; Reynolds, R.; Hohenester, E.; Saffell, J. L. A Peptide from the First Fibronectin Domain of NCAM Acts as an Inverse Agonist and Stimulates FGF Receptor Activation, Neurite Outgrowth and Survival. *J. Neurochem.* **2005**, *95*, 570–583.
 - (29) Lin, X.; Takahashi, K.; Champion, S. L.; Liu, Y.; Gustavsen, G. G.; Peña, L. A.; Zamora, P. O. Synthetic Peptide F2A4-K-NS Mimics Fibroblast Growth Factor-2 in Vitro and Is Angiogenic in Vivo. *Int. J. Mol. Med.* **2006**, *17*, 833–839.
 - (30) Jacobsen, J.; Kiselyov, V.; Bock, E.; Berezin, V. A Peptide Motif from the Second Fibronectin Module of the Neural Cell Adhesion Molecule, NCAM, NLIKQDDGGSPIRHY, Is a Binding Site for the FGF Receptor. *Neurochem. Res.* **2008**, *33*, 2532–2539.

- (31) Li, S.; Christensen, C.; Kiselyov, V. V.; K hler, L. B.; Bock, E.; Berezin, V. Fibroblast Growth Factor-Derived Peptides: Functional Agonists of the Fibroblast Growth Factor Receptor. *J. Neurochem.* **2008**, *104*, 667–682.
- (32) Li, S.; Christensen, C.; K hler, L. B.; Kiselyov, V. V.; Berezin, V.; Bock, E. Agonists of Fibroblast Growth Factor Receptor Induce Neurite Outgrowth and Survival of Cerebellar Granule Neurons. *Dev. Neurobiol.* **2009**, *69*, 837–854.
- (33) Manf , V.; Kochoyan, A.; Bock, E.; Berezin, V. Peptides Derived from Specific Interaction Sites of the Fibroblast Growth Factor 2-FGF Receptor Complexes Induce Receptor Activation and Signaling. *J. Neurochem.* **2010**, *114*, 74–86.
- (34) Kiselyov, V.; Skladchikova, G.; Hinsby, A.; Jensen, P.; Kulahin, N.; Soroka, V.; Pedersen, N.; Tsetlin, V.; Poulsen, F.; Berezin, V. Structural Basis for a Direct Interaction between FGFR1 and NCAM and Evidence for a Regulatory Role of ATP. *Structure* **2003**, *11*, 691–701.
- (35) Neiiendam, J. L.; K hler, L. B.; Christensen, C.; Li, S.; Pedersen, M. V.; Ditlevsen, D. K.; Kornum, M. K.; Kiselyov, V. V.; Berezin, V.; Bock, E. An NCAM-Derived FGF-Receptor Agonist, the FGL-Peptide, Induces Neurite Outgrowth and Neuronal Survival in Primary Rat Neurons. *J. Neurochem.* **2004**, *91*, 920–935.
- (36) Sadick, M. D.; Galloway, A.; Shelton, D.; Hale, V.; Weck, S.; Anicetti, V.; Wong, W. L. Analysis of Neurotrophin/receptor Interactions with a gD-Flag-Modified Quantitative Kinase Receptor Activation (gD.KIRA) Enzyme-Linked Immunosorbent Assay. *Exp. Cell Res.* **1997**, *234*, 354–361.
- (37) Gonzalez, A. M.; Berry, M.; Maher, P. A.; Logan, A.; Baird, A. A Comprehensive Analysis of the Distribution of FGF-2 and FGFR1 in the Rat Brain. *Brain Res.* **1995**, *701*, 201–226.
- (38) Lin, H. Y.; Xu, J.; Ornitz, D. M.; Halegoua, S.; Hayman, M. J. The Fibroblast Growth Factor Receptor-1 Is Necessary for the Induction of Neurite Outgrowth in PC12 Cells by aFGF. *J. Neurosci.* **1996**, *16*, 4579–4587.
- (39) Franklin, R. A.; Tordai, A.; Patel, H.; Gardner, A. M.; Johnson, G. L.; Gelfand, E. W. Ligation of the T Cell Receptor Complex Results in Activation of the Ras/Raf-1/MEK/MAPK Cascade in Human T Lymphocytes. *J. Clin. Invest.* **1994**, *93*, 2134–2140.
- (40) Lee, F. S.; Rajagopal, R.; Kim, A. H.; Chang, P. C.; Chao, M. V. Activation of Trk Neurotrophin Receptor Signaling by Pituitary Adenylate Cyclase-Activating Polypeptides. *J. Biol. Chem.* **2002**, *277*, 9096–9102.
- (41) Graham, D. L.; Edwards, S.; Bachtell, R. K.; DiLeone, R. J.; Rios, M.; Self, D. W. Dynamic BDNF Activity in Nucleus Accumbens with Cocaine Use Increases Self-Administration and Relapse. *Nat. Neurosci.* **2007**, *10*, 1029–1037.
- (42) Drubin, D. G.; Feinstein, S. C.; Shooter, E. M.; Kirscher, M. W. Nerve Growth Factor-Induced Neurite Outgrowth in PC12 Cells Involves the Coordinate Induction of Microtubule Assembly-Promoting Factors. *J. Cell Biol.* **1985**, *1985*, 1799–1807.
- (43) Rydel, R. E.; Greene, L. A. Acidic and Basic Fibroblast Growth Factors Promote Stable Neurite Outgrowth and Neuronal Differentiation in Cultures of PC12 Cells. *J. Neurosci.* **1987**, *7*, 3639–3653.
- (44) Lin, H.; Xu, J.; Ischenko, I.; Ornitz, D. M.; Halegoua, S.; Hayman, M. J. Identification of the Cytoplasmic Regions of Fibroblast Growth Factor (FGF) Receptor 1 Which Play Important Roles in Induction of Neurite Outgrowth in PC12 Cells by FGF-1 Identification of the Cytoplasmic Regions of Fibroblast Growth Factor (FGF) Receptor. *Molecular Cell.*

- Biol.* **1998**, *18*, 3762–3770.
- (45) Powers, C. J.; McLeskey, S. W.; Wellstein, A. Fibroblast Growth Factors, Their Receptors and Signaling. *Endocr. Relat. Cancer* **2000**, *7*, 165–197.
- (46) Zhang, J.-H. A Simple Statistical Parameter for Use in Evaluation and Validation of High Throughput Screening Assays. *J. Biomol. Screen.* **1999**, *4*, 67–73.
- (47) Iversen, P. W.; Beck, B.; Chen, Y. F.; Dere, W.; Devanarayan, V.; Eastwood, B. J.; Farmen, M. W.; Iturria, S. J.; Montrose, C.; Moore, R. A.; Weidner, J. R.; Sittampalam, G. S. *HTS Assay Validation*; Sittampalam, G. S.; Gal-Edd, N.; Arkin, M.; Auld, D.; Austin, C.; Bejcek, B.; Glicksman, M.; Inglese, J.; Lemmon, V.; Li, Z.; McGee, J.; McManus, O.; Minor, L.; Napper, A.; Riss, T.; Trask, O. J.; Weidner, J., Eds.; Eli Lilly & Company and the National Center for Advancing Translational Sciences: Bethesda, Maryland, 2012.
- (48) Inglese, J.; Auld, D. S.; Jadhav, A.; Johnson, R. L.; Simeonov, A.; Yasgar, A.; Zheng, W.; Austin, C. P. Quantitative High-Throughput Screening: A Titration-Based Approach That Efficiently Identifies Biological Activities in Large Chemical Libraries. *Proc. Natl. Acad. Sci. U. S. A.* **2006**, *103*, 11473–11478.
- (49) Bhattacharyya, N.; Hu, X.; Chen, C. Z.; Mathews Griner, L. A.; Zheng, W.; Inglese, J.; Austin, C. P.; Marugan, J. J.; Southall, N.; Neumann, S.; Northup, J. K.; Ferrer, M.; Collins, M. T. A High Throughput Screening Assay System for the Identification of Small Molecule Inhibitors of Gsp. *PLoS One* **2014**, *9*, e90766.
- (50) Wang, Y.; Jadhav, A.; Southal, N.; Huang, R.; Nguyen, D.-T. A Grid Algorithm for High Throughput Fitting of Dose-Response Curve Data. *Curr. Chem. Genomics* **2010**, *4*, 57–66.
- (51) Hahn, E. F.; Pasternak, G. W. Naloxonazine, a Potent, Long-Lasting Inhibitor of Opiate Binding Sites. *Life Sci.* **1982**, *31*, 1385–1388.
- (52) Hahn, E. F.; Carroll-Buatti, M.; Pasternak, G. W. Irreversible Opiate Agonists and Antagonists: The 14-Hydroxydihydromorphinone Azines. *J. Neurosci.* **1982**, *2*, 572–576.
- (53) Ling, G. S.; Simantov, R.; Clark, J. A.; Pasternak, G. W. Naloxonazine Actions in Vivo. *Eur. J. Pharmacol.* **1986**, *129*, 33–38.
- (54) Yoshii, A.; Constantine-Paton, M. Postsynaptic BDNF-TrkB Signaling in Synapse Maturation, Plasticity, and Disease. *Dev. Neurobiol.* **2010**, *70*, 304–322.
- (55) Rantamäki, T.; Hendolin, P.; Kankaanpää, A.; Mijatovic, J.; Piepponen, P.; Domenici, E.; Chao, M. V.; Männistö, P. T.; Castrén, E. Pharmacologically Diverse Antidepressants Rapidly Activate Brain-Derived Neurotrophic Factor Receptor TrkB and Induce Phospholipase-Cgamma Signaling Pathways in Mouse Brain. *Neuropsychopharmacology* **2007**, *32*, 2152–2162.
- (56) Li, Y.; Luikart, B. W.; Birnbaum, S.; Chen, J.; Kwon, C.-H.; Kernie, S. G.; Bassel-Duby, R.; Parada, L. F. TrkB Regulates Hippocampal Neurogenesis and Governs Sensitivity to Antidepressive Treatment. *Neuron* **2008**, *59*, 399–412.
- (57) May, L. T.; Leach, K.; Sexton, P. M.; Christopoulos, A. Allosteric Modulation of G Protein-Coupled Receptors. *Annu. Rev. Pharmacol. Toxicol.* **2007**, *47*, 1–51.
- (58) Kenakin, T. Allosteric Agonist Modulators. *J. Recept. Signal Transduct. Res.* **2007**, *27*, 247–259.
- (59) Mohammadi, M.; Dikic, I.; Sorokin, A.; Burgess, W. H.; Jaye, M.; Schlessinger, J. Identification of Six Novel Autophosphorylation Sites on Fibroblast Growth Factor Receptor 1 and Elucidation of Their Importance in Receptor Activation and Signal Transduction. *Mol. Cell. Biol.* **1996**, *16*, 977–989.
- (60) Reynolds, A. R.; Tischer, C.; Verveer, P. J.; Rocks, O.; Bastiaens, P. I. H. EGFR

- Activation Coupled to Inhibition of Tyrosine Phosphatases Causes Lateral Signal Propagation. *Nat. Cell Biol.* **2003**, *5*, 447–453.
- (61) Haj, F. G.; Markova, B.; Klamann, L. D.; Bohmer, F. D.; Neel, B. G. Regulation of Receptor Tyrosine Kinase Signaling by Protein Tyrosine Phosphatase-1B. *J Biol Chem* **2003**, *278*, 739–744.
- (62) Kalra, S.; Genge, A.; Arnold, D. L. A Prospective, Randomized, Placebo-Controlled Evaluation of Corticoneuronal Response to Intrathecal BDNF Therapy in ALS Using Magnetic Resonance Spectroscopy: Feasibility and Results. *Amyotroph. Lateral Scler. Other Motor Neuron Disord.* **2003**, *4*, 22–26.
- (63) Beck, M.; Flachenecker, P.; Magnus, T.; Giess, R.; Reiners, K.; Toyka, K. V.; Naumann, M. Autonomic Dysfunction in ALS: A Preliminary Study on the Effects of Intrathecal BDNF. *Amyotroph. Lateral Scler. Other Motor Neuron Disord.* **2005**, *6*, 100–103.
- (64) Salvatore, M. F.; Ai, Y.; Fischer, B.; Zhang, A. M.; Grondin, R. C.; Zhang, Z.; Gerhardt, G. a; Gash, D. M. Point Source Concentration of GDNF May Explain Failure of Phase II Clinical Trial. *Exp. Neurol.* **2006**, *202*, 497–505.
- (65) Miller, R. G.; Petajan, J. H.; Bryan, W. W.; Armon, C.; Barohn, R. J.; Goodpasture, J. C.; Hoagland, R. J.; Parry, G. J.; Ross, M. A.; Stromatt, S. C. A Placebo-Controlled Trial of Recombinant Human Ciliary Neurotrophic (rhCNTF) Factor in Amyotrophic Lateral Sclerosis. rhCNTF ALS Study Group. *Ann. Neurol.* **1996**, *39*, 256–260.
- (66) Rives, M.-L.; Rossillo, M.; Liu-Chen, L.-Y.; Javitch, J. A. 6'-Guanidinonaltrindole (6'-GNTI) Is a G Protein-Biased κ -Opioid Receptor Agonist That Inhibits Arrestin Recruitment. *J. Biol. Chem.* **2012**, *287*, 27050–27054.
- (67) Chen, D.; Brahim, F.; Angell, Y.; Li, Y.-C.; Moskowicz, J.; Saragovi, H. U.; Burgess, K. Bivalent Peptidomimetic Ligands of TrkC Are Biased Agonists and Selectively Induce Neuritogenesis or Potentiate Neurotrophin-3 Trophic Signals. *ACS Chem. Biol.* **2009**, *4*, 769–781.
- (68) Lin, B.; Pirrung, M. C.; Deng, L.; Li, Z.; Liu, Y.; Webster, N. J. G. Neuroprotection by Small Molecule Activators of the Nerve Growth Factor Receptor. *J. Pharmacol. Exp. Ther.* **2007**, *322*, 59–69.
- (69) Longo, F. M.; Massa, S. M. Small-Molecule Modulation of Neurotrophin Receptors: A Strategy for the Treatment of Neurological Disease. *Nat. Rev. Drug Discov.* **2013**, *12*, 507–525.
- (70) Arrowsmith, C. H.; Audia, J. E.; Austin, C.; Baell, J.; Bennett, J.; Blagg, J.; Bountra, C.; Brennan, P. E.; Brown, P. J.; Bunnage, M. E.; Buser-Doepner, C.; Campbell, R. M.; Carter, A. J.; Cohen, P.; Copeland, R. a; Cravatt, B.; Dahlin, J. L.; Dhanak, D.; Edwards, A. M.; Frye, S. V.; Gray, N.; Grimshaw, C. E.; Hepworth, D.; Howe, T.; Huber, K. V. M.; Jin, J.; Knapp, S.; Kotz, J. D.; Kruger, R. G.; Lowe, D.; Mader, M. M.; Marsden, B.; Mueller-Fahrnow, A.; Müller, S.; O'Hagan, R. C.; Overington, J. P.; Owen, D. R.; Rosenberg, S. H.; Roth, B.; Ross, R.; Schapira, M.; Schreiber, S. L.; Shoichet, B.; Sundström, M.; Superti-Furga, G.; Taunton, J.; Toledo-Sherman, L.; Walpole, C.; Walters, M. a; Willson, T. M.; Workman, P.; Young, R. N.; Zuercher, W. J. The Promise and Peril of Chemical Probes. *Nat. Chem. Biol.* **2015**, *11*, 536–541.
- (71) Lin, B.; Li, Z.; Park, K.; Deng, L.; Pai, A.; Zhong, L.; Pirrung, M. C.; Webster, N. J. G. Identification of Novel Orally Available Small Molecule Insulin Mimetics. *J. Pharmacol. Exp. Ther.* **2007**, *323*, 579–585.
- (72) Maliartchouk, S.; Feng, Y.; Ivanisevic, L.; Debeir, T.; Cuello, a C.; Burgess, K.;

- Saragovi, H. U. A Designed Peptidomimetic Agonistic Ligand of TrkA Nerve Growth Factor Receptors. *Mol. Pharmacol.* **2000**, *57*, 385–391.
- (73) Jacquemier, J.; Adelaide, J.; Parc, P.; Penault-Llorca, F.; Planche, J.; DeLapeyriere, O.; Birnbaum, D. Expression of the FGFR1 Gene in Human Breast-Carcinoma Cells. *Int. J. cancer* **1994**, *59*, 373–378.
- (74) Gorringer, K. L.; Jacobs, S.; Thompson, E. R.; Sridhar, A.; Qiu, W.; Choong, D. Y. H.; Campbell, I. G. High-Resolution Single Nucleotide Polymorphism Array Analysis of Epithelial Ovarian Cancer Reveals Numerous Microdeletions and Amplifications. *Clin. Cancer Res.* **2007**, *13*, 4731–4739.
- (75) Simon, R.; Richter, J.; Wagner, U.; Fijan, A.; Bruderer, J.; Schmid, U.; Ackermann, D.; Maurer, R.; Alund, G.; Knönagel, H.; Rist, M.; Wilber, K.; Anabitarte, M.; Hering, F.; Hardmeier, T.; Schönenberger, A.; Flury, R.; Jäger, P.; Fehr, J. L.; Schraml, P.; Moch, H.; Mihatsch, M. J.; Gasser, T.; Sauter, G. High-Throughput Tissue Microarray Analysis of 3p25 (RAF1) and 8p12 (FGFR1) Copy Number Alterations in Urinary Bladder Cancer. *Cancer Res.* **2001**, *61*, 4514–4519.
- (76) Dutt, A.; Ramos, A. H.; Hammerman, P. S.; Mermel, C.; Cho, J.; Sharifnia, T.; Chande, A.; Tanaka, K. E.; Stransky, N.; Greulich, H.; Gray, N. S.; Meyerson, M. Inhibitor-Sensitive *fgfr1* Amplification in Human Non-Small Cell Lung Cancer. *PLoS One* **2011**, *6*, 1–10.
- (77) Tiong, K. H.; Mah, L. Y.; Leong, C.-O. Functional Roles of Fibroblast Growth Factor Receptors (FGFRs) Signaling in Human Cancers. *Apoptosis* **2013**, *18*, 1447–1468.
- (78) Missiaglia, E.; Selfe, J.; Hamdi, M.; Williamson, D.; Schaaf, G.; Fang, C.; Koster, J.; Summersgill, B.; Messahel, B.; Versteeg, R.; Pritchard-Jones, K.; Kool, M.; Shipley, J. Genomic Imbalances in Rhabdomyosarcoma Cell Lines Affect Expression of Genes Frequently Altered in Primary Tumors: An Approach to Identify Candidate Genes Involved in Tumor Development. *Genes. Chromosomes Cancer* **2009**, *48*, 455–467.
- (79) Hojjat-Farsangi, M. Small-Molecule Inhibitors of the Receptor Tyrosine Kinases: Promising Tools for Targeted Cancer Therapies. *Int. J. Mol. Sci.* **2014**, *15*, 13768–13801.
- (80) Yeung, Y.; Stanley, E. R. A Solution for Stripping Antibodies from Polyvinylidene Fluoride Immunoblots for Multiple Reprobing. *Anal. Biochem.* **2009**, *389*, 89–91.
- (81) Hayashi, H.; Ishisaki, A.; Suzuki, M.; Imamura, T. BMP-2 Augments FGF-Induced Differentiation of PC12 Cells through Upregulation of FGF Receptor-1 Expression. *J. Cell Sci.* **2001**, *114*, 1387–1395.